Mission-Oriented Seismic Research Program

Annual Report

2013-2014

M-OSRP

University of Houston

Sponsors and Advisory Board representatives

May 21, 2014

Corporate Sponsors

Anadarko ..... Yafei Wu
BGP/CNPC ..... Shaohua Zhang, Lei Na
BHP Billiton ..... Corey Morgan
BP ..... Imtíaz Ahmed
Chevron ..... Debbie Bones
ConocoPhillips ..... Haiyan Zhang, Robert Stolt
Devon Energy ..... Alex Bridge
Encana ..... David Bonar
ExxonMobil ..... Ramesh Neelamani, Peter Traynin
Hess ..... Scott Morton
IBM ..... Tom McClure
Ion ..... Jacques Leveille
Pemex ..... Pamela Diaz
Petrobras ..... Paulo M. Carvalho, Neiva Zago
PGS ..... Nizar Chemingui, Sverre Brandsberg-Dahl
Repsol ..... Gladys Gonzalez, Francisco Ortigosa
Saudi Aramco ..... Yi Luo, Tim Keho
Shell ..... Jonathan Sheiman
Statoil ..... Marianne Houbiers, Lasse Amundsen
Total ..... Bertrand Duquet, Wafik Beydoun
WesternGeco ..... Clement Kostov, Richard Coates

Federal Support

DOE Basic Sciences award DE-FG02-05ER15697 ..... Nick Woodward
NSF-CMG award DMS-0327778 ..... Henry A. Warchall

M-OSRP Personnel

Faculty, Adjunct Faculty, Research Faculty, Postdocs

Lasse Amundsen (Statoil) ..... Adjunct Professor (Physics)
Douglas J. Foster (ConocoPhillips) ..... Adjunct Professor (Physics)
Kristopher A. Innanen (Associate Professor, University of Calgary) .. Adjunct Professor (Physics)
Robert G. Keys (ConocoPhillips) ..... Adjunct Professor (Physics)
Jacques Leveille (Ion) ..... Adjunct Professor (Physics)
Fang Liu ..... Research Assistant Professor (Physics)
Ken H. Matson (Shell) ..... Adjunct Associate Professor (Physics)
James D. Mayhan ..... Post Doctoral Fellow 1 (Physics)
Mark Meier (ExxonMobil) ..... Adjunct Professor (Physics)
Jon Sheiman (Shell) ..... Adjunct Professor (Physics)
Robert H. Stolt (ConocoPhillips) ..... Adjunct Professor (Physics)
T. Hing Tan (Shell) ..... Adjunct Professor (Physics)
Arthur B. Weglein ..... Cullen Professor (Physics)
Daniel Whitmore (PGS) ..... Adjunct Professor (Physics)

Graduate Students (PhD candidates)

Qiang Fu ..... Physics
Xinglu Lin ..... Physics
Chao Ma ..... Physics
Lin Tang ..... Physics
Jing Wu ..... Physics
Jinlong Yang ..... Physics
Yanglei Zou ..... Physics

Recent Alumni

Hichem Ayadi ..... Physics
Andre Ferreira[2] ..... Geosciences
Zhiqiang Guo ..... Geosciences
Wilberth Herrera ..... Physics
Shih-Ying Hsu ..... Physics
Xu Li ..... Physics
Hong Liang ..... Physics
Jose Eduardo Lira[2] ..... Geosciences
Fang Liu ..... Physics
James D. Mayhan ..... Physics
Francisco Miranda ..... Physics
Mozhdeh Niazmand ..... Physics
Adriana Citlali Ramírez ..... Physics
Simon A. Shaw ..... Geosciences
Zhiqiang Wang ..... Physics
Haiyan Zhang ..... Physics
Jingfeng Zhang ..... Physics

Administrative Support

Jennifer Chin-Davis ..... Associate Director, Physics Department
Andrew Fortney ..... Computer/IT Support
Chris Watts ..... Webmaster/NSM IT
Andrea Arias-Rodriguez ..... NSM IT
Anne Thomas ..... Copy Editor

[2]Petrobras, Brazil

Table of Contents

Introduction

Arthur B. Weglein

May 21, 2014

M-OSRP's research objective and goal: identify and address seismic processing challenges

The research objective of M-OSRP is to identify and address outstanding, pressing and prioritized seismic exploration challenges. M-OSRP develops and delivers step-change improved capability to the seismic processing tool-box. That goal delivers new options and processing methods that will be successful and effective when the methods and choices within the current tool-box can and will have difficulty and/or fail. What we provide will not always be the appropriate choice within the toolbox; but what we provide increases the number and types of options, and allows new capability, when needed. That new set of options then facilitates and supports exploring and producing in offshore and on-shore areas and types of plays that are currently too technically challenging, high risk, and unreasonable as investments and to help make those currently difficult or precluded E&P areas, plays and opportunities more reasonable, accessible and manageable.

What's behind seismic processing challenges? Why do we drill dry holes; why do we drill suboptimal development wells? Why do seismic processing methods have problems and fail?

Seismic processing methods are effective and successful when their assumptions and prerequisites are satisfied. When assumptions behind processing methods are not satisfied, these methods can fail. That, in turn, contributes to dry hole drilling and sub-optimal development well drilling decisions.

There are different categories of assumptions, among them are: (1) acquiring the required/adequate seismic data, and (2) required preprocessing, subsurface information, interpretive intervention, needed for methods to be effective.

The M-OSRP strategy and plan

The industry trend to more complicated and challenging offshore and on-shore plays demands more sophisticated and effective seismic processing and imaging methods, with more physically

complete and realistic descriptions and concepts. Historically, at every stage of seismic processing and imaging evolution and advancement there has been a concomitant greater demand on providing more detailed and accurate subsurface information (for example, the evolution of seismic migration from post-stack migration, to pre-stack time migration, to pre-stack depth migration, to pre-stack migration-inversion, to RTM for heterogeneous anisotropic media) where each step was, at once, both more complete, effective and more demanding.

The confluence of seismic methods that make increasing demands for detailed and accurate subsurface information, together with the industry trend to regions and plays where providing that level of subsurface information is, in general, increasingly difficult to satisfy, and therefore represents a significant challenge at the present time and for the foreseeable future.

The inability to adequately provide that accurate and detailed subsurface information is a contributing factor to seismic processing, imaging and inversion breakdown and failure and subsequent dry hole drilling. There are two ways to address that type of challenge: (1) remove the assumption violation by finding, *e.g.*, new methods and approaches for satisfying the prerequisites, data acquisition assumptions, and accurate velocity models and other subsurface information, or (2) remove the assumption, by developing new methods that do not make that assumption.

Methods have assumptions and requirements: How does M-OSRP decide whether to advance seismic capability by: (a) developing new methods/approaches to provide what a current method requires or (b) developing fundamentally new methods that do not have those requirements/assumptions?

M-OSRP adopts one or the other of these attitudes and approaches for different assumptions, requirements, steps, and links in the seismic processing chain that's under stress and duress and is in need of attention and improvement.

We describe here the basic strategy that M-OSRP adopts in deciding between: (a) finding a better way of satisfying a current method's assumptions and requirements, and (b) developing new and more effective methods that do not require those assumptions.

If the method requires, *e.g.*, adequate data collected or a better description of the seismic experiment (*e.g.*, the source signature and radiation pattern and deghosted data) then find an approach and method to satisfy those requirements. However, if the method requires detailed subsurface information, or interpretive intervention, to be effective and successful then develop a direct method that doesn't require that subsurface information.

Why the aversion to providing subsurface information?

As the petroleum industry trend world-wide moves to ever more complex and challenging plays, the ability to provide subsurface information has become (and will continue to become) an increasingly serious impediment to effectiveness. That fact, explains the reasonableness and (in fact) the necessity of seeking new methods that can be more effective than current capability, and without subsurface information.

A central purpose of M-OSRP has been, and remains, to provide a consistent and comprehensive set of seismic processing methods, for every link in the processing chain, that are direct and do not require any knowledge of subsurface information.

The tools

The methods M-OSRP develops to satisfy prerequisites, *e.g.*, (reference wave prediction separation, source signature and radiation pattern, and source and receiver deghosting) benefit from forms of wave field separation methods derived from Green's theorem (the extinction theorem). Recent papers on this subject can be found in
`http://mosrp.uh.edu/news/recent-published-papers-deghosting`

Those preprocessing methods do not require subsurface information. All ISS subseries require these preprocessing prerequisites (provided by variants of Green's theorem) to achieve ISS processing objectives.

The inverse scattering series communicates that all processing objectives are achievable directly and without subsurface information. Isolated task ISS subseries are identified that directly and without subsurface information achieve free surface and internal multiple removal, depth imaging, target identification and Q compensation without Q.

The combination of Green's theorem preprocessing and ISS processing provides every link in the processing chain with methods that are direct, and do not require subsurface information.

M-OSRP and Multiples

The early history of multiple removal methods required at every step a more detailed and accurate velocity model (for example, stacking, to FK filters, to Radon, and high resolution Radon or 1D earth and statistical assumptions concerning primaries and multiples (Deconvolution)). A sea-change in multiple removal capability arrived with methods that to one extent or another didn't require subsurface information or interpretive intervention. Methods from the Delphi consortium depended on either subsurface information and/or interpretive intervention, whereas the inverse scattering series (ISS) methods from M-OSRP did not. That is the reason that the ISS internal multiple attenuator has assumed a mainstream industry status and recognition as the high water mark of internal multiple capability. There is ample evidence to support the latter claim, including the 2013 SEG (Thursday, September 26, 2013) Internal Multiple Workshop where 9 of the 10 presenters showed ISS internal multiple results as the state of the art available capability for that seismic internal multiple goal and objective. ISS internal multiple attenuation has become fully mainstream.

Challenge we face

However, we also recognize, report and emphasize that the current industry portfolio/trend and focus today (and for the foreseeable future) makes it clear that there is a large and significant

gap between the current challenge for the removal of free surface and internal multiples, where the specific issues are that: (1) the multiple generators and the subsurface properties are ill-defined and complex and (2) *the multiple can too often be proximal to or interfering with primaries.* That type of challenge of removing multiples proximal to, and/or overlapping with, primaries (without damaging primaries) is well beyond the collective capability of the petroleum industry, service companies and academic research groups and consortia—in their ability to effectively address that issue today.

There is a need for new basic concepts, and fundamental theory development that will first need to take place, and following that delivery the practical application issues will need to be addressed.

The plan

At the 2013 SEG, we proposed and described a three pronged strategy (please see the link and slides below) to address that challenge, that M-OSRP will pursue—with the potential to provide the step-change increased and necessary capability. That strategy and plan responds to this outstanding, pressing and prioritized challenge. That level and magnitude of challenge (and the potential opening and delineation of new petroleum reserves and the scale of the opportunity that overcoming it represents) resides behind our commitment to develop and deliver fundamental new concepts, algorithms with step change increased capability, and has returned multiple removal (from its being viewed as a relatively mature subject and project that helps "pay the rent") back to center stage as a major research project and focus within the Mission-Oriented Seismic Research Program. We feel that our background and experience gives us a good chance to develop, and to deliver, the next level of required capability.

Below please find links for the 2013 SEG abstracts/posters/presentations and slides that relate to this communication.
`http://mosrp.uh.edu/events/event-news/seg-annual-meeting-2013`
`http://mosrp.uh.edu/news/seg-annual-meeting-2013`

In the table of contents, we have divided the contributions to this Annual Report into categories:
(1) (a) Prerequisite satisfaction and ISS multiple removal, (b) case studies
(2) Beyond internal multiple attenuation: (a) Removing artifacts/spurious events, (b) internal multiple elimination
(3) ISS depth imaging without the velocity model: update
(4) Analysis and tests of amplitude information at the image point from asymptotic and wave equation migration: implications for RTM.

2014 SEG Expanded Abstracts that relate to these topics can be found in the link:
`http://mosrp.uh.edu/research/publications/seg-abstracts-2014`

What is asymptotic and wave equation migration amplitude analysis with a velocity model doing in an M-OSRP report? What are our objectives, what have we contributed and what are our plans?

While deriving preprocessing methods (described above), and one-way-wave Stolt pre-stack wave equation migration (WEM) from Green's theorem, for our class at UH in Seismic Physics, it was

natural to consider how to derive a wave equation migration for two way propagating waves (for RTM) from Green's theorem. That produced the first WEM RTM.

Please see the link
`http://mosrp.uh.edu/news/wave-equation-migration-RTM`

Wave equation migration (WEM) consists of predicting a source and receiver experiment at depth, and then a coincident source and receiver experiment at time equals zero. There are two other original and classic migration imaging conditions, (1) the space and time coincidence of up and down going waves and (2) the exploding reflector model.

These three migration/imaging conditions are not equivalent, with the latter two representing asymptotic (Kirchhoff) approximations of the WEM concept and algorithms. There are several advantages to WEM compared to asymptotic forms of migration: (1) a definitive answer as to whether a subsurface point is an image point; (2) the amplitude analysis at the image point, and (3) the ubiquitous wave coverage and illumination of WEM compared to asymptotic ray based methods. Those advantages and differences between asymptotic and WEM are present for both one way and two-way (RTM) methods.

The first definitive examination and comparison of WEM and asymptotic (Kirchhoff) migration, for one-way-waves, and their respective amplitude information and analysis at the target is reported in this Annual Report. The asymptotic approximate image is useful for structure maps, but doesn't provide an angle dependent reflection coefficient. WEM provides both structure and amplitude information at the image point.

Asymptotic (Kirchhoff) approximate migration doesn't provide an approximate experiment of a predicted coincident source and receiver at time equals zero at an image point.

Asymptotic migration loses that definiteness and meaning of WEM at the image point and provides instead a fixed travel-time curve with "candidate" image points. The physical meaning and amplitude benefits of the WEM experiment at the image point are lost in asymptotic migration, whether for one way waves or for RTM (all current RTM methods are asymptotic migration).

This has important implications for all current RTM methods, which are asymptotic migration, and suggests and encourages a look at the first WEM RTM that M-OSRP has pioneered, and will keep developing. There are also implications for those looking at increased *illumination* by imaging primaries and multiples separately, since all current approaches to that problem use asymptotic RTM methods, which are intrinsically illumination challenged to begin with. Once again, that's an opportunity for WEM RTM.

M-OSRP doesn't plan to be involved long term in the RTM business, because it's a velocity dependent method.

Every year those pursuing RTM methods describe their need for a yet more complicated and accurate set of heterogeneous and anisotropic velocities. We have no special concept, or idea (or interest) to

compete in that "provide the velocity" arena, where many capable and resourceful and hard-working researchers now reside. Our goal is to examine and define the potential and the added-value of WEM RTM compared to asymptotic RTM, in some simple but meaningful two dimensional examples, and then encourage others to pursue the further development, where their experience and expertise will expedite that continued development, application and delivery. That's our current plan for RTM.

ISS depth imaging without the velocity model

In this Report, HOIS, a ISS direct depth imaging algorithm without a velocity model is applied to the Marmousi model.

The results are very encouraging and the computer run time is 30% longer than a single Stolt pre-stack water speed migration.

Our prediction for the future is that ISS depth imaging will enter the seismic imaging tool box with stand-alone imaging capability in the next 5-10 years. Our first published field data test of ISS imaging on the Kristin North Sea data set demonstrated concept and method viability.

The technical steps needed between viability and providing a new and more effective seismic imaging option within the seismic toolbox are understood, and will be taken. ISS depth imaging will in the future have the same mainstream role for depth imaging under the most challenging and daunting subsurface complexity that ISS multiple removal plays today, and will be the new and necessary option available for exactly those same daunting circumstances. Those who understand the derivations and logic behind the ISS free surface and internal multiple attenuation methods, will have no problem with the logic that leads to ISS depth imaging. The ISS multiple removal methods and the ISS depth imaging and inversion algorithms derive from the same single set of ISS equations.

Summary/Focus

M-OSRP is pleased to see the mainstream usage and application of the ISS internal multiple attenuator.

However, the current challenges frequently faced with on-shore plays and complex off-shore plays to remove multiples of different orders, and, proximal to, or interfering with, primaries, and without damaging primaries, raises the bar on needed multiple removal capability. That new level of multiple removal challenge is currently beyond the collective capability of the petroleum industry to address. M-OSRP has a three pronged strategy and plan to address that challenge and to develop and deliver an effective response. That is currently (and near term will remain) our central and principle focus and resource allocation. That new algorithmic strength and capability developed within M-OSRP will have a commensurate higher level of compute demand. Our collaboration/cooperation/partnership with IBM connects the "what to compute" for more effectiveness from M-OSRP with new visions of "how to compute" from IBM. That combination of "what" and "how" are essential for providing a new, more effective and relevant capability to our sponsors.

We plan to continue our research in WEM RTM (with a velocity model) and ISS direct imaging (without a velocity model).

For the near future, these imaging projects, will move forward, but with somewhat less resource allocation in comparison to the serious and unfinished business of removing multiples.

There are several reasons for this relative emphasis of projects within M-OSRP: (1) there are numerous regions in the world (*e.g.*, the Middle East, Central North Sea, ...) where without more capability and effectiveness in removing multiples, making advances in imaging (that depend on multiples having been removed) are irrelevant or useless; and (2) there is often a resistance among researchers in seismic imaging to recognize and acknowledge an imaging challenge as existing, beyond the one that they are currently able to address.

M-OSRP has a portfolio of projects that takes ownership of all the links in the seismic processing chain. Some of our projects are embryonic, whereas others are more "mature" and help "pay the rent". M-OSRP is very aware that some of the concepts we develop and methods we pursue, and messages we communicate, are at variance with the conventional, the consensus view and mainstream concepts and thinking. To provide fundamental new step change capability requires the ability to be resolute and to flourish and to succeed in the face of considerable doubt and skepticism.

No real advance in science ever occurred without running into issues and obstacles from the "consensus view"

It wasn't too long ago that a statement like "multiples can be predicted directly and without subsurface information" was greeted with eyes rolling and disbelief. Now that idea and methodology have become mainstream. Today, saying it will be possible to "directly depth image without a velocity model" generally elicits that same incredulous response.

We are enormously fortunate and deeply grateful for your encouragement and support. Your support and confidence allows us the opportunity to perform fundamental directed "mission-oriented" seismic research that will continue to deliver effective responses to pressing and prioritized seismic processing challenges.

Arthur B. Weglein
May, 2014

(a) Prerequisite satisfaction and ISS multiple removal, (b) case studies

Short note: Multiple removal and prerequisite satisfaction: Current status and future plans

James D. Mayhan and Arthur B. Weglein

May 21, 2014

Abstract

In exploration seismology, as the geology that seismic waves probe becomes more complex, the untangling of multiples and primaries becomes more challenging. The inverse scattering series (ISS) has provided distinct algorithms for eliminating free-surface multiples and attenuating internal multiples without needing any subsurface information. For these two algorithms to deliver on their promise, however, it is important that we satisfy their prerequisites. The free-surface-multiple-elimination algorithm assumes that its input has had the source wavelet deconvolved and ghosts removed. The internal-multiple algorithm also requires deghosting and source-wavelet deconvolution and further assumes that its input data have had free-surface multiples removed. Fortunately, Green's theorem provides algorithms for estimating the source wavelet and removing ghosts that are consistent with the ISS algorithms — *i.e.*, those algorithms need no subsurface information and are multidimensional. The effects of meeting and not meeting the prerequisites of the demultiple algorithms are exemplified here, and the current status and future plans for demultiple algorithms are discussed.

1 Introduction

The purposes of this paper are (1) to show some results of Green's-theorem preprocessing (required by ISS algorithms), (2) to review and exemplify the influence that results from satisfying the prerequisites for free-surface-multiple and internal-multiple algorithms with synthetic data corresponding to offshore plays, and (3) to motivate onshore methods for satisfying the prerequisites and to describe early efforts to reach that goal.

As exploration for hydrocarbons has moved into areas with increasingly complex geology, there are more instances in which multiples are proximal to or even overlap the primaries. Hence, demultiple algorithms are challenged to remove multiples without damaging proximal primaries. The inverse scattering series (ISS) can achieve all processing objectives directly and without subsurface information. In particular, the ISS free-surface-multiple-elimination method can accurately predict the phase and amplitude of free-surface multiples, if its prerequisites (source signature and deghosted data) are satisfied (Carvalho et al., 1992; Weglein et al., 1997, 2003). This has been demonstrated on marine field data (Carvalho, 1992; Carvalho et al., 1992; Carvalho and Weglein, 1994; Weglein et al., 2003; Ferreira, 2011). The current ISS internal-multiple-attenuation algorithm can predict the

exact phase (time) and an approximate amplitude of all internal multiples, at once, automatically, and without subsurface information (Araújo et al., 1994; Weglein et al., 2003), as has been demonstrated on marine field data (Matson et al., 1999; Terenghi et al., 2011; Ferreira, 2011; Weglein, 2013; Goodway and Mackidd, 2013; Kelamis and Yi Luo, 2013; Ferreira et al., 2013; Dragoset, 2013; Brookes and Jenner, 2013; Griffiths et al., 2013; Hegge et al., 2013). Those ISS properties are what all other current demultiple methods (*e.g.*, Feedback-loop methods, modeling and subtraction of multiples, and filter methods) do not possess and cannot deliver (Weglein, 1999; Weglein and Dragoset, 2005; Qiang Fu et al., 2010; Yi Luo et al., 2011; Weglein et al., 2011; Ferreira, 2011; Kelamis et al., 2013). Details concerning the ISS free-surface-multiple-elimination method and the internal-multiple-attenuation algorithm can be found in the Appendix.

The prerequisites for ISS demultiple algorithms can be met by Green's-theorem-based algorithms (Weglein and Secrest, 1990; Weglein et al., 2002; Jingfeng Zhang and Weglein, 2005, 2006; Jingfeng Zhang, 2007). The ability of Green's theorem to meet prerequisites has been tested on SEAM and field data (Mayhan and Weglein, 2013a; Mayhan, 2013); we show examples in Figures 1-3. When the prerequisites are satisfied, the prediction improves, as is shown in Figures 5-12. Background on Green's-theorem-based algorithms can be found in the Appendix.

Zhiqiang Wang (now at PGS) tested Green's-theorem deghosting while an intern at Total (Figure 4).

Free-surface-multiple removal without and with prior removal of ghosts is shown in Figures 6 and 7, respectively. Using the model shown in Figure 5, Figures 6a and 7a are the input data with and without ghosts, respectively. Inputting those data into the ISS free-surface-multiple-elimination algorithm, Figures 6b and 7b are the corresponding free-surface-multiple predictions. After subtraction of the predicted free-surface multiples from the input data, Figures 6c and 7c show the corresponding results. If the input data are not deghosted, the ISS free-surface-multiple-removal method can predict the exact phase but only an approximate amplitude of free-surface multiples. After deghosting the data, we can see that all free-surface multiples are predicted exactly, and, through a simple subtraction, all are well eliminated, and, most importantly, primaries are not touched, as is shown in Figure 6c. For simple synthetic data, other examples of removing free-surface multiples, with and without deghosting, are given in Jingfeng Zhang (2007) and Zhiqiang Wang et al. (2012) .

Free-surface-multiple elimination and internal-multiple attenuation with and without first removing the source wavelet are shown in Figures 8-12. Figures 8-9 uses the model in Figure 5, and Figures 11-12 use a model with no free surface and with two reflectors (Figure 10). Figures 8 and 9 show the input data, the predicted free-surface multiples using the ISS free-surface-multiple-elimination algorithm, and the results of simple subtraction without and with source-wavelet deconvolution. Figures 11 and 12 show the input data, the predicted internal multiples using the ISS internal-multiple-attenuation algorithm, and the results of simple subtraction without and with source-wavelet deconvolution. In Figure 12, the amplitude of the predicted internal multiple is comparable to the internal multiple in the input data, while the amplitude is totally different from that of the internal multiple in the input data in Figure 11. Deconvolution of the source wavelet, as required by the internal-multiple-attenuation algorithm, significantly improves the amplitude and shape of the predicted internal multiple.

ISS free-surface-multiple elimination assumes (1) Carvalho's obliquity factor, q, given (in 2D) by $q = sgn(\omega)\sqrt{\omega^2/c_0^2 - k^2}$, which is not available in other methods including Delft SRME, (2) the

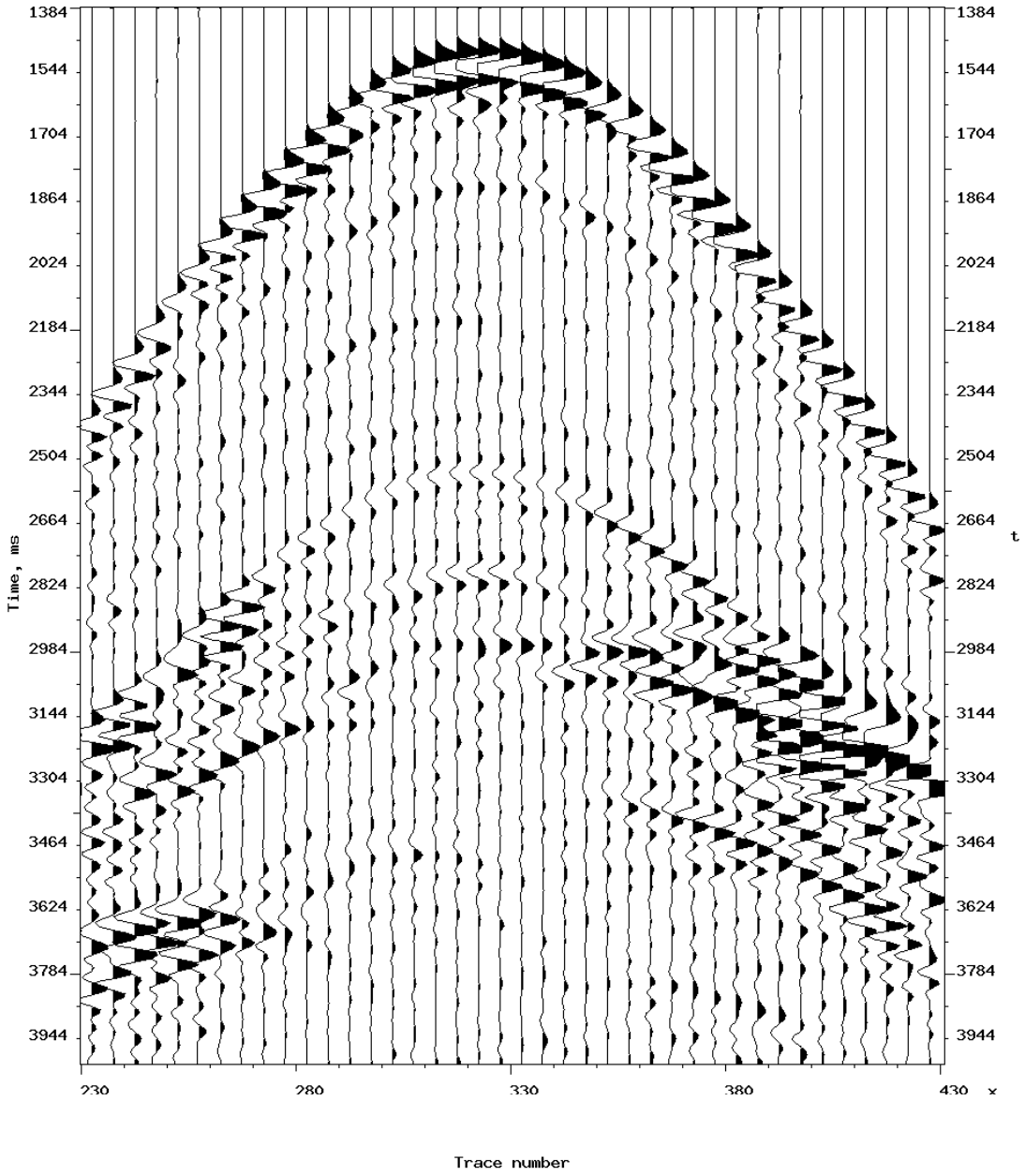

Figure 1: *SEAM data, example shot (131373), recorded data at 17 m. Tested while an intern at PGS.*

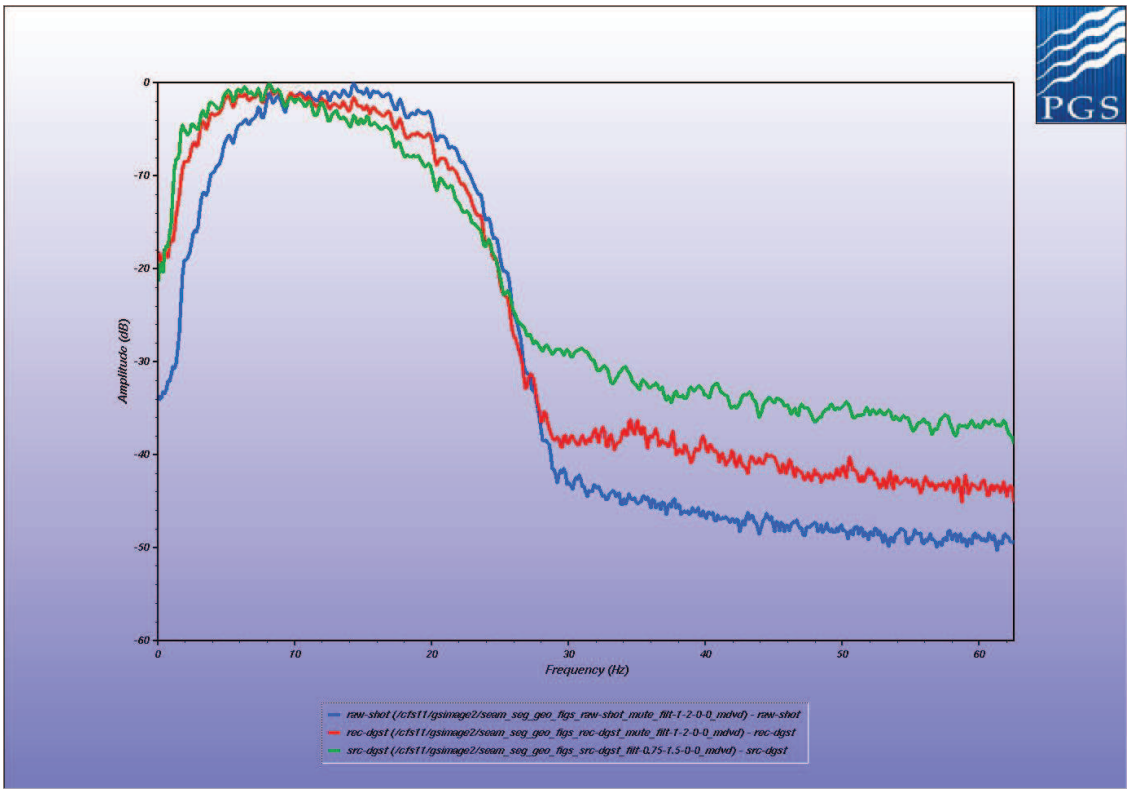

Figure 2: *Green's-theorem deghosting on SEAM data (Mayhan and Weglein, 2013b). Shot 131373, frequency spectra: blue=P at 17 m, red=receiver deghosted at 10 m using Green's theorem, green=source and receiver deghosted at 10 m using Green's theorem. Vertical axis=amplitude (dB), horizontal axis=frequency (Hz). The first source notch is at 44 Hz, which lies above the source frequency range (1–30 Hz). Note the shift of the spectrum towards lower frequencies (which may be of interest to FWI).*

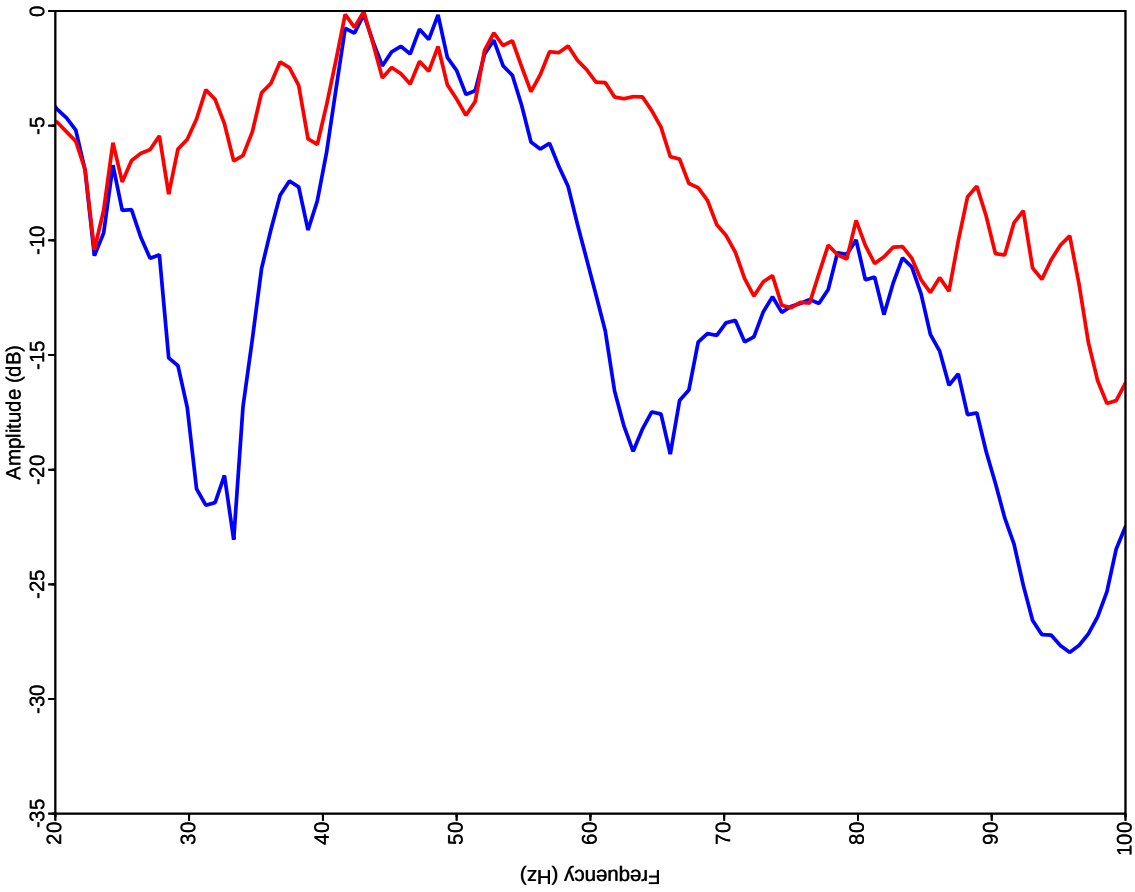

Figure 3: *Green's-theorem deghosting on field data (Mayhan et al., 2011). Shot 841, frequency spectra: blue=P at 25 m, red=receiver deghosted at the air-water boundary using Green's theorem. Vertical axis=amplitude (dB), horizontal axis=frequency (Hz). The receiver notches around 30 Hz, 60 Hz, and 90 Hz have been filled in. Input data courtesy of PGS.*

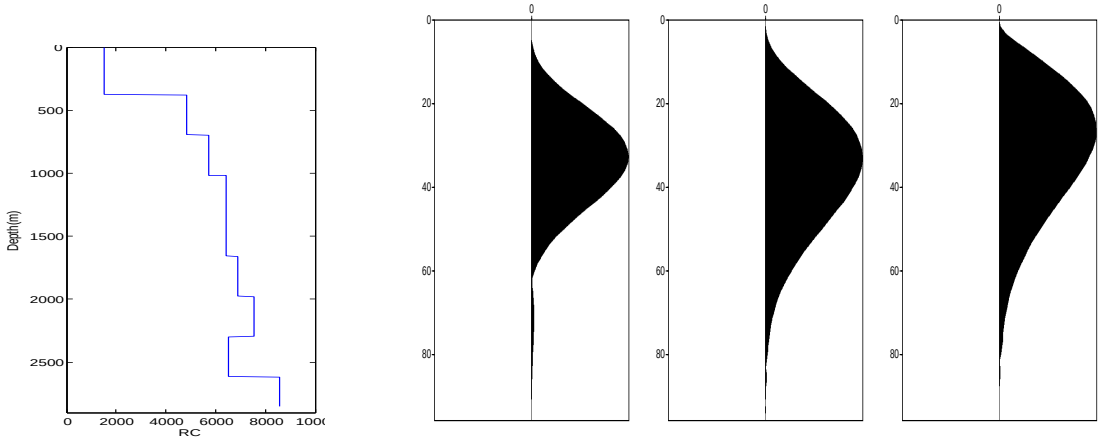

(a) *Velocity model (provided by Total)*

(b) *Spectrum plots of the wavelets*

Figure 4: *In (b), the left panel is before deghosting, the middle panel is receiver deghosted, and the right panel is source and receiver deghosted. Both receiver deghosting and source deghosting recover more low-frequency information. (Zhiqiang Wang et al., 2012)*

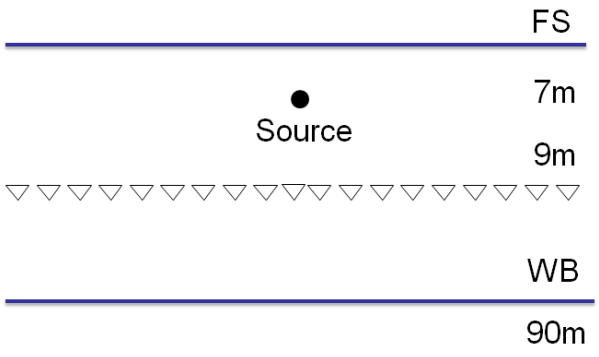

Figure 5: *Model used for Figures 6 - 9*

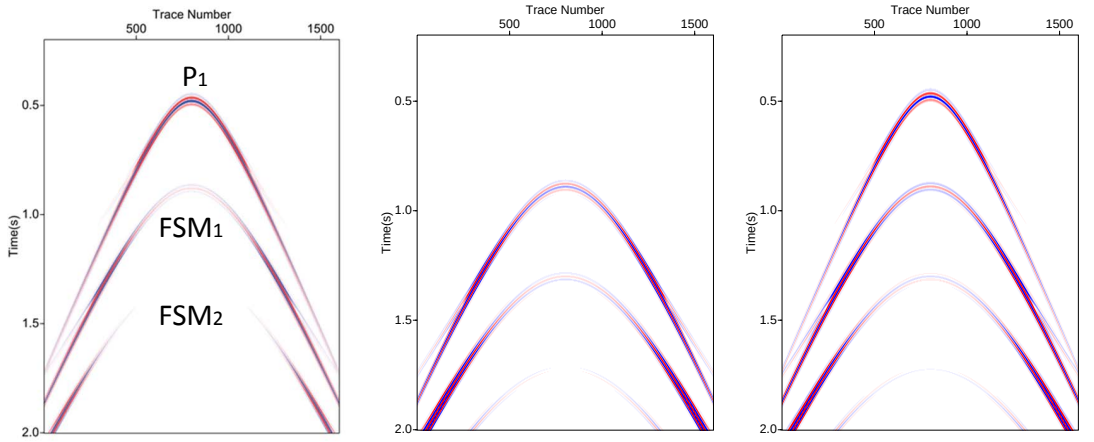

(a) *Input data* (b) *ISS FSM prediction* (c) *After a simple subtraction*

Figure 6: *Free-surface-multiple elimination without prior removal of ghosts (Jinlong Yang reported in Lin Tang et al., 2013)*

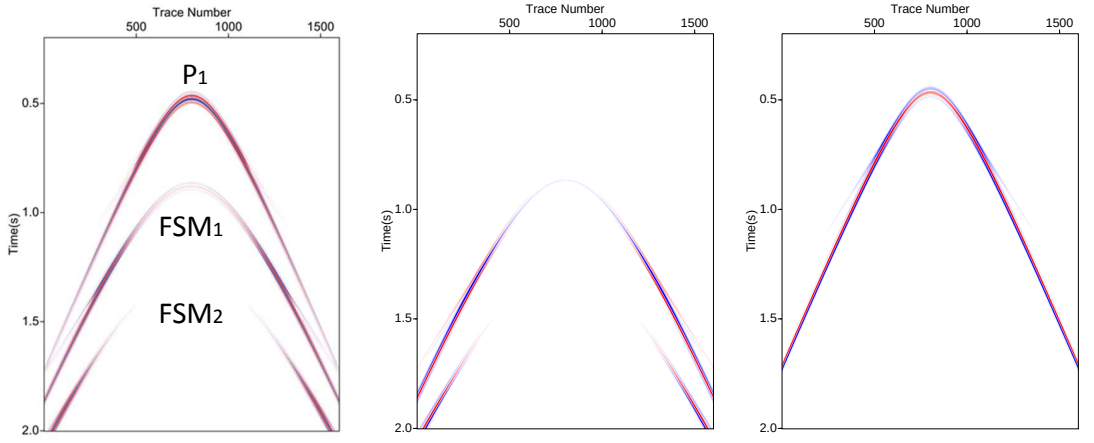

(a) *Input data* (b) *ISS FSM prediction* (c) *After a simple subtraction*

Figure 7: *Free-surface-multiple elimination with prior removal of ghosts (Jinlong Yang reported in Lin Tang et al., 2013)*

wavelet has been removed, and (3) receiver and source deghosting has been performed.

2 Current status

The current status of multiple removal for marine seismic data is summarized in Table 1. Row (1): Satisfaction of the prerequisites of the ISS (using Green's theorem) is relatively mature. Estimation

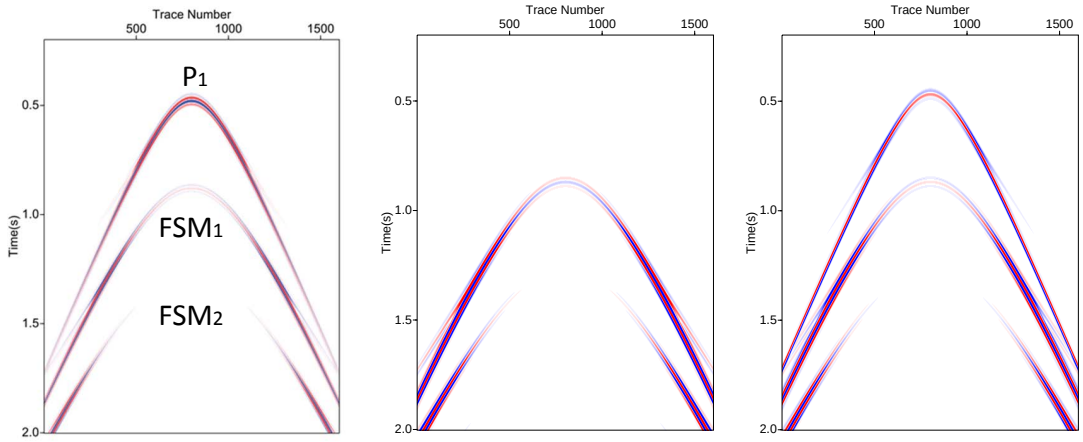

(a) *Input data* (b) *ISS FSM prediction* (c) *After a simple subtraction*

Figure 8: *Impact of the source wavelet on ISS free-surface-multiple elimination without wavelet deconvolution (Jinlong Yang and Weglein, 2012).*

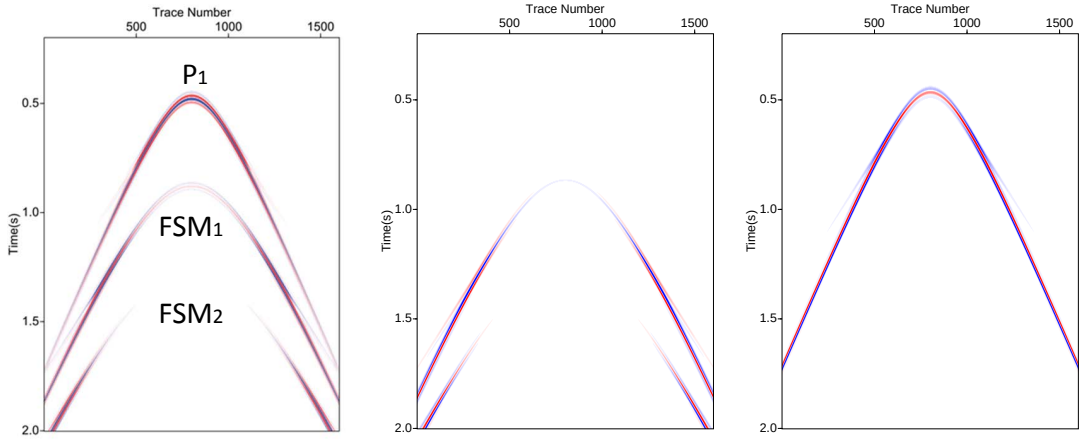

(a) *Input data* (b) *ISS FSM prediction* (c) *After a simple subtraction*

Figure 9: *Impact of the source wavelet on ISS free-surface-multiple elimination with wavelet deconvolution (Jinlong Yang and Weglein, 2012).*

of the source wavelet and removal of ghosts have been tested on simple synthetic data, SEAM data, and field data (Jingfeng Zhang, 2007; Mayhan, 2013). Row (2): Free-surface-multiple elimination is also mature. In principle, the ISS free-surface-multiple-prediction algorithm (equations 1 and 2) gives the exact amplitude and phase of the free-surface multiples. Row (3): Internal-multiple attenuation is also mature; it was tested on field data by Matson et al. (1999), Terenghi et al. (2011), and Ferreira (2011). Work is underway to eliminate spurious events (Chao Ma and Weglein, 2014a) and to move attenuation to elimination (Yanglei Zou and Weglein, 2014a,b). Row (4): Adaptive

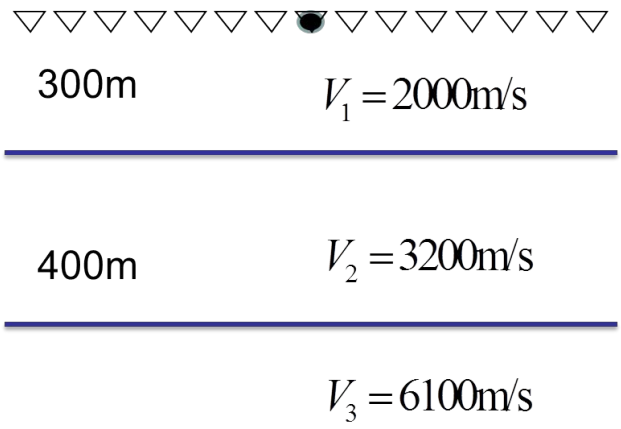

Figure 10: *Model used for Figures 11 and 12*

subtraction using energy minimization is inconsistent; if multiples and primaries are separated, it works, but if multiples are proximal to or overlap the primaries, it fails. A possible replacement for energy-minimization adaptive subtraction has been proposed for free-surface-multiples (Weglein, 2012).

	Method	Comment/status
1	Prerequisites (estimate wavelet, deghost)	Relatively mature
2	Free-surface multiples	Eliminate
3	Internal multiples	Attenuate
4	Adaptive steps	Energy minimization

Table 1: *The current status of multiple removal (marine seismic data).*

The current capability of multiple removal for onshore seismic data is summarized in Table 2. Row (1): Use of Green's theorem to satisfy ISS prerequisites, as is currently performed for marine seismic data, is discussed in Jing Wu and Weglein (2014b), and a method for finding the reference velocity in the near surface is discussed in Lin Tang and Weglein (2014). Row (3): The results of testing ISS internal-multiple attenuation on land are encouraging; its "performance was demonstrated with complex synthetic and challenging land field data sets with encouraging results, where other internal multiple suppression methods were unable to demonstrate similar effectiveness." (Qiang Fu et al., 2010, page 3457) Row (4): "The examples of this paper point to the pressing need to improve the prediction and reduce the reliance on adaptive steps, since the latter can fail precisely when you have interfering events." (Qiang Fu et al., 2010, page 3458)

Code currently available on the sponsors-only portion of mosrp.uh.edu includes Cagniard-de Hoop forward modeling (1D acoustic earth, line source), finite-difference forward modeling (2D acoustic

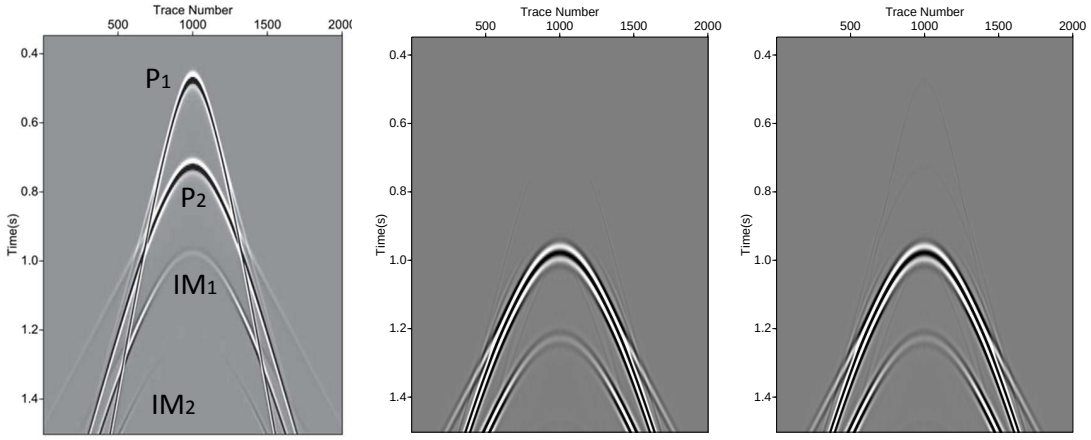

(a) *Input data* (b) *ISS IM prediction* (c) *After a simple subtraction*

Figure 11: *Impact of the source wavelet on ISS internal-multiple attenuation without wavelet deconvolution (Jinlong Yang and Weglein, 2014).*

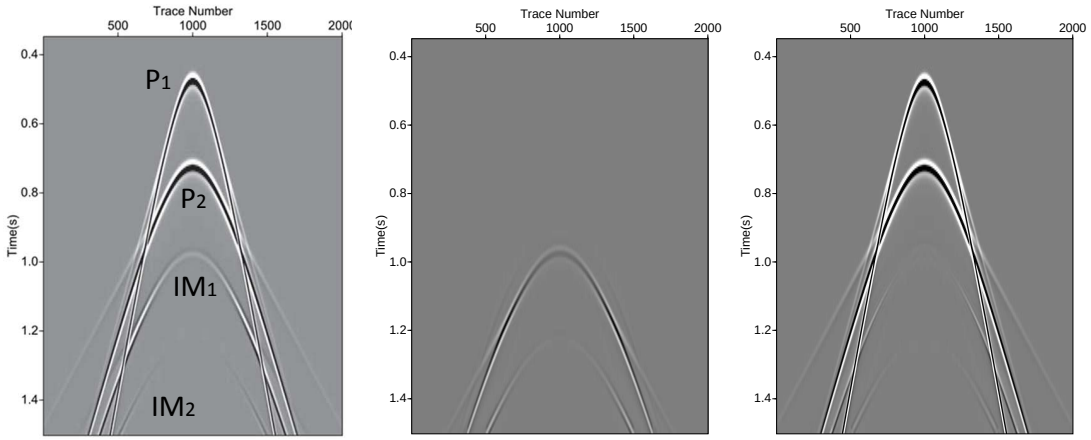

(a) *Input data* (b) *ISS IM prediction* (c) *After a simple subtraction*

Figure 12: *Impact of the source wavelet on ISS internal-multiple attenuation with wavelet deconvolution (Jinlong Yang and Weglein, 2014).*

earth, line source), Green's-theorem marine-data preprocessing (2D or 3D data sets), ISS free-surface-multiple elimination (3D data sets), ISS internal-multiple attenuation (1.5D or 2D data sets), and adaptive-subtraction (applicable to ISS free-surface-multiple elimination).

Data sampling issues are in the Appendix.

	Method	Comment/status
1	Prerequisites (estimate wavelet, deghost)	Find reference velocity iteratively
2	Free-surface multiples	Eliminate
3	Internal multiples	Attenuate
4	Adaptive steps	Energy minimization

Table 2: *The current capability of multiple removal (onshore seismic data).*

3 Future plans

A three-pronged strategy will address the current outstanding issues listed in Tables 1 and 2 (Weglein, 2014a,b). (1) Develop the ISS prerequisites that are direct and do not require subsurface information to predict the reference wavefield (wavelet and radiation pattern) and produce deghosted data (in particular, for onshore and ocean-bottom acquisition); (2) Develop ISS algorithms to reduce/eliminate so-called spurious events (Appendix) and to eliminate (rather than attenuate) internal multiples; and (3) Develop a replacement for the energy-minimization criterion for adaptive subtraction; that replacement should derive from, and always align with and serve, the inverse-scattering-series free-surface and internal-multiple algorithms. This three-pronged strategy represents a consistent and aligned processing chain, with one single objective: providing a direct and practical solution to the removal of all multiples, without requiring any subsurface information and without damaging primaries. All three prongs are being progressed: (1) in Jing Wu and Weglein (2014a,b), (2) in Yanglei Zou and Weglein (2014a,b) and Chao Ma and Weglein (2014a), and (3) in Weglein (2012). This ideal status of multiple removal (for marine seismic data) is summarized in Table 3.

	Method	Comment/status
1	Prerequisites (estimate wavelet, deghost)	Mature
2	Free-surface multiples	Eliminate
3	Internal multiples	Eliminate
4	Adaptive steps	Consistent with 1-3

Table 3: *The ideal status of multiple removal (for marine seismic data).*

The energy-minimization adaptive-subtraction criterion, while not derived as a property of the free-surface-multiple-elimination or the internal-multiple-attenuation criteria, is useful for completing the matching between multiple prediction and the actual multiple, when events are separated and there are no higher-order multiples in the vicinity, and only a first-order algorithm is being used. Part of the three-pronged strategy is to use the terms in the respective ISS subseries that can

accommodate the order of multiple that is anticipated in the target region. Given deghosted and wavelet-deconvolved data, there is a stable closed form that eliminates all orders of free-surface multiples at once (Weglein and Dragoset, 2005). With proximal and/or interfering events the energy-minimization criterion fails, independently of how it is implemented (because of interfering proximal events), and a new set of criteria is sought for the adaptive step that derives from, aligns with, and always supports the multiple subseries. (A candidate to replace energy-minimization adaptive subtraction for free-surface multiples is given in Weglein (2012).)

4 Conclusions

This paper provides (1) an overview of removal of multiples from marine data and (2) a motivation and a preview for removal of multiples from onshore data. In principle, the ISS free-surface-multiple-prediction algorithm (equations 1 and 2) gives the exact amplitude and phase of the free-surface multiples, and the ISS internal-multiple-attenuation algorithm (equation 3) is the high-water mark of current internal-multiple-attenuation capability. The quality of their output assumes that their requirements are met — *i.e.*, that the source wavelet has been deconvolved and ghosts have been removed.

5 Acknowledgements

We thank the M-OSRP sponsors for their encouragement and support.

Appendix

A ISS free-surface-multiple elimination

A so-called isolated-task subseries to predict free-surface multiples is extracted from the ISS. For example, the 2D form of the subseries is

$$D'(k_g, k_s, \omega) = \sum_{n=1}^{\infty} D'_n(k_g, k_s, \omega), \text{ where} \tag{1}$$

$$D'_n(k_g, k_s, \omega) = \frac{1}{i\pi\rho_0 A(\omega)} \int_{-\infty}^{\infty} dk\, q \exp\left(iq(\epsilon_g + \epsilon_s)\right) D'_1(k_g, k, \omega) D'_{n-1}(k, k_s, \omega) \tag{2}$$

for $n = 2, 3, 4, \ldots$ k_g, k_s, and the ω values represent the Fourier conjugates of receiver x coordinate, source x coordinate, and time; ϵ_g and ϵ_s are the (fixed) receiver and source depths below the free surface; the obliquity factor, q, is given by $q = sgn(\omega)\sqrt{\omega^2/c_0^2 - k^2}$; and c_0 is the reference velocity. This algorithm requires only the source signature $A(\omega)$ and source- and receiver-deghosted (and source-wavelet deconvolved) data $D'_1(k_g, k, \omega)$ as its input. The free-surface multiples are predicted order-by-order (for $n = 2, 3, 4, \ldots$) and then are added together (equation 1) to give the deghosted and free-surface-demultipled data. For a more detailed discussion please see Section 5.4 of Weglein et al. (2003). Equation 2 can be modified to accommodate an anisotropic extended source $\rho(k, q, \omega)$ (Jinlong Yang et al., 2013).

B ISS internal-multiple attenuation

The 2D form of the ISS internal-multiple leading-order attenuator is (Araújo, 1994; Weglein et al., 2003)

$$\begin{aligned}
&b_3(k_g,k_s,q_g+q_s)\\
=&\frac{1}{(2\pi)^2}\int_{-\infty}^{\infty}\int_{-\infty}^{\infty}dk_1\exp\left(iq_1(\epsilon_s-\epsilon_g)\right)dk_2\exp\left(iq_2(\epsilon_g-\epsilon_s)\right)\\
\times&\int_{-\infty}^{\infty}dz_1\exp\left(i(q_g+q_1)z_1\right)b_1(k_g,-k_1,z_1)\\
\times&\int_{-\infty}^{z_1-\varepsilon_2}dz_2\exp\left(i(-q_1-q_2)z_2\right)b_1(k_1,-k_2,z_2)\\
\times&\int_{z_2+\varepsilon_1}^{\infty}dz_3\exp\left(i(q_2+q_s)z_3\right)b_1(k_2,-k_s,z_3).
\end{aligned}\tag{3}$$

The vertical wave numbers are defined by $q_i=sgn(\omega)\sqrt{\omega^2/c_0^2-k_i^2}$ for $i=s,g,1,2$; in practice $\varepsilon_1,\varepsilon_2$ are chosen to be the wavelet; and b_1 represents the data that would result from a single-frequency incident plane wave imaged with water speed. For a more detailed discussion please see Section 6 of Weglein et al. (2003). Equation 3 can be modified to suppress spurious predictions (Chao Ma and Weglein, 2014b,c). (The internal-multiple-attenuation algorithm assumes only primaries in its input. the presence of internal multiples can result in the prediction of internal multiples that do not correspond to internal multiples in the seismic data.) A new ISS algorithm is being developed to eliminate (rather than attenuate) internal multiples (Yanglei Zou and Weglein, 2014a,b).

C Green's-theorem wavefield separation

As is the case with the inverse scattering series, Green's theorem also requires no *a priori* knowledge of the subsurface (when used for wavefield separation). Green's theorem can be used to remove the reference wavefield and to estimate the source wavelet (Weglein and Secrest, 1990), and also to remove ghosts (Weglein et al., 2002; Jingfeng Zhang and Weglein, 2005, 2006; Jingfeng Zhang, 2007; Mayhan et al., 2011, 2012; Mayhan and Weglein, 2013; Mayhan, 2013). The key equation for Green's-theorem wavefield separation is

$$P_R'(\mathbf{r}_g',\mathbf{r}_s,\omega)=\int_{MS}dS\,\hat{\mathbf{n}}\cdot[P(\mathbf{r},\mathbf{r}_s,\omega)\nabla G_0^{d+}(\mathbf{r},\mathbf{r}_g',\omega)-G_0^{d+}(\mathbf{r},\mathbf{r}_g',\omega)\nabla P(\mathbf{r},\mathbf{r}_s,\omega)],\tag{4}$$

where P and $\hat{\mathbf{n}}\cdot\nabla P$ are the measured values of the pressure wavefield and its derivative normal to the measurement surface; $\mathbf{r}_s$, $\mathbf{r}$, and $\mathbf{r}_g'$ are the locations of the source, receivers, and output point, respectively; G_0^{d+} is a known analytic Green's function; and the integration is performed over the measurement surface. The data used in the integral in equation 4 are Fourier transformed from $\mathbf{r},t$ to $\mathbf{r},\omega$; given the dense time samplings characteristic of field acquisitions, the required Fourier transforms have not been an issue.

Capturing $\hat{\mathbf{n}}\cdot\nabla P$ requires over-under streamers with hydrophones, a dual-sensor streamer with hydrophones and geophones, or a dual-sensor streamer with hydrophones and accelerometers. If

measurements of $\hat{\mathbf{n}} \cdot \nabla P$ are not available and the source wavelet can be independently estimated, yet another choice of Green's function allows equation 4 to predict $\hat{\mathbf{n}} \cdot \nabla P$ (and a new estimate of P), which can be used as input to equation 4 for receiver deghosting. Similarly, if over-under sources are not available, this process can be repeated for source deghosting, but in that case independent estimates of the source wavelet are not needed.

D Data sampling issues

We conducted a literature search to better understand WesternGeco's IsoMetrix acquisition, WesternGeco's simultaneous sources, and ocean-bottom acquisition in order to evaluate their impact on Green's-theorem wavefield separation (*e.g.*, on deghosting) and on ISS free-surface-multiple removal. Seismic data are a function of seven variables, the source coordinates (x_s, y_s, z_s), the receiver coordinates (x_g, y_g, z_g),, and time t. Seismic data are often properly sampled in time and the receiver inline direction but are undersampled in the receiver crossline direction and source inline and crossline directions (Moldoveanu, 2010). Undersampling in the crossline direction impacts Green's-theorem receiver deghosting and wavelet estimation, and undersampling of shots impacts Green's-theorem source deghosting. Undersampling also impacts ISS free-surface-multiple removal because this algorithm works with shots and receivers at every station point of the processing lattice.

The PGS GeoStreamer® measures pressure, P, using hydrophones and measures the vertical component of particle velocity, V_z, using geophones (Carlson et al., 2007; Tenghamn et al., 2007). The IsoMetrix streamer measures pressure and vertical and crossline components of particle acceleration, A_z and A_y, by using a micro-electro-mechanical system (MEMS) (Harries, 2012; Bunting et al., 2013; El Yadari et al., 2013; van Manen et al., 2013; WesternGeco, 2013). Hydrophone data are good down to a couple of Hz (Long, 2014), geophone data are reliable down to something less than 20 Hz (Cambois et al., 2009), and MEMS data are accurate down to 3 Hz (Harries, 2012). In the range of 3 Hz to <20 Hz, it appears that the IsoMetrix streamer captures three independent measurements (P, A_z, A_y) whereas the GeoStreamer® captures one (P).

The WesternGeco IsoMetrix acquisition uses measurements of crossline particle acceleration and sinc interpolation to provide more "streamers" and hence a denser grid of receiver data points. A 6.25 m × 6.25 m surface grid will give better resolution than will a 12.5 m × 75 or 100 m. (1) The advantage of Green's-theorem wavefield separation is that a smaller Δx offers more flexibility (Mayhan, 2013, section 2.3). The vertical distance between the output point and the measurement point, $\Delta z = |z'_g - z|$, is related to the horizontal distance between traces, Δx, by $\Delta z \gtrsim 0.5\Delta x$. As the output point approaches the measurement point — *i.e.*, as Δz gets smaller — G_0^{d+} and especially $\partial G_0^{d+}/\partial z$ become narrower in width. For a given Δx, too few data points may fall inside $\partial G_0^{d+}/\partial z$, and the output of equation 4 becomes less accurate. (A more detailed explanation is given in Weglein et al., 2013.) The WesternGeco IsoMetrix streamer helps Green's-theorem wavefield separation by yielding a smaller Δx. (2) However, a smaller Δx gives a larger data set. We can take advantage of the narrowness of G_0^{d+} and $\partial G_0^{d+}/\partial z$ to save computation time (with little loss of accuracy) by restricting the Green's theorem integral (equation 4) to a radius of (*e.g.*) 100 Δx instead of integrating over the whole measurement surface (Mayhan, 2013, section 2.3).

The method of simultaneous sources provides better-sampled data by firing two shots close in time. For example, a standard "flip-flop" acquisition may alternately fire the sources every 18.75 m, which

gives a 37.5 m shot interval in each shot line. In the method of simultaneous sources, both sources are fired every 18.75 m, which cuts in half the inline shot interval (Beasley et al., 2012). The sources are not quite fired simultaneously. One source is fired every 18.75 m, but the other shot is fired with a time difference chosen randomly from a small time window. (Beasley et al. (2011) report a time window 300 ms wide.)

The cost of placing sensors on the ocean bottom means a larger grid may be used (400 m×400 m in deep water, Maver, 2011). Data is undersampled and less useful as input to Green's-theorem preprocessing and ISS processing.

References

Araújo, F. V. *Linear and non-linear methods derived from scattering theory: backscattering tomography and internal-multiple attenuation.* PhD thesis, Universidade Federal da Bahía, Brazil, 1994. In Portuguese.

Araújo, F. V., A. B. Weglein, P. M. Carvalho, and R. H. Stolt. "Inverse scattering series for multiple attenuation: An example with surface and internal multiples." *64th Annual International Meeting, SEG, Expanded Abstracts.* 1994, 1039–1041.

Beasley, C., A. Salama, and W. H. Dragoset. "A 3D Simultaneous Source Field Test Processed by Active Separation." *73rd EAGE Conference & Exhibition, Extended Abstracts.* 2011.

Beasley, Craig, Ian Moore, David Monk, and Laurence Hansen. "Simultaneous sources: The inaugural full-field, marine seismic case history." *82nd Annual International Meeting, SEG, Expanded Abstracts.* 2012, 1–5.

Brookes, D. and Ed Jenner. An Onshore example of 3D Interbed Multiple Attenuation. Presentation given at the Post SEG Convention Workshop on Internal Multiples, Houston, Texas, September 2013.

Bunting, Tim, Pete Watterson, and Massimiliano Vassallo. "IsoMetrix; Isometrically sampled towed-streamer marine seismic data." *Thirteenth International Congress of the Brazilian Geophysical Society.* Sociedade Brasileira de Geofísica, 2013.

Cambois, Guillaume, David Carlson, Craig Jones, Marina Lesnes, Walter Söllner, and Hocine Tabti. "Dual-sensor streamer data: Calibration, acquisition QC and attenuation of seismic interferences and other noises." *79th Annual International Meeting, SEG, Expanded Abstracts.* 2009, 142–146.

Carlson, David, Walter Söllner, Hocine Tabti, Eli Brox, and Martin Widmaier. "Increased resolution of seismic data from a dual-sensor streamer cable." *77th Annual International Meeting, SEG, Expanded Abstracts.* 2007, 994–998.

Carvalho, P. M. and A. B. Weglein. "Wavelet estimation for surface multiple attenuation using a simulated annealing algorithm." *64th Annual International Meeting, SEG, Expanded Abstracts.* 1994, 1481–1484.

Carvalho, P. M., A. B. Weglein, and R. H. Stolt. "Nonlinear inverse scattering for multiple suppression: Application to real data. Part I." *62nd Annual International Meeting, SEG, Expanded Abstracts*. 1992, 1093–1095.

Carvalho, Paulo Marcos. *Free-surface multiple reflection elimination method based on nonlinear inversion of seismic data*. PhD thesis, Universidade Federal da Bahia, 1992. In Portuguese.

Dragoset, W. Internal Multiple Attenuation for Land Data: Requirements for Success. Presentation given at the Post SEG Convention Workshop on Internal Multiples, Houston, Texas, September 2013.

El Yadari, N., M. Vassallo, K. Eggenberger, S. Rentsch, S. Gupta, D. J. van Manen, A. Özbek, and S. Zeroug. "Impact of Streamer Spacing on the Reconstruction Using Multimeasurement Seismic Data — Study Before and After Imaging." *75th EAGE Conference & Exhibition, Extended Abstracts*. June 2013.

Ferreira, A., P. Terenghi, A. Weglein, and A. Oliveira. Internal Multiple Removal in Offshore Brazil Seismic Data Using the Inverse Scattering Series. Presentation given at the Post SEG Convention Workshop on Internal Multiples, Houston, Texas, September 2013.

Ferreira, Andre. Internal multiple removal in offshore Brazil seismic data using the inverse scattering series. Master's thesis, University of Houston, 2011.

Fu, Qiang, Yi Luo, Panos G. Kelamis, ShouDong Huo, Ghada Sindi, Shih-Ying Hsu, and Arthur B. Weglein. "The inverse scattering series approach towards the elimination of land internal multiples." *80th Annual International Meeting, SEG, Expanded Abstracts*. 2010, 3456–3461.

Goodway, W. and D. Mackidd. Multiples... The Elephant in the Room. Presentation given at the Post SEG Convention Workshop on Internal Multiples, Houston, Texas, September 2013.

Griffiths, M., A. Pica, and B. Hung. Internal Multiple removal solutions for multiple environments. Presentation given at the Post SEG Convention Workshop on Internal Multiples, Houston, Texas, September 2013.

Harries, Steve. "Isometric in-line and cross-line sampling advances marine 3D seismic." *World Oil* (October 2012): 73–78.

Hegge, R., A. Klaedtke, R. van Borselen, and E. Otnes. Aspects of standard practice and possible enhancements to 3D IME. Presentation given at the Post SEG Convention Workshop on Internal Multiples, Houston, Texas, September 2013.

Kelamis, P. and Yi Luo. Myths & Realities of Land Internal Multiple Elimination Technologies. Presentation given at the Post SEG Convention Workshop on Internal Multiples, Houston, Texas, September 2013.

Kelamis, Panos G., Yi Luo, and Arthur B. Weglein. "Strategies of Land Internal Multiple Elimination based on Inverse Scattering Series." *Technical Session 21: Recent Development in Seismic Imaging/Processing, International Petroleum Technology Conference, Beijing, China, 26-28 March 2013*. 2013, 1–4.

Long, Andrew. Really Low Frequency Seismic: The Next Wave? SEG Professional Development eLearning Course, Society of Exploration Geophysicists, February 2014.

Luo, Yi, Panos G. Kelamis, Qiang Fu, Shoudong Huo, Ghada Sindi, Shih-Ying Hsu, and Arthur B. Weglein. "Elimination of land internal multiples based on the inverse scattering series." *The Leading Edge* 30 (August 2011): 884–889.

Ma, Chao and Arthur B. Weglein. "Including higher-order Inverse Scattering Series (ISS) terms to address a serious shortcoming/problem of the ISS internal-multiple attenuator: exemplifying the problem and its resolution." *84th Annual International Meeting, SEG, Expanded Abstracts.* Submitted, 2014.

Ma, Chao and Arthur B. Weglein. "Inverse Scattering Series (ISS) leading-order internal-multiple-attenuation algorithm and higher-order modification to accommodate primaries and internal multiples as input: 1-D normal incident test on interfering events, and extension to multi-D." *M-OSRP 2013-2014 Annual Report.* 2014.

Ma, Chao and Arthur B. Weglein. "Short note: Lower-order internal multiples act as subevents in the ISS internal-multiple-attenuation algorithm in a three-reflector example." *M-OSRP 2013-2014 Annual Report.* 2014.

Matson, Ken, Dennis Corrigan, Arthur Weglein, Chi-Yuh Young, and Paulo Carvalho. "Inverse scattering internal multiple attenuation: Results from complex synthetic and field data examples." *69th Annual International Meeting, SEG, Expanded Abstracts.* 1999, 1060–1063.

Maver, Kim Gunn. "Ocean bottom seismic: strategic technology for the oil industry." *First Break* 29 (December 2011): 75–80.

Mayhan, James D. *Wave theoretic preprocessing to allow the Inverse Scattering Series methods for multiple removal and depth imaging to realize their potential and impact: Methods, examples, and added value.* PhD thesis, University of Houston, December 2013.

Mayhan, James D., Paolo Terenghi, Arthur B. Weglein, and Nizar Chemingui. "Green's theorem derived methods for preprocessing seismic data when the pressure P and its normal derivative are measured." *81st Annual International Meeting, SEG, Expanded Abstracts.* 2011, 2722–2726.

Mayhan, James D. and Arthur B. Weglein. "First application of Green's theorem-derived source and receiver deghosting on deep-water Gulf of Mexico synthetic (SEAM) and field data." *Geophysics* 78 (March 2013): WA77–WA89.

Mayhan, James D. and Arthur B. Weglein. Source and Receiver De-Ghosting of SEAM Dual Sensor Data. Invited presentation given at the SEG SEAM Workshop, San Antonio, Texas, May 2013.

Mayhan, James D., Arthur B. Weglein, and Paolo Terenghi. "First application of Green's theorem derived source and receiver deghosting on deep water Gulf of Mexico synthetic (SEAM) and field data." *82nd Annual International Meeting, SEG, Expanded Abstracts.* 2012, 1–5.

Moldoveanu, Nick. "Random Sampling: A New Strategy for Marine Acquisition." *80th Annual International Meeting, SEG, Expanded Abstracts.* 2010, 51–55.

Tang, Lin, James D. Mayhan, Jinlong Yang, and Arthur B. Weglein. "Using Green's theorem to satisfy data requirements of multiple removal methods: The impact of acquisition design." *83rd Annual International Meeting, SEG, Expanded Abstracts*. 2013, 4392–4396.

Tang, Lin and Arthur B. Weglein. "Predicting reference medium properties from invariances in Green's theorem reference wave prediction: Towards an on-shore near surface medium and reference wave prediction." *84th Annual International Meeting, SEG, Expanded Abstracts*. Submitted, 2014.

Tenghamn, Rune, Svein Vaage, and Claes Borresen. "A Dual-Sensor Towed Marine Streamer: Its Viable Implementation and Initial Results." *77th Annual International Meeting, SEG, Expanded Abstracts*. 2007, 989–993.

Terenghi, P., X. Li, Shih-Ying Hsu, and Arthur B. Weglein. "1D preprocessing of Kristin data." *M-OSRP 2010-2011 Annual Report*. 2011, 35–49.

van Manen, D. J., M. Vassallo, A. K. Özdemir, A. Özbek, and J. O. A. Robertsson. "Crossline Reconstruction Using Aliased 3D Deghosted Up- and Downgoing Wavefields." *75th EAGE Conference & Exhibition, Extended Abstracts*. June 2013.

Wang, Zhiqiang, Arthur B. Weglein, James D. Mayhan, Paolo Terenghi, and Christian Rivera. "Green's theorem derived deghosting: fundamental analysis, numerical test results, and impact on ISS free-surface multiple elimination." *82nd Annual International Meeting, SEG, Expanded Abstracts*. 2012, 1–5.

Weglein, A. B. and W. Dragoset, editors. *Multiple Attenuation*. SEG Geophysics Reprint Series. Society of Exploration Geophysicists, 2005.

Weglein, A. B., S. A. Shaw, K. H. Matson, J. L. Sheiman, R. H. Stolt, T. H. Tan, A. Osen, G. P. Correa, K. A. Innanen, Z. Guo, and J. Zhang. "New approaches to deghosting towed-streamer and ocean-bottom pressure measurements." *72nd Annual International Meeting, SEG, Expanded Abstracts*. 2002, 2114–2117.

Weglein, Arthur B. "Multiple attenuation: an overview of recent advances and the road ahead (1999)." *The Leading Edge* 18 (January 1999): 40–44.

Weglein, Arthur B. "Short note: An alternative adaptive subtraction criteria (to energy minimization) for free surface multiple removal." *M-OSRP 2011-2012 Annual Report*. 2012, 375.

Weglein, Arthur B. Multiple Attenuation: Recent Advances and the Road Ahead (2013). Keynote presentation given at the Post SEG Convention Workshop on Internal Multiples, Houston, Texas, September 2013.

Weglein, Arthur B. "Multiple attenuation: strategy that addresses current challenges." *E&P Magazine* 87 (April 2014): 132–135.

Weglein, Arthur B. "Removing multiples without subsurface data." *E&P Magazine* 87 (May 2014): 154–156.

Weglein, Arthur B., Fernanda V. Araújo, Paulo M. Carvalho, Robert H. Stolt, Kenneth H. Matson, Richard T. Coates, Dennis Corrigan, Douglas J. Foster, Simon A. Shaw, and Haiyan Zhang. "Inverse Scattering Series and Seismic Exploration." *Inverse Problems* 19 (October 2003): R27–R83.

Weglein, Arthur B., Fernanda Araújo Gasparotto, Paulo M. Carvalho, and Robert H. Stolt. "An Inverse-Scattering Series Method for Attenuating Multiples in Seismic Reflection Data." *Geophysics* 62 (November-December 1997): 1975–1989.

Weglein, Arthur B., Shih-Ying Hsu, Paolo Terenghi, Xu Li, and Robert H. Stolt. "Multiple attenuation: Recent advances and the road ahead (2011)." *The Leading Edge* 30 (August 2011): 864–875.

Weglein, Arthur B., James D. Mayhan, Lasse Amundsen, Hong Liang, Jing Wu, Lin Tang, Yi Luo, and Qiang Fu. "Green's theorem de-ghosting algorithms in k, ω (e.g., $P - V_z$ de-ghosting) as a special case of x, ω algorithms (based on Green's theorem) with: (1) significant practical advantages and disadvantages of algorithms in each domain, and (2) a new message, implication and opportunity for marine towed streamer, ocean bottom and on-shore acquisition and applications." *Journal of Seismic Exploration* 22 (September 2013): 389–412.

Weglein, Arthur B. and Bruce G. Secrest. "Wavelet estimation for a multidimensional acoustic or elastic earth." *Geophysics* 55 (July 1990): 902–913.

WesternGeco. 2013 "IsoMetrix Marine Seismic Technology.". Available online at `http://www.slb.com/services/westerngeco/services/marine/technologies/isometrix.aspx`.

Wu, Jing and Arthur B. Weglein. "The First Test and Evaluation of the ISS Internal Multiple Attenuation Algorithm for the Attenuating Medium." *84th Annual International Meeting, SEG, Expanded Abstracts*. Submitted, 2014.

Wu, Jing and Arthur B. Weglein. "Green's Theorem Based Wavefield Separation Application on Elastic/Land." *84th Annual International Meeting, SEG, Expanded Abstracts*. Submitted, 2014.

Yang, J. and A. B. Weglein. "Incorporating source and receiver arrays in the Inverse Scattering Series free-surface multiple elimination algorithm: Theory and examples that demonstrate impact." *M-OSRP 2011-2012 Annual Report*. 2012, 114–132.

Yang, Jinlong, James D. Mayhan, Lin Tang, and Arthur B. Weglein. "Accommodating the source (and receiver) array in free-surface multiple elimination algorithm: Impact on interfering or proximal primaries and multiples." *83rd Annual International Meeting, SEG, Expanded Abstracts*. 2013, 4184–4189.

Yang, Jinlong and Arthur B. Weglein. "Incorporating source wavelet and radiation pattern into the ISS internal multiple attenuation algorithm." *84th Annual International Meeting, SEG, Expanded Abstracts*. Submitted, 2014.

Zhang, Jingfeng. *Wave theory based data preparation for inverse scattering multiple removal, depth imaging and parameter estimation: analysis and numerical tests of Green's theorem deghosting theory*. PhD thesis, University of Houston, 2007.

Zhang, Jingfeng and Arthur B. Weglein. "Extinction theorem deghosting method using towed streamer pressure data: analysis of the receiver array effect on deghosting and subsequent free surface multiple removal." *75th Annual International Meeting, SEG, Expanded Abstracts*. 2005, 2095–2098.

Zhang, Jingfeng and Arthur B. Weglein. "Application of extinction theorem deghosting method on ocean bottom data." *76th Annual International Meeting, SEG, Expanded Abstracts*. 2006, 2674–2678.

Zou, Yanglei and Arthur B. Weglein. "The pre-stack 1D ISS internal multiple elimination algorithm for all reflectors Part I: strengths and limitations." *84th Annual International Meeting, SEG, Expanded Abstracts*. Submitted, 2014.

Zou, Yanglei and Arthur B. Weglein. "The pre-stack 1D ISS internal multiple elimination algorithm for all reflectors Part II: addressing the limitations." *84th Annual International Meeting, SEG, Expanded Abstracts*. Submitted, 2014.

Predicting reference-medium properties from invariances in Green's theorem reference-wave prediction: towards an on-shore near surface medium and reference wave prediction

Lin Tang and Arthur B. Weglein

May 21, 2014

Abstract

The Inverse Scattering Series (ISS) methods require prerequisites to reach their potentials. Seismic data preprocessing for ISS includes identifying and removing the reference wave, estimating the source wavelet and radiation pattern, and deghosting source and receiver. For onshore seismic exploration, these preprocessing steps still have many serious challenges. To study how to determine the reference velocity for land applications, I use a marine environment as a starting point, and show that the invariance of the estimated source signature for a point source could be a criterion for finding the correct reference velocity. In addition, for the case of a source array, the invariance of the source wavelet in one radiation angle could be the criterion for verifying that we have the right reference velocity.

1 Introduction

The current trend in the petroleum industry is to explore in deep water and in areas that have complex geology, where primary and multiple events often may be interfering with or proximal to each other. In such cases, removal of the multiple events becomes a big challenge. Inverse Scattering Series (ISS) methods offer a direct way of removing free-surface multiples and attenuating internal multiples without requiring any subsurface information. However, these methods have prerequisites that need to be satisfied. The prerequisites include identifying and removing the reference wave, estimating the source wavelet and radiation pattern, and deghosting source and receiver. In order to deliver the high fidelity expected of ISS multiple predictions, effective preprocessing methods need to be developed and improved (Zhang (2007), Mayhan et al. (2011), Mayhan and Weglein (2013), Tang et al. (2013), Yang et al. (2013)).

As seismic exploration moves to increasingly complex and difficult onshore and offshore plays, there are additional fundamental issues and challenges that need to be resolved. Among these issues and challenges, removal of the reference wave on land is a pressing and interesting topic. Scattering theory separates the real world into two parts: the reference medium, whose property is known, plus a perturbation. ISS methods require that the reference medium agree with the actual medium on

and above the measurement surface. The wave that travels in the reference medium is the reference wave, and it does not experience the earth in its history, so it contains no subsurface information. It is important to identify and remove reference waves before the following data-processing steps. In inverse scattering series, the data D on the measurement surface is,

$$\begin{aligned} D &= (G - G_0)_{m.s.} \\ &= G_0 V G \\ &= G_0 V G_0 + G_0 V G_0 V G_0 + ... \end{aligned}$$

As the above equation shows, the very first step of any ISS methods (free surface multiple removal, internal multiple removal and depth imaging) is to remove G_0. From the wave equation

$$L_0 G_0 = \delta,$$

in order to predict and remove G_0, we need to know L_0, which is the reference medium. ISS methods only require the reference medium information at and above the measurement surface. For marine environment, the property of water is relatively easy to define. However, for on-shore seismic applications, the near surface properties are often complicated and difficult to determine, e.g., because the conditions of rocks, soil or minerals in the near surface are not easy to define due to weathering. Strong ground roll can be generated, and it can obscure reflected seismic data. To remove the ground roll/reference wave, the physical properties of the near surface is needed.

Green's theorem provides a good mathematical tool for achieving these prerequisites, which are consistent with the ISS methods they are meant to serve. My purpose in looking for a way to determine the velocity of near surface medium on land, is to provide a foundation for the study of onshore seismic data preprocessing methods. That task is part of the comprehensive Inverse Scattering Series multiple removal strategy.

In order to study the complex on-shore or ocean bottom near surface property, we propose to start from seeking criteria which can determine whether we have the correct reference medium information or not. The criteria could be the presence of some invariance that only the correct reference velocity would satisfy. We use a marine seismic application as a starting point to pursue this idea. First, consider an isotropic point source, which has an isotropic source wavelet in every radiation direction. Using Green's theorem, we can estimate the wavelet signature everywhere below the measurement surface. When using the correct reference velocity, the results for the wavelet should be invariant for all output points below the measurement surface. Thus, the value of reference velocity we use in the wavelet calculation that leads to an invariance of the estimated source wavelet is the correct reference velocity. Furthermore, instead of a single point source, in practice, source arrays which have angle radiation pattern are widely used in industry (Loveridge et al. (1984)). Then the invariance of the estimated wavelet will happen when estimating the wavelet at different points along one radiation angle. Similarly, only the correct reference velocity can lead to the invariance. Thus, the invariances of the source wavelet indicate that we have found the correct reference velocity.

This report will discuss the criteria of predicting the reference medium properties from invariances in Green's theorem-based wavelet estimation, for both point source and for source array cases. A 1D

analytic example will be shown first to explain the idea of invariance. For a point source, the source wavelet estimated at any point beneath the measurement surface should stay the same; while for source array data, the estimated source wavelet in one radiation angle should be invariant. These invariances could be criteria for verifying that we have the correct reference velocity. Future study will extend this research from the marine example to a complex, onshore elastic model.

2 Theory

2.1 Green's theorem for wavelet estimation

The theory of wavelet estimation using Green's theorem is first described in Weglein and Secrest (1990). Assume that source $A(\omega)$ is placed at $\vec{r_s}$ and the receiver is at $\vec{r}$. The pressure wavefield P satisfies the constant density acoustic wave equation in the frequency domain:

$$\left(\nabla^2 + \frac{\omega^2}{c^2(\vec{r})}\right) P(\vec{r}, \vec{r}_s, \omega) = A(\omega)\delta(\vec{r} - \vec{r_s}). \tag{1}$$

In scattering theory, we treat the actual medium as if it were a combination of an unperturbed medium, called the reference medium, and a perturbation. Induce perturbation α defined by

$$\frac{1}{c^2(\vec{r})} = \frac{1}{c_0^2}[1 - \alpha(\vec{r})],$$

where c_0 is the velocity in a homogeneous reference medium. Then Equation 1 becomes

$$\left(\nabla^2 + \frac{\omega^2}{c_0^2}\right) P(\vec{r}, \vec{r}_s, \omega) = \underbrace{\frac{\omega^2}{c_0^2}\alpha(\vec{r})P(\vec{r}, \vec{r}_s, \omega) + A(\omega)\delta(\vec{r} - \vec{r_s})}_{\rho}. \tag{2}$$

The right-hand side of the equation can be viewed as the source of the wavefield P, which has two terms: the perturbation α, which generates the scattered wave P_s, and the active source $A(\omega)$, the energy source that generates the wave P. The corresponding Green's function satisfies,

$$\left(\nabla^2 + \frac{\omega^2}{c_0^2}\right) G_0(\vec{r}, \vec{r'}, \omega) = \delta(\vec{r} - \vec{r'}). \tag{3}$$

Having a causal Green's function G_0^+, we can obtain wavefield P,

$$\begin{aligned} P(\vec{r}, \omega) &= \int_\infty G_0^+(\vec{r}, \vec{r'}, \omega)\rho(\vec{r'}, \omega)d\vec{r'} \\ &= \int_\infty G_0^+(\vec{r}, \vec{r'}, \omega)\frac{\omega^2}{c_0^2}\alpha(\vec{r'})P(\vec{r'}, \omega)d\vec{r'} + A(\omega)G_0^+(\vec{r}, \vec{r_s}, \omega). \end{aligned} \tag{4}$$

The first term on the right-hand side of Equation 4 is the source that generates the difference between the total wavefield P and the reference wavefield P_0. Therefore, P_0 is given by

$$P_0(\vec{r}, \vec{r_s}, \omega) = A(\omega) G_0^+(\vec{r}, \vec{r_s}, \omega). \tag{5}$$

The difference between P and P_0 is defined as the scattered wavefield P_s, which is

$$P_s = P - P_0. \tag{6}$$

Thus, P_s satisfies

$$P_s(\vec{r}, \vec{r_s}, \omega) = \int_\infty G_0(\vec{r}, \vec{r'}, \omega) \frac{\omega^2}{c_0^2} \alpha(\vec{r'}) P(\vec{r'}, \vec{r_s}, \omega) d\vec{r'}. \tag{7}$$

On the other hand, from Green's second identity, we have

$$\int_V (\phi \nabla'^2 \psi - \psi \nabla'^2 \phi) d\vec{r'} = \oint_S [\phi \nabla' \psi - \psi \nabla' \phi] \cdot \hat{n} dS. \tag{8}$$

Now suppose that $\phi = P$ and $\psi = G_0$. Plugging Equation 2 and Equation 3 into Equation 8, we have

$$\begin{aligned}
&\int_V (P \nabla'^2 G_0 - G_0 \nabla'^2 P) d\vec{r'} \\
= &\int_V \left(P(\vec{r'}, \vec{r_s}, \omega) \left[-\frac{\omega^2}{c_0^2} G_0(\vec{r'}, \vec{r}, \omega) + \delta(\vec{r} - \vec{r'}) \right] - G_0(\vec{r'}, \vec{r}, \omega) \left[-\frac{\omega^2}{c_0^2} P(\vec{r'}, \vec{r_s}, \omega) + \rho(\vec{r'}) \right] \right) d\vec{r'} \\
= &\int_V P(\vec{r'}, \vec{r_s}, \omega) \delta(\vec{r} - \vec{r'}) d\vec{r'} - \int_V G_0(\vec{r'}, \vec{r}, \omega) \left[\frac{\omega^2}{c_0^2} \alpha(\vec{r'}) P(\vec{r'}, \vec{r_s}, \omega) + \delta(\vec{r'} - \vec{r_s}) A(\omega) \right] d\vec{r'} \\
= &\oint_S \left[P(\vec{r'}, \vec{r_s}, \omega) \nabla' G_0(\vec{r'}, \vec{r}, \omega) - G_0(\vec{r'}, \vec{r}, \omega) \nabla' P(\vec{r'}, \vec{r_s}, \omega) \right] \cdot \hat{n} dS.
\end{aligned} \tag{9}$$

We choose the volume as the infinite space below the measurement surface, and $\vec{r}$ is chosen to be below the measurement surface (inside the volume V), as Figure 1 shows. Equation 9 becomes

$$P(\vec{r}, \vec{r_s}, \omega) = \int_V G_0(\vec{r}, \vec{r'}, \omega) \frac{\omega^2}{c_0^2} \alpha(\vec{r'}) P(\vec{r'}, \vec{r_s}, \omega) d\vec{r'} + \oint_S \left[P \nabla' G_0 - G_0 \nabla' P \right] \cdot \hat{n} dS. \tag{10}$$

When choosing G_0^+ in Equation 10, let us compare Equation 10 and Equation 4. When the support of perturbation $\alpha(\vec{r})$ is within the volume V, the integral of α over infinity equals the integral over volume V. Thus, with $\vec{r}$ inside the volume, the support of α is within the volume, and both Equations 10 and 4 should give the same wavefield. Therefore,

$$A(\omega) G_0^+(\vec{r}, \vec{r_s}, \omega) = \oint_S \left[P(\vec{r'}, \vec{r_s}, \omega) \nabla' G_0^+(\vec{r'}, \vec{r}, \omega) - G_0^+(\vec{r'}, \vec{r}, \omega) \nabla' P(\vec{r'}, \vec{r_s}, \omega) \right] \cdot \hat{n} dS. \tag{11}$$

Thus, source signature $A(\omega)$ can be estimated by a surface integral and then divided by the Green's function. Using Sommerfeld's radiation condition for G_0^+, the wavefield contribution at $\vec{r}$ in V from at the infinitely far away boundary vanishes. Then,

$$A(\omega) = \frac{1}{G_0^+(\vec{r}, \vec{r_s}, \omega)} \cdot \int_{m.s.} \left[P(\vec{r'}, \vec{r_s}, \omega) \nabla' G_0^+(\vec{r'}, \vec{r}, \omega) - G_0^+(\vec{r'}, \vec{r}, \omega) \nabla' P(\vec{r'}, \vec{r_s}, \omega) \right] \cdot \hat{n} dS. \tag{12}$$

In marine seismic exploration as shown in Figure 2, for the purpose of estimating wavelet, we choose the reference medium as a half-space of air plus a half-space of water. Thus, Green's function is consist of two parts,

$$G_0 = G_0^d + G_0^{FS}. \tag{13}$$

Equation 12 is the equation of Green's theorem-based wavelet estimation method. $\vec{r'}$ is on the measurement surface, and $\vec{r}$ is the observation point, which need to be chosen as below the measurement surface. This equation is valid for any points below the cable. Both the numerator and denominator of Equation 12 are functions of $\vec{r}$, $\vec{r_s}$ and ω. However, their quotient $A(\omega)$ is not a function of the observation point $\vec{r}$, when we are calculating it correctly. Using this property, we can have the criterion for having the correct reference velocity. If we use a wrong reference velocity in the Green's function, it will break this property. The quotient will become a function of $\vec{r}$. Next, an analytic example in 1D earth will be shown to illustrate this idea.

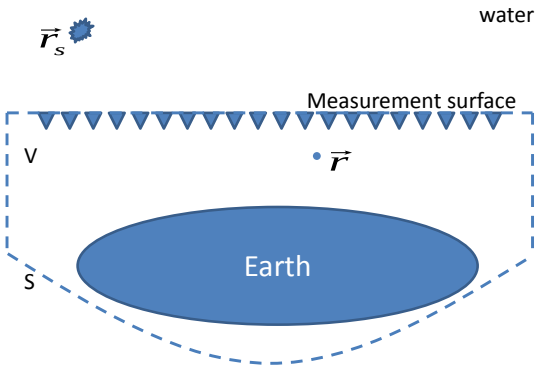

Figure 1: Choosing V as the infinite space below the measurement surface and $\vec{r}$ below the cable (inside the volume).

3 1D analytical example

In this section, a 1D analytical example of wavelet estimation will be given. 1D means the wave propagates only in z direction, and the Earth is also only has z direction variance. Therefore, the measurement surface is one point at depth $z' = a$. The surface integral changes to the value of $(P\nabla G_0 - G_0\nabla P)$ at the two ends: infinite $z' = \infty$ and the measurement surface $z' = a$. The configuration is shown in Figure 3. As discussed above, the prediction point z is chosen as below the measurement surface $z' = a$. Therefore, $z > a > z_s$. The existence of free surface is equal to an image source. Therefore, the Green's function satisfies the wave equation,

$$(\frac{d^2}{dz^2} + k^2)G_0(z, z', \omega) = \delta(z - z') - \delta(z + z'). \tag{14}$$

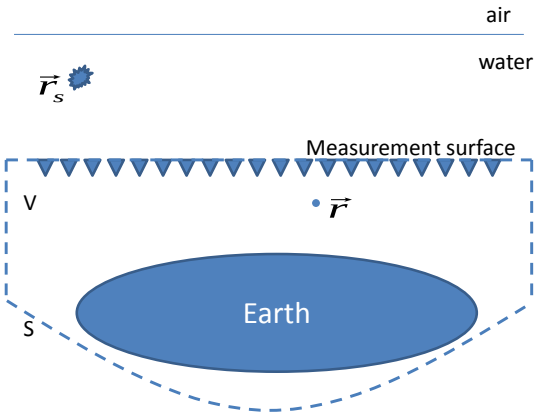

Figure 2: Marine seismic exploration configuration.

So Green's function G_0 and its normal derivative dG_0/dz' in 1D become,

$$\begin{aligned} G_0(z,z',\omega) &= \frac{\exp(ik|z-z'|)}{2ik} \\ &= \frac{\exp(ik(z-z')) - \exp(ik(z+z'))}{2ik}, \qquad (15) \\ \frac{d}{dz'}G_0(z,z',\omega) &= \frac{-\exp(ik(z-z')) - \exp(ik(z+z'))}{2}. \qquad (16) \end{aligned}$$

In this example, there is no perturbation below the measurement surface. Therefore, the measured wavefield P equals the reference wave P_0. On the measurement surface $z' = a$, the wavefield P and its normal derivative dP/dz' are,

$$\begin{aligned} P(z',z_s,\omega) &= A(\omega)G_0(z',z_s,\omega) \qquad (17) \\ &= A(\omega)\frac{\exp(ik(z'-z_s)) - \exp(ik(z'+z_s))}{2ik}, \qquad (18) \\ \frac{d}{dz'}P(z',z_s,\omega) &= A(\omega)\frac{d}{dz'}G_0(z',z_s,\omega) \qquad (19) \\ &= A(\omega)\frac{\exp(ik(z'-z_s)) - \exp(ik(z'+z_s))}{2}. \qquad (20) \end{aligned}$$

So the predicted reference wave $P_0(z,z_s,\omega)$ is,

$$P_0(z,z_s,\omega) = |_{z'=a}^{\infty}\left[(z',z_s,\omega)\frac{d}{dz'}G_0(z,z',\omega) - G_0(z,z',\omega)\frac{d}{dz'}P(z',z_s,\omega)\right]$$

$$
\begin{aligned}
&= 0 - \Bigg[A(\omega)\frac{[\exp(ik(a-z_s)) - \exp(ik(a+z_s))]}{2ik}\frac{[-\exp(ik(z-a)) - \exp(ik(z+a))]}{2} \\
&- \frac{[\exp(ik(z-a)) - \exp(ik(z+a))]}{2ik}A(\omega)\frac{[\exp(ik(a-z_s)) - \exp(ik(a+z_s))]}{2}\Bigg] \\
&= A(\omega)\frac{1}{2ik}[\exp(ik(z-z_s)) - \exp(ik(z+z_s))]. \qquad (21)
\end{aligned}
$$

$$(22)$$

Therefore,

$$\frac{P_0(z,z_s,\omega)}{G_0(z,z_s,\omega)} = \frac{A(\omega)\frac{1}{2ik}[\exp(ik(z-z_s)) - \exp(ik(z+z_s))]}{\frac{1}{2ik}[\exp(ik(z-z_s)) - \exp(ik(z+z_s))]} = A(\omega) \qquad (23)$$

The above equation shows that even though both P_0 and G_0 depend on the prediction point z, their quotient $A(\omega)$ is independent of z. When a wrong reference velocity c_0' is used to predict the wavelet, Green's functions in the above equation contains a wrong wavenumber $k' = \omega/c_0'$. We now have,

$$
\begin{aligned}
P_0(z,z_s,\omega) = &\ |_{z'=a}^{\infty} P(z',z_s,\omega)\tfrac{d}{dz'}G_0(z,z',\omega) - G_0(z,z',\omega)\tfrac{d}{dz'}P(z',z_s,\omega) \\
= 0 - &\Bigg[A(\omega)\frac{[\exp(ik(a-z_s)) - \exp(ik(a+z_s))]}{2ik}\frac{[-\exp(ik'(z-a)) - \exp(ik'(z+a))]}{2} \\
- &\frac{[\exp(ik'(z-a)) - \exp(ik'(z+a))]}{2ik'}A(\omega)\frac{[\exp(ik(a-z_s)) - \exp(ik(a+z_s))]}{2}\Bigg] \\
= A(\omega)&(\frac{1}{4ik} + \frac{1}{4ik'})[\exp(i(k'z - kz_s + (k-k')a)) - \exp(i(k'z + kz_s) + (k-k')a))].
\end{aligned} \qquad (24)
$$

So the wavelet becomes,

$$\frac{P_0(z,z_s,\omega)}{G_0(z,z_s,\omega)} = \frac{A(\omega)(\frac{1}{4ik} + \frac{1}{4ik'})[\exp(i(k'z - kz_s + (k-k')a)) - \exp(i(k'z + kz_s) + (k-k')a))]}{\frac{1}{2ik'}[\exp(ik'(z-z_s)) - \exp(ik'(z+z_s))]} \qquad (25)$$

Now using the wrong reference velocity to calculate the wavelet, the result of $A(\omega)$ depends on the observation point z. So the property of invariance no longer exists. By observing the invariance of predicted wavelet at different output point under the cable, we can determine if we have the correct reference velocity or not. We use a marine environment as an example to test this idea.

3.1 Radiation pattern

In the previous section, we focused on solving the wavelet from a point source at $\delta(\vec{r}-\vec{r_s})$. In a more general case, a extended source array that consists of several point source could be used in seismic exploration. In this case, the source displays a radiation pattern in different radiation angles. The

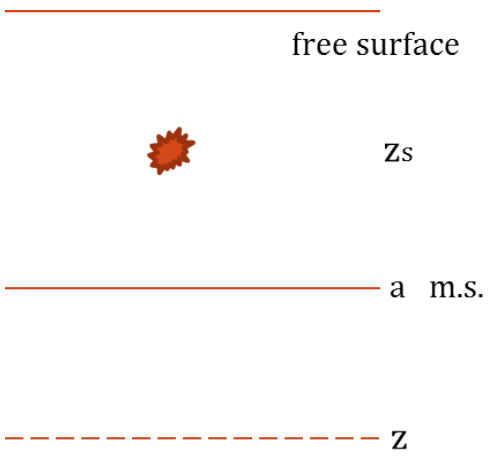

Figure 3: A 1D example

radiation pattern from a single effective point source could be estimated by assuming that $A(\omega)$ is a function of the radiation angle θ (using far field approximation).

Assume that a general extended source $\rho(\vec{r})$ as Figure 4 shows. Wavefield at $\vec{r}$ generated from this source array can be calculated from the integral,

$$P_0(\vec{r},\omega) = \int G_0(\vec{r},\vec{r'},\omega)\rho(\vec{r'})d\vec{r'}. \tag{26}$$

In 3D propagation, Green's function in frequency domain can be written as

$$G_0(\vec{r},\vec{r'},\omega) = \frac{e^{ik|\vec{r}-\vec{r'}|}}{|\vec{r}-\vec{r'}|}. \tag{27}$$

In the far field, $|\vec{r}| >> |\vec{r'}|$, we have approximation,

$$\begin{aligned} |\vec{r}-\vec{r'}| &= \sqrt{(\vec{r}-\vec{r'})^2} \\ &= \sqrt{r^2 - 2\vec{r}\cdot\vec{r'} + r'^2} \\ &= r[1 - \frac{2\vec{r}\cdot\vec{r'}}{r^2} + \frac{r'^2}{r^2}]^{1/2} \\ &= r(1 - \frac{\vec{r}\cdot\vec{r'}}{r^2} + \frac{r'^2}{2r^2} + ...) \\ &= r - \hat{n}\cdot\vec{r'} + O(\frac{1}{r}). \end{aligned} \tag{28}$$

The above equation uses Taylor series $(1+x)^{1/2} = 1 + \frac{1}{2}x + O(x^2)$, and $\hat{n}$ is the unit vector in the

direction of $\vec{r}$. And similarly,

$$\frac{1}{|\vec{r}-\vec{r'}|} = \frac{1}{r} + \frac{\hat{n}\cdot\vec{r'}}{r^2} + ... = \frac{1}{r} + O(\frac{1}{r^2}). \tag{29}$$

Then in the far field, Equation 26 becomes

$$\begin{aligned} P_0(\vec{r},\omega) &= \int \frac{e^{ik(r-\hat{n}\cdot\vec{r'})}}{r}\rho(\vec{r'})d\vec{r'} \\ &= \frac{e^{ikr}}{r}\int e^{-ik\hat{n}\cdot\vec{r'}}\rho(\vec{r'})d\vec{r'} \\ &= \frac{e^{ikr}}{r}\tilde{\rho}(k\hat{n}). \end{aligned} \tag{30}$$

Therefore, in the far field if we process seismic data generated from the source array as if a point source, we can get the source wavelet

$$A(\omega,\theta) = \frac{P_0}{G_0} = \tilde{\rho}(k\hat{n}).$$

Since $\hat{n}$ is the direction from the source to the observation point, the estimated wavelet result will display variances in different radiation angle. While in one radiation angle, wavelet $A(\omega,\theta)$ will be the same. This could be a criterion of determining the correct reference velocity. If using a wrong reference velocity, this invariance at one radiation angle will not be satisfied.

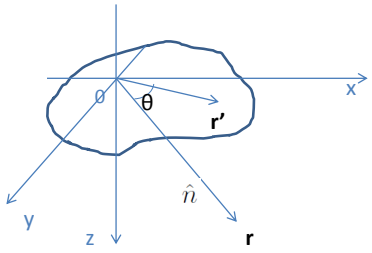

Figure 4: A general extended source.

4 Point source

In this test, we use the Cagniard-de Hoop method to model over-under cable data. Then using the Green's theorem of Equation 12, we estimate wavelet $A(\omega)$, at different points at a fixed depth. We predict the estimated wavelet results by using different reference velocities:
(1) the correct reference velocity $c_0 = 1500m/s$;

(2) a wrong reference velocity $c_0 = 1490m/s$;
(3) an additional wrong reference velocity $c_0 = 1450m/s$.
The estimated reference wavefields P_0 are shown in Figure 3, and the corresponding wavelet are presented in Figure 4. Figure 5 indicates that the wrong reference velocities also lead to errors in the prediction of P_0. The estimated source wavelet results show that when using the correct reference velocity, the wavelet displays invariance at different offset, while wrong velocities give different wavelet prediction at different output points.

Therefore, only the correct reference velocity can result in the invariance of estimated wavelet. When the reference velocities become progressively more incorrect, the errors of the wavelet invariance also become larger. This conclusion will also help us in finding the correct reference velocity.

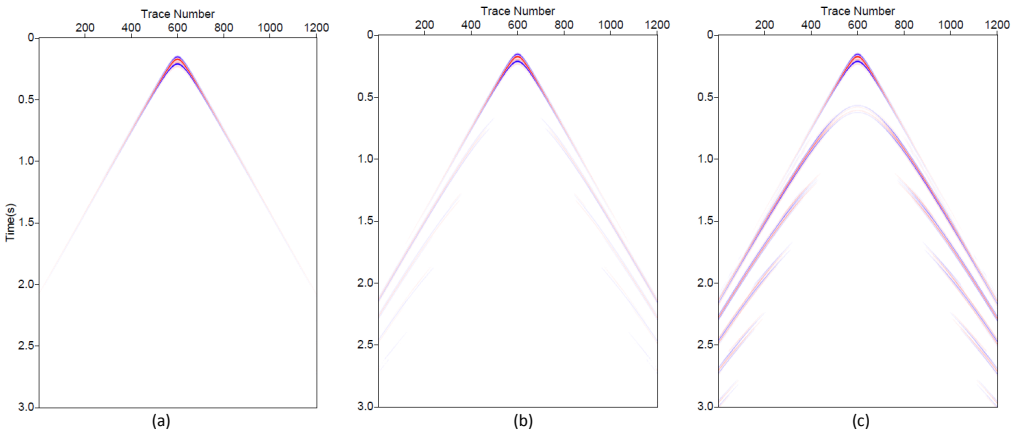

Figure 5: P_0 estimated using (a) correct $c_0 = 1500m/s$, (b) wrong $c_0 = 1490m/s$, (c) wrong $c_0 = 1450m/s$

5 Source array

In this section, instead of using a point source, I will test data generated by a source array. The source array consists of 7 point sources separated at 3 m, as shown in Figure 7. First, we will estimate source wavelet along a horizontal cable, whose radiation angles are different. We predict source wavelet at depth 56 m, from offset 0 m to 606 m, whose radiation angles are from 0° to 85°. The results in Figure 7 show the radiation pattern in different offset (radiation angle). Next, we estimate the wavelet $A(\omega, \theta)$ in one radiation angle. The estimated wavelet in angle 5.8°, using different velocities, is shown in Figure 9. As with the conclusion above, we can see that only the

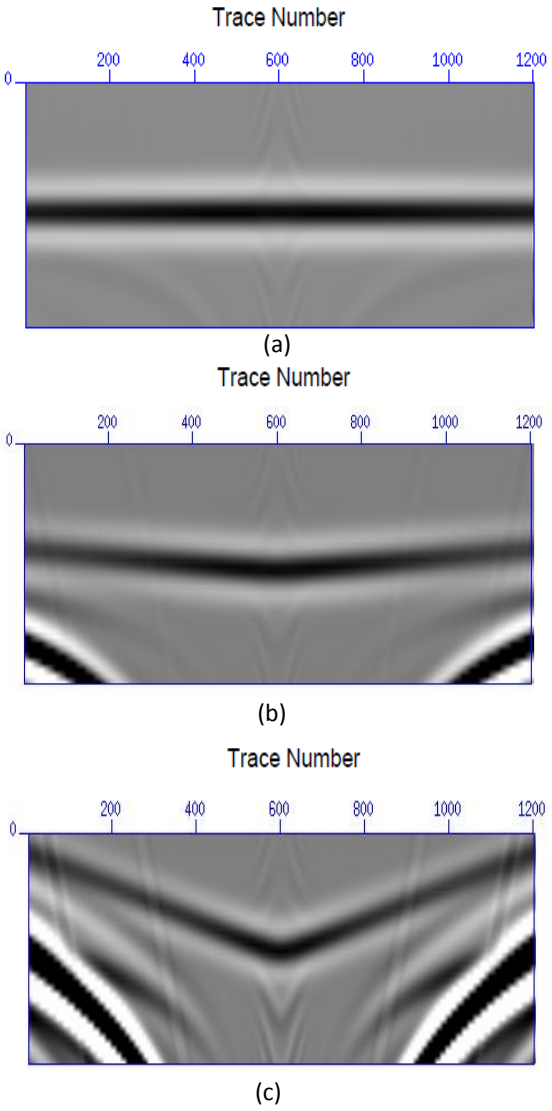

Figure 6: $A(t)$ estimated using (a) correct $c_0 = 1500m/s$, (b) wrong $c_0 = 1490m/s$, and (c) wrong $c_0 = 1450m/s$

correct velocity gives us the invariance of the source array wavelet in one angle, while the wrong reference velocity will lead to differences of the wavelet in one radiation angle.

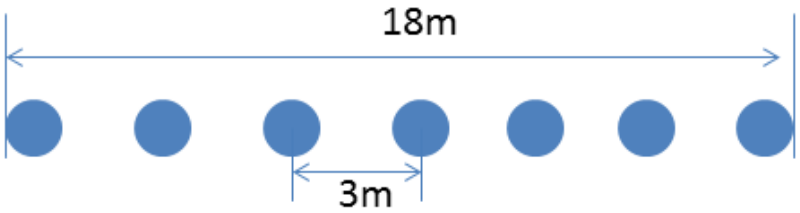

Figure 7: Source array

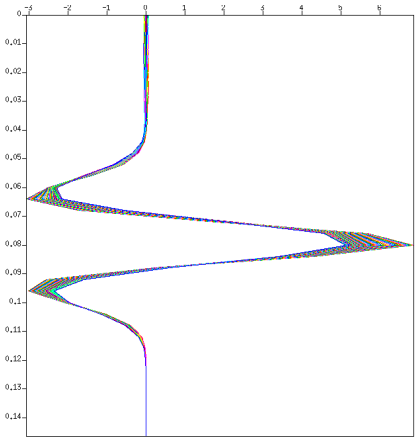

Figure 8: Radiation pattern of the source array in Figure 7, estimated from offset 0m to 606m.

6 Conclusions

We have shown that an output point invariance of a wavelet estimated by using Green's theorem could be a criterion for determining the correct reference velocity. For a point source, the invariance occurs for the output point anywhere below the measurement surface, while for data with source array and radiation pattern, the invariance is for output points along one radiation angle. Using marine seismic application as a starting point, this paper shows that invariances of Green's theorem-based wavelet estimation could be a criterion of determining the reference velocity. Using similar thinking, in the future study we will focus on solving the complex onshore or ocean-bottom near surface medium problems. For on-shore or ocean bottom problems, understanding of the near surface property could enable us to predict and remove the ground roll/reference wave on land, and thereby enhance the capability of subsequent multiple removal processing steps for the challenge of on-shore multiple attenuation.

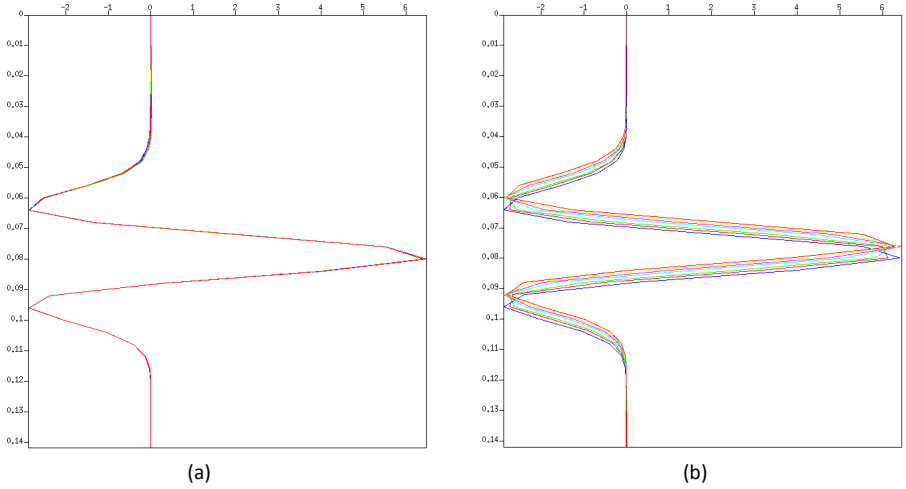

Figure 9: Wavelet estimated at depths 36m, 56m, 76m, 96m, 116m, 136m, and 156m, at the same radiation angle and using (a) the correct reference wave $c_0 = 1500m/s$ and (b) a wrong reference velocity $c_0 = 1450m/s$.

7 Acknowledgements

We are grateful to all M-OSRP sponsors for their encouragement and support in this research. The first author would like to thank Jinlong Yang and Chao Ma for reviewing this report, and Professor Weglein for his guidance and discussions.

References

Loveridge, M.M., G.E. Parks, L. Hatton, and M.H. Worthington. "Effects of marine source array directivity on seismic data and source signature deconvlution." *First Break* 2 (1984): 16–22.

Mayhan, J., P. Terenghi, A. Weglein, and N. Chemingui. "Green's theorem derived methods for preprocessing seismic data when the pressure P and its normal derivative are measured.." *SEG Expanded Abstracts.* (2011): 2722–2726.

Mayhan, J. and A. Weglein. "First application of Green's theorem-derived source and receiver deghosting on deep-water Gulf of Mexico synthetic (SEAM) and field data.." *Geophysics* 78 (2013): WA77–WA89.

Tang, L., J. Mayhan, J. Yang, and A. Weglein. "Using Green's theorem to satisfy data requirements of multiple removal methods: The impact of acquisition design.." *SEG Expanded Abstracts.* (2013): 4392–4396.

Weglein, Arthur B. and Bruce G. Secrest. "Wavelet estimation for a multidimensional acoustic earth model." *Geophysics* 55 (July 1990): 902–913.

Yang, J., J. Mayhan, L. Tang, and A. Weglein. "Accommodating the source (and receiver) array in free-surface multiple elimination algorithm: Impact on interfering or proximal primaries and multiples.." *SEG Expanded Abstracts.* (2013): 4184–4189.

Zhang, Jingfeng. *Wave theory based data preparation for inverse scattering multiple removal, depth imaging and parameter estimation: analysis and numerical tests of Green's theorem deghosting theory.* PhD thesis, University of Houston, 2007.

Elastic Green's theorem preprocessing for on-shore internal multiple attenuation: theory and initial synthetic data tests

Jing Wu and Arthur B. Weglein

May 21, 2014

Abstract

Prerequisites are important for the Inverse Scattering Series (ISS) multiple removal method that assumes the reference wavefield has been removed and the source wavelet has been deconvolved. This paper derives the elastic Green's theorem reference wave prediction algorithm, which extends the off-shore acoustic to the on-shore elastic wavefield separation, in preparation for on-shore ISS internal multiple attenuation.

1 Introduction

Weglein (2013) proposes a three-pronged strategy to respond to the current pressing challenges in removing multiples: (1) develop the ISS prerequisites for predicting the reference wavefield and producing deghosted data that are direct and do not require subsurface information; (2) develop internal multiple elimination algorithms from the ISS; and (3) develop a replacement for the energy-minimization criteria for adaptive subtraction. For part (1), Green's theorem preprocessing has documented effectiveness for off-shore plays (e.g., Weglein et al., 2002; Zhang, 2007; Mayhan et al., 2012; Mayhan and Weglein, 2013; Tang et al., 2013; Yang et al., 2013).

For on-shore plays, because of their complex structures with lateral variation, as well as significant ground roll, there are more fundamental issues and challenges for resolving the near surface problem. Among these issues and challenges, identification and removal of the reference wave is one pressing and essential topic. Scattering theory separates the real world into two parts: the reference medium, whose property is known, plus a perturbation. The wave that travels in the reference medium is called the reference wave, which does not experience the earth that we are interested in (Weglein et al., 2003; Tang and Weglein, 2014). Especially for on-shore, the ground roll is the main energy of the reference wave and can obscure the reflections. In addition, the reference wave contains the source signature information, which is important and will be used for deconvolution before the subsequent ISS multiple removal. Therefore, it is an important step to identify and remove the reference wavefield on land.

Matson (1997) provides the ISS free surface multiple elimination algorithm and internal multiple attenuation algorithm in PS space, i.e., by using potentials rather than displacements. He assumes the reference wave has been removed by using a linear mute; however, the linear mute may harm/destroy useful information, especially when the reference wave and the scattering wave are seriously interfering with each other. Weglein and Secrest (1990) propose the reference wave prediction method for elastic media based on Green's theorem, and following that they derive the wavelet estimation algorithm in displacement space. When the medium is assumed to consist of a homogeneous elastic whole-space, Jiang et al. (2013) test the algorithm.

In order to simulate the land acquisition situation, we choose two homogeneous half spaces as the reference medium, an acoustic half-space over an elastic half-space. We locate the source in the acoustic medium and receivers in the elastic medium. The perturbation will be in the lower elastic half-space. By using Green's second identity, we derive the algorithm to separate the reference wave and scattering wave in PS space. In this paper, the algorithms are derived in both the space-frequency domain and the wavenumber-frequency domain. The wavelet can be estimated from the predicted reference wave. Numerical tests are shown to evaluate the accuracy of the algorithm for predicting the source wavelet for this acoustic over elastic half-space problem that models the on-shore play acquisition. The results are positive and encouraging.

2 Background for 2D Elastic Medium

We are deriving the wavefield-separation method for on-shore application and we start with the elastic formulation. For convenience, the basis is changed from $\mathbf{u} = \begin{pmatrix} u_x \\ u_z \end{pmatrix}$ to $\Phi = \begin{pmatrix} \phi^P \\ \phi^S \end{pmatrix}$. $\mathbf{u}$ represents the displacement, constituting with x and z components; whereas Φ has potential components for P wave and S wave. The detail for the basis transform is shown in appendix A.

In PS space, the basic wave equations (Weglein and Stolt, 1995; Zhang, 2006) are

$$\hat{L}\Phi = \mathbf{F}, \tag{1}$$

$$\hat{L}\hat{G} = \delta, \tag{2}$$

$$\hat{L}_0\Phi_0 = \mathbf{F}, \tag{3}$$

$$\hat{L}_0\hat{G}_0 = \delta, \tag{4}$$

where $\hat{L}$ and $\hat{L}_0$ are the differential operators that describe the wave propagation in the actual medium and the reference medium, respectively. $\mathbf{F}$ is the source term. $\hat{G}$ and $\hat{G}_0$ are the corresponding Green's function operators for the actual and reference media.

For a homogeneous medium,

$$\hat{L}_0 = \begin{pmatrix} \nabla^2 + \frac{\omega^2}{\alpha_0^2} & \\ & \nabla^2 + \frac{\omega^2}{\beta_0^2} \end{pmatrix} = \begin{pmatrix} \hat{L}_0^P & \\ & \hat{L}_0^S \end{pmatrix}, \tag{5}$$

where α_0 and β_0 are P wave velocity and S wave velocity, respectively,

and

$$\hat{G}_0 = \begin{pmatrix} \hat{G}_0^P & \\ & \hat{G}_0^S \end{pmatrix}. \tag{6}$$

Equations 5 and 6 are diagonal and zeros are omitted for clarity. However, in an actual inhomogeneous medium, $\hat{G}$ is no longer a diagonal matrix, but has a form

$$\hat{G} = \begin{pmatrix} \hat{G}^{PP} & \hat{G}^{PS} \\ \hat{G}^{SP} & \hat{G}^{SS} \end{pmatrix}. \tag{7}$$

For the superscripts, the right one represents the wave type of source side, whereas the left one represents the wave type of receiver side.

3 Green's Theorem Wavefield Separation Algorithm in PS Space

3.1 Description of the Problem

Transforming the elastic wave equations from displacement space to PS space, we have

$$\hat{L}\Phi = \mathbf{F},$$

$$\hat{L}_0\hat{G}_0 = \delta,$$

$$\hat{L} = \hat{L}_0 - \hat{V}. \tag{8}$$

The basic form of these equations is the same as that for the acoustic case. On the basis of the successful applications of Green's theorem wavefield separation to the acoustic case (e.g., Zhang, 2007; Mayhan et al., 2012), it is feasible to apply the Green's theorem wavefield separation algorithm to the elastic medium in a similar way. The reference medium ($\hat{L}_0$) can be chosen for different objectives. To separate the reference wavefield and the scattering wavefield, the portion of the reference medium above the measurement surface should have the same properties that the actual medium has.

For on-shore acquisition, we assume that the source is located slightly above the earth's surface (e.s.), and the geophone is in the earth but close to the earth's surface as shown in Fig.1. Actually, because of weathered layer and tundra, the properties of the near surface can be complicated, with laterally varying densities and velocities. For this initial study, we assume that the medium, which is below the earth's surface and above the measurement surface (m.s.), is homogeneous. The reference wave can be predicted in any point inside the volume in Fig.1 by using Green's theorem.

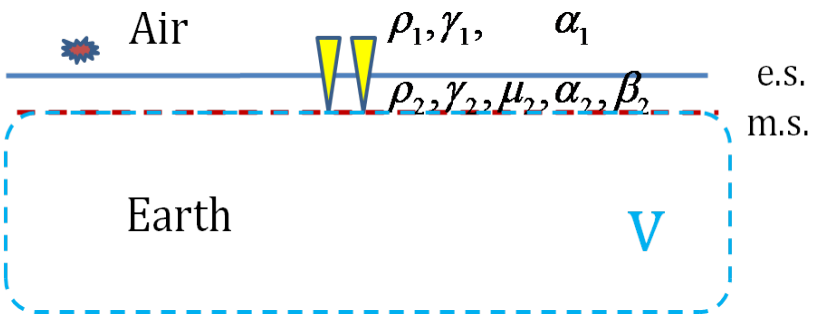

Figure 1: On-shore acquisition. ρ is the density, γ is the bulk modulus, μ is the shear modulus, α is the P wave velocity, and β is the S wave velocity

3.2 Reference Wavefield Prediction in PS Space

In Fig.2, the source ($\mathbf{r}_s$) is above the earth's surface, i.e., the boundary, receiver ($\mathbf{r}'$) is on the measurement surface, and the prediction location is represented by $\mathbf{r}$. The reference medium is chosen as a discontinuous two-half-space medium; above the boundary is homogeneous air and below is homogeneous elastic. A hemispherical surface integral upper bounded by the measurement surface will separate the total wave Φ into the reference wave Φ_0 and the scattering wave Φ_S. The prediction in the volume is the reference wave Φ_0 as shown in Fig.2.

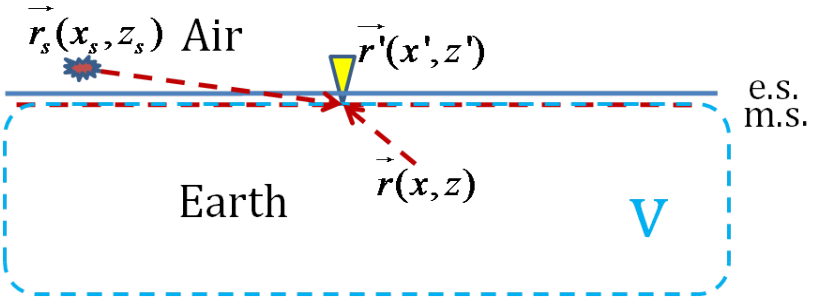

Figure 2: Volume enclosed (blue dashed line) for reference wavefield prediction at $\mathbf{r}$ in the volume and $\mathbf{r}$ is under the measurement surface that is represented by $\mathbf{r}'$.

The elastic Green's theorem algorithm in the space-frequency domain for the reference wave prediction in the volume is

$$\Phi_0(\mathbf{r}, \mathbf{r}_s) = \oint \left(\Phi(\mathbf{r}', \mathbf{r}_s) \cdot \nabla' \hat{G}_0(\mathbf{r}', \mathbf{r}) - \nabla' \Phi(\mathbf{r}', \mathbf{r}_s) \cdot \hat{G}_0(\mathbf{r}', \mathbf{r}) \right) \cdot \hat{n} dS', \tag{9}$$

where $\Phi_0(\mathbf{r}, \mathbf{r}_s) = \begin{pmatrix} \Phi_0^P(\mathbf{r}, \mathbf{r}_s) \\ \Phi_0^S(\mathbf{r}, \mathbf{r}_s) \end{pmatrix}$, $\Phi(\mathbf{r}, \mathbf{r}_s) = \begin{pmatrix} \Phi^P(\mathbf{r}, \mathbf{r}_s) \\ \Phi^S(\mathbf{r}, \mathbf{r}_s) \end{pmatrix}$, and Green's function for the reference

medium in the ($\mathbf{r}$,ω) domain is

$$\begin{aligned}
&\hat{G}_0(\mathbf{r}^{'},\mathbf{r}) \\
=&\begin{pmatrix} \hat{G}_0^P(\mathbf{r}^{'},\mathbf{r}) + \hat{G}_0^{PP}(\mathbf{r}^{'},\mathbf{r}) & \hat{G}_0^{PS}(\mathbf{r}^{'},\mathbf{r}) \\ \hat{G}_0^{SP}(\mathbf{r}^{'},\mathbf{r}) & \hat{G}_0^S(\mathbf{r}^{'},\mathbf{r}) + \hat{G}_0^{SS}(\mathbf{r}^{'},\mathbf{r}) \end{pmatrix} \\
=&\frac{1}{2\pi}\int e^{ik_x(x'-x)}dk_x \\
&\left(\begin{pmatrix} \frac{e^{i\nu_2|z'-z|}}{2i\nu_2} & 0 \\ 0 & \frac{e^{i\eta_2|z'-z|}}{2i\eta_2} \end{pmatrix} + \begin{pmatrix} \acute{P}\grave{P}\frac{e^{i\nu_2 z}e^{i\nu_2 z'}}{2i\nu_2} & \acute{S}\grave{P}\frac{e^{i\eta_2 z}e^{i\nu_2 z'}}{2i\eta_2} \\ \acute{P}\grave{S}\frac{e^{i\nu_2 z}e^{i\eta_2 z'}}{2i\nu_2} & \acute{S}\grave{S}\frac{e^{i\eta_2 z}e^{i\eta_2 z'}}{2i\eta_2} \end{pmatrix}\right),
\end{aligned} \tag{10}$$

where $\acute{P}\grave{P}$, $\acute{P}\grave{S}$, $\acute{S}\grave{P}$, $\acute{S}\grave{S}$ represent the reflection coefficients along the boundary, respectively, and

$$\nu_2 = \begin{cases} \sqrt{k_{\alpha_2}^2 - k_x^2} & if \quad k_x < k_{\alpha_2} \\ i\sqrt{k_x^2 - k_{\alpha_2}^2} & if \quad k_x > k_{\alpha_2} \end{cases} \qquad k_{\alpha_2} = \frac{\omega}{\alpha_2} \quad ,$$

$$\eta_2 = \begin{cases} \sqrt{k_{\beta_2}^2 - k_x^2} & if \quad k_x < k_{\beta_2} \\ i\sqrt{k_x^2 - k_{\beta_2}^2} & if \quad k_x > k_{\beta_2} \end{cases} \qquad k_{\beta_2} = \frac{\omega}{\beta_2} \quad .$$

Since both Φ and $\hat{G}_0$ in the integral are tensors, the symbol $'\cdot'$ represents a tensor product. (The derivation of the Green's function in PS space and Green's theorem reference wavefield separation in PS space are shown in the appendixes B and C.)

If the measurement surface is horizontal, $\hat{n} = (0, -1)$ and represents the outward normal vector directed upward. Equation 9 can be simplified as:

$$\Phi_0(\mathbf{r}, \mathbf{r}_s) = -\int \left(\Phi(\mathbf{r}^{'}, \mathbf{r}_s) \cdot \partial_{z'} \hat{G}_0(\mathbf{r}^{'}, \mathbf{r}) - \partial_{z'}\Phi(\mathbf{r}^{'}, \mathbf{r}_s) \cdot \hat{G}_0(\mathbf{r}^{'}, \mathbf{r})\right) dx'. \tag{11}$$

Using the reciprocity of the Green's function and Fourier transforming over x, the algorithm in the wavenumber-frequency domain for the reference wave prediction in the volume can be obtained:

$$\tilde{\Phi}_0(k_x, z, \mathbf{r}_s) = -\tilde{\Phi}(k_x, z, \mathbf{r}_s) \cdot \partial_{z'} \tilde{\hat{G}}_0^T(k_x, z, z') + \partial_{z'}\tilde{\Phi}(k_x, z, \mathbf{r}_s) \cdot \tilde{\hat{G}}_0^T(k_x, z, z'), \tag{12}$$

where $\tilde{\hat{G}}_0^T$ is the transpose of $\tilde{\hat{G}}_0$.

With the reference wave separated from the total wave, the wavelet $A(\omega)$ can be estimated. A point isotropic source is used here. Since

$$\begin{pmatrix} \Phi_0^P(\mathbf{r}, \mathbf{r}_s, \omega) \\ \Phi_0^S(\mathbf{r}, \mathbf{r}_s, \omega) \end{pmatrix} = \begin{pmatrix} A(\omega)\hat{G}_0^{PP}(\mathbf{r}, \mathbf{r}_s, \omega) \\ A(\omega)\hat{G}_0^{SP}(\mathbf{r}, \mathbf{r}_s, \omega) \end{pmatrix}, \tag{13}$$

$A(\omega)$ can be obtained by either

$$A(\omega) = \frac{\Phi_0^P(\mathbf{r}, \mathbf{r}_s, \omega)}{\hat{G}_0^{PP}(\mathbf{r}, \mathbf{r}_s, \omega)} \quad \text{or} \quad A(\omega) = \frac{\Phi_0^S(\mathbf{r}, \mathbf{r}_s, \omega)}{\hat{G}_0^{SP}(\mathbf{r}, \mathbf{r}_s, \omega)}, \tag{14}$$

where

$$\hat{G}_0^{PP}(\mathbf{r},\mathbf{r}_s,\omega) = \frac{1}{2\pi}\int \grave{P}\grave{P}\frac{e^{-i\nu_1 z_s}e^{i\nu_2 z}}{2iv_1}e^{ik_x(x-x_s)}dk_x,$$
$$\hat{G}_0^{SP}(\mathbf{r},\mathbf{r}_s,\omega) = \frac{1}{2\pi}\int \grave{P}\grave{S}\frac{e^{-i\nu_1 z_s}e^{i\eta_2 z}}{2i\nu_1}e^{ik_x(x-x_s)}dk_x, \tag{15}$$

and $\nu_1 = \begin{cases} \sqrt{k_{\alpha_1}^2 - k_x^2} & if \quad k_x < k_{\alpha_1} \\ i\sqrt{k_x^2 - k_{\alpha_1}^2} & if \quad k_x > k_{\alpha_1} \end{cases} \qquad k_{\alpha_1} = \frac{\omega}{\alpha_1} \quad ,$

and $\grave{P}\grave{P}$, $\grave{P}\grave{S}$ represent the transmission coefficients along the boundary, respectively.

4 Numerical Evaluation

Since the methodology in this paper chooses the reference medium above the earth's surface to be acoustic, either fluid (water) or air can be chosen as the medium above the earth's surface. Those two cases would correspond to ocean bottom and on-shore applications, respectively. In this section, two models are chosen to evaluate Green's theorem wavefield separation algorithm, one is water/elastic, and the other is air/elastic.

4.1 Water/Elastic Model

A water/elastic model is first selected to examine the accuracy of the algorithm. The parameters are listed in Table 1. The water/elastic boundary is at depth 0m, the source's depth is -5m, and the measurement's depth is 0m (on the boundary) but coupled with the lower elastic. The trace interval is 2m.

Layer Number	P Velocity (m/s)	S Velocity (m/s)	Density (kg/m^3)
1	1500	0	1000
2	2250	1200	2000

Table 1: The water/elastic model parameters

Since there is no perturbation from earth in this model, the reference medium is the same as the actual one. Therefore, if the prediction point in the elastic medium is close to depth 0m, the predicted reference wave should be the same as the total wave. This will serve as a criteria later to test the algorithm.

The P wave is produced by source in the water, and the transmitted P and S waves will be collected by the receivers in the elastic medium. The synthetic data are generated by multiplying a wavelet with the analytical forms of Green's function in the frequency domain (equation 13), shown in Fig.3(a) for total P wave and Fig.4(a) for total S wave. The most significant energy of the total wave is surface waves since the source and receivers are very close to the boundary. Here the surface wave is Scholte wave, which are generated at the boundary between the fluid and elastic earth.

The predicted reference P wave (P_0) and S wave (S_0) are listed in Fig.3(b) and Fig.4(b), respectively, and as anticipated are similar to the input data. There are some artifacts with weak energy, which can be seen in Fig.3(b) and Fig.4(b). They are caused by the truncation on wavenumber (k_x) during the calculations to keep the stability of the numerical results. The differences between total waves and predicted reference waves are obtained by subtracting the reference waves from total waves and they are shown as Fig.3(c) and Fig.4(c). It's clearly to find Scholte waves have been effectively removed.

After obtaining the reference wave, the wavelet can be estimated by using equation 14. The results of comparisons between the actual wavelet (the one used to generate the total wavefield and represented by red line in Fig.3(d)) and the wavelet estimated from P_0 at offset 400m (blue line in Fig.3(d)), and the actual wavelet (red line in Fig.4(d)) and the wavelet estimated from S_0 at offset 400m (blue line in Fig.4(d)) further confirm the accuracy of the wavelet estimation algorithm.

4.2 Air/Elastic Model

An air/elastic model is also selected to examine the accuracy of the algorithm. The parameters are listed in Table 2. Same as previous air/water model, the water/elastic boundary is at depth 0m, the source's depth is -5m, the measurement's depth is 0m (on the boundary) but coupled with the lower elastic, and the prediction point is located on the measurement surface, so the predicted reference wave should also be the same as the total wave for this example, without the perturbation existing under the measurement surface.

Layer Number	P Velocity (m/s)	S Velocity (m/s)	Density (kg/m^3)
1	340	0	3
2	2250	1200	2000

Table 2: The air/elastic model parameters

The synthetic input data for total P and total S are similarly generated as in the first case, as shown in Fig.5(a) and Fig.5(d). The predicted reference waves are shown in Fig.5(b) for P_0 and Fig.5(e) for S_0. The subtraction results between total waves and reference waves are shown as Fig.5(c) and Fig.5(f). Similar to the previous example, the surface waves have been effectively removed and they're actually Rayleigh waves which are existing on the boundary between air and elastic earth.

5 Conclusion and Future Plan

From the theoretical derivation and numerical tests in this paper, we understand that it is possible to apply the Green's theorem wavefield separation algorithm on land. For on-shore application, the reference medium consists of two half spaces: one acoustic and the other elastic. This will provide a possible way to remove ground roll, which has the majority of the energy of the reference wave for on-shore acquisition. In order to apply Green's theorem to remove ground roll for practical complicated land acquisition data, a modified reference model and further research are required.

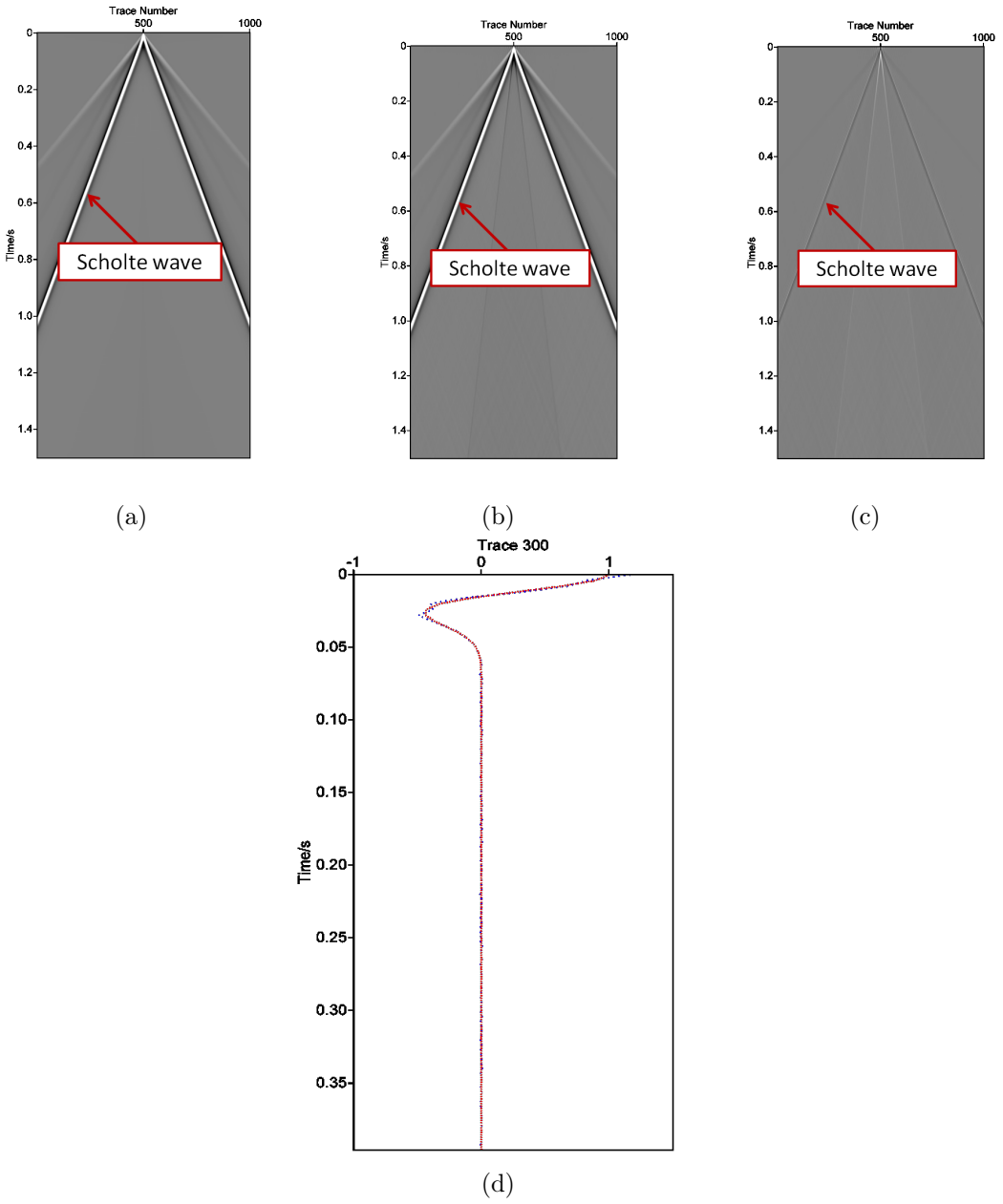

Figure 3: Numerical result for water/elastic model. (a): input total P wave; (b): predicted reference wave P_0 at depth 0m; (c): P-P_0; (d): actual wavelet (red line) and wavelet estimated from P_0 at offset 400m (blue line). Figures in (a), (b) and (c) are in the same scales.

6 Acknowledgements

We are grateful to all M-OSRP sponsors for their encouragement and support in this research.

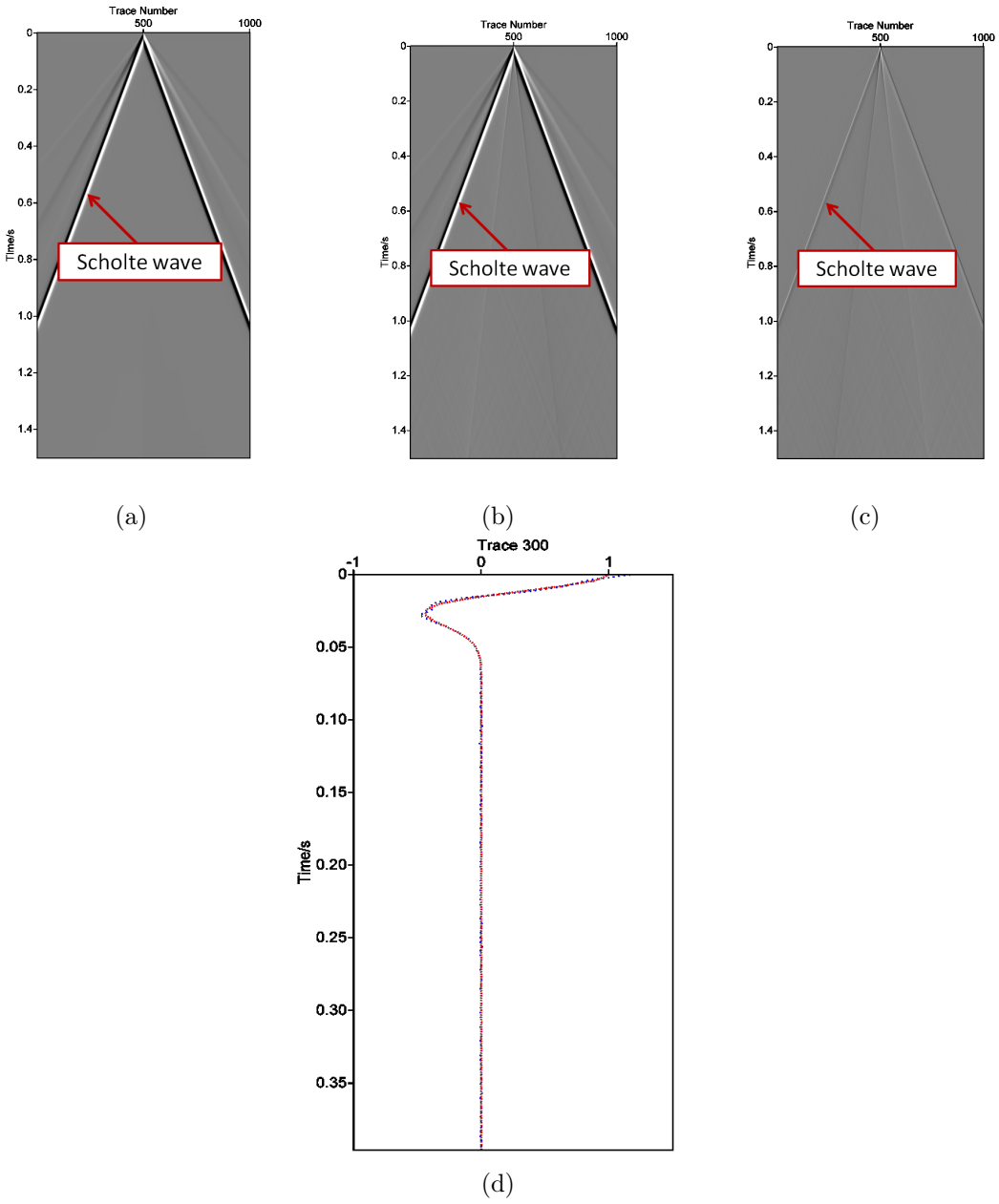

Figure 4: Numerical result for water/elastic model. (a): input total S wave; (b): predicted reference wave S_0 at depth 0m; (c): S-S_0; (d): actual wavelet (red line) and wavelet estimated from S_0 at offset 400m (blue line). Figures in (a), (b) and (c) are in the same scales.

Appendix

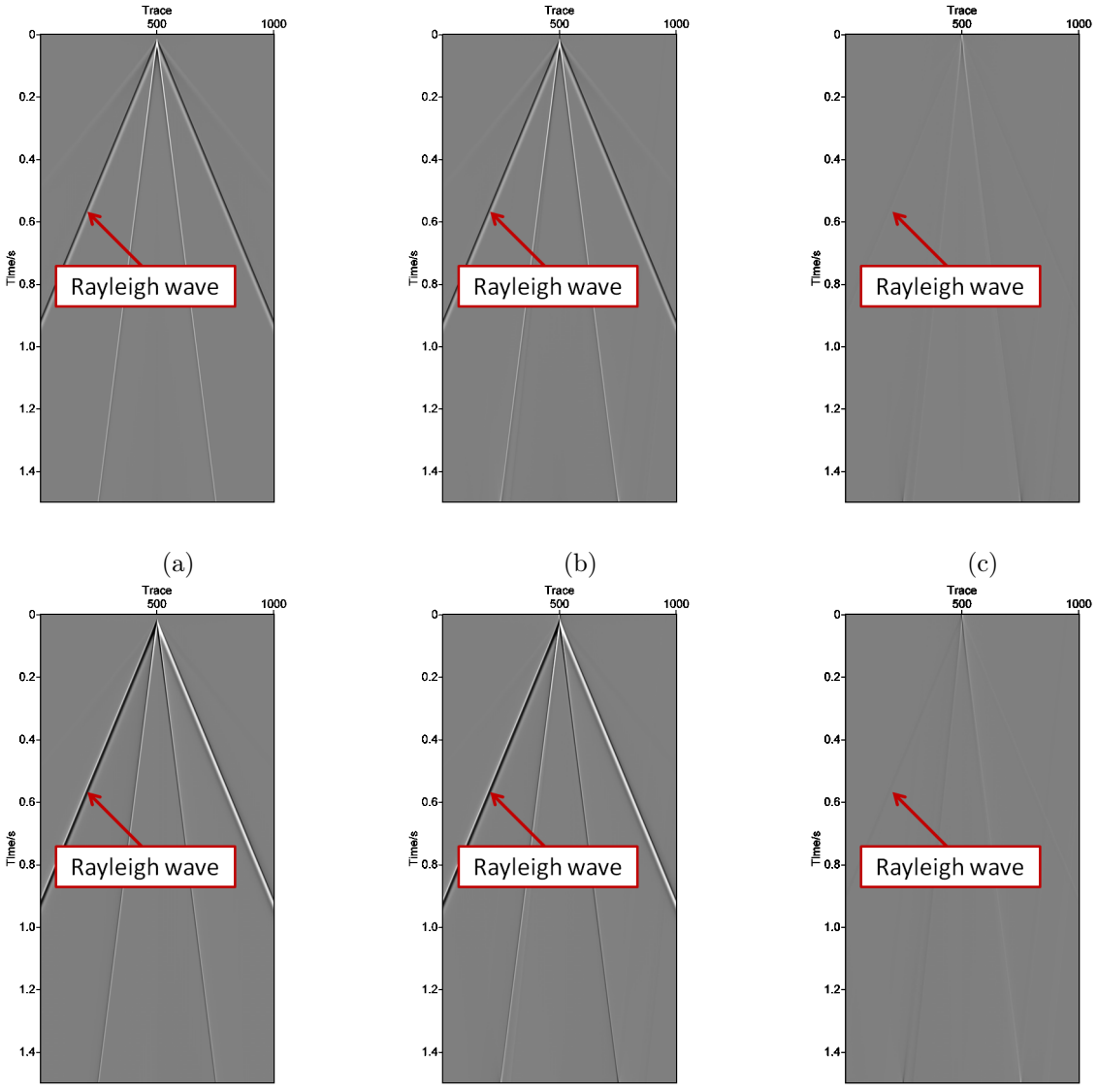

Figure 5: Numerical result for air/elastic model. (a): input total P wave; (b): predicted reference wave P_0; (c): P-P_0; (d): input total S wave; (e): predicted reference wave S_0; (f): S-S_0. All the figures are in the same scales.

A 2D Elastic Wave Equation and Basis Transform

A.1 In Displacement Space

In displacement space, the basic wave equations (Matson (1997), Zhang (2006)) are

$$L\mathbf{u} = \mathbf{f}, \tag{16}$$

$$L_0\mathbf{u}_0 = \mathbf{f}, \tag{17}$$

$$LG = \delta, \tag{18}$$

$$L_0G_0 = \delta, \tag{19}$$

where L and L_0 are the differential operators that describe the wave propagation in the actual medium and the reference medium, respectively, $\mathbf{u}$ is the displacement and $\mathbf{f}$ is source term, and G and G_0 are the corresponding Green's operators for the actual medium and the reference medium, respectively.

In the actual medium, the 2D isotropic elastic wave equation is (Weglein and Stolt (1995))

$$L\mathbf{u} = \left(\rho\omega^2 \begin{pmatrix} 1 & 0 \\ 0 & 1 \end{pmatrix} + \begin{pmatrix} \partial_x\gamma\partial_x + \partial_z\mu\partial_z & \partial_x(\gamma - 2\mu)\partial_z + \partial_z\mu\partial_x \\ \partial_z(\gamma - 2\mu)\partial_x + \partial_x\mu\partial_z & \partial_z\gamma\partial_z + \partial_x\mu\partial_x \end{pmatrix}\right) = \mathbf{f}, \tag{20}$$

where

$\mathbf{u} = \begin{pmatrix} u_x \\ u_z \end{pmatrix}$=displacement,

ρ=density,

γ=bulk modulus ($\gamma \equiv \rho\alpha^2$, where α is P-wave velocity),

μ=shear modulus ($\mu \equiv \rho\beta^2$, where β is S-wave velocity),

and

$\mathbf{f} = \begin{pmatrix} f_x \\ f_z \end{pmatrix}$=source term.

For an isotropic homogeneous medium, $(\rho, \gamma, \mu) = (\rho_0, \gamma_0, \mu_0)$, $(\alpha, \beta) = (\alpha_0, \beta_0)$, and

$$L_0 = \left(\rho_0\omega^2 \begin{pmatrix} 1 & 0 \\ 0 & 1 \end{pmatrix} + \begin{pmatrix} \gamma_0\partial_x^2 + \mu_0\partial_z^2 & (\gamma_0 - \mu_0)\partial_x\partial_z \\ (\gamma_0 - \mu_0)\partial_x\partial_z & \mu_0\partial_x^2 + \gamma_0\partial_z^2 \end{pmatrix}\right). \tag{21}$$

A.2 In PS space

For convenience, we can change the basis from $\mathbf{u} = \begin{pmatrix} u_x \\ u_z \end{pmatrix}$ to $\Phi = \begin{pmatrix} \phi^P \\ \phi^S \end{pmatrix}$.

For homogeneous reference medium, L_0 can be diagonalized in a new basis via transformation (Weglein and Stolt (1995))

$$\hat{L}_0 \equiv \Pi L_0 \Pi^{-1}\Gamma_0^{-1} = \begin{pmatrix} \bigtriangledown^2 + \frac{\omega^2}{\alpha_0^2} & \\ & \bigtriangledown^2 + \frac{\omega^2}{\beta_0^2} \end{pmatrix} = \begin{pmatrix} \hat{L}_0^P & \\ & \hat{L}_0^S \end{pmatrix}, \tag{22}$$

where $\hat{L}_0$ corresponds to L_0 transformed to PS space, $\Pi = \begin{pmatrix} \partial_x & \partial_z \\ -\partial_z & \partial_x \end{pmatrix}$, and $\Gamma_0 = \begin{pmatrix} \gamma_0 & \\ & \mu_0 \end{pmatrix}$.

Then we have

$$\Phi_0 = \begin{pmatrix} \phi^P \\ \phi^S \end{pmatrix} = \Gamma_0 \Pi \mathbf{u}_0 \tag{23}$$

and

$$\mathbf{F} = \begin{pmatrix} F^P \\ F^S \end{pmatrix} = \Pi \mathbf{f}. \tag{24}$$

The wave equation can then be written as

$$\hat{L}_0 \Phi_0 = \begin{pmatrix} \hat{L}_0^P & \\ & \hat{L}_0^S \end{pmatrix} \begin{pmatrix} \phi^P \\ \phi^S \end{pmatrix} = \mathbf{F}. \tag{25}$$

Since $G_0 \equiv L_0^{-1}$, Green's Function in the PS space is

$$\hat{G}_0 \equiv \Gamma_0 \Pi G_0 \Pi^{-1} = \begin{pmatrix} \hat{G}_0^P & \\ & \hat{G}_0^S \end{pmatrix}, \tag{26}$$

and

$$\hat{L}_0 \hat{G}_0 = \delta. \tag{27}$$

For an actual inhomogeneous medium, on the basis of scattering theory, Weglein et al. (2003) give,

$$G = G_0 + G_0 V G, \tag{28}$$

where V is the perturbation satisfying $V = L_0 - L$.

Using the same form to transform the basis of G,

$$\hat{G} = \Gamma_0 \Pi G \Pi^{-1} = \Gamma_0 \Pi (G_0 + G_0 V G) \Pi^{-1} = \hat{G}_0 + \hat{G}_0 \hat{V} \hat{G}, \tag{29}$$

where Green's operator in the PS space is $\hat{G} = \begin{pmatrix} \hat{G}^{PP} & \hat{G}^{PS} \\ \hat{G}^{SP} & \hat{G}^{SS} \end{pmatrix}$ and$\hat{V} = \Pi V \Gamma_0^{-1} \Pi^{-1} = \begin{pmatrix} \hat{V}^{PP} & \hat{V}^{PS} \\ \hat{V}^{SP} & \hat{V}^{SS} \end{pmatrix}$.

The elastic wave equations in PS space are

$$\hat{L} \Phi = \mathbf{F}, \tag{30}$$

$$\hat{L} \hat{G} = \delta. \tag{31}$$

B Green's Function in PS Space with an Air/Elastic Reference Medium

In the air/elastic reference medium ($\hat{L}_0'$), there are three possible sources. From Fig.6, we understand that different wavefields will be generated by sources located in different media. For a P source located in the air, PP reflected wave and PP and SP transmitted waves will be generated; for a P source located in the elastic earth, PP transmitted wave and PP and SP reflected waves will be generated; and for a S source located in the elastic earth, PS transmitted wave and PS and SS reflected waves will be generated. The reflection/transmission coefficients should be calculated in order to find the Green's functions.

The boundary condition should be used to confirm the reflection and transmission coefficients. The normal and shear stresses and vertical displacements should be continuous along the air/elastic boundary. If we assume that the air is medium (1) and the earth is medium (2), we have

$$\begin{aligned} \tau_{zz}^{(1)} &= \tau_{zz}^{(2)}, \\ \tau_{zx}^{(1)} &= \tau_{zx}^{(2)} = 0, \\ u_z^{(1)} &= u_z^{(2)}, \end{aligned} \tag{32}$$

where $\tau_{zz}^{(1)}$ is the normal stress and $\tau_{zx}^{(1)}$ is the shear stress.

On the basis of the constitutive relations that

$$\begin{aligned} \tau_{zz} &= \gamma \frac{\partial u_z}{\partial z} + (\gamma - 2\mu)\frac{\partial u_x}{\partial x}, \\ \tau_{zx} &= \mu(\frac{\partial u_z}{\partial x} + \frac{\partial u_x}{\partial z}), \end{aligned}$$

and on the relation between potential and displacement that

$$\Phi = \Gamma \Pi \mathbf{u},$$

we can obtain

$$\begin{cases} \tau_{zz}^{(1)} = \phi_1^P, \\ \tau_{zz}^{(2)} = \frac{1}{\rho_2 \omega^2}[(\gamma_2 - 2\mu_2)k_{\alpha_2}^2 \phi_2^P - 2\mu_2(\frac{\partial^2 \phi_2^P}{\partial z^2} + \frac{\partial^2 \phi_2^S}{\partial x \partial z})], \\ \tau_{zx}^{(2)} = -\frac{1}{\rho_2 \omega^2}[2\frac{\partial^2 \phi_2^P}{\partial x \partial z} + (\frac{\partial^2 \phi_2^S}{\partial x^2} - \frac{\partial^2 \phi_2^S}{\partial z^2})], \\ u_z^{(1)} = -\frac{1}{\rho_1 \omega^2}\frac{\partial \phi_1^P}{\partial z}, \\ u_z^{(2)} = -\frac{1}{\rho_2 \omega^2}(\frac{\partial \phi_2^P}{\partial z} + \frac{\partial \phi_2^S}{\partial x}). \end{cases} \tag{33}$$

Combining equation 32 and equation 33, the reflection and transmission coefficients can be confirmed.

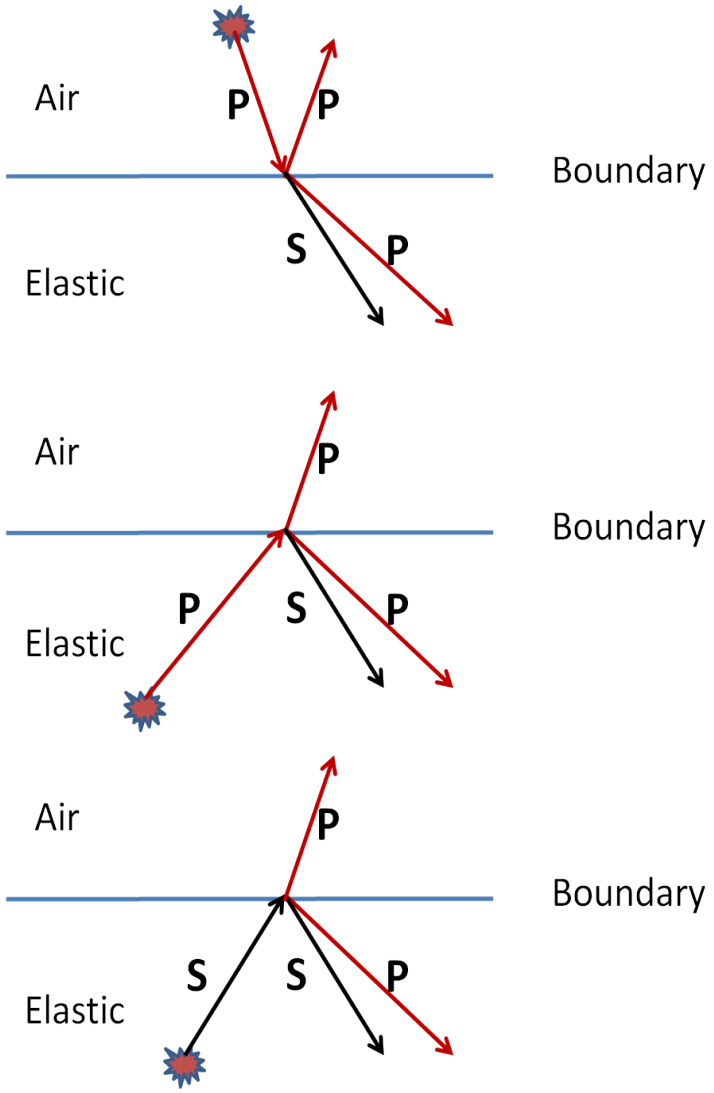

Figure 6: Three types of source located in different media and their corresponding waves. (a): a P source located in the air; (b): a P source located in the earth; (c): a S source located in the earth.

From Fig.6, there should be three Green's functions. Here we assume that the boundary is located at depth 0 and the source and receiver locations are given by $\mathbf{r}_s(x_s, z_s)$ and $\mathbf{r}_(x, z)$, respectively.

For the first situation (Fig.6(a)), the incident P-wave ($z < 0$) can be represented by

$$(\nabla^2 + \frac{\omega^2}{\alpha_1^2})\hat{G}_0^P(x, z) = \delta(x - x_s)\delta(z - z_s), \tag{34}$$

$$\hat{G}_0^P(x, z, \omega) = \frac{1}{2\pi}\int \frac{e^{i\nu_1|z-z_s|}}{2i\nu_1} e^{ik_x(x-x_s)} dk_x, \tag{35}$$

where the vertical wavenumber in the air is

$$\nu_1 = \begin{cases} \sqrt{k_{\alpha_1}^2 - k_x^2} & if \quad k_x < k_{\alpha_1} \\ i\sqrt{k_x^2 - k_{\alpha_1}^2} & if \quad k_x > k_{\alpha_1} \end{cases} \qquad k_{\alpha_1} = \frac{\omega}{\alpha_1}.$$

The reflected and transmitted waves can be represented as

$$\begin{cases} \hat{G}_0^{PP(1)}(x,z,\omega) = \frac{1}{2\pi}\int \grave{P}\acute{P}\frac{e^{-i\nu_1 z_s}e^{-i\nu_1 z}}{2i\nu_1}e^{ik_x(x-x_s)}dk_x, \\ \hat{G}_0^{PP(2)}(x,z,\omega) = \frac{1}{2\pi}\int \grave{P}\grave{P}\frac{e^{-i\nu_1 z_s}e^{i\nu_2 z}}{2i\nu_1}e^{ik_x(x-x_s)}dk_x, \\ \hat{G}_0^{SP(2)}(x,z,\omega) = \frac{1}{2\pi}\int \grave{P}\grave{S}\frac{e^{-i\nu_1 z_s}e^{i\eta_2 z}}{2i\nu_1}e^{ik_x(x-x_s)}dk_x, \end{cases} \tag{36}$$

where the vertical wavenumbers in the elastic medium are

$$\nu_2 = \begin{cases} \sqrt{k_{\alpha_2}^2 - k_x^2} & if \quad k_x < k_{\alpha_2} \\ i\sqrt{k_x^2 - k_{\alpha_2}^2} & if \quad k_x > k_{\alpha_2} \end{cases} \qquad k_{\alpha_2} = \frac{\omega}{\alpha_2},$$

$$\eta_2 = \begin{cases} \sqrt{k_{\beta_2}^2 - k_x^2} & if \quad k_x < k_{\beta_2} \\ i\sqrt{k_x^2 - k_{\beta_2}^2} & if \quad k_x > k_{\beta_2} \end{cases} \qquad k_{\beta_2} = \frac{\omega}{\beta_2}.$$

When z is close to 0 on both sides, by using the boundary condition, we can confirm the coefficients are

$$\begin{cases} \grave{P}\acute{P} = \frac{\nu_1 D - \nu_2 n k_{\beta_2}^4}{D_1}, \\ \grave{P}\grave{P} = \frac{-2\nu_1 k_{\beta_2}^2 (2k_x^2 - k_{\beta_2}^2)}{D_1}, \\ \grave{P}\grave{S} = \frac{4k_x \nu_1 \nu_2 k_{\beta_2}^2}{D_1}, \end{cases}$$

where

$$\begin{cases} n = \rho_1/\rho_2, \\ D = (2k_x^2 - k_{\beta_2}^2)^2 + 4k_x^2 \nu_2 \eta_2, \\ D_1 = \nu_1 D + \nu_2 n k_{\beta_2}^4. \end{cases}$$

For the second situation (Fig.6(b)), the incident P-wave ($z > 0$) can be represented by

$$(\nabla^2 + \frac{\omega^2}{\alpha_2^2})\hat{G}_0^P(x,z) = \delta(x - x_s)\delta(z - z_s), \tag{37}$$

$$\hat{G}_0^P(x,z,\omega) = \frac{1}{2\pi}\int \frac{e^{i\nu_2|z-z_s|}}{2i\nu_2}e^{ik_x(x-x_s)}dk_x. \tag{38}$$

The reflected and transmitted waves can be represented as

$$\begin{cases} \hat{G}_0^{PP(1)}(x,z,\omega) = \frac{1}{2\pi}\int \acute{P}\acute{P}\frac{e^{i\nu_2 z_s}e^{-i\nu_1 z}}{2i\nu_2}e^{ik_x(x-x_s)}dk_x, \\ \hat{G}_0^{PP(2)}(x,z,\omega) = \frac{1}{2\pi}\int \acute{P}\grave{P}\frac{e^{i\nu_2 z_s}e^{i\nu_2 z}}{2i\nu_2}e^{ik_x(x-x_s)}dk_x, \\ \hat{G}_0^{SP(2)}(x,z,\omega) = \frac{1}{2\pi}\int \acute{P}\grave{S}\frac{e^{i\nu_2 z_s}e^{i\eta_2 z}}{2i\nu_2}e^{ik_x(x-x_s)}dk_x, \end{cases} \tag{39}$$

$$\text{where} \begin{cases} \acute{P}\acute{P} = \frac{-2n\nu_2 k_{\beta_2}^2 (2k_x^2 - k_{\beta_2}^2)}{D_1}, \\ \acute{P}\grave{P} = \frac{-\nu_1((2k_x^2 - k_{\beta_2}^2)^2 - 4k_x^2\nu_2\eta_2) + \nu_2 n k_{\beta_2}^4}{D_1}, \\ \acute{P}\grave{S} = \frac{4k_x\nu_1\nu_2(2k_x^2 - k_{\beta_2}^2)}{D_1}. \end{cases}$$

For the third situation (Fig.6(c)), the incident S-wave ($z > 0$) can be represented by

$$(\nabla^2 + \frac{\omega^2}{\beta_2^2})\hat{G}_0^S(x,z) = \delta(x - x_s)\delta(z - z_s), \tag{40}$$

$$\hat{G}_0^S(x,z,\omega) = \frac{1}{2\pi}\int \frac{e^{i\eta_2|z-z_s|}}{2i\eta_2} e^{ik_x(x-x_s)} dk_x. \tag{41}$$

The reflected and transmitted waves can be represented as

$$\begin{cases} \hat{G}_0^{PS(1)}(x,z,\omega) = \frac{1}{2\pi}\int \acute{S}\acute{P}\frac{e^{i\eta_2 z_s} e^{-i\nu_1 z}}{2i\eta_2} e^{ik_x(x-x_s)} dk_x, \\ \hat{G}_0^{PS(2)}(x,z,\omega) = \frac{1}{2\pi}\int \acute{S}\grave{P}\frac{e^{i\eta_2 z_s} e^{i\nu_2 z}}{2i\eta_2} e^{ik_x(x-x_s)} dk_x, \\ \hat{G}_0^{SS(2)}(x,z,\omega) = \frac{1}{2\pi}\int \acute{S}\grave{S}\frac{e^{i\eta_2 z_s} e^{i\eta_2 z}}{2i\eta_2} e^{ik_x(x-x_s)} dk_x, \end{cases} \tag{42}$$

$$\text{where} \begin{cases} \acute{S}\acute{P} = \frac{-4nk_{\beta_2}^2 k_x\nu_2\eta_2}{D_1}, \\ \acute{S}\grave{P} = \frac{4k_x\nu_1\eta_2(2k_x^2 - k_{\beta_2}^2)}{D_1}, \\ \acute{S}\grave{S} = \frac{-\nu_1((2k_x^2 - k_{\beta_2}^2)^2 - 4k_x^2\nu_2\eta_2) - \nu_2 n k_{\beta_2}^4}{D_1}. \end{cases}$$

If both the source and the receiver are located below the boundary, for equation

$$\hat{L}_0'\hat{G}_0 = \delta, \tag{43}$$

$$\begin{aligned} &\hat{G}_0(x,z,x_s,z_s,\omega) \\ =&\begin{pmatrix} \hat{G}_0^P & \\ & \hat{G}_0^S \end{pmatrix} + \begin{pmatrix} \hat{G}_0^{PP} & \hat{G}_0^{PS} \\ \hat{G}_0^{SP} & \hat{G}_0^{SS} \end{pmatrix} \\ =&\frac{1}{2\pi}\int e^{ik_x(x-x_s)} \left(\begin{pmatrix} \frac{e^{i\nu_2|z-z_s|}}{2i\nu_2} & 0 \\ 0 & \frac{e^{i\eta_2|z-z_s|}}{2i\eta_2} \end{pmatrix} + \begin{pmatrix} \acute{P}\grave{P}\frac{e^{i\nu_2 z_s} e^{i\nu_2 z}}{2i\nu_2} & \acute{S}\grave{P}\frac{e^{i\eta_2 z_s} e^{i\nu_2 z}}{2i\eta_2} \\ \acute{P}\grave{S}\frac{e^{i\nu_2 z_s} e^{i\eta_2 z}}{2i\nu_2} & \acute{S}\grave{S}\frac{e^{i\eta_2 z_s} e^{i\eta_2 z}}{2i\eta_2} \end{pmatrix} \right) dk_x. \end{aligned} \tag{44}$$

C Derivation of Green's Theorem Reference Wavefield Prediction in PS Space

Let us define $\hat{L}_0, \hat{L}_0', \hat{L}$ as the differential operators, in turn describing the whole-space homogeneous elastic medium, the air/elastic reference medium and the actual medium; and let $\hat{V}_{air}, \hat{V}_{earth}$ represent the perturbations of air and earth relative to the whole-space homogeneous elastic condition,

respectively. Then we have

$$\begin{cases} \hat{L}_0^{'} = \hat{L}_0 - \hat{V}_{air}, \\ \hat{L}\Phi = (\hat{L}_0 - \hat{V}_{air} - \hat{V}_{earth})\Phi = \mathbf{F}, \\ \hat{L}_0^{'}\hat{G}_0 = \delta. \end{cases} \tag{45}$$

If it is written explicitly, we have

$$\begin{pmatrix} \nabla'^2 + \frac{\omega^2}{\alpha_2^2} & \\ & \nabla'^2 + \frac{\omega^2}{\beta_2^2} \end{pmatrix} \begin{pmatrix} \phi^P(\mathbf{r}^{'}, \mathbf{r}_s) \\ \phi^S(\mathbf{r}^{'}, \mathbf{r}_s) \end{pmatrix} = \begin{pmatrix} A(\omega)\delta(\mathbf{r}^{'} - \mathbf{r}_s) \\ 0 \end{pmatrix} + (\hat{V}_{air} + \hat{V}_{earth}) \begin{pmatrix} \phi^P(\mathbf{r}^{'}, \mathbf{r}_s) \\ \phi^S(\mathbf{r}^{'}, \mathbf{r}_s) \end{pmatrix}, \tag{46}$$

$$\begin{aligned} &\begin{pmatrix} \nabla'^2 + \frac{\omega^2}{\alpha_2^2} & \\ & \nabla'^2 + \frac{\omega^2}{\beta_2^2} \end{pmatrix} \begin{pmatrix} \hat{G}_0^P(\mathbf{r}^{'}, \mathbf{r}) + \hat{G}_0^{PP}(\mathbf{r}^{'}, \mathbf{r}) & \hat{G}_0^{PS}(\mathbf{r}^{'}, \mathbf{r}) \\ \hat{G}_0^{SP}(\mathbf{r}^{'}, \mathbf{r}) & \hat{G}_0^S(\mathbf{r}^{'}, \mathbf{r}) + \hat{G}_0^{SS}(\mathbf{r}^{'}, \mathbf{r}) \end{pmatrix} \\ =&\begin{pmatrix} \delta(\mathbf{r}^{'} - \mathbf{r}) & \\ & \delta(\mathbf{r}^{'} - \mathbf{r}) \end{pmatrix} + \hat{V}_{air} \begin{pmatrix} \hat{G}_0^P(\mathbf{r}^{'}, \mathbf{r}) + \hat{G}_0^{PP}(\mathbf{r}^{'}, \mathbf{r}) & \hat{G}_0^{PS}(\mathbf{r}^{'}, \mathbf{r}) \\ \hat{G}_0^{SP}(\mathbf{r}^{'}, \mathbf{r}) & \hat{G}_0^S(\mathbf{r}^{'}, \mathbf{r}) + \hat{G}_0^{SS}(\mathbf{r}^{'}, \mathbf{r}) \end{pmatrix}. \end{aligned} \tag{47}$$

If we choose the volume as is shown in Fig.2, by using Green's Second Identity, we have

$$\begin{aligned} &\int_V \left(\Phi(\mathbf{r}^{'}, \mathbf{r}_s) \cdot \nabla'^2 \hat{G}_0(\mathbf{r}^{'}, \mathbf{r}) - \nabla'^2 \Phi(\mathbf{r}^{'}, \mathbf{r}_s) \cdot \hat{G}_0(\mathbf{r}^{'}, \mathbf{r}) \right) dV \\ =&\int_V \left(\begin{array}{l} \Phi(\mathbf{r}^{'}, \mathbf{r}_s) \cdot \begin{pmatrix} \delta(\mathbf{r}^{'} - \mathbf{r}) & \\ & \delta(\mathbf{r}^{'} - \mathbf{r}) \end{pmatrix} + \Phi(\mathbf{r}^{'}, \mathbf{r}_s) \cdot \hat{V}_{air}(\mathbf{r}^{'}) \hat{G}_0(\mathbf{r}^{'}, \mathbf{r}) \\ + \Phi(\mathbf{r}^{'}, \mathbf{r}_s) \cdot \begin{pmatrix} \frac{\omega^2}{\alpha_2^2} & \\ & \frac{\omega^2}{\beta_2^2} \end{pmatrix} \hat{G}_0(\mathbf{r}^{'}, \mathbf{r}) \\ - \left(\begin{pmatrix} A(\omega)\delta(\mathbf{r}^{'} - \mathbf{r}_s) \\ 0 \end{pmatrix} \cdot \hat{G}_0(\mathbf{r}^{'}, \mathbf{r}) + \hat{V}_{air}(\mathbf{r}^{'}) \Phi(\mathbf{r}^{'}, \mathbf{r}_s) \cdot \hat{G}_0(\mathbf{r}^{'}, \mathbf{r}) \right. \\ \left. + \hat{V}_{earth}(\mathbf{r}^{'}) \Phi(\mathbf{r}^{'}, \mathbf{r}_s) \cdot \hat{G}_0(\mathbf{r}^{'}, \mathbf{r}) + \begin{pmatrix} \frac{\omega^2}{\alpha_2^2} & \\ & \frac{\omega^2}{\beta_2^2} \end{pmatrix} \Phi(\mathbf{r}^{'}, \mathbf{r}_s) \cdot \hat{G}_0(\mathbf{r}^{'}, \mathbf{r}) \right) \end{array} \right) dV \\ =&\Phi(\mathbf{r}, \mathbf{r}_s) - \int_V \hat{V}_{earth}(\mathbf{r}^{'}) \Phi(\mathbf{r}^{'}, \mathbf{r}_s) \cdot \hat{G}_0(\mathbf{r}^{'}, \mathbf{r}) dV \\ =&\Phi(\mathbf{r}, \mathbf{r}_s) - \Phi_S(\mathbf{r}, \mathbf{r}_s) \\ =&\oint \left(\Phi(\mathbf{r}^{'}, \mathbf{r}_s) \cdot \nabla^{'} \hat{G}_0(\mathbf{r}^{'}, \mathbf{r}) - \nabla^{'} \Phi(\mathbf{r}^{'}, \mathbf{r}_s) \cdot \hat{G}_0(\mathbf{r}^{'}, \mathbf{r}) \right) \cdot \hat{n} dS', \end{aligned} \tag{48}$$

where $\Phi_S(\mathbf{r}, \mathbf{r}_s)$ represents the scattering wavefield caused by the earth perturbation.

Finally, we can obtain the reference wavefield as

$$\begin{aligned}\Phi_0(\mathbf{r},\mathbf{r}_s) &= \oint \Big(\Phi(\mathbf{r}',\mathbf{r}_s)\cdot\nabla'\hat{G}_0(\mathbf{r}',\mathbf{r}) - \nabla'\Phi(\mathbf{r}',\mathbf{r}_s)\cdot\hat{G}_0(\mathbf{r}',\mathbf{r})\Big)\cdot\hat{n}dS' \\ &\quad \text{or, if the measurement surface is horizontal,} \\ &= -\int\left(\Phi(\mathbf{r}',\mathbf{r}_s)\cdot\begin{pmatrix}\partial_{z'} & \\ & \partial_{z'}\end{pmatrix}\hat{G}_0(\mathbf{r}',\mathbf{r}) - \begin{pmatrix}\partial_{z'} & \\ & \partial_{z'}\end{pmatrix}\Phi(\mathbf{r}',\mathbf{r}_s)\cdot\hat{G}_0(\mathbf{r}',\mathbf{r})\right)dx'.\end{aligned} \tag{49}$$

The reference wavefield in the $(\mathbf{r},\omega)$ domain can be obtained as

$$\begin{aligned}&\begin{pmatrix}\phi_0^P(\mathbf{r},\mathbf{r}_s)\\ \phi_0^S(\mathbf{r},\mathbf{r}_s)\end{pmatrix} \\ &= -\int\left(\begin{array}{l}\begin{pmatrix}\partial_{z'} & \\ & \partial_{z'}\end{pmatrix}\begin{pmatrix}\hat{G}_0^P(\mathbf{r}',\mathbf{r})+\hat{G}_0^{PP}(\mathbf{r}',\mathbf{r}) & \hat{G}_0^{SP}(\mathbf{r}',\mathbf{r}) \\ \hat{G}_0^{PS}(\mathbf{r}',\mathbf{r}) & \hat{G}_0^{S}(\mathbf{r}',\mathbf{r})+\hat{G}_0^{SS}(\mathbf{r}',\mathbf{r})\end{pmatrix}\begin{pmatrix}\phi^P(\mathbf{r},\mathbf{r}_s)\\ \phi^S(\mathbf{r},\mathbf{r}_s)\end{pmatrix} \\ -\begin{pmatrix}\hat{G}_0^P(\mathbf{r}',\mathbf{r})+\hat{G}_0^{PP}(\mathbf{r}',\mathbf{r}) & \hat{G}_0^{SP}(\mathbf{r}',\mathbf{r}) \\ \hat{G}_0^{PS}(\mathbf{r}',\mathbf{r}) & \hat{G}_0^{S}(\mathbf{r}',\mathbf{r})+\hat{G}_0^{SS}(\mathbf{r}',\mathbf{r})\end{pmatrix}\begin{pmatrix}\partial_{z'} & \\ & \partial_{z'}\end{pmatrix}\begin{pmatrix}\phi^P(\mathbf{r},\mathbf{r}_s)\\ \phi^S(\mathbf{r},\mathbf{r}_s)\end{pmatrix}\end{array}\right)dx' \\ &\quad \text{and using the reciprocity of the Green's function} \\ &= -\int\left(\begin{array}{l}\begin{pmatrix}\partial_{z'} & \\ & \partial_{z'}\end{pmatrix}\begin{pmatrix}\hat{G}_0^P(\mathbf{r},\mathbf{r}')+\hat{G}_0^{PP}(\mathbf{r},\mathbf{r}') & \hat{G}_0^{PS}(\mathbf{r},\mathbf{r}') \\ \hat{G}_0^{SP}(\mathbf{r}',\mathbf{r}) & \hat{G}_0^{S}(\mathbf{r},\mathbf{r}')+\hat{G}_0^{SS}(\mathbf{r},\mathbf{r}')\end{pmatrix}\begin{pmatrix}\phi^P(\mathbf{r},\mathbf{r}_s)\\ \phi^S(\mathbf{r},\mathbf{r}_s)\end{pmatrix} \\ -\begin{pmatrix}\hat{G}_0^P(\mathbf{r},\mathbf{r}')+\hat{G}_0^{PP}(\mathbf{r},\mathbf{r}') & \hat{G}_0^{PS}(\mathbf{r},\mathbf{r}') \\ \hat{G}_0^{SP}(\mathbf{r},\mathbf{r}') & \hat{G}_0^{S}(\mathbf{r},\mathbf{r}')+\hat{G}_0^{SS}(\mathbf{r},\mathbf{r}')\end{pmatrix}\begin{pmatrix}\partial_{z'} & \\ & \partial_{z'}\end{pmatrix}\begin{pmatrix}\phi^P(\mathbf{r},\mathbf{r}_s)\\ \phi^S(\mathbf{r},\mathbf{r}_s)\end{pmatrix}\end{array}\right)dx'.\end{aligned} \tag{50}$$

Fourier transforming over x, we can obtain the algorithm for predicting the reference wavefield in the (k_x,ω) domain:

$$\begin{aligned}&\begin{pmatrix}\tilde{\phi}_0^P(k_x,z,\mathbf{r}_s)\\ \tilde{\phi}_0^S(k_x,z,\mathbf{r}_s)\end{pmatrix} \\ &= -\left(\begin{pmatrix}\partial_{z'} & \\ & \partial_{z'}\end{pmatrix}\begin{pmatrix}\tilde{\hat{G}}_0^P(k_x,z,\mathbf{r}')+\tilde{\hat{G}}_0^{PP}(k_x,z,\mathbf{r}') & \tilde{\hat{G}}_0^{PS}(k_x,z,\mathbf{r}') \\ \tilde{\hat{G}}_0^{SP}(k_x,z,\mathbf{r}') & \tilde{\hat{G}}_0^{SS}(k_x,z,\mathbf{r}')+\tilde{\hat{G}}_0^{SS}(k_x,z,\mathbf{r}')\end{pmatrix}\right)\begin{pmatrix}\tilde{\phi}^P(k_x,z,\mathbf{r}_s)\\ \tilde{\phi}^S(k_x,z,\mathbf{r}_s)\end{pmatrix} \\ &\quad + \begin{pmatrix}\tilde{\hat{G}}_0^P(k_x,z,\mathbf{r}')+\tilde{\hat{G}}_0^{PP}(k_x,z,\mathbf{r}') & \tilde{\hat{G}}_0^{PS}(k_x,z,\mathbf{r}') \\ \tilde{\hat{G}}_0^{SP}(k_x,z,\mathbf{r}') & \tilde{\hat{G}}_0^{SS}(k_x,z,\mathbf{r}')+\tilde{\hat{G}}_0^{SS}(k_x,z,\mathbf{r}')\end{pmatrix}\left(\begin{pmatrix}\partial_{z'} & \\ & \partial_{z'}\end{pmatrix}\begin{pmatrix}\tilde{\phi}^P(k_x,z,\mathbf{r}_s)\\ \tilde{\phi}^S(k_x,z,\mathbf{r}_s)\end{pmatrix}\right).\end{aligned} \tag{51}$$

References

Jiang, T., P. Terenghi, and A. B. Weglein. "Wavelet estimation and wavefield reconstruction in elastic media, without a subsurface model." *Mission-Oriented Seismic Research Program (M-OSRP) Annual Report*. 2013.

Matson, K. H. *An inverse-scattering series method for attenuating elastic multiples from multi-component land and ocean bottom seismic data.* PhD thesis, University of British Columbia, 1997.

Mayhan, J. D., P. Terenghi, A. B. Weglein, and C. Nizar. "Green's theorem derived methods for preprocessing seismic data when the pressure P and its normal derivative are measured." *SEG Technical Program Expanded Abstracts. .* Soc. Expl. Geophys., 2012. 2722–2726.

Mayhan, J. D. and A. B. Weglein. "First application of Green's theorem-derived source and receiver deghosting on deep-water Gulf of Mexico synthetic (SEAM) and field data.". Volume 78 . 2013. WA77–WA89.

Tang, L., J. D. Mayhan, J. Yang, and A. B. Weglein. "Using Green's theorem to satisfy data requirements of multiple removal methods: The impact of acquisition design." *SEG Technical Program Expanded Abstracts. .* Soc. Expl. Geophys., 2013. 4392–4395.

Tang, L. and A. B. Weglein. "Predicting reference medium properties from invariances in Green's theorem reference wave prediction: towards an on-shore near surface medium and reference wave prediction." *SEG Technical Program Expanded Abstracts. .* Soc. Expl. Geophys., 2014. TBD.

Weglein, A. B. "The multiple attenuation toolbox: Progress, challenges and open issues." *SEG Technical Program Expanded Abstracts. .* Soc. Expl. Geophys., 2013. 4493–4499.

Weglein, A. B., F. V. Araújo, P. M. Carvalho, R. H. Stolt, K. H. Matson, R. T. Coates, D. Corrigan, D. J. Foster, S. A. Shaw, and H. Zhang. "Inverse Scattering Series and Seismic Exploration." *Inverse Problems* (2003): R27–R83.

Weglein, A. B. and R. H. Stolt. "I. The wave physics of downward continuation, wavelet estimation and volume and surface scattering. II. Approaches to linear and nonlinear migration inversion." *Mathematical Frontiers in Reflection Seismology: SEG/SIAM publication* (1995).

Weglein, Arthur B. and Bruce G. Secrest. "Wavelet estimation for a multidimensional acoustic earth model." *Geophysics* 55 (July 1990): 902–913.

Weglein, Arthur B., S. .A. Shaw, K. H. Matson, J. L. Sheiman, R. H. Solt, T. H. Tan, A. Osen, G. P. Correa, K. A. Innanen, Z. Guo, and J. Zhang. "New approaches to deghosting towed-streamer and ocean-bottem pressure measurements." *72nd Annual International Meeting, SEG, Expanded Abstracts* (2002): 1016–1019.

Yang, J., J. D. Mayhan, L. Tang, and A. B. Weglein. "Accommodating the source (and receiver) array in free-surface multiple elimination algorithm: Impact on interfering or proximal primaries and multiples." *SEG Technical Program Expanded Abstracts. .* Soc. Expl. Geophys., 2013. 4184–4189.

Zhang, H. *Direct non-linear acoustic and elastic inversion: Towards fundamentally new comprehensive and realistic target identification.* PhD thesis, University of Houston, 2006.

Zhang, J. *Wave theory based data preparation for inverse scattering multiple removal, depth imaging and parameter estimation: analysis and numerical tests of Green's theorem deghosting theory*. PhD thesis, University of Houston, 2007.

Incorporating the source wavelet and radiation pattern into the ISS internal multiple attenuation algorithm: theory and examples

Jinlong Yang and Arthur B. Weglein

May 21, 2014

Abstract

The ISS internal multiple attenuation algorithm is modified and improved in order to enhance the fidelity of the amplitude and phase predictions of the internal multiple, by incorporating the source wavelet and radiation pattern. The modified ISS internal multiple attenuation algorithm is fully data-driven to predict all first-order internal multiples for all horizons at once, without requiring any subsurface information. In synthetic data tests, for data generated by a point source with a wavelet, the amplitudes and shapes of the predicted internal multiples are significantly improved by incorporating the deconvolution of the source wavelet into the ISS internal multiple attenuation algorithm. For data generated by a general source with a radiation pattern, the prediction is further improved by incorporating the source wavelet and radiation pattern. Therefore, the modified ISS internal multiple attenuation algorithm produces more accurate results when the data are generated by a frequency and angle dependent source.

1 Introduction

In seismic exploration, seismic reflection events are classified as primary or multiple, depending on whether the energy arriving at the receiver has experienced one or more upward reflections, respectively. Depending on the location of the downward reflections, multiples are divided into free-surface multiples and internal multiples. Free-surface multiples are multiples that have experienced at least one downward reflection at the free surface (a free surface is either an air-water surface or an air-land surface). Multiples that have experienced all their downward reflections below the free surface are called internal multiples. Methods for seismic imaging and parameter estimation (inversion) assume that the data contain only primaries. Multiples are considered to be noise because they can interfere with primaries and/or be misinterpreted as primaries. Hence, multiple removal is a prerequisite to seismic imaging and inversion.

In this report, we will focus on internal multiple attenuation and will analyze and test the impact of incorporating the source wavelet and radiation pattern on internal multiple prediction. The ISS internal multiple attenuation algorithm was first proposed by Araújo et al. (1994) and Weglein et al.

(1997). It is a fully data-driven and model-type independent algorithm (Weglein et al., 2003), and it predicts the correct traveltimes and approximate amplitudes of all the internal multiples at all depths at once. Matson (1997) extended the theory for land and OBC applications (Matson and Weglein, 1996) and presented the first towed-streamer field-data example using the $2D$ version of the algorithm (Matson et al., 1999). Ramírez and Weglein (2005) discussed how to extend the ISS internal multiple attenuation algorithm from attenuator toward eliminator of multiples. Herrera and Weglein (2013) developed the 1-D ISS internal multiple elimination algorithm for internal multiple generated by a single shallowest reflector and Zou and Weglein (2013) further derived a general form of the ISS internal multiple elimination algorithm. Other implementations and improvements have also been achieved by Hsu et al. (2011), Terenghi et al. (2011), Weglein et al. (2011), and Luo et al. (2011). Ma et al. (2012) and Liang et al. (2012) discussed how to remove spurious events.

The ISS internal multiple attenuation algorithm has certain data requirements: (1) removal of the reference wavefield, (2) an estimation of the source wavelet and radiation pattern, (3) source and receiver deghosting, and (4) removal of the free-surface multiples. The first three requirements can be obtained by Green's theorem methods (Zhang and Weglein, 2005; Mayhan et al., 2012; Tang et al., 2013) and the free-surface multiples can be removed by the ISS free-surface multiple elimination algorithm (Carvalho, 1992; Weglein et al., 2003; Yang et al., 2013). Green's theorem methods and the ISS free-surface multiple elimination algorithm are consistent with the ISS internal multiple attenuation algorithm, since all are multidimensional wave-theoretic preprocessing methods and do not require subsurface information.

The ISS internal multiple attenuation algorithm (Araújo, 1994; Weglein et al., 1997) assumes that the input data are spike wave. In other words, the input data have been deconvolved by a source wavelet. If the input data are generated by a source wavelet instead of by a spike wave, the predicted internal multiple has convolved at least three source wavelets. Hence, the source wavelet has a significant effect on the amplitude and shape of the predicted internal multiple. In this report, to improve the amplitude and the shape of a predicted internal multiple, the ISS internal multiple attenuation algorithm is extended to accommodate a source wavelet.

In addition, the ISS internal multiple attenuation algorithm assumes an isotropic point source, i.e., it assumes that the source has no variation of amplitude or phase with take-off angle. A large marine air-gun array will exhibit directivity and produce variations of the source signature (Loveridge et al., 1984). In on-shore exploration, even if there is no source array, the source can have radiation pattern or directivity. That directivity has significant effects on multiple removal or attenuation and AVO analysis. In seismic data processing, it is important that we characterize the source array's effect on any seismic processing methods. Therefore, to further improve the effectiveness of the ISS internal multiple attenuation algorithm, it is extended to accommodate a source wavelet and radiation pattern. The synthetic data tests show that accommodating the source wavelet and radiation pattern can enhance the fidelity of the amplitude and phase predictions of internal multiples.

The report is arranged as follows: First, the ISS internal multiple attenuation algorithm is briefly reviewed and analyzed. Second, the ISS internal multiple attenuation algorithm is modified and extended by incorporating the source wavelet and radiation pattern. Third, the synthetic data

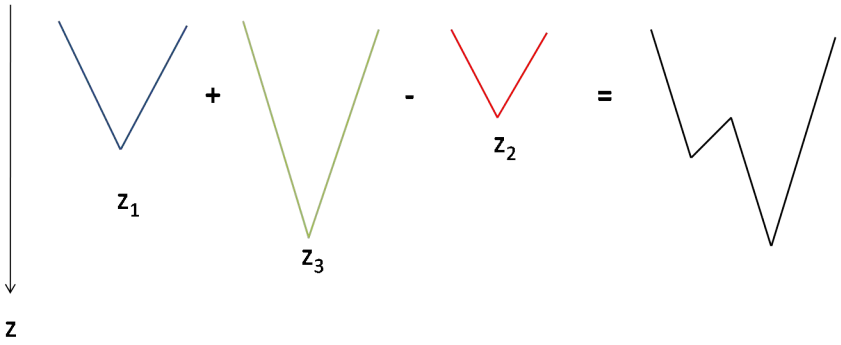

Figure 1: Subevents of an internal multiple. The internal multiple (black) is constructed by three arrivals (blue, green and red) that satisfy a lower-higher-lower relationship in pseudodepths, z_i.

generated by a point source and by a general source with a radiation pattern are tested by this modified algorithm. Finally, we offer a discussion and conclusions.

2 The ISS internal multiple attenuation algorithm

The ISS internal multiple attenuation algorithm assumes that the input data $D(k_g, k_s, \omega)$ have been deghosted and the reference wavefield and free-surface multiples have been removed. The terms ω, k_s and k_g are temporal frequency, and the horizontal wavenumbers for source and receiver coordinates, respectively. The algorithm (Araújo, 1994; Weglein et al., 1997; 2003) for first-order internal multiple prediction in a $2D$ earth is given by

$$\begin{aligned} b_3(k_g, k_s, \omega) = \frac{1}{(2\pi)^2} \int_{-\infty}^{\infty} \int_{-\infty}^{\infty} dk_1 e^{-iq_1(z_g - z_s)} dk_2 e^{iq_2(z_g - z_s)} \\ \times \int_{-\infty}^{\infty} dz_1 b_1(k_g, k_1, z_1) e^{i(q_g + q_1)z_1} \\ \times \int_{-\infty}^{z_1 - \epsilon} dz_2 b_1(k_1, k_2, z_2) e^{-i(q_1 + q_2)z_2} \\ \times \int_{z_2 + \epsilon}^{\infty} dz_3 b_1(k_2, k_s, z_3) e^{i(q_2 + q_s)z_3}, \end{aligned} \tag{1}$$

where q_s and q_g are the vertical source and vertical receiver wavenumbers, respectively. The wavenumbers are given by the dispersion relation $q_i = sgn(\omega)\sqrt{\frac{\omega^2}{c_0^2} - k_i^2}$ for $i = (g, s)$; c_0 is the reference velocity. The terms z_s and z_g are the source and receiver depths, respectively; and z_i $(i = 1, 2, 3)$ represents pseudodepth. The parameter ϵ is introduced to insure that the relations $z_1 > z_2$ and $z_3 > z_2$ are satisfied. The input b_1 represents effective plane-wave incident data and will be discussed and analyzed in detail in the next section.

Figure 1 illustrates how the algorithm constructs a first-order internal multiple. The first-order internal multiple is created by using convolutions and crosscorrelations to combine three events.

The traveltime of the internal multiple is predicted by adding the traveltimes of the two deeper events and subtracting the traveltime of the shallower one. Since not all combinations of subevents will generate an internal multiple, the depth integrals in equation 1 are constrained to impose a lower-higher-lower relationship among the three subevents, as represented in Figure 1. Therefore, the third subevent in Figure 1 has a pseudodepth z_2 above the other two events, such that $z_2 < z_3$ and $z_2 < z_1$. To impose the strict lower-higher-lower relationship, a parameter ϵ is introduced to preclude $z_1 = z_2$ and $z_2 = z_3$ in the integrals. For band-limited data, ϵ relates to the width of the wavelet.

3 Incorporating the source wavelet and radiation pattern into the ISS internal multiple attenuation algorithm

In the previous section, the input b_1 of the ISS internal multiple attenuation algorithm represents effective plane-wave incident data, which can be defined from the first-order equation of the inverse scattering series (Weglein et al., 2003),

$$\begin{aligned} D(x_g, \epsilon_g, x_s, \epsilon_s, \omega) = & \int dx_1 \int dz_1 \int dx_2 \int dz_2 \\ & G_0^d(x_g, \epsilon_g, x_1, z_1, \omega) V_1(x_1, z_1, x_2, z_2, \omega) P_0^d(x_2, z_2, x_s, \epsilon_s, \omega), \end{aligned} \tag{2}$$

where the data D have been deghosted and the reference wavefield and free-surface multiples have been removed (Mayhan et al., 2012; Yang et al., 2013). G_0^d and P_0^d are the direct reference Green's function and the direct reference wavefield, respectively.

The direct reference wavefield is govern by wave equation in the reference medium,

$$(\nabla^2 + \omega^2/c_0^2) P_0^d = \begin{cases} \delta, & unit, \\ A\delta, & point, \\ \rho, & general, \end{cases} \tag{3}$$

where c_0 is the reference velocity. The terms δ, $A\delta$, and ρ are unit source, point source, and general source, respectively.

For a unit source, $P_0^d = G_0^d$. We take a Fourier transform over x_s and x_g on both sides of equation 2 and define b_1 as

$$b_1(k_g, k_s, q_g + q_s) = \frac{V_1(k_g, q_g, k_s, q_s, \omega)}{-2iq_g} = -2iq_s D(k_g, k_s, \omega), \tag{4}$$

where $D(k_g, k_s, \omega)$ is the Fourier-transformed prestack data. The effective plane-wave incident data b_1 are introduced into equation 1 after an uncollapsed Stolt migration (Weglein et al., 1997) that takes $b_1(k_g, k_s, q_g + q_s)$ into the pseudodepth domain, $b_1(k_g, k_s, z_i)$, by using the reference velocity,

c_0. Then, the first-order internal multiples $D_3(k_g, k_s, \omega)$, which are predicted by the ISS internal multiple attenuation algorithm (equation 1), are obtained by

$$D_3(k_g, k_s, \omega) = (-2iq_s)^{-1} b_3(k_g, k_s, q_g + q_s). \tag{5}$$

For an isotropic point source, $P_0^d = A(\omega)G_0^d$. Fourier transforming over x_g and x_s on both sides of equation 2 gives

$$b_1(k_g, k_s, q_g + q_s) = -2iq_s D(k_g, k_s, \omega)/A(\omega), \tag{6}$$

where $A(\omega)$ is the source signature for a point source. After b_3 has been predicted by equation 1, the first-order internal multiple is achieved by convolving the source wavelet $A(\omega)$ back

$$D_3(k_g, k_s, \omega) = (-2iq_s)^{-1} A(\omega) b_3(k_g, k_s, q_g + q_s). \tag{7}$$

For a general source with a radiation pattern (e.g., a source array), the direct reference wavefield P_0^d for a 2D case can be expressed as an integral of the direct reference Green's function G_0^d over all air-guns in an array,

$$P_0^d(x, z, x_s, z_s, \omega) = \int dx' dz' \rho(x', z', \omega) G_0^d(x, z, x' + x_s, z' + z_s, \omega), \tag{8}$$

where (x, z) and (x_s, z_s) are the prediction point and source point, respectively. (x', z') is the distribution of the source with respect to the source locator (x_s, z_s). Using the bilinear form of Green's function and Fourier transforming over x, we obtain the relationship between ρ and P_0^d as

$$P_0^d(k, z, x_s, z_s, \omega) = \rho(k, q, \omega) \frac{e^{iq|z - z_s|}}{2iq} e^{ikx}. \tag{9}$$

On the other hand, the direct reference wavefield P_0^d is obtained by deghosting the reference wavefield P_0 that is separated from the total measured data by using Green's theorem method (Weglein and Secrest, 1990).

Since $k^2 + q^2 = \omega^2/c_0^2$, q is not a free variable, hence, we can not obtain $\rho(x, z, \omega)$ in space-frequency domain by taking an inverse Fourier transform on $\rho(k, q, \omega)$. However, the projection of the source signature $\rho(k, q, \omega)$ can be achieved directly from the direct reference wavefield P_0^d in the f-k domain, where the variable k or q represent the amplitude variations of the source signature with angles.

Substituting the projection of the source signature ρ into equation 2 and Fourier transforming over x_s and x_g gives

$$b_1(k_g, k_s, q_g + q_s) = -2iq_s D(k_g, k_s, \omega)/\rho(k_g, q_g, \omega). \tag{10}$$

Further details of obtaining ρ can be found in Yang et al. (2013) and Yang and Weglein (2013). The first-order internal multiple is calculated from b_3,

$$D_3(k_g, k_s, \omega) = (-2iq_s)^{-1} \rho(k_g, q_g, \omega) b_3(k_g, k_s, q_g + q_s), \tag{11}$$

where b_3 is predicted by equation 1.

All above derivations are 2D cases, and they can be directly extended to 3D. From the derivations, we can see that the kernel of the ISS internal multiple attenuation algorithm (equation 1) is not change and the source wavelet and radiation pattern are imported by equations 6 and 10. The predicted internal multiples D_3 are also affected by the source wavelet and radiation pattern in equations 7 and 11. When adding the predicted internal multiple D_3 to the input data D, all the first-order internal multiples are attenuated, and higher-order internal multiples are altered. If the source wavelet is not incorporated into the ISS internal multiple attenuation algorithm, the amplitudes and shapes of the predicted internal multiples are not comparable with those of the internal multiples in the input data. To improve the prediction of amplitude and shape, the internal multiple attenuation algorithm should be modified for its input and output by accommodating the source wavelet and radiation pattern. This accommodation can enhance the fidelity of predictions of the amplitude and shape of internal multiples. In Liang and Weglein (2013), the author also discussed the effects of the source wavelet on the higher-order terms and on the spurious events in the internal multiple prediction.

4 Numerical tests on the synthetic data

In this section, I will present the numerical tests of the internal multiple attenuation for the data generated by a point source and a general source with a radiation pattern. The numerical tests are based on a simple $1D$ acoustic model with varying velocity and constant density, as shown in Figure 2a. The synthetic data are generated by the finite-difference method shown in Figure 3a. The synthetic data have one shot gather with 2001 traces, and each trace has 301 time samples, with $dt = 5ms$. The trace interval is $5m$. Figure 2b shows the source wavelet that we applied in the finite-difference modeling code.

4.1 The source wavelet effect on internal multiple prediction

For the data generated by a point source, the internal multiple will be predicted by using the ISS internal multiple attenuation algorithm with and without source wavelet deconvolution. Figure 3 shows the input data and their corresponding predicted internal multiples. They are plotted using the same scale. In the input data, the first two strongest events are the primaries, and the other events are internal multiples. Figures 3b and 3c show the predicted internal multiples using the ISS internal multiple attenuation algorithm with and without source wavelet deconvolution. From Figures 3b and 3c, we can see that both algorithms predict the correct traveltimes, but they predict different amplitudes and shapes for the internal multiples. In Figure 3b, the amplitude of the predicted internal multiple is comparable with the internal multiple in the input data, while the amplitude is totally different from that of the internal multiple in the input data in Figure 3c.

To see the details of the predicted internal multiples, we pick the middle trace (offset = 0) and the far trace (offset = $1700m$) from each image in Figure 3. To compare the internal multiples from the input data with the predicted results, the time windows are chosen at $0.85s \sim 1.10s$ for the middle

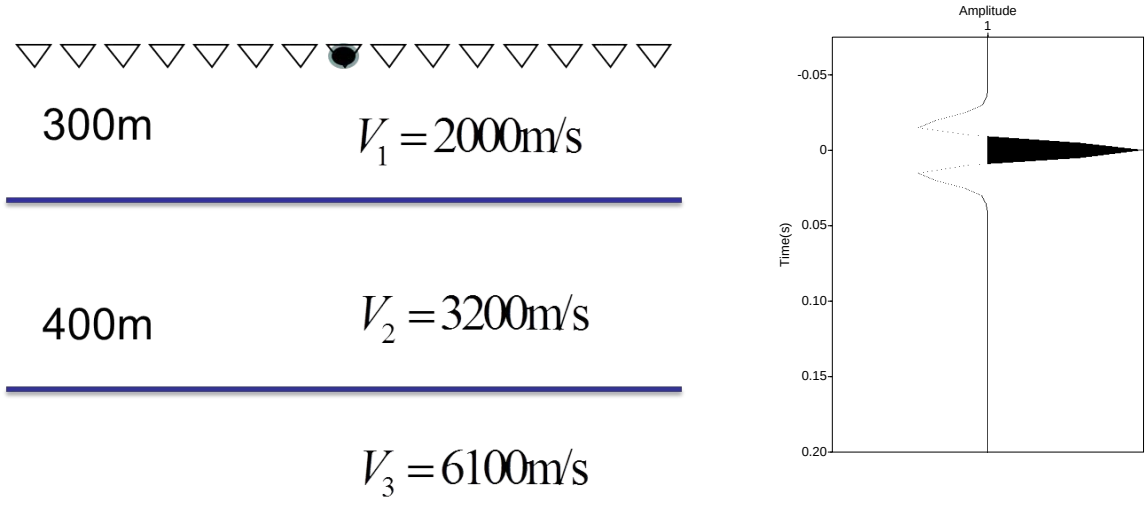

(a) (b)

Figure 2: (a) The earth model that we used to generate the synthetic data. It is a one-dimensional acoustic constant-density medium. (b) A Ricker wavelet.

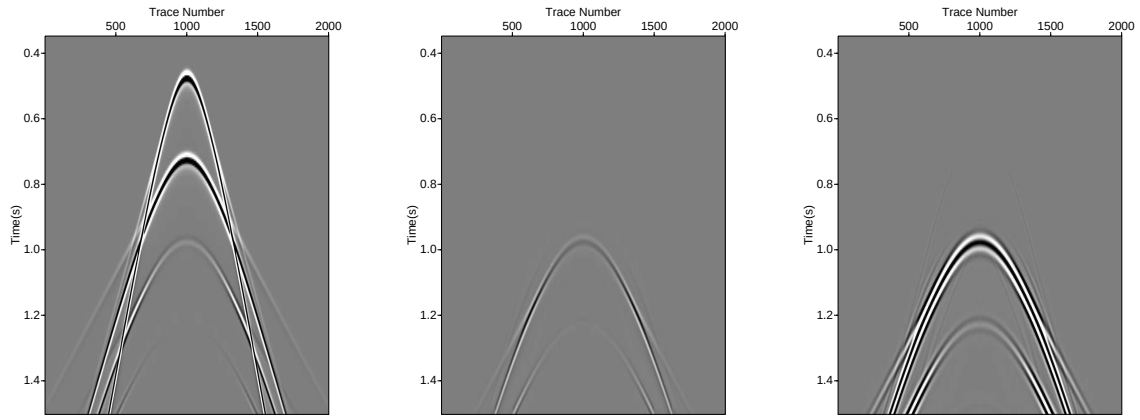

(a) (b) (c)

Figure 3: (a) The input data; (b) and (c) The internal multiples predicted by the ISS internal multiple attenuation algorithm with and without source wavelet deconvolution.

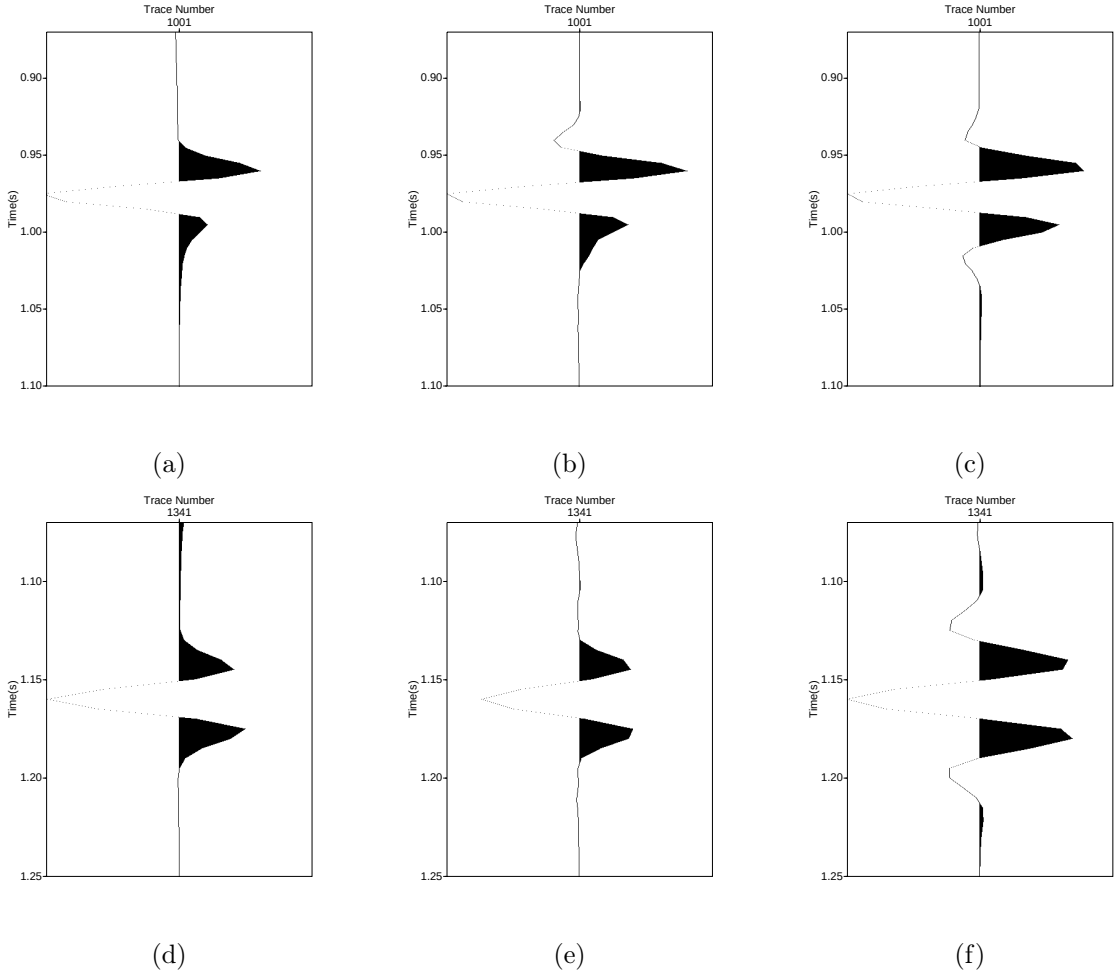

Figure 4: (a), (b), (c) The middle traces, and (d), (e), (f) the far traces, picked from the input data and the internal multiples predicted by the ISS internal multiple attenuation algorithm with and without source wavelet deconvolution.

trace and at $1.05s \sim 1.25s$ for the far trace, as shown in Figure 4. For the middle trace, comparing Figure 4c with Figure 4a, we can see that the shape of the internal multiple predicted by the ISS internal multiple attenuation algorithm without source wavelet deconvolution is totally different from that of the true internal multiple. The predicted and true amplitudes are not comparable, either. The predicted amplitudes and shapes are so different from the true ones in this case because the predicted internal multiples convolve three wavelets (Equation 1). However, comparing Figure 4b with Figure 4a, we can see that the amplitude and shape of the internal multiple predicted by the ISS internal multiple attenuation algorithm with source wavelet deconvolution are similar to those for the true internal multiple. Their comparison is plotted in Figure 5a. It demonstrates that by accommodating the source wavelet deconvolution, the amplitude and shape of the predicted internal multiple are significantly improved. For the far-offset traces, we obtain the similar results, as are shown in Figures 4e and 5b.

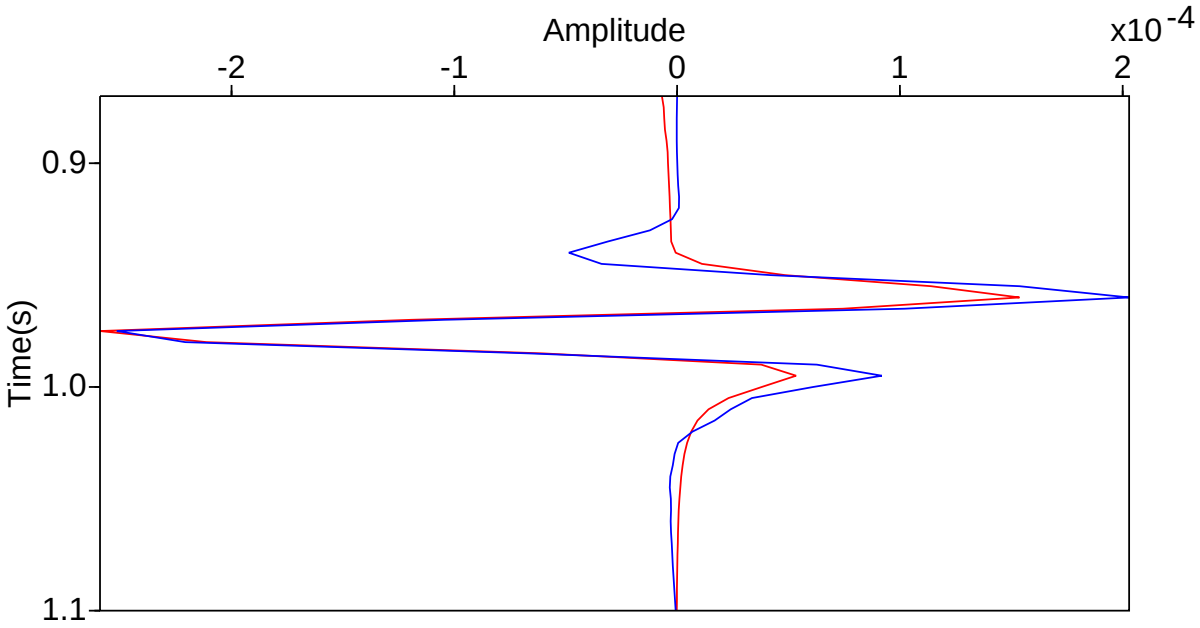

(a)

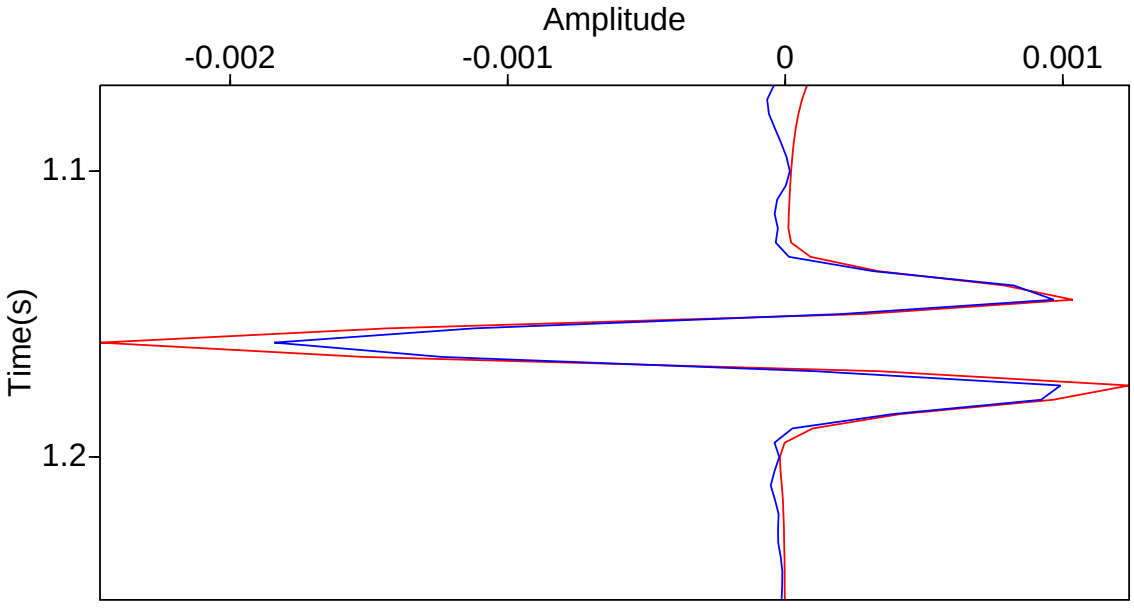

(b)

Figure 5: The comparison between the internal multiple (red) in the input data and the internal multiple (blue) predicted by the ISS internal multiple attenuation algorithm with source wavelet deconvolution at (a) zero offset and at (b) far offset (1700m).

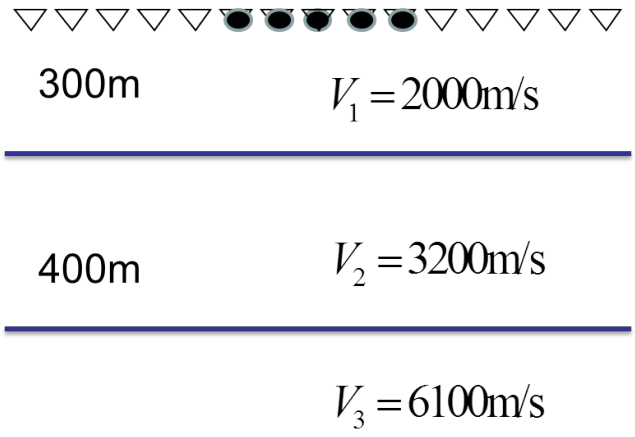

Figure 6: (a) The earth model with a source array.

From the numerical test, we conclude that by incorporating the source wavelet deconvolution, the ISS internal multiple attenuation algorithm produces more accurate and encouraging results. The predicted internal multiple has the correct traveltime, and the amplitude and shape are significantly improved.

4.2 The radiation pattern effect on internal multiple prediction

For the data generated by a general source with a radiation pattern (e.g., source array), we will predict the internal multiple using the ISS internal multiple attenuation algorithm with and without incorporating the source wavelet and radiation pattern. The synthetic data are generated by a source array with five point sources, using the finite-difference method in the same model, as shown in Figure 6.

Figure 7a shows the input data generated by the source array. Similar with the data generated by the point source, the first two strongest events are the primaries, and the other events are internal multiples. Figures 7b and 7c show the internal multiples predicted by using the ISS internal multiple attenuation algorithm with and without incorporating the source wavelet and radiation pattern. From Figures 7b and 7c, we can see that both algorithms can predict the correct traveltime and an acceptable amplitude of the internal multiple.

To compare the predictions of internal multiples in detail, the middle trace (offset = 0) and the far trace (offset = $1700m$) are picked from each figure in Figure 7. We choose the time windows at $0.85s \sim 1.10s$ for the middle trace and at $1.05s \sim 1.25s$ for the far trace, as shown in Figure 8. Comparing the middle and far traces, we can see that the amplitude and shape of the internal multiple predicted by the ISS internal multiple attenuation algorithm with and without incorporating the radiation pattern are very similar to those for the internal multiple in the input data. Their comparisons are plotted in Figure 9. At zero offset, there are no visible differences, as is shown in Figure 9a, while at far offset, Figure 9b demonstrates that the amplitude of the internal multiple

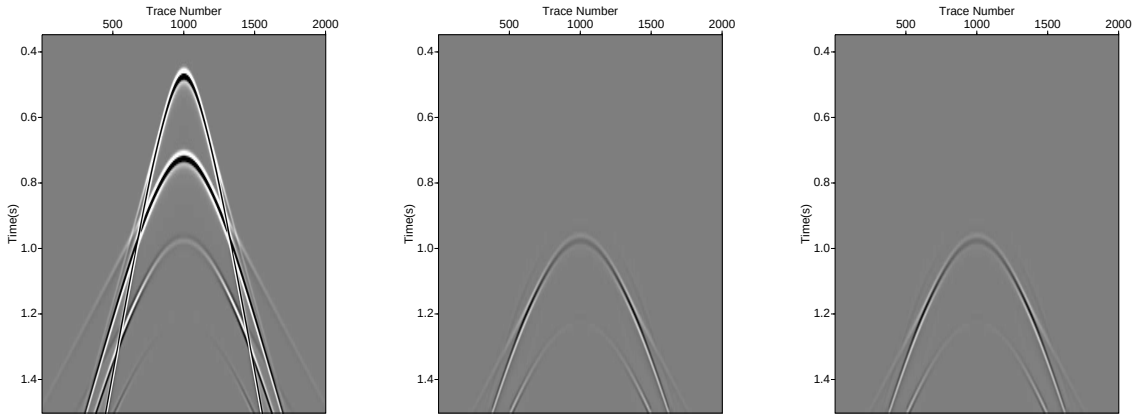

(a) (b) (c)

Figure 7: (a) The input data; (b) and (c) the internal multiples predicted by the ISS internal multiple attenuation algorithm with and without incorporating the source wavelet and radiation pattern.

prediction is further improved by accommodating the source array. Therefore, for the general source data, the modified ISS internal multiple attenuation algorithm that incorporates the source wavelet and radiation pattern can enhance the accuracy of the amplitude prediction of the internal multiple.

5 Conclusions

The ISS internal multiple attenuation algorithm is modified and extended by accommodating the source wavelet and radiation pattern, which can be provided by the prerequisite. The modified ISS internal multiple attenuation algorithm enhances the fidelity of amplitude and phase predictions of the internal multiple. It can provide added value compared to previous methods for the effectiveness of the internal multiple prediction. The modified ISS internal multiple attenuation algorithm retains all the merits of the original algorithm that is fully data-driven and does not require subsurface information. In synthetic data tests, for the data generated by a point source with a wavelet, the predictions of the amplitudes and shapes of internal multiples are significantly improved by incorporating the source wavelet deconvolution into the ISS internal multiple attenuation algorithm. For the data generated by a general source with a radiation pattern, the prediction is further improved by incorporating the source wavelet and radiation pattern. We expect this extended ISS internal multiple attenuation algorithm to be relevant and useful for on-shore application, as well.

6 ACKNOWLEDGMENTS

The first author is grateful to all M-OSRP sponsors for their support of this research, and to Lin Tang and Chao Ma for their reviews. Special thanks go to my advisor, Dr. Arthur B. Weglein, for

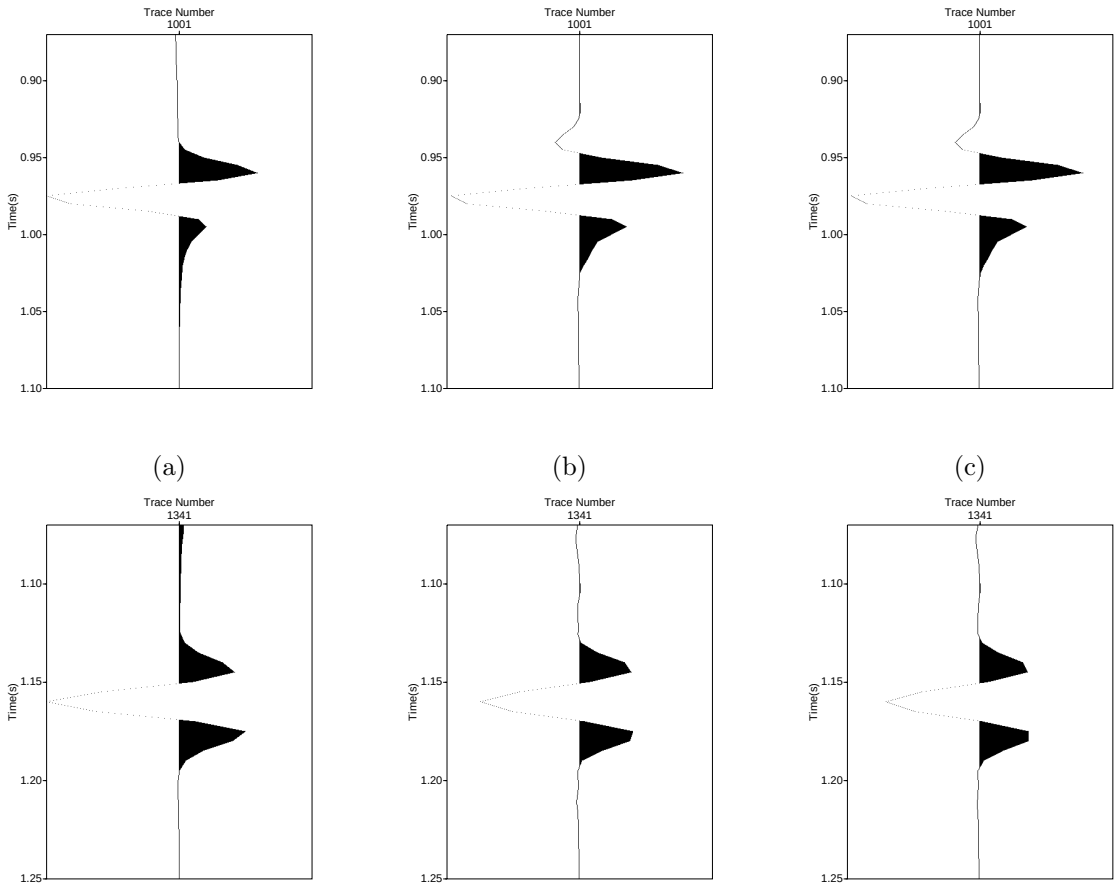

Figure 8: (a), (b), (c) The middle traces, and (d), (e), (f) the far traces, picked from the input data and the internal multiples predicted by the ISS internal multiple attenuation algorithm with and without incorporating the source wavelet and radiation pattern.

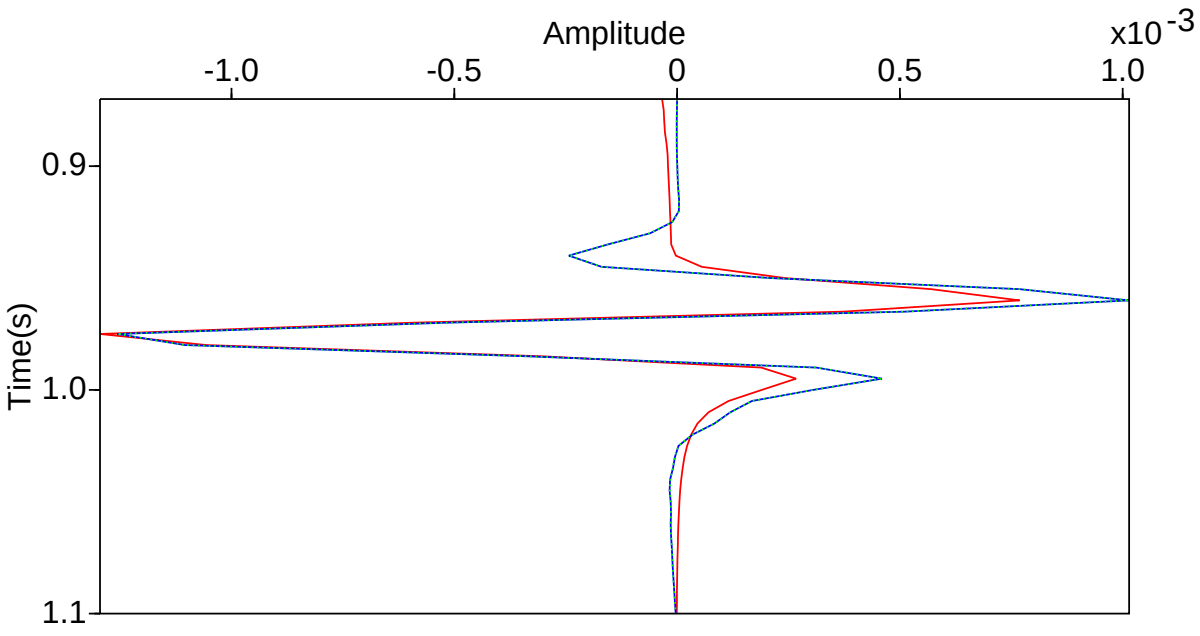

(a)

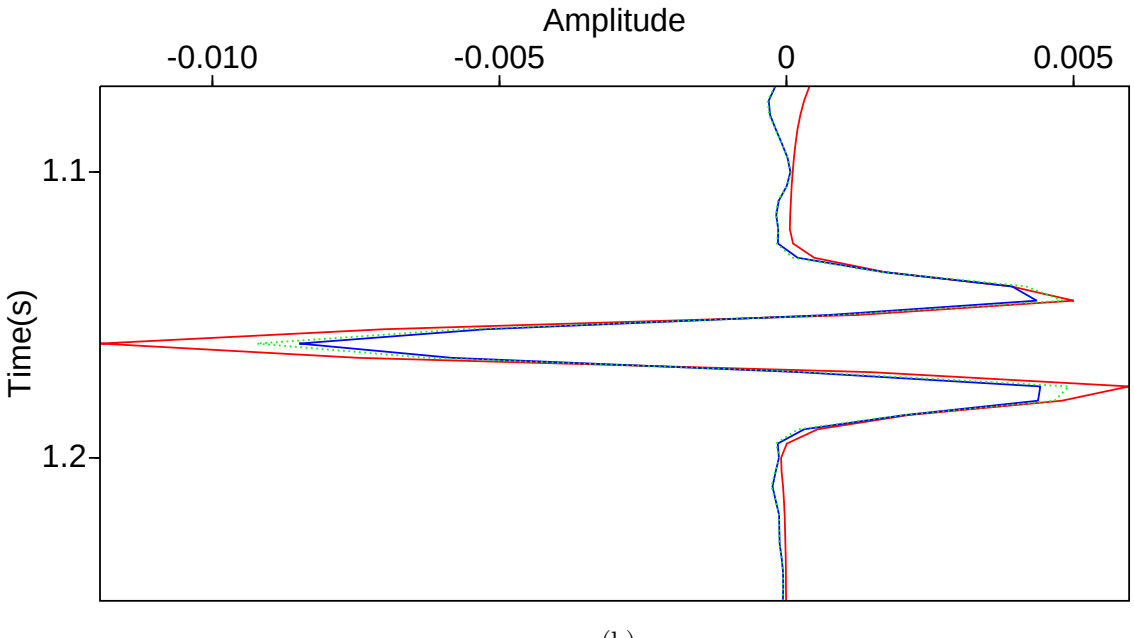

(b)

Figure 9: The comparison between the true internal multiple (red) in the input data and the internal multiple predicted by the ISS internal multiple attenuation algorithm with (green dash) and without (blue) incorporating the source wavelet and radiation pattern at (a) zero offset and at (b) far offset ($1700m$).

his teaching and guidance.

References

Araújo, F. V. *Linear and non-linear methods derived from scattering theory: backscattered tomography and internal multiple attenuation.* PhD thesis, Universidade Federal da Bahia, 1994.

Araújo, F. V., A. B. Weglein, P. M. Carvalho, and R. H. Stolt. "Inverse scattering series for multiple attenuation: An example with surface and internal multiples." *64th Annual International Meeting, SEG, Expanded Abstracts* (1994): 1039–1042.

Carvalho, P. M. *Free-surface multiple reflection elimination method based on nonlinear inversion of seismic data.* PhD thesis, Universidade Federal da Bahia, 1992.

Herrera, W. and A. B. Weglein. "Eliminating first-order internal multiples with downward reflection at the shallowest interface: Theory and initial examples." *83rd International Annual Meeting, SEG, Expanded Abstracts* (2013): 4131–4135.

Hsu, S., P. Terenghi, and A. B. Weglein. "The properties of the inverse scattering series internal multiple attenuation algorithm: Analysis and evaluation on synthetic data with lateral variations, choosing reference velocity and examining its sensitivity to near surface properties." *M-OSRP Annual Report* (2011): 16–28.

Liang, H., C. Ma, and A. B. Weglein. "A further general modification of the leading order ISS attenuator of first order internal multiples to accommodate primaries and internal multiples when an arbitrary number of reflectors generate the data: theory, development, and examples." *M-OSRP Annual Report* (2012): 148–166.

Liang, H. and A. B. Weglein. "Source wavelet effects on the ISS internal multiple leading order attenuation algorithm and its higher order modification." *M-OSRP Annual Report* (2013).

Loveridge, M. M., G. E. Parkes, L. Hatton, and M. H. Worthington. "Effects of marine source array directivity on seismic data and source signature deconvolution." *First Break* 2 (1984): 16–22.

Luo, Y., P. G. Kelamis, Q. Fu, G. Sindi, S. Hsu, and A. B. Weglein. "Elimination of land internal multiple based on the inverse scattering series." *The Leading Edge* (2011): 884–889.

Ma, C., H. Liang, and A. B. Weglein. "Modifying the leading order ISS attenuator of first-order internal multiples to accommodate primaries and internal multiples: fundamental concept and theory, development, and examples exemplified when three reflectors generate the data." *M-OSRP Annual Report* (2012): 133–147.

Matson, K. and A. B. Weglein. "Removal of elastic interface multiples from land and ocean bottom data using inverse scattering." *66th Annual International Meeting, SEG, Expanded Abstracts.* (1996): 1526–1529.

Matson, K. H. *An inverse-scattering series method for attenuating elastic multiples from multi-component land and ocean bottom seismic data.* PhD thesis, University of British Columbia, 1997.

Matson, K. H., D. C. Corrigan, A. B. Weglein, C. Y. Young, and P. M. Carvalho. "Inverse scattering internal multiple attenuation: results from complex synthetic and field data examples." *69th Annual International Meeting, SEG, Expanded Abstracts* (1999): 1060–1063.

Mayhan, James D., Arthur B. Weglein, and Paolo Terenghi. "First application of Green's theorem derived source and receiver deghosting on deep water Gulf of Mexico synthetic (SEAM) and field data." *82nd Annual International Meeting, SEG, Expanded Abstracts* (2012): 1–5.

Ramírez, A. C. and A.B. Weglein. "An inverse scattering internal multiple elimination method: Beyond attenuation, a new algorithm and initial tests." *75th International Annual Meeting, SEG, Expanded Abstracts* (2005): 2115–2118.

Tang, Lin, James D. Mayhan, Jinlong Yang, and Arthur B. Weglein. "Using Green's theorem to satisfy data requirements of inverse scattering series multiple removal methods." *83rd International Annual Meeting, SEG, Expanded Abstracts* (2013): 4392–4396.

Terenghi, P., S. Hsu, A. B. Weglein, and X. Li. "Exemplifying the specific properties of the inverse scattering series internal-multiple attenuation method that reside behind its capability for complex onshore and marine multiples." *The Leading Edge* (2011): 876–882.

Weglein, A. B., F. V. Araújo, P. M. Carvalho, R. H. Stolt, K. H. Matson, R. T. Coates, D. Corrigan, D. J. Foster, S. A. Shaw, and H. Zhang. "Inverse Scattering Series and Seismic Exploration." *Inverse Problems* (2003): R27–R83.

Weglein, A. B., F. A. Gasparotto, P. M. Carvalho, and R. H. Stolt. "An Inverse-Scattering Series Method for Attenuating Multiples in Seismic Reflection Data." *Geophysics* 62 (November-December 1997): 1975–1989.

Weglein, A. B., S. Hsu, P. Terenghi, X. Li, and R. H. Stolt. "Multiple attenuation: Recent advances and the road adead 2011." *The Leading Edge* (2011): 864–875.

Weglein, Arthur B. and Bruce G. Secrest. "Wavelet estimation for a multidimensional acoustic earth model." *Geophysics* 55 (July 1990): 902–913.

Yang, Jinlong, James D. Mayhan, Lin Tang, and Arthur B. Weglein. "Accommodating the source (and receiver) array in free-surface multiple elimination algorithm: impact on interfering or proximal primaries and multiples." *83rd International Annual Meeting, SEG, Expanded Abstracts* (2013): 4184–4189.

Yang, Jinlong and Arthur B. Weglein. "Incorporating the source array in the free-surface multiple elimination algorithm: impact on removing a multiple that interferes with a primary and first test of the source deconvolution on the internal multiple attenuation algorithm." *M-OSRP Annual Report* (2013).

Zhang, Jingfeng and Arthur B. Weglein. "Extinction theorem deghosting method using towed streamer pressure data: Analysis of the receiver array effect on deghosting and subsequent free surface multiple removal." (2005): 2095–2100.

Zou, Y. and A. B. Weglein. "A new method to eliminate first order internal multiples for a normal incidence plane wave on a 1D earth." *83rd International Annual Meeting, SEG, Expanded Abstracts* (2013): 4136–4140.

Internal-multiple attenuation on Encana data

Qiang Fu and Arthur B. Weglein

May 21, 2014

Abstract

The attenuation of internal-multiple energy on land data is currently one of the most challenging tasks in seismic data preprocessing. In general, poor data quality and the lack of velocity information for complicated geological structure (especially in the near surface) in land data often result in poor predictions by the internal multiple attenuation methods requiring subsurface information. Inverse Scattering Series (ISS) internal-multiple attenuation is a very promising algorithm for attenuating internal-multiple energy on land seismic exploration data. The key characteristic of the ISS-based methods is that they do not require any information about the subsurface– i.e., they are fully data driven. Internal multiples from all possible generators are predicted simultaneously from the input data. In this paper we apply Inverse Scattering Series (ISS) internal- multiple-attenuation algorithms on land seismic data from Canada.

1 Introduction

Inverse Scattering Series (ISS) internal multiple-attenuation is a data-driven internal-multiple-attenuation algorithm (Araújo et al., 1994; Weglein et al., 1997). The lack of any need for information about the medium through which the seismic wave propagates or the reflectors from which the internal multiples generate makes the algorithm feasible in areas with complicated geological structure. The algorithm predicts internal multiples for all horizons at once, with no intervention required in the whole procedure. Weglein et al. (2003) provided a review of applications of the inverse scattering series in seismic exploration.

This ISS internal-multiple-attenuation algorithm is the first term in a subseries of the ISS that predicts the exact time and amplitude of all internal multiples without subsurface information. The ISS attenuation algorithm predicts the correct traveltimes and approximate amplitudes of all the internal multiples in the data, including converted-wave internal multiples (Coates and Weglein, 1996). Carvalho et al. (1992) pioneered the free-surface ISS method and applied it to field

data. Matson et al. (1999) were the first to apply the ISS internal-multiple algorithm to marine towed-streamer field data. Matson (1997) and Weglein et al. (1997) extended the ISS methods for removing free-surface and internal multiples from ocean-bottom and land data. Fu et al. (2010) presented the first example of using land field data with the ISS internal-multiple attenuation algorithm. Terenghi (2011) showed a result of pre-stack field data internal-multiple attenuation on Encana on-shore data.

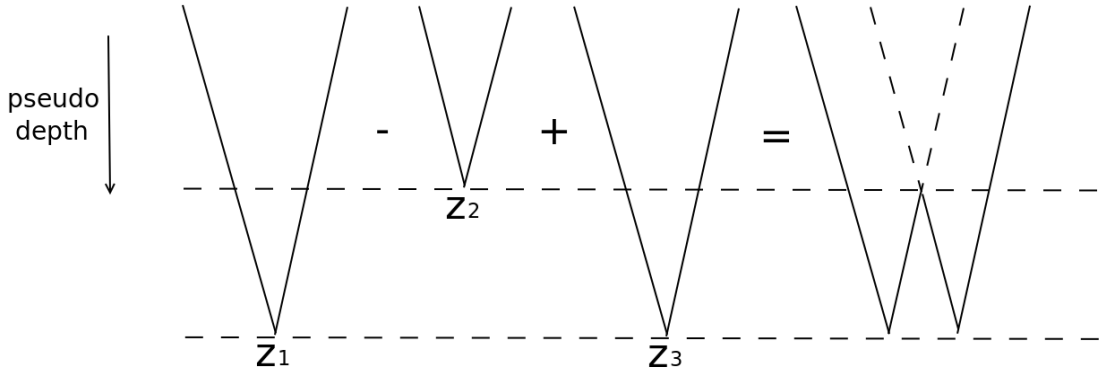

Figure 1: The sub-events of an internal-multiple event. The internal multiple (rightmost one) is constructed by three sub-events (the left three) that satisfy the lower-higher-lower relationship in pseudodepth z_i $(i = 1, 2, 3)$.

2 Theory

The ISS internal-multiple-attenuation algorithm in 2D starts with the input data, $D(k_g, k_s, \omega)$, which are deghosted and have had all free-surface multiples eliminated. The parameters, k_g, k_s, and ω represent the Fourier conjugates to receiver, source and time, respectively. The ISS internal-multiple-attenuation algorithm for first-order internal-multiple prediction in a 2D earth is given by Araújo et al. (1994); Weglein et al. (1997):

$$\begin{aligned} b_3^{2D}(k_g, k_s, q_g + q_s) = \frac{1}{(2\pi)^2} \int_{-\infty}^{+\infty} \int_{-\infty}^{+\infty} dk_1 e^{-iq_1(z_g - z_s)} \\ dk_2 e^{-iq_2(z_g - z_s)} \\ \times \int_{-\infty}^{+\infty} dz_1 e^{i(q_g + q_1)z_1} b_1(k_g, k_1, z_1) \\ \times \int_{-\infty}^{z_1 - \epsilon} dz_2 e^{i(-q_1 - q_2)z_2} b_1(k_1, k_2, z_2) \\ \times \int_{z_2 + \epsilon}^{+\infty} dz_3 e^{i(q_2 + q_s)z_3} b_1(k_2, k_s, z_3). \end{aligned} \quad (1)$$

The quantity $b_1(k_g, k_s, z)$ corresponds to an un-collapsed migration (Weglein et al., 1997) of an effective incident-plane-wave data that is given by $-2iq_s D(k_g, k_s, \omega)$. The vertical wavenumbers for receiver q_g and source q_s are given by $q_i = sqn(\omega)\sqrt{\frac{\omega^2}{c_0^2} - k_i^2}$ for $i = (q, s)$; c_0 is the constant reference velocity; z_s and z_g are source and receiver depths, respectively; and z_i $(i = 1, 2, 3)$ represents pseudodepth.

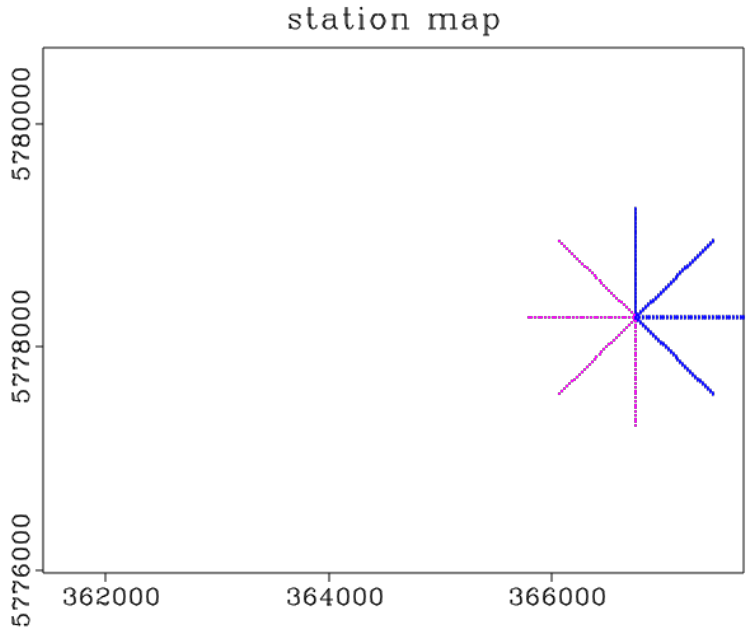

Figure 2: Acquisition-geometry map of the first CMP gather of the data set. Red dots represent the source locations, and blue dots represent the receiver locations.

The construction of a first-order internal multiple is illustrated in Figure 1. The first-order internal multiple is composed of three sub-events that satisfy $z_1 > z_2$ and $z_3 > z_2$. The traveltime of the internal multiple is the sum of the traveltimes of the two deeper sub-events, minus the traveltime of the shallower one. The parameter ϵ is introduced in equation 1 to preclude $z_1 = z_2$ and $z_2 = z_3$ in the integrals. For band-limited data, ϵ is related to the width of the wavelet. The output of equation 1, b_3, is divided by the obliquity factor and transformed back to the space-time domain. When we subtract the predicted internal multiples from the original input data (by adaptive subtraction), all first-order internal multiples are attenuated and higher-order internal multiples are altered.

3 Data and method chosen to accommodate the data

The Encana data are from the Western Canadian Sedimentary Basin, and are situated over a restricted Devonian shelf basin. This shallow basin was initially connected to open marine waters. Pinnacle reefs grew in this marine environment and later filled with oil, making them a prime exploration target. The connection to the open marine water later became restricted, causing the basin to fill with evaporates that today consist primarily of anhydrite. The anhydrite acts as a lateral seal and cap rock for the porous reef reservoirs.

The reefs should be very easy to find in the seismic data. The basinal anhydrite produces a very

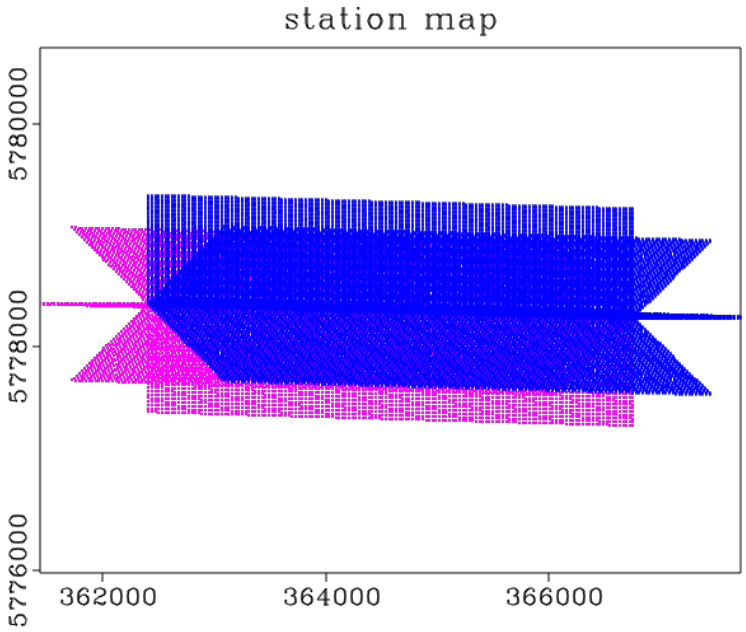

Figure 3: Acquisition-geometry map of the whole Encana data set. Red dots represent the source locations, and blue dots represent the receiver locations

strong peak reflection, but the response is almost reversed when there is a reef present because the reef porosity has a much lower acoustic impedance than the anhydrite porosity does. This is the case with the western part of the basin, where all the reefs have all been found. On the eastern side of the basin, the situation is quite different. There, a Lower Cretaceous coal, which reaches 15 meters in thickness, produces severe multiple interferences that obscure the entire Paleozoic section. Many reefs have been found there, but many more dry holes than successes have been drilled there because of this interference. Most commercial multiple-attenuation algorithms fail to remove this interference. Our goal here is to make the reefs as clearly visible in the seismic data from the eastern side of the basin as they are in the western side.

As was mentioned in the previous section, Fu et al. (2010) tested the ISS internal-multiple attenuation algorithm on Arabian Peninsula land field data. Although the Arabian Peninsula land field data in Fu et al. (2010) are off better quality, that region also has much more complicated geological features. Thus, it is hard to pick a single clear target there with which to judge the internal-multiple-attenuation result. The Encana data are inferior in data quality (with lower S/N ratio) and have poorer acquisition geometry (limited fold and offset range) compared with the Arabian Peninsula data, but there is a very simple target in the Encana data: the disappeared target layer (the reef). The Encana data contain four different azimuths, but that does not provide much help for the internal-multiple-attenuation task. Terenghi (2011) tested the same method on another Canadian field data set, but those data have large offset coverage.

The Encana data we use here are from a multi-azimuth 2D survey line. Figure 3 shows the acquisition geometry of the data. The geometry of the first CMP gather of these data is shown in Figure 2. All CMP stations of the data compose a straight line on the map, so this is a 2D survey line even though there are multiple azimuths in the data. The data area relatively old (from the mid 1990s), so they have a very low fold for each CMP gather (32 traces). The 2D ISS internal-multiple-prediction algorithm requires a full-coverage input (each shot gather has all receivers on the exact same stations, and we have a shot gather for each station– e.g., there is a trace between every station pair.). If we want to perform the 2D ISS internal- multiple-prediction, we would need to carry out a large amount of extrapolation to obtain full 2D data coverage from the low-fold data that we have. That would not only be expensive for computation, it also would be unreliable to "make" such a large amount of data by extrapolation. Given the fact that the subsurface structures of the whole survey line is fairly flat, the 1.5D pre-stack method would be a suitable choice for the internal-multiple-attenuation task on these data. In equation 1 we show the 2D ISS internal-multiple-attenuation algorithm. The 1.5D ISS internal-multiple-attenuation algorithm is a straightforward extension the of 2D algorithm, and can be described as

$$\begin{aligned} b_3^{1.5D}(k_x;\omega) = \frac{1}{(2\pi)^4} e^{-iq(z_g-z_s)} e^{iq(z_g-z_s)} \\ \times \int_{-\infty}^{+\infty} dz_1 b_1(k_x,z_1) e^{2iqz_1} \\ \times \int_{-\infty}^{z_1-\epsilon} dz_2 b_1(k_x,z_2) e^{-2iqz_2} \end{aligned}$$

$$\times \int_{z_2+\epsilon}^{+\infty} dz_3 b_1(k_x, z_3) e^{2iqz_3}. \quad (2)$$

The notation in equation 2 is the same as that in equation 1. If we compare the 1.5D version in equation 2 with the 2D version in equation 1, the only difference is that in the 1.5D formula the output has only one horizontal spatial wavenumber index k_x rather than two (k_g and k_s). This is obvious since under the 1.5D assumption (flat-layer medium assumption), all horizontal incident wavenumbers should be equal to the reflected wavenumber ($k_g = k_1 = k_2 = k_s = k_x$). Hence, there is only one horizontal spatial wavenumber k_x in equation 2.

4 Results

Figures 4 and 5 show the input data in the pre-stack and post-stack domains, respectively. As the ISS internal multiple attenuation algorithm requires, the data have first been deghosted and have all free-surface multiples eliminated. In this case, the major multiple generator is the coal layer. We can see the reflector clearly in Figure 5 (in the vicinity of 1s), and the target layer (the reef), which should be around 1.15s, cannot be seen in Figure 5.

Figures 6 and 7 show the internal-multiple-attenuation results in the pre-stack and post-stack domains, respectively. The reference velocity c_0 used is the shallowest layer's NMO velocity (averaged horizontally). After internal-multiple attenuation, we can see that a significant amount of internal-multiple energy is removed in the vicinity of 1.15s. However, we can still barely discern the reef clearly. The results show that there is marginal improvement of the target event after ISS internal-multiple attenuation with these limited offset data.

Figures 8 and 9 are the predicted internal multiples in the pre-stack and post-stack domains, respectively. Although the method knows nothing about the generator, the predicted internal multiples only appear below the main generator. Figure 8 shows that the predicted internal multiples have primarily far-offset component (with some near-offset component still visible). However, the near-offset component is critical to obtaining an effective internal-multiple-attenuation result.

Therefore, the lack of the near-offset portion of the internal-multiple prediction is an important reason why we do not obtain a very satisfactory result in this case. The severely limited offset coverage of the input data is responsible for the absence of a predicted near-offset multiple, and that negatively impacts the results of our internal-multiple-attenuation.

The data-acquisition geometry consists of four different azimuths. We also tried to use the data of each azimuth separately, but the results are not significantly different from the result obtained by using data of all azimuths together. The use of all azimuth data results in a little better quality in the post-stack section and has four times higher fold than the single azimuth data have, and that increases the S/N ratio.

5 Conclusions

We applied 1.5D pre-stack ISS internal-multiple attenuation on Encana land seismic data and obtained marginal improvement in discerning the target event. The result is not as satisfactory as that from the same ISS internal-multiple-attenuation algorithm used on the Arabian Peninsula data (Fu et al., 2010). This is because the ISS internal-multiple-attenuation algorithm requires that a Fourier transform be performed along the offset axis. That in turn requires a reasonable offset range in the input data, in order to avoid truncated effects. Considering the data-acquisition geometry (32 traces per CMP gather and a maximum offset of 2000m), this is a positive and encouraging result. The ISS algorithm for attenuation of the surface and internal multiples requires reasonable data collection in terms of sampling and offset in order for it to be effective and to deliver its promise.

6 Acknowledgment

We thank David Mackidd and David Bonar of Encana for providing the data used in this paper and for encouraging (1) the ISS internal-multiple attenuation tests and (2) communicating these results to the geophysical community. We thank Dr. P. Terenghi for his useful and worthwhile comments and suggestions. We thank the M-OSRP sponsors for their encouragement and their support for our research. M-OSRP would like to thank Bill Goodway, of Apache Corp, for his constant, strong and much appreciated encouragement and support for all the projects in our program.

References

Araújo, F. V., A. B. Weglein, P. M. Carvalho, and R. H. Stolt. "Inverse scattering series for multiple attenuation: An example with surface and internal multiples." *64th Annual International Meeting, SEG, Expanded Abstracts* (1994): 1039–1042.

Carvalho, P. M., A. B. Weglein, and R. H. Stolt. "Nonlinear inverse scattering for multiple suppression: Application to real data. Part I." *62nd Annual International Meeting, SEG, Expanded Abstracts* (1992): 1093–1095.

Coates, R. T. and Aurther B. Weglein. "Internal multiple attenuation using inverse scattering: Results from prestack 1 and 2D acoustic and elastic synthetics." *66th Annual International Meeting, SEG, Expanded Abstracts* (1996): 1522–1525.

Fu, Qiang, Yi Luo, Panos G. Kelamis, ShouDong Huo, Ghada Sindi, Shih-Ying Hsu, and Arthur B. Weglein. "The inverse scattering series approach towards the elimination of land internal multiples." *80th Annual International Meeting, SEG, Expanded Abstracts* (2010).

Matson, K. "An inverse scattering series method for attenuating elastic multiples from multicomponent land and ocean bottom seismic data." *Ph. D. thesis, The University of British Columbia* (1997).

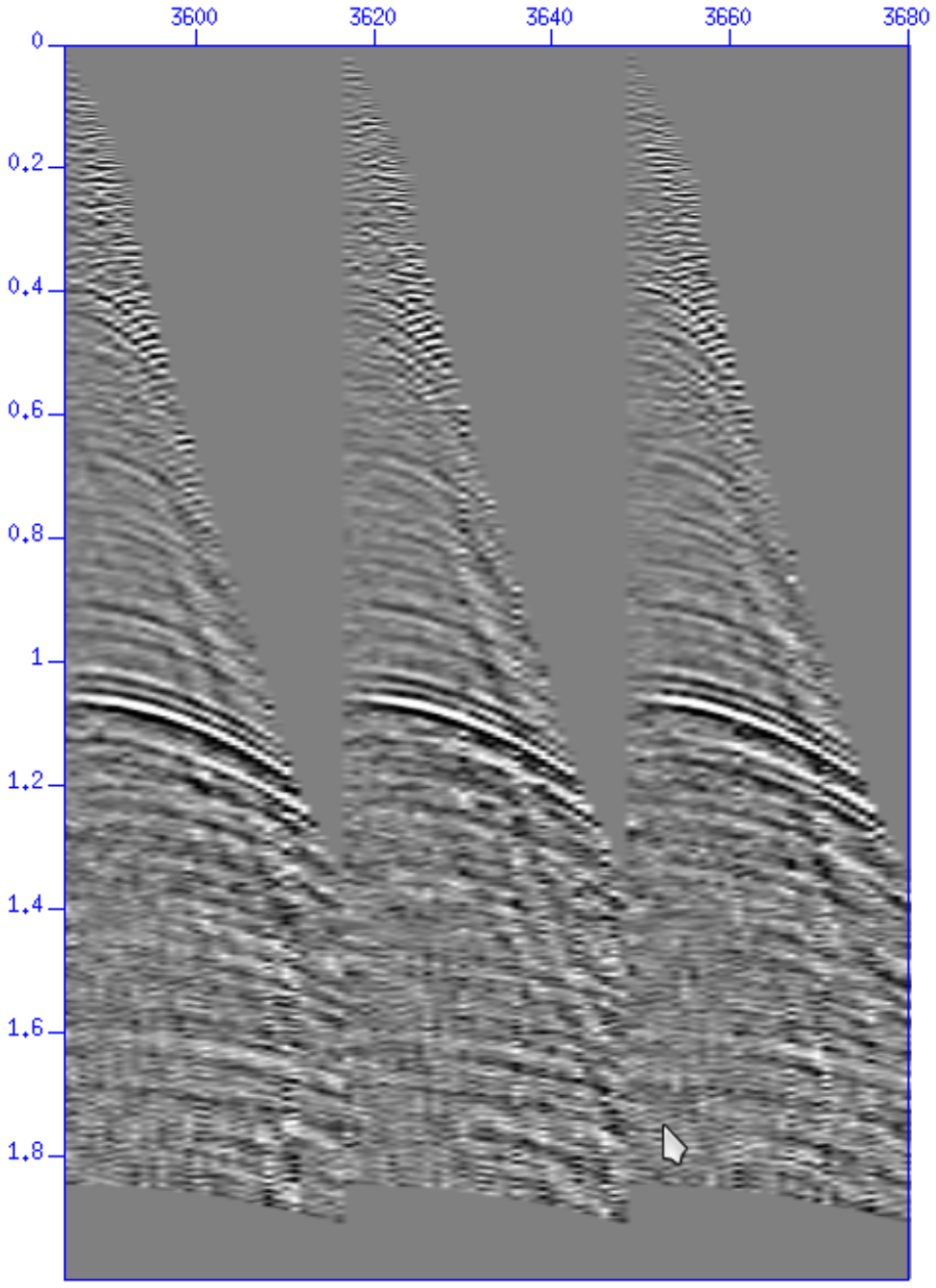

Figure 4: Three pre-stack gathers of input data.

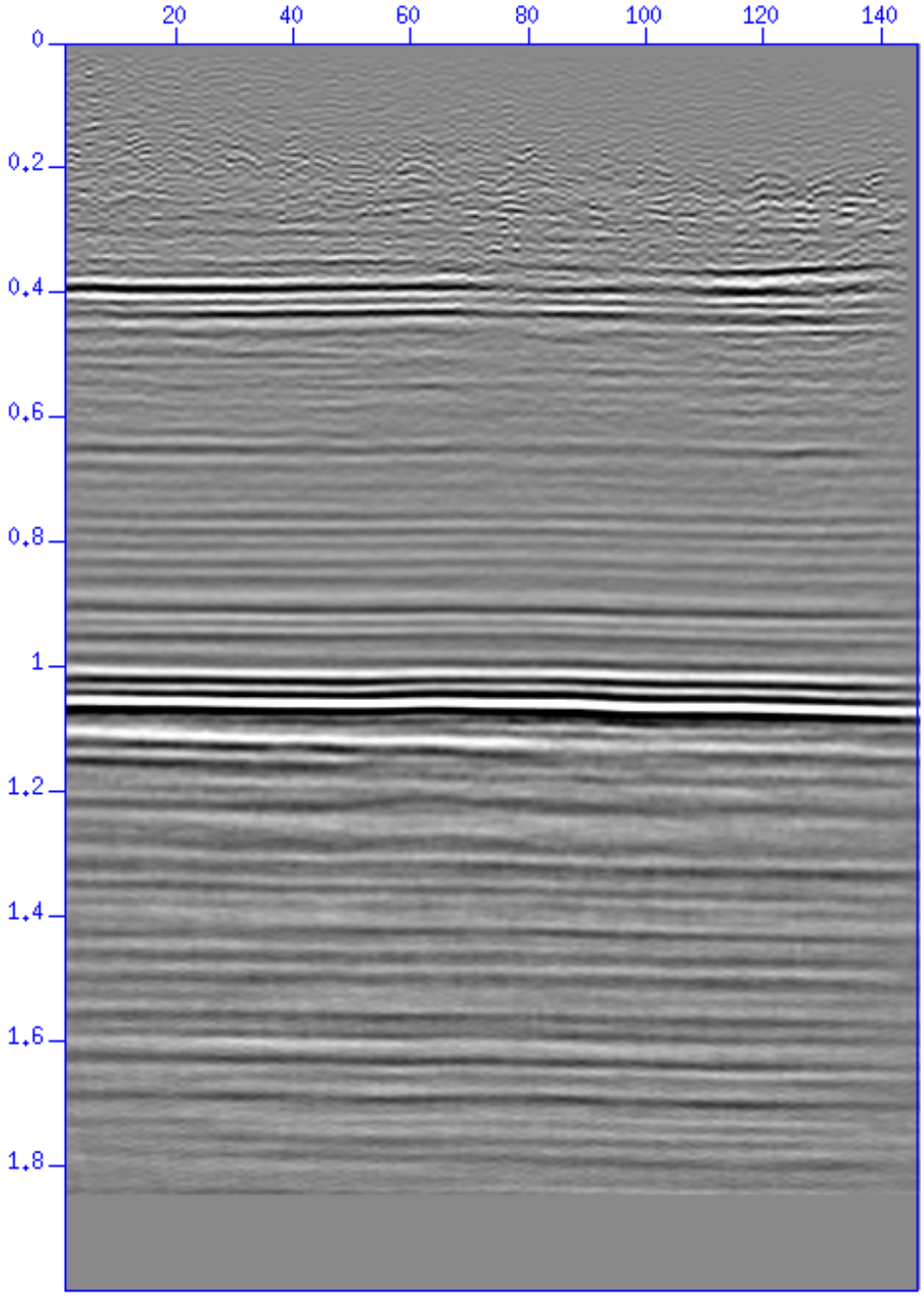

Figure 5: Stack section of input data.

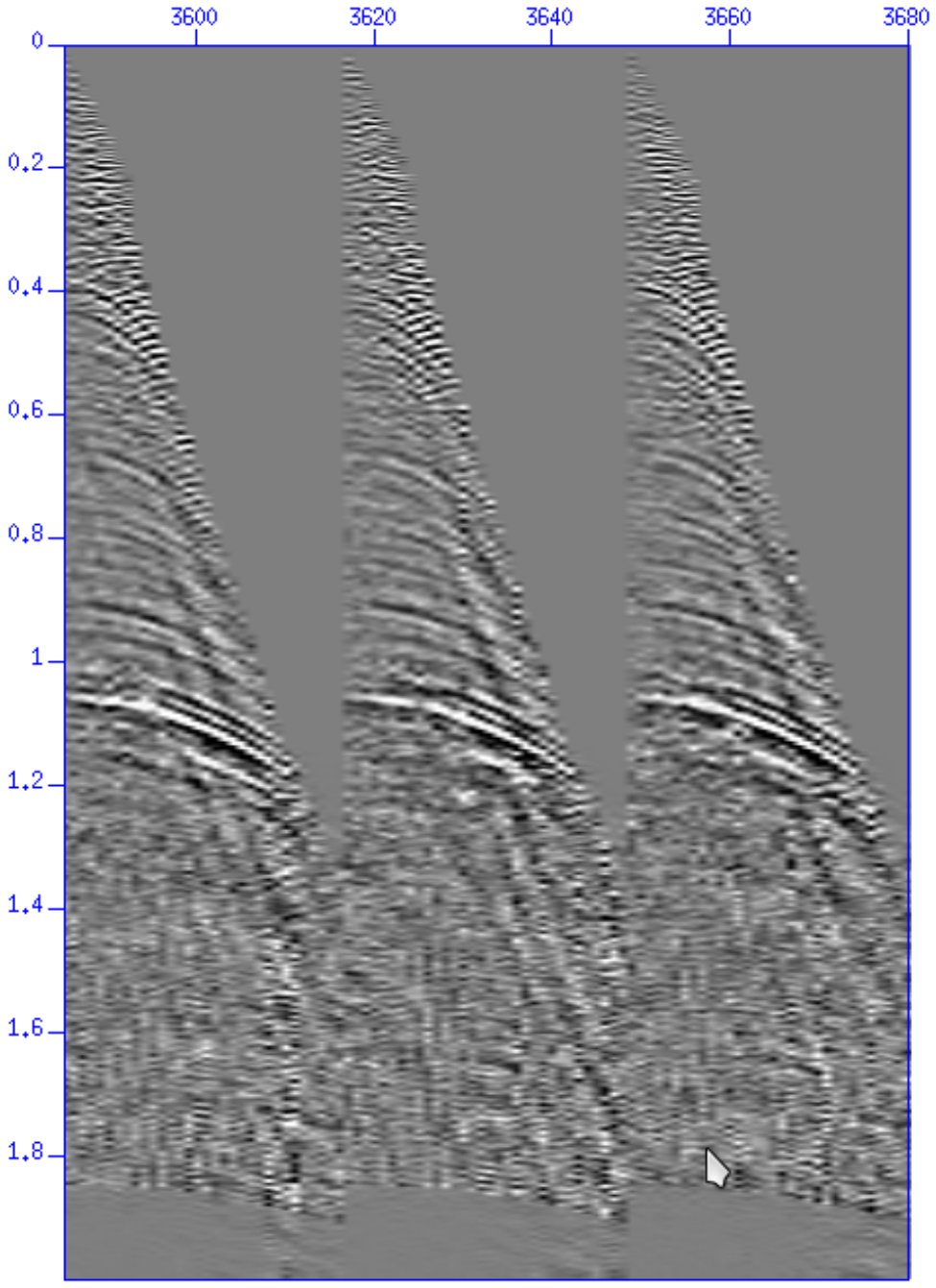

Figure 6: Three pre-stack gathers of internal multiple attenuation result.

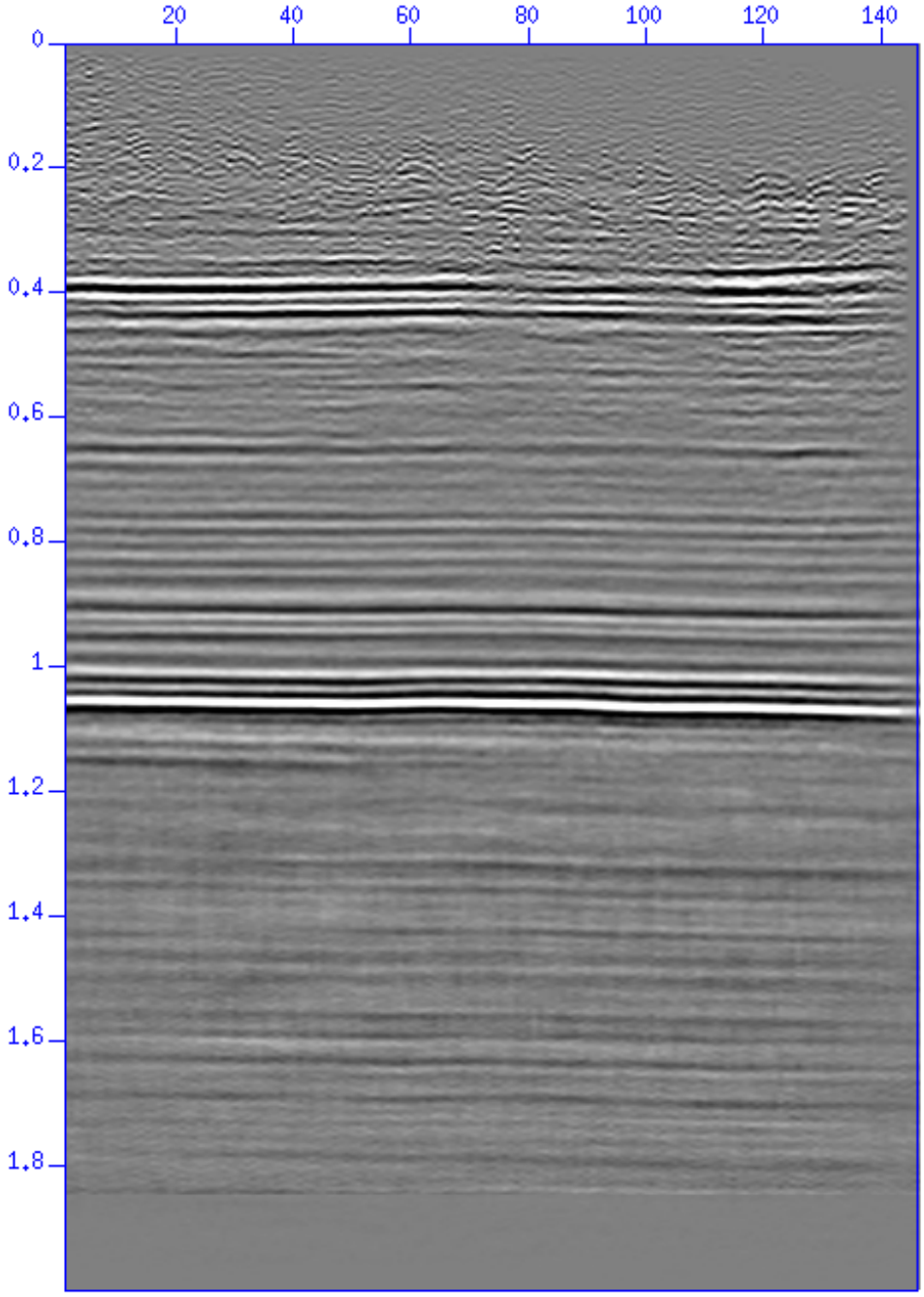

Figure 7: Stack section of internal multiple attenuation result.

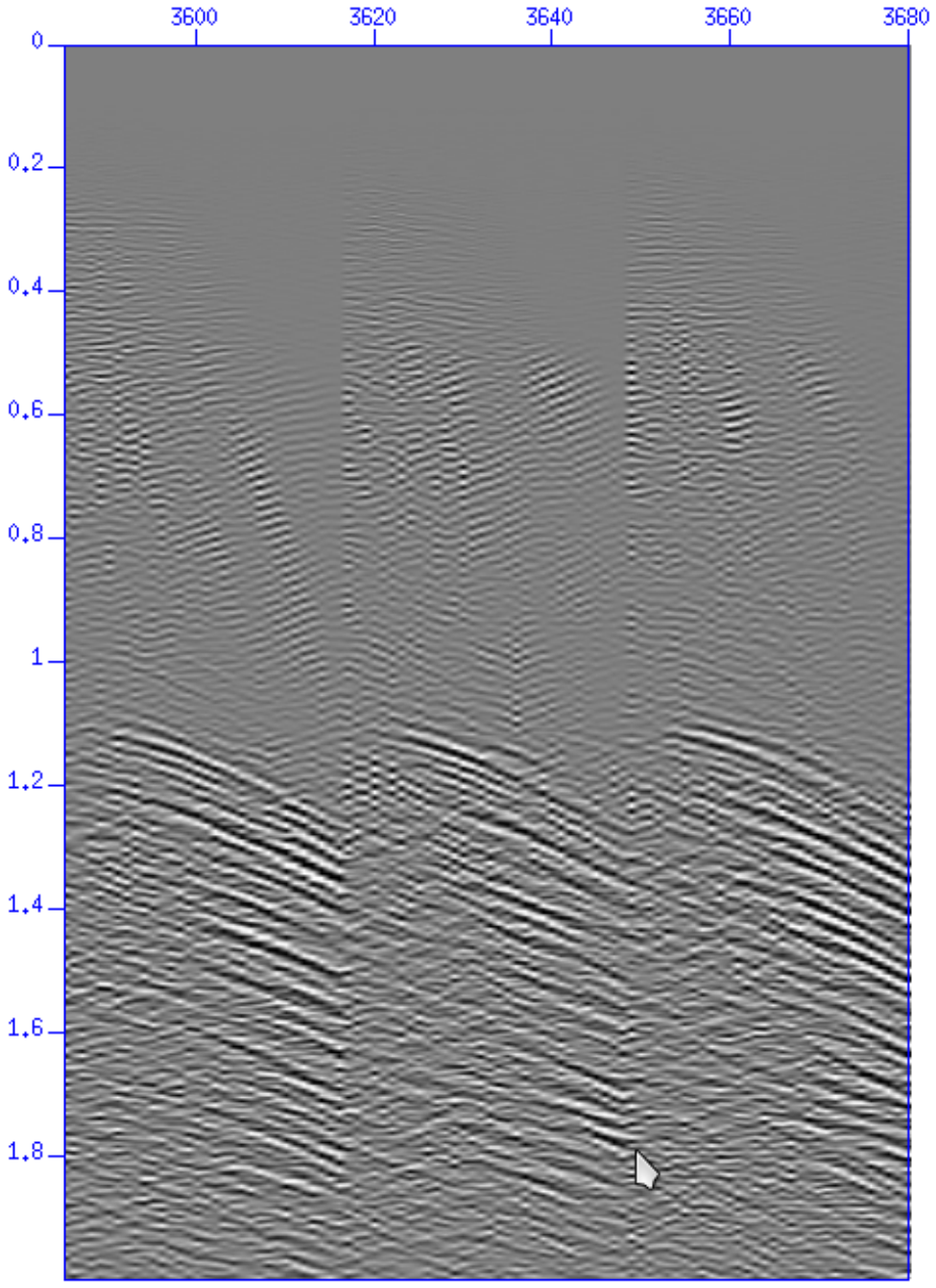

Figure 8: Three pre-stack gathers of internal multiple prediction.

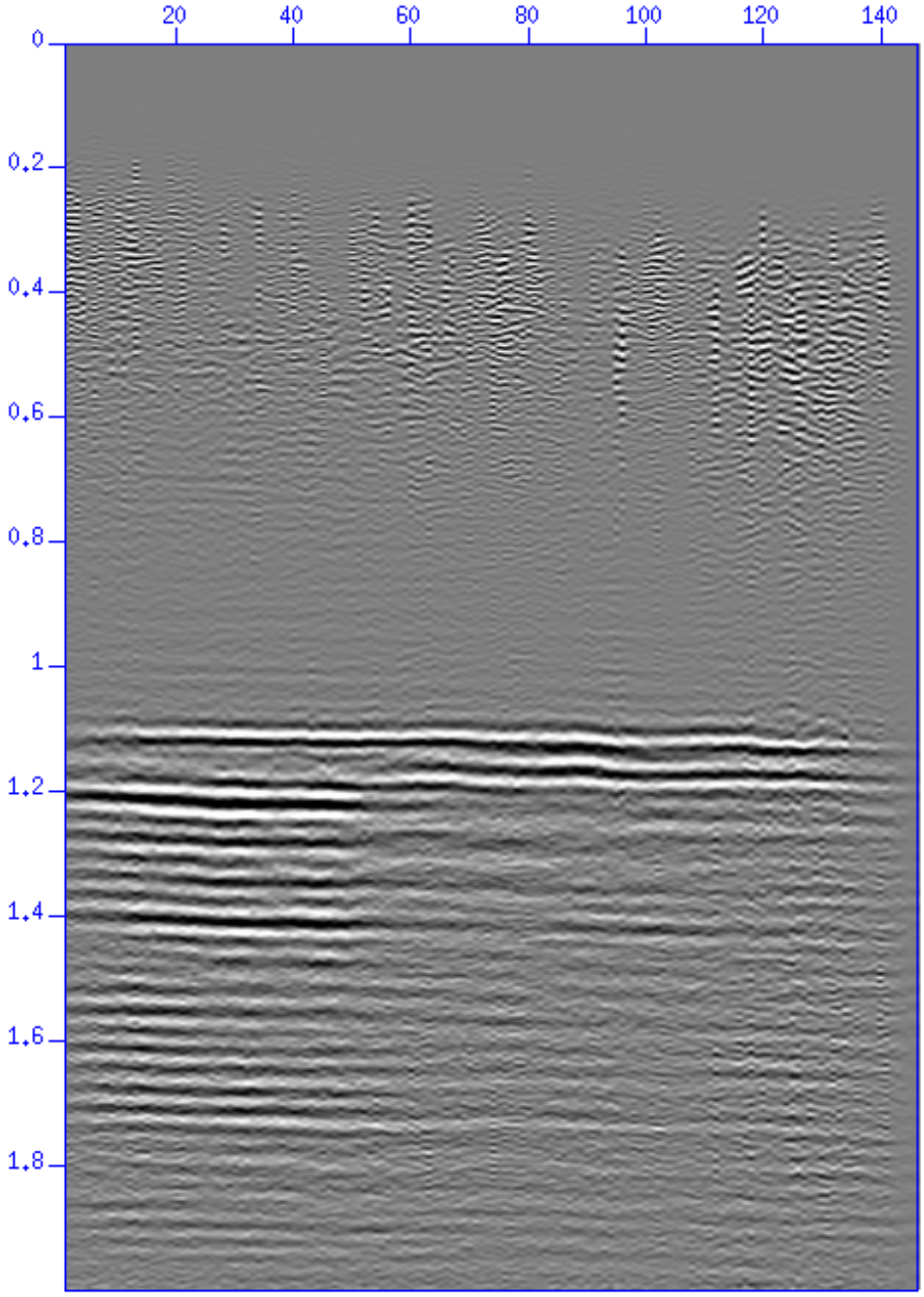

Figure 9: Stack section of internal multiple prediction.

Matson, K., D. Corrigan, A. B. Weglein, C. Y. Young, and P. Carvalho. "Inverse scattering internal multiple attenuation: Results from complex synthetic and field data examples." *69th Annual International Meeting, SEG, Expanded Abstracts* (1999): 1060–1063.

Terenghi, Paolo. "Informal M-OSRP memo on 'initial EnCana post-stack data ISS attenuation tests'." (2011).

Weglein, A. B., F. V. Araújo, P. M. Carvalho, R. H. Stolt, K. H. Matson, R. T. Coates, D. Corrigan, D. J. Foster, S. A. Shaw, and H. Zhang. "Inverse Scattering Series and seismic exploration." *Inverse Problems* (2003): R27–R83.

Weglein, A. B., F. A. Gasparotto, P. M. Carvalho, and R. H. Stolt. "An Inverse-Scattering Series method for attenuating multiples in seismic reflection data." *Geophysics* 62 (November-December 1997): 1975–1989.

Beyond internal multiple attenuation: (a) Removing artifacts/spurious events, (b) internal multiple elimination

Inverse Scattering Series (ISS) leading-order internal-multiple-attenuation algorithm and higher-order modification to accommodate primaries and internal multiples as input: 1-D normal incident test on interfering events, and extension to multi-D

Chao Ma and Arthur B. Weglein

May 21, 2014

Abstract

The strength of the ISS internal-multiple-attenuation algorithm is that it can predict all internal multiples with accurate time and approximate amplitude generated by any reflectors below the free surface at once, directly and without any sub-surface information and interpretative intervention. That strength is always present, independent of the circumstances and complexity of the geology, and enables this algorithm to be the most capable algorithm currently available for attenuating internal multiples. However, this algorithm also has limitations. For example, one open issue is that it can produce spurious events (events that do not exist in the data) when the input data are generated by three or more reflectors and internal multiples in the input are treated as subevents. That spurious-events issue is a problem only for the ISS leading-order term (the term used to derive the current ISS internal-multiple-attenuation algorithm); specific higher-order terms from ISS will remove those spurious events. A new higher-order ISS internal-multiple-attenuation algorithm is developed to effectively address the spurious predictions generated by the current leading-order ISS internal-multiple-attenuation algorithm while at the same time retaining the current algorithm's recognized strength.

In last year's Annual Report, the higher-order ISS internal-multiple-attenuation algorithm for addressing spurious predictions is tested using analytic and synthetic data generated from a three-reflector model. In this report, we focus on examining the effects of spurious predictions by using realistic well-log-based data sets and show the significance and value of including higher-order ISS terms to address the spurious predictions.

1 Introduction

The ISS internal-multiple-attenuation algorithm was first developed by Araújo (1994) and Weglein et al. (1997). The first term in this algorithm is the input data consisting of primaries and internal multiples. The second term is called the first-order internal-multiple attenuator; it uses the input data to predict the first-order internal multiples with accurate time and approximate amplitude.

The third term is called the second-order internal-multiple attenuator; it uses the input data to predict the second-order internal multiples with accurate time and approximate amplitude. In the same manner, the following terms in this algorithm use the input data to predict the third-order, fourth-order and higher-order internal multiples with accurate time and approximate amplitude. These predictions of internal multiples of different orders effectively attenuate internal multiples of different orders in the input data.

In this report, we restrict our analysis to the prediction and attenuation of first-order internal multiples. To predict the first-order internal multiples, the first-order internal-multiple attenuator treats all the events in the input data as subevents and combines three subevents nonlinearly (Weglein et al., 2003). When all three subevents are primaries, a first-order internal multiple with accurate time and approximate amplitude will be predicted (see Figure 1 and more details in the next section). This prediction will attenuate the first-order internal multiples in the data.

When internal multiples in the input data themselves act as subevents in the first-order internal-multiple attenuator, two types of events are predicted. One type is higher-order internal multiples (Zhang and Shaw, 2010); the other type is spurious/false events that do not exist in the data (Weglein et al., 2011; Ma et al., 2011; Liang et al., 2011) (see more details in section 3).

It can be shown that the first type of events (i.e., higher-order internal multiples predicted by the first-order internal-multiple attenuator) will alter the higher-order internal multiples and thereby assist the higher-order internal-multiple attenuator to attenuate the higher-order internal multiples in the data. Therefore, the prediction of higher-order internal multiples from the first-order internal-multiple attenuator is a benefit and asset.

It can also be shown that the second type of events (i.e., spurious events) is fully anticipated by the Inverse Scattering Series, and specific higher-order terms from the ISS will precisely address those spurious events (Weglein et al., 2011; Ma et al., 2011; Liang et al., 2011), and taken together with the first-order internal-multiple attenuator, first-order internal multiples will be predicted (with accurate time and approximate amplitude) for effectively attenuating the first-order internal multiples in the data, and no spurious events will be produced at the same time.

2 The ISS leading-order internal-multiple-attenuation algorithm

The ISS leading-order internal-multiple-attenuation algorithm starts with the input data, $D(k_g, k_s, \omega)$, in 2D, which are the Fourier transform of the deghosted prestack data with the wavelet deconvolved and the free-surface multiples removed. The second term is the first-order internal-multiple attenuator for the prediction of the first-order internal multiples. In a 2D earth, this prediction is (Weglein et al., 2003)

$$b_3(k_g, k_s, \omega) = \frac{1}{(2\pi)^2} \int_{-\infty}^{\infty} dk_1 \int_{-\infty}^{\infty} dk_2 e^{-iq_1(z_g - z_s)} e^{iq_2(z_g - z_s)} \times \int_{-\infty}^{\infty} dz_1 b_1(k_g, k_1, z_1) e^{i(q_g + q_1)z_1}$$

$$\times \int_{-\infty}^{z_1-\epsilon} dz_2 b_1(k_1, k_2, z_2) e^{-i(q_1+q_2)z_2}$$
$$\times \int_{z_2+\epsilon}^{\infty} dz_3 b_1(k_2, k_s, z_3) e^{i(q_2+q_s)z_3}, \quad (1)$$

where ω is temporal frequency; k_s and k_g are the horizontal wavenumbers for the source and receiver coordinates, respectively; q_g and q_s are the vertical source and receiver wavenumbers defined by $q_i = sgn(\omega)\sqrt{\frac{\omega^2}{c_0^2} - k_i^2}$ for $i \in \{g, s\}$; z_s and z_g are source and receiver depths; and z_j ($i \in \{1, 2, 3\}$) represents pseudo-depth by using a reference velocity migration. The quantity $b_1(k_g, k_s, z)$ corresponds to an uncollapsed migration (Weglein et al., 1997) of effective plane-wave incident data.

The data with their first-order internal multiple attenuated are

$$D(k_g, k_s, \omega) + D_3(k_g, k_s, \omega), \quad (2)$$

where $b_3(k_g, k_s, \omega) = -2iq_s D_3(k_g, k_s, \omega)$.

For a 1-D earth and a normal incident plane wave, equation 1 reduces to

$$b_3(k) = \int_{-\infty}^{\infty} dz_1 e^{ikz_1} b_1(z_1) \int_{-\infty}^{z_1-\epsilon} dz_2 e^{-ikz_2} b_1(z_2) \int_{z_2+\epsilon}^{\infty} dz_3 e^{ikz_3} b_1(z_3). \quad (3)$$

The deghosted data, $D(t)$, for an incident spike wave, satisfy $D(\omega) = b_1(\frac{2\omega}{c_0})$, $D(\omega)$ is the temporal Fourier transform of $D(t)$, $b_1(z) = \int_{-\infty}^{\infty} e^{ikz} b_1(k) dk$, and $k = \frac{2\omega}{c_0}$ is the vertical wavenumber.

Equation 2 then reduces to

$$D(t) + D_3(t), \quad (4)$$

where $D_3(t)$ is Inverse Fourier transform of $D_3(\omega)$, and $D_3(\omega) = b_3(k)$ for incident spike data.

The idea behind using equation 1 or 3 to predict the first-order internal multiple is treating events in the data as subevents, and combining different primary subevents satisfying " lower(A)-higher(B)-lower(C) " requirement in pseudo-depth domain, see Figure 1.

We denote the three primary-subevents combination as "PPP", where P stands for primary.

As its distinct advantages are recognized in Weglein et al. (2011), challenges and limitations are also pointed out in that paper. For example, spurious prediction can be produced at time when there are three or more reflectors and internal multiples themselves act as subevents. In next section, we will briefly review the generation of those spurious prediction and proposed algorithms to reduce them (Ma et al., 2011; Liang et al., 2011).

3 The higher-order modification of the ISS internal-multiple leading-order algorithm

Early work of Araújo (1994) and Weglein et al. (1997) focuses on the analysis of the leading-order prediction of first-order internal multiples by treating primaries in the data as subevents. However,

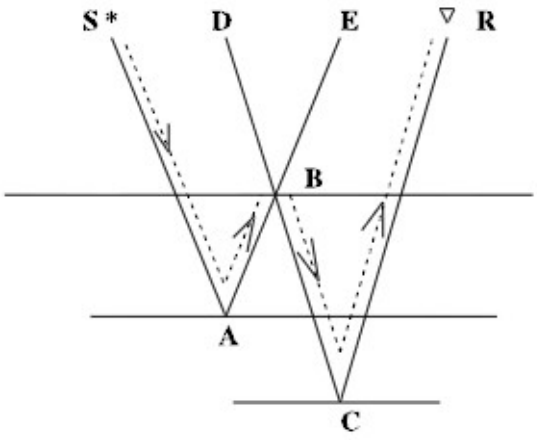

Figure 1: Combination of subevents for the first-order internal multiple (dashed line), $(SABE)_{time}+(DBCR)_{time}-(DBE)_{time}=(SABCR)_{time}$, figure adapted from Weglein et al. (2003)

data consist of both primaries and internal multiples. Hence the internal multiples are inevitably also treated as subevents. There are many other possible subevent combinations in addition to PPP, when both primaries and internal multiples are treated as subevents:

$$\begin{aligned} b_3 &= b_1 * b_1 * b_1 \\ &= (P+I)(P+I)(P+I) \\ &= PPP + PPI + PIP + IPP + PII + IPI + IIP + III, \end{aligned} \tag{5}$$

where $*$ stands for the nonlinear interaction between the data in equation 1, and P and I stand for primaries and internal multiples. Notice that we use the above expression to categorize different possible subevent combinations.

When internal multiples are treated as subevents, Zhang and Shaw (2010) use a two-reflector model to show that a second-order internal multiple can be predicted (see Figure 2); Ma et al. (2011) and Liang et al. (2011) use three-reflector and four-reflector examples to show that spurious events are generated, respectively (see Figures 3 and 4).

It is worth noting that because of the "lower-higher-lower" requirement of the algorithm (see Figure 1), the spurious event in Figure 3 (i.e., P_3–I_{212}–P_3), can be generated only when the arrival time of the third primary (P_3) is greater than that of the internal multiple (I_{212}). Otherwise, this spurious event would not be produced.

In Figure 4, the condition for the prediction of spurious event (i.e., P_4–P_3–I_{212}) is that the arrival time of the third primary (P_3) is smaller than that of the internal multiple (I_{212}).

Ma et al. (2011) and Liang et al. (2011) also isolated higher-order terms in 1-D from ISS to address the two types of spurious events, see equation 6 and 7,

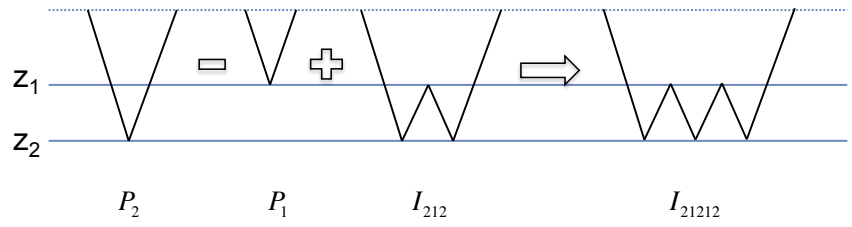

In a two reflector example, a "Primary-Primary-Internal multiple (***PPI***)" combination predicts a second-order internal multiple.

Figure 2: Subevent diagram for the prediction of a second-order internal multiple.

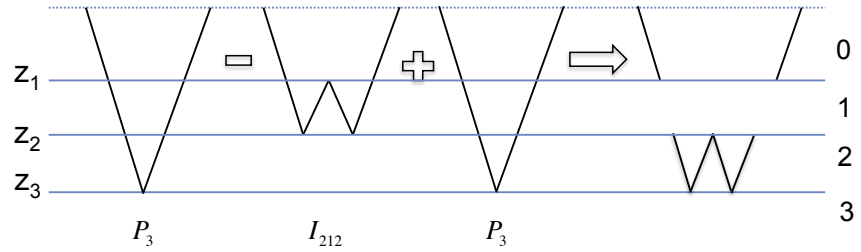

In a three reflector example, a "Primary-Internal multiple-Primary (***PIP***)" combination predicts a spurious event.

Figure 3: Subevent diagram for the prediction of a ***PIP*** spurious event, where $z_3 > (2z_2 - z_1)$.

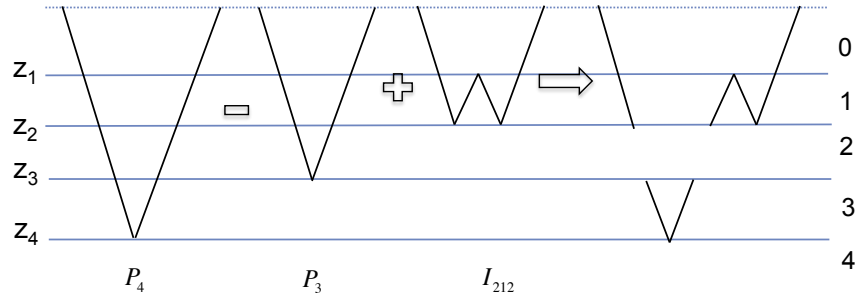

In a four reflector example, a "Primary-Primary-Internal multiple (***PPI***)" combination predicts another type of spurious event.

Figure 4: Subevent diagram for the prediction of a ***PPI*** spurious event, where $z_3 < (2z_2 - z_1)$.

$$b_5^{PIP}(k) = \int_{-\infty}^{\infty} dz_1 e^{ikz_1} b_1(z_1) \int_{-\infty}^{z_1-\epsilon} dz_2 e^{-ikz_2} b_3(z_2) \int_{z_2+\epsilon}^{\infty} dz_3 e^{ikz_3} b_1(z_3), \tag{6}$$

and

$$b_5^{PPI}(k) = 2\int_{-\infty}^{\infty} dz_1 e^{ikz_1} b_3(z_1) \int_{-\infty}^{z_1-\epsilon} dz_2 e^{-ikz_2} b_1(z_2) \int_{z_2+\epsilon}^{\infty} dz_3 e^{ikz_3} b_1(z_3), \tag{7}$$

where $b_1(z)$ is the same as in equation 3, and $b_3(z) = \int_{-\infty}^{\infty} e^{ikz} b_3(k) dk$. The superscripts PIP and PPI in equations 6 and 7 indicate that higher-order terms, b_5^{PIP} and b_5^{PPI}, are included to address the spurious prediction generated by Primary–Internal multiple–Primary and Primary-Primary-Internal multiple, respectively. The factor of 2 is used in equation 7 because an internal multiple can act as a subevent in either the innermost integral or the outermost integral.

By including the higher-order terms in equations 6 and 7, the proposed new algorithm in 1-D is (Liang et al., 2011):

$$D(t) + D_3(t) + D_5^{PIP}(t) + D_5^{PPI}(t), \tag{8}$$

where $D_3(t)$, $D_5^{PIP}(t)$ and $D_5^{PPI}(t)$ are Inverse Fourier transforms of $D_3(\omega)$, $D_5^{PIP}(\omega)$ and $D_5^{PPI}(\omega)$, respectively, and $D_5^{PIP}(\omega) = b_5^{PIP}(k)$ and $D_5^{PPI}(\omega) = b_5^{PPI}(k)$ for incident spike data, $k = \frac{2\omega}{c_0}$.

It should be mentioned that, in the cases where there are only three reflectors, only D_5^{PIP} is needed because PPI-type spurious events arise only when there are four or more reflectors.

4 1-D normal incident example with interfering primaries and internal multiples

In Ma et al. (2011) and Liang et al. (2011), the term D_5^{PIP} term (equation 6) is tested in a three-reflector example by using analytic and synthetic data, respectively. In this section, we test both the D_5^{PIP} and D_5^{PPI} terms by using more realistic and practical synthetic data (generated by many reflectors with interfering primaries and internal multiples), compare the reference internal multiples to the prediction results with/without the inclusion of higher-order terms.

The model (see Figure 5) used to generate the 1-D normal incident data is from blocked velocity and density well-log data (courtesy of Kuwait Oil Company). It has more than 30 layers, so that primaries and internal multiples are no longer isolated from each other. The reflectivity method is used to generate the primary-only and primary-and-internal-multiple synthetic data with a source ricker wavelet of peak frequency at 25Hz.

The comparison among the true/reference internal multiples (blue line), leading-order prediction (red line), and leading-order plus higher-order prediction (green line) is shown in Figure 6, where black arrows point to the significant improvement. The top panel and bottom panel traveltime ranges are from 3.6s to 4.2s and 4.2s to 4.9s, respectively. It is worth noting (for the purpose of comparison with the true internal multiples) that the red and green plots are the negatives of the leading-order prediction and the leading-order plus higher-order prediction, respectively — i.e., the red plot is $-D_3(t)$ and the green plot is $-(D_3(t) + D_5^{PIP} + D_5^{PPI})$.

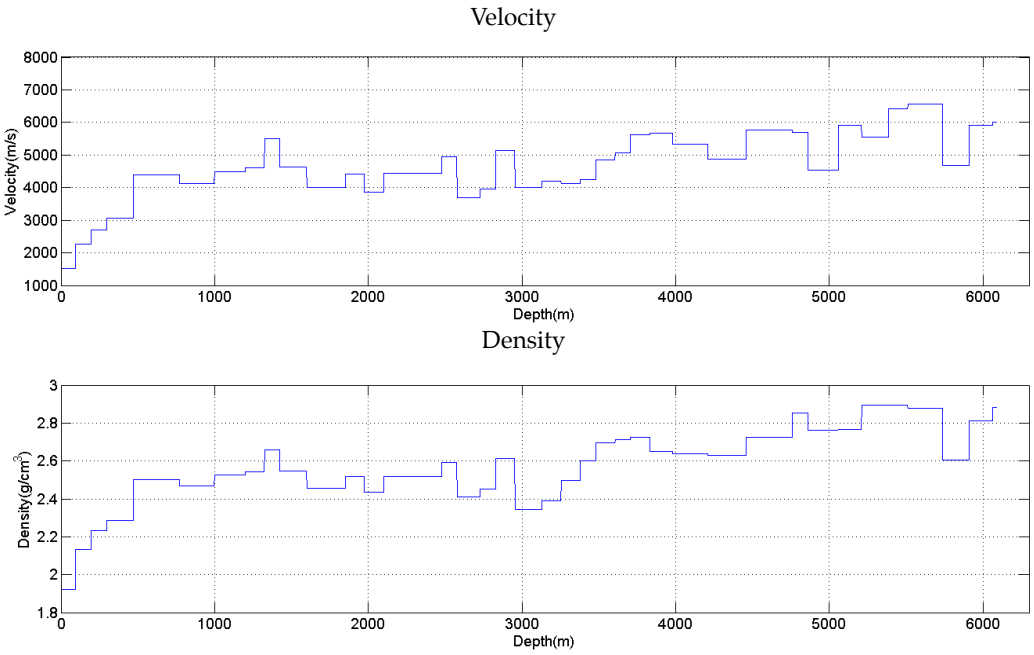

(data courtesy of KOC)

Figure 5: Velocity and density blocking from well-log data.

5 Extension to multi-D

The proposed algorithm and tests in Ma et al. (2011) and Liang et al. (2013) assume that earth properties vary only in depth — i.e., that the earth is 1-D. In this section, we propose the algorithm for use in multiple dimensions. Extending the derivation of equation 1 in Araújo (1994), we provide the higher-order term D_5^{PIP} in 2D,

$$\begin{aligned} b_5^{PIP}(k_g,k_s,\omega) = \frac{1}{(2\pi)^2}\int_{-\infty}^{\infty} dk_1 \int_{-\infty}^{\infty} dk_2 e^{-iq_1(z_g-z_s)} e^{iq_2(z_g-z_s)} \\ \times \int_{-\infty}^{\infty} dz_1 b_1(k_g,k_1,z_1) e^{i(q_g+q_1)z_1} \\ \times \int_{-\infty}^{z_1-\epsilon} dz_2 b_3(k_1,k_2,z_2) e^{-i(q_1+q_2)z_2} \\ \times \int_{z_2+\epsilon}^{\infty} dz_3 b_1(k_2,k_s,z_3) e^{i(q_2+q_s)z_3}, \end{aligned} \tag{9}$$

where $b_3(k_g,k_s,z)$ is an uncollapsed migration of the leading-order prediction. As in the 1-D case, the difference between equation 1 and 9 is the middle integrand.

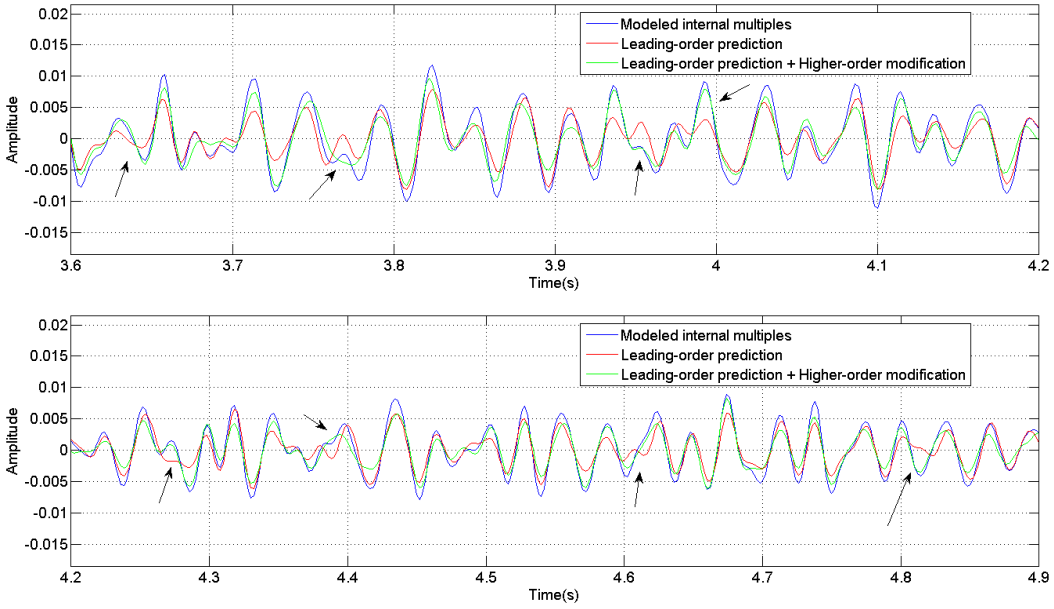

(data courtesy of KOC)

Figure 6: A comparison among the true internal multiples in blue, the leading-order prediction in red, and the leading-order plus higher-order prediction in green.

In a three-reflector case, the algorithm in multi-D is

$$D(k_g, k_s, \omega) + D_3(k_g, k_s, \omega) + D_5^{PIP}(x_g, x_s, \omega) \tag{10}$$

where $b_5^{PIP}(k_g, k_s, \omega) = -2iq_s D_5^{PIP}(k_g, k_s, \omega)$.

To test the algorithm in 2-D — i.e., equation 9 — we need to first modify the current code of leading-order prediction (equation 1) to produce the higher-order prediction (equation 9). The modification is based on the code of ISS leading-order internal-multiple prediction with angle constraint, by Terenghi and Weglein (2011).

6 Conclusions and Future plan

In this paper, we exemplified a serious shortcoming (i.e., spurious predictions) of the current ISS leading-order internal-multiple-attenuation algorithm. We develop, test and analyze the resolution with a new higher-order ISS algorithm that anticipates and removes the spurious events. This higher-order ISS internal-multiple-attenuation algorithm retains the strengths of the current leading-order ISS internal-multiple-attenuation algorithm and addresses one of its limitations.

The synthetic tests on the realistic well-log based data sets in this paper show the significance and value of including the higher-order ISS terms to address the spurious predictions.

7 Acknowledgements

We are grateful to all M-OSRP sponsors for their encouragement and support of this research. We thank: (1) the Kuwait Oil Company (KOC) Exploration/Geosolution for permission to use their well log data in studies on the ISS method (in Figure 5); (2) KOC and WesternGeco/Schlumberger management for permission to cite the results of the study; (3) Clement Kostov and WG/SLB for a very valuable internship opportunity and experience during which Chao Ma carried out the study on the KOC data. M-OSRP appreciates the close cooperation and collaboration with Panos Kelamis and his EXPEC ARC Geophysical Team, Saudi Arabian Oil Co..

References

Araújo, F. V. *Linear and non-linear methods derived from scattering theory: backscattered tomography and internal multiple attenuation.* PhD thesis, Universidade Federal da Bahia, 1994. In Portuguese.

Liang, H., C. Ma, and A.B.Weglein. "A further general modification of the leading order ISS attenuator of first order internal multiples to accommodate primaries and internal multiples when an arbitrary number of reflectors generate the data: theory, development, and examples." *Mission-Oriented Seismic Research Program (M-OSRP) Annual Report* (2011): 148–166.

Liang, H., C. Ma, and A. Weglein. "General theory for accommodating primaries and multiples in internal multiple algorithm: Analysis and numerical tests." *SEG Technical Program Expanded Abstracts* (2013): 4178–4183.

Ma, C., H. Liang, and A. Weglein. "Modifying the leading order ISS attenuator of first-order internal multiples to accommodate primaries and internal multiples: fundamental concept and theory, development, and examples exemplified when three reflectors generate the data." *Mission-Oriented Seismic Research Program (M-OSRP) 2011 Annual Report* (2011): 133–147.

Terenghi, P. and A. B. Weglein. "ISS internal multiple attenuation with angle constraints." *Mission-Oriented Seismic Research Program (M-OSRP) Annual Report* (2011): 242–266.

Weglein, A., Shih-Ying Hsu, Paolo Terenghi, Xu Li, and Robert H. Stolt. "Multiple attenuation: Recent advances and the road ahead (2011)." *The Leading Edge* (2011): 864–875.

Weglein, A. B., F. V. Araújo, P. M. Carvalho, R. H. Stolt, K. H. Matson, R. T. Coates, D. Corrigan, D. J. Foster, S. A. Shaw, and H. Zhang. "Inverse Scattering Series and Seismic Exploration." *Inverse Problems* (2003): R27–R83.

Weglein, A. B., F. A. Gasparotto, P. M. Carvalho, and R. H. Stolt. "An Inverse-Scattering Series Method for Attenuating Multiples in Seismic Reflection Data." *Geophysics* 62 (November-December 1997): 1975–1989.

Zhang, H. and S. Shaw. "1-D analytic analysis of higher order internal multiples predicted via the inverse scattering series based algorithe." *SEG Expanded Abstracts* 29 (2010): 3493–3498.

Short note: Lower-order internal multiples act as subevents in the ISS internal-multiple-attenuation algorithm in a three-reflector example

Chao Ma and Arthur B. Weglein

May 21, 2014

Abstract

The Inverse Scattering Series (ISS) first-order internal-multiple attenuator (the second term in the ISS internal-multiple-attenuation algorithm) predicts the first-order internal multiples with accurate time and approximate amplitude, directly and without subsurface information, by treating events in the input data as subevents and combining three primary subevents nonlinearly (Weglein et al., 2003). This prediction of first-order internal multiples effectively attenuates the first-order internal multiples in the data. However, the input data contain both primaries and internal multiples. When internal multiples themselves act as subevents in the first-order internal-multiple attenuator, two different types of events will be produced. The first type is higher-order internal multiples (for example, second-order internal multiples), and the second type is spurious events (events that do not exist in the data). For the second type of events, Ma et al. (2011) and Liang et al. (2011) show that the spurious events are fully foreseen by the ISS and specific terms from the ISS will precisely address that spurious-events issue. For the first type of events, we will show in this report that the prediction of higher-order internal multiples is a benefit and asset. In other words, the first-order internal-multiple attenuator not only predicts and attenuates the first-order internal multiples in the data, but also predicts higher-order internal multiples and cooperatively assists and benefits the ISS higher-order internal-multiple attenuators for attenuating of higher-order internal multiples in the data.

1 Introduction

The ISS internal-multiple-attenuation algorithm starts with the input data, $D(k_g, k_s, \omega)$ in 2D, which are the Fourier transform of the deghosted prestack data with the wavelet deconvolved and the free-surface multiples removed. In a 2D earth, the second term is the ISS first-order internal-multiple attenuator is (Araújo, 1994)

$$b_3(k_g, k_s, \omega) = \frac{1}{(2\pi)^2} \int_{-\infty}^{\infty} dk_1 \int_{-\infty}^{\infty} dk_2 e^{-iq_1(z_g - z_s)} e^{iq_2(z_g - z_s)} \times \int_{-\infty}^{\infty} dz_1 b_1(k_g, k_1, z_1) e^{i(q_g + q_1)z_1}$$

$$\times \int_{-\infty}^{z_1-\epsilon} dz_2 b_1(k_1, k_2, z_2) e^{-i(q_1+q_2)z_2}$$
$$\times \int_{z_2+\epsilon}^{\infty} dz_3 b_1(k_2, k_s, z_3) e^{i(q_2+q_s)z_3}, \quad (1)$$

where ω is temporal frequency; k_s and k_g are the horizontal wavenumbers for the source and receiver coordinates, respectively; q_g and q_s are the vertical source and receiver wavenumbers defined by $q_i = sgn(\omega)\sqrt{\frac{\omega^2}{c_0^2} - k_i^2}$ for $i \in \{g, s\}$; z_s and z_g are source and receiver depths; and z_j ($i \in \{1, 2, 3\}$) represents pseudo-depth using a reference velocity migration. The quantity $b_1(k_g, k_s, z)$ corresponds to an uncollapsed migration (Weglein et al., 1997) of effective plane-wave incident data.

The data with their first-order internal multiples attenuated are

$$D(k_g, k_s, \omega) + D_3(k_g, k_s, \omega), \quad (2)$$

where $b_3(k_g, k_s, \omega) = -2iq_s D_3(k_g, k_s, \omega)$.

Early work of Araújo (1994) focused on combining primaries as subevents to predict first-order internal multiples. However, the input data contain both primaries and internal multiples. Internal multiples acting as subevents in the ISS internal-multiple-attenuation algorithm were first studied by Zhang and Shaw (2010) using a two-reflector example. Their work shows that a second-order internal multiple is predicted by b_3 (the leading-order prediction of first-order internal multiples) when a first-order internal multiple acts as one subevent. Ma and Weglein (2012) further point out that this prediction of second-order internal multiples from b_3, combined with the second-order internal-multiple prediction from b_5, is useful for attenuating the second-order internal multiples in the data (see equation (3.11) in Ma and Weglein (2012)). This shows the cooperative nature/property of the ISS internal-multiple-attenuation algorithm. It should be mentioned that the analyses in Zhang and Shaw (2010) and Ma and Weglein (2012) use a two-reflector example. In this work, we extend the analysis to a three-reflector example. It should be mentioned that in a three-reflector example, spurious events can be produced when an internal multiple acts as a subevent. In the next section, we purposefully design the three-reflector example so that when the data generated by that three-reflector model are input in to the ISS internal multiple attenuation algorithm, the ISS first-order internal-multiple attenuator (b_3) will produce spuriou events. We will examine the effects of the prediction of second-order internal multiples from b_3 in the presence of spurious events.

2 The prediction result of ISS first-order internal-multiple attenuator in a three-reflector example

In this short note, we examine the prediction of first-order internal-multiple attenuator using a three-reflector example. The input data contain three primaries and four first-order internal multiples generated by this example, see Figure 1. Notice that, in Figure 1, only three primaries and a first-order internal multiple are plotted.

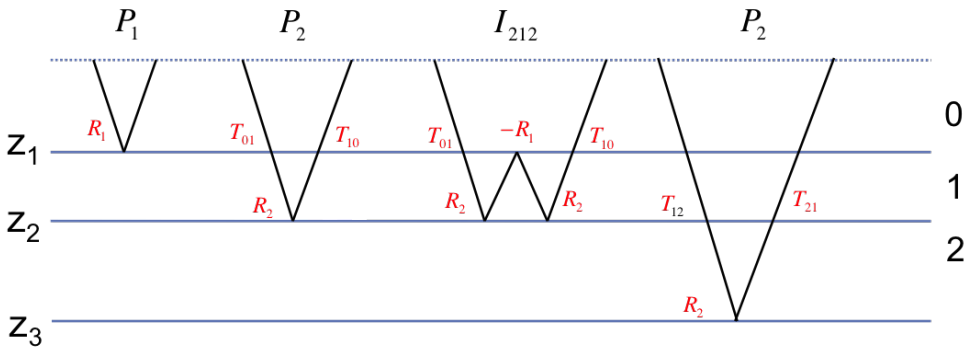

Figure 1: Definition of reflection and transmission coefficients

The arrival times of the primaries and internal multiples are t_1, t_2, $(2t_2 - t_1)$, t_3, $(t_2 + t_3 - t_1)$, $(2t_3 - t_2)$, and $(2t_3 - t_1)$. The three red terms are the arrival times of three primaries, whereas the four blue terms are the arrival times of four first-order internal multiples. The reflection coefficient from the nth reflector is defined as R_n, and the transmission coefficient from the mth medium to the nth medium is defined as T_{mn}, as shown in Figure 1.

The input data in the pseudo-depth domain are

$$\begin{aligned} D(z) = {} & R_1\delta(z - z_1) + T_{01}R_2T_{10}\delta(z - z_2) + T_{01}T_{12}R_3T_{21}T_{10}\delta(z - z_3) - R_1R_2^2T_{01}T_{10}\delta(z - (2z_2 - z_1)) \\ & - R_1R_3^2T_{01}T_{10}T_{12}^2T_{21}^2\delta(z - (2z_3 - z_1)) - R_2R_3^3T_{01}T_{10}T_{12}T_{21}\delta(z - (2z_3 - z_2)) \\ & - 2R_1R_2R_3T_{01}T_{10}T_{12}T_{21}\delta(z - (z_3 + z_2 - z_1)), \end{aligned} \tag{3}$$

where $z_i \equiv t_i \times c_0/2$, and c_0 is the reference velocity for Stolt migration. With a total of seven terms as input, we can calculate the prediction results from b_3 using

$$b_3(k) = \int_{-\infty}^{\infty} dz_1 e^{ikz_1} b_1(z_1) \int_{-\infty}^{z_1-\epsilon} dz_2 e^{-ikz_2} b_1(z_2) \int_{z_2+\epsilon}^{\infty} dz_3 e^{ikz_3} b_1(z_3). \tag{4}$$

We design the model so that $(2t_2 - t_1) < t_3$ for the production of spurious events. With the assumption of $(2t_2 - t_1) < t_3$, the explicit result [1] of b_3 using equation 3 is shown in Figure 4.

In Figure 4, the terms in green are three first-order internal multiples, the terms in orange are six second-order internal multiples, the terms in yellow are the first-order internal multiple and second-order internal multiple that have the same arrival time (see Figure 2), and the terms in red are spurious events (see Ma et al. (2011) and Liang et al. (2011)). All the other terms that are not highlighted are third-order or fourth-order internal multiples. Notice that in the result of Figure 4, we do not combine the terms that have the same arrival time for third-order or fourth-order internal multiples.

[1] We use *Mathematica* software to perform the analytic calculation

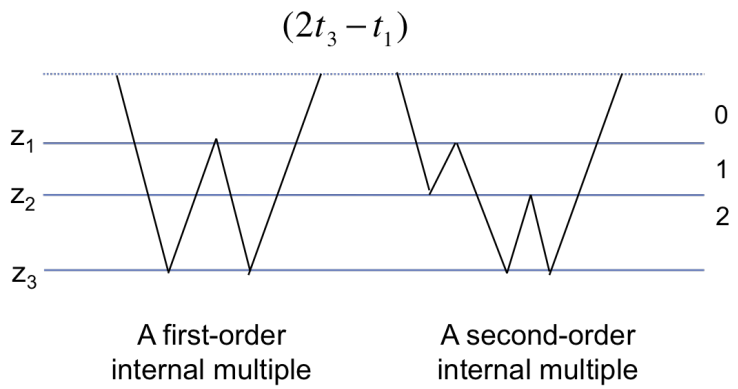

Figure 2: A same arrival time for a first-order internal multiple $(2t_3 - t_1)$ and second-order internal multiple $(2t_3 + t_2 - t_2 - t_1)$.

In this three-reflector example, both second-order internal multiples and spurious events are predicted by b_3 when internal multiples act as subevents. To examine the effects of the second-order internal-multiple prediction and spurious events from b_3 in a three reflector example, we assign $R_1 = 0.5\,(T_{01} = 1 - R_1 = 0.5; T_{10} = 1 + R_1 = 1.5), R_2 = 0.5\,(T_{12} = 1 - R_2 = 0.5; T_{21} = 1 + R_2 = 1.5), Z_1 = 10, Z_2 = 13$, and $Z_3 = 20$ in the result of Figure 4, and compare between the refere-cen/true internal multiple in the data and the reference/true internal multiple plus the prediction of b_3 (see Figure 3). In Figure 3, the three green arrows point to three first-order internal multiples, and the six orange arrows point to six second-order internal multiples. The yellow arrow points to the first-order internal multiple and the second-order internal multiple that have the same arrival time. The red arrows point to the spurious events that do not exist in the data.

Primary-only input will not predict spurious events, but then the useful second-order internal-multiple prediction also will not be predicted. Further studies are needed to help us understand how the Inverse Scattering Series overall addresses the problem. If we restrict our goal to one of effectively attenuating the first-order internal multiple, we must remove the effects of internal multiples acting as subevents in order to eliminate the prediction of spurious events.

3 Conclusion and Future plan

To conclude, on one hand internal multiples acting as subevents in b_3 will benefit the attenuation of second-order internal multiples. However, on the other hand, internal multiples acting as subevents will also produce spurious events. Further work is needed to understand how the inverse scattering series addresses this problem overall. If we restrict our goal to one of achieving attenuation of first-order internal multiples without at the same time obtaining spurious prediction, the effect of internal multiples acting as subevents should be removed.

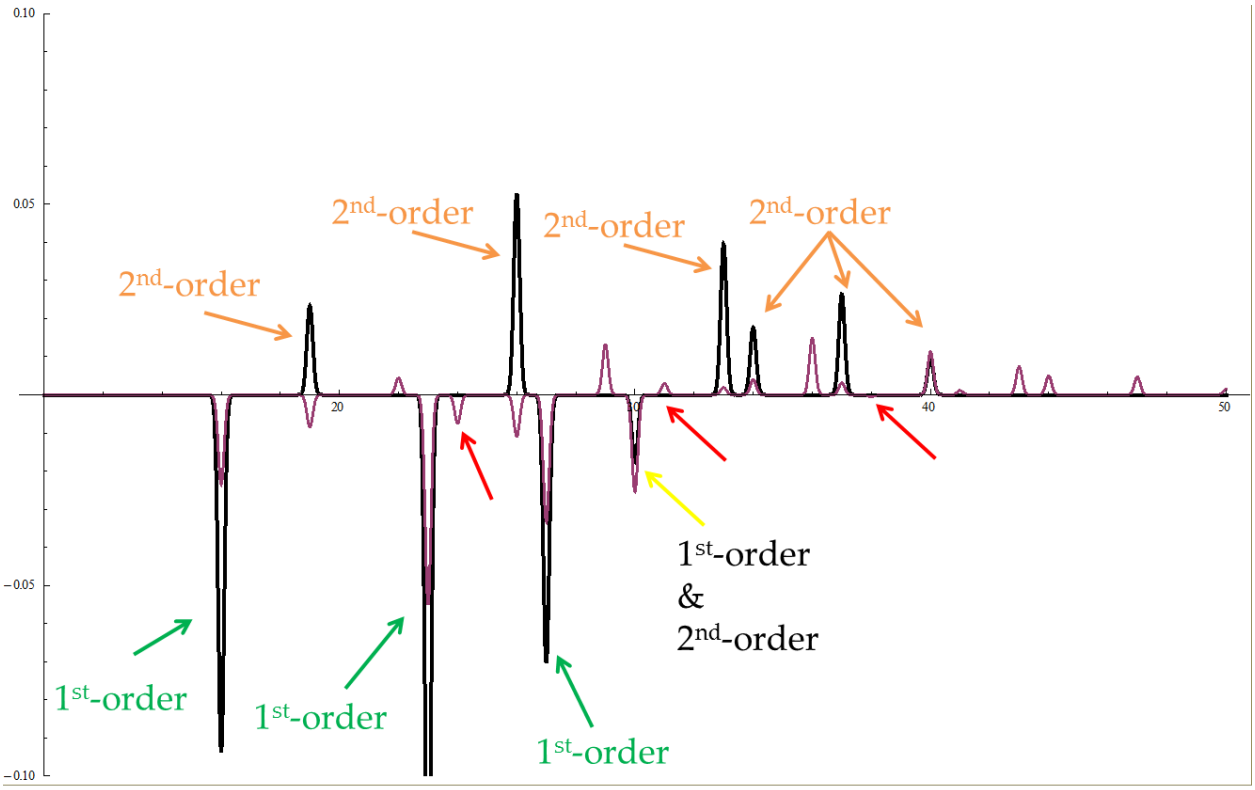

Figure 3: Comparison between the internal multiples in black (containing first-order internal multiple and second-order internal multiples) and internal multiples plus b_3 prediction in purple.

4 Acknowledgements

We are grateful to all M-OSRP sponsors for long-term encouragement and support in this research. All members in M-OSRP are thanked for their help towards finishing this report and for valuable discussions in this research program.

```
R1^3 R2^4 T01^2 T10^2 DiracDelta[z + 3 Z1 - 4 Z2] + (-2 R1^2 R2^3 T01^2 T10^2 + R1^2 R2^5 T01^3 T10^3) DiracDelta[z + 2 Z1 - 3 Z2] +
R1 R2^2 T01^2 T10^2 DiracDelta[z + Z1 - 2 Z2] + R1^3 R3^4 T01^2 T10^2 T12^4 T21^4 DiracDelta[z + 3 Z1 - 4 Z3] +
2 R1^2 R2 R3^4 T01^2 T10^2 T12^3 T21^3 DiracDelta[z + 2 Z1 + Z2 - 4 Z3] + R1^2 R2 R3^4 T01^3 T10^3 T12^4 T21^4 DiracDelta[z + 2 Z1 + Z2 - 4 Z3] +
R1 R2^2 R3^4 T01^2 T10^2 T12^2 T21^2 DiracDelta[z + Z1 + 2 Z2 - 4 Z3] + 2 R1 R2^2 R3^4 T01^3 T10^3 T12^3 T21^3 DiracDelta[z + Z1 + 2 Z2 - 4 Z3] -
R1^3 R2^2 R3^4 T01^3 T10^3 T12^4 T21^4 DiracDelta[z + Z1 + 2 Z2 - 4 Z3] + R2^3 R3^4 T01^3 T10^3 T12^2 T21^2 DiracDelta[z + 3 Z2 - 4 Z3] -
2 R1^2 R2^3 R3^4 T01^3 T10^3 T12^3 T21^3 DiracDelta[z + 3 Z2 - 4 Z3] - R1 R2^4 R3^4 T01^3 T10^3 T12^2 T21^2 DiracDelta[z - Z1 + 4 Z2 - 4 Z3] +
(4 R1^2 R2^2 R3^3 T01^2 T10^2 T12^2 T21^2 - 2 R1^2 R3^3 T01^2 T10^2 T12^3 T21^3 + 4 R1^2 R2^2 R3^3 T01^3 T10^3 T12^3 T21^3 + R1^2 R3^5 T01^3 T10^3 T12^5 T21^5)
 DiracDelta[z + 2 Z1 - 3 Z3] + 4 R1^3 R2 R3^3 T01^2 T10^2 T12^3 T21^3 DiracDelta[z + 3 Z1 - Z2 - 3 Z3] +
(-2 R1 R2 R3^3 T01^2 T10^2 T12^2 T21^2 + 4 R1 R2^3 R3^3 T01^3 T10^3 T12^2 T21^2 - 2 R1 R2 R3^3 T01^3 T10^3 T12^3 T21^3 -
   4 R1^3 R2^3 R3^3 T01^3 T10^3 T12^3 T21^3 + 2 R1 R2 R3^5 T01^3 T10^3 T12^4 T21^4 - 2 R1^3 R2 R3^5 T01^3 T10^3 T12^5 T21^5)
 DiracDelta[z + Z1 + Z2 - 3 Z3] +
(-2 R2^2 R3^3 T01^3 T10^3 T12^2 T21^2 - 4 R1^2 R2^4 R3^3 T01^3 T10^3 T12^2 T21^2 + 2 R1^2 R2^2 R3^3 T01^3 T10^3 T12^3 T21^3 +
   R2^2 R3^5 T01^3 T10^3 T12^3 T21^3 - 4 R1^2 R2^2 R3^5 T01^3 T10^3 T12^4 T21^4) DiracDelta[z + 2 Z2 - 3 Z3] +
2 R1 R2^3 R3^3 T01^3 T10^3 T12^2 T21^2 DiracDelta[z - Z1 + 3 Z2 - 3 Z3] - 2 R1 R2^3 R3^5 T01^3 T10^3 T12^3 T21^3 DiracDelta[z - Z1 + 3 Z2 - 3 Z3] +
(-2 R1 R2^2 R3^2 T01^2 T10^2 T12 T21 + 2 R1 R2^4 R3^2 T01^3 T10^3 T12 T21 + R1 R3^2 T01^2 T10^2 T12^2 T21^2 - 4 R1 R2^2 R3^2 T01^3 T10^3 T12^2 T21^2 -
   4 R1^3 R2^4 R3^2 T01^3 T10^3 T12^2 T21^2 + 4 R1 R2^2 R3^4 T01^3 T10^3 T12^3 T21^3) DiracDelta[z + Z1 - 2 Z3] +
(2 R1^2 R2^3 R3^2 T01^2 T10^2 T12 T21 - 6 R1^2 R2 R3^2 T01^2 T10^2 T12^2 T21^2 + 6 R1^2 R2^3 R3^2 T01^3 T10^3 T12^2 T21^2 +
   4 R1^2 R2 R3^4 T01^3 T10^3 T12^4 T21^4 - R1^2 R2 R3^6 T01^3 T10^3 T12^5 T21^5) DiracDelta[z + 2 Z1 - Z2 - 2 Z3] +
(R2 R3^2 T01^3 T10^3 T12^2 T21^2 + 4 R1^2 R2^3 R3^2 T01^3 T10^3 T12^2 T21^2) DiracDelta[z + Z2 - 2 Z3] -
R1 R2^2 R3^2 T01^3 T10^3 T12^2 T21^2 DiracDelta[z - Z1 + 2 Z2 - 2 Z3] + 4 R1^3 R2^3 R3 T01^2 T10^2 T12 T21 DiracDelta[z + 3 Z1 - 3 Z2 - Z3] +
(-6 R1^2 R2^2 R3 T01^2 T10^2 T12 T21 + 4 R1^2 R2^4 R3 T01^3 T10^3 T12 T21 + 4 R1^2 R2^2 R3^3 T01^3 T10^3 T12^3 T21^3) DiracDelta[z + 2 Z1 - 2 Z2 - Z3] +
(2 R1 R2 R3 T01^2 T10^2 T12 T21 - 2 R1 R2^3 R3 T01^3 T10^3 T12 T21) DiracDelta[z + Z1 - Z2 - Z3] +
6 R1^3 R2^2 R3^2 T01^2 T10^2 T12^2 T21^2 DiracDelta[z + 3 Z1 - 2 (Z2 + Z3)]
```

Figure 4: Prediction results of ISS internal-multiple attenuation for first-order internal multiples, b_3.

References

Araújo, F. V. *Linear and non-linear methods derived from scattering theory: backscattered tomography and internal multiple attenuation.* PhD thesis, Universidade Federal da Bahia, 1994.

Liang, H., C. Ma, and A.B.Weglein. "A further general modification of the leading order ISS attenuator of first order internal multiples to accommodate primaries and internal multiples when an arbitrary number of reflectors generate the data: theory, development, and examples." *Mission-Oriented Seismic Research Program (M-OSRP) Annual Report* (2011): 148–166.

Ma, C., H. Liang, and A. Weglein. "Modifying the leading order ISS attenuator of first-order internal multiples to accommodate primaries and internal multiples: fundamental concept and theory, development, and examples exemplified when three reflectors generate the data." *Mission-Oriented Seismic Research Program (M-OSRP) 2011 Annual Report* (2011): 133–147.

Ma, C. and A. Weglein. "One-dimensional analytic analysis of the effects of treating internal multiples in the data as subevents in the leading-order inverse scattering series (ISS) internal-multiple attenuation algorithm: analogues between free-surface and internal-multiple algorithms." *Mission-Oriented Seismic Research Program (M-OSRP) Annual Report* (2012): 123–145.

Weglein, A. B., F. V. Araújo, P. M. Carvalho, R. H. Stolt, K. H. Matson, R. T. Coates, D. Corrigan, D. J. Foster, S. A. Shaw, and H. Zhang. "Inverse Scattering Series and Seismic Exploration." *Inverse Problems* (2003): R27–R83.

Weglein, A. B., F. A. Gasparotto, P. M. Carvalho, and R. H. Stolt. "An Inverse-Scattering Series Method for Attenuating Multiples in Seismic Reflection Data." *Geophysics* 62 (November-December 1997): 1975–1989.

Zhang, H. and S. Shaw. "1-D Analytical Analysis of Higher Order Internal Multiples Predicted Via the Inverse Scattering Series Based Algorithm." *SEG Expanded Abstracts* 29 (2010): 3493–3498.

The internal-multiple elimination algorithm for all first-order internal multiples[†] generated from all reflectors for a 1D earth: algorithm, discussion and numerical tests

Yanglei Zou and Arthur B. Weglein

May 21, 2014

Abstract

The ISS (Inverse-Scattering-Series) internal-multiple attenuation algorithm (Araújo et al. (1994) and Weglein et al. (1997)) can predict the correct time and approximate amplitude for all first-order internal multiples without any information of the earth. This algorithm is effective and can attenuate internal multiples in many cases. However, in certain places, both on-shore and off-shore, the multiple is often proximal to or interfering with the primaries. Therefore, the task of completely removing internal multiples without damaging primaries becomes more challenging and subtle and currently beyond the collective capability of the petroleum industry. Weglein (2014) proposed a three-pronged strategy for providing an effective response to this pressing and prioritized challenge. One part of the strategy is to develop an internal-multiple elimination algorithm that can predict both the correct amplitude and the correct time for all internal multiples. The ISS internal-multiple elimination algorithm for all first-order internal multiples generated from all reflectors in a 1D earth is proposed in this report. The primaries in the reflection data that enters the algorithm provides that elimination capability, automatically without our requiring the primaries to be identified or in any way separated. The other events in the reflection data, that is, the internal multiples, will not be helpful in this elimination scheme. That is a limitation of this algorithm. We will propose a modified strategy for providing the elimination ability without the current shortcoming. We note that this elimination algorithm based on the ISS internal-multiple attenuation algorithm is derived by using reverse engineering to provide the difference between elimination and attenuation for a 1D earth. This particular elimination algorithm is model type dependent since the reverse engineering method is model type dependent. The ISS internal-multiple attenuation algorithm is completely model type independent and in future work we will pursue the development of an eliminator for a multi-dimensional earth by identifying terms in the inverse scattering series that have that purpose.

[†]A first-order internal multiple is an internal multiple with only one downward reflection in its history.

1 Introduction

The inverse-scattering-series allows all seismic processing objectives, such as free-surface-multiple removal and internal-multiple removal to be achieved directly in terms of data, without any estimation of the earth's properties. For internal-multiple removal, the ISS internal-multiple attenuation algorithm can predict the correct time and an approximate and well-understood amplitude for all first-order internal multiples generated from all reflectors without requiring any subsurface information. If the events in the data are isolated, the energy-minimization adaptive subtraction can fix the gap between the attenuation algorithm and the elimination algorithm, plus all factors that are outside the assumed physics of the subsurface and acquisition. However, in certain places, events often interfere with each other in both on-shore and off-shore seismic data. In these cases, the criteria of energy minimization adaptive subtraction may fail and the task for completely removing internal multiples becomes more challenging and beyond the current capability of the petroleum industry.

For dealing with this challenging problem, Weglein (2014) proposed a three-pronged strategy including (1)Develop the ISS prerequisites for predicting the reference wave field and to produce de-ghosted data Mayhan and Weglein (2014). (2)Develop internal-multiple elimination algorithms from ISS. (3)Develop a replacement for the energy-minimization criteria for adaptive subtraction. For the second part of the strategy, that is, to upgrade the ISS internal-multiple attenuator to eliminator, the strengths and limitations of the ISS internal-multiple attenuator are noted and reviewed. The ISS internal-multiple attenuator always attenuates all first-order internal multiples from all reflectors at once, automatically and without subsurface information. That is a tremendous strength, and is a constant and holds independent of the circumstances and complexity of the geology and the play. The primaries in the reflection data that enters the algorithm provides that delivery, automatically without our requiring the primaries to be identified or in any way separated. The other events in the reflection data (the internal multiples) when they enter the ISS internal-multiple algorithm will alter the higher order internal multiples and thereby assist and cooperate with higher order ISS internal-multiple attenuation terms, to attenuate higher order internal multiples. However, there is a downside, a limitation. There are cases when internal multiples that enter the attenuator can predict spurious events. That is a well-understood shortcoming of the leading order term, when taken in isolation, but is not an issue for the entire ISS internal-multiple capability. It is anticipated by the ISS and higher order ISS internal multiple terms exist to precisely remove that issue of spurious event prediction, and taken together with the first order term, no longer experiences spurious event prediction. Ma et al. (2012) and Ma and Weglein (2014) provided those higher order terms and for spurious events removal. In a similar way, there are higher order ISS internal multiple terms that provide the elimination of internal multiples when taken together with the leading order attenuator term. There are early discussions in Ramírez (2007). And Wilberth Herrera and Weglein (2012) has derived an algorithm that can eliminate all first-order internal multiples generated at the shallowest reflector for 1D normal incidence. In this report we proposes a general elimination algorithm for all first-order internal-multiples generated from all reflectors in a 1D earth. Similarly as the attenuator, the primaries in the reflection data that enters the elimination algorithm provides that elimination capability, automatically without our requiring the primaries to be identified or in any

way separated. The internal multiples in the reflection data will not be helpful in this elimination scheme. We will show how the ISS anticipate that shortcoming and propose a modified strategy for providing elimination ability without this shortcoming. This elimination algorithm based on the ISS internal-multiple attenuation algorithm is derived by using reverse engineering method. It is model type dependent since the reverse engineering method is model type dependent. The ISS internal-multiple attenuation algorithm is model type independent.

2 The ISS internal-multiple attenuation algorithm and Attenuation Factor for 1D normal incidence

First, we will give a review of the ISS internal-multiple attenuation algorithm before introducing the elimination algorithm. The ISS internal-multiple attenuation algorithm was first given by Araújo (1994) and Weglein et al. (1997). The 1D normal-incidence version of the algorithm is presented as follows:

$$b_3^{IM}(k) = \int_{-\infty}^{\infty} dz e^{ikz} b_1(z) \int_{-\infty}^{z-\varepsilon_2} dz' e^{-ikz'} b_1(z') \int_{z'+\varepsilon_1}^{\infty} dz'' e^{ikz''} b_1(z''), \tag{1}$$

Where $b_1(z)$, which is closely related to the data, is the water-speed migration of the data due to a 1D normal-incidence spike plane wave. In the following example, we will show how to obtain $b_1(z)$ from data and predict internal multiples. The terms ε_1 and ε_2 are two small positive numbers introduced to avoid self interaction. This equation can predict the correct time and an approximate amplitude of all first-order internal multiples.

To demonstrate explicitly the mechanism of the ISS internal-multiple attenuation algorithm and to examine its properties, Weglein et al. (2003) considered the simplest two-layer model that can produce an internal multiple. For this model, the reflection data caused by an impulsive incident wave $\delta(t - \frac{z}{c})$ is:

$$D(t) = R_1\delta(t - t_1) + T_{01}R_2T_{10}\delta(t - t_2) + \cdots,$$

where t_1, t_2 and R_1, R_2 are the two-way travel times and the reflection coefficients from the two reflectors,respectively; and T_{01} and T_{10} are the coefficients of transmission between model layers 0 and 1 and 1 and 0, respectively. Then

$$D(\omega) = R_1e^{i\omega t_1} + T_{01}R_2T_{10}e^{i\omega t_2} + \cdots,$$

where$D(\omega)$ is the temporal Fourier transform of $D(t)$.
Given a 1D medium and a normal incident wave, $k_z = \frac{2\omega}{c_0}$ and $b_1(k_z) = D(\omega)$, and the following is obtained:

$$b_1(k_z) = R_1e^{i\frac{2\omega}{c_0}\frac{c_0t_1}{2}} + T_{01}R_2T_{10}e^{i\frac{2\omega}{c_0}\frac{c_0t_2}{2}} + \cdots.$$

The pseudo-depths z_1 and z_2 in the reference medium are defined as follows:

$$z_1 = \frac{c_0t_1}{2} \quad z_2 = \frac{c_0t_2}{2}.$$

The input data can now be expressed in terms of $k = k_z$, z_1, and z_2:

$$b_1(k) = R_1 e^{ikz_1} + T_{01}R_2T_{10}e^{ikz_2} + \cdots .$$

The date are now ready for the internal-multiple attenuation algorithm.
Substituting $b_1(k)$ into the algorithm, we derive the prediction:

$$b_3^{IM}(k) = R_1R_2^2T_{01}^2T_{10}^2e^{2ikz_2}e^{-ikz_1},$$

which in the time domain is:

$$b_3^{IM}(t) = R_1R_2^2T_{01}^2T_{10}^2\delta(t-(2t_2-t_1)).$$

From the example it is easy to compute the actual first-order internal multiple precisely:

$$-R_1R_2^2T_{01}T_{10}\delta(t-(2t_2-t_1)).$$

Therefore, the time prediction is precise, and the amplitude of the prediction has an extra power of $T_{01}T_{10}$, which is called the attenuation factor, thus defining exactly the difference between attenuation (represented by b_3^{IM}) and elimination.

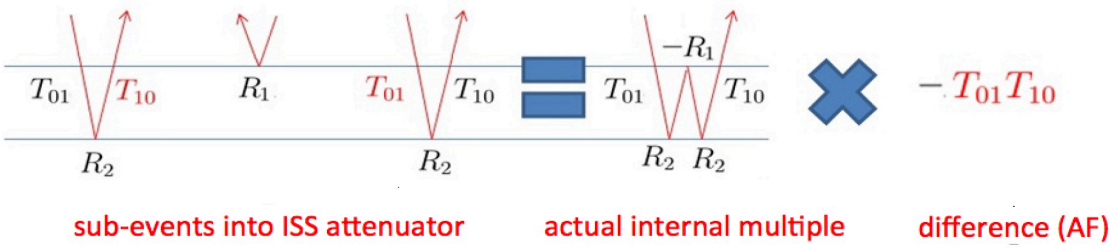

Figure 1: An example of the attenuation factor of a first-order internal multiple generated at the shallowest reflector. Notice that all red terms are extra transmission coefficients

The procedure for predicting a first-order internal multiple generated at the shallowest reflector is shown in Figure 1. The ISS internal-multiple attenuation algorithm uses three primaries in the data to predict a first-order internal multiple. From the figure we can see that, every sub-event on the left-hand side experiences several phenomena as it makes its way down to the earth then back to the receiver. When compared with the internal multiple on the right-hand side, the events on the left-hand side have extra transmission coefficients, which are shown in red. Multiplying all of those extra transmission coefficients, we get the attenuation factor $T_{01}T_{10}$ for this first-order internal multiple generated at the shallowest reflector. And all first-order internal multiples generated at the shallowest reflector have the same attenuation factor.

Figure 2 shows the procedure for predicting a first-order internal multiple generated at the next shallowest reflector. In this example, the attenuation factor is $(T_{01}T_{10})^2(T_{12}T_{21})$.

To derive a general formula for the amplitude prediction of the algorithm, Ramírez (2007) analyzed a model with n layers and respective velocities C_n, n being an integer. By using the definitions

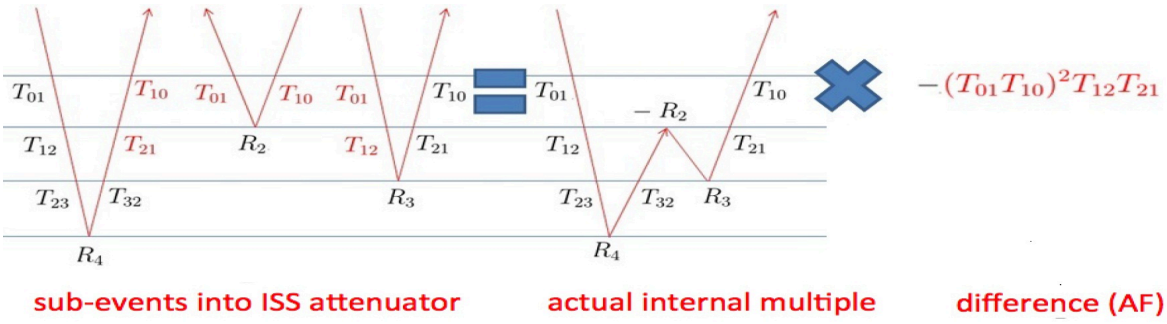

Figure 2: An example of the attenuation factor of a first-order internal multiple generated at the next shallowest reflector. Notice that all red terms are extra transmission coefficients

$R_1 = R_1'$, $R_N' = R_N \prod_{i=1}^{N-1}(T_{i-1,i}T_{i,i-1})$, and Einstein's summation, and we apply them to the reflection data from a normal-incident spike wave, we can obtain the following:

$$D(t) = R_n'\delta(t - t_n) + internal\ multiples. \tag{2}$$

The generalized prediction of the attenuation algorithm is obtained by

$$b_3^{IM}(k) = R_i'R_j'R_k'e^{ikz_i}e^{ikz_j}e^{ikz_k}, \tag{3}$$

which in the time domain becomes

$$b_3^{IM}(t) = R_i'R_j'R_k'\delta(t - (t_i + t_k - t_j)) \tag{4}$$

By evaluating equation (3) for different values of i, j, and k, the amplitude prediction of first-order internal multiples is obtained and can be generalized for any number of layers in a 1D model. The generalization of the internal-multiple's amplitude states that the overabundance of transmission coefficients depends on the position of the generating reflector (i.e., where the downward reflection took place). Compared with the real amplitude of internal multiples in the data, we can obtain the attenuation factor.

The attenuation factor, AF_j, in the prediction of internal multiples, is given by the following:

$$AF_j = \begin{cases} T_{0,1}T_{1,0} & (for\ j = 1) \\ \prod_{i=1}^{j-1}(T_{i-1,i}^2T_{i,i-1}^2)T_{j,j-1}T_{j-1,j} & (for\ 1 < j < J) \end{cases} \tag{5}$$

The attenuation factor AF_j can also be rewritten by using reflection coefficients:

$$AF_j = \begin{cases} 1 - R_1^2 & (for\ j = 1) \\ (1 - R_1^2)^2(1 - R_2^2)^2 \cdots (1 - R_{j-1}^2)^2(1 - R_j^2) & (for\ 1 < j < J) \end{cases} \tag{6}$$

The subscript j represents the generating reflector, and J is the total number of interfaces in the model. The interfaces are numbered starting with the shallowest location. The attenuation algorithm b_3^{IM} predicts a first-order internal multiple by using three events within the data. The attenuation factor is directly related to the trajectory of the events, and that trajectory forms the prediction of the internal multiple.

3 The ISS internal-multiple elimination algorithm for 1D normal incidence

The discussion above demonstrates that all first-order internal multiples generated at the same reflector have the same attenuation factor. Also, we derived a generalized formula for the attenuation factor for all reflectors. We can see that the attenuation factor contains all transmission coefficients, from the shallowest reflector down to the reflector generating the multiple. From the examples (shown in Figure 1 and 2), we can also see that the middle event contains all those transmission coefficients. Therefore, our idea is to modify the middle term in the attenuation algorithm to remove the attenuation factor and make the attenuation algorithm an eliminator. That is, we go from

$$b_3^{IM}(k) = \int_{-\infty}^{\infty} dz e^{ikz} b_1(z) \int_{-\infty}^{z-\varepsilon_2} dz' e^{-ikz'} b_1(z') \int_{z'+\varepsilon_1}^{\infty} dz'' e^{ikz''} b_1(z'') \tag{7}$$

to

$$b_E^{IM}(k) = \int_{-\infty}^{\infty} dz e^{ikz} b_1(z) \int_{-\infty}^{z-\varepsilon_2} dz' e^{-ikz'} F[b_1(z')] \int_{z'+\varepsilon_1}^{\infty} dz'' e^{ikz''} b_1(z'') \tag{8}$$

For 1D normal incidence, $b_1(z)$ is expressed as:

$$b_1(z) = R_1\delta(z-z_1) + R_2'\delta(z-z_2) + R_3'\delta(z-z_3) + \cdots + R_n'\delta(z-z_n) + \cdots . \tag{9}$$

To remove all attenuation factors in the prediction, the term $F[b_1(z)]$ should be written as:

$$\begin{aligned} F[b_1(z')] =& \frac{R_1}{AF_{j=1}}\delta(z'-z_1) + \frac{R_2'}{AF_{j=2}}\delta(z'-z_2) + \cdots + \frac{R_n'}{AF_{j=n}}\delta(z'-z_n) + \cdots \\ =& \frac{R_1}{1-R_1^2}\delta(z'-z_1) + \frac{R_2'}{(1-R_1^2)^2(1-R_2^2)}\delta(z'-z_2) + \cdots \\ &+ \frac{R_n'}{(1-R_1^2)^2(1-R_2^2)^2\cdots(1-R_{n-1}^2)^2(1-R_n^2)}\delta(z'-z_n) + \cdots . \end{aligned} \tag{10}$$

The basic strategy to construct $F[b_1(z)]$ in terms of $b_1(z)$ is to first construct the attenuation factor by $b_1(z)$, and then to construct $F[b_1(z)]$ by using $b_1(z)$ and attenuation factor. The attenuation factor can be written in reflection coefficients, and then we can map the reflection coefficients to R's ($R's$ are the amplitudes of the events in data), finally construct the R's by $b_1(z)$, as shown in Figure 3 . However, we have tried this approach and found that it is difficult to achieve.

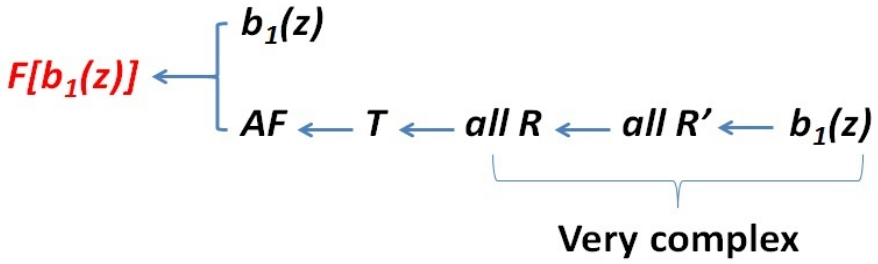

Figure 3: The straight forward strategy

Next, we propose another way to achieve the goal. By introducing a new function called g(z) in which the amplitude of each event corresponds to a reflection coefficient, we find a way to construct $F[b_1(z)]$ by using $b_1(z)$ and g(z). After that, we find an integral equation about $b_1(z)$ and g(z). If we can solve the latter equation for g(z) and integrate it into the first part, we can achieve our goal (as shown in Figure 4).

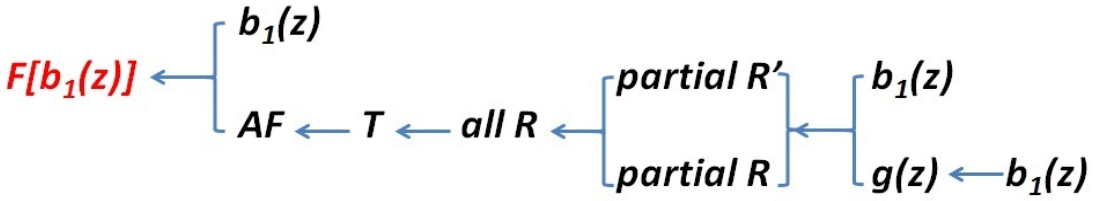

Figure 4: Modified strategy

By using that modified strategy, the $F[b_1(z)]$ is discovered (See Appendix A for the derivation):

$$F[b_1(z)] = \frac{b_1(z)}{[1-(\int_{z-\varepsilon}^{z+\varepsilon} dz' g(z'))^2][1-\int_{-\infty}^{z-\varepsilon} dz' b_1(z') \int_{z'-\varepsilon}^{z'+\varepsilon} dz'' g(z'')]^2} \tag{11}$$

$$g(z) = \frac{b_1(z)}{1-\int_{-\infty}^{z-\varepsilon} dz' b_1(z') \int_{z'-\varepsilon}^{z'+\varepsilon} dz'' g(z'')} \tag{12}$$

To derive the $F[b_1(z)]$ from $b_1(z)$, g(z) must first be solved in equation (12). Thereafter, g(z) is integrated into equation (11).

Equation (12) is an integral equation. Generally speaking, this kind of equation does not have analytical solutions; hence, an approximation must be made for this equation.

3.1 The First Type of Equation Approximation for g(z)

The simplest approximation for g(z) is:

$$\begin{aligned} g(z) =& \frac{b_1(z)}{1 - \int_{-\infty}^{z-\varepsilon} dz' b_1(z') \int_{z'-\varepsilon}^{z'+\varepsilon} dz'' g(z'')} \\ \approx& \frac{b_1(z)}{1-0} \\ \approx& b_1(z) \end{aligned} \tag{13}$$

3.2 The Second Type of Equation Approximation for g(z)

A more accurate approximation for g(z) is presented as follows:

$$\begin{aligned} g(z) =& \frac{b_1(z)}{1 - \int_{-\infty}^{z-\varepsilon} dz' b_1(z') \int_{z'-\varepsilon}^{z'+\varepsilon} dz'' g(z'')} \\ \approx& \frac{b_1(z)}{1 - \int_{-\infty}^{z-\varepsilon} dz' b_1(z') \int_{z'-\varepsilon}^{z'+\varepsilon} dz'' b_1(z'')} \end{aligned} \tag{14}$$

3.3 Higher-order approximations

By iterating $g(z)$ in (12), we can obtain a more accurate approximation, as shown in Figure 5. If we substitute more accurate approximations of $g(z)$ into $F[b_1(z)]$, we will get higher orders of approximation of the elimination algorithm which can predict the correct amplitude of first-order internal multiples generated at deeper reflectors.

3.4 A modified strategy of using b_1+b_3 instead of b_1 for the elimination algorithm

The primaries in the reflection data that enters the elimination algorithm (both 1D normal incidence and 1D pre-stack) provide that elimination capability, automatically without our requiring the primaries to be identified or in any way separated. The internal multiples in the data will not be helpful in this elimination scheme. That is a limitation of current algorithm. Now, we will show the modified strategy for the internal-multiple elimination algorithm that can address the limitation. As shown in figure 6, b_1, which is very close to data, contains primaries, first-order internal multiples, and higher-order internal multiples. We use the attenuation algorithm to predict first-order internal multiples (that is b_3) with the correct time and the approximate amplitude. Due to the multiples in the data, the attenuation algorithm also generates spurious events (Ma et al.

First type approximation for $g(z)$	$g(z) = \frac{b_1(z)}{1 - \int_{-\infty}^{z-\varepsilon} dz' b_1(z') \int_{z'-\varepsilon}^{z'+\varepsilon} dz'' g(z'')}$ $\approx \frac{b_1(z)}{1-0}$ $\approx b_1(z)$
Second type approximation for $g(z)$	$g(z) = \frac{b_1(z)}{1 - \int_{-\infty}^{z-\varepsilon} dz' b_1(z') \int_{z'-\varepsilon}^{z'+\varepsilon} dz'' g(z'')}$ $\approx \frac{b_1(z)}{1 - \int_{-\infty}^{z-\varepsilon} dz' b_1(z') \int_{z'-\varepsilon}^{z'+\varepsilon} dz'' b_1(z'')}$
Third type approximation for $g(z)$	$g(z) = \frac{b_1(z)}{1 - \int_{-\infty}^{z-\varepsilon} dz' b_1(z') \int_{z'-\varepsilon}^{z'+\varepsilon} dz'' g(z'')}$ $\approx \frac{b_1(z)}{1 - \int_{-\infty}^{z-\varepsilon} dz' b_1(z') \int_{z'-\varepsilon}^{z'+\varepsilon} dz'' \frac{b_1(z'')}{1 - \int_{-\infty}^{z''-\varepsilon} dz''' b_1(z''') \int_{z'''-\varepsilon}^{z'''+\varepsilon} dz^{(4)} b_1(z^{(4)})}}$
• • •	• • •

Figure 5: different approximations for g(z)

(2012)) and makes prediction for higher-order multiples at the same time. Similarly, the internal multiples entering the elimination algorithm will cause an error . Here is the strategy for addressing this shortcoming, since in $b_1 + b_3$ the first-order internal multiples are attenuated and it is a good approximation for data with only primaries. If we use $b_1 + b_3$ instead of b_1 for the input data for the elimination algorithm, the predicted spurious events and higher-order multiples due to first-order internal multiples in the data are also attenuated. All events in the red circle are small compared with the predicted first-order internal multiples and can be ignored.

3.5 Numerical tests for the modified strategy applied to a 34-reflector model that is based on well log velocity data

In this section, we will test the modified strategy for a 34-reflector model under 1D normal incidence. And the modified strategy we proposed in this paper can be easily extended to the 1D pre-stack version. Figure 7 shows the 34-reflector model and Figure 8 shows the input data. In this test we used a 40th approximation of the algorithm by iterations, as is shown in:

$$g_1(z) = b_1(z) \tag{15}$$

$$g_{n+1}(z) = \frac{b_1(z)}{1 - \int_{-\infty}^{z-\varepsilon} dz' b_1(z') \int_{z'-\varepsilon}^{z'+\varepsilon} dz'' g_n(z'')} \tag{16}$$

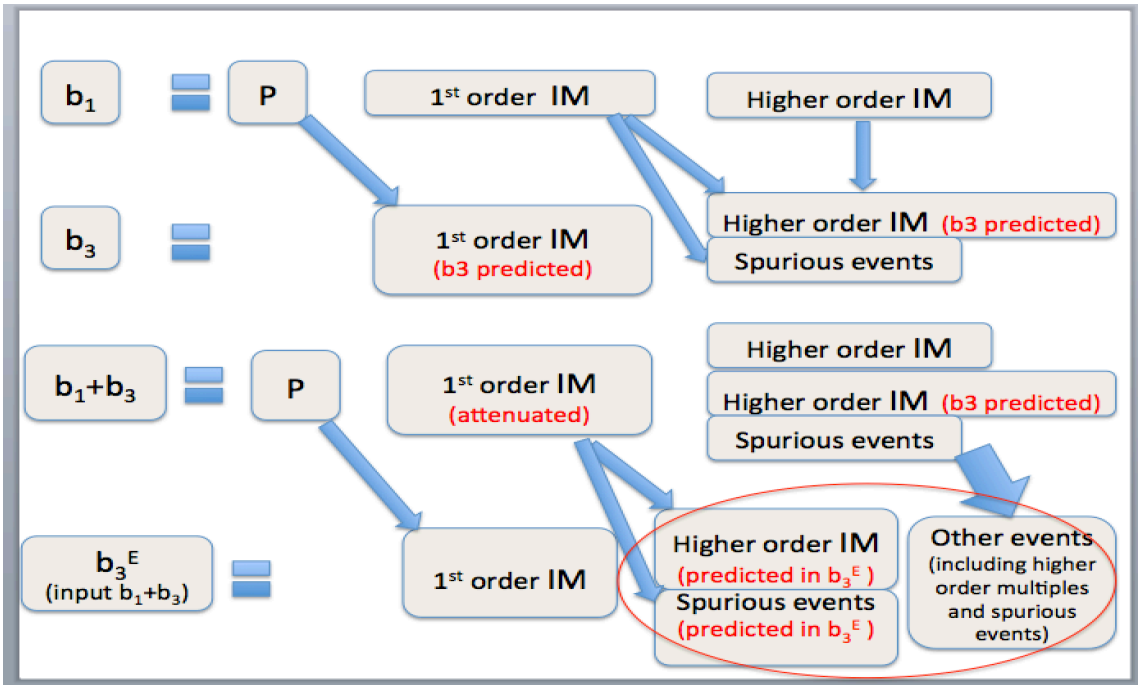

Figure 6: using $b_1 + b_3$ instead of b_1 as the input data for the elimination algorithm

We tested the ISS internal-multiple attenuation algorithm, the elimination algorithm and the modified strategy for the elimination algorithm. From the result we conclude that using b_1+b_3 as the input significantly reduced errors and generates better prediction for all first-order internal multiples generated from all reflectors.

Figure 9,11,13 show the prediction of different algorithms/strategies compared with the input data. Figure 10,12,14 shows a small time interval of figure 9,11,13 respectively.

4 The ISS internal-multiple elimination algorithm for 1D pre-stack data

4.1 A 2-reflector analytic example for the ISS internal-multiple attenuation algorithm in a 1D pre-stack acoustic medium

Now we will go on to extend the elimination algorithm for a 1D pre-stack data. Before that we need to better understand the mechanism of the attenuation algorithm for a 1D pre-stack data. What does b_1 looks like for a 1D pre-stack data? Is there any analog of the attenuation factors in 1D pre-stack acoustic medium? If yes, what is it?

In order to answer these questions, we will look at an analytic example for a 2-reflector acoustic medium in 1D pre-stack.

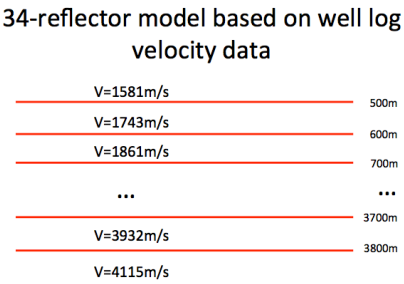

Figure 7: model

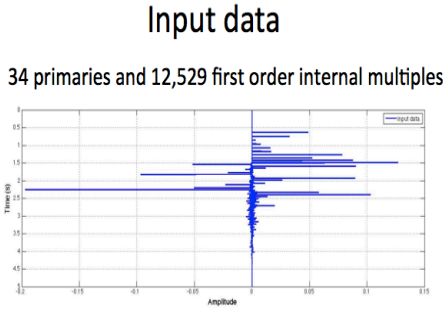

Figure 8: input data

The first question is what is b_1 in 1D pre-stack? We know that b_1 is closely related to the measured data D. If we can get the data, we can obtain b_1. Thus, first we need to obtain the data. Let us consider a delta source at (x_s, z_s), wherein the wave generated at (x_g, z_g) by this source is the Green's function:

$$G_0(x_g, z_g, x_s, z_s, \omega) = \frac{1}{2\pi}\int_{-\infty}^{\infty} dk'_s \frac{e^{ik'_s(x_g - x_s)} e^{iq'_s|z_g - z_s|}}{2iq'_s} \tag{17}$$

Let us set $z_s = 0$ and let z_g be positive, so that we can evaluate the absolute value,

$$G_0(x_g, z_g > 0, x_s, z_s = 0, \omega) = \frac{1}{2\pi}\int_{-\infty}^{\infty} dk'_s \frac{e^{-ik'_s x_s}}{2iq'_s} e^{ik'_s x_g + iq'_s z_g}. \tag{18}$$

Then, for simplicity, we will ignore the evanescent part, which means $k'_s < \omega/c$. That does not mean the algorithm can not handle the evanescent part. However, for many cases the evanescent part is small and can be ignored, and the math will be much simpler and easier to understand. Now the Green's function is:

$$G_0(x_g, z_g > 0, x_s, z_s = 0, \omega) = \frac{1}{2\pi}\int_{-\omega/c}^{\omega/c} dk'_s \frac{e^{-ik'_s x_s}}{2iq'_s} e^{ik'_s x_g + iq'_s z_g}. \tag{19}$$

At this point, G_0 can be regarded as a superposition of plane waves $e^{ik'_s x + iq'_s z}$ with weights $\frac{e^{-ik'_s x_s}}{2iq'_s}$. For a plane wave $e^{ik'_s x + iq'_s z}$ incident in an acoustic medium, the reflected wavefield is: (Note that It can be calculated by using the forward scattering series, as in Nita et al. (2004))

$$D(k'_s, q'_s, x_g, z_g = 0) = R(k'_s, q'_s) e^{ik'_s x_g} e^{2iq'_s z_1}. \tag{20}$$

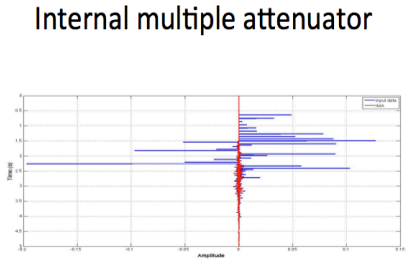

Figure 9: attenuator(red) compared with the input data(blue)

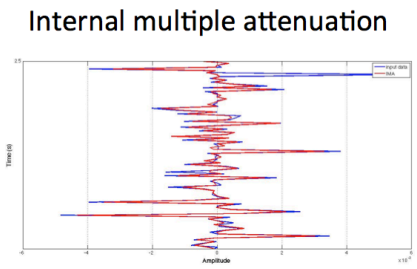

Figure 10: A small time interval of figure 9

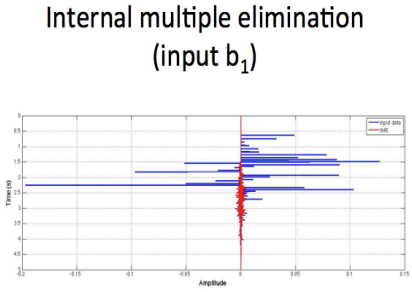

Figure 11: elimination(red) compared with the input data(blue), input b_1.

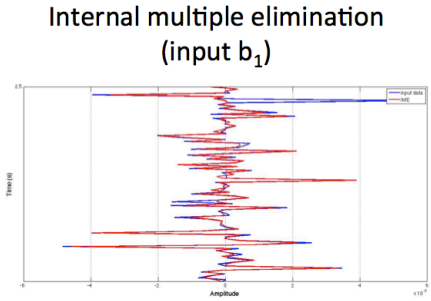

Figure 12: A small time interval of figure 11

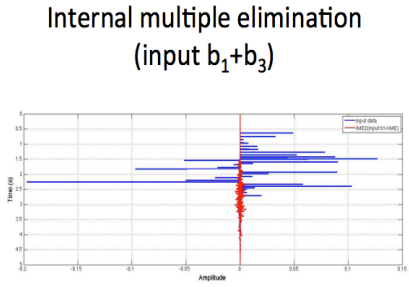

Figure 13: elimination(red) compared with the input data(blue), input $b_1 + b_3$.

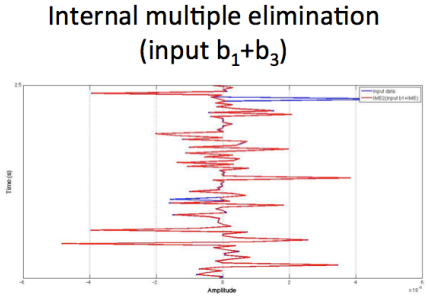

Figure 14: A small time interval of figure 13

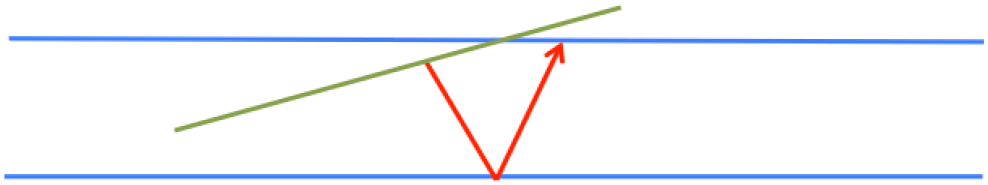

Figure 15: prestack

Then the total wave-field is (we set $z_g = z_s = 0$):

$$D(x_s, z_s = 0, x_g, z_g = 0, \omega) = \frac{1}{2\pi} \int_{-\omega/c}^{\omega/c} dk'_s \frac{e^{-ik'_s x_s}}{2iq'_s} D(k'_s, q'_s, x_g, z_g = 0). \tag{21}$$

Now we get the data at one receiver (x_g,0) from one delta source (x_s,0) and rewrite it as:

$$D(x_s, x_g, \omega) = \frac{1}{2\pi} \int_{-\omega/c}^{\omega/c} dk'_s \frac{e^{-ik'_s x_s}}{2iq'_s} R(k'_s, q'_s) e^{ik'_s x_g} e^{2iq'_s z_1} \tag{22}$$

This is in the frequency-space domain, whereas the attenuation algorithm works in the frequency-wavenumber domain. After Fourier transforming over the source and receivers, we convert the data to the frequency-wavenumber domain[1].

$$D(k_s, k_g, \omega) = \delta(k_s - k_g) \frac{R(k_s, q_s) e^{2iq_s z_1}}{4\pi i q_s} (-\omega/c < k_s < \omega/c) \tag{23}$$

Now we define $b_1(k_s, k_g, \omega)$ as (in the following discussion, we assume that $-\omega/c < k_s < \omega/c$):

$$\begin{aligned} b_1(k_s, k_g, \omega) &= -2iq_s D(k_s, k_g, \omega) & (24) \\ &= -\frac{1}{2\pi} \delta(k_s - k_g) R(k_s, q_s) e^{2iq_s z_1}. & (25) \end{aligned}$$

Then, $b_1(k_s, k_g, \omega)$ and the attenuation algorithm prediction $b_3(k_s, k_g, \omega)$ are related by the 2D internal-multiple attenuation algorithm:

$$b_3(k_g, k_s, \omega) = \int_{-\infty}^{\infty} \int_{-\infty}^{\infty} dk_1 dk_2 \int_{-\infty}^{\infty} dz e^{i(q_g + q_1)z} b_1(k_g, k_1, z) \int_{-\infty}^{z} dz' e^{i(-q_1 - q_2)z'} b_1(k_1, k_2, z')$$

[1] See appendix B for derivation

$$\times \int_{z'}^{\infty} dz'' e^{i(q_2+q_s)z''} b_1(k_2, k_s, z'')$$

Next with the definition of $b_1(k_s, 2q_s)$ and its prediction $b_3(k_s, 2q_s)$ for 1D pre-stack data, we have:

$$b_1(k_s, k_g, \omega) = -\frac{1}{2\pi}\delta(k_s - k_g) b_1(k_s, 2q_s) \quad (26)$$

$$b_3(k_g, k_s, q_g + q_s) = -\frac{1}{(2\pi)^3}\delta(k_g - k_s) b_3(k_s, 2q_s). \quad (27)$$

Then, $b_1(k_s, 2q_s)$ and $b_3(k_s, 2q_s)$ are related by the 1D pre-stack algorithm:

$$b_3(k_s, 2q_s) = \int_{-\infty}^{\infty} dz e^{2iq_s z} b_1(k_s, z) \int_{-\infty}^{z} dz' e^{-2iq_s z'} b_1(k_s, z') \int_{z'}^{\infty} dz'' e^{2iq_s z''} b_1(k_s, z'') \quad (28)$$

Ignoring the subscript s, we have

$$b_3(k, 2q) = \int_{-\infty}^{\infty} dz e^{2iqz} b_1(k, z) \int_{-\infty}^{z} dz' e^{-2iqz'} b_1(k, z') \int_{z'}^{\infty} dz'' e^{2iqz''} b_1(k, z''). \quad (29)$$

In the equation, for the first primary, we have

$$b_1(k, 2q) = R(k, q) e^{2iqz_1}, \quad (30)$$

and $b_1(k, z)$ is the Fourier transform of $b_1(k, 2q)$ from 2q to z.

We can also get the reflection data from the second reflector, and we can obtain a first order internal multiple as shown in Figure 16

Now, b_1 can be written as,

$$\begin{aligned} b_1(k_1, 2q_1) = & R_1(k_1, q_1) e^{2iq_1 z_1} \\ & + T_{01} R_2(k_2, q_2) T_{10} e^{2iq_1 z_1} e^{2iq_2(z_2 - z_1)} \\ & - T_{01} R_2 R_1 R_2 T_{10} e^{2iq_1 z_1} e^{4iq_2(z_2 - z_1)} \end{aligned}$$

Here, q_1 and q_2 are vertical wavenumbers at each layer, and q_2 is a function of q_1. To Fourier transform from q_1 to z, first we need to substitute q_2 with q_1.

Using the relation,

$$\begin{aligned} q_1^2 + k_1^2 &= (\frac{\omega}{c_1})^2 \\ q_2^2 + k_2^2 &= (\frac{\omega}{c_2})^2 \\ k_1 &= k_2, \end{aligned}$$

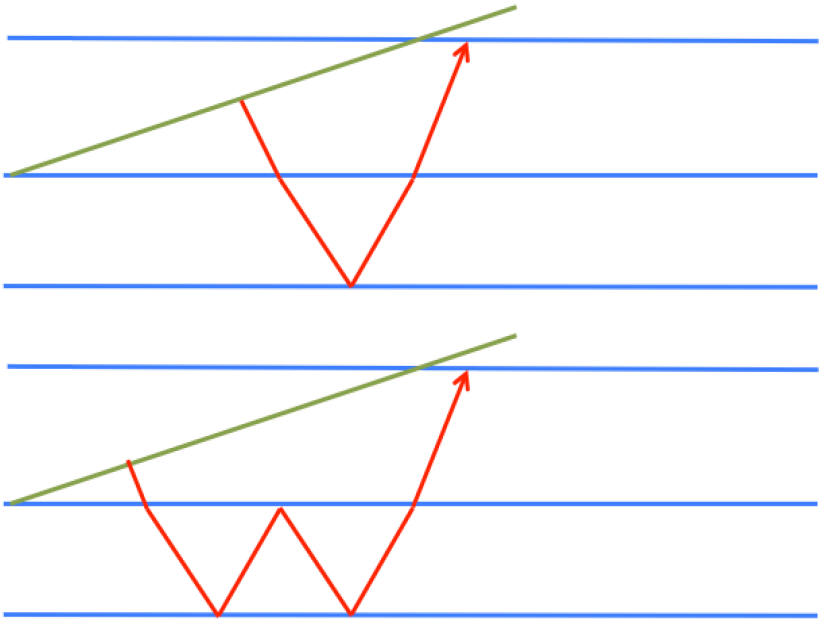

Figure 16: prestack

we can express q_2 in q_1 and k_1:

$$\begin{aligned} q_2 &= \sqrt{(\frac{c_1^2}{c_2^2}-1)k_1^2+\frac{c_1^2}{c_2^2}q_1^2} \\ &= \frac{c_1}{c_2}q_1+[\sqrt{(\frac{c_1^2}{c_2^2}-1)k_1^2+\frac{c_1^2}{c_2^2}q_1^2}-\frac{c_1}{c_2}q_1] \\ &= \frac{c_1}{c_2}q_1+\frac{(\frac{c_1^2}{c_2^2}-1)k_1^2}{\sqrt{(\frac{c_1^2}{c_2^2}-1)k_1^2+\frac{c_1^2}{c_2^2}q_1^2}+\frac{c_1}{c_2}q_1} \\ &= \frac{c_1}{c_2}q_1+S(k_1,q_1) \end{aligned}$$

Now we substitute q_2 with q_1:

$$\begin{aligned} b_1(k_1,2q_1) &= R_1(k_1,q_1)e^{2iq_1z_1} \\ &\quad +R_2'(k_1,q_1)e^{2i(z_2-z_1)S(k_1,q_1)}e^{2iq_1(z_1+\frac{c_1}{c_2}(z_2-z_1))} \end{aligned}$$

$$\begin{aligned} & -R'_{212}(k_1,q_1)e^{4i(z_2-z_1)S(k_1,q_1)}e^{2iq_1(z_1+\frac{2c_1}{c_2}(z_2-z_1))} \\ = \; & R_1(k_1,q_1)e^{2iq_1z_1} \\ & +R'_2(k_1,q_1)e^{2i(z_2-z_1)S(k_1,q_1)}e^{2iq_1z'_2} \\ & -R'_{212}(k_1,q_1)e^{4i(z_2-z_1)S(k_1,q_1)}e^{2iq_1(2z'_2-z_1)} \end{aligned}$$

The predicted internal multiple should be:

$$b_3(k_1,2q_1) = R'_2(k_1,q_1)R_1(k_1,q_1)R'_2(k_1,q_1)e^{4i(z_2-z_1)S(k_1,q_1)}e^{2iq_1(2z'_2-z_1)}$$

Comparing the predicted amplitude of the internal multiple with the actual amplitude of the internal multiple, we have:

$$\begin{aligned} R'_{212}(k_1,q_1) &= T_{01}R_2R_1R_2T_{10} \\ &= \frac{R'_2(k_2,q_2)R_1(k_1,q_1)R'_2(k_2,q_2)}{T_{01}(k_1,q_1)T_{10}(k_1,q_1)} \end{aligned}$$

We can see that they differed by a factor $T_{01}(k_1,q_1)T_{10}(k_1,q_1)$. That is the attenuation factor for the 1D pre-stack acoustic medium.

4.2 The ISS internal-multiple elimination algorithm for 1D pre-stack data

Now we have the attenuation factor for the 1D pre-stack acoustic medium and it lights the way to extending the 1D normal-incidence algorithm to 1D pre-stack data. Below shows the 1D pre-stack acoustic algorithm. In the 1D pre-stack elimination algorithm, due to the angle-dependent reflection coefficients, we can no longer just integrate the data in the k-z domain to get the reflection coefficients-we need to go to the k-q domain in which each pair k-q corresponds to a reflection coefficient. The differences between the 1D pre-stack algorithm and the 1D normal incidence algorithm are that the 1D pre-stack algorithm has one more variable k, and it uses the reflection coefficients in the k-q domain instead of the direct integral in the k-z domain.

$$b_E^{IM}(k,2q) = \int_{-\infty}^{\infty} dz e^{2iqz} b_1(k,z) \int_{-\infty}^{z-\varepsilon_1} dz' e^{-2iqz'} F[b_1(k,z')] \int_{z'+\varepsilon_2}^{\infty} dz'' e^{2iqz''} b_1(k,z'')$$

$$F[b_1(k,z)] = \frac{1}{2\pi}\int_{-\infty}^{\infty}\int_{-\infty}^{\infty} dz'dq' \times \frac{e^{-iq'z}e^{iq'z'}b_1(k,z')}{[1-\int_{-\infty}^{z'-\varepsilon} dz'' b_1(k,z'')e^{iq'z''}\int_{z''-\varepsilon}^{z''+\varepsilon} dz''' g^*(k,z''')e^{-iq'z'''}]^2[1-|\int_{z'-\varepsilon}^{z'+\varepsilon} dz'' g(k,z'')e^{iq'z''}|^2]}$$

$$g(k,z) = \frac{1}{2\pi}\int_{-\infty}^{\infty}\int_{-\infty}^{\infty} dz'dq' \frac{e^{-iq'z}e^{iq'z'}b_1(k,z')}{1-\int_{-\infty}^{z'-\varepsilon} dz'' b_1(k,z'')e^{iq'z''}\int_{z''-\varepsilon}^{z''+\varepsilon} dz''' g^*(k,z''')e^{-iq'z'''}}$$

4.3 Initial numerical tests for the ISS internal-multiple elimination algorithm for a 1D pre-stack data

We now test the 1D pre-stack algorithm for a two-reflector model.

We test the 1D pre-stack acoustic internal multiple elimination algorithm for a two-reflector model. The layers have densities $1.0g/cm^3$, $1.2g/cm^3$, $2.0g/cm^3$ and velocities 1500m/s, 3000m/s, and 4500m/s respectively. Figure 17 shows the data and figure 18 and 19 show the attenuation and elimination algorithm predictions respectively. Figure 20 to Figure 27 show different traces in different offsets (the elimination algorithm prediction (red) and attenuation algorithm prediction (green) compared to data (blue)). We can see the elimination algorithm keeps the correct time and can generate better amplitude.

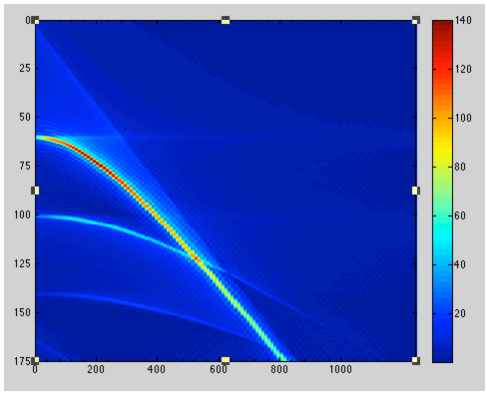

Figure 17: data

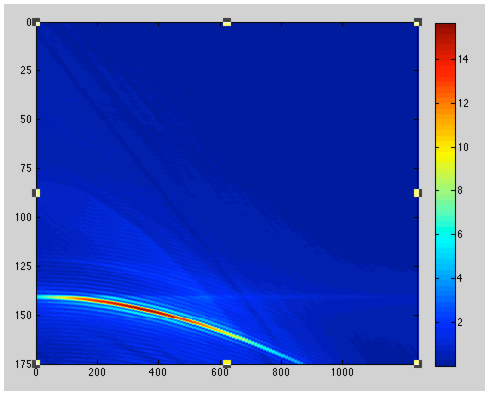

Figure 18: internal multiple attenuation prediction

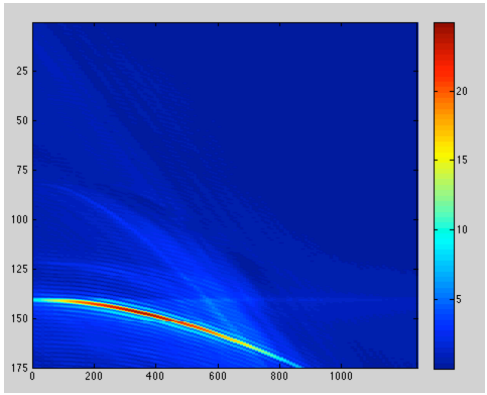

Figure 19: internal multiple elimination prediction

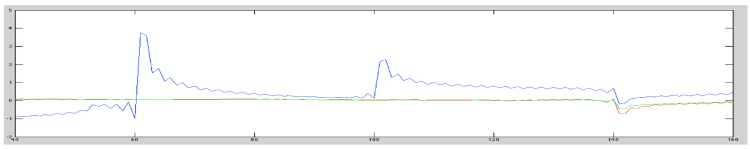

Figure 20: the elimination algorithm prediction (red) and attenuation algorithm prediction (green) compared to data (blue) at offset = 0m

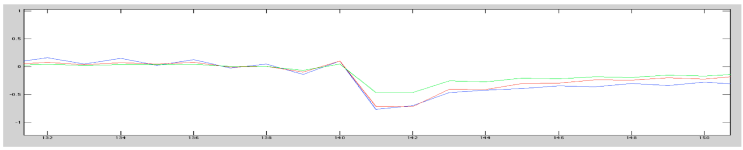

Figure 21: the elimination algorithm prediction (red) and attenuation algorithm prediction (green) compared to data (blue) at offset = 0m. After compensating for the tails of primaries.

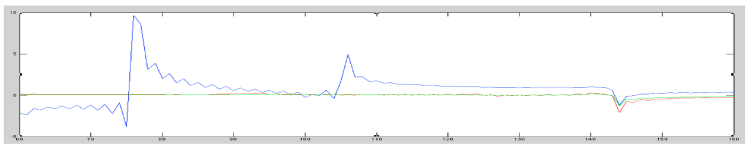

Figure 22: the elimination algorithm prediction (red) and attenuation algorithm prediction (green) compared to data (blue) at offset = 200m

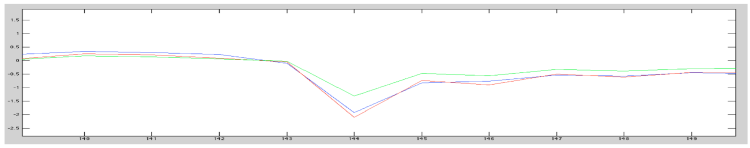

Figure 23: the elimination algorithm prediction (red) and attenuation algorithm prediction (green) compared to data (blue) at offset = 200m. After compensating for the tails of primaries.

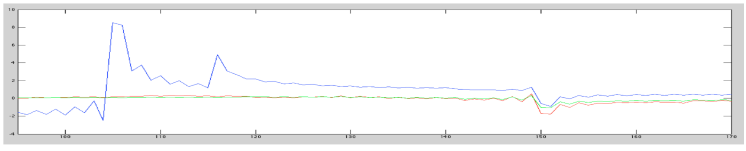

Figure 24: the elimination algorithm prediction (red) and attenuation algorithm prediction (green) compared to data (blue) at offset = 400m

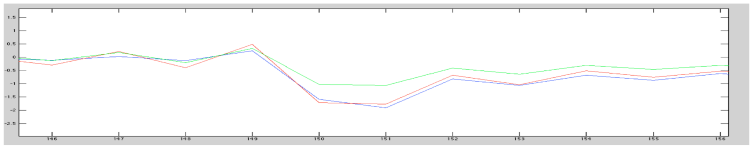

Figure 25: the elimination algorithm prediction (red) and attenuation algorithm prediction (green) compared to data (blue) at offset = 400m. After compensating for the tails of primaries.

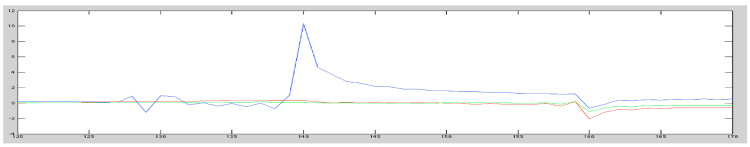

Figure 26: the elimination algorithm prediction (red) and attenuation algorithm prediction (green) compared to data (blue) at offset = 600m

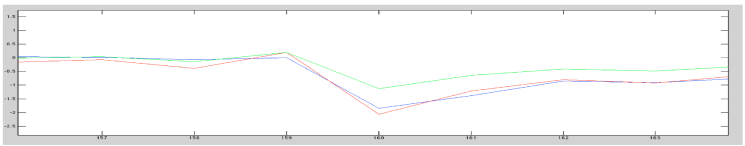

Figure 27: the elimination algorithm prediction (red) and attenuation algorithm prediction (green) compared to data (blue) at offset = 600m. After compensating for the tails of primaries.

5 Conclusion

The pre-stack 1D ISS internal multiple elimination algorithm for all first-order internal multiples from all reflectors is proposed in this report. Numerical tests are carried out to evaluate this new algorithm and to determine the strengths and limitations. The results shows that given no wavelet data with perfect preprocessing work finished (deghosting, free-surface multiple removal, et al.) the elimination algorithm can predict better amplitude of the internal multiples than the attenuation algorithm. In discussing the elimination algorithm, the primaries in the reflection data that enters the algorithm provide that elimination capability, automatically without our requiring the primaries to be identified or in any way separated. The other events (internal multiples) in the reflection data will not be helpful in this elimination scheme. We also propose a modified strategy for dealing with this issue. This algorithm is a part of the three-pronged strategy for elimination of all internal multiples which is especially relevant and provide value when primaries and internal multiples are proximal to and/or interfere with each other in both on-shore and off-shore data. We note that this particular elimination algorithm is model type dependent since the reverse engineering method is model type dependent. The ISS internal-multiple attenuation algorithm is model type independent and in future work we will pursue the development of an eliminator for a multi-dimensional earth by identifying terms in the inverse scattering series that have that purpose.

6 Acknowledgements

We are grateful to all M-OSRP sponsors for their encouragement and support in this research. I would like to thank Professor Arthur B. Weglein for his mentoring, and I thank all my coworkers for their help toward my finishing this paper and also for their valuable discussions in this research program.
I extend a special thanks to Saudi Arabian Oil Co. for the use of their well log velocity data.

Appendix

A Derivation of the algorithm for the elimination of all first-order internal multiples from all reflectors in a 1D medium

The algorithm is given by:

$$F[b_1(z)] = \frac{b_1(z)}{[1-(\int_{z-\varepsilon}^{z+\varepsilon} dz' g(z'))^2][1-\int_{-\infty}^{z-\varepsilon} dz' b_1(z') \int_{z'-\varepsilon}^{z'+\varepsilon} dz'' g(z'')]^2}$$

$$g(z) = \frac{b_1(z)}{1-\int_{-\infty}^{z-\varepsilon} dz' b_1(z') \int_{z'-\varepsilon}^{z'+\varepsilon} dz'' g(z'')}$$

with

$$\begin{aligned} b_1(z) =& R_1\delta(z-z_1) + R_2'\delta(z-z_2) + R_3'\delta(z-z_3) + \cdots + R_n'\delta(z-z_n) + \cdots \\ g(z) =& R_1\delta(z-z_1) + R_2\delta(z-z_2) + R_3\delta(z-z_3) + \cdots + R_n\delta(z-z_n) + \cdots \end{aligned}$$

($\int_{z-\varepsilon}^{z+\varepsilon} dz'' g(z'')$ is a function of z)

First Let us calculate $\int_{z-\varepsilon}^{z+\varepsilon} dz'' g(z'')$ for the given g(z):

$$\begin{aligned} \int_{z-\varepsilon}^{z+\varepsilon} dz'' g(z'') =& \int_{z-\varepsilon}^{z+\varepsilon} dz''[R_1\delta(z''-z_1) + R_2\delta(z''-z_2) + \cdots + R_n\delta(z''-z_n) + \cdots] \\ =& \int_{-\infty}^{\infty} dz''[R_1\delta(z''-z_1) + R_2\delta(z''-z_2) + \cdots + R_n\delta(z''-z_n) + \cdots] \\ & \times H(z''-(z-\varepsilon))H((z+\varepsilon)-z'') \\ =& R_1 H(z_1-(z-\varepsilon))H((z+\varepsilon)-z_1) + R_2 H(z_2-(z-\varepsilon))H((z+\varepsilon)-z_2) \\ & + \cdots + R_n H(z_n-(z-\varepsilon))H((z+\varepsilon)-z_n) + \cdots \\ =& R_1 H((z_1+\varepsilon)-z)H(z-(z_1-\varepsilon)) + R_2 H((z_2+\varepsilon)-z)H(z-(z_2-\varepsilon)) \\ & + \cdots + R_n H((z_n+\varepsilon)-z)H(z-(z_n-\varepsilon)) + \cdots \end{aligned}$$

$$\begin{aligned} & (\int_{z-\varepsilon}^{z+\varepsilon} dz'' g(z''))^2 \\ =& R_1^2 H((z_1+\varepsilon)-z)H(z-(z_1-\varepsilon)) + R_2^2 H((z_2+\varepsilon)-z)H(z-(z_2-\varepsilon)) \\ & + \cdots + R_n^2 H((z_n+\varepsilon)-z)H(z-(z_n-\varepsilon)) + \cdots \end{aligned}$$

$$
\begin{aligned}
& b_1(z') \int_{z'-\varepsilon}^{z'+\varepsilon} dz'' g(z'') \\
=& R_1^2 \delta(z'-z_1) + R_2 R_2' \delta(z'-z_2) + R_3 R_3' \delta(z'-z_3) + \cdots + R_n R_n' \delta(z'-z_n) + \cdots
\end{aligned}
$$

$$
\begin{aligned}
& \int_{-\infty}^{z-\varepsilon} dz' b_1(z') \int_{z'-\varepsilon}^{z'+\varepsilon} dz'' g(z'') \\
=& \int_{-\infty}^{z-\varepsilon} dz' [R_1^2 \delta(z'-z_1) + R_2 R_2' \delta(z'-z_2) + \cdots + R_n R_n' \delta(z'-z_n) + \cdots] \\
=& \int_{-\infty}^{\infty} dz' H((z-\varepsilon)-z') [R_1^2 \delta(z'-z_1) + R_2 R_2' \delta(z'-z_2) + \cdots + R_n R_n' \delta(z'-z_n) + \cdots] \\
=& R_1^2 H((z-\varepsilon)-z_1) + R_2 R_2' H((z-\varepsilon)-z_2) + \cdots + R_n R_n' H((z-\varepsilon)-z_n) + \cdots \\
=& R_1^2 H(z-(z_1+\varepsilon)) + R_2 R_2' H(z-(z_2+\varepsilon)) + \cdots + R_n R_n' H(z-(z_n+\varepsilon)) + \cdots
\end{aligned}
$$

Now we can prove the first part of the equation:

$$
\begin{aligned}
& F[b_1(z)] \\
=& \frac{b_1(z)}{[1-(\int_{z-\varepsilon}^{z+\varepsilon} dz' g(z'))^2][1-\int_{-\infty}^{z-\varepsilon} dz' b_1(z') \int_{z'-\varepsilon}^{z'+\varepsilon} dz'' g(z'')]^2} \\
=& \frac{b_1(z)}{[1-R_1^2 H((z_1+\varepsilon)-z) H(z-(z_1-\varepsilon)) - \cdots][1-R_1^2 H(z-(z_1+\varepsilon)) - R_2 R_2' H(z-(z_2+\varepsilon)) - \cdots]^2} \\
=& \frac{R_1}{1-R_1^2} \delta(z-z_1) + \frac{R_2'}{(1-R_1^2)^2(1-R_2^2)} \delta(z-z_2) + \cdots \\
& + \frac{R_n'}{(1-R_1^2)^2(1-R_2^2)^2 \cdots (1-R_{n-1}^2)^2(1-R_n^2)} \delta(z-z_n) + \cdots \\
=& \frac{R_1}{AF_{j=1}} \delta(z-z_1) + \frac{R_2'}{AF_{j=2}} \delta(z-z_2) + \cdots + \frac{R_n'}{AF_{j=n}} \delta(z-z_n) + \cdots
\end{aligned}
$$

For the second part of the equation, we have:

$$
g(z) = \frac{b_1(z)}{1-\int_{-\infty}^{z-\varepsilon} dz' b_1(z') \int_{z'-\varepsilon}^{z'+\varepsilon} dz'' g(z'')}
$$

$$
b_1(z') \int_{z'-\varepsilon}^{z'+\varepsilon} dz'' g(z'')
$$

$$=R_1^2\delta(z'-z_1)+R_2R_2'\delta(z'-z_2)+R_3R_3'\delta(z'-z_3)+\cdots+R_nR_n'\delta(z'-z_n)+\cdots$$

$$\begin{aligned}
&\int_{-\infty}^{z-\varepsilon}dz'b_1(z')\int_{z'-\varepsilon}^{z'+\varepsilon}dz''g(z'')\\
=&\int_{-\infty}^{z-\varepsilon}dz'[R_1^2\delta(z'-z_1)+R_2R_2'\delta(z'-z_2)+\cdots+R_nR_n'\delta(z'-z_n)+\cdots]\\
=&\int_{-\infty}^{\infty}dz'H((z-\varepsilon)-z')[R_1^2\delta(z'-z_1)+R_2R_2'\delta(z'-z_2)+\cdots+R_nR_n'\delta(z'-z_n)+\cdots]\\
=&R_1^2H((z-\varepsilon)-z_1)+R_2R_2'H((z-\varepsilon)-z_2)+\cdots+R_nR_n'H((z-\varepsilon)-z_n)+\cdots\\
=&R_1^2H(z-(z_1+\varepsilon))+R_2R_2'H(z-(z_2+\varepsilon))+\cdots+R_nR_n'H(z-(z_n+\varepsilon))+\cdots
\end{aligned}$$

$$\begin{aligned}
&\frac{b_1(z)}{1-\int_{-\infty}^{z-\varepsilon}dz'b_1(z')\int_{z'-\varepsilon}^{z'+\varepsilon}dz''g(z'')}\\
=&R_1\delta(z-z_1)+\frac{R_2'}{1-R_1R_1}\delta(z-z_2)+\frac{R_3'}{1-R_1R_1-R_2'R_2}\delta(z-z_3)+\cdots\\
&+\frac{R_n'}{1-R_1R_1-R_2'R_2-\cdots-R_{n-1}'R_{n-1}}\delta(z-z_n)\\
=&R_1\delta(z-z_1)+R_2\delta(z-z_2)+R_3\delta(z-z_3)+\cdots+R_n\delta(z-z_n)+\cdots\\
=&g(z)
\end{aligned}$$

Thus the second equation is proved.

In the derivation we used:$R_i=\frac{R_i'}{1-R_1R_1-R_2'R_2-\cdots-R_{i-1}'R_{i-1}}$ It can be proved:

$$\begin{aligned}
R_i=&\frac{R_i'}{(1-R_1^2)(1-R_2^2)\cdots(1-R_{i-2}^2)(1-R_{i-1}^2)}\\
=&\frac{R_i'}{(1-R_1^2)(1-R_2^2)\cdots(1-R_{i-2}^2)-(1-R_1^2)(1-R_2^2)\cdots(1-R_{i-2}^2)R_{i-1}^2}\\
=&\frac{R_i'}{(1-R_1^2)(1-R_2^2)\cdots(1-R_{i-2}^2)-(1-R_1^2)(1-R_2^2)\cdots(1-R_{i-2}^2)R_{i-1}R_{i-1}}\\
=&\frac{R_i'}{(1-R_1^2)(1-R_2^2)\cdots(1-R_{i-2}^2)-R_{i-1}'R_{i-1}}\\
=&\frac{R_i'}{1-R_1R_1-R_2'R_2-\cdots-R_{i-1}'R_{i-1}}
\end{aligned}$$

B Fourier transform of the data from the frequency-space domain to the frequency-wavenumber domain

$$D(x_s, x_g, \omega) = \frac{1}{2\pi} \int_{-\omega/c}^{\omega/c} dk'_s \frac{e^{-ik'_s x_s}}{2iq'_s} R(k'_s, q'_s) e^{ik'_s x_g} e^{2iq'_s z_1} \tag{31}$$

$$\begin{aligned} D(k_s, x_g, \omega) &= \frac{1}{2\pi} \int_{-\infty}^{\infty} dx_s e^{ik_s x_s} \int_{-\omega/c}^{\omega/c} dk'_s \frac{e^{-ik'_s x_s}}{2iq'_s} R(k'_s, q'_s) e^{ik'_s x_g} e^{2iq'_s z_1} \\ &= \frac{1}{2\pi} \int_{-\omega/c}^{\omega/c} \int_{-\infty}^{\infty} dx_s e^{i(k_s - k'_s)x_s} dk'_s \frac{R(k'_s, q'_s) e^{ik'_s x_g} e^{2iq'_s z_1}}{2iq'_s} \\ &= \frac{1}{2\pi} \int_{-\omega/c}^{\omega/c} dk'_s \delta(k_s - k'_s) \frac{R(k'_s, q'_s) e^{ik'_s x_g} e^{2iq'_s z_1}}{2iq'_s} \\ &= \frac{R(k_s, q_s) e^{ik_s x_g} e^{2iq_s z_1}}{4\pi i q_s} (-\omega/c < k_s < \omega/c) \end{aligned}$$

$$\begin{aligned} D(k_s, k_g, \omega) &= \int_{-\infty}^{\infty} dx_g e^{-ik_g x_g} \frac{R(k_s, q_s) e^{ik_s x_g} e^{2iq_s z_1}}{4\pi i q_s} (-\omega/c < k_s < \omega/c) \\ &= \delta(k_s - k_g) \frac{R(k_s, q_s) e^{2iq_s z_1}}{4\pi i q_s} (-\omega/c < k_s < \omega/c) \end{aligned}$$

References

Araújo, F. V. *Linear and non-linear methods derived from scattering theory: backscattered tomography and internal multiple attenuation.* PhD thesis, Universidade Federal da Bahia, 1994.

Araújo, F. V., A. B. Weglein, P. M. Carvalho, and R. H. Stolt. "Inverse scattering series for multiple attenuation: An example with surface and internal multiples." *SEG Technical Program Expanded Abstracts* (1994): 1039–1041.

Ma, C., H. Liang, and A. B. Weglein. "Modifying the leading order ISS attenuator of first-order internal multiples to accommodate primaries and internal multiples: fundamental concept andtheory, development, and examples exemplified when three reflectors generatethe data." *Mission Oriented Seismic Research Program Annual Report* (2012): 133–147.

Ma, C. and A. B. Weglein. "Including higher-order Inverse Scattering Series (ISS) terms to address a serious shortcoming/problem of the ISS internal-multiple attenuator: exemplifying the problem and its resolution." *SEG Technical Program Expanded Abstracts* (2014).

Mayhan, J. and A. B. Weglein. "Multiple removal and prerequisite satisfaction: current status and future plans." *SEG Technical Program Expanded Abstracts* (2014).

Nita, B. G., K. H. Matson, and A. B. Weglein. "Forward scattering series and seismic events: Far field approximations, critical and postcritical events." *SIAM Journal of Applied Mathematics* 64 (2004): 2167–2185.

Ramírez, A. C. *1.-Inverse scattering subseries for removal of internal multiples and depth imaging primaries; 2.-Green's theorem as the foundation of interferometry and guiding new practical methods and applications.* PhD thesis, University of Houston, 2007.

Weglein, A. B., F. V. Araújo, P. M. Carvalho, R. H. Stolt, K. H. Matson, R. T. Coates, D. Corrigan, D. J. Foster, S. A. Shaw, and H. Zhang. "Inverse Scattering Series and Seismic Exploration." *Inverse Problems* (2003): R27–R83.

Weglein, A. B., F. A. Gasparotto, P. M. Carvalho, and R. H. Stolt. "An Inverse-Scattering Series Method for Attenuating Multiples in Seismic Reflection Data." *Geophysics* 62 (November-December 1997): 1975–1989.

Weglein, Arthur B. "Multiple attenuation: The status and a strategy that identifies and addresses current challenges." *SEG Technical Program Expanded Abstracts* (2014).

Wilberth Herrera, Hong Liang Paolo Terenghi,Chao Ma and Arthur B. Weglein. "Progressing amplitude issues for testing 1D analytic data in leading order internal multiple algorithms." *Mission Oriented Seismic Research Program Annual Report* (2012): 167–188.

Short note: Inverse scattering series internal multiple attenuation algorithm for a 3-D source and 1-D subsurface

Xinglu Lin and Arthur B. Weglein

May 21, 2014

Abstract

The ISS internal multiple attenuator was developed in Cartesian coordinates (Araújo (1994),Weglein et al. (2003)) and demands a "complete" dataset for a 3-D source and 3-D earth. Even for a 3-D source and 1-D earth (a realistic case in Central North Sea, Canada, and Middle East), the areal coverage of receivers in acquisition is required for one shot gather in Cartesian coordinates. In this shot note, the ISS internal multiple attenuator will be changed into polar coordinates for a 3-D source and 1-D earth, which allows a single source and receivers on a single line, rather than a full surface of receivers. The reduced form will benefit the 3-D source application and computational costs of ISS internal multiple eliminator in the future, which is a step in the M-OSRP three-pronged strategy to address the pressing challenges with multiples.

1 Introduction

In the M-OSRP three-pronged strategy, which is proposed by Weglein (2013), the pressing challenges in current internal multiple removal technologies are, (1) preprocessing for on-shore application, (2) developing internal multiple eliminator and (3) finding a replacement for the energy-minimization criteria for adaptive subtraction. In order to solve the second problem, Herrera and Weglein (2013) and Zou and Weglein (2013) in M-OSRP group have proposed the ISS leading-order internal multiple eliminator, which can compensate the transmission loss in attenuator, and the algorithm has been extended to 1.5-D (Y. Zou, A. Weglein,13-14 M-OSRP Annual Report). Since the study naturally starts from a 1-D earth and the real source in acquisition has a 3-D signature, it is necessary to consider a 3-D source and 1-D earth attenuator for the initial investigation of eliminator. In addition, we would like to point out that there are on-shore and off-shore regions in 1-D structure where the seismic data suffers from serious internal multiple problems, for instance, Central North Sea (Duquet et al. (2013)), Canada and Middle East.

Current ISS internal multiple 2-D source attenuator has the ability to solve the internal multiple problems in a field data. For example, the 1-D earth-2-D source algorithm, which is derived from 2-D source algorithm with the assumption of a 1-D layered earth, has been successfully applied on Encana data and produces a positive result (Q. Fu, 2014). The original 2-D earth-2-D source algorithm demands a collection of shot records on a line, however, the 1-D earth-2-D source reduces the requirement to only one shot record. For a more realistic world of 3-D earth-3-D source, the algorithm needs the sources everywhere on the measurement plane and each source needs the receivers everywhere on the plane. For a 3-D source and 2-D earth, where the properties do not vary in y-direction, the algorithm still asks for sources on a line (x-direction) and an areal coverage of receivers on the plane for each source. Even with 1-D earth assumption in Cartesian coordinates, the attenuator requires one shot record with an areal coverage, namely the information from all the receivers in this area, for a fixed source.

In this report, the ISS algorithm for a 3-D source and 1-D earth will be rewritten in polar coordinates, which allows a single 3-D source and the receivers on one line, rather than a full surface of receivers. The numerical tests are shown, as an initial comparison of the 2-D source internal multiple prediction, 3-D source internal multiple prediction and 3-D source internal multiple prediction with an asymptotic Bessel function for a 3-D data set. The results indicate that the reduced form can save the computational costs and preserve the internal multiple prediction from the risks of wrongly assuming 2-D line sources with applying 2-D ISS internal multiple attenuation algorithm to a 3-D dataset. Also, the difference in results will be amplified when the attenuator (b_3) enters the eliminator algorithm, e.g. that Yanglei Zou is developing, which is a crucial step in M-OSRP three-pronged strategy.

2 Circular symmetry under the cylindrical coordinate in 1-D earth

3-D data generated by 1-D earth only depends on the source-receiver offset and the frequency, which has a spatial circular symmetry under cylindrical coordinate (independence of azimuth angle). That symmetry makes it convenient to study the 1-D earth problem under cylindrical coordinate, in which the position in a 3-D world is characterized by a radial length, an azimuth angle and a vertical position. Let us define the 3-D vector in a cylindrical coordinate as (r_i, θ_i, z_i) in spatial domain and (k_{ri}, ϕ_i, k_{zi}) in wave-number domain, separately. The diagram for a 3-D vector is shown in figure 1.

The dependence of 3-D data for a 1-D earth can be expressed as $D^{1DE}(|\vec{r_g} - \vec{r_s}|, \epsilon_g, \epsilon_s; \omega)$ or $D^{1DE}(r_h, \epsilon_g, \epsilon_s, \omega)$, where the $\vec{r_g}$ and $\vec{r_s}$ are the horizontal projection of the receivers and the source separately, and r_h is the magnitude of the difference between $\vec{r_g}$ and $\vec{r_s}$. And the ϵ_g and ϵ_s are the constant depths of receivers and sources, which are omitted in later discussion. For convenience, the superscript $1DE$ represent the 1-D earth assumption for different sources (For example, line source: 2D-1DE; point source: 3D-1DE). In the next step, we will show the symmetry of the data under the two-dimensional Fourier transform. The 3-D data for 1-D earth can be transformed to

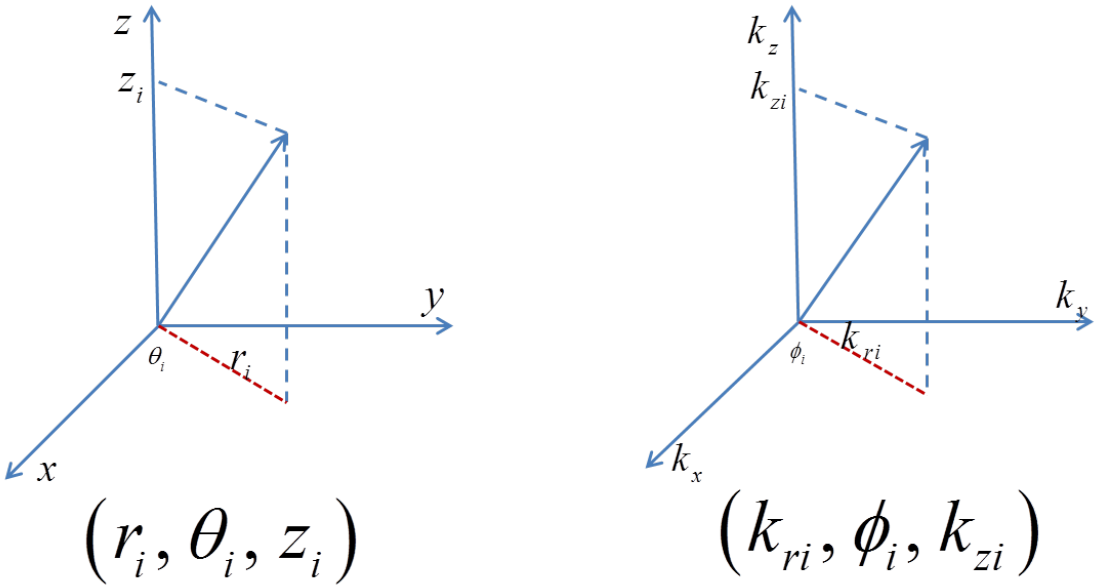

Figure 1: Figure 1: Cylindrical coordinates for spatial domain (left) and wave-number domain (right).

$k_{ri} - \omega$ domain as,

$$
\begin{aligned}
& D(\vec{k_g}, \vec{k_s}; \omega) && (1)\\
&= FT[D^{1DE}(|\vec{r_g} - \vec{r_s}|; \omega)] && (2)\\
&= \iint \iint e^{i\vec{k_{rg}} \cdot \vec{r_g}} D^{1DE}(|\vec{r_g} - \vec{r_s}|; \omega) e^{-i\vec{k_{rs}} \cdot \vec{r_s}} d\vec{r_g} d\vec{r_s} && (3)\\
&= \iint \iint e^{i\vec{k_{rg}} \cdot (\vec{r_g} - \vec{r_s})} D^{1DE}(|\vec{r_g} - \vec{r_s}|; \omega) e^{i(\vec{k_r g} - \vec{k_{rs}}) \cdot \vec{r_s}} d\vec{r_g} d\vec{r_s} && (4)\\
&= \iint \iint e^{i\vec{k_{rg}} \cdot \vec{r_h}} D^{1DE}(|\vec{r_h}|; \omega) e^{i(\vec{k_r g} - \vec{k_{rs}}) \cdot \vec{r_s}} d\vec{r_h} d\vec{r_s} && (5)\\
&= \iint e^{i\vec{k_{rg}} \cdot \vec{r_h}} D^{1DE}(|\vec{r_h}|; \omega) d\vec{r_h} \cdot \iint e^{i(\vec{k_r g} - \vec{k_{rs}}) \cdot \vec{r_s}} d\vec{r_s} && (6)\\
&= D^{1DE}(k_{rg}, \omega)(2\pi)^2 \frac{\delta(k_{rg} - k_{rs})\delta(\phi_g - \phi_s)}{k_{rg}}. && (7)
\end{aligned}
$$

The step in equation 5 can be proven by Jacobian determinant in appendix A. And the symmetry factor in equation 7 contains the Dirac delta in cylindrical coordinate, which is equivalent to $\delta(k_{xg} - k_{xs})\delta(k_{yg} - k_{ys})$ (appendix B). In order to apply 1-D earth symmetry in the 3-D algorithm, we continue with the definition of $b_1(\vec{k_g}, \vec{k_s}, q_s + q_s)$, which leads to

$$b_1(\vec{k_g}, \vec{k_s}, q_g + q_s) \quad (8)$$

$$= -2iq_s \cdot D(\vec{k_g}, \vec{k_s}; \omega) \tag{9}$$

$$= -2iq_s \cdot D^{1DE}(k_{rg}; \omega)(2\pi)^2 \frac{\delta(k_{rg} - k_{rs})\delta(\phi_g - \phi_s)}{k_{rg}} \tag{10}$$

$$= b_1^{1DE}(k_{rg}, q_g + q_s)(2\pi)^2 \frac{\delta(k_{rg} - k_{rs})\delta(\phi_g - \phi_s)}{k_{rg}}, \tag{11}$$

where $q_i = sgn(\omega)\sqrt{(\omega/c_0)^2 - k_{ri}^2}$. The symmetry factor in equation 11 is independent of $k_z = q_g + q_s$. In the following step, b_1 needs to be transformed back to depth domain:

$$b_1(\vec{k_g}, \vec{k_s}, z) = b_1^{1DE}(k_{rg}, z)(2\pi)^2 \frac{\delta(k_{rg} - k_{rs})\delta(\phi_g - \phi_s)}{k_{rg}}, \tag{12}$$

which is an un-collapsed Stolt migration. In the next section, the structure of 1-D earth symmetry will be applied into current 3-D ISS internal multiple attenuation algorithm.

3 3-D ISS internal multiple attenuation algorithm for 1-D earth

The inverse scattering subseries for internal multiples provides a comprehensive theory for removing all multiples from an arbitrary earth without requiring any subsurface information. The 3-D leading-order internal multiple prediction term in this infinite subseries is (Weglein et al. (2003),Terenghi and Weglein (2009)):

$$\begin{aligned}
& b_3^{3D}(k_{x_g}, k_{y_g}, k_{x_s}, k_{y_s}, \omega) \\
= & \frac{1}{(2\pi)^4} \iint dk_{x_1} dk_{x_2} \iint dk_{y_1} dk_{y_2} e^{-iq_1(\epsilon_g - \epsilon_s)} e^{iq_2(\epsilon_g - \epsilon_s)} \\
& \times \int_{-\infty}^{+\infty} dz_1 b_1^{3D}(k_{x_g}, k_{y_g}, k_{x_1}, k_{y_1}, z_1) e^{i(q_g + q_1)z_1} \\
& \times \int_{-\infty}^{z_1 - \epsilon} dz_2 b_1^{3D}(k_{x_1}, k_{y_1}, k_{x_2}, k_{y_2}, z_2) e^{-i(q_1 + q_2)z_2} \\
& \times \int_{z_2 + \epsilon}^{+\infty} dz_3 b_1^{3D}(k_{x_2}, k_{y_2}, k_{x_s}, k_{y_s}, z_2) e^{i(q_2 + q_s)z_3},
\end{aligned} \tag{13}$$

where the vertical wavenumber is $q_i = sgn(\omega)\sqrt{\frac{\omega^2}{c_0^2} - k_{x_{(i)}}^2 - k_{y_{(i)}}^2}$. Using the symmetry of 1-D earth presented in equation 12, the reduced 3-D algorithm in a cylindrical coordinate can be obtained as,

$$\begin{aligned}
& b_3^{3D-1DE} \cdot \frac{\delta(k_{rg} - k_{rs})\delta(\phi_g - \phi_s)}{k_{rg}} \\
= & \int_0^{\infty} k_{r1} dk_{r1} \int_0^{2\pi} d\phi_1 \int_0^{\infty} k_{r2} dk_{r2} \int_0^{2\pi} d\phi_2 \\
& \times \int_{-\infty}^{+\infty} dz_1 b_1^{3D-1DE}(k_{rg}, z_1) e^{i(q_g + q_1)z_1} \frac{\delta(k_{rg} - k_{r1})\delta(\phi_g - \phi_1)}{k_{rg}}
\end{aligned}$$

$$\times \int_{-\infty}^{z_1-\epsilon} dz_2 b_1^{3D-1DE}(k_{r1}, z_2) e^{-i(q_1+q_2)z_2} \frac{\delta(k_{r1}-k_{r2})\delta(\phi_1-\phi_2)}{k_{r1}}$$
$$\times \int_{z_2+\epsilon}^{+\infty} dz_3 b_1^{3D-1DE}(k_{r2}, z_3) e^{i(q_2+q_s)z_3} \frac{\delta(k_{r2}-k_{rs})\delta(\phi_2-\phi_s)}{k_{r2}}, \quad (14)$$

where the receivers and sources are located at the same depth ($\epsilon_g = \epsilon_s$). The lateral integrals vanish because of the Dirac delta. The reduced form of the 3-D algorithm is

$$b_3^{3D-1DE}(k_{rh}.\omega) \quad (15)$$
$$= \int_{-\infty}^{+\infty} dz_1 b_1^{3D-1DE}(k_{rh}, z_1) e^{i2qz_1} \int_{-\infty}^{z_1-\epsilon} dz_2 b_1^{3D-1DE}(k_{rh}, z_2) e^{-i2qz_2} \int_{z_2+\epsilon}^{+\infty} dz_3 b_1^{3D-1DE}(k_{rh}, z_3) e^{i2qz_3},$$

where $k_{rh} = k_{rg} = k_{rs}$ and $q = sgn(\omega)\sqrt{\frac{\omega^2}{c_0^2} - k_{rh}^2}$. Here, the simplified 3-D algorithm for 1-D earth has the same structure as a reduced 2-D algorithm (Y. Zou, A. B. Weglein, 13-14 M-OSRP annual report), but dimension of inverse Fourier transform is different. Applying the two-dimensional Fourier transform or the Bessel-Fourier transform on both sides of equation 16, we can obtain

$$\begin{aligned} b_3^{3D-1DE}(r_h;\omega) &= (\frac{1}{2\pi})^2 \iint d\vec{k_h} e^{i\vec{k_h}\cdot\vec{r_h}} b_3^{3D-1DE}(k_{rh};\omega) \\ &= (\frac{1}{2\pi})^2 \int_0^{\infty} k_{rh} dk_{rh} \int_0^{2\pi} d\phi_h \cdot e^{ik_{rh}r_h cos(\phi_h-\theta_h)} \cdot b_3^{3D-1DE}(k_{rh};\omega) \\ &= \frac{1}{2\pi} \int_0^{\infty} J_0(k_{rh}\cdot r_h) b_3^{3D-1DE}(k_{rh};\omega) k_{rh} dk_{rh} \\ &= \frac{1}{2\pi} \int_{-\infty}^{+\infty} \frac{1}{2} H_0^+(k_{rh}\cdot r_h) b_3^{3D-1DE}(k_{rh};\omega) k_{rh} dk_{rh}, \end{aligned} \quad (16)$$

where the H_0^+ is the Bessel function of third kind (Hankel function) and $q = sgn(\omega)\sqrt{\frac{\omega^2}{c_0^2} - k_{rh}^2}$. Considering the computational costs in Hankel transform, we can use the asymptotic Hankel function to improve the efficiency by FFT. Then the asymptotic Hankel transform is

$$\begin{aligned} b_3^{3D-1DE}(r_h;\omega) &= \frac{1}{2\pi} \int_{-\infty}^{+\infty} \frac{1}{2} \sqrt{\frac{2}{\pi k_{rh} r_h}} b_3^{3D-1DE}(k_{rh};\omega) k_{rh} dk_{rh} \\ &= \frac{1}{2\pi} \int_{-\infty}^{+\infty} \sqrt{\frac{k_{rh}}{2\pi r_h}} b_3^{3D-1DE}(k_{rh};\omega) dk_{rh}, \end{aligned} \quad (17)$$

where the offset is defined as $r_h = |\vec{r_g} - \vec{r_s}|$. In a specified acquisition geometry that sources and receivers are on the same streamer line in 3-D survey, we can make $k_{rh} = k_x$, which means, the 3-D algorithm can be reduced dramatically in $k-\omega$ domain. The efficiency of predicting multiples in a 3-D data for a 1-D earth is comparable to processing a 2-D data set.

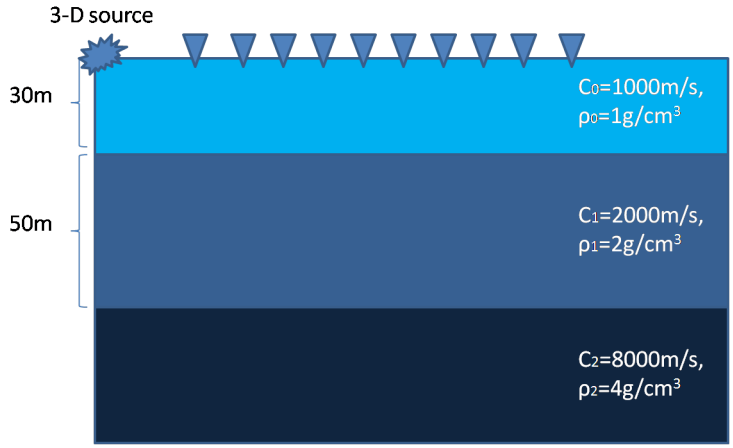

Figure 2: Acoustic model for modeling a synthetic 3-D data

4 Numerical tests

In order to evaluate the reduced form of 3-D ISS internal multiple attenuation algorithm (equation 16), we generate a synthetic 3-D data in a two-reflector acoustic medium. Before we start the prediction of internal multiple, here are three prior assumptions. Firstly, the earth is assumed to be a 1-D layered medium. Secondly, the 3-D source is located on the receiver streamer, which means that there is no crossline offset. In addition, since the synthetic data is generated in (k_{rh}, q) domain, we assume that the 3-D data must be transformed to wave-number-frequency domain correctly. The transformation from spatial to wave-number domain demands a 2-dimensional Fourier transform or a Fourier-Bessel transform for a 1-D earth model.

The (a) part in figure 3 shows the 3-D data, which is simulated by a two-reflector model (figure 2). The internal multiple predictions generated by the 2-D algorithm (Y. Zou, 2014 M-OSRP annual report) and the reduced 3-D internal multiple algorithms with (equation 17) or without (equation 16) an asymptotic Bessel function are separately shown in (b), (c) and (d). Efficiency of 2-D source-1-D earth algorithm and 3-D source-1-D earth algorithm are the same when we use an asymptotic Bessel function in the Hankel transform.

The trace comparisons are shown in figure 4 (near-offset, trace 2) and figure 5 (far-offset, trace 50). In each figure, there are four different traces involved in the comparison: red line represents the dataset, black line represents the 3-D prediction that is transformed back to spatial domain by a Hankel transform (equation 16), green line represents the 3-D prediction with an asymptotic Bessel function (equation 17), and the blue line represents a 2-D prediction using a Fourier transform. From these figures, we conclude that even though the prediction is still an attenuator, the shape of wavelet and approximated amplitude can be preserved by using the reduced 3-D ISS internal multiple algorithm with or without asymptotic Bessel. Due to the far field approximation, the

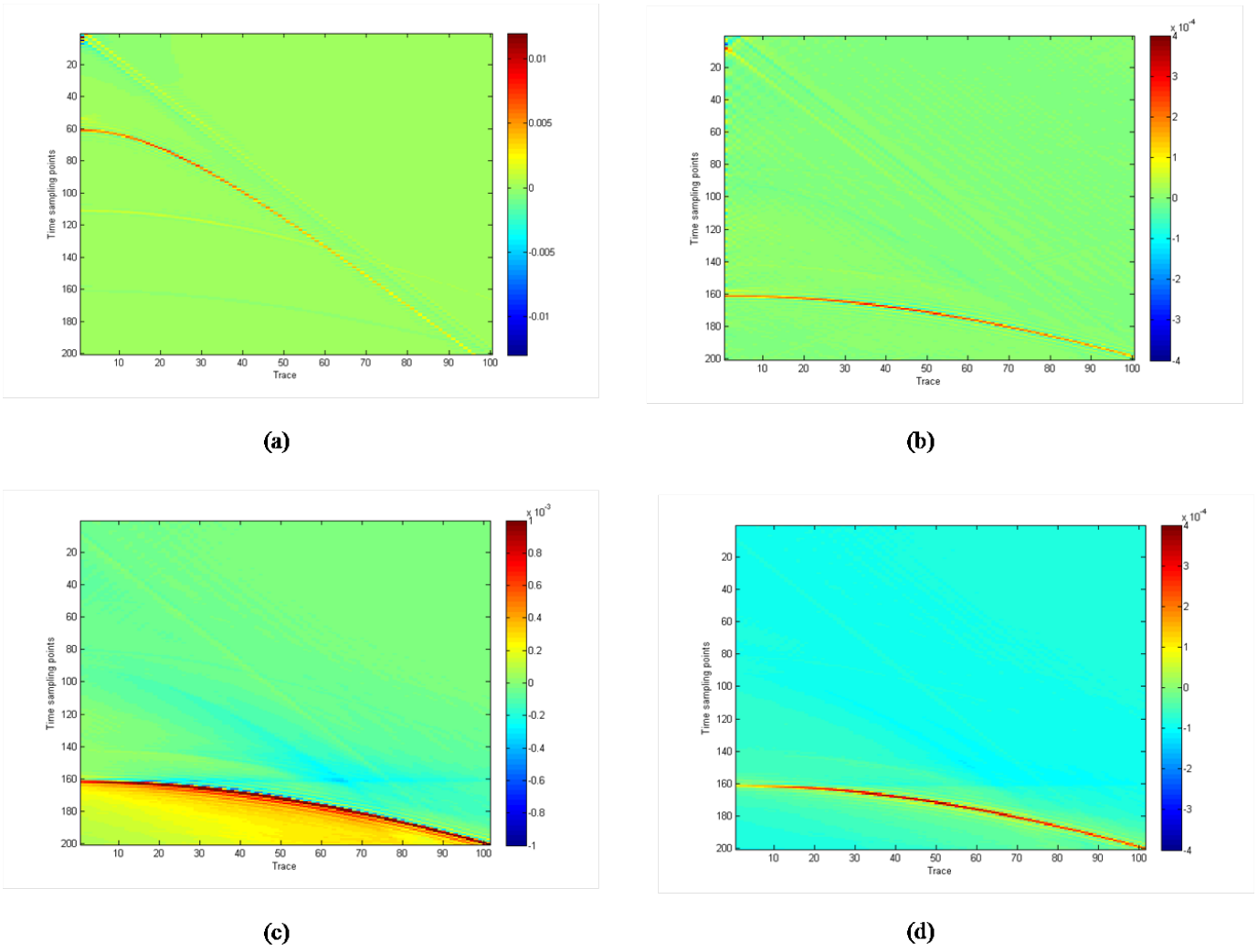

Figure 3: (a) 3-D Data set (one streamer, courtesy of Yanglei Zou); (b) Leading-order internal multiple prediction using the reduced 3-D algorithm and the inverse Hankel transformation; (c) Leading-order internal multiple prediction using 2-D algorithm and FFT; (d) Leading-order internal multiple prediction using the reduced 3-D algorithm and FFT (asymptotic Bessel function).

transform with asymptotic Bessel function fails to generate the same amplitude as an attenuator for the near-offset prediction. On the other hand, the 2-D algorithm, which use a Fourier transform, produces a spike wavelet with a tail in prediction and a boosted amplitude. The over-estimated amplitude of 2-D prediction will damage the primary-events, especially when there is an interference of primaries and internal multiples in data set.

5 Conclusions and future work

This report demonstrates the 3-D source and 1-D earth ISS internal multiple attenuator in cylindrical coordinates. Attenuating internal multiples without knowing subsurface information is the greatest strength of ISS subseries algorithm; nevertheless, the adequate full 3-D data is required by the algorithm. In Cartesian coordinates, even for a 3-D source and 1-D earth, the prediction needs one source and an areal coverage of receivers. We accommodate the 3-D source-3D earth algorithm to a reduced 3-D source-1-D earth form under a circular symmetry in cylindrical coordinates, which allows a single source and receivers on a single line, rather than a full surface of receivers.

The results of 3-D source and 1-D earth b_3 will be applied into other stronger but expensive algorithm, such as the high-dimensional ISS internal multiple eliminator that Yanglei Zou and Dr. Weglein are developing. The elimination of internal multiple is a challenge in the second part of the three-pronged strategy.

6 Acknowledgements

We are grateful to all M-OSRP sponsors for their encouragement and support. All members in the M-OSRP group are thanked for their help of valuable discussions and shared information.

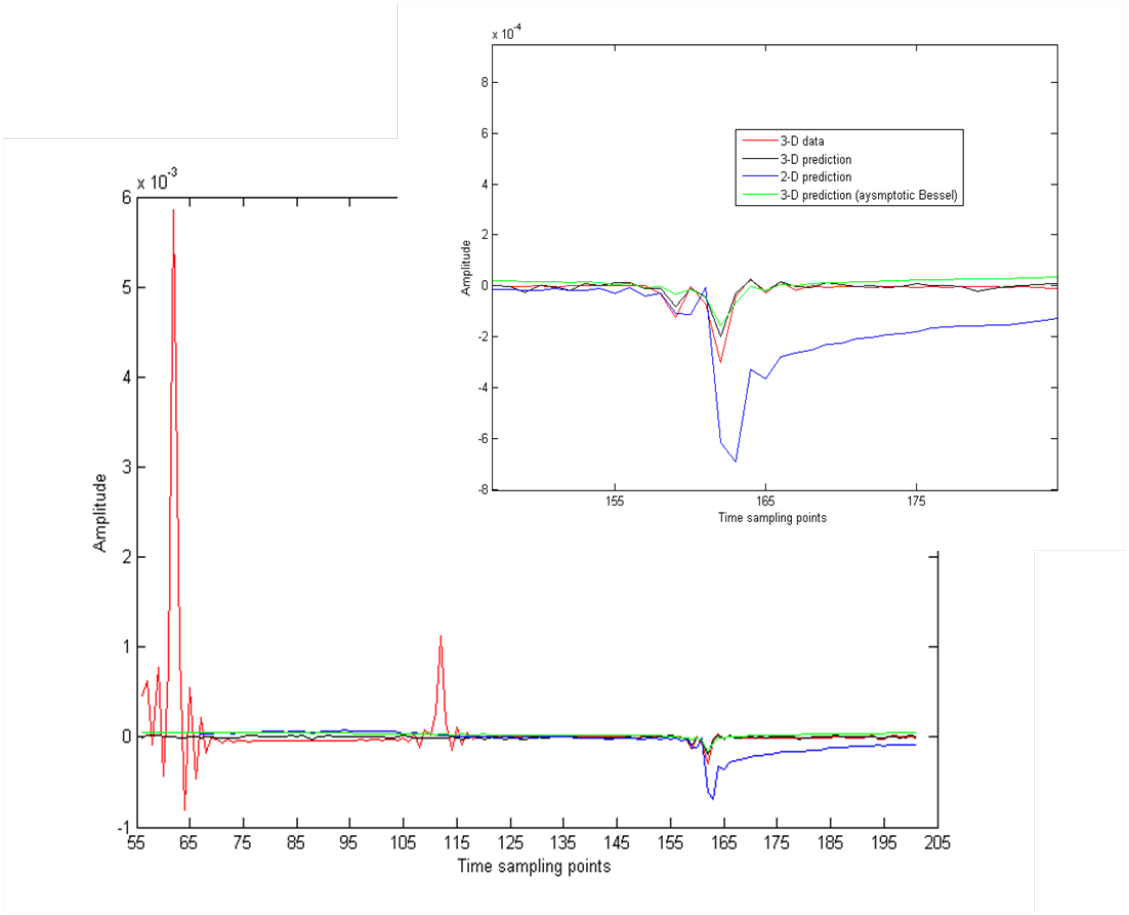

Figure 4: Trace 2 comparison of the data (red line), the 2-D algorithm prediction (blue line), the 3-D algorithm prediction (black line) the 3-D algorithm prediction with asymptotic Bessel function (green line). Figure shown on the right top is the enlarged internal multiple event.

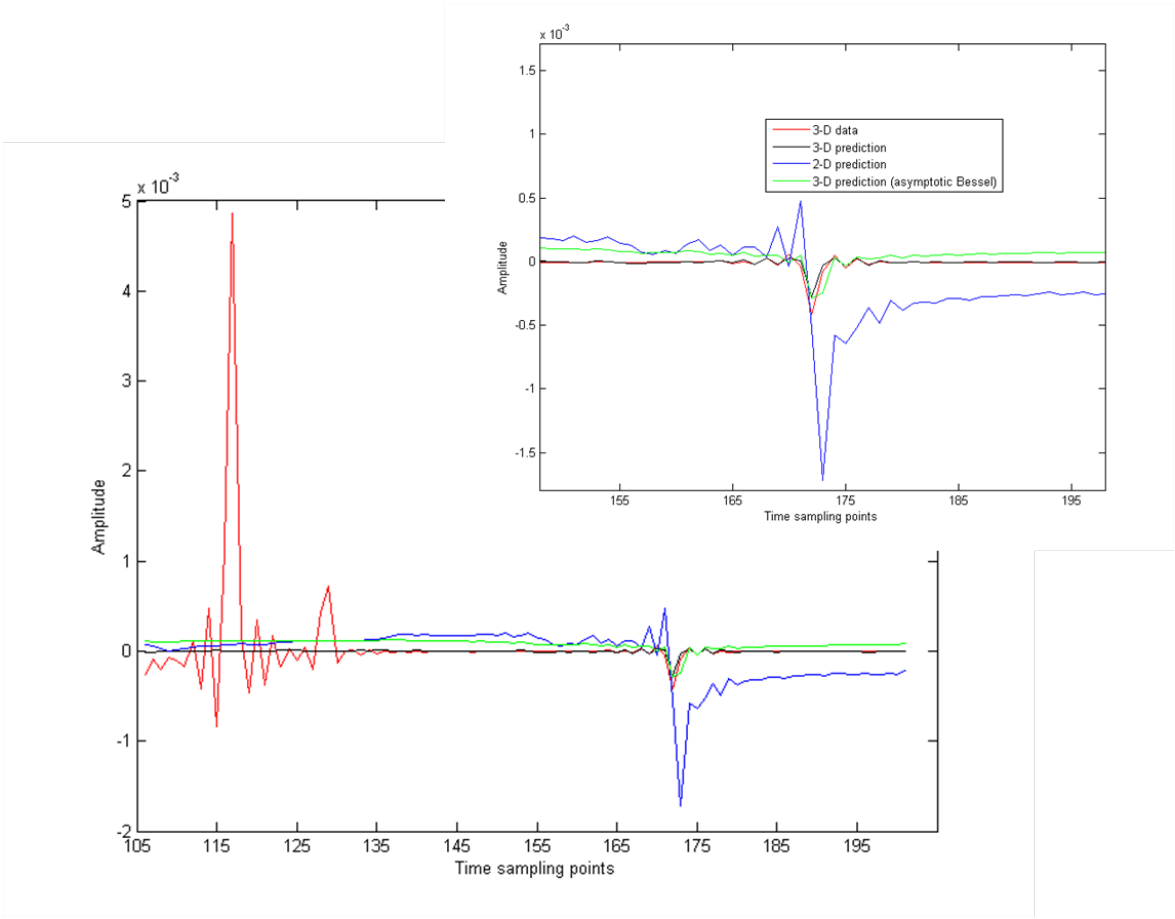

Figure 5: Trace 50 comparison of the data (red line), the 2-D algorithm prediction (blue line), the 3-D algorithm prediction (black line) the 3-D algorithm prediction with asymptotic Bessel function (green line). Figure shown on the right top is the enlarged internal multiple event.

Appendix A

A Transformation of integral variables

The transformation from the integrand over the vector $\vec{r_g}$ to the other vector $\vec{r_h}$ can be obtained by Jacobian determinant. The definition of two vectors under cylindrical coordinate can be expressed by $\vec{r_g} = (r_g, \theta_g)$ and $\vec{r_h} = (r_h, \theta_h)$. Because of the $\vec{r_h} = \vec{r_g} - \vec{r_s}$, where the $\vec{r_g}$ is the location of receivers and the $\vec{r_s}$ is the location of sources, we have the relation between two vectors:

$$r_h = \sqrt{r_g^2 + r_s^2 - 2r_g r_s cos(\theta_g - \theta_s)} \tag{18}$$

$$\theta_h = \arctan(\frac{r_g sin\theta_g - r_s sin\theta_s}{r_s cos\theta_g - r_g cos\theta_s}). \tag{19}$$

The relation can be represented by a Jacobian determinant,

$$dr_h d\theta_h = |J| dr_g d\theta_g = \begin{vmatrix} \frac{\partial r_h}{\partial r_g} & \frac{\partial r_h}{\partial \theta_g} \\ \frac{\partial \theta_h}{\partial r_g} & \frac{\partial \theta_h}{\partial \theta_g} \end{vmatrix}. \tag{20}$$

Solve the determinant through the derivative values given by,

$$\frac{\partial r_h}{\partial r_g} = \frac{r_g - r_s cos(\theta_g - \theta_s)}{\sqrt{r_g^2 - r_s^2 - 2r_g r_s cos(\theta_g - \theta_s)}} \tag{21}$$

$$\frac{\partial r_h}{\partial \theta_g} = \frac{r_g r_s sin(\theta_g - \theta_s)}{\sqrt{r_g^2 - r_s^2 - 2r_g r_s cos(\theta_g - \theta_s)}} \tag{22}$$

$$\frac{\partial \theta_h}{\partial r_g} = \frac{b sin\theta_g - a cos\theta_g}{a^2 + b^2} \tag{23}$$

$$\frac{\partial \theta_h}{\partial \theta_g} = \frac{b r_g cos\theta_g - a r_g sin\theta_g}{a^2 + b^2}, \tag{24}$$

where $a = r_g sin\theta_g - r_s sin\theta_s$ and $b = r_g cos\theta_g - r_s cos\theta_s$. The J determinant can be calculated as,

$$|J| = \frac{\partial r_h}{\partial r_g}\frac{\partial \theta_h}{\partial \theta_g} - \frac{\partial r_h}{\partial \theta_g}\frac{\partial \theta_h}{\partial r_g} = \frac{r_g}{r_h}. \tag{25}$$

We obtain the relation between two integral variables, as

$$dr_h d\theta_h = |J| dr_g d\theta_g \tag{26}$$

$$r_h dr_h d\theta_h = r_g dr_g d\theta_g. \tag{27}$$

B Dirac delta in cylindrical coordinates

Prove the Dirac delta from a general formula,

$$\iint e^{i(\vec{k_{r1}}-\vec{k_{r2}})\cdot\vec{r_2}}d\vec{r_2} = (2\pi)^2\delta(k_{x1}-k_{x2})\delta(k_{y1}-k_{y2}). \tag{28}$$

Convert the Dirac delta on the right side from Cartesian coordinate to cylindrical coordinate, as

$$\delta(k_{r1}-k_{r2})\delta(\phi_1-\phi_2) = |\frac{\partial(k_{x1},k_{y1})}{\partial(\phi_1-\phi_2)}|\delta(k_{x1}-k_{x2})\delta(k_{y1}-k_{y2}) \tag{29}$$

$$\delta(k_{r1}-k_{r2})\delta(\phi_1-\phi_2) = \begin{vmatrix} cos\phi_1 & sin\phi_1 \\ -k_{r1}sin\phi_1 & k_{r1}cos\phi_1 \end{vmatrix}\delta(k_{x1}-k_{x2})\delta(k_{y1}-k_{y2}) \tag{30}$$

$$\frac{\delta(k_{r1}-k_{r2})\delta(\phi_1-\phi_2)}{k_{r1}} = \delta(k_{x1}-k_{x2})\delta(k_{y1}-k_{y2}). \tag{31}$$

The 2-dimensional Fourier transform over a constant can give us

$$\iint e^{i(\vec{k_{r1}}-\vec{k_{r2}})\cdot\vec{r_2}}d\vec{r_2} = (2\pi)^2\frac{\delta(k_{r1}-k_{r2})\delta(\phi_1-\phi_2)}{k_{r1}}. \tag{32}$$

References

Araújo, F. V. *Linear and non-linear methods derived from scattering theory: backscattered tomography and internal multiple attenuation.* PhD thesis, Universidade Federal da Bahia, 1994.

Duquet, B., A. Chavanne, P. Poupion, M. Rowlands, B. Santos-Luis, and J. M. Ugolini. "Seismic Processing and Imaging in Central North Sea Area - Recents Advances and Remaining Challenges." *75th EAGE conference* (2013).

Herrera, W. and A. Weglein. "Eliminating first-order internal multiples with downward reflection at the shallowest interface: Theory and initial examples." *SEG Technical Program Expanded Abstracts* (2013): 4131–4135.

Terenghi, P. and A.B. Weglein. "3D Internal Multiple Prediction coding project: preliminary notes." *Mission-Oriented Seismic Research Program Annual Report* (2009): 364–370.

Weglein, A. B. "The multiple attenuation toolbox: Progress, challenges and open issues." *SEG Technical Program Expanded Abstracts. .* Soc. Expl. Geophys., 2013. 4493–4499.

Weglein, A. B., F. V. Araújo, P. M. Carvalho, R. H. Stolt, K. H. Matson, R. T. Coates, D. Corrigan, D. J. Foster, S. A. Shaw, and H. Zhang. "Inverse Scattering Series and Seismic Exploration." *Inverse Problems* (2003): R27–R83.

Zou, Y. and A. Weglein. "A new method to eliminate first order internal multiples for a normal incidence plane wave on a 1D earth." *SEG Technical Program Expanded Abstracts* (2013): 4136–4140.

The first test and evaluation of the inverse scattering series internal multiple attenuation algorithm for an attenuating medium

Jing Wu and Arthur B. Weglein

May 21, 2014

Abstract

In this paper, the Inverse Scattering Series (ISS) internal multiple attenuation algorithm is analytically and numerically evaluated on reflection data from an attenuating medium. All previous synthetic data tests on this algorithm have involved multidimensional acoustic and elastic media. The results for an attenuating medium show that the method retains its value to directly predict internal multiples (IM) with the exact phase and an approximate amplitude, without knowing the medium and its anelastic properties.

1 Introduction

The inverse scattering series can achieve all processing objectives directly by using distinct isolated task-specific subseries and without subsurface information (Weglein et al. (2003)). The ISS internal multiple attenuator has shown stand-alone capabilities on both marine and on-shore plays (e.g., Ferreira, 2011; Fu et al., 2010). To extend the attenuation method to elimination, Zou and Weglein (2013) propose a new algorithm to compensate for transmission loss in the attenuator. This new elimination method requires the input data to be wavelet deconvolved and assumes an elastic subsurface. Obviously, if the data are attenuated and broadened because of their propagation in an anelastic medium, Q compensation is the conventional step to recover the amplitudes before substituting the data into ISS internal multiple elimination algorithm. That can be a difficult step to effectively achieve in practice, because: (1) it requires an accurate knowledge of the attenuation factor Q, and (2) the method is sensitive to small errors in the estimated Q.

An alternative approach, Q compensation based on the ISS without Q information of the subsurface has demonstrated an early but encouraging effectiveness (e.g., Innanen and Weglein, 2003; 2005; Innanen and Lira, 2008). The current ISS Q compensation without Q method assumes that the input data contain primaries only, i.e., that the internal multiples have been attenuated or eliminated for best before stepping into Q compensation algorithm.

This paper demonstrates that applying the industry standard ISS internal multiple attenuator to data from an anelastic earth will attenuate the multiples. The data with primary and relatively weak residual internal multiple can be substituted into the ISS Q compensation algorithm to obtain effective elastic data and then insert that data into the new elastic internal multiple elimination algorithm.

In this paper, for the first time the ISS internal multiple attenuator is tested on data from an attenuating medium. A two-reflector model with constant Q in each layer is used for analytical and numerical testing and evaluation. The result indicates that the prediction has the correct phase and an approximate amplitude. That is positive news for the ISS internal multiple attenuator and encourages developing an elimination method for the exploration plays where absorption is significant, e.g., pre-salt plays in the deep water Gulf of Mexico, off-shore Brazil, the Red Sea and the North Sea.

2 Analytical Test of ISS Internal Multiple Attenuation Algorithm on Data with Q

2.1 Wavefield expression for an attenuating medium

Based on Aki and Richards (2002), assuming a constant Q model, the 1D wave equation can be written as

$$\frac{d^2P}{dx^2} + \frac{\omega^2}{c_0^2}\left(1 + \frac{F(\omega)}{Q}\right)^2 P = 0, \tag{1}$$

where

$$F(\omega) = \frac{i}{2}\,\mathrm{sgn}(\omega) - \frac{1}{\pi}\log(|\frac{\omega}{\omega_r}|)$$

; it's constitute of two terms: the first term is related to the energy attenuation, and the second term is related to velocity dispersion. ω_r here is the reference frequency, and it could be chosen as the maximum frequency in the experiment; c_0 is the constant velocity at the reference frequency.

Q here is used to represent the energy loss for a wave-field propagating, in one wave length, and is defined as

$$Q = \frac{2\pi E}{\Delta E}, \tag{2}$$

where E is the energy of the wave-field, and ΔE is the energy loss in a wavelength of propagation.

If we define a frequency dependent velocity $c(\omega)$ as

$$\frac{1}{c(\omega)} = \frac{1}{c_0}\left(1 + \frac{F(\omega)}{Q}\right), \tag{3}$$

then the wavefield $P(x, \omega)$ can be expressed as

$$P(x,\omega) = e^{i\frac{\omega}{c(\omega)}x} = e^{i\frac{\omega}{c_0}x} e^{-\frac{\omega\,\mathrm{sgn}(\omega)}{2c_0Q}x} e^{-i\frac{\omega}{c_0\pi Q}\log(|\frac{\omega}{\omega_r}|)x}. \tag{4}$$

From the formula, we understand the wavefield is influenced by three terms: the first term is contributing to the phase with the velocity of c_0, the second term is contributing to the energy attenuation, and the third term is contributing to the phase delay with velocity dispersion. Only the first term is left when Q is increased to infinity; i.e, the medium is back to elastic.

2.2 Analytical Test Under 1D Normal Incidence

Following the explanation in the previous section, we can express the wave-field in an anelastic medium analytically. In this section, the anelastic data will be used as input to test the ISS internal multiple attenuation algorithm analytically.

For 1D normal incidence, the ISS internal multiple attenuation algorithm (e.g., Araújo, 1994; Weglein et al., 1997; 2003) can be expressed as:

$$b_3(k_z) = \int_{-\infty}^{\infty} b_1(z) e^{ik_z z} dz \int_{-\infty}^{z-\epsilon} b_1(z_1) e^{-ik_z z_1} dz_1 \int_{z_1+\epsilon}^{\infty} b_1(z_2) e^{ik_z z_2} dz_2, \tag{5}$$

where the deghosted data, $D(t)$, for an incident spike wave, satisfies $D(\omega) = b_1(2\omega/c_0)$, and $b_1(z) = \int_{-\infty}^{\infty} b_1(k_z) e^{-ik_z z} dk_z$, $k_z = 2\omega/c_0$ is the vertical wavenumber, and $b_1(z)$ corresponds to an uncollapsed FK migration of the normal-incident spike plane-wave data. ϵ in the formula is used to make sure the events satisfy the lower-higher-lower relationship, and its value is chosen on the basis of the length of the wavelet.

A two-reflector model is provided below as an example, with the parameters listed in Fig.1, and with the depths of source and receiver both assumed to be zero.

For a 1D model and a 1D normal-incident plane wave, two primaries in the data $D(\omega)$ can be represented as:

$$\begin{aligned} P^{(1)}(\omega) &= R_1(\omega) e^{i\frac{\omega}{c_1(\omega)}2z_1}, \\ P^{(2)}(\omega) &= T_{12}(\omega) T_{21}(\omega) R_2(\omega) e^{i\frac{\omega}{c_1(\omega)}2z_1} e^{i\frac{\omega}{c_2(\omega)}2(z_2-z_1)}, \end{aligned} \tag{6}$$

where $\frac{1}{c_1(\omega)} = \frac{1}{c_1}\left(1 + \frac{F(\omega)}{Q_1}\right)$ and $\frac{1}{c_2(\omega)} = \frac{1}{c_2}\left(1 + \frac{F(\omega)}{Q_2}\right)$, the velocities in both layers are frequency dependent. And the primaries are both suffered from the absorption.

After migrating the data into the pseudo depth domain to get $b_1(z)$, we can substitute it into eqn.4. We further assume that the two primaries in $b_1(z)$ are isolated and ϵ is chosen reasonably to make sure there is no overlap between the two events among the integrals. The predicted internal multiple $b_3(k_z)$ can be obtained:

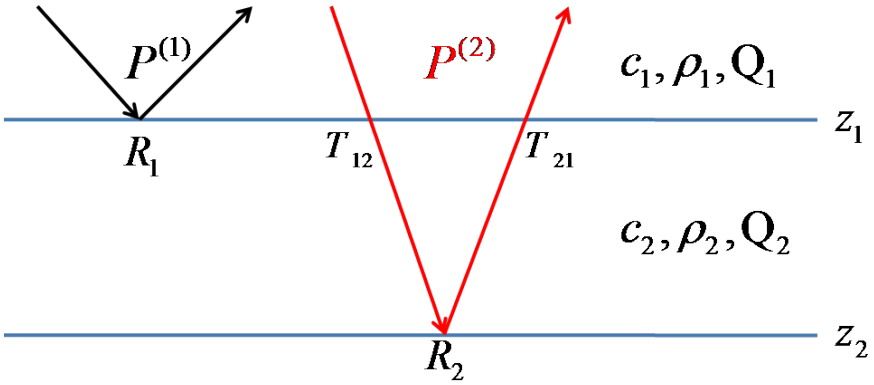

Figure 1: A two-reflector 1D model. $P^{(1)}$ and $P^{(2)}$ are primaries from the first and the second interface, respectively; R_1 and R_2 are reflection coefficients; T_{12} and T_{21} are transmission coefficients; c_1 and c_2 are the velocities; ρ_1 and ρ_2 are densities; and Q_1 and Q_2 are quality factors.

$$b_3(k_z) = (T_{12}(k_z)T_{21}(k_z)R_2(k_z))^2 {R_1}^*(k_z) e^{-\frac{|k_z|}{Q_1}z_1} e^{ik_z\left(1+\frac{F(k_z)}{Q_1}\right)z_1} e^{i2k_z\frac{c_1}{c_2}\left(1+\frac{F(k_z)}{Q_2}\right)(z_2-z_1)}, \quad (7)$$

where $F(k_z) = \frac{i}{2}\,\mathrm{sgn}\,(k_z) - \frac{1}{\pi}\log(|\frac{k_z}{k_{zr}}|)$, and $k_{zr} = 2\omega_r/c_1$.

The actual first-order internal multiple in the k_z domain is

$$IM(k_z) = -T_{12}(k_z)T_{21}(k_z)(R_2(k_z))^2 R_1(k_z) e^{ik_z\left(1+\frac{F(k_z)}{Q_1}\right)z_1} e^{i2k_z\frac{c_1}{c_2}\left(1+\frac{F(k_z)}{Q_2}\right)(z_2-z_1)}. \quad (8)$$

The relation between the predicted internal multiple and the actual internal multiple is

$$b_3(k_z) = -T_{12}(k_z)T_{21}(k_z)\frac{{R_1}^*(k_z)}{R_1(k_z)} e^{-\frac{|k_z|}{Q_1}z_1} IM(k_z). \quad (9)$$

In this formula, the phase related to the product between the transmission and reflection coefficients can be neglected, since it's too small to make effective contribution, and the later numerical results can further confirm this view point.

Until now, we understand that, by using the ISS internal multiple attenuation algorithm, the multiple can be predicted with the correct phase and an approximate amplitude.

If the data are without the influence of Q absorption, i.e., Q is increasing to infinity and the medium is acoustic/elastic, then from Weglein et al. (2003), we can obtain the relation between predicted and actual internal multiple as

$$b_3(k_z) = -T_{12}T_{21}IM(k_z). \quad (10)$$

Comparing equation 9 and equation 10, it can be seen that the predicted amplitude is less accurate for input data with Q absorption than it is for data without Q; however, still the correct phase under both situations. Actually, for the elastic medium, the transmission coefficients on the interfaces that are above and at the multiple generator are over predicted and the first interface is the multiple generator for this model; however, for the anelastic medium, besides the transmission coefficients on those related interfaces, the energy attenuation caused by absorption in the layers that are above the multiple generator is also over estimated and only the first layer is above the multiple generator for this model. This is reasonable, since for the attenuating medium, both the layer and interface will make contribution to the transmission loss.

3 Numerical Test of ISS Internal Multiple Attenuation Algorithm on Data with Q

Two two-reflector 1D models (Fig.1) will be used as examples to numerically test the effectiveness of ISS internal multiple attenuator on anelastic data.

For the first model, the parameters are listed in Fig.2(a). We know from the Q values that the wavefield will experience light absorption during the propagation, and the events will still be very narrow. The synthetic data with the parameters are generated with two primaries and one first-order internal multiple which is encountering downward reflection at the first interface.

Substituting the input data b_1, shown as the blue line in Fig.2(b), into ISS internal multiple attenuation algorithm, we can predict internal multiple b_3, shown as the red line in Fig.2(b). Actually, the red line in Fig.2(b) is -b_3. It can be seen from equation 9 that the polarity of b_3 is opposite to that of the actual internal multiple. In order to show the result more clearly, the predicted internal multiple and the actual internal multiple are compared in Fig.2(c). From the result, we further confirm that the prediction result matches well in phase and approximately in amplitude even with data from an attenuating medium, without knowing absorptive and dispersive properties.

For the second model, the parameters are listed in Fig.3(a). Here we only decrease Q in the second layer to be a very small value, and keep the other parameters to be the same as the first model. With such a small Q in the second layer, the primaries from the second interface and the internal multiple propagating two cycles in the second layer will suffer seriously from the absorption. This can be seen from the blue line in Fig.3(b), representing the input data b_1. Even with significant energy attenuation and velocity dispersion, the prediction result from the ISS attenuator is still satisfied, which can be clearly confirmed from Fig.3(c), the comparison between the predicted and actual internal multiple.

4 Discussion

In this paper, the ISS internal multiple attenuation algorithm is tested analytically and numerically using Q-influenced data, with the conclusion that the prediction will have the correct phase and an

approximate amplitude.

The discussion in this paper gives us confidence that even for an attenuating medium, the ISS internal multiple attenuator can provide a result that retains the primary and partially removes the internal multiple. This is an important step in a strategy to eliminate internal multiples for both elastic and anelastic media. That will allow application for exploration plays where the geology exhibits significant absorption, e.g., pre-salt plays in the deep water Gulf of Mexico, off-shore Brazil, the Red Sea and the North Sea.

5 Acknowledgements

We are grateful to all M-OSRP sponsors for encouragement and support in this research.

Layer	Velocity(m/s)	Q	Density(kg/m^3)
1	1500	100	1000
2	2500	100	1000
3	6000	200	1000

(a)

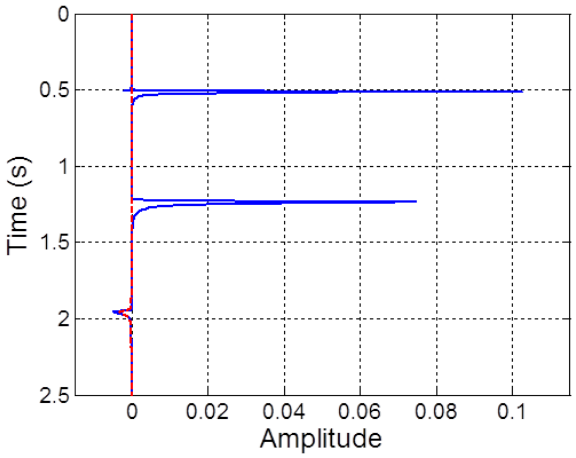

(b)

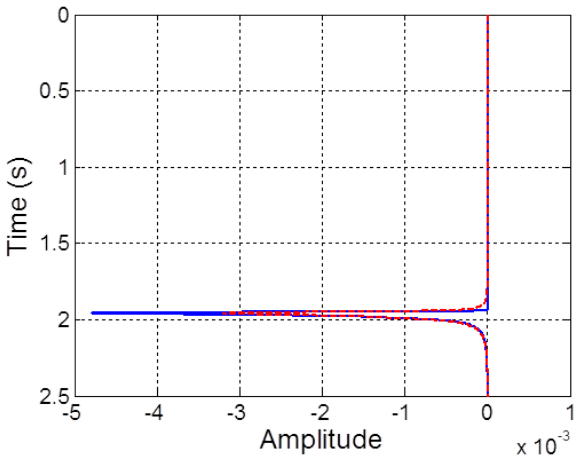

(c)

Figure 2: The numerical result of ISS internal multiple attenuation algorithm with anelastic data. (a) the parameters for the first model; (b): the input data b_1 (blue line) and the predicted multiple -b_3 (red line); (c): the actual internal multiple (blue line) and the predicted internal multiple -b_3 (red line).

Layer	Velocity(m/s)	Q	Density(kg/m^3)
1	1500	100	1000
2	2500	20	1000
3	6000	200	1000

(a)

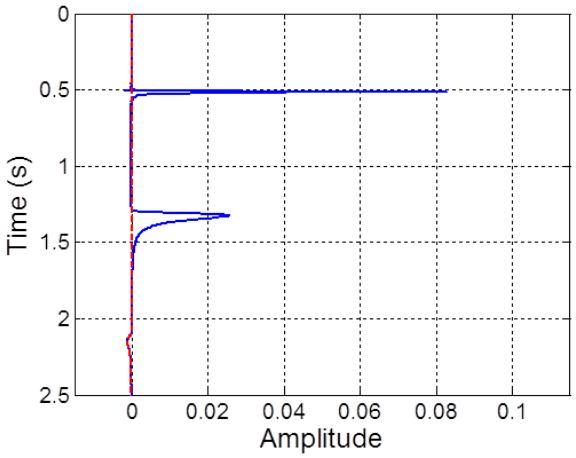

(b)

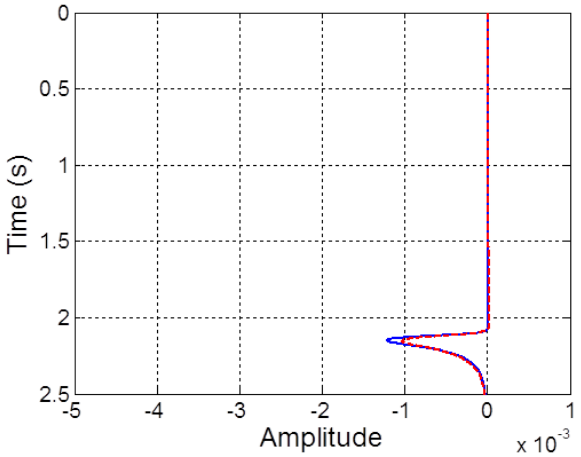

(c)

Figure 3: The numerical result of ISS internal multiple attenuation algorithm with anelastic data. (a) the parameters for the second model; (b): the input data b_1 (blue line) and the predicted multiple -b_3 (red line); (c): the actual internal multiple (blue line) and the predicted internal multiple -b_3 (red line).

Appendix

A B3 Calculation

The primaries in frequency domain can be expressed from equation 6. Since the migrated data in pseudo depth domain are required to substitute into the internal multiple attenuation algorithm, the variable should be changed from ω to $k_z = \frac{2\omega}{c_1}$:

$$\begin{aligned} P^{(1)}(k_z) &= R_1(k_z)e^{ik_z\left(1+\frac{F(k_z)}{Q_1}\right)z_1}, \\ P^{(2)}(k_z) &= T_{12}(k_z)T_{21}(k_z)R_2(k_z)e^{ik_z\left(1+\frac{F(k_z)}{Q_1}\right)z_1}e^{ik_z\frac{c_1}{c_2}\left(1+\frac{F(k_z)}{Q_2}\right)(z_2-z_1)}. \end{aligned} \tag{11}$$

We obtain $b_1(k_z) = P^{(1)}(k_z) + P^{(2)}(k_z)$.

Then, Fourier transform is applied over k_z to pseudo depth domain to obtain

$$b_1(z) = P^{(1)}(z) + P^{(2)}(z), \tag{12}$$

which will be substituted into ISS internal multiple attenuation algorithm to predict the internal multiple $b_3(k_z)$.

Based on Weglein et al. (2003), the 1D ISS internal multiple attenuation algorithm is

$$b_3(k_z) = \int_{-\infty}^{\infty} b_1(z)e^{ik_z z}dz \int_{-\infty}^{z-\epsilon} b_1(z_1)e^{-ik_z z_1}dz_1 \int_{z_1+\epsilon}^{\infty} b_1(z_2)e^{ik_z z_2}dz_2, \tag{13}$$

where ϵ is used to make sure the events satisfy the lower-higher-lower relationship, and its value is chosen on the basis of the length of the wavelet.

For this model, there are two primaries in the data. Now we assume that these two events are isolated (Fig.4). The pseudo depth of the first event is z_1' with a length of 2a, whereas the pseudo depth of the second event is z_2' with a length of 2b. For ϵ in equation 13 , it is chosen to satisfy $\epsilon \geq max(2a, 2b)$ and $\epsilon \leq (z_2' - b - (z_1' + a))$.

Kaplan et al. (2004) change the integral order of equation 13 and rewrite the formula as:

$$b_3(k_z) = \int_{-\infty}^{\infty} b_1(z)e^{-ik_z z}[\int_{z+\epsilon}^{\infty} b_1(z')e^{ik_z z'}dz']^2 dz. \tag{14}$$

Since $b_1(z) = P^{(1)}(z) + P^{(2)}(z)$, equation 14 can be divided into two parts:

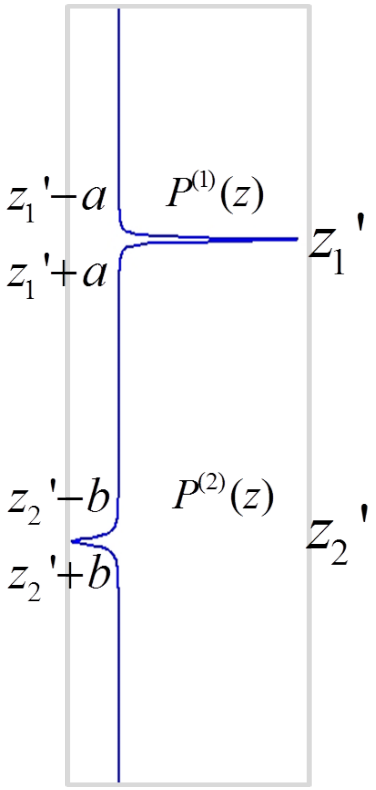

Figure 4: A two-reflector 1D model. $P^{(1)}$ and $P^{(2)}$ are primaries from the first and the second interface, respectively; R_1 and R_2 are reflection coefficients; T_{12} and T_{21} are transmission coefficients; c_1 and c_2 are the velocities; ρ_1 and ρ_2 are densities; and Q_1 and Q_2 are quality factors.

$$
\begin{aligned}
& b_3(k_z) \\
&= \int_{-\infty}^{\infty} P^{(1)}(z) e^{-ik_z z} [\int_{z+\epsilon}^{\infty} b_1(z') e^{ik_z z'} dz']^2 dz \\
&+ \int_{-\infty}^{\infty} P^{(2)}(z) e^{-ik_z z} [\int_{z+\epsilon}^{\infty} b_1(z') e^{ik_z z'} dz']^2 dz \\
&= \int_{z_1'-a}^{z_1'+a} P^{(1)}(z) e^{-ik_z z} [\int_{z+\epsilon}^{\infty} b_1(z') e^{ik_z z'} dz']^2 dz \qquad (15.1) \\
&+ \int_{z_2'-b}^{z_2'+b} P^{(2)}(z) e^{-ik_z z} [\int_{z+\epsilon}^{\infty} b_1(z') e^{ik_z z'} dz']^2 dz. \qquad (15.2)
\end{aligned}
$$

For (15.1), the integral limitation of z is $[z_1' - a, z_1' + a]$. Consider the lower limit of the integral of z' and the constraint of ϵ,

$z+\epsilon \geq z_1' - a + \epsilon \geq z_1' + a + 2a = z_1' + a,$

and

$z+\epsilon \leq z_1' + a + \epsilon \leq z_1' + a + z_2' - b - (z_1' + a) = z_2' - b.$

We can see that the lower limit of the second integral should be after the end of the first event and before the beginning of the second event, i.e., in $[z+\epsilon, \infty)$, the kernel of the second integral is $b_1(z') = P^{(2)}(z')$.

So

$$\begin{aligned}
&(15.1)\\
=&\int_{z_1'-a}^{z_1'+a} P^{(1)}(z) e^{-ik_z z} [\int_{z+\epsilon}^{\infty} b_1(z') e^{ik_z z'} dz']^2 dz\\
=&\int_{z_1'-a}^{z_1'+a} P^{(1)}(z) e^{-ik_z z} [\int_{z+\epsilon}^{\infty} P^{(2)}(z') e^{ik_z z'} dz']^2 dz\\
=&\int_{-\infty}^{\infty} P^{(1)}(z) e^{-ik_z z} [\int_{-\infty}^{\infty} P^{(2)}(z') e^{ik_z z'} dz']^2 dz\\
=&(T_{12}(k_z)T_{21}(k_z)R_2(k_z))^2 {R_1}^*(k_z) e^{-\frac{|k_z|}{Q_1} z_1} e^{ik_z\left(1+\frac{F(k_z)}{Q_1}\right)z_1} e^{i2k_z \frac{c_1}{c_2}\left(1+\frac{F(k_z)}{Q_2}\right)(z_2-z_1)}.
\end{aligned}$$

Similarly, for (15.2), the integral limitation of z is $[z_2' - b, z_2' + b]$. Consider the lower limit of the integral of z' and the constraint of ϵ,

$z+\epsilon \geq z_2' - b + \epsilon \geq z_2' + b + 2b = z_2' + b.$

The lower limit of the second integral should be after the end of the second event, i.e., in $[z+\epsilon, \infty)$, the kernel the of second integral is $b_1(z') = 0$.

So

$$\begin{aligned}
&(15.2)\\
=&\int_{z_2'-b}^{z_2'+b} P^{(2)}(z) e^{-ik_z z} [\int_{z+\epsilon}^{\infty} b_1(z') e^{ik_z z'} dz']^2 dz\\
=&0.
\end{aligned}$$

Now

$$\begin{aligned}
&b_3(k_z)\\
=&(15.1)\\
=&(T_{12}(k_z)T_{21}(k_z)R_2(k_z))^2 {R_1}^*(k_z) e^{-\frac{|k_z|}{Q_1} z_1} e^{ik_z\left(1+\frac{F(k_z)}{Q_1}\right)z_1} e^{i2k_z \frac{c_1}{c_2}\left(1+\frac{F(k_z)}{Q_2}\right)(z_2-z_1)}.
\end{aligned}$$

References

Aki, Keiiti and Paul G. Richards. *Quantitative Seismology.* Second edition. University Science Books, 2002.

Araújo, F. V. *Linear and non-linear methods derived from scattering theory: backscattered tomography and internal multiple attenuation.* PhD thesis, Universidade Federal da Bahia, 1994.

Ferreira, A. Internal multiple removal in offshore Brazil seismic data using the inverse scattering series. Master's thesis, University of Houston, 2011.

Fu, Q., Y. Luo, P. G. Kelamis, S. Huo, G. Sindi, S.-Y. Hsu, and A. B.Weglein. "The inverse scattering series approach towards the elimination of land internal multiples." *SEG Technical Program Expanded Abstracts.* 2010, 3456–3461.

Innanen, K. A. and J.E. Lira. "Direct non-linear Q compensation of primaries in layered media: Theory and synthetic examples." *SEG Technical Program Expanded Abstracts.* . Soc. Expl. Geophys., 2008. 2957–2962.

Innanen, K. A. and A. B. Weglein. "Construction of absorptive/dispersive wave fields with the forward scattering series." *Journal of Seismic Exploration* 12 (2003): 259–282.

Innanen, K. A. and A. B. Weglein. "Towards non-linear construction of a Q-compensation operator directly from reflection seismic data." *SEG Technical Program Expanded Abstracts.* . Soc. Expl. Geophys., 2005. 1693–1696.

Kaplan, Sam T., Kristopher A. Innanen, Einar Otnes, and Arthur Weglein. "Internal multiple attenuation code-development and implementation." *Mission-Oriented Seismic Research Program (M-OSRP) Annual Report.* 2004, 83–102.

Weglein, A. B., F. V. Araújo, P. M. Carvalho, R. H. Stolt, K. H. Matson, R. T. Coates, D. Corrigan, D. J. Foster, S. A. Shaw, and H. Zhang. "Inverse Scattering Series and Seismic Exploration." *Inverse Problems* (2003): R27–R83.

Weglein, A. B., F. A. Gasparotto, P. M. Carvalho, and R. H. Stolt. "An Inverse-Scattering Series Method for Attenuating Multiples in Seismic Reflection Data." *Geophysics* 62 (November-December 1997): 1975–1989.

Zou, Y. and A.B. Weglein. "A new method to eliminate first order internal multiples for a normal incidence plane wave on a 1D earth." *SEG Technical Program Expanded Abstracts.* 2013, 4136–4140.

Short note: Progress in ISS internal-multiple removal: Computational requirements

Qiang Fu, Chao Ma, Yanglei Zou, James D. Mayhan, and Fang Liu

May 21, 2014

Abstract

The leading-order ISS internal-multiple-attenuation algorithm computes the exact time and the approximate amplitude of internal multiples using a compute-intensive algorithm. This algorithm plus adaptive subtraction might be effective enough for areas with few strong reflectors — *e.g.*, the deep-water Gulf of Mexico. However, areas with many strong reflectors, where most primaries have an adjacent or overlying internal multiple — *e.g.*, Saudi Arabia and western Canada — need additional accuracy in computing amplitudes. This accuracy can be provided by removing so-called "spurious" predictions and by completely eliminating internal multiples by using the respective ISS algorithms. An approach to estimating the compute requirements of this additional capability is discussed and compared with the compute requirements of the leading-order ISS internal-multiple-attenuation algorithm.

1 Introduction

M-OSRP algorithms for depth imaging and inversion for properties across subsurface boundaries assume that only primaries from the measured wavefield, P, are used as input — *i.e.*, that the reference wavefield, P_0, ghosts, and multiples have been removed from P. The leading-order ISS internal-multiple-attenuation algorithm (Araújo, 1994; Weglein et al., 1997) computes the exact time and the approximate amplitude of internal multiples by using a compute-intensive algorithm. New algorithms to converge on the exact amplitude are expected to be even more compute-intensive. The compute requirements of the leading-order ISS internal-multiple-attenuation algorithm are estimated in Kaplan et al. (2005). We report first-pass estimates of the compute requirements for the new algorithms.

An infinite series is required to compute both the exact time and the exact amplitude of internal multiples embedded in seismic data. The leading-order ISS internal-multiple-attenuation algorithm is the first term in that series (hence the term "leading order" in its description). Approximate amplitudes are computed because higher-order terms (beyond first order) are not present.

The new algorithms take two approaches to the missing higher-order terms. (1) The ISS higher-order internal-multiple-attenuation algorithm removes the spurious predictions (normally eliminated by higher-order terms) by taking the output of the leading-order ISS internal-multiple-attenuation algorithm and using it as part of the input to another calculation by the leading-order ISS internal-multiple-attenuation algorithm. (2) The internal-multiple-elimination algorithm solves an integral equation by iteration. The advantage of approach 2 is that, as is the case with the free-surface-multiple algorithm, it can use as many terms as are needed to eliminate all orders of internal multiples that are present in P.

2 What are internal multiples?

In a marine experiment, an air-gun array (towed by a survey boat) periodically releases compressed air underwater to create intense sound waves. The sound waves reflect from the ocean surface, ocean bottom, and boundaries between underground rock layers. Reflected sound waves are recorded by underwater microphones (hydrophones), which are also towed by the survey boat.[1] The recorded sound waves are processed to infer information about the structure and properties of the underground rock layers. One component of the recorded sound waves (internal multiples) is computed and removed from the recorded sound waves.

M-OSRP processing of marine seismic data includes the following steps. (1) The total pressure wavefield P measured by the hydrophones is considered to be the sum of a reference pressure wavefield P_0 and a scattered pressure wavefield P_s, which is $P - P_0$. All events that are reflected from the Earth are in the measured values of the scattered wave, P_s. (2) After P_0 is removed, M-OSRP defines ghosts. Ghosts are the events in P_s that begin their propagation by moving upward from the source (source ghosts) or end their propagation by moving downward to the receiver (receiver ghosts) or both (source-receiver ghosts) and that have at least one upward reflection from the Earth. (3) After the reference wavefield and all ghosts have been removed, M-OSRP defines multiples and primaries. Free-surface multiples have at least one downward reflection from the air-water boundary and at least one upward reflection from the Earth. Internal multiples have no downward reflections from the air-water boundary, have more than one upward reflection from the Earth, and at have least one downward reflection from inside the Earth. An nth-order free-surface multiple has n downward reflections from the air-water boundary, and an nth-order internal multiple has n downward reflections from reflector(s) inside the Earth. Primaries have only one upward reflection from the Earth and no other reflections.

3 Why are internal multiples so compute intensive?

An internal multiple can be pictured as one or more W's.[2] Sound moves down, is reflected upward, then downward, then upward, and so on. We don't know *a priori* where the reflections take place, so

[1] The towed streamers may also include geophones or accelerometers.

[2] Similarly, a primary can be pictured as a V.

the algorithm combs through the recorded data looking for upward and downward reflections at all possible depths (with the restriction that downward reflections are at shallower depths than upward reflections are). Kaplan et al. (2005) and Perrone (2007) performed the early work estimating compute requirements for the internal-multiple-attenuation algorithm. This algorithm is but the first term in a subseries; hence, it requires modification. Ma and Weglein (2014) are improving the algorithm to suppress so-called "spurious" events. Zou and Weglein (2014a;b;c) are improving the algorithm to more accurately compute amplitudes of internal multiples. However, each improvement in accuracy increases the algorithmic complexity and compute time.

4 Why improve the internal multiple algorithm?

M-OSRP's toolbox approach recognizes that each method for attenuating multiples has strengths and limitations and that, for a given prospect and play, one chooses the appropriate method from a cost-effectiveness perspective (Weglein, 2013). The petroleum industry's current worldwide portfolio of both conventional and unconventional onshore plays, and of increasingly complex offshore plays — with new and unforeseen, daunting challenges — has returned and rejuvenated an interest in multiple removal (and has stimulated a demand for substantially increased effectiveness). Multiple removal has come back to center stage, both for our sponsors and concomitantly as a key and fundamental research project (once again) for M-OSRP (Weglein, 2014). To adequately address the current industry challenge, we will need to be able to predict exactly the phase and amplitude of all internal multiples and thereby to surgically remove (eliminate) the multiples at all offsets, directly, and without subsurface information (Weglein, 2014).

For example, in the deep-water Gulf of Mexico, an area with few strong reflectors, the 3D internal-multiple-attenuation algorithm plus adaptive subtraction might be enough. However, in Saudi Arabia and western Canada, where there are many strong reflectors and most primaries have an adjacent or overlying internal multiple, spurious predictions must be removed and internal multiples must be completely eliminated. If we can not separate primaries and multiples, how can we do AVO analysis?

5 Compute requirements of the Inverse-Scattering-Series (ISS) higher-order internal-multiple-attenuation algorithm to accommodate primaries and internal multiples as input

The current leading-order Inverse-Scattering-Series internal-multiple-attenuation algorithm (Araújo, 1994; Weglein et al., 1997) is among the most compute-intensive processes in seismic exploration. Its computational costs and optimization on large distributed systems are reported in Kaplan et al. (2005) and Terenghi (2011). The new higher-order ISS internal-multiple-attenuation algorithm accommodates the input data containing both primaries and internal multiples and addresses the so-called "spurious" predictions that the current leading-order algorithm can produce. In the following,

we will provide a brief summary of the computational requirements of the new higher-order algorithm compared with that of the current leading-order algorithm.

In two dimensions, the current leading-order ISS internal-multiple-attenuation algorithm is (Weglein et al., 2003; Kaplan et al., 2005)

$$b_{3IM}(k_g,k_s,\omega) = \frac{1}{(2\pi)^2}\int_{-\infty}^{\infty}\int_{-\infty}^{\infty}\int_{-\infty}^{\infty} b_1(k_1,k_2,z_1)e^{-i(k_{1z}+k_{2z})z_1} \left[\int_{z_1+\epsilon}^{\infty} b_1(k_g,k_1,z_2)e^{i(k_{gz}+k_{1z})z_2}dz_2\right]\left[\int_{z_1+\epsilon}^{\infty} b_1(k_g,k_1,z_2)e^{i(k_{2z}+k_{sz})z_2}dz_2\right]dz_1dk_1dk_2. \quad (1)$$

The proposed higher-order algorithms to address spurious predictions are (Ma et al., 2011; Liang et al., 2011)

$$b_5^{PIP}(k_g,k_s,\omega) = \frac{1}{(2\pi)^2}\int_{-\infty}^{\infty}\int_{-\infty}^{\infty}\int_{-\infty}^{\infty} b_{3IM}(k_1,k_2,z_1)e^{-i(k_{1z}+k_{2z})z_1} \left[\int_{z_1+\epsilon}^{\infty} b_1(k_g,k_1,z_2)e^{i(k_{gz}+k_{1z})z_2}dz_2\right]\left[\int_{z_1+\epsilon}^{\infty} b_1(k_g,k_1,z_2)e^{i(k_{2z}+k_{sz})z_2}dz_2\right]dz_1dk_1dk_2, \quad (2)$$

and

$$b_5^{PPI}(k_g,k_s,\omega) = \frac{1}{(2\pi)^2}\int_{-\infty}^{\infty}\int_{-\infty}^{\infty}\int_{-\infty}^{\infty} b_1(k_1,k_2,z_1)e^{-i(k_{1z}+k_{2z})z_1} \left[\int_{z_1+\epsilon}^{\infty} b_{3IM}(k_g,k_1,z_2)e^{i(k_{gz}+k_{1z})z_2}dz_2\right]\left[\int_{z_1+\epsilon}^{\infty} b_1(k_g,k_1,z_2)e^{i(k_{2z}+k_{sz})z_2}dz_2\right]dz_1dk_1dk_2. \quad (3)$$

Equations 2 and 3 show that the output of the leading-order algorithm, Equation 1, acts as one of the integrands in the higher-order algorithm.

Following the calculations in Kaplan et al. (2005), we estimate the required floating-point operations. For example, for a 2D data set with 100 shots, 100 receivers, 1000 pseudo-depth points, 1000 output frequencies, and a sampling interval in time of 0.001 s,[3] the data set requires about 3×10^{15} floating-point operations for both the leading-order algorithm and the higher-order term in equation 2. It is worth pointing out that the higher-order term, Equation 2, cannot be calculated until the required value for $b_3(k_g,k_s,z)$ is made available by Equation 1. The same calculation applies for the other higher-order term, Equation 3. For a 3D data set, using the same parameters as in the 2D example (*i.e.*, 100 shots, 100 receivers, *etc.*), the floating-point operations number approximately 10^{23} for the current leading-order algorithm, Equation 1. Calculation of Equations 2 and 3 will triple the required number of floating-point operations.

[3]Note, however, that this example is a tiny fraction of a typical modern seismic survey (thousands of shots each with hundreds of receivers generating terabytes of data).

6 Compute requirements of the internal-multiple-elimination algorithm that is based on the ISS

The ISS internal-multiple-attenuation algorithm is a compute-intensive algorithm. However, it is an attenuation algorithm. In order to completely remove all internal multiples, especially when internal multiples are proximal to and/or interfering with primaries, M-OSRP proposes a three-pronged strategy (please refer to Weglein, 2014) for providing an effective response to this pressing and prioritized challenge. One part of the strategy is to find an elimination algorithm, which probably needs more compute power than the attenuation algorithm. A straight-forward implementation of the recently developed elimination algorithm for 1D pre-stack data (please refer to Zou and Weglein, 2014a;b;c) needs approximately 10-30 times more floating-point operations than the attenuation algorithm requires. The need for more floating-point operations is mainly due to the small integrals that represent the self-interactions; that is, if you include more points in the small integrals, the algorithm will need more floating-point operations, and *vice versa*.

The elimination algorithms under 2D and 3D are currently in development. These algorithms probably need more floating-point operations than the attenuation algorithm does. A rough guess is that they can be hundreds of times more compute-intensive than the attenuation algorithm is. Meanwhile, we note that for the same algorithm, different methods of implementation may need quite different numbers of floating-point operations.

7 Additional remarks on testing

Generally, there are two approaches to evaluating the cost of our algorithms: static analysis and dynamic analysis. Static analysis is the analysis of implementing the algorithm (computer program), without actually executing the program. We can count all computational operations required in the program (FLOPS) during its implementation and compare that with capability of our target (hardware and software). Dynamic analysis is performed by executing programs on a real or virtual target environment. In a modern high-performance computation environment, the bottleneck of performance usually is not the capability of computational operations (FLOPS) itself but is instead the data-transfer bandwidth between CPU and memory. The data-transfer time is not ignorable when we consider the total run time of a program. Furthermore, memory access (to obtain a high cache-hit ratio) is critical to improving performance. The aspect of data transfer is relatively difficult to evaluate in static analysis (by only counting memory access), so a dynamic analysis is preferable in our situation. Because some of our algorithms are currently in the development stage, their final implementation is not available. This, one way to evaluate their actual costs is to make model programs that simulate the same logic structure, number of operations and memory access strategy and then to test those model programs on a real or virtual target environment.

7.1 Computational cost (measured by floating-point operations) required by current implementation of the 2D ISS internal-multiple-attenuation algorithm

In the current implementation of the 2D ISS internal-multiple-attenuation algorithm, the whole procedure is divided into two steps (modules): (1) obtaining the b_1 term from the data and (2) calculating the b_3 term (predicted internal multiples) from the b_1 term. The first step (module) is actually a constant-velocity Stolt migration, whose computational cost is negligible compared with that of the second step. Thus, we consider the cost of only the second step: the prediction.

In the second module, there are also some auxiliary jobs, such as data-file input/output, memory allocation/freeing, reading/calculation of parameters, data sorting/regularization, fast Fourier transform/inverse fast Fourier transform, error checking, *etc.* We will ignore the cost of these auxiliary jobs, and will concentrate on the kernel of the prediction.

The pseudo code for the kernel of the ISS internal-multiple prediction and FLoating-point Operations (FLOs) estimation is

```
for all ks
  for all kg
    some preparation jobs (about 30 FLOs)
    for all frequencies (omega)
      for all k2
        for all k1
          some preparation jobs (about 130 FLOs)
            for all z2
              calculating the initial values of the exponential factors
                  and the increments of the exponential factors (about
                 150 FLOs)
              for all z1
                calculating the prediction and accumulating the
                   exponential factors (about 40 FLOs)
              for all z3
                calculating the prediction and accumulating the
                   exponential factors (about 40 FLOs)
              shift the output to output depth (about 30 FLOs)
```

Note:

1. The FLOs comprise an approximate estimate based on source code only; the actual FLOs of the binary executable will depend on the compiler optimization in the binary executable generation.

2. The number of iterations for all loops are the upper limit. In some cases (*e.g.*, the evanescent

part in the wavenumber/frequency domain), the iterations executed for each loop may be fewer than the upper limit.

3. It is assumed that some complicated math functions (such as real square root, complex exponential) take 10 FLOs, that complex addition and subtraction take 2 FLOs, and that complex multiplication and division take 6 FLOs. The actual costs of these functions will depend on the implementation of the math library.

4. All FLOs estimates for each step are rounded to the nearest ten.

Thus, the total cost for the kernel will be

$$FLOs = nks \times nkg \times (30 + nw \times nk2 \times nk1 \times (130 + nz2 \times (150 + nz1 \times 40 + nz3 \times 40 + 30))). \quad (4)$$

This FLOs calculation is an estimate of the order of magnitude (rather than an accurate number) of the floating-point operations that we need for the ISS internal-multiple-prediction kernel.

Here we estimate the computational cost by the number of FLOs. However, it is not a linear conversion to determine runtime by multiplying FLOs by a constant factor such as the FLoating-point Operations Per Second (FLOPS) of a certain machine. As we mentioned above, the memory-access time and cache-hit ratio will play important roles for the total runtime. Such an estimate of the number of FLOs is intended to help us understand the scale of the computational cost of the ISS internal-multiple-attenuation problem, rather than to evaluate the actual runtime or performance of the ISS internal-multiple-attenuation code.

7.2 Estimating computational cost for a specific 2D marine-field-data set

Now, let us evaluate the FLOs for a 2D marine-field-data set. Some parameters of the geometry or size of the data set are given in the following table.

Parameter	Value
Number of shots	374
Number of traces per shot	960
Shot interval	32 m
Trace interval	12.5 m
Number of time samples per trace	3585
Time sampling	4 ms
Maximum measured frequency	assume 100 Hz

The 2D ISS attenuation algorithm requires "full coverage" geometry in the input data set. The algorithm requires that all sources and receivers be located on the same surface grid with an equal number of sources and receivers. For the above 2D marine-field-data set, given the fact that the

shot interval is 32 m but the receiver interval is 12.5 m, we need to interpolate to get more source stations. To obtain a good result and to avoid the boundary effect of the data set, we need padding on the data set in both space directions and also in the time direction. This is to avoid the boundary effect and aliasing in the wavenumber domain. The padding factor is a parameter that depends on the data set on a case-by-case basis.

These two aspects (regularization and padding) make the actual input data set bigger than the original data set. Here we assume that we have 1700 stations after the regularization and that we will do 1.5 times padding; the data set then will be 2550×2550 traces (compared with 374×960 traces before regularization and padding). The data will occupy $2550 \times 2550 \times (3585 \times 4 + 240) \times 2 \approx= 200$ GB in memory. We understand that this amount of memory per node is commonly available in modern compute clusters.

Now we can use equation 4 to get the order of magnitude of the floating-point operations necessary for this 2D marine-field-data set. Here we assume that for each trace we have the prediction result that is as long as the input data (3585 samples), and we do not know the depth range of the multiple generators (nz1=nz2=nz3=3585). All wavenumber samples are equal to the conjugate spatial samples (nks=nkg=nk1=nk2=2550), hence we get

$$\begin{aligned} FLOs &= nks \times nkg \times (30 + nw \times nk2 \times nk1 \times (130 + nz2 \times (150 + nz1 \times 40 + nz3 \times 40 + 30))) \\ &= 2550 \times 2550 \times (30 + 3585 \times 2550 \times 2550 \times (130 + 3585 \times (150 + 3585 \times 40 + 3585 \times 40 + 30))) \\ &= 1.6 \times 10^{26}, \end{aligned}$$

which is larger than the above synthetic example by a factor of approximately 5×10^{10}.

8 Conclusions

The compute requirements of the ISS internal-multiple-attenuation algorithm are estimated in Kaplan et al. (2005). We update the estimate for a 2D marine-field-data set.

9 Acknowledgements

We thank the M-OSRP sponsors for their encouragement and support.

References

Araújo, F. V. *Linear and non-linear methods derived from scattering theory: backscattered tomography and internal multiple attenuation.* PhD thesis, Universidade Federal da Bahia, 1994. In Portuguese.

Kaplan, Sam T., Billy Robinson, Kristopher A. Innanen, and Arthur B. Weglein. "Optimizing internal multiple attenuation algorithms for large distributed computing systems." *Mission-Oriented Seismic Research Program (M-OSRP) Annual Report.* 2005, 158–170.

Liang, H., C. Ma, and A.B.Weglein. "A further general modification of the leading order ISS attenuator of first order internal multiples to accommodate primaries and internal multiples when an arbitrary number of reflectors generate the data: theory, development, and examples." *Mission-Oriented Seismic Research Program (M-OSRP) Annual Report* (2011): 148–166.

Ma, C., H. Liang, and A. Weglein. "Modifying the leading order ISS attenuator of first-order internal multiples to accommodate primaries and internal multiples: fundamental concept and theory, development, and examples exemplified when three reflectors generate the data." *Mission-Oriented Seismic Research Program (M-OSRP) 2011 Annual Report* (2011): 133–147.

Ma, Chao and Arthur B. Weglein. "Inverse Scattering Series (ISS) leading-order internal-multiple-attenuation algorithm and higher-order modification to accommodate primaries and internal multiples as input: 1-D normal incident test on interfering events, and extension to multi-D." *M-OSRP 2013-2014 Annual Report.* 2014.

Perrone, Michael. Accelerating IMA: A Processor Performance Comparison of the Internal Multiple Attenuation Algorithm. Presentation given at the 2007 M-OSRP Annual Meeting, available online at mosrp.uh.edu, June 2007.

Terenghi, Paolo. Overview of M-OSRP coding projects. Presentation at M-OSRP Annual Meeting, June 1-3, 2011, available to sponsors at mosrp.uh.edu, 2011.

Weglein, Arthur B. "The multiple attenuation toolbox: Progress, challenges and open issues." *83rd Annual International Meeting, SEG, Expanded Abstracts.* 2013, 4493–4499.

Weglein, Arthur B. "Multiple attenuation: strategy that addresses current challenges." *E&P Magazine* 87 (April 2014): 132–135.

Weglein, Arthur B., Fernanda V. Araújo, Paulo M. Carvalho, Robert H. Stolt, Kenneth H. Matson, Richard T. Coates, Dennis Corrigan, Douglas J. Foster, Simon A. Shaw, and Haiyan Zhang. "Inverse Scattering Series and Seismic Exploration." *Inverse Problems* 19 (October 2003): R27–R83.

Weglein, Arthur B., Fernanda Araújo Gasparotto, Paulo M. Carvalho, and Robert H. Stolt. "An Inverse-Scattering Series Method for Attenuating Multiples in Seismic Reflection Data." *Geophysics* 62 (November-December 1997): 1975–1989.

Zou, Yanglei and Arthur B. Weglein. "The internal-multiple elimination algorithm for all first-order internal multiples generated from all reflectors for a 1D earth: algorithm, discussion and numerical tests." *M-OSRP 2013-2014 Annual Report.* Submitted, 2014.

Zou, Yanglei and Arthur B. Weglein. "The pre-stack 1D ISS internal multiple elimination algorithm for all reflectors Part I: strengths and limitations." *84th Annual International Meeting, SEG, Expanded Abstracts*. Submitted, 2014.

Zou, Yanglei and Arthur B. Weglein. "The pre-stack 1D ISS internal multiple elimination algorithm for all reflectors Part II: addressing the limitations." *84th Annual International Meeting, SEG, Expanded Abstracts*. Submitted, 2014.

ISS depth imaging without the velocity model: update

Short note: Inverse Scattering series direct depth imaging without the velocity model: test on the Marmousi model

Fang Liu and Arthur B. Weglein

May 21, 2014

Abstract

This short note presents the recent inverse scattering series seismic imaging efforts of M-OSRP on the well-known Marmousi model. The α_1 results (similar to FK migration with fixed angle p_h) and our current higher-order imaging subseries (HOIS) results are shown. Further experiments are in progress.

1 The Marmousi model and our finite-difference modeling procedure

The Marmousi model is one of the well know benchmark seismic imaging challenges. The original model is sampled every $1.25(m)$ in both the vertical and the horizontal directions. In the modeling procedure we resample it at $5(m)$ and boost the wave speed of a low velocity region to water velocity ($1500m/s$) to accommodate the coarser $5(m)$ sampling. In the framework set up in Weglein et al. (2000; 2002), α_1 is the first term in the seismic imaging subseries and is essentially equivalent to a prestack Stolt migration with constant velocity. In this note, α_1 (the first term of ISS) and the subsequent higher-order imaging subseries are shown. For this model with very big velocity contrast (the highest velocity being $4700m/s$ vs the reference $1500m/s$ water speed) and large lateral variation, the idea of purposeful perturbation (see Weglein (2006) for detail) observed in all previous simpler imaging challenges still holds for the much more complicated Marmousi model.

There are hundreds of reflectors (horizons) in the Marmousi model, to display all of them at the same time will block a significant portion of the data. Therefore in each figure we selected only the major reflectors for display.

The original Marmousi model (see Fig. (1)) has a small region of very low velocity. Since the wavelength of seismic wave is shorter in the low velocity zone, the extreme low velocity requires very fine sampling in both the x and z directions. Since this low velocity zone is located in the portion of the model with very mild lateral variation, the low velocity contrast by itself (without large lateral variation) was not a major challenge for HOIS. This modification (shown in Fig. (2)) does not reduce the imaging challenge for our ISS imaging.

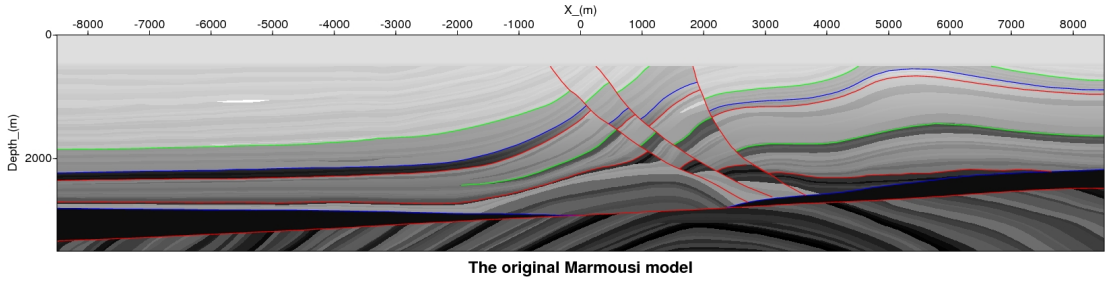

Figure 1: The original Marmousi model. The wave speed of the low velocity region in this model (shown by the bright zone with x-coordinate between $-6000(m)$ and $-5000(m)$) will be boosted to water speed ($1500m/s$). The colored horizons are major reflectors in the model.

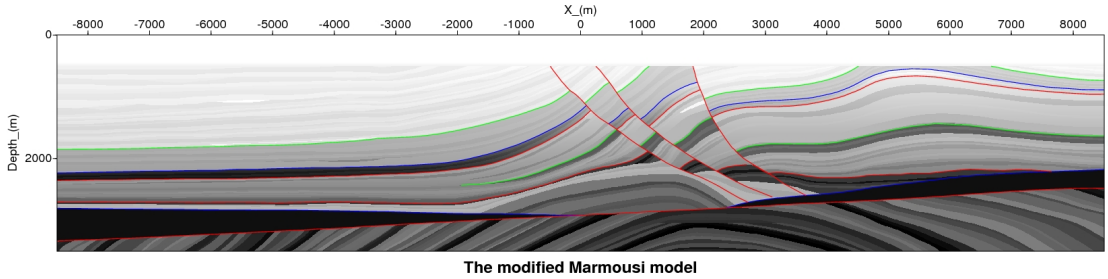

Figure 2: The modified Marmousi model. The modification happened between $x = -6000m$ and $x = -5000m$ where the lateral variation is mild. The low velocity values are boosted to water speed ($1500m/s$). The colored horizons are major reflectors in the model.

In the finite difference modeling procedure, the interval between two adjacent time step is $0.5ms$, but the sampling interval in the output is $2ms$ to follow the standard choice in seismic data. A typical shot gather is shown in Fig. (3). In the modeling procedure, only the P-wave velocity is used.

2 ISS imaging results

The physical meaning of the angle θ in this note is as follows: if k_h is the wavenumber conjugate to offset $x_h = x_g - x_s$, and we define $k_h = \omega p_h$, then θ is associated with k_h and p_h in the following relagtionship:

$$k_h = \omega p_h = \omega \frac{\sin\theta}{c_0}, \tag{1}$$

where c_0 is the reference velocity (in our case a constant with value $1500m/s$).

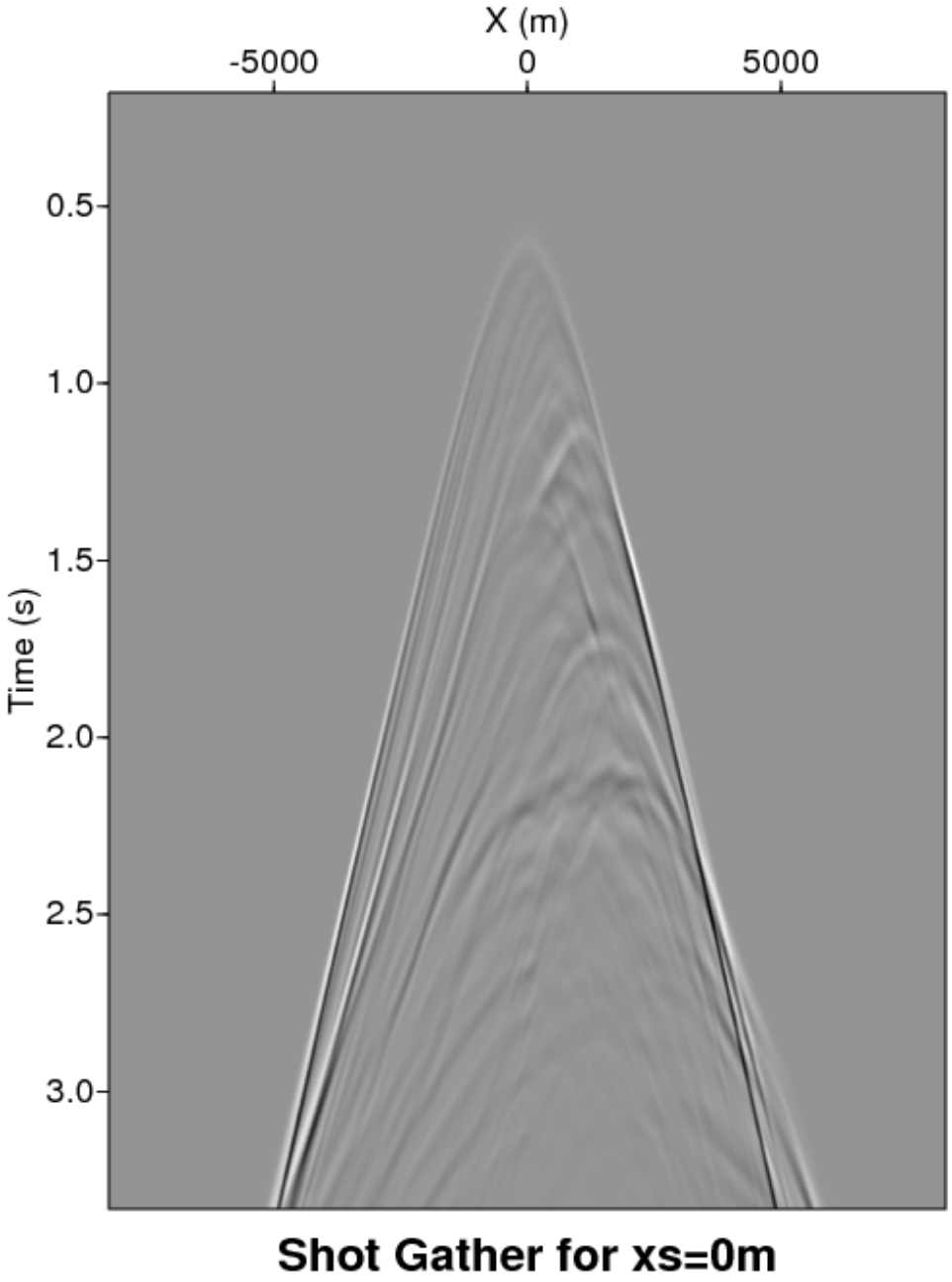

Figure 3: The shot gather with $x_s = 0(m)$.

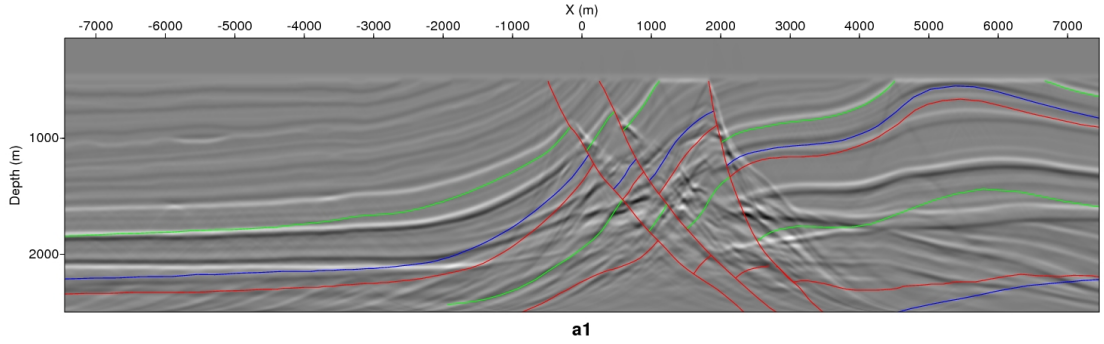

Figure 4: The α_1 imaging result (equivalent with FK migration with $p_h = 0$ or $k_h = 0$). The detail can be found in equation (2.22) of Liu (2006).

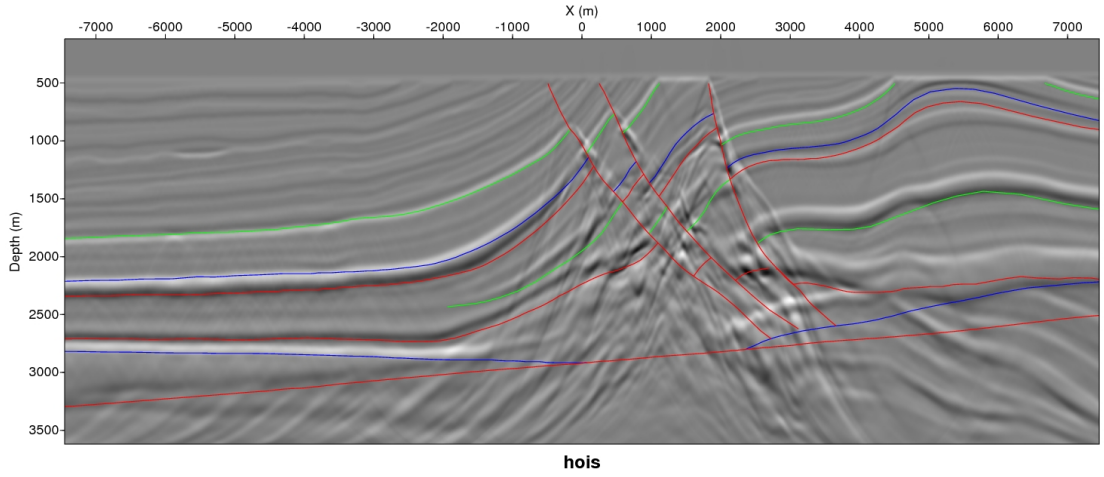

Figure 5: The HOIS imaging result after the calculation of α_1 in Fig. (4). The formula to compute this term can be found in equation (2.34) of Liu (2006).

α_1 is only the first term in the seismic imaging series. Its subsequent step HOIS does not include ISS imaging terms exclusively required for lateral variations in the medium. Diffractions are a phenomena that requires a laterally variable subsurface. Therefore there are diffractions in the final HOIS result.

3 Conclusions

The initial test of the ISS imaging subseries on the Marmousi model is very encouraging: a constant water speed migration is input to the closed form HOIS algorithm. The HOIS image has most of

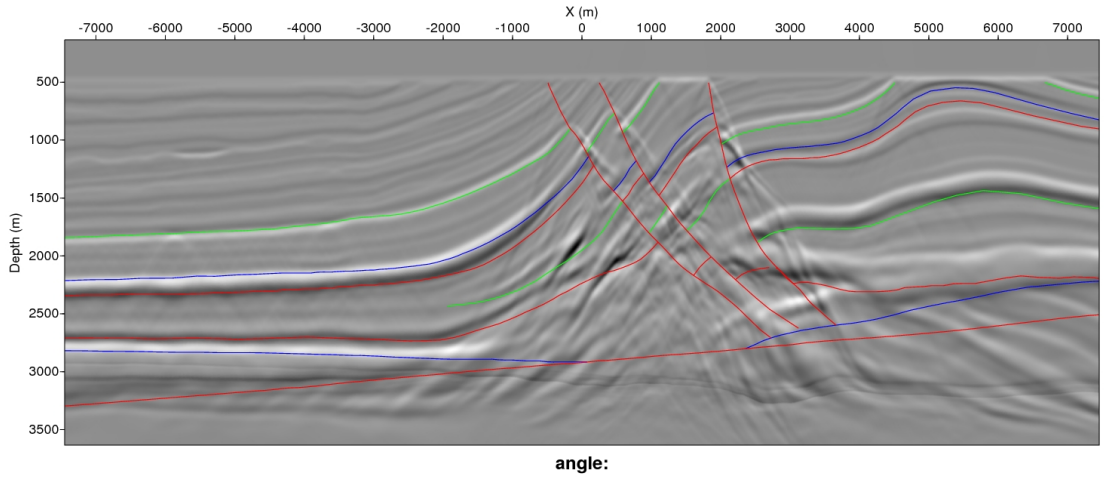

Figure 6: HOIS imaging result for angle $\theta = 9°$.

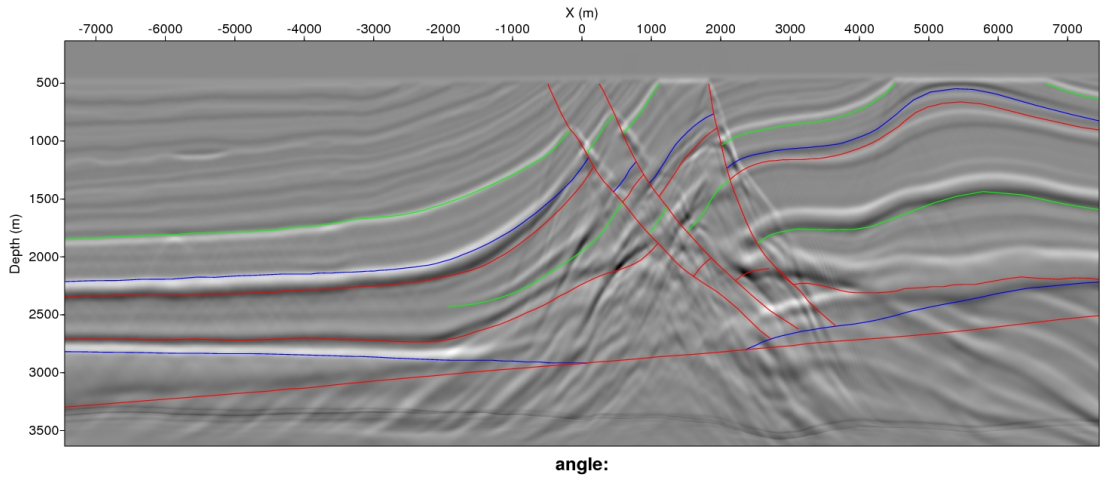

Figure 7: HOIS imaging result for angle $\theta = 4.5°$.

the reflectors very close their actual location. HOIS represents only a small fraction of ISS imaging terms. Therefore further ISS terms, especially HOIS+LE will add further imaging capability and the laterally exclusive term in α_{23} will be studied and evaluated to incorporate and capture new imaging capability. The latter study is on going with Dr. Zhiqiang Wang, and will be subject of future communication.

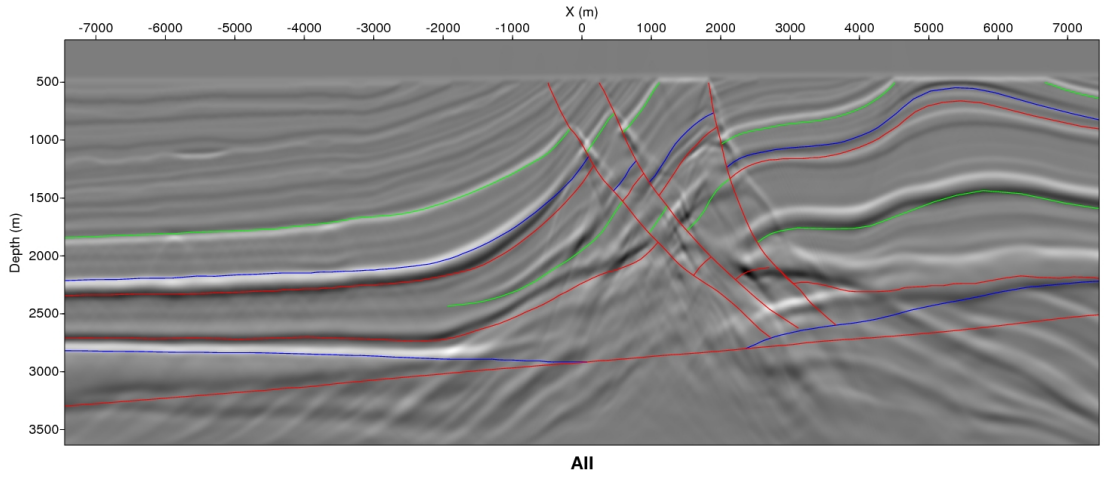

Figure 8: The sum of all HOIS imaging results from all 101 angles between $\theta = 0^\circ$ and $\theta = 9^\circ$.

4 ACKNOWLEDGMENTS

The authors would like to thank all M-OSRP members and sponsors. This work has been partially funded by NSFCMG award DMS-0327778 and DOE Basic Energy Sciences Award DE-FG02-05ER15697. The Marmousi model was downloaded by the first author from the website of the Allied Geophysical Laboratory of University of Houston.

References

Liu, Fang. *Multi-dimensional depth imaging without an adequate velocity model.* PhD thesis, University of Houston, 2006.

Weglein, A. B. "Introduction and overview: MOSRP06." *M-OSRP 2005-2006 Annual Report.* 2006, 1–4.

Weglein, A. B., D. J. Foster, K. H. Matson, S. A. Shaw, P. M. Carvalho, and D. Corrigan. "Predicting the correct spatial location of reflectors without knowing or determining the precise medium and wave velocity: initial concept, algorithm and analytic and numerical example." *Journal of Seismic Exploration* 10 (2002): 367–382.

Weglein, A. B., K. H. Matson, D. J. Foster, P. M. Carvalho, D. Corrigan, and S. A. Shaw. "Imaging and inversion at depth without a velocity model: Theory, concepts and initial evaluation." *70th Annual International Meeting, SEG, Expanded Abstracts.* 2000, 1016–1019.

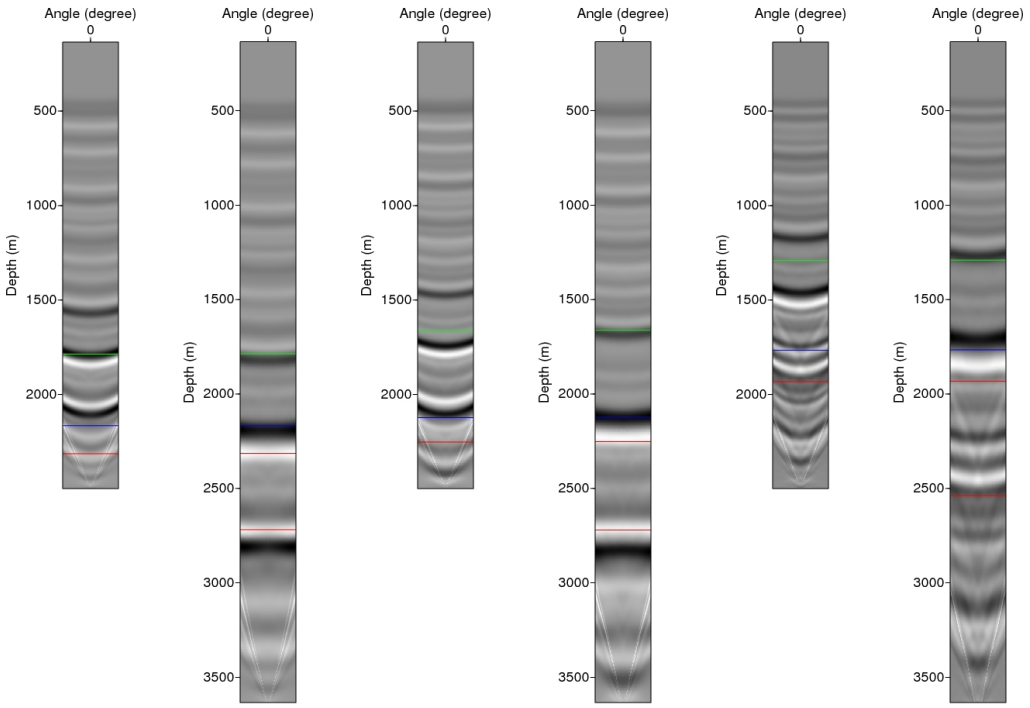

Figure 9: Angle gathers, from left to right: $alpha_1$ at $x_s = -5000(m)$, HOIS at $x_s = -5000(m)$; $alpha_1$ at $x_s = -3000(m)$, HOIS at $x_s = -3000(m)$; $alpha_1$ at $x_s = -1000(m)$, HOIS at $x_s = -1000(m)$.

Analysis and tests of amplitude information at the image point from asymptotic and wave equation migration: implications for RTM

Initial analysis and comparison of the amplitude properties/information of asymptotic and wave equation migration for one-way propagating waves: implications for RTM

Qiang Fu, Yanglei Zou, Arthur B. Weglein and Robert H. Stolt

May 21, 2014

Abstract

In this paper, we provide the first analysis and comparison between wave equation migration and asymptotic migration in terms of providing amplitude information at the target. Wave equation migration provides the angle dependent reflection coefficient at the image point, whereas the asymptotic migration does not.

1 Introduction

We compare wave equation migration and asymptotic migration for the simplest possible overburden, providing each algorithm with perfect data in the domain it requires. That allows us to isolate and examine only the differences of the migration methods. There are several substantive differences between asymptotic (Kirchhoff) and wave equation migration. This paper focuses only on the difference in the amplitude information provided by each method at the image point.

2 Background

Let's begin by discussing the various concepts, objectives, and levels of ambition for seismic imaging. This section borrows freely from the 2014 SEG expanded abstract for the invited recent advances and the Road ahead presentation "Multiples: Signal or noise?". Methods that use the wave equation to perform seismic migration have two ingredients: (1) a wave propagation component and (2) an imaging principle or concept. Jon Claerbout (Claerbout, 1971; Riley and Claerbout, 1976) was the initial and key wave-equation-migration imaging-concept pioneer and algorithm developer, and together with Stolt (1978) and Lowenthal et al. (1985), they introduced imaging conditions for locating reflectors at depth from surface-recorded data.

2.1 Imaging conditions

The three key imaging conditions that were introduced are:

1. time and space coincidence of up and downgoing waves,
2. the exploding-reflector model, and
3. predicting a source and receiver experiment at a coincident-source-and-receiver subsurface point, and asking for time equals zero (the definition of Wave-Equation Migration (WEM)).

For a normal-incident spike plane wave on a horizontal reflector, these three imaging concepts are totally equivalent. However, a key point to make clear for this paper, is that for a non-zero-offset surface seismic-data experiment they are no longer equivalent, for either a one-dimensional or a multi-dimensional subsurface. For the purposes of determining quantitative information on the physical meaning of the image, the clear choice is predicting a source and receiver experiment at depth. Wave-equation migration (WEM) (see e.g. Stolt (1978), Stolt and Benson (1986), Stolt and Weglein (2012)) is defined as using the third imaging condition, (3), the predicted source and receiver experiment at depth at time equals zero. In anything beyond 1D normal-incidence or zero-offset data, the other two imaging concepts (for example, time coincidence of up and downgoing waves) turn out to be asymptotic ray travel-time-curve "Kirchhoff" algorithms with a trajectory of image candidates, that are summed, looking for constructive addition for structural determination. Lost is the definitive "yes" or "no" to a point being an image provided by a source and receiver experiment at a coincident subsurface point. Stolt and his colleagues (Clayton and Stolt, 1981; Stolt and Weglein, 1985; Stolt and Benson, 1986) extended the experiment-at-depth concept to allow a separated source and receiver at time equals zero, to not only provide a definitive "yes" or "no" to any given subsurface point being a reflector, but, in addition, provide the angle-dependent reflection coefficient. The other imaging concepts cannot provide that imaging definitiveness nor the quantitative angle-dependent reflection-coefficient information at the image point. In addition, and in general all pre-stack versions, variants, and extensions of the first two imaging conditions listed above, whether for one-way waves or two-way waves, or for data consisting of primaries, or primaries and multiples, are always asymptotic or ray approximates of the third imaging condition. Asymptotic migration, resulting from adopting imaging conditions (1) or (2), will impose asymptotic forms of wave propagation that relate to ray theory and do not satisfy the ubiquitous space-filling propagation and illumination of wave theory and wave-theory migration.

The properties and benefits of Wave-Equation Migration (WEM) in comparison to asymptotic "Kirchhoff-like" migration are:

1. Definitiveness of a subsurface point corresponding to (or not corresponding to) structure from a predicted source and receiver experiment at that point;
2. Quantitative angle-dependent reflection coefficient information at the imaged point; and

3. Ubiquitous volume-filling wave propagation, coverage and illumination, compared to the limited propagation and illumination of ray theory.

This paper examine the second of these three issues.

2.2 RTM

When two-way migration was introduced by Whitmore, McMechan and their colleagues (Whitmore, 1983; McMechan, 1983), it was formulated and carried out first in post-stack and then in the pre-stack domain by running the data back in time (hence reversed time migration, or RTM) and the source field forward in time, and then cross-correlating the two fields at zero lag. The post-stack and pre-stack versions were basically the earlier exploding-reflector model and the time coincidence of up and downgoing wave-imaging concepts, respectively. That formulation of asymptotic RTM has become so widespread that it has been adopted even for one-way migration, where too often the very meaning of migration has come to be defined as:

$$\mathbf{I}(\mathbf{x}) = \sum_{\mathbf{x_s}} \sum_{\omega} \frac{\mathbf{S}'(\mathbf{x}, \mathbf{x_s}; \omega)\mathbf{R}(\mathbf{x}, \mathbf{x_s}; \omega)}{\mathbf{S}'(\mathbf{x}, \mathbf{x_s}; \omega)\mathbf{S}(\mathbf{x}, \mathbf{x_s}; \omega) + \varepsilon^2}, \tag{1}$$

where R is the back-propagated reflection data, S is the forward-propagated source wavefield, the zero-lag cross-correlation is indicated by the sum over angular frequency, ω, and the sum over sources adds candidate-image travel-time trajectories. S' is the complex conjugate of S, and ε is a stabilization parameter.

The conventional RTM method represented by equation (1), consists of back propagating the receiver field and forward propagating the source field, where each is carried out using the wave equation. However, the cross-correlation at zero lag is the grown-up version of imaging condition (1) and the imaging condition (1) is the place that the method entered the land of asymptotic and "Kirchhoff" ray theory.

All current RTM methods (for primaries, multiples, primaries and multiples) use variants and extensions or higher-order terms based on equation (1), are asymptotic ray-based migration, and hence do not correspond to wave-equation migration.

That might come as a surprise to the very large number of researchers and those who apply equation (1) in oil and service companies, that with all the wave-equation computer effort and expense to implement and utilize equation (1) that it doesn't correspond to wave-equation migration. The use of equation (1) is ubiquitous, but the imaging method it employs and represents and the RTM migration itself is ray-theoretic and is therefore not ubiquitous in its subsurface coverage and illumination.

2.3 Wave-equation migration (WEM) for two-way waves, for diving waves, or for migrating primaries and multiples

Neither the post- nor pre-stack current versions of RTM (captured in equation (1)) correspond to predicting a source and receiver experiment at depth and hence neither is WEM RTM. We suspect that many researchers that begin with migration forms such as equation (1) today, have no idea that they are starting with and remain in asymptotic rather than wave-equation migration concepts and algorithms. Weglein and his colleagues (Weglein et al., 2011a;b; Liu and Weglein, 2013) provided for two-way wave propagation the first predicted source and receiver experiment at depth and wave-equation migration, i.e., WEM RTM. Green's theorem provides a solid basis and firm foundation for predicting a source and receiver experiment at depth from the wavefield on an upper surface of a volume. That's how wave-equation migration RTM is formulated for either: (1) turning-wave primaries, and (2) for reflection data consisting of both primaries and multiples. The benefits and added value of WEM RTM compared to all current and conventional RTM methods (equation (1)) are the same benefits as between wave-equation migration and asymptotic or Kirchhoff forms for one-way waves for one-way-wave migration: (1) definitiveness on whether a point in the subsurface corresponds to structure, (2) the angle-dependent reflection coefficient at the image point, and (3) the subsurface coverage, and illumination of waves versus rays. Equation (2) describes the predicted source and receiver experiment at depth for WEM migration for one-way waves, where D inside the integral is the surface data, and G_0^{-D} is the anti-causal Green's function that vanishes on the measurement surface. Equation (3) is the analogous predicted source and receiver experiment step in WEM RTM where D in the integral is the surface data, and G_0^{DN} is the Green's function that along with its normal derivative vanishes on the lower surface and the walls of the volume.

$$D = \int_{S_s} \frac{\partial G_0^{-D}}{\partial z_s} \int_{S_g} \frac{\partial G_0^{-D}}{\partial z_g} D \, dS_g \, dS_s$$

(Green, 1-way waves) (2)

$$D = \int_{S_s} \left[\frac{\partial G_0^{DN}}{\partial z_s} \int_{S_g} \left\{ \frac{\partial G_0^{DN}}{\partial z_g} D + \frac{\partial D}{\partial z_g} G_0^{DN} \right\} dS_g \right.$$
$$\left. + G_0^{DN} \frac{\partial}{\partial z_s} \int_{S_g} \left\{ \frac{\partial G_0^{DN}}{\partial z_g} D + \frac{\partial D}{\partial z_g} G_0^{DN} \right\} dS_g \right] dS_s$$

(Green, 2-way waves) (3)

Equation 2 is Stolt prestack one-way wave-equation migration (see also Schneider, 1978, figure 40), and equation 3 is wave-equation-migration RTM.

These new wave-equation-migration RTM methods (equation 3) provide for two-way wave propagation what earlier wave-equation migration methods (e.g., Stolt, 1978) provided for one-way propagation (Weglein et al., 2011a; Stolt and Weglein, 2012).

In this paper, we examine WEM for one-way propagating waves (equation 2), and its asymptotic (Kirchhoff) approximation to analyze and examine, in detail, the second of the three claimed benefits provided by WEM compared to its asymptotic (Kirchhoff) forms.

This paper provides an indication of the analogous benefit provided by equation 3 compared to equation 1 for two way propagating waves and WEM and asymptotic RTM methods.

The RTM specific comparison will be the subject of a future work.

2.4 Wave-equation migration for one-way wave

Following Stolt (1978), Stolt and Benson (1986), and Stolt and Weglein (2012), we implement the imaging concept described in imaging condition 3. In a 2D world, the acoustic wave equation is

$$\left(\nabla^2 + \frac{\omega^2}{c_0^2}\right) P(x, z|x_s, z_s; \omega) = 0. \tag{4}$$

The data, D, are the measurements of the wave field on the surface

$$D(x_g|x_s; \omega) = P(x_g, 0|x_s, 0; \omega). \tag{5}$$

We begin by Fourier transforming the data into wavenumber-frequency domain

$$D(k_{gx}|k_{sx}; \omega) = \int dx_g \int dx_s \int dt D(x_g|x_s; \omega) e^{i(k_{xs}x_s - k_{xg}x_g + \omega t)}. \tag{6}$$

Then, we predict the experiment where the source is at depth z,

$$P(k_{gx}, 0|k_{sx}, z; \omega) = D(k_{gx}|k_{sx}; \omega) e^{-ik_{sz}z}, \tag{7}$$

where the vertical wavenumber component k_{sz} for a down-going source wave is

$$k_{sz} = +\frac{\omega}{c}\sqrt{1 - \frac{{k_{sz}}^2 c^2}{\omega^2}}, \tag{8}$$

and similarly we predict the receiver at depth z;

$$P(k_{gx}, z\,|k_{sx}, z; \omega\,) = P(k_{gx}, z|k_{sx}, 0; \omega) e^{ik_{gz}z} \tag{9}$$

$$= D(k_{gx}|k_{sx}; \omega) e^{i(k_{gz} - k_{sz})z}, \tag{10}$$

where the vertical wavenumber component k_{gz} for an up-going receiver wave is

$$k_{gz} = -\frac{\omega}{c}\sqrt{1 - \frac{{k_{gz}}^2 c^2}{\omega^2}}. \tag{11}$$

Figure 1 shows a cartoon of these first two steps of the three-step wave-equation migration scheme. Now we have the experiment with source and receiver both at depth z, and we can apply the imaging

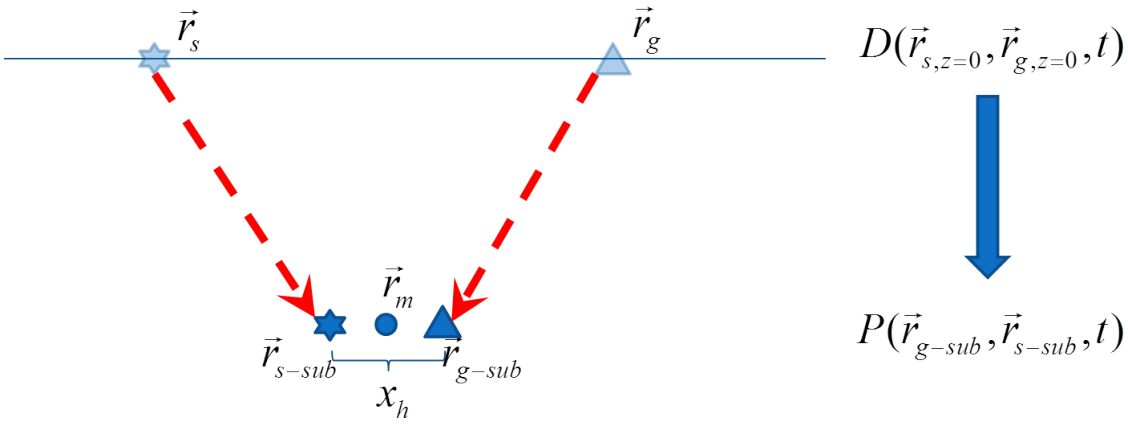

Figure 1: The first two steps of the three-step wave-equation migration scheme.

condition, that is, predicting both source and receiver at the image location and letting time be zero.

$$M(x,z) \equiv P(x_g = x, z_g = z \,|x_s = x, z_s = z; t = 0) \tag{12}$$

$$= \frac{1}{(2\pi)^3} \int d\omega \int dk_{sx} \int dk_{gx} D(k_{gx}|k_{sx};\omega) e^{i(k_{gz}-k_{sz})z} e^{i(k_{gz}-k_{sz})x}. \tag{13}$$

$M(x,z)$ is the imaging result from wave-equation migration. Wave-equation migration (see e.g. Clayton and Stolt (1980), Stolt and Weglein (1985), Weglein and Stolt (1999)), can be extended to predict imaging result non-zero offset data at time equals zero. In order to obtain the subsurface offset information, we first change the integral variables in the wave equation migration formula from k_{sx}, k_{gx}, ω to k_x, k_h, k_z. With the definition of k_x, k_h, k_z,

$$k_z \equiv k_{gz} - k_{sz} \tag{14}$$

$$= -\frac{\omega}{c}\left(\sqrt{1 - \frac{{k_{gx}}^2 - c^2}{\omega^2}} + \sqrt{1 - \frac{{k_{sx}}^2 - c^2}{\omega^2}}\right) \tag{15}$$

$$k_x \equiv k_{gx} - k_{sx} \tag{16}$$

$$k_h \equiv k_{gx} + k_{sx} \tag{17}$$

the Jacobian for a change of variables in equation 13 is

$$\text{Det}\left[\frac{\partial(k_x, k_h, k_z)}{\partial(k_{sx}, k_{gx}, \omega)}\right] = \frac{2\omega k_z}{c^2 k_{sx} k_{gx}}, \tag{18}$$

and the result can be rewritten as

$$M(x,z) = \frac{c^2}{2(2\pi)^3} \int dk_z \int dk_x \int dk_h D(k_{gx}|k_{sx};\omega) \frac{k_{sx}k_{gx}}{\omega k_z} e^{ik_z z} e^{ik_x x}. \tag{19}$$

In equation 19, since two of the integrals are Fourier transform, we can obtain the image result in k_x, k_z domain

$$M(k_x, k_z) = \frac{c^2}{4\pi^2} \int dk_h D(k_{gx}|k_{sx};\omega) \frac{k_{sx}k_{gx}}{\omega k_z}. \tag{20}$$

Now the formula only contains an integral of k_h, which is the Fourier conjugate of subsurface offset x_h. We obtain the migration imaging result with subsurface offset information,

$$M(k_x, k_z, k_h) = \frac{c^2}{4\pi^2} \frac{k_{sx}k_{gx}}{\omega k_z} D(k_{gx}|k_{sx};\omega). \tag{21}$$

2.5 Asymptotic migration for one-way wave propagating

Following Stolt and Weglein (2012) (p.75) We start with the one-way wave equation migration formula and rearrange the formula with the data in the space-time domain,

$$\begin{aligned} M(x,z) =& \frac{1}{(2\pi)^3} \int d\omega \int dk_{sx} \int dk_{gx} D(k_{gx}|k_{sx};\omega) e^{i(k_{gz}-k_{sz})z} e^{i(k_{gz}-k_{sz})x} \qquad (22) \\ =& \frac{1}{(2\pi)^3} \int dx_g \int dx_s \int dt D(x_g|x_s;t) \int d\omega e^{i\omega t} \\ & \times \int dk_{sx} \int dk_{gx} e^{-i(k_{sz}z + k_{sx}(x-x_s))} e^{i(k_{gz}z + k_{gx}(x-x_g))}. \qquad (23) \end{aligned}$$

Then we apply the asymptotic approximation for the integral of k_{sx} and k_{gx} as shown in the following,

$$\int dk_{sx} e^{-i(k_{sz}z + k_{sx}(x-x_s))} \simeq e^{i\omega r_s/c} \sqrt{\frac{2\pi i \omega z^2}{c {r_s}^3}} \tag{24}$$

$$\int dk_{gx} e^{i(k_{gz}z + k_{gx}(x-x_g))} \simeq e^{i\omega r_g/c} \sqrt{\frac{2\pi i \omega z^2}{c {r_g}^3}}, \tag{25}$$

where

$$\begin{aligned} r_s &= \sqrt{z^2 + (x-x_s)^2} \\ r_g &= \sqrt{z^2 + (x-x_g)^2}. \end{aligned} \tag{26}$$

Substituting the stationary phase approximations in equation 23, we obtain the asymptotic migration result, M^A,

$$M^A(x,z) = \frac{1}{(2\pi)^3} \int dx_g \int dx_s \int dt D(x_g|x_s;t) \int d\omega e^{i\omega t}$$

$$
\begin{aligned}
&\times \int dk_{sx} \int dk_{gx} e^{-i(k_{sz}z + k_{sx}(x-x_s))} e^{i(k_{gz}z + k_{gx}(x-x_g))} \\
=&\frac{z^2}{(2\pi)^2 c} \int dx_s \int dx_g \frac{\frac{\partial}{\partial t} D(x_g|\, x_s; t = r/c)}{(r_g r_s)^{3/2}} \\
=&\frac{z^2}{(2\pi)^2 c} \int d\tilde{x}_h \int d\tilde{x}_m \frac{\frac{\partial}{\partial t} D(\tilde{x}_m, \tilde{x}_h; t = r/c)}{(r_g r_s)^{3/2}}.
\end{aligned} \tag{27}
$$

This asymptotic migration formula is a weighted summation of the data along a trajectory of travel-times corresponding to ray-paths from the source to image point and then to receiver.

A general ray theory based Kirchhoff migration formula is

$$
I(x,z) = \int d\tilde{x}_h \int d\tilde{x}_m W(\vec{r}_m, \tilde{x}_m, \tilde{x}_h) D(\tilde{x}_m, \tilde{x}_h, t = R/c), \tag{28}
$$

where the W is a weighting function (see e.g. Biondi (2006), Stolt and Benson (1986) (chapter 3)).

The asymptotic migration (equation 27) is the prototype Kirchhoff migration (equation 28). It is derived as an asymptotic approximation of the clearest and most transparent form of WEM for one-way waves, equation 23.

2.6 Subsurface information from asymptotic one-way migration

The asymptotic migration formula (equation 27) has $\tilde{x}_h$ and $\tilde{x}_m$ integrals quite similar to the wave equation migration. Can we obtain the subsurface offset information from this formula? The answer is no.

$M^A(x,z)$ is the output of interfering travel time curves. Although it is a function of x and z, $M^A(x,z)$ is <u>not</u> the output at the midpoint coordinates (x_m, z_m) of a coincident (zero offset) source-receiver experiment. It has limited value (if any) in being interpreted as a reflection coefficient, let alone as the angle dependence of a reflection coefficient. A coincident source and receiver experiment, directly above a reflector at small positive time, is related to the reflection coefficient of that local reflection point. If the migration concept does not correspond to that experiment at depth, one can correctly locate structure but cannot obtain the local reflection coefficient. If you nevertheless decide to interpret $M^A(x,z)$ in equation 27 as though it was the output of an imagined or fictitious zero offset experiment at $t = 0$, then taking that leap we would write

$$
M^A(x,z) = M^A(x_m, z_m, x_h = 0, t = 0). \tag{29}
$$

Furthermore, and in addition for the interpretation of the right hand member of equation 27 we will assume by causality that for $x_h \neq 0$ at $t = 0$ the measurement would be zero, that is

$$
M^A(x_m, z_m, x_h, t = 0) = 0 \quad \text{for} \quad x_h \neq 0. \tag{30}
$$

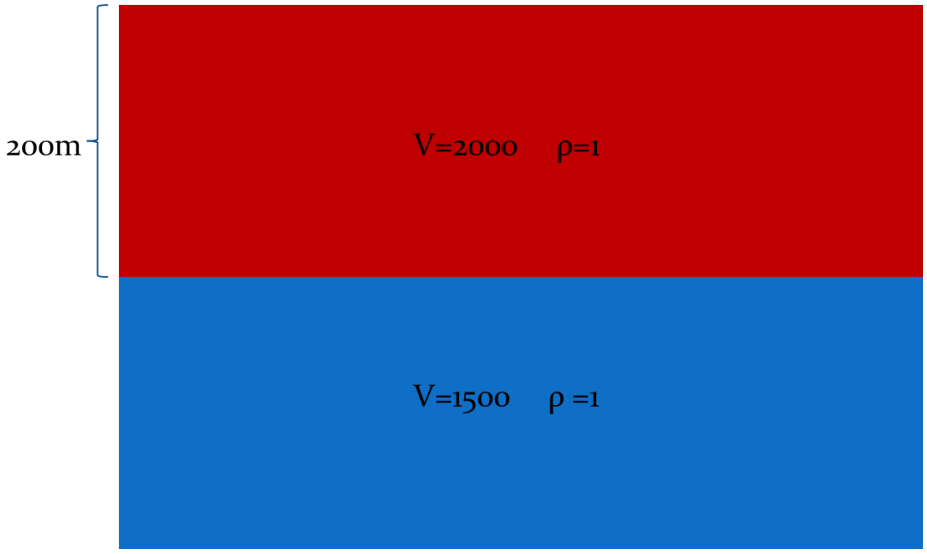

Figure 2: Simple two-layer model we use to generate data.

By assuming that interpretation to equation 27, we bent over backwards to allow a way to compare $M(x,z,x_h)$ with $M^A(x,z,x_h)$ (or $M(k_x,k_z,k_h)$ with $M^A(k_x,k_z,k_h)$) in terms of amplitude information from the actual and fictitious experiment output by WEM and asymptotic migration, respectively.

Alternatively, further stretching credulity to provide an assist for interpreting the asymptotic migration $M^A(x,z)$, we could treat the $M^A(x,z,\tilde{x_h})$ from equation 27

$$M^A(x,z,\tilde{x}_h) = \frac{z^2}{(2\pi)^2 c}\int d\tilde{x}_m \frac{\frac{\partial}{\partial t}D(\,x_g|\,x_s;t=r/c)}{(r_g r_s)^{3/2}} \tag{31}$$

where $\tilde{x}_h$ is a fixed offset of the surface data, not the offset of the experiment initialize at depth, as though it corresponded to x_h in $M(x,z,x_h,t=0)$ (although it doesn't). We will show that does not correspond even for the simplest possible imaging example, as exemplified in the result section.

3 A test and comparison with the simplest possible imaging problem

In the following section, we will demonstrate the differences between the wave equation migration and the asymptotic migration in the simplest possible case with offset data.

The simplest scenario for such a test would be one-way wave-equation migration and its asymptotic form in a two-layer acoustic model, in which each layer is homogeneous. Figure 2 shows the model we used to generate the data.

We test the amplitudes of both wave-equation migration and its asymptotic approximation to see how the amplitudes of their images relate to the angle dependent reflection coefficient. We use

	wave-equation migration	asymptotic migration
migration method	one-way Stolt migration	asymptotic approximation of one-way Stolt migration
data	analytic data (reflectivity method in wavenumber-frequency domain)	analytic data (Cagniard-de Hoop method in space-time domain)
migration procedure	step 1: downward continuation of source step 2: downward continuation of receiver step 3: apply imaging condition	step 1: start with one-way Stolt migration formula step 2: apply stationary phase approximation
imaging result	$M(x,z)$	$M^A(x,z)$
imaging result with subsurface offset information	$M(k_x,k_h,k_z)$ or $M(x,x_h,z)$	N/A (requires introduction of an imaginary experiment corresponding to the asymptotic imaging result)

Table 1: Test procedure for wave-equation migration and its asymptotic form

analytic data for both wave-equation migration and its asymptotic approximation. Using analytic data will avoid the effect of any numerical inaccuracy in the data generating procedure and all differences will be attributable to the processing methods being compared.

Table 1 shows the migration procedure for wave-equation migration and its asymptotic form.

3.1 Data for wave-equation migration

For the wave equation migration, we use the analytic data generated by the reflectivity method in the frequency-wave number domain (e.g., in Ewing, Jardetzky and Press (1957))

$$\begin{aligned} D(k_s,k_g,\omega) =& \int_{-\infty}^{+\infty} dx_g e^{-ik_g x_g} \frac{r(k_s,q_s)e^{ik_s x_g} e^{2iq_s z_1}}{4\pi i q_s} \\ =& \delta(k_s-k_g)\frac{r(k_s,q_s)e^{2iq_s z_1}}{4\pi i q_s}. \end{aligned} \tag{32}$$

3.2 Data for asymptotic migration

For the asymptotic migration, we use the analytic data generated by Cagniard-de Hoop method in space-time domain (as utilized inZhang and Weglein (2006)). The analytic data for this model are

$$D(x_s,x_g,z_s,z_g,t) = \frac{1}{2\pi}\mathrm{Re}(\widehat{pp})\frac{H(t-R/c_0)}{\sqrt{t-R^2/{c_0}^2}}, \tag{33}$$

with

$$R = \sqrt{(x_s-x_g)^2+(z_s+z_g-2z_r)^2}, \tag{34}$$

where z_r is the depth of the reflector.

Note that since in the model the velocity in the first layer is greater than the velocity of the second layer, the reflection data does not have a post-critical component.

3.3 Results

We compare the results from the two different migration in the same domain.

Figure 3 – 5 show the results of one-way wave equation migration and asymptotic migration in different domains, respectively. Figure 3 shows the results in space domain (x_h, z), figure 4 shows the results in wavenumber-depth domain (k_h, z) and figure 5 shows the results in wavenumber domain (k_h, k_z).

We can analytically calculate the angle dependent reflection coefficient for the model shown in figure 2 by using the equation 35

$$r(k_{sx}, k_{sz}) = \frac{\rho_2 k_{sz1} - \rho_1 k_{sz2}}{\rho_2 k_{sz1} + \rho_1 k_{sz2}}. \tag{35}$$

Figure 6 shows the result of this analytic calculation.

We can also retrieve the angle dependent reflection coefficients from WEM result (equation 36) as well.

$$M(k_m, k_z, k_h) = \frac{c^2}{4\pi} dk_h D(\, k_{gx} |\, k_{sx}; \omega) \frac{k_{gz} k_{sz}}{\omega k_z}. \tag{36}$$

And then we can simplify the formula for a 1D medium. For a 1D medium, the k_{gx} and k_{sx} will be equal,

$$D(k_{gx}\,|k_{sx}\,;\omega) = \delta(k_{gx} - k_{sx}) D(k_{gx}\,|k_{sx}\,;\omega) \tag{37}$$

$$= \delta(k_m) D(k_{gx}\,|k_{sx}\,;\omega). \tag{38}$$

We plug the analytic form of the data into equation 36, and then obtain the angle dependent reflection coefficient

$$r(k_{sx}, k_{sz}) = -\frac{\pi\omega}{c^2} \frac{4\pi i}{e^{2ik_{sz}z_r}} M(k_z, k_h). \tag{39}$$

The angle dependent reflection coefficient should be a real number by definition, so equation 39 should give us a real number for result. In ideal case that will not be a problem, all phase factors inside the formula will cancel each other and a real value result will be obtained. However in

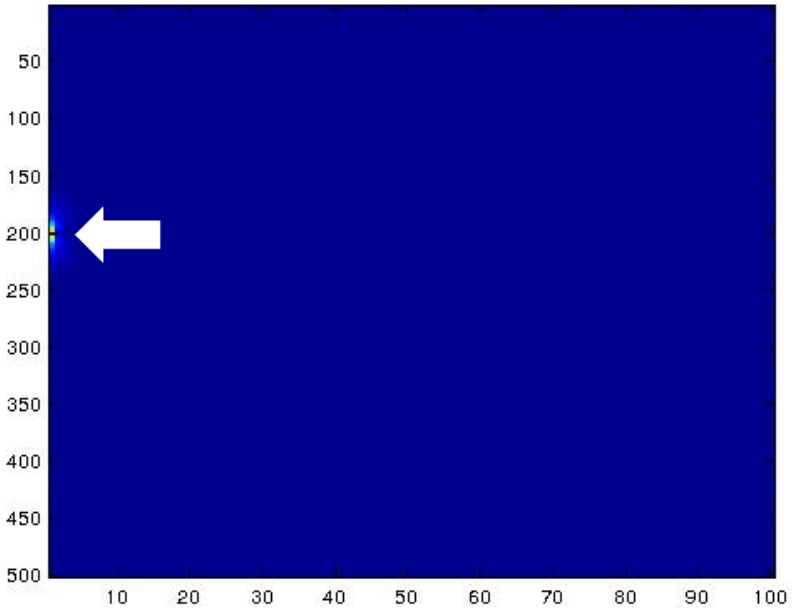

(d)

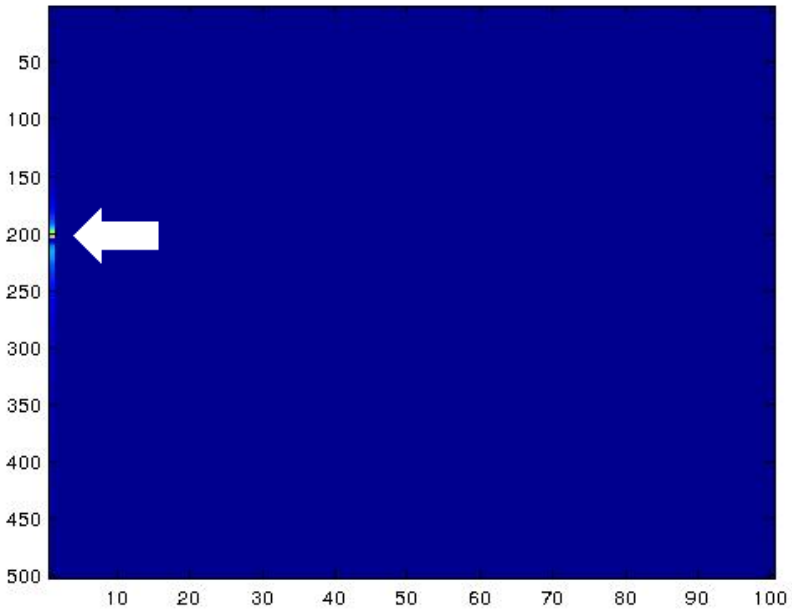

(e)

Figure 3: (a) wave-equation migration image in x_h-z domain; (b) asymptotic migration image in x_h-z domain.

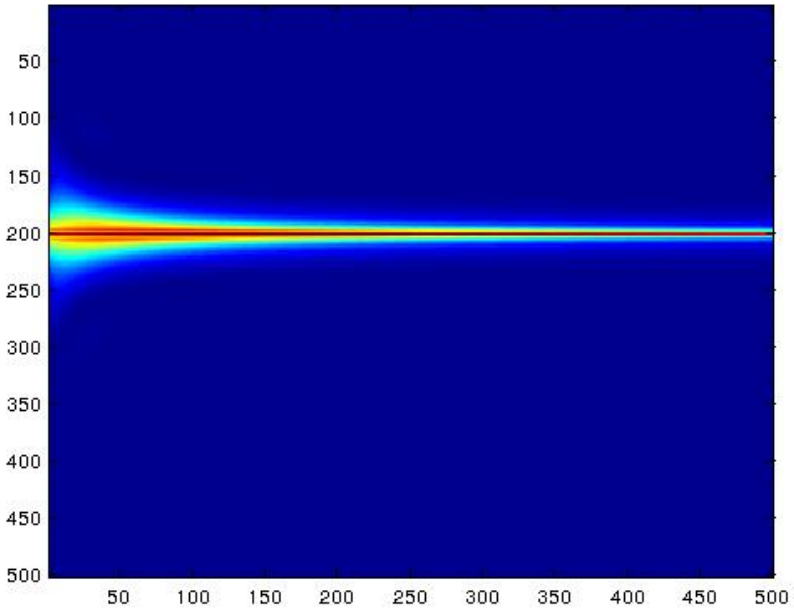

(a)

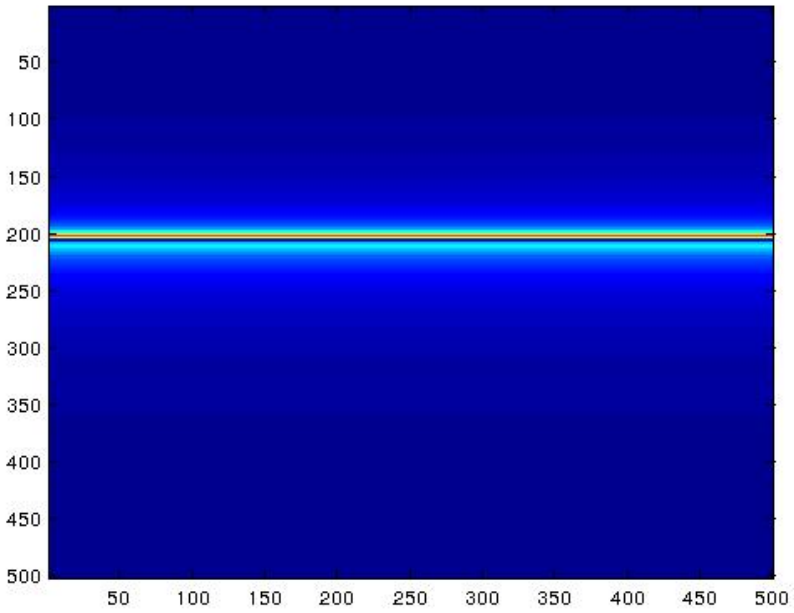

(b)

Figure 4: (a) wave-equation migration image in k_h-z domain; (b)asymptotic migration image in k_h-z domain.

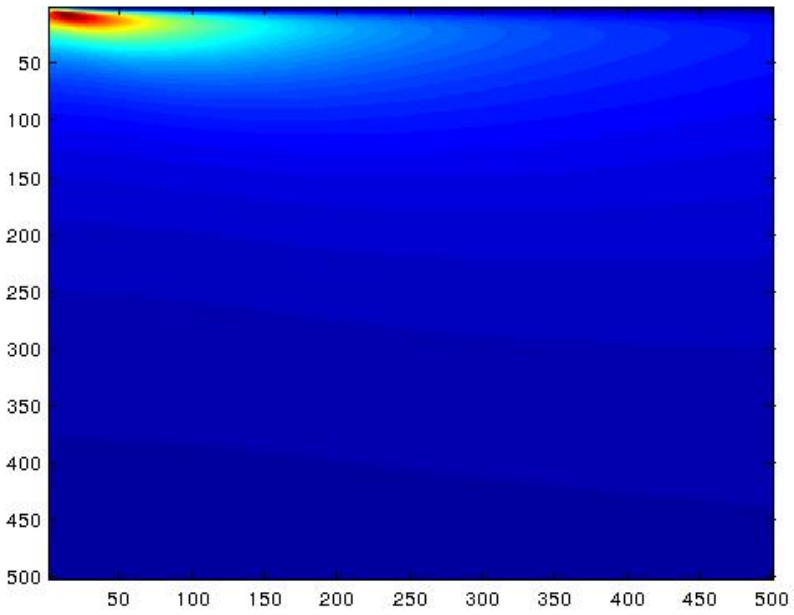

(a)

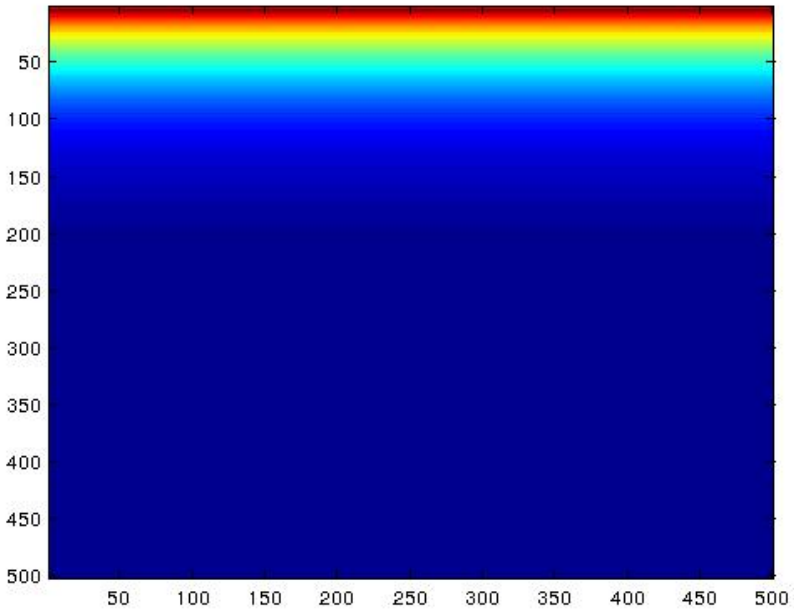

(b)

Figure 5: (a) wave-equation migration image in k_h-k_z domain; (b)asymptotic migration image in k_h-k_z domain.

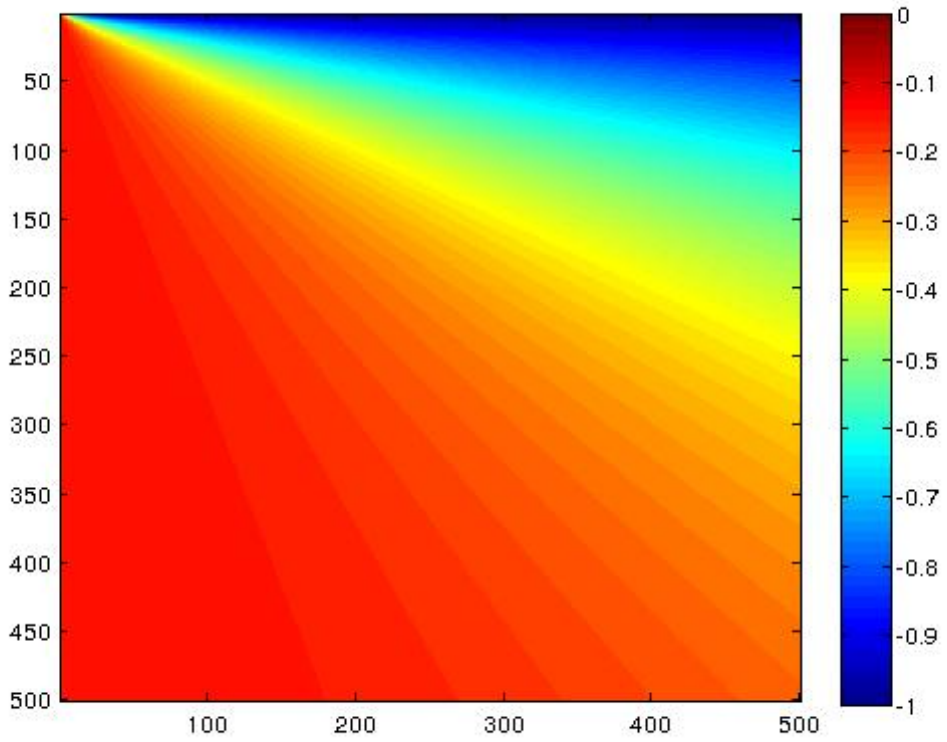

Figure 6: The angle dependent reflection coefficient by analytic calculation $r(k_{sx}, k_{sz}) = \frac{\rho_2 k_{sz1} - \rho_1 k_{sz2}}{\rho_2 k_{sz1} + \rho_1 k_{sz2}}$

numerical calculation, the numerical inaccuracy will cause a complex result of equation 39. Hence, we use the amplitude (module of the complex number) of the result instead of the value itself,

$$|r(k_{sx}, k_{sz})| = \left| \frac{\pi\omega 4\pi}{c^2} \right| |M(k_z, k_h)| \,. \tag{40}$$

We use equation 40 to calculate the angle dependent reflection coefficient from wave-equation and asymptotic migration result (figure 5) respectively, and figure 7 shows the results.

By comparing figures 6 and 7a, we find the inverted angle dependent reflection coefficient from wave-equation migration image is almost identical as the theoretical value except for the small vertical wavenumber part. The differences are due to the numerical stabilizing scheme for the division by small vertical wavenumber. Besides these differences, the result is perfect.

However, the inverted angle dependent reflection coefficient from asymptotic migration image (figures 6) is not even close to the theoretical value.

As mentioned previously, we could treat the $M^A(x, z, \tilde{x_h})$ from equation 31 where $\tilde{x_h}$ is a fixed offset of the surface data, not the offset of the experiment at depth, as though it corresponded to

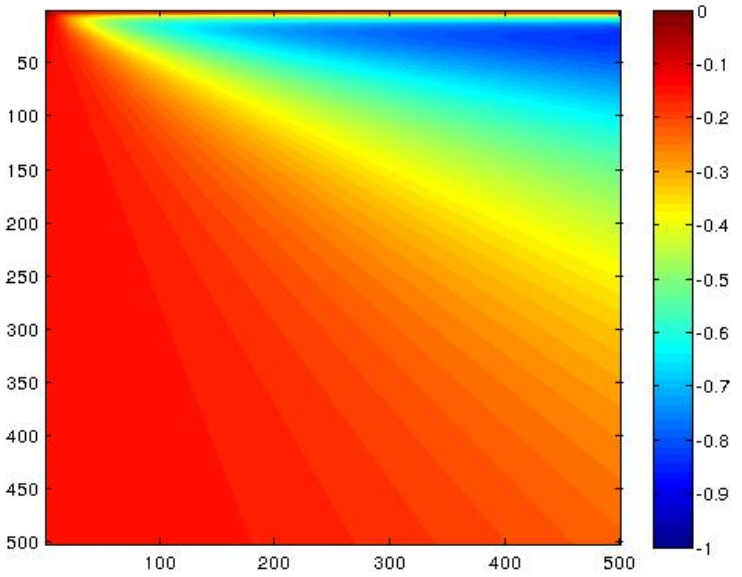

(a)

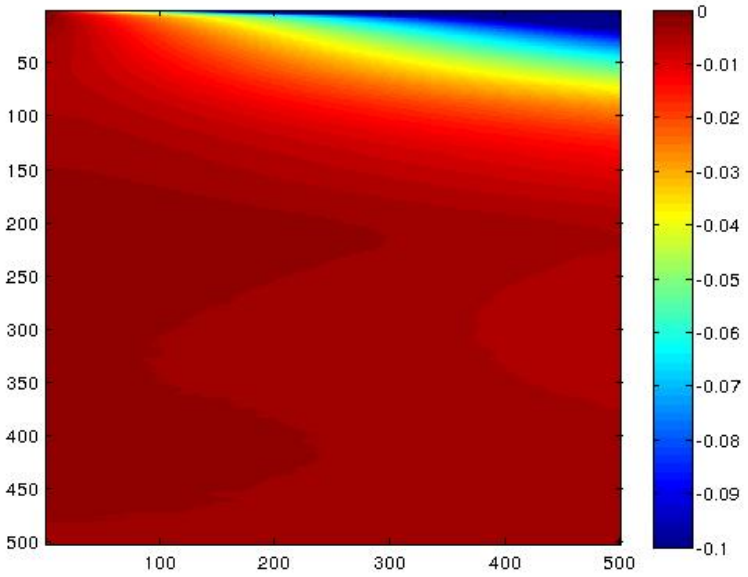

(b)

Figure 7: (a) The angle dependent reflection coefficient inverted from wave-equation migration imaging (figure 5a); (b) The angle dependent reflection coefficient inverted from asymptotic migration imaging (figure 5b)

x_h in $M(x, z, x_h, t = 0)$ while it doesn't. We compare that result $M^A(k_x, k_z, \tilde{k_h})$ in figure 8a and the angle dependent reflection coefficient in figure 8b. We can see even for the simplest possible imaging example, the equation 31 could not provide any angle dependent information at all.

4 Conclusions

We compare the amplitudes of the wave equation migration and the asymptotic migration for the simplest possible overburden, with both perfect data in the domain each requires, and attempt to retrieve the angle dependent reflection coefficient from both migration methods. The amplitude of wave-equation migration is closely related to the angle dependent reflection coefficient of the reflector, thus angle dependent reflection coefficient can be retrieved from wave-equation migration imaging. The asymptotic approximation does not correspond to a coincident source and receiver experiment at depth. We cannot retrieve the angle dependent reflection coefficient after the asymptotic approximation comes into the migration scheme. Attempts to attribute/interpret the asymptotic migration result as due to an imaginary source and receiver experiment at the image point, does not provide the angle dependent reflection coefficient. This is an important lesson to keep in mind when examining the amplitude information contained in all current (asymptotic) RTM methods.

5 Acknowledgment

We thank the M-OSRP sponsors for their encouragement and their support for our research.

References

Biondi, Biondo L. *3D Seismic Imaging.* Investigations in Geophysics. Society of Exploration Geophysicists, 2006.

Claerbout, Jon F. "Toward a unified theory of reflector mapping." *Geophysics* 36 (June 1971): 467–481.

Clayton, Robert W. and Robert H. Stolt. An Inversion Method for Acoustic Wave Fields. Technical Report 24, SEP, Tulsa, OK, 1980.

Clayton, Robert W. and Robert H. Stolt. "A Born-WKBJ inversion method for acoustic reflection data." *Geophysics* 46 (November 1981): 1559–1567.

Ewing, W. Maurice, Wenceslas S. Jardetzky, and Frank Press. *Elastic Waves in Layered Media.* McGraw-Hill Book Company, 1957.

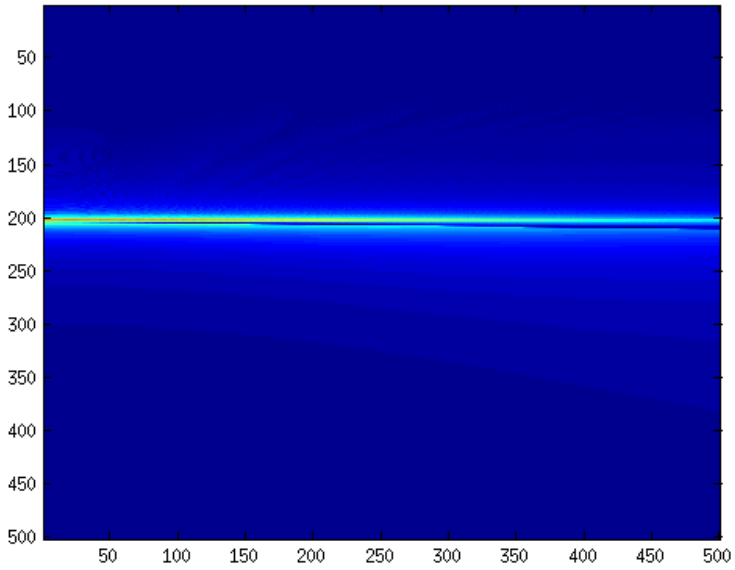

(a)

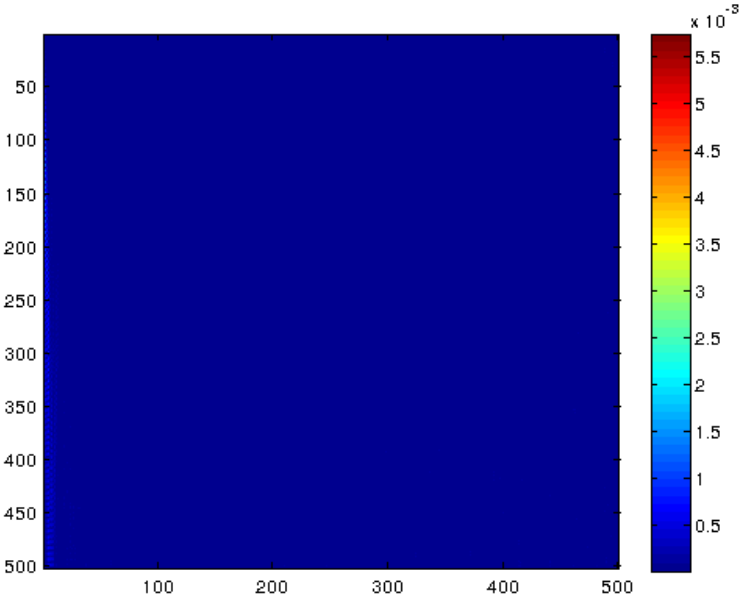

(b)

Figure 8: (a) Asymptotic migration result in as function of surface offset $\tilde{x_h}$ rather than function of subsurface offset x_h in space (x_h, z) domain. (b) the angle dependent reflection coefficient retrieved from that surface offset migration result.

Liu, Fang and Arthur B. Weglein. "The first *wave theory* RTM, examples with a layered medium, predicting the source and receiver at depth and then imaging, providing the correct location and reflection amplitude at every depth location, and where the data includes primaries and all internal multiples.." *M-OSRP 2012-2013 Annual Report.* 2013, 284–335.

Lowenthal, D., L. Lu, R. Roberson, and J. W. C. Sherwood. "The wave equation applied to migration." *Geophysical Prospecting* 24 (1985): 380–399.

McMechan, G. A. "Migration by extrapolation of time dependent boundary values." *Geophysical Prospecting* 31 (1983): 413–420.

Riley, D. C. and J. F. Claerbout. "2D multiple reflections." *Geophysics* 41 (1976): 592–620.

Schneider, William A. "Integral formulation for migration in two and three dimensions." *Geophysics* 43 (February 1978): 49–76.

Stolt, R. H. "Migration by Fourier transform." *Geophysics* 43 (1978): 23–48.

Stolt, R. H. and A. B. Weglein. "Migration and inversion of seismic data." *Geophysics* 50 (1985): 2458–2472.

Stolt, Robert H. and Alvin K. Benson. *Seismic migration: theory and practice.* London—Amsterdam: Geophysical Press, 1986.

Stolt, Robert H. and Arthur B. Weglein. *Seismic Imaging and Inversion: Application of Linear Inverse Theory.* Cambridge University Press, February 2012.

Weglein, A. B. and R. H. Stolt. "Migration-inversion revisited (1999)." *The Leading Edge* 18 (August 1999): 950–952, 975.

Weglein, A. B., R. H. Stolt, and J. D. Mayhan. "Reverse-time migration and Green's theorem: Part I — The evolution of concepts, and setting the stage for the new RTM method." *Journal of Seismic Exploration* 20 (February 2011): 73–90.

Weglein, A. B., R. H. Stolt, and J. D. Mayhan. "Reverse time migration and Green's theorem: Part II — A new and consistent theory that progresses and corrects current RTM concepts and methods." *Journal of Seismic Exploration* 20 (May 2011): 135–159.

Whitmore, D. N. "Iterative depth imaging by back time propagation." *53rd Annual International Meeting, SEG, Expanded Abstracts.* 1983, 382–385.

Zhang, Jingfeng and Arthur B. Weglein. "A note on data modelling using the Cagniard-de Hoop method." *M-OSRP 2005-2006 Annual Report.* 2006, 126–138.

Short note: Initial analysis and comparison of the wave equation and asymptotic prediction of a receiver experiment at depth for one-way propagating waves

Chao Ma, Jing Wu, and Arthur B. Weglein

May 21, 2014

Abstract

In a companion paper, Fu et al. (2014) examine the amplitude information at the image that derives from a wave equation method and its corresponding asymptotic form. The operator that is asymptotically approximated contains wave equation migration (WEM) ingredients as the prediction of a source and receiver experiment at depth. The purpose of this note is to isolate and examine the impact of the asymptotic approximation on the production of a receiver at depth. The spectral difference between the wave and asymptotic receiver experiment is consistent with the corresponding migration difference.

1 Introduction

The work of Fu et al. (2014) provide the first analysis and comparison between wave equation migration and asymptotic migration in terms of providing amplitude information at the target. We focus on one part of that procedure, i.e., the step of predicting the receiver at depth using a wave-equation prediction method and its asymptotic prediction counterpart, providing complimentary understanding of the work done by Fu et al. (2014).

2 Theory

2.1 Wave-equation method prediction

Following Stolt (1978); Stolt and Benson (1986); Stolt and Weglein (2012), and assuming only upgoing wave existing in the medium, the wave-equation migration method to predict the experiment with receiver at depth is: (1) Fourier transforming data generated by Cagniard-de Hoop method, $D^{CdH}(x_g, z_g|x_s, z_s; t)$, on t and x_g, to obtain the data in frequency-wavenumber domain,

$D(k_g, z_g|x_s, z_s; \omega)$; (2) applying phase-shift factor $e^{ik_z(z-z_g)}$ to $D(k_g, z_g|x_s, z_s; \omega)$, where z is the predicted receiver depth, and $k_z = -\frac{\omega}{c_0}\sqrt{1 - \frac{k_g^2 c_0^2}{\omega}}$; (3) Inverse Fourier transforming the phase-shifted data from k_g to x, see equation 1.

$$D^W(x, z\,|x_s, z_s; \omega\,) = \frac{1}{(2\pi)} \int\int D(x_g, z_g|x_s, z_s; \omega) e^{-ik_g x_g} dx_g e^{ik_z(z-z_g)} e^{ik_g x} dk_g, \tag{1}$$

where $D^W(x, z\,|x_s, z_s; \omega\,)$ is the predicted receiver at (x, z) using a wave-equation prediction method.

2.2 Asymptotic method prediction

Using stationary phase approximation, the k_g integral in equation 1 can be approximated as

$$\int e^{i(k_g(x-x_g)+k_z(z-z_g))} dk_g = \sqrt{\frac{2\pi i\omega(z-z_g)^2}{c r_g^3}}, \tag{2}$$

where $r_g = \sqrt{(z-z_g)^2 + (x-x_g)^2}$. Then, equation 1 becomes

$$\begin{aligned} D^A(x, z\,|x_s, z_s; \omega\,) &= \frac{1}{(2\pi)} \int\int D(x_g, z_g|x_s, z_s; \omega) e^{-ik_g x_g} dx_g e^{ik_z(z-z_g)} e^{ik_g x} dk_g \\ &= \frac{1}{(2\pi)} \int D(x_g, z_g|x_s, z_s; \omega) dx_g \underline{\int e^{i(k_g(x-x_g)+k_z(z-z_g))} dk_g} \\ &\simeq \frac{1}{(2\pi)} \int D(x_g, z_g|x_s, z_s; \omega) dx_g e^{-i\omega r_g/c} \underline{\sqrt{\frac{2\pi i\omega(z-z_g)^2}{c r_g^3}}}. \end{aligned} \tag{3}$$

$D^A(x, z\,|x_s, z_s; \omega\,)$ from equation 3 is the predicted receiver at (x, z) using an asymptotic prediction method.

3 Numerical tests

3.1 Synthetic data generation by Cagniard-de Hoop method

We use the Cagniard-de Hoop (CdH) method to generate the test data in the space-time domain in two dimensions. In an acoustic medium, for a source at $(0, z_s)$, and the receiver at (x_g, z_g) (see Fig 1), the pre-critical reflection Green's function is (e.g., Zhang and Weglein (2005))

$$D^{CdH}(x_g, z_g|0, z_s, t) = \frac{-1}{2\pi} ReP P \frac{H(t - \frac{R}{c_0})}{\sqrt{t^2 - \frac{R^2}{c_0^2}}} \tag{4}$$

where

$$PP = \frac{\eta_0 - \eta_1}{\eta_0 + \eta_1};$$
$$\eta_i = \sqrt{c_i^{-2} - p^2};$$

$$p = \begin{cases} \frac{x_g t - |z_g + z_s - 2z_d|\sqrt{R^2/c_2^2 - t^2}}{R^2}, t <= \frac{R}{c_0} \\ \\ \frac{x_g t + i|z_g + z_s - 2z_d|\sqrt{R^2/c_2^2 - t^2}}{R^2}, t >= \frac{R}{c_0} \end{cases}$$

$$R = \sqrt{x_g^2 + (z_g + z_s - 2z_d)^2}.$$

3.2 Test results

We use equation 4 to generate the synthetic data based on the model shown in Figure 1. Reflector depth is at $z_d = 2,000m$, source is located at $(x_s = 0, z_s = 0)$, offset of receivers is from $x_g = -20,000m$ to $x_g = 20,000m$ at depth $z_g = 400m$, receiver interval, dx, is 4m, time sampling interval, dt, is 0.001s ($T_{max} = 5s$). Velocities are $2,000m/s$ and $1,000m/s$ in the first and second medium, respectively. The generated synthetic data are shown in Figure 3.

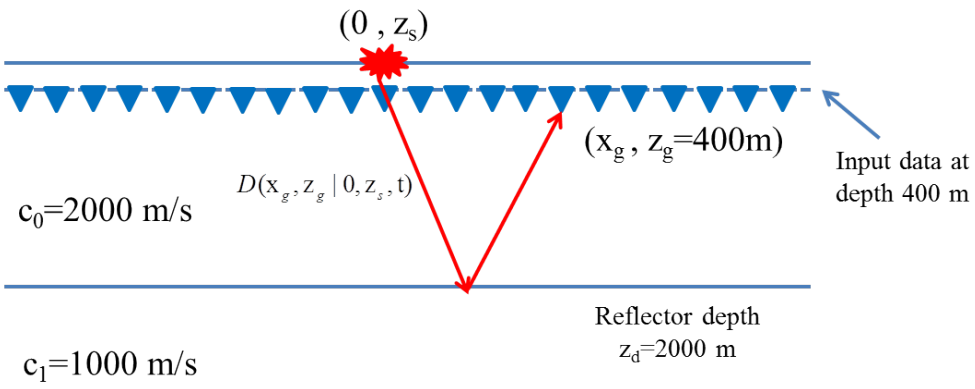

Figure 1: Model to generate CdH synthetic test data as input.

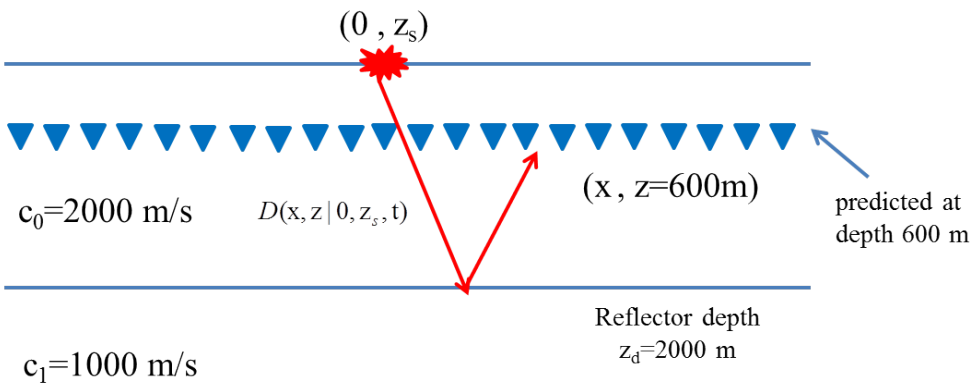

Figure 2: Predicted wavefield at depth 600 m.

We use this data set (receiver depth $z_g = 400m$) to predict the receiver at depth $z = 600m$ (see Figure 2) using both wave-equation prediction method (equation 1) and its asymptotic prediction counterpart (equation 3). We compare the predicted results of D^W and D^A at depth $z = 600m$ with the exact D^{CdH} at depth z=600m at 0m offset and 2,000m offset. In all these figures, the black line is the exact data generated by using the Cagniard-de Hoop method at depth $z = 600m$, the red line is the asymptotic prediction result, and the blue line is the wave-equation prediction result, respectively.

4 Conclusion

The asymptotic approximation of the prediction of receiver experiment at depth takes a highly nonlinear dependence of the phase in equation 1 [from k_z] and replace it with a liner dependence on the phase in equation 3. The resultant difference in spectrum at the low end has a dramatic impact

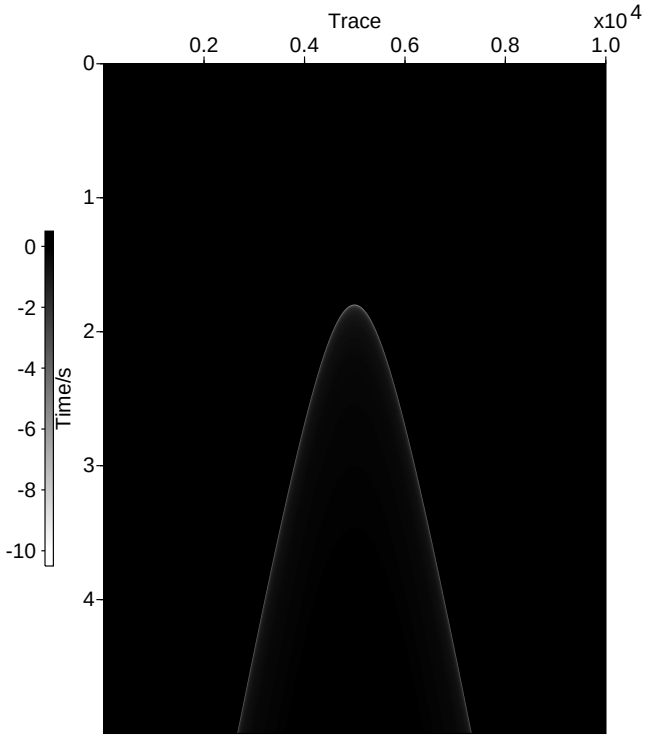

Figure 3: CdH synthetic test data generated from the one reflector model in Figure 1.

on subsequent imaging step, and makes the asymptotic migration method not an approximated source and receiver coincident at time equals zero.

References

Fu, Qiang, Yanglei Zou, Arthur B. Weglein, and Robert H. Stolt. "Initial analysis and comparison of the amplitude properties/information of asymptotic and wave equation migration for one-way propagating waves: implications for RTM." *M-OSRP Annual report* (2014).

Stolt, R. H. "Migration by Fourier transform." *Geophysics* 43 (1978): 23–48.

Stolt, Robert H. and Alvin K. Benson. *Seismic Migration: Theory and Practice.* Ed. Klaus Helbig and Sven Treitel. Volume 5 of Seismic Exploration. Geophysical Press, 1986.

Stolt, Robert H. and Arthur B. Weglein. *Seismic Imaging and Inversion: Application of Linear Inverse Theory.* February 2012.

Zhang, Jingfeng and Arthur B. Weglein. "A note on data modelling using the Cagniard-de Hoop method." *M-OSRP Annual report* (2005): 126–138.

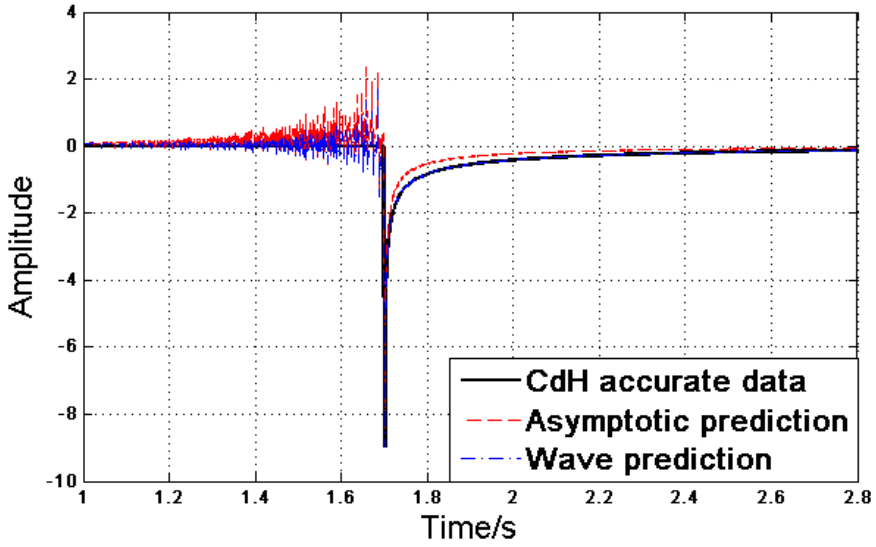

Figure 4: Space-time domain comparison at x=0m, z=600m (1.0s to 2.8s).

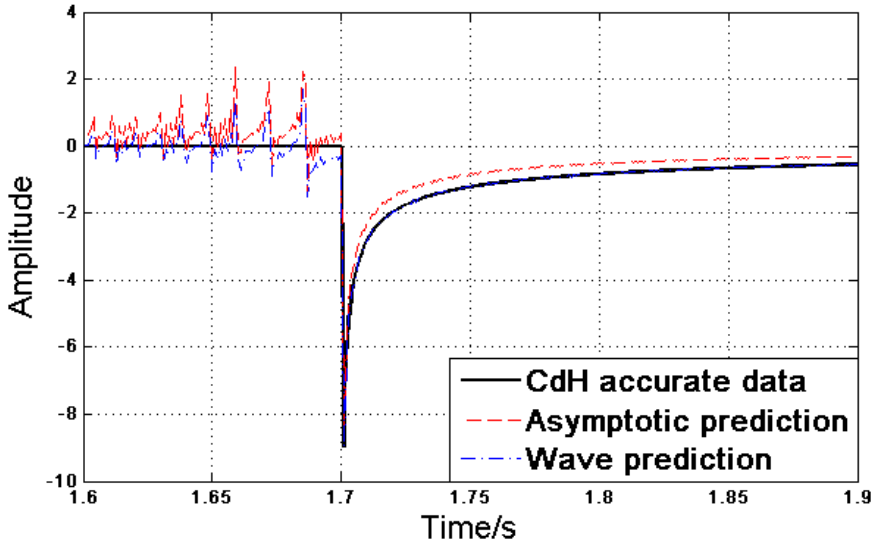

Figure 5: (Zoom-in of Figure 4) Space-time domain comparison at x=0m, z=600m (1.6s to 1.9s).

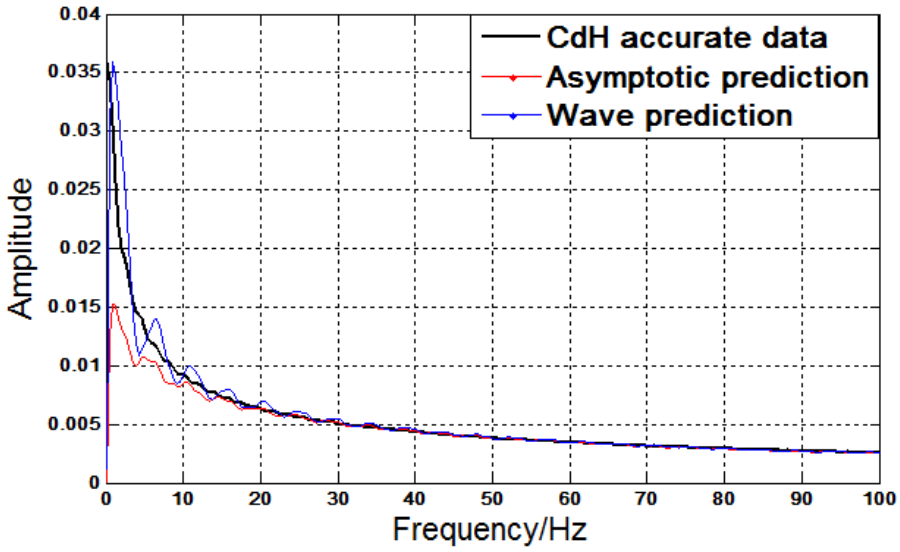

Figure 6: Space-frequency domain comparison at x=0m, z=600m (0Hz-100Hz).

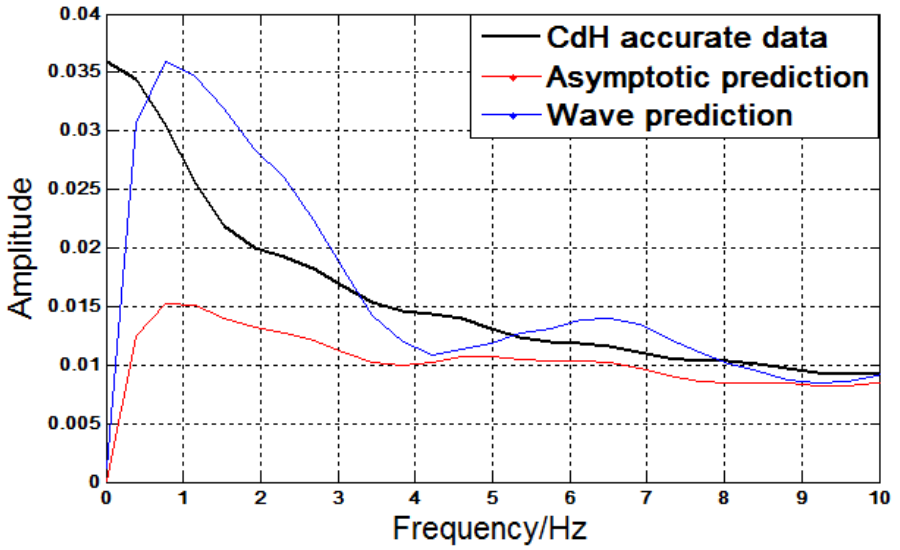

Figure 7: (Zoom-in of Figure 6) Space-frequency domain comparison at x=0m, z=600m (0Hz-100Hz).

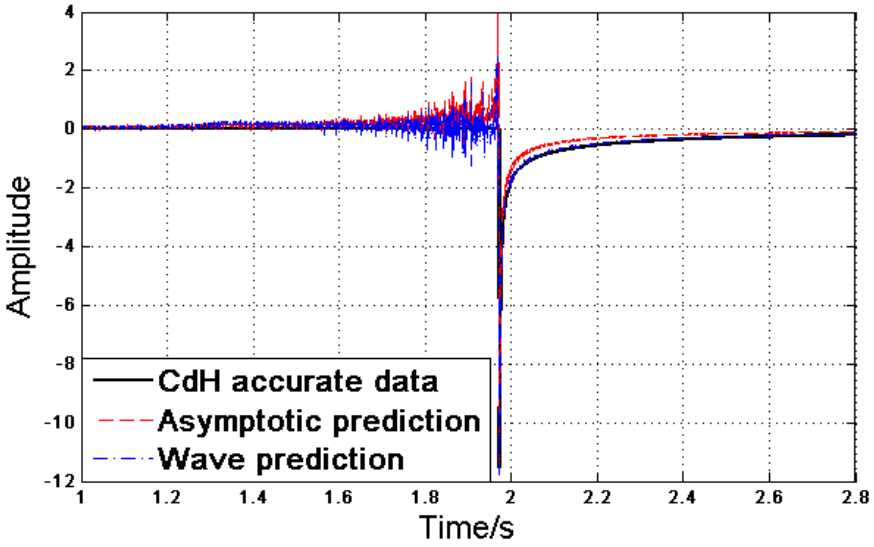

Figure 8: Space-time comparison at x=2,000m, z=600m (1.0s to 2.8s).

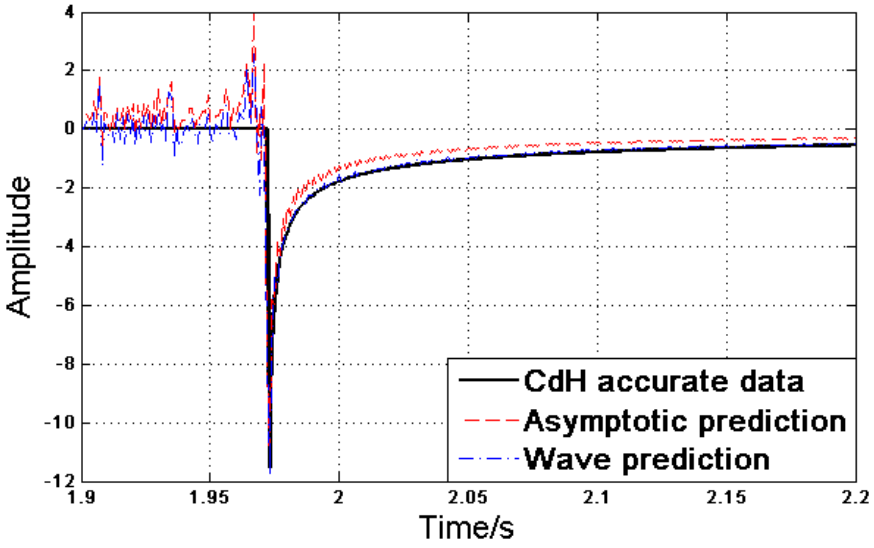

Figure 9: (Zoom-in of Figure 8) Space-time comparison at x=2,000m, z=600m (1.9s to 2.2s).

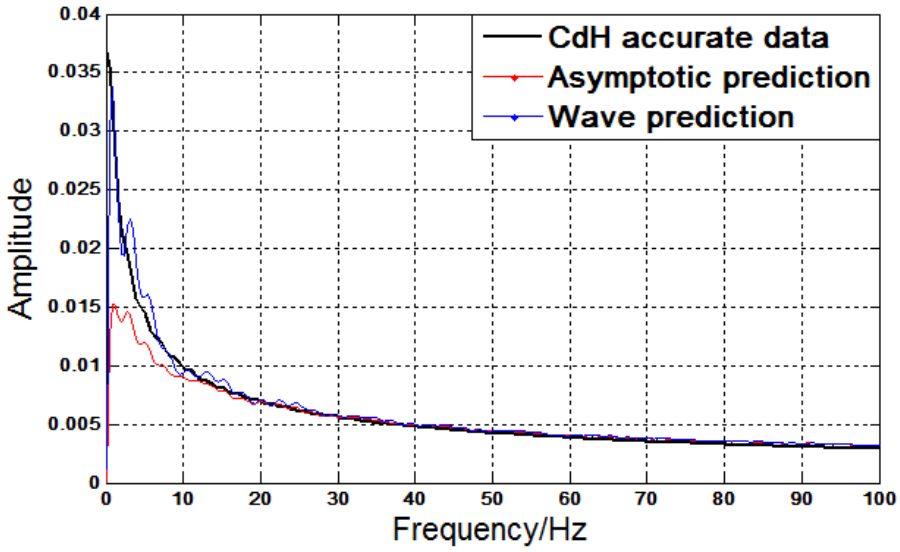

Figure 10: Space-frequency domain comparison at x=2,000m, z=600m (0Hz-100Hz).

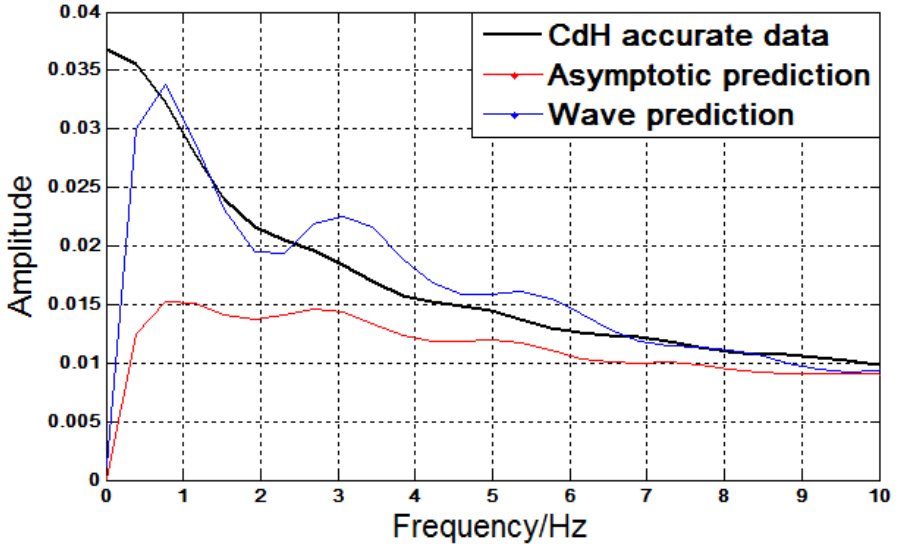

Figure 11: (Zoom-in of Figure 10) Space-frequency domain comparison at x=2000m, z=600m (0Hz-100Hz).

The first *wave theory* RTM, examples with a layered medium, predicting the source and receiver at depth and then imaging, providing the correct location and reflection amplitude at every depth location, and where the data includes primaries and all internal multiples.

Fang Liu and Arthur B. Weglein

April 29, 2013

Abstract

Reverse time migration (RTM) is the cutting-edge imaging method used in seismic exploration. In earlier RTM publications, density was often used to balance a medium with velocity variation, such that the acoustic impedance − the product of velocity and density − stays constant. Thus, reflections from sharp boundaries are avoided. In order to be more complete, consistent, realistic, and predictive, density variation is intentionally included in our study so that we can test its impact on the Green's theorem-based wave-theory RTM algorithms.

The major objectives of this article are to advance our understanding and to provide concepts, added imaging capabilities, and new algorithms for RTM. Although our objective of extracting useful subsurface information from recorded data is not different from that of well-known previous RTM publications, our approach is different: we use wave theory as much as possible to maximize the benefit from the Green's function and Green's theorem, rather than use the more popular methodology of running finite-difference modeling backwards in time.

A significant artifact in RTM is caused by the fact that numerous subsurface seismic events necessary for backward propagation never return to the measurement surface. This unwanted phenomenon also exists for the wave-field-prediction method formulated from Green's theorem: Green's formula (in its general form, i.e., equation (2.5)), which links the wave field on the entire outer surface with interior field values, also requires data from everywhere on the surface. Weglein et al. (2011a) and Weglein et al. (2011b) proposed a special Green's function with vanishing Dirichlet and Neumann boundary conditions at the deeper boundary to cope with that issue. This article provides a natural extension of the two aforementioned papers, into a medium with density variation and more complicated geological structures.

The major advantage of RTM over many other seismic imaging methods is its additional ability to handle two-way propagation without assuming that the events in the input data are only up-going and that all multiples have been removed. This article demonstrates with numerical examples that both up- and down-going waves can be precisely predicted from the data (including internal multiples) on the top surface only. In our example, the contribution of the transmission events that never return to the measurement surface is deliberately eliminated, and it is not necessary for those events to enter the calculation.

The Green's function with vanishing Dirichlet and Neumann boundary conditions at the deeper boundary demonstrates many remarkable properties. For example, it vanishes if the receiver is deeper than the source, it violates reciprocity, and its value is not affected by any heterogeneity outside the region between the source and receiver. The double vanishing boundary condition also leads us to a wave-theory solution for a model that has many reflectors and lacks internal multiples.

In this paper, two approaches have been used to derive the Green's function with vanishing Dirichlet and Neumann boundary conditions at the deeper boundary. The first is an analytical boundary-matching method in the frequency domain, and the second is the numerical finite-difference approach identical to many current finite-difference forward-modeling procedures in the industry. The second method can be extended to multiple dimensions with lateral variation in the medium properties. We find these two methods agree with each other with regard to the intrinsic accuracy issue of the finite-difference approximation to differential equations.

In this paper, we also have some very early and very positive news on the first wave theory RTM imaging tests, with a discontinuous reference medium and images that have the correct depth and amplitude (that is, producing the reflection coefficient at the correctly located target) with primaries and multiples in the data. That is an implementation of Weglein et al. (2011a;b) with creative implementation and testing and analysis.

1 Introduction

One of the major early objectives of Reverse Time Migration (RTM) is to obtain a better image of salt flanks through diving waves than is obtained by directly imaging through the complex overburden. The key new capability of the RTM method compared with one-way migration algorithms is to allow two-way wave propagation in the imaging procedure. This article follows closely the idea established in Weglein et al. (2011a;b): achieving a Green's function with vanishing Dirichlet and Neumann boundary conditions at the deeper boundary, to eliminate the need for measurement at depth.

To achieve the two-way imaging, we study the behavior of our Green's function in three examples: (1) a homogeneous model, (2) a single reflector model, and (3) a two-reflector model with internal multiples. In order to get two-way propagation without complexity and approximation, we study 1D examples with both up- and down-going wave propagation. We provide the details to demonstrate the underlying physics.

As stated in Whitmore (1983); Baysal et al. (1983); Luo and Schuster (2004); Fletcher et al. (2006); Liu et al. (2009) and Vigh et al. (2009), accurate medium properties above the target are required for the RTM procedure discussed in this article. The major difference is that in most RTM algorithms in the industry, a smoothed version of the velocity is used in the imaging procedure to avoid reflections from the velocity model itself, while the exact velocity models (often discontinuous) are used in all three examples in this article.

To apply the firm footing and math-physics foundation established in Weglein et al. (2011a;b) in an arbitrary medium, we first study in detail the properties of the Green's functions with vanishing boundary conditions at the deeper boundary $z' = \mathcal{B}$. The understanding of the aforementioned

properties provides us with a straightforward procedure for constructing a Green's function with the double vanishing boundary condition for a 1D medium with arbitrary complexity. We adopt the notations of the aforementioned articles as much as possible while introducing some minor modifications to allow smooth expansions into new territories.

One of the remarkable properties of the Green's function in this article is that, although both the causal Green's function G_0^+ and the anti-causal Green's function G_0^- vary with the medium below the source, the Green's function with both vanishing Dirichlet and Neumann boundary conditions does not. The implications are that if we want to predict the wave field at depth z, the medium's properties deeper than z are not required. Such a property is very difficult to visualize if G_0^+ or G_0^- is used to make the prediction, since both of them will change with the medium's properties deeper than z. It is worthwhile to note that this property of the Green's function with vanishing boundary conditions is also demonstrated by the WKBJ Green's function used in the derivation of FK and phase-shift migrations. While the WKBJ Green's function is an approximate solution for a medium with smooth variations, and the Green's function with double vanishing boundary conditions in this report is exact and for a discontinuous medium, nevertheless we find their similarity worth reporting.

The property that allows an easy iterative procedure for constructing a Green's function with double vanishing boundary conditions is the following: the field values of the Green's function vanishing at the deeper surface are not affected by heterogeneity beyond the region between the field point and the source. Consequently, we can start the calculation from a field location sufficiently close to the source that the medium in between is homogeneous. In this case, the initial field value (for all time and frequency values) can be calculated from a much simpler medium obtained by extending the homogeneity to the entire space*. This initial field value contains two parts: the first part† is the out-going G_0^+ and is produced by the actual source, and the second term is the downward propagation portion‡ that will cancel with the downward propagation energy of G_0^+. Consequently, it will give a solution that vanishes completely below the source, satisfying both Dirichlet and Neumann boundary conditions. For the solution of the wave field above the initial field, standard analytic boundary-matching methods or discrete finite-difference procedures can be used to iteratively extrapolate the function values to locations further and further away from the source location.

Another property of the Green's function with both Dirichlet and Neumann boundary conditions vanishing is that it contains no multiples or reflections from the energy produced by the source, even for models with an arbitrary number of reflectors. This property, derived from precise Green's theory, agrees with many methodologies in the current seismic imaging procedures (which are often derived with some approximation to the wave equation): a smooth model is preferred, in order to exclude reflections and multiples caused by the velocity model.

The major contributions of this article are:

*For example, equation (14) of Weglein et al. (2011b) or equation (3.1) in this paper.

†The second term of equation (14) of Weglein et al. (2011b).

‡The first term of equation (14) of Weglein et al. (2011b).

- It provides two methods to calculate the Green's function with vanishing Dirichlet and Neumann boundary conditions for arbitrary 1D medium.
- It incorporates the density variation for Green's theorem RTM.
- It provides the finite-difference scheme for calculating the Green's function that vanishes at the deeper boundary.
- It provides a two-way propagation and downward continuation of wave fields, by using Green's function with double vanishing boundary conditions.
- It demonstrates remarkable properties of the precise analytical Green's function that coincide with many existing seismic imaging ideas derived with different degrees of approximation.

The following notations are worth mentioning at the beginning: G_0^+ and G_0^- are used to denote causal and anti-causal Green's functions, respectively. G_0^{DN} is used to denote the Green's function with vanishing Dirichlet and Neumann boundary conditions at the deeper boundary. $k = \omega/c_0$ where c_0 is the constant velocity of the reference medium, and ω is the angular frequency.

Although Green's theorem and Green's functions are more often discussed in the frequency domain, in this paper the Green's functions and wave field prediction examples are always graphed in the time domain since this domain is more easily accessible (without expressing the values in complex numbers). A very straightforward Fourier transform is sufficient to make the domain change:

$$f(t) = \frac{1}{2\pi} \int_{-\infty}^{\infty} \widetilde{f}(\omega) e^{-i\omega t} d\omega. \tag{1.1}$$

The Green's function, resulting from an ideal impulsive source, contains frequency information of an arbitrary frequency. For display, we convolve it with a band-limited wavelet (the first derivative of a Gaussian function[§]) to avoid aliasing beyond the Nyquist frequency.

2 Green's theorem wave-field prediction with density variation

In many migration methods, density variation is often left out of the acoustic wave equation since it does not affect the travel time. In reverse time migration, however, density serves a very important role even in the early stage: in order to have a reflectionless medium with velocity variations, a counterbalancing density variation is introduced to make sure the acoustic impedance is constant. Therefore in our derivation of Green's theorem-based RTM, we explicitly incorporate the density variations in the acoustic medium. First, let us assume the wave propagation problem in a volume V bounded by a shallower depth $\mathcal{A}$ and deeper depth $\mathcal{B}$:

[§]The wavelet is $i\omega e^{-\omega^2/\beta}$ in the frequency domain or $\frac{1}{2}\sqrt{\frac{\beta}{\pi}} e^{-\beta t^2/4}$ in the time domain, where $\beta = (20\pi)^2$

$$\left\{\frac{\partial}{\partial z'}\frac{1}{\rho(z')}\frac{\partial}{\partial z'}+\frac{\omega^2}{\rho(z')c^2(z')}\right\}P(z',\omega)=0 \qquad , \qquad \mathcal{A}<z'<\mathcal{B}, \tag{2.1}$$

where z' is the depth, and $\rho(z')$ and $c(z')$ are the density and velocity fields, respectively. In exploration seismology, we let the shallower depth $\mathcal{A}$ be the measurement surface where the seismic acquisition can be accomplished economically. The volume V is the finite volume defined in the "finite volume model" for migration, the details of which can be found in Weglein et al. (2011a). We measure P at the measurement surface $z'=\mathcal{A}$, and the objective is to predict P anywhere between the shallower surface and another surface with greater depth, $z'=\mathcal{B}$. This can be achieved via the solution of the wave-propagation equation in the same medium by an idealized impulsive source or Green's function:

$$\left\{\frac{\partial}{\partial z'}\frac{1}{\rho(z')}\frac{\partial}{\partial z'}+\frac{\omega^2}{\rho(z')c^2(z')}\right\}G_0(z,z',\omega)=\delta(z-z') \qquad , \qquad \mathcal{A}<z'<\mathcal{B}, \tag{2.2}$$

where z is the location of the source, and z' and z increase in a downward direction. It can be achieved as follows:

- Multiply equation (2.2) by $P(z',\omega)$.
- Multiply equation (2.1) by $G_0(z,z',\omega)$.
- Integrate the difference of the two aforementioned products (both are functions of z') over the variable z' from $\mathcal{A}$ to $\mathcal{B}$.

The right-hand side of the operation above is:

$$\int_{\mathcal{A}}^{\mathcal{B}} P(z',\omega)\delta(z-z')dz'=P(z,\omega), \tag{2.3}$$

where in the derivation above we assume z is inside the volume V (i.e., $\mathcal{A}<z<\mathcal{B}$). Omitting the arguments of the following functions: $P(z',\omega)$, $G_0(z,z',\omega)$, $c(z')$ and $\rho(z')$, since their arguments will not be changed in the derivation process, the left-hand side of the operation above is:

$$
\begin{aligned}
&\int_{\mathcal{A}}^{\mathcal{B}} \left[P \frac{\partial}{\partial z'} \left\{ \frac{1}{\rho} \frac{\partial G_0}{\partial z'} \right\} + \frac{\omega^2 P G_0}{\rho c^2} - G_0 \frac{\partial}{\partial z'} \left\{ \frac{1}{\rho} \frac{\partial P}{\partial z'} \right\} - \frac{\omega^2 P G_0}{\rho c^2} \right] dz' \\
=&\int_{\mathcal{A}}^{\mathcal{B}} \left[P \frac{\partial}{\partial z'} \left\{ \frac{1}{\rho} \frac{\partial G_0}{\partial z'} \right\} - G_0 \frac{\partial}{\partial z'} \left\{ \frac{1}{\rho} \frac{\partial P}{\partial z'} \right\} \right] dz' \\
=&\int_{\mathcal{A}}^{\mathcal{B}} \left[P \frac{\partial}{\partial z'} \left\{ \frac{1}{\rho} \frac{\partial G_0}{\partial z'} \right\} + \frac{\partial P}{\partial z'} \frac{1}{\rho} \frac{\partial G_0}{\partial z'} - G_0 \frac{\partial}{\partial z'} \left\{ \frac{1}{\rho} \frac{\partial P}{\partial z'} \right\} - \frac{\partial G_0}{\partial z'} \frac{1}{\rho} \frac{\partial P}{\partial z'} \right] dz' \\
=&\int_{\mathcal{A}}^{\mathcal{B}} \left[\frac{\partial}{\partial z'} \left\{ \frac{P}{\rho} \frac{\partial G_0}{\partial z'} \right\} - \frac{\partial}{\partial z'} \left\{ \frac{G_0}{\rho} \frac{\partial P}{\partial z'} \right\} \right] dz' = \int_{\mathcal{A}}^{\mathcal{B}} \frac{\partial}{\partial z'} \left\{ \frac{P}{\rho} \frac{\partial G_0}{\partial z'} - \frac{G_0}{\rho} \frac{\partial P}{\partial z'} \right\} dz' \\
=&\int_{\mathcal{A}}^{\mathcal{B}} \frac{\partial}{\partial z'} \left\{ \frac{1}{\rho} \left[P \frac{\partial G_0}{\partial z'} - G_0 \frac{\partial P}{\partial z'} \right] \right\} dz' \\
=&\frac{1}{\rho} \left\{ P \frac{\partial G_0}{\partial z'} - G_0 \frac{\partial P}{\partial z'} \right\} \Bigg|_{z'=\mathcal{A}}^{z'=\mathcal{B}}.
\end{aligned}
\tag{2.4}
$$

Equating the results obtained by the left- and right-hand-side operations, and restoring the specific arguments of each function, we have:

$$
P(z,\omega) = \frac{1}{\rho(z')} \left\{ P(z',\omega) \frac{\partial G_0(z,z',\omega)}{\partial z'} - G_0(z,z',\omega) \frac{\partial P(z',\omega)}{\partial z'} \right\} \Bigg|_{z'=\mathcal{A}}^{z'=\mathcal{B}}, \tag{2.5}
$$

where $\mathcal{A}$ and $\mathcal{B}$ are the shallower and deeper boundaries, respectively, of the volume to which the Green's theorem is applied. It is identical to equation (43) of Weglein et al. (2011a), except for the additional density contribution to the Green's theorem. Similar density contributions can be found in many seismic imaging procedures, such as equation (21) of Clayton and Stolt (1981).

In the arguments of G_0, z is the location of the source, and z' is the location of the receiver. The Green's theorem given in equation (2.5) predicts the data $P(z,\omega)$ in an arbitrary location using the data $P(z',\omega)$ at the measurement surface. In this specific application, z is the depth at which the wave-field prediction is carried out.

Note that in equation (2.5), the field values at the surface of the volume V are necessary for predicting the field value inside V. The surface of V contains two parts: the shallower portion $z' = \mathcal{A}$ and the deeper portion $z' = \mathcal{B}$. In seismic exploration, the need for data at $z' = \mathcal{B}$ is often the issue. For example, one of the significant artifacts of the current RTM procedures is caused by

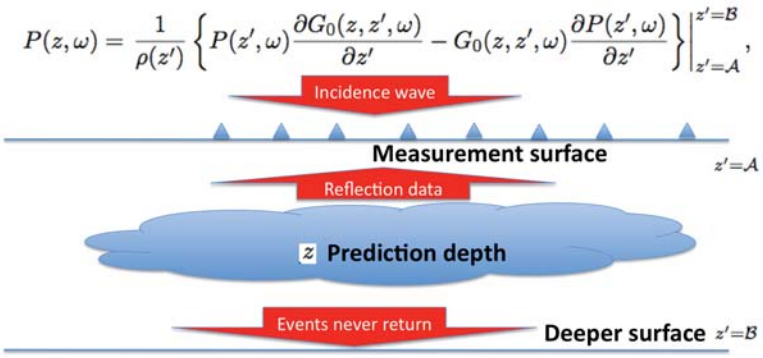

Figure 1: Green's theorem predicts the wave field at an arbitrary depth z between the shallower depth $\mathcal{A}$ and deeper depth $\mathcal{B}$.

this phenomenon: there are events necessary for accurate wave-field prediction that reach $z' = \mathcal{B}$ but never return to $z' = \mathcal{A}$, as is demonstrated in Figure 1. The solution, based on Green's theorem without any approximation, was first published in Weglein et al. (2011a) and Weglein et al. (2011b), the basic idea can be summarized as the following.

Since the wave equation is a second-order differential equation, its solution is not unique. In other words, for a wave equation with a specific medium property, there are an infinite number of solutions. This freedom in choosing the Green's function has been taken advantage of in many seismic-imaging procedures. For example, the most popular choice in wave-field prediction is the physical solution G_0^+. In downward continuing an up-going wave field to a subsurface, the anti-causal solution G_0^- is often used.

If both G_0 and $\partial G_0/\partial z'$ vanish at the deeper boundary $z' = \mathcal{B}$, where measurement is often much more expensive than acquiring data at the shallower boundary $z' = \mathcal{A}$, then only the data at the shallower surface (i.e., the actual measurement surface) is needed in the calculation. We use G_0^{DN} to denote the Green's function with vanishing Dirichlet and Neumann boundary conditions at the deeper boundary.

3 The vanishing property of G_0^{DN} and its independence of the medium's properties below the source

First, let us look at some properties of the Green's function detailed in equation (14) of Weglein et al. (2011b):

$$G_0^{DN}(z,z',\omega) = \frac{-1}{2ik}\left(e^{-ik(z-z')} - e^{ik|z-z'|}\right), \tag{3.1}$$

where $k = \omega/c_0$ and the quantity c_0 is the unchanged homogeneous velocity in the entire space, and z and z' are the locations of the source and receiver, respectively. This Green's function is

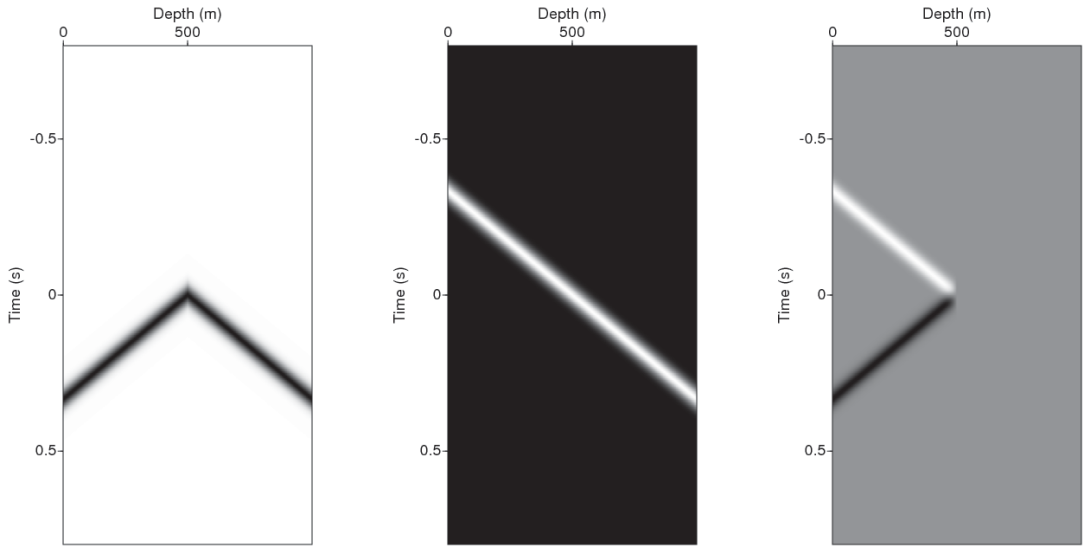

Figure 2: The construction of G_0^{DN} for a homogeneous medium with constant velocity $1500m/s$. The source depth is 500m. The left panel is the causal solution (if we denote $k = \omega/c_0$ and H is the Heaviside function, the causal Green's function is $G_0^+(z, z', \omega) = e^{ik|z-z'|}/(2ik)$ in the frequency domain or $G_0^+(z, z', t) = \frac{-c_0}{2} H(t - |z - z'|/c_0)$ in the time domain). The middle panel shows the homogeneous solution $(-e^{ik(z'-z)}/(2ik)$ in the frequency domain or $\frac{c_0}{2} H(t - (z' - z)/c_0)$ in the time domain) that cancels with the left panel below the source. The right panel results from summing the two panels on its left and is the desired Green's function with double vanishing boundary conditions.

for a whole-space homogeneous medium with c_0 as its velocity. It also satisfies the Dirichlet and Neumann boundary conditions at the deeper boundary $\mathcal{B}$:

$$G_0^{DN}(z,z',\omega)\Big|_{z'=\mathcal{B}} = 0,$$
$$\frac{\partial G_0^{DN}(z,z',\omega)}{\partial z'}\bigg|_{z'=\mathcal{B}} = 0.$$

The construction of equation (3.1) (i.e., G_0^{DN} in a homogeneous medium) is detailed in Weglein et al. (2011b); we only provide its graphic version in this article in Figure 2.

In equation (3.1), the second term is the causal solution for the same homogeneous medium, and the first term is a specific solution to the homogeneous[¶] wave equation, introduced to perfectly cancel the causal solution at the deeper boundary. The major objective of this Green's function is to eliminate the need for measurement at the deeper surface: $z' = \mathcal{B}$.

According to equation (2.5), for arbitrary values of the wave field $P(z',\omega)$, this objective implies $G_0(z,z',\omega)|_{z'=\mathcal{B}} = \frac{\partial G_0(z,z',\omega)}{\partial z'}\Big|_{z'=\mathcal{B}} = 0$, since normally the data are available only at the measurement surface: $z' = \mathcal{A}$. The variable z is used to denote the depth to which we want to continue the wave field downward. It is obvious that $\mathcal{A} < z' < \mathcal{B}$. First, if $z < z'$, this Green's operator vanishes, since

$$\begin{aligned} G_0^{DN}(z,z',\omega) &= \frac{-1}{2ik}\left(e^{-ik(z-z')} - e^{ik|z-z'|}\right) \\ &\overset{z<z'}{=} \frac{-1}{2ik}\left(e^{ik(z'-z)} - e^{ik(z'-z)}\right) \\ &\equiv 0. \end{aligned} \tag{3.2}$$

According to equation (3.2), this Green's function vanishes not only for the isolated location at $\mathcal{B}$, but also in the extended entire half-space below the source, which include $z' = \mathcal{B}$.

Obviously this Green's function satisfies the wave equation of the whole-space homogeneous medium (i.e., equation (7) of Weglein et al. (2011b)):

$$\left(\frac{d^2}{dz'^2} + \frac{\omega^2}{c_0^2}\right) G_0^{DN}(z,z',\omega) = \delta(z-z'). \tag{3.3}$$

If we have an inhomogeneous medium $c(z')$ such that $c(z') = c_0$ when $z' < z$, the Helmholtz equation for this inhomogeneous medium is

[¶]In this article the adjective homogeneous has different meaning when it acts on medium or equation. In the first case it means medium with constant acoustic property in the entire space, while in the second case it means a wave equation without the source term.

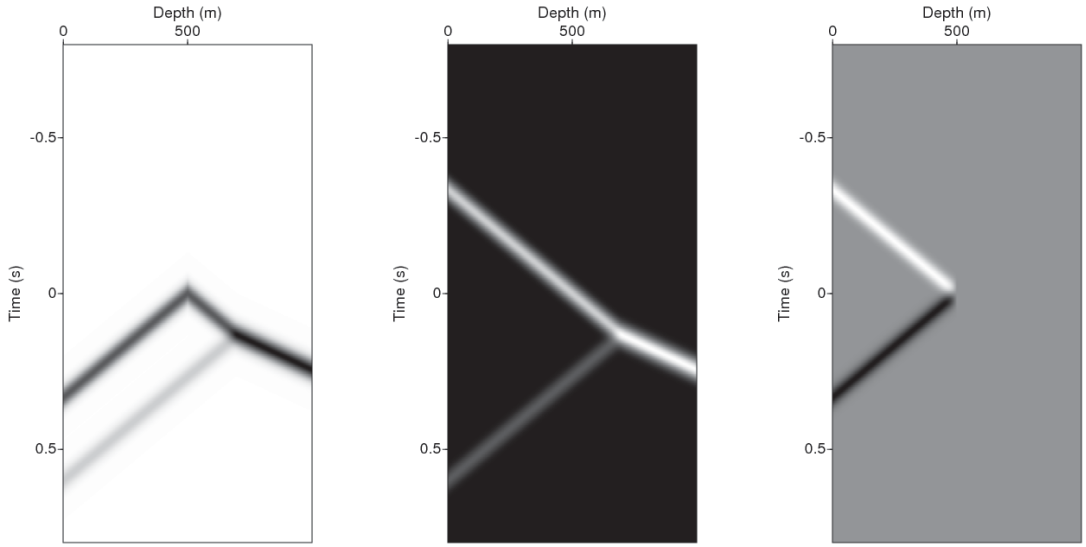

Figure 3: The construction of G_0^{DN} for a medium with one reflector (the velocities above and below the reflector are $1500m/s$ and $2700m/s$, respectively). The source depth is 500m and is above the single reflector at $700m$. The left panel is the causal solution G_0^+, and the middle panel shows the homogeneous solution that cancels with the left panel below the source. The right panel results from summing the two panels on its left and is the desired Green's function with double vanishing boundary conditions.

$$\left(\frac{d^2}{dz'^2} + \frac{\omega^2}{c^2(z')}\right) \mathcal{G}_0(z, z', \omega) = \delta(z - z'). \tag{3.4}$$

When $z' < z$, wave equation (3.4) is satisfied by Green's function (3.1) since it satisfies the homogeneous wave equation (3.3), which is identical to the inhomogeneous equation (3.4) when $z' < z$.

For the other possibility, that $z' > z$, wave equation (3.4) is also satisfied by Green's function (3.1) since it completely vanishes in this region. If we substitute G_0^{DN} for $\mathcal{G}_0$, left-hand side of equation (3.4) vanishes since the spatial partial derivative is zero, while the right-hand side vanishes due to the fact that the source z is located outside the region of interest. Consequently, equation (3.4) is satisfied by the Green's function in equation (3.3).

As an example, introducing a single reflector below the source for the Green's function in equation (16) of Weglein et al. (2011b) will not change the value of the Green's function. The construction of G_0^{DN} with its source located above the single reflector is detailed in Weglein et al. (2011b); here we provide its graphical version in Figure 3. The equivalence of the Green's function (3.1) to

equation (39) in Weglein et al. (2011b) can be demonstrated as follows. Since a is the depth of the reflector, and we consider the case in which the source is above the reflector, we have $z < a$ and $\mathtt{sgn}(a - z) = 1$. According to Appendix B of Weglein et al. (2011b), we have: $D_1 = 0$, $C_1 = -\frac{T}{2ik}e^{ik|a-z|}e^{-ik_1 a} = -\frac{T}{2ik}e^{ik(a-z)}e^{-ik_1 a}$. Thus, the wave field below the reflector (i.e., $z' > a$, the transmitted wave) can be simplified as:

$$\begin{aligned}
&\frac{T}{2ik}e^{ik|a-z|}e^{ik_1(z'-a)} + C_1 e^{ik_1 z'} + D_1 e^{-ik_1 z'} \\
=&\frac{T}{2ik}e^{ik|a-z|}e^{ik_1(z'-a)} - \frac{T}{2ik}e^{ik|a-z|e^{-ik_1 a}}e^{ik_1 z'} + 0 \times e^{-ik_1 z'} \\
=&\frac{T}{2ik}e^{ik|a-z|}e^{ik_1(z'-a)} - \frac{T}{2ik}e^{ik|a-z|}e^{ik_1(z'-a)} \equiv 0.
\end{aligned} \tag{3.5}$$

Obviously, this Green's function vanishes if $z' > a$ (is deeper than the reflector). The same vanishing property is also displayed for G_0^{DN} without the single reflector below the source; the details can be found in equation (3.2).

Since $A_1 = \frac{-1}{2ik}e^{-ikz}$, and $B_1 = \frac{-R}{2ik}e^{ik(2a-z)}$, and if $z' < a$ is above the reflector, the reflected wave in equation (39) of Weglein et al. (2011b) can be simplified as follows:

$$\begin{aligned}
&\frac{e^{ik|z'-z|}}{2ik} + R\frac{e^{-ik(z'-a)}}{2ik}e^{ik(a-z)} + A_1 e^{ikz'} + B_1 e^{-ikz'} \\
=&\frac{e^{ik|z'-z|}}{2ik} + R\frac{e^{ik(2a-z'-z)}}{2ik} + A_1 e^{ikz'} + B_1 e^{-ikz'} \\
=&\frac{e^{ik|z'-z|}}{2ik} + R\frac{e^{ik(2a-z'-z)}}{2ik} - \frac{e^{ik(z'-z)}}{2ik} - \frac{R}{2ik}e^{ik(2a-z)}e^{-ikz'} \\
=&\frac{e^{ik|z'-z|}}{2ik} + R\frac{e^{ik(2a-z'-z)}}{2ik} - \frac{e^{ik(z'-z)}}{2ik} - R\frac{e^{ik(2a-z'-z)}}{2ik} \\
=&\frac{e^{ik|z'-z|}}{2ik} - \frac{e^{ik(z'-z)}}{2ik} = \frac{-1}{2ik}\left(e^{ik(z'-z)} - e^{ik|z'-z|}\right).
\end{aligned} \tag{3.6}$$

Consequently, it is identical to the Green's function (3.1) for $z' < a$ (i.e., to equation (14) of Weglein et al. (2011b), the Green's function with the same vanishing Dirichlet and Neumann boundary conditions at the deeper boundary for a whole-space homogeneous medium). In other words, the reflector below the source will not change the values of the Green's function with vanishing Dirichlet and Neumann boundary conditions at the deeper boundary.

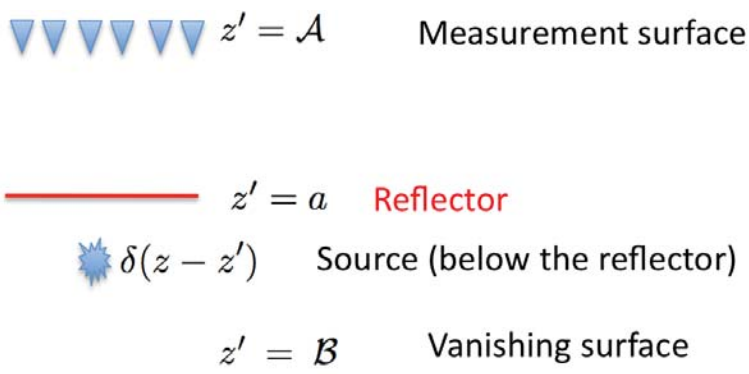

Figure 4: The configuration of the experiment with the source below a single reflector.

4 G_0^{DN} for a model with a single reflector

4.1 Case I: source above the reflector

This case had been derived and documented in detail in Weglein et al. (2011b). The only additional contribution we have in this article is the density term in the amplitude of the Green's function:

$$G_0^{DN}(z, z', \omega) = \frac{\rho_0}{2ik}\left(e^{ik|z-z'|} - e^{-ik(z-z')}\right). \tag{4.1}$$

In the equation above, the density at the source location is the extra contribution in extending the Green's function in equation (39) of Weglein et al. (2011b). A similar density term can be found in the Green's function of Clayton and Stolt (1981).

We can also Fourier transform equation (4.1) to the time domain to have:

$$G_0^{DN}(z, z', t) = \frac{\rho_0 c_0}{2}\left(H\left[t - \frac{z' - z}{c_0}\right] - H\left[t - \frac{|z' - z|}{c_0}\right]\right). \tag{4.2}$$

4.2 Case II: source below the reflector

From the previous section, if $z < a$, the solution is trivial since $G_0^{DN}(z, z', \omega) = G_0^{DN}(z, z', \omega)$. It is critical to derive G_0^{DN} for $z > a$. The physical experiment is the following (see Figure 4): The locations of the measurement surface and the deeper surface are $\mathcal{A}$ and $\mathcal{B}$, respectively. The depth of the single reflector and source are a and z, respectively. The causal Green's function with the source located at depth z and receiver at depth z' is denoted as $G_0^{+}(z, z', \omega)$.

If the impulsive source is below the reflector, it will produce an out-going wave $\frac{\rho_1 e^{ik_1|z'-z|}}{2ik_1}$ in the second medium; i.e., the Green's function with homogeneous properties (ρ_1, c_1). After the out-going

field is obtained, the reflection in the second medium and the transmission in the first medium can be solved as a classical reflection problem, as is presented in equations (12.5) and (12.8), and the final result is:

$$\frac{1}{\rho_1}G_0^+(z,z',\omega)=\begin{cases}\frac{1-R}{2ik_1}e^{ik_1(z-a)}e^{ik(a-z')} & \texttt{if } (z'<a)\\ \frac{1}{2ik_1}\left(e^{ik_1|z'-z|}-Re^{ik_1(z'+z-2a)}\right) & \texttt{if } (z'>a)\end{cases}, \tag{4.3}$$

where $R=\frac{\rho_1c_1-\rho_0c_0}{\rho_1c_1+\rho_0c_0}$ is the reflection coefficient of a plane wave incident from above. Since $\mathcal{B}$ is the depth of the deeper surface, for our wave-field prediction purpose we have $\mathcal{A}<z<\mathcal{B}$. Consequently, G_0^+ will produce two packets of down-going waves at the deeper surface $\mathcal{B}$: $\frac{\rho_1e^{ik_1(\mathcal{B}-z)}}{2ik_1}$ (the direct wave or the homogeneous propagation as if the entire space is filled with the second medium) and $-R\frac{\rho_1e^{ik_1(\mathcal{B}+z-2a)}}{2ik_1}$ (the reflection wave$^{\|}$).

For $z'>z$, G_0^+ can be expressed as:

$$\frac{e^{ik_1|z'-z|}-Re^{ik_1(z'+z-2a)}}{2ik_1/\rho_1}=\frac{e^{ik_1(z'-z)}-Re^{ik_1(z'+z-2a)}}{2ik_1/\rho_1}=\frac{e^{-ik_1z}-Re^{ik_1(z-2a)}}{2ik_1/\rho_1}e^{ik_1z'}.$$

In order to have a Green's function that vanishes at the deeper boundary $z'=\mathcal{B}$, we can introduce a homogeneous solution that cancels with the causal solution. As a result, the desired homogeneous solution, denoted as $\phi(z,z',\omega)$, must be

$$\phi(z,z',\omega)=\frac{Re^{ik_1(z-2a)}-e^{-ik_1z}}{2ik_1/\rho_1}e^{ik_1z'}\qquad\texttt{if } (z'>z). \tag{4.4}$$

We denote the amplitude factor of the down-going wave $e^{ik_1z'}$ as $F_1(z,\omega)=\frac{e^{-ik_1z}-Re^{ik_1(z-2a)}}{2ik_1/\rho_1}$. Our objective is to produce a homogeneous propagation that will produce $-F_1(z,\omega)e^{ik_1z'}$ for $z'>z$ that cancels G_0^+ at the deeper boundary $z'=\mathcal{B}$. Since the actual medium has a single invariant velocity c_1 for $z'>a$ and there is no velocity change at the source location, $z'=z$, this implies that it is also the solution for a broader region (i.e., $z'>a$):

$$\phi(z,z',\omega)=\frac{Re^{ik_1(z-2a)}-e^{-ik_1z}}{2ik_1/\rho_1}e^{ik_1z'}\qquad\texttt{if } (z'>a). \tag{4.5}$$

With the solution for $z'>a$, the wave propagation for $z'<a$ can be unambiguously solved via boundary conditions detailed in Appendix A. The medium's properties are listed in Table 1, and R is used to denote the reflection coefficient of this model when the incident wave is coming from above:

Depth Range	Velocity	Density
$(-\infty, a)$	c_0	ρ_0
(a, ∞)	c_1	ρ_1

Table 1: The properties of an acoustic medium with a single reflector at depth a.

$R = \frac{\rho_1 c_1 - \rho_0 c_0}{\rho_1 c_1 + \rho_0 c_0}$; other coefficients such as the reflection coefficient from below, and the transmission coefficients, can all be easily expressed as a simple function** of R.

According to the classical reflection problem listed in Appendix A, the incident wave (i.e., for $z' < a$) intended to produce the transmission packet in equation (4.5) for the purpose of canceling the boundary values of G_0^+ at the deeper boundary $z' = \mathcal{B}$ is:

$$\frac{-F_1}{1+R} e^{ik_1 a} e^{ik(z'-a)} = \frac{R e^{ik_1(z-a)} - e^{ik_1(a-z)}}{2ik_1(1+R)/\rho_1} e^{ik(z'-a)}. \tag{4.6}$$

However, the above incident wave will produce a corresponding reflection wave in the upper medium (i.e., $z' < a$) as a byproduct:

$$\frac{-F_1 R}{1+R} e^{ik_1 a} e^{ik(a-z')} = \frac{R^2 e^{ik_1(z-a)} - R e^{ik_1(a-z)}}{2ik_1(1+R)/\rho_1} e^{ik(a-z')}. \tag{4.7}$$

We can summarize the solution below the reflector in equation (4.5) and the solution above the reflector in equations (4.6) and (4.7) to have:

$$\phi(z, z', \omega) = \begin{cases} \frac{R e^{ik_1(z-a)} - e^{ik_1(a-z)}}{2ik_1(1+R)/\rho_1} e^{ik(z'-a)} + \frac{R^2 e^{ik_1(z-a)} - R e^{ik_1(a-z)}}{2ik_1(1+R)/\rho_1} e^{ik(a-z')} & \texttt{if } (z' < a) \\ \frac{R e^{ik_1(z-2a)} - e^{-ik_1 z}}{2ik_1/\rho_1} e^{ik_1 z'} & \texttt{if } (z' > a) \end{cases}. \tag{4.8}$$

Combining equations (4.3) and (4.8), the Green's function that satisfies the Dirichlet and Neumann boundary conditions at the deeper boundary $z' = \mathcal{B}$ is:

$$\frac{1}{\rho_1} G_0^{DN}(z, z', \omega) = \frac{G_0^+(z, z', \omega) + \phi(z, z', \omega)}{\rho_1} =$$
$$\begin{cases} \frac{1-R}{2ik_1} e^{ik_1(z-a)} e^{ik(a-z')} + \\ \frac{R e^{ik_1(z-a)} - e^{ik_1(a-z)}}{2ik_1(1+R)} e^{ik(z'-a)} + \frac{R^2 e^{ik_1(z-a)} - R e^{ik_1(a-z)}}{2ik_1(1+R)} e^{ik(a-z')} & \texttt{if } (z' < a) \\ \frac{e^{ik_1|z'-z|} - R e^{ik_1(z'+z-2a)}}{2ik_1} + \frac{R e^{ik_1(z-2a)} - e^{-ik_1 z}}{2ik_1} e^{ik_1 z'} & \texttt{if } (z' > a) \end{cases}. \tag{4.9}$$

‖The amplitude factor is $-R$ instead of R since the incident wave comes from the second medium (below) rather than the first medium (above).

**For example, the reflection coefficient from below is $-R$, and the transmission coefficients from above and below are $1 + R$ and $1 - R$, respectively.

The above expression can be simplified as:

$$G_0^{\overset{D}{\mathcal{N}}}(z,z',\omega)=\begin{cases}\frac{Re^{ik_1(z-a)}-e^{ik_1(a-z)}}{2ik_1(1+R)/\rho_1}e^{ik(z'-a)}+\frac{e^{ik_1(z-a)}-Re^{ik_1(a-z)}}{2ik_1(1+R)/\rho_1}e^{ik(a-z')} & \texttt{if } (z'<a)\\ \frac{e^{ik_1|z'-z|}-e^{ik_1(z'-z)}}{2ik_1/\rho_1} & \texttt{if } (z'>a)\end{cases}. \quad (4.10)$$

The procedure above is shown in Figure 5 in the time domain.

Let us study the vanishing property of $G_0^{\overset{D}{\mathcal{N}}}$ with the source location z below a reflector. If $z'>z$ (which automatically implies the solution in equation (4.10), since the source is located below the reflector: $z>a$), we have:

$$G_0^{\overset{D}{\mathcal{N}}}(z,z',\omega)=\frac{e^{ik_1|z'-z|}-e^{ik_1(z'-z)}}{2ik_1/\rho_1}=\frac{e^{ik_1(z'-z)}-e^{ik_1(z'-z)}}{2ik_1/\rho_1}\equiv 0 \quad (4.11)$$

According to equation (4.11), $G_0^{\overset{D}{\mathcal{N}}}$ for $z>a$ also vanishes in the half-space below the source, which includes $z'=\mathcal{B}$, a behavior demonstrated by $G_0^{\overset{D}{\mathcal{N}}}$ for $z<a$ as well.

Following the argument for $G_0^{\overset{D}{\mathcal{N}}}$ for $z<a$, it is obvious that any variations of $c(z')$ below the source location z will not change the value of the Green's function with double vanishing boundary conditions. A very important consequence is that any heterogeneity below the prediction point (i.e., the source depth z) will not have any impact on $G_0^{\overset{D}{\mathcal{N}}}$ and consequently will not affect the imaging result at z. It is worthwhile to remind the reader that this fact had already been in many publications − for example in "Finite Volume Model for Migration" from Weglein et al. (2011a).

In summary, combining equations (4.1) and (4.10), the frequency domain solution for $G_0^{\overset{D}{\mathcal{N}}}$ with a single reflector located at depth a is:

$$G_0^{\overset{D}{\mathcal{N}}}(z,z',\omega)=\begin{cases}\frac{\rho_0}{2ik}\left(e^{ik|z-z'|}-e^{ik(z'-z)}\right) & \texttt{if } (z<a),\\ \frac{\rho_1}{2ik_1}\left(e^{ik_1|z'-z|}-e^{ik_1(z'-z)}\right) & \texttt{if } (a<z' \texttt{ and } a<z),\\ \frac{Re^{ik_1(z-a)}-e^{ik_1(a-z)}}{2ik_1(1+R)/\rho_1}e^{ik(z'-a)}+ & \\ \frac{e^{ik_1(z-a)}-Re^{ik_1(a-z)}}{2ik_1(1+R)/\rho_1}e^{ik(a-z')} & \texttt{if } (z'<a \texttt{ and } a<z).\end{cases} \quad (4.12)$$

It can be transformed into the time domain via equation (1.1) to have:

$$G_0^{DN}(z,z',t) = \begin{cases} \frac{\rho_0 c_0}{2}\left(H\left[t+\frac{z-z'}{c_0}\right] - H\left[t-\frac{|z-z'|}{c_0}\right]\right) & \texttt{if } (z<a), \\ \frac{\rho_1 c_1}{2}\left(H\left[t+\frac{z-z'}{c_1}\right] - H\left[t-\frac{|z-z'|}{c_1}\right]\right) & \texttt{if } (a<z' \texttt{ and } a<z), \\ \frac{\rho_1 c_1}{2(1+R)}\left\{\begin{array}{r} H\left(t+\frac{z'-a}{c_0}+\frac{z-a}{c_1}\right) \\ -H\left(t-\frac{z'-a}{c_0}-\frac{z-a}{c_1}\right) \\ +RH\left(t+\frac{z'-a}{c_0}-\frac{z-a}{c_1}\right) \\ -RH\left(t-\frac{z'-a}{c_0}+\frac{z-a}{c_1}\right) \end{array}\right\} & \texttt{if } (z'<a \texttt{ and } a<z). \end{cases} \tag{4.13}$$

Another important property of G_0^{DN} for a model with a single reflector is that, from both equations (4.12) and (4.13), G_0^{DN} for $a<z$ and for $a<z'$ is the same even if the single reflector does not exist[††]. Note that in this case the additional heterogeneity (i.e., the single reflector) is outside the interval (z',z), and it is obvious that the geologic complexity beyond the (z',z) zone will not affect the value of G_0^{DN}.

The independence of G_0^{DN} from the heterogeneity outside the interval (z',z) agrees with the WKBJ Green's function. The WKBJ Green's function is derived as an approximate solution for a smoothed medium and is not a function of any heterogeneity outside (z',z).

In the procedure to construct G_0^{DN}, we start from the causal solution in equation (4.3). Here the last term is a reflection resulting from the up-going wave produced by the source. Note that this term is canceled after adding the homogeneous solution ϕ in equation (4.8). Consequently, their sum G_0^{DN} contains no reflection generated from the source.

It is well-known that reflections are omitted in both the WKBJ approximation and in many current seismic imaging procedures that prefer a smooth and reflectionless velocity model. In many current imaging algorithms, the velocity field is smoothed to minimize the reflections caused by the velocity, whereas in the logic for Green's function with double vanishing boundary conditions, the discontinuous model is kept intact. Nevertheless, both approaches yield the same reflectionless conclusion.

The procedure in this section to calculate G_0^{DN} for a simple single-reflector model is already very tedious. The major difficulty is to find a homogeneous solution ϕ that will cancel both the downward reflection originating from the source and the downward propagation of the source below the source location. For more complicated geological models, the procedure will be much more demanding.

Fortunately, a much simpler procedure, easily generalizable to more complicated models, can be derived from the fact that the values of G_0^{DN} are not affected by any heterogeneity outside the interval (z',z).

[††]This solution is the same as in equation (3.1) if (1) c_0 is replaced by c_1, and (2) the trivial density contribution at the source ρ_1 is added. And consequently this solution is equivalent with G_0^{DN} with a homogeneous velocity c_1 and constant density ρ_1 that contains no reflector.

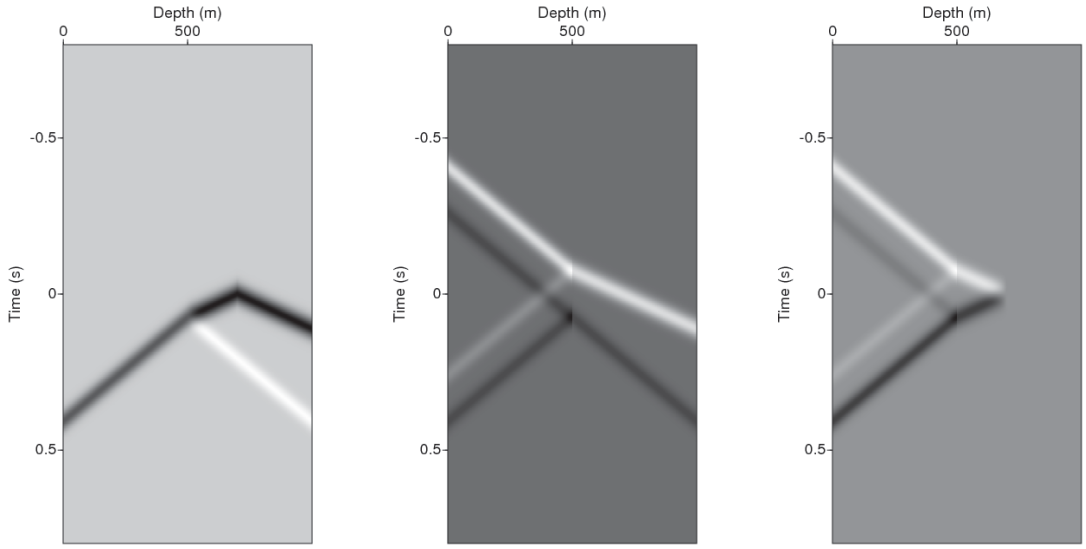

Figure 5: The construction of G_0^{DN} for a medium with one reflector (the velocities above and below the reflector are $1500m/s$ and $2700m/s$, respectively). The source depth is 700m and is below the single reflector at $500m$. The left panel is the causal solution G_0^+, and the middle panel shows the homogeneous solution that cancels with the left panel below the source. The right panel results from summing the two panels on its left and is the desired Green's function with double vanishing boundary conditions.

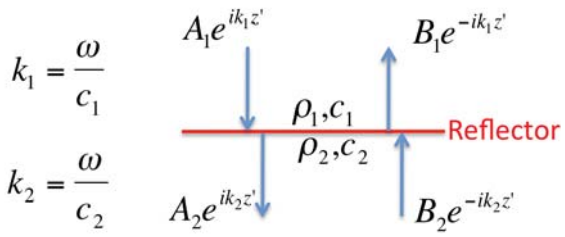

Figure 6: The diagram for upward continuation. A reflector is located at depth a, the medium properties above and below the reflector are (ρ_1, c_1) and (ρ_2, c_2), respectively. In this case we assume that the wave below the reflector $A_2 e^{ik_2 z'} + B_2 e^{-ik_2 z'}$ is known, the objective is to compute the wave above the reflector $A_1 e^{ik_1 z'} + B_1 e^{-ik_1 z'}$.

5 Upward continuation procedure: wave-theory approach

In the process of calculating G_0^{DN} with the source below many reflectors, we start from the wave field of the layer that contains the source. The wave field in this layer can be calculated through equation (4.1), and can be expressed as:

$$A_n e^{ik_n z'} + B_n e^{-ik_n z'},$$

where the source is assumed to be in the n^{th}-layer (with velocity c_n and density ρ_n, respectively), $k_n = \frac{\omega}{c_n}$, $A_n = -\frac{\rho_n}{2ik_n} e^{-iz}$, $B_n = \frac{\rho_n}{2ik_n} e^{iz}$. The objective is to find the wave field at the $(n-1)^{\text{th}}$ layer: $A_{n-1} e^{ik_{n-1} z'} + B_{n-1} e^{-ik_{n-1} z'}$, as shown in Figure 6. The theory is listed below. The continuity of the wave field and its derivatives requires:

$$\begin{aligned} A_1 e^{ik_1 a} + B_1 e^{-ik_1 a} &= A_2 e^{ik_2 a} + B_2 e^{-ik_2 a}, \\ \frac{ik_1}{\rho_1}\left(A_1 e^{ik_1 a} - B_1 e^{-ik_1 a}\right) &= \frac{ik_2}{\rho_2}\left(A_2 e^{ik_2 a} - B_2 e^{-ik_2 a}\right). \end{aligned} \tag{5.1}$$

If we define: $\gamma = \frac{\rho_1 k_2}{\rho_2 k_1} = \frac{\rho_1 c_1}{\rho_2 c_2}$, equation (5.1) can be written in matrix form:

$$\begin{pmatrix} e^{ik_1 a} & -e^{-ik_1 a} \\ e^{ik_1 a} & e^{-ik_1 a} \end{pmatrix} \begin{pmatrix} A_1 \\ B_1 \end{pmatrix} = \begin{pmatrix} \gamma & 0 \\ 0 & 1 \end{pmatrix} \begin{pmatrix} e^{ik_2 a} & -e^{-ik_2 a} \\ e^{ik_2 a} & e^{-ik_2 a} \end{pmatrix} \begin{pmatrix} A_2 \\ B_2 \end{pmatrix}, \tag{5.2}$$

with the solution:

$$\begin{aligned}\begin{pmatrix} A_1 \\ B_1 \end{pmatrix} &= \frac{1}{2}\begin{pmatrix} e^{-ik_1a} & e^{-ik_1a} \\ -e^{ik_1a} & e^{ik_1a} \end{pmatrix}\begin{pmatrix} \gamma & 0 \\ 0 & 1 \end{pmatrix}\begin{pmatrix} e^{ik_2a} & -e^{-ik_2a} \\ e^{ik_2a} & e^{-ik_2a} \end{pmatrix}\begin{pmatrix} A_2 \\ B_2 \end{pmatrix} \\ &= \frac{1}{2}\begin{pmatrix} \gamma e^{-ik_1a} & e^{-ik_1a} \\ -\gamma e^{ik_1a} & e^{ik_1a} \end{pmatrix}\begin{pmatrix} e^{ik_2a} & -e^{-ik_2a} \\ e^{ik_2a} & e^{-ik_2a} \end{pmatrix}\begin{pmatrix} A_2 \\ B_2 \end{pmatrix} \\ &= \frac{1}{2}\begin{pmatrix} (1+\gamma)e^{i(k_2-k_1)a} & (1-\gamma)e^{-i(k_1+k_2)a} \\ (1-\gamma)e^{i(k_1+k_2)a} & (1+\gamma)e^{i(k_1-k_2)a} \end{pmatrix}\begin{pmatrix} A_2 \\ B_2 \end{pmatrix}.\end{aligned} \tag{5.3}$$

Since $\frac{1+\gamma}{2} = \frac{1}{2} + \frac{\rho_1 c_1}{2\rho_2 c_2} = \frac{\rho_2 c_2 + \rho_1 c_1}{2\rho_2 c_2} = \frac{1}{1+R}$, and $\frac{1-\gamma}{2} = \frac{1}{2} - \frac{\rho_1 c_1}{2\rho_2 c_2} = \frac{\rho_2 c_2 - \rho_1 c_1}{2\rho_2 c_2} = \frac{R}{1+R}$, the above results can be rewritten as:

$$\begin{pmatrix} A_1 \\ B_1 \end{pmatrix} = \frac{1}{1+R}\begin{pmatrix} e^{i(k_2-k_1)a} & Re^{-i(k_1+k_2)a} \\ Re^{i(k_1+k_2)a} & e^{i(k_1-k_2)a} \end{pmatrix}\begin{pmatrix} A_2 \\ B_2 \end{pmatrix}. \tag{5.4}$$

For example, for G_0^{DN} with $z > a$, the wave field immediately below the single reflector is $\frac{\rho_1}{2ik_1}\left(-e^{ik_1(z'-z)} + e^{ik_1(z-z')}\right)$. If it is expressed in the form $A_2 e^{ik_1 z'} + B_2 e^{-ik_1 z'}$, we have $A_2 = -\frac{\rho_1 e^{-ik_1 z}}{2ik_1}$, $B_2 = \frac{\rho_1 e^{ik_1 z}}{2ik_1}$ and consequently we have:

$$\begin{aligned}\begin{pmatrix} A_1 \\ B_1 \end{pmatrix} &= \frac{1}{1+R}\begin{pmatrix} e^{i(k_1-k)a} & Re^{-i(k+k_1)a} \\ Re^{i(k+k_1)a} & e^{i(k-k_1)a} \end{pmatrix}\frac{\rho_1}{2ik_1}\begin{pmatrix} -e^{-ik_1 z} \\ e^{ik_1 z} \end{pmatrix} \\ &= \frac{\rho_1}{2ik_1}\frac{1}{1+R}\begin{pmatrix} \left\{Re^{ik_1(z-a)} - e^{ik_1(a-z)}\right\}e^{-ika} \\ \left\{e^{ik_1(z-a)} - Re^{ik_1(a-z)}\right\}e^{ika} \end{pmatrix}.\end{aligned} \tag{5.5}$$

From equation (5.5), we can easily produce the wave field above the reflector: $A_1 e^{ikz'} + B_1 e^{-ikz'} = \frac{\rho_1}{2ik_1}\frac{\left\{Re^{ik_1(z-a)} - e^{ik_1(a-z)}\right\}e^{ik(z'-a)} + \left\{e^{ik_1(z-a)} - Re^{ik_1(a-z)}\right\}e^{ik(a-z')}}{1+R}$.

Compared with the previous section, the example above is a much simpler derivation of G_0^{DN} with a single reflector above the source.

For example, for G_0^{DN} in a two-reflector model, the wave field immediately below the second reflector is $A_3 e^{ik_2 z'} + B_3 e^{-ik_2 z'} = \frac{\rho_2}{2ik_2}\left(-e^{ik_2(z'-z)} + e^{ik_2(z-z')}\right)$. It is obvious that in this case $A_3 = -\frac{\rho_2 e^{-ik_2 z}}{2ik_2}$, $B_2 = \frac{\rho_2 e^{ik_2 z}}{2ik_2}$ and consequently, we have:

$$\begin{pmatrix} A_2 \\ B_2 \end{pmatrix} = \frac{1}{1+R_2} \begin{pmatrix} e^{i(k_2-k_1)a_2} & R_2 e^{-i(k_1+k_2)a_2} \\ R_2 e^{i(k_1+k_2)a_2} & e^{i(k_1-k_2)a_2} \end{pmatrix} \frac{\rho_2}{2ik_2} \begin{pmatrix} -e^{-ik_2 z} \\ e^{ik_2 z} \end{pmatrix}$$
$$= \frac{\rho_2}{2ik_2} \frac{1}{1+R_2} \begin{pmatrix} \left\{R_2 e^{ik_2(z-a_2)} - e^{ik_2(a_2-z)}\right\} e^{-ik_1 a_2} \\ \left\{e^{ik_2(z-a_2)} - R_2 e^{ik_2(a_2-z)}\right\} e^{ik_1 a_2} \end{pmatrix}. \tag{5.6}$$

Renaming $R = R_1$, and $a = a_1$, the combination of equations (5.4) and (5.6) gives:

$$\begin{pmatrix} A_1 \\ B_1 \end{pmatrix} = \frac{1}{1+R_1} \begin{pmatrix} e^{i(k_1-k)a_1} & R_1 e^{-i(k+k_1)a_1} \\ R_1 e^{i(k+k_1)a_1} & e^{i(k-k_1)a_1} \end{pmatrix} \begin{pmatrix} A_2 \\ B_2 \end{pmatrix}$$
$$= \frac{\rho_2/(1+R_2)}{2ik_2(1+R_1)} \begin{pmatrix} e^{i(k_1-k)a_1} & R_1 e^{-i(k+k_1)a_1} \\ R_1 e^{i(k+k_1)a_1} & e^{i(k-k_1)a_1} \end{pmatrix} \begin{pmatrix} \left\{R_2 e^{ik_2(z-a_2)} - e^{ik_2(a_2-z)}\right\} e^{-ik_1 a_2} \\ \left\{e^{ik_2(z-a_2)} - R_2 e^{ik_2(a_2-z)}\right\} e^{ik_1 a_2} \end{pmatrix}$$
$$= \frac{\rho_2}{2ik_2(1+R_1)(1+R_2)} \times$$
$$\begin{pmatrix} \left[e^{ik_1(a_1-a_2)} \left\{R_2 e^{ik_2(z-a_2)} - e^{ik_2(a_2-z)}\right\} + e^{ik_1(a_2-a_1)} \left\{R_1 e^{ik_2(z-a_2)} - R_1 R_2 e^{ik_2(a_2-z)}\right\}\right] e^{-ika_1} \\ \left[e^{ik_1(a_1-a_2)} \left\{R_1 R_2 e^{ik_2(z-a_2)} - R_1 e^{ik_2(a_2-z)}\right\} + e^{ik_1(a_2-a_1)} \left\{e^{ik_2(z-a_2)} - R_2 e^{ik_2(a_2-z)}\right\}\right] e^{ika_1} \end{pmatrix}. \tag{5.7}$$

If we define: $\lambda \equiv e^{ik_2(z-a_2)}$, $\mu \equiv e^{ik(z'-a_1)}$ and $\nu \equiv e^{ik_1(a_2-a_1)}$, the Green's function can be expressed as:

$$\frac{\left[\nu^{-1}(R_2\lambda - \lambda^{-1}) + R_1\nu(\lambda - R_2\lambda^{-1})\right]\mu + \left[R_1\nu^{-1}(R_2\lambda - \lambda^{-1}) + \nu(\lambda - R_2\lambda^{-1})\right]\mu^{-1}}{2ik_2(1+R_1)(1+R_2)/\rho_2} \tag{5.8}$$

6 Upward continuation: finite-difference approach

In order to demonstrate the general philosophy of our method, we study wave propagation in an arbitrary acoustic medium $c(z)$ (with only velocity variation). It can be extended to a medium with density variation as well. First we have the equation for the causal Green's function with source located at depth z_s:

$$\left(\frac{\partial^2}{\partial z^2} - \frac{1}{c^2(z)}\frac{\partial^2}{\partial t^2}\right) G_0^+(z, z_s, t) = \delta(z - z_s)\delta(t). \tag{6.1}$$

We then consider a homogeneous equation (without the source) in the same velocity field $c(z)$:

$$\left(\frac{\partial^2}{\partial z^2} - \frac{1}{c^2(z)}\frac{\partial^2}{\partial t^2}\right)\phi(z,t) = 0. \tag{6.2}$$

Note that for a small positive number ε, and for $z > z_s + \varepsilon$, the source term of equation (6.1) vanishes: $\delta(z - z_s)\delta(t) = 0$. Consequently, equation (6.1) is a homogeneous wave equation for $z > z_s + \varepsilon$, i.e., identical to equation (6.2).

In the aforementioned source-free region, the difference scheme (with second-order accuracy in both space and time) is:

$$\frac{\phi_{m+1,n} + \phi_{m-1,n} - 2\phi_{m,n}}{(\Delta z)^2} - \frac{1}{c^2}\frac{\phi_{m,n+1} + \phi_{m,n-1} - 2\phi_{m,n}}{(\Delta t)^2} = 0, \tag{6.3}$$

where in the subscript, the variable m denotes the index for depth z, and the variable n denotes the index for time t: $\phi_{m,n} = \phi(m\Delta z, n\Delta t)$. If we define $p \overset{\Delta}{=} \frac{c\Delta t}{\Delta z}$, we have:

$$\phi_{m,n+1} = (2 - 2p^2)\phi_{m,n} - \phi_{m,n-1} + p^2(\phi_{m+1,n} + \phi_{m-1,n}), \tag{6.4}$$

for forward marching in time, and

$$\phi_{m-1,n} = (2 - 2p^{-2})\phi_{m,n} - \phi_{m+1,n} + p^{-2}(\phi_{m,n+1} + \phi_{m,n-1}), \tag{6.5}$$

for upward marching in depth. Since both difference schemes with second-order accuracy in equations (6.4) and (6.5) are of the same type, according to the analysis in Alford et al. (1974), equation (6.4) is stable for $\frac{c\Delta t}{\Delta z} \leq \sqrt{0.5}$, and equation (6.5) is stable for $\frac{c\Delta t}{\Delta z} \geq \sqrt{2}$.

Since the value of $G_0^{DN}(z, z')$ is completely determined by the medium in the interval (z', z), if the medium between z' and z is homogeneous, we can extend the local homogeneous medium to the entire space and we have a much simpler problem already solved in equation (14) of Weglein et al. (2011b). In equation (6.5), the initial values are listed on the right-hand side of the formula, with depth levels that have indices m and $m + 1$, respectively. The field values for the depth level with index $m - 1$ can be straightforwardly computed by using equation (6.5), and by using the values at depth indices $m - 1$ and m, the field at depth index $m - 2$ can be likewise calculated. That procedure is very similar to the scheme popularly implemented in finite-difference forward-modeling algorithms that march forward in time.

The two levels of initial field values are from equation (14) of Weglein et al. (2011b), which satisfies the double vanishing Green's function at the lower boundary. These initial field values will not be changed by the scheme in equation (6.5); all the complexity to match the boundary conditions at the current level is carried on to the next depth level with index $m - 1$. It guarantees that both Dirichlet and Neumann boundary conditions at $z' = \mathcal{B}$ are satisfied.

Note that in equation (6.5), the velocity field c is a function of depth and can be arbitrary, enabling the flexibility of the scheme for a medium with any spatially varying velocities.

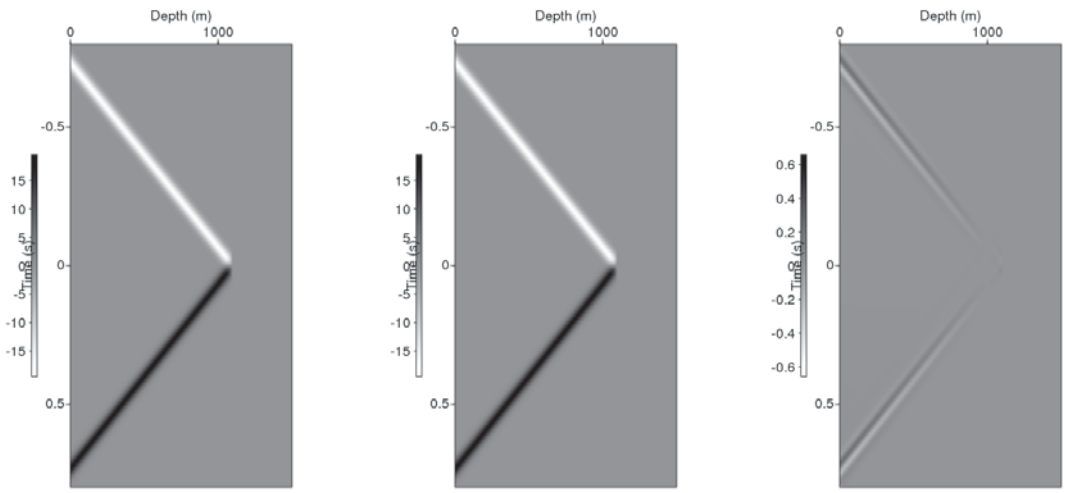

Figure 7: $G_0^{DN}(z = 1100m, z', t)$ for a homogeneous medium with velocity $1500m/s$. The left panel is generated through the finite-difference scheme from equation (6.5). The middle panel is computed from the analytic method and is presented in equation (4.1). The difference between the left and middle panels is shown in the right panel.

7 G_0^{DN} for a model with two reflectors

The G_0^{DN} in this case is for the medium listed in Table 2. The final result is:

$$G_0^{DN}(z,z',\omega) = \begin{cases} \frac{\rho_0}{2ik}\left(e^{ik|z-z'|} - e^{ik(z'-z)}\right) & \texttt{if } (z < a_1) \\ \frac{\rho_1}{2ik_1}\left(e^{ik_1|z'-z|} - e^{ik_1(z'-z)}\right) & \texttt{if } (z' > a_1 \texttt{ and } a_1 < z < a_2) \\ \frac{R_1 e^{ik_1(z-a_1)} - e^{ik_1(a_1-z)}}{2ik_1(1+R_1)/\rho_1} e^{ik_1(z'-a_1)} + & \\ \frac{e^{ik_1(z-a_1)} - R_1 e^{ik_1(a_1-z)}}{2ik_1(1+R_1)/\rho_1} e^{ik_1(a_1-z')} & \texttt{if } (z' < a_1 \texttt{ and } a_1 < z < a_2), \\ \frac{\rho_2}{2ik_2}\left(e^{ik_2|z-z'|} - e^{ik_2(z'-z)}\right) & \texttt{if } (a_2 < z' \texttt{ and } a_2 < z), \\ \frac{R_2 e^{ik_2(z-a_2)} - e^{ik_2(a_2-z)}}{2ik_1(1+R_2)/\rho_2} e^{ik_1(z'-a_2)} + & \\ \frac{e^{ik_2(z-a_2)} - R_2 e^{ik_2(a_2-z)}}{2ik_1(1+R_2)/\rho_2} e^{ik_1(a_2-z')} & \texttt{if } (a_1 < z' < a_2 \texttt{ and } a_2 < z), \\ \frac{\rho_2}{2i(1+R_1)(1+R_2)} \left\{ \begin{array}{r} \nu^{-1}(R_2\lambda - \lambda^{-1})\mu \\ +R_1\nu(\lambda - R_2\lambda^{-1})\mu \\ +R_1\nu^{-1}(R_2\lambda - \lambda^{-1})\mu^{-1} \\ +\nu(\lambda - R_2\lambda^{-1})\mu^{-1} \end{array} \right\} & \texttt{if } (a_2 < z \texttt{ and } z' < a_1). \end{cases} \tag{7.1}$$

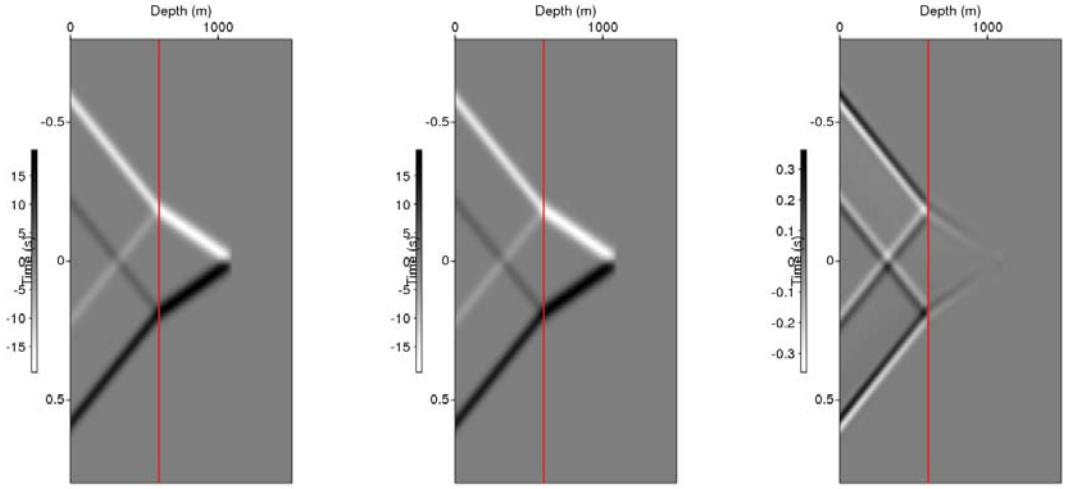

Figure 8: $G_0^{DN}(z = 1100m, z', t)$ for a medium with a reflector at a depth of $600m$. The velocities above and below the reflector are $1500m/s$ and $2700m/s$, respectively. The left panel is generated through the finite-difference scheme from equation (6.5). The middle panel is computed from the analytic method and is presented in equation (4.10). The difference between the left and middle panels is shown in the right panel.

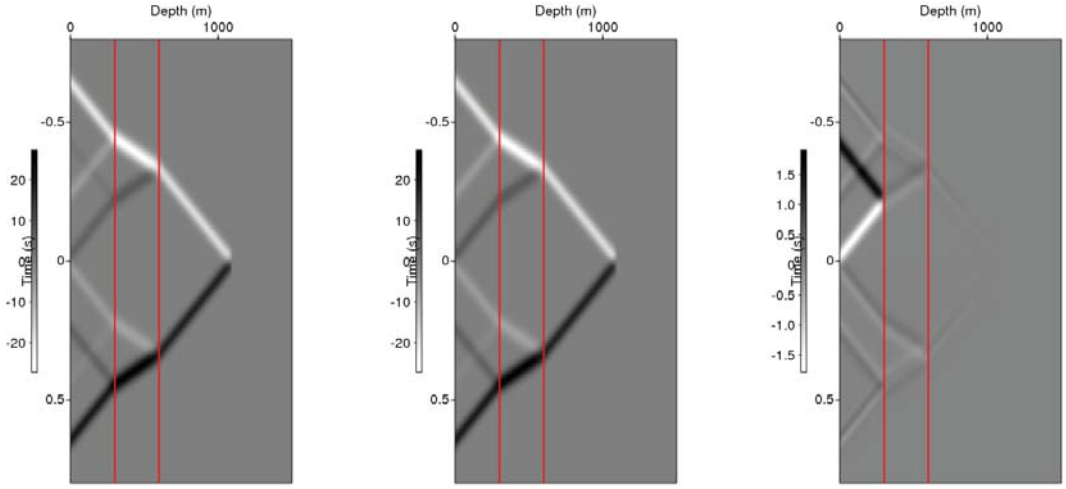

Figure 9: $G_0^{DN}(z = 1100m, z', t)$ for a medium with two reflectors, located at depths of $300m$ and $600m$, respectively. The medium velocities are (from top to bottom) $1500m/s$, $2700m/s$, and $1500m/s$. The left panel is generated through the finite-difference scheme from equation (6.5). The middle panel is computed from the analytic method and is presented in equation (7.1). The difference between the left and middle panels is shown in the right panel.

In the equation above: $\lambda \equiv e^{ik_2(z-a_2)}$, $\mu \equiv e^{ik(z'-a_1)}$, and $\nu \equiv e^{ik_1(a_2-a_1)}$. The details of the above result are listed below:

- Case 1, the source is above the first reflector (i.e., $z < a_1$): the solution in this case is essentially for a whole-space homogeneous medium with velocity c_0 and density ρ_0. The Green's function in this case is the simplest (identical to that for equation (4.1)) and has only two events.
- Case 2, the source is between the first and second reflectors and the receiver is below the first reflector (i.e., $a_1 < z < a_2$ and $a_1 < z'$): the solution in this case is exactly the same as that for a simpler medium that lacks the shallower reflector. It is obtained from equation (4.1), with (c_0, ρ_0) being replaced by (c_1, ρ_1), or the second case of equation (4.10). The G_0^{DN} in this case has two events.
- Case 3, the source is between the first and second reflectors and the receiver is above the first reflector (i.e., $a_1 < z < a_2$ and $z' a_1$. It is the first case of equation (4.10). The G_0^{DN} in this case has four events).
- Case 4, the source and receiver are both below the second reflector (i.e., $a_2 < z$ and $a_2 < z'$): the solution in this case is exactly the same as that for a simpler medium that lacks the shallower reflectors. It is obtained from equation (4.1), with (c_0, ρ_0) being replaced by (c_2, ρ_2).
- Case 5, the source is below the second reflector and the receiver is between the first and second reflectors (i.e., $a_2 < z$ and $a_1 < z' < a_2$). It is obtained from equation (4.10) with (c_1, ρ_1) being replaced by (c_2, ρ_2) and with (c_0, ρ_0) being replaced by (c_1, ρ_1). There are four events in this situation.
- Case 6, the source is below the second reflector and the receiver is above the first reflector (i.e., $a_2 < z$ and $z' < a_1$): this is the most complicated situation and contains eight events. It is calculated by using equation (5.7).

8 Wave-field prediction with the RTM Green's function

In this section, we demonstrate the behavior of the Green's function that satisfies both Dirichlet and Neumann boundary conditions at the deeper boundary. The study consists of three geological models with progressive complexity.

8.1 Example I: homogeneous case

This example had already been documented in Appendix A of Weglein et al. (2011b) for an acoustic medium without density variation; it is given here to make a smooth transition into more complicated examples and to demonstrate the impact of density in the algorithms. With $k = \omega/c_0$, the general solution of a wave propagating in the whole space homogeneous medium with velocity c_0 is:

$$P(z',\omega) = \alpha e^{ikz'} + \beta e^{-ikz'}, \tag{8.1}$$

where α and β can be any value. At the measurement surface $z' = \mathcal{A}$, we will detect the wave field and its partial derivative over z' as follows:

$$\begin{aligned} P(z')\big|_{z'=\mathcal{A}} &= \alpha e^{ik\mathcal{A}} + \beta e^{-ik\mathcal{A}}, \\ \left.\frac{\partial P(z',\omega)}{\partial z'}\right|_{z'=\mathcal{A}} &= ik\left(\alpha e^{ik\mathcal{A}} - \beta e^{-ik\mathcal{A}}\right). \end{aligned} \tag{8.2}$$

From equation (4.1), the values of the Green's function needed on the boundary $z' = \mathcal{A}$ are:

$$\begin{aligned} G_0^{DN}(z,z',\omega)\big|_{z'=\mathcal{A}} &= \frac{\rho(z)}{2ik}\left[e^{ik|z-z'|} - e^{ik(z'-z)}\right]_{z'=\mathcal{A}} = \frac{\rho_0}{2ik}\left[e^{ik|z-\mathcal{A}|} - e^{ik(\mathcal{A}-z)}\right], \\ \left.\frac{\partial}{\partial z'}G_0^{DN}(z,z',\omega)\right|_{z'=\mathcal{A}} &= \frac{\rho(z)}{2}\left[\mathtt{sgn}(z'-z)e^{ik|z-z'|} - e^{ik(z'-z)}\right]_{z'=\mathcal{A}} \\ &= \frac{\rho_0}{2}\left[\mathtt{sgn}(\mathcal{A}-z)e^{ik|z-\mathcal{A}|} - e^{ik(\mathcal{A}-z)}\right]. \end{aligned} \tag{8.3}$$

Using the boundary values of the wave field P and Green's operator G_0^{DN} at the boundary $z' = \mathcal{A}$ (in equations (8.2) and (8.3)), we can predict the wave field as follows,

$$\begin{aligned} P(z,\omega) =& \frac{1}{\rho(z')}\left[P(z',\omega)\frac{\partial G_0^{DN}(z,z',\omega)}{\partial z'} - G_0^{DN}(z,z',\omega)\frac{\partial P(z',\omega)}{\partial z'}\right]_{z'=\mathcal{A}}^{z'=\mathcal{B}} \\ =& -\frac{1}{\rho_0}\left[P(z',\omega)\frac{\partial G_0^{DN}(z,z',\omega)}{\partial z'} - G_0^{DN}(z,z',\omega)\frac{\partial P(z',\omega)}{\partial z'}\right]_{z'=\mathcal{A}} \\ =& -\frac{\alpha e^{ik\mathcal{A}} + \beta e^{-ik\mathcal{A}}}{2}\left[\mathtt{sgn}(\mathcal{A}-z)e^{ik|z-\mathcal{A}|} - e^{ik(\mathcal{A}-z)}\right] \\ &+\frac{\alpha e^{ik\mathcal{A}} - \beta e^{-ik\mathcal{A}}}{2}\left[e^{ik|z-\mathcal{A}|} - e^{ik(\mathcal{A}-z)}\right]. \end{aligned} \tag{8.4}$$

For the purpose of predicting the wave field below the measurement surface $z' = \mathcal{A}$, we obviously have the situation $z > \mathcal{A}$. Consequently, the equation above can be simplified as,

$$\begin{aligned} P(z,\omega) =& \frac{\alpha e^{ik\mathcal{A}} + \beta e^{-ik\mathcal{A}}}{2}\left[e^{ik(z-\mathcal{A})} + e^{ik(\mathcal{A}-z)}\right] + \frac{\alpha e^{ik\mathcal{A}} - \beta e^{-ik\mathcal{A}}}{2}\left[e^{ik(z-\mathcal{A})} - e^{ik(\mathcal{A}-z)}\right] \\ =& \alpha e^{ik\mathcal{A}}e^{ik(z-\mathcal{A})} + \beta e^{-ik\mathcal{A}}e^{ik(\mathcal{A}-z)} \\ =& \alpha e^{ikz} + \beta e^{-ikz}. \end{aligned} \tag{8.5}$$

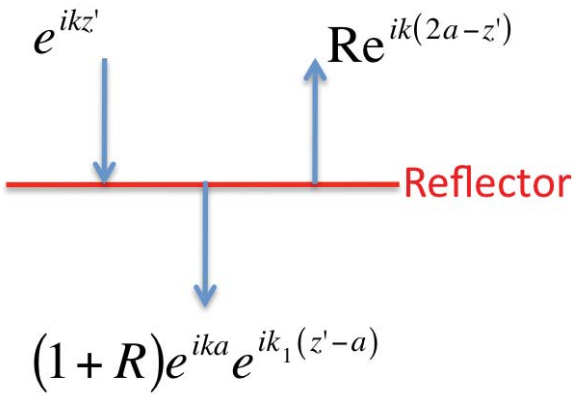

Figure 10: The incident, reflection, and transmission waves in example II. Here $k = \omega/c_0$, $k_1 = \omega/c_1$, and a is the depth of the single reflector. $R = (\rho_1 c_1 - \rho_0 c_0)/(\rho_1 c_1 + \rho_0 c_0)$ is the reflection coefficient for a down-going incident plane wave. $e^{ikz'}$ is the incident wave. $Re^{ik(2a-z')}$ is the reflection data. $(1+R)e^{ika}e^{ik_1(z'-a)}$ is the transmission wave.

The above expression is exactly the actual wave field that we assumed in equation (8.1). In other words, the original wave field, with both up-going and down-going waves, is perfectly reconstructed at an arbitrary depth.

It would sound irrational that we can also perfectly predict the wave field if there are reflectors below z. However, according to d'Alembert's formula for a 1D wave equation for any interval, the introduction of additional reflectors into the homogeneous reference medium below z will not alter the possible type of waves between a and z, which remains homogeneous: $\alpha e^{ikz} + \beta e^{-ikz}$, where α and β are arbitrary numbers. The examples of using this Green's function derived from homogeneous media for nonhomogeneous velocity models can be found in Examples II and III.

8.2 Example II: a single reflector

With the models listed in Table 1, an incident plane wave $e^{ikz'}$ will produce various waves, as shown in Figure 10. Obviously the wave at the measurement surface is:

$$\begin{aligned} P(z' = \mathcal{A}, \omega) &= e^{ik\mathcal{A}} + Re^{ik(2a-\mathcal{A})}, \\ \left.\frac{P(z' = \mathcal{A}, \omega)}{\partial z'}\right|_{z'=\mathcal{A}} &= ik\left(e^{ik\mathcal{A}} - Re^{ik(2a-\mathcal{A})}\right). \end{aligned} \tag{8.6}$$

First let us consider the simpler situation, predicting the wave field above the reflector: $P(z, \omega)$ where $z < a$. The Green's function can be found in equation (4.1). Note that in this case, we use a reflectionless Green's function to downward continue a reflection.

$$
\begin{aligned}
G_0^{DN}(z,z',\omega)\big|_{z'=\mathcal{A}} &= \frac{\rho(z)}{2ik}\left[e^{ik|z-z'|}-e^{ik(z'-z)}\right]_{z'=\mathcal{A}} = \frac{\rho_0}{2ik}\left[e^{ik(z-\mathcal{A})}-e^{ik(\mathcal{A}-z)}\right], \\
\frac{\partial}{\partial z'}G_0^{DN}(z,z',\omega)\Big|_{z'=\mathcal{A}} &= \frac{\rho_0}{2}\left[-e^{ik(z-\mathcal{A})}-e^{ik(\mathcal{A}-z)}\right].
\end{aligned}
\tag{8.7}
$$

In the equation above, we take advantage of the fact that $\mathtt{sgn}(\mathcal{A}-z)=-1$. With the boundary values from equations (8.6) and (8.7), we can predict the wave field at arbitrary location z using equation (2.5):

$$
\begin{aligned}
P(z,\omega) =& \frac{e^{ik\mathcal{A}}+Re^{ik(2a-\mathcal{A})}}{2}\left[e^{ik(z-\mathcal{A})}+e^{ik(\mathcal{A}-z)}\right]+\frac{e^{ik\mathcal{A}}-Re^{ik(2a-\mathcal{A})}}{2}\left[e^{ik(z-\mathcal{A})}-e^{ik(\mathcal{A}-z)}\right] \\
=& e^{ik\mathcal{A}}e^{ik(z-\mathcal{A})}+Re^{ik(2a-\mathcal{A})}e^{ik(\mathcal{A}-z)} \\
=& e^{ikz}+Re^{ik(2a-z)}.
\end{aligned}
\tag{8.8}
$$

Next let us predict the wave field below the reflector: $P(z,\omega)$, where $z>a$. The value of Green's function at the measurement surface, needed in equation (2.5), can be found in equation (4.10) and is given as:

$$
\begin{aligned}
G_0^{DN}(z,z',\omega)\big|_{z'=\mathcal{A}} &= \frac{\rho_1}{2ik_1}\left\{\frac{R\lambda-\lambda^{-1}}{1+R}\mu+\frac{\lambda-R\lambda^{-1}}{1+R}\mu^{-1}\right\}, \\
\frac{\partial}{\partial z'}G_0^{DN}(z,z',\omega)\Big|_{z'=\mathcal{A}} &= \frac{\rho_1 k}{2k_1}\left\{\frac{R\lambda-\lambda^{-1}}{1+R}\mu-\frac{\lambda-R\lambda^{-1}}{1+R}\mu^{-1}\right\},
\end{aligned}
\tag{8.9}
$$

where $\lambda\equiv e^{ik_1(z-a)}$ and $\mu\equiv e^{ik(\mathcal{A}-a)}$. With all the terms in equations (8.6) and (8.9), we can predict the wave field below the reflector using equation (2.5):

Depth Range	Velocity	Density
$(-\infty, a_1)$	c_0	ρ_0
(a_1, a_2)	c_1	ρ_1
(a_2, ∞)	c_1	ρ_1

Table 2: The properties of an acoustic medium with two reflectors, at depth a_1 and a_2.

$$
\begin{aligned}
P(z,\omega) &= \frac{1}{\rho(z')}\left\{P(z',\omega)\frac{\partial G_0^{DN}(z,z',\omega)}{\partial z'} - G_0^{DN}(z,z',\omega)\frac{\partial P(z',\omega)}{\partial z'}\right\}\Bigg|_{z'=\mathcal{A}}^{z'=\mathcal{B}} \\
&= \frac{1}{\rho(z')}\left[G_0^{DN}(z,z',\omega)\frac{\partial P(z',\omega)}{\partial z'} - P(z',\omega)\frac{\partial G_0^{DN}(z,z',\omega)}{\partial z'}\right]_{z'=\mathcal{A}} \\
&= \frac{\rho_1 k}{\rho_0 k_1}\left\{\frac{\lambda - R\lambda^{-1}}{1+R}\mu^{-1}e^{ik\mathcal{A}} - \frac{R\lambda - \lambda^{-1}}{1+R}\mu R e^{ik(2a-\mathcal{A})}\right\} \\
&= \frac{\rho_1 k}{\rho_0 k_1}e^{ika}\left\{\frac{\lambda - R\lambda^{-1}}{1+R} - \frac{R^2\lambda - R\lambda^{-1}}{1+R}\right\} \\
&= \frac{\rho_1 c_1}{\rho_0 c_0 (1+R)}e^{ika}\left\{\left[1-R^2\right]\lambda + \left[R-R\right]\lambda^{-1}\right\} \\
&= \frac{\rho_1 c_1}{\rho_0 c_0}(1-R)\lambda e^{ika} = \frac{\rho_1 c_1}{\rho_0 c_0}\frac{2\rho_0 c_0}{\rho_1 c_1 + \rho_0 c_0}\lambda e^{ika} = \frac{2\rho_1 c_1}{\rho_1 c_1 + \rho_0 c_0}\lambda e^{ika} \\
&= (R+1)\lambda e^{ika} = (1+R)e^{ika}e^{ik_1(z-a)}.
\end{aligned}
\tag{8.10}
$$

In the derivation above, we take advantage of the fact that $\mu \cdot e^{ik(2a-\mathcal{A})} = \mu^{-1}e^{ik\mathcal{A}} = e^{ika}$. The final result above is exactly the transmission wave in the second medium illustrated in Figure 10. Note that the down-going incident wave and the up-going reflection data act together to produce the down-going transmission data in the second medium, with correct amplitude and phase.

In the G_0^{DN} expression in equation (8.9), the λ terms are for the down-going wave, and the λ^{-1} terms are for the up-going wave. In other words, both down-going and up-going energy is present in the formalism. However, the action of the data cancels the up-going terms (i.e., the terms containing λ^{-1}) in the second medium, as it should.

8.3 Example III: a model with two reflectors: reconstruction of internal multiples in the subsurface

As was chosen in Example II, the incident wave here is $e^{ikz'}$, and the reflection data contain two primaries, corresponding to each reflector, and an infinite number of internal multiples. The measurement at $z' = \mathcal{A}$ is:

$$
\begin{aligned}
P(z'=\mathcal{A},\omega) &= e^{ik\mathcal{A}} + R_1 e^{ik(2a_1-\mathcal{A})} \\
&\quad + \left(1-R_1^2\right) e^{ik(2a_1-\mathcal{A})} \sum_{n=0}^{\infty} (-1)^n R_1^n R_2^{n+1} e^{ik_1(2n+2)[a_2-a_1]}, \\
\frac{1}{ik}\left.\frac{P(z'=\mathcal{A},\omega)}{\partial z'}\right|_{z'=\mathcal{A}} &= e^{ik\mathcal{A}} - R_1 e^{ik(2a_1-\mathcal{A})} \\
&\quad - \left(1-R_1^2\right) e^{ik(2a_1-\mathcal{A})} \sum_{n=0}^{\infty} (-1)^n R_1^n R_2^{n+1} e^{ik_1(2n+2)[a_2-a_1]},
\end{aligned}
\tag{8.11}
$$

where $R_1 = \frac{\rho_1 c_1 - \rho_0 c_0}{\rho_1 c_1 + \rho_0 c_0}$ and $R_2 = \frac{\rho_2 c_2 - \rho_1 c_1}{\rho_2 c_2 + \rho_1 c_1}$ are the reflection coefficients for the first and second reflectors, respectively. Since $1+R_1$ and $1-R_1$ are the transmission coefficients for a down-going and an up-going wave through the first reflector, respectively, $1-R_1^2 = (1+R_1)(1-R_1)$ is the total transmission loss for seismic energy passing through the first reflector. To predict the wave field in the second medium (i.e., $a_1 < z' < a_2$), the Green's function can be found in equation (4.12) and is:

$$
\begin{aligned}
G_0^{DN}(z,z',\omega)\big|_{z'=\mathcal{A}} &= \frac{\rho_1}{2ik_1}\left\{\frac{R_1\lambda-\lambda^{-1}}{1+R_1}\mu + \frac{\lambda-R_1\lambda^{-1}}{1+R_1}\mu^{-1}\right\}, \\
\left.\frac{\partial}{\partial z'}G_0^{DN}(z,z',\omega)\right|_{z'=\mathcal{A}} &= \frac{\rho_1 k}{2k_1}\left\{\frac{R_1\lambda-\lambda^{-1}}{1+R_1}\mu - \frac{\lambda-R_1\lambda^{-1}}{1+R_1}\mu^{-1}\right\},
\end{aligned}
\tag{8.12}
$$

where in the equation above $\lambda \equiv e^{ik_1(z-a_1)}$ and $\mu \equiv e^{ik(\mathcal{A}-a_1)}$. With all the terms in equations (8.11) and (9.34), we can predict the wave field below the reflector using equation (2.5):

$$
\begin{aligned}
P(z,\omega) &= \frac{1}{\rho(z')}\left\{P(z',\omega)\frac{\partial G_0^{DN}(z,z',\omega)}{\partial z'} - G_0^{DN}(z,z',\omega)\frac{\partial P(z',\omega)}{\partial z'}\right\}\Bigg|_{z'=\mathcal{A}}^{z'=\mathcal{B}} \\
&= \frac{1}{\rho(z')}\left[G_0^{DN}(z,z',\omega)\frac{\partial P(z',\omega)}{\partial z'} - P(z',\omega)\frac{\partial G_0^{DN}(z,z',\omega)}{\partial z'}\right]_{z'=\mathcal{A}} \\
&= \frac{\rho_1 k}{\rho_0 k_1}\left\{\frac{\lambda - R_1\lambda^{-1}}{1+R_1}\mu^{-1}e^{ik\mathcal{A}} - \frac{R_1\lambda - \lambda^{-1}}{1+R_1}\mu R_1 e^{ik(2a_1-\mathcal{A})}\right\} \\
&- \frac{\rho_1 k}{\rho_0 k_1}\left\{\frac{R_1\lambda - \lambda^{-1}}{1+R_1}\mu\left(1-R_1^2\right)e^{ik(2a_1-\mathcal{A})}\sum_{n=0}^{\infty}(-1)^n R_1^n R_2^{n+1} e^{ik_1(2n+2)[a_2-a_1]}\right\} \\
&= \frac{\rho_1 k}{\rho_0 k_1}e^{ika_1}\left\{\frac{\lambda - R_1\lambda^{-1}}{1+R_1} - \frac{R_1^2\lambda - R_1\lambda^{-1}}{1+R_1}\right\} \\
&- e^{ika_1}\frac{\rho_1 k}{\rho_0 k_1}\left(1-R_1\right)\left\{R_1\lambda - \lambda^{-1}\right\}\sum_{n=0}^{\infty}(-1)^n R_1^n R_2^{n+1} e^{ik_1(2n+2)[a_2-a_1]} \\
&= \frac{\rho_1 c_1}{\rho_0 c_0(1+R_1)}e^{ika_1}\left\{\left[1-R_1^2\right]\lambda + \left[R_1 - R_1\right]\lambda^{-1}\right\} \\
&+ e^{ika_1}\frac{\rho_1 k}{\rho_0 k_1}\left(1-R_1\right)\left\{e^{ik_1(a_1-z)} - R_1 e^{ik_1(z-a_1)}\right\}\sum_{n=0}^{\infty}(-1)^n R_1^n R_2^{n+1} e^{ik_1(2n+2)[a_2-a_1]}. \\
&= \frac{\rho_1 c_1}{\rho_0 c_0}\left(1-R_1\right)\lambda e^{ika_1} \\
&+ e^{ika_1}\frac{\rho_1 k}{\rho_0 k_1}\left(1-R_1\right)\left\{e^{ik_1(a_1-z)} - R_1 e^{ik_1(z-a_1)}\right\}\sum_{n=0}^{\infty}(-1)^n R_1^n R_2^{n+1} e^{ik_1(2n+2)[a_2-a_1]}. \\
&= (1+R_1)e^{ika_1}e^{ik_1(z-a_1)} \\
&+ e^{ika_1}\frac{\rho_1 k}{\rho_0 k_1}\left(1-R_1\right)\left\{e^{ik_1(a_1-z)} - R_1 e^{ik_1(z-a_1)}\right\}\sum_{n=0}^{\infty}(-1)^n R_1^n R_2^{n+1} e^{ik_1(2n+2)[a_2-a_1]}.
\end{aligned}
\tag{8.13}
$$

In the derivation above we take advantage of the fact that $\mu e^{ik(2a_1-A)} = e^{ika_1}$. Also, many simplifications are detailed in the process of deriving equation (8.10). Since $\frac{\rho_1 k}{\rho_0 k_1}\left(1-R_1\right) = \frac{\rho_1 c_1}{\rho_0 c_0}\frac{2\rho_0 c_0}{\rho_1 c_1+\rho_0 c_0} = \frac{2\rho_1 c_1}{\rho_1 c_1+\rho_0 c_0} = 1+R_1$, the expression above can be simplified as:

$$
\begin{aligned}
P(z,\omega) &= (1+R_1)e^{ika_1}e^{ik_1(z-a_1)} \\
&+ e^{ika_1}(1+R_1)\sum_{n=0}^{\infty}(-1)^n R_1^n R_2^{n+1} e^{ik_1[(2n+2)a_2-(2n+1)a_1-z]} \\
&+ e^{ika_1}(1+R_1)\sum_{n=0}^{\infty}(-1)^{n+1} R_1^{n+1} R_2^{n+1} e^{ik_1[z+(2n+2)a_2-(2n+3)a_1]}.
\end{aligned}
\tag{8.14}
$$

It is very interesting to look each term of the expression above.

- $(1+R_1)e^{ika_1}e^{ik_1(z-a_1)}$ is the down-going wave straight from the source.
- For the simplest case, $n=0$, the results are:

$$e^{ika_1}(1+R_1)R_2e^{ik_1(2a_2-a_1-z)} - e^{ika_1}(1+R_1)R_1R_2e^{ik_1(z+2a_2-3a_1)},$$

  where the first term is the up-going primary reflected from the second reflector, and the second term is the down-going leg of the first-order internal multiple.

- For the case $n=1$, we have:

$$-e^{ika_1}(1+R_1)R_1R_2^2e^{ik_1(4a_2-3a_1-z)} + e^{ika_1}(1+R_1)R_1^2R_2^2e^{ik_1(z+4a_2-5a_1)},$$

  where the first term is the up-going leg of the first-order internal multiple, and the second term is the down-going leg of the second-order internal multiple.

The details to predict the wave field below the second reflector are as follows:

$$\begin{aligned}
G_0^{DN}(z,z',\omega)\big|_{z'=\mathcal{A}} &= \frac{\left[\nu^{-1}(R_2\lambda-\lambda^{-1})+R_1\nu(\lambda-R_2\lambda^{-1})\right]\mu+\left[R_1\nu^{-1}(R_2\lambda-\lambda^{-1})+\nu(\lambda-R_2\lambda^{-1})\right]\mu^{-1}}{2ik_2(1+R_1)(1+R_2)/\rho_2},\\
\frac{\partial}{\partial z'}G_0^{DN}(z,z',\omega)\bigg|_{z'=\mathcal{A}} &= \frac{\left[\nu^{-1}(R_2\lambda-\lambda^{-1})+R_1\nu(\lambda-R_2\lambda^{-1})\right]\mu-\left[R_1\nu^{-1}(R_2\lambda-\lambda^{-1})+\nu(\lambda-R_2\lambda^{-1})\right]\mu^{-1}}{2k_2(1+R_1)(1+R_2)/(k\rho_2)},
\end{aligned} \tag{8.15}$$

where $\lambda \equiv e^{ik_2(z-a_2)}$, $\mu \equiv e^{ik(\mathcal{A}-a_1)}$, and $\nu \equiv e^{ik_1(a_2-a_1)}$. The wave field from Example III (i.e., equation (8.11)) can be rewritten as:

$$\begin{aligned}
P(z'=\mathcal{A},\omega) &= e^{ik\mathcal{A}} + R_1e^{ik(2a_1-\mathcal{A})}\\
&\quad + \left(1-R_1^2\right)e^{ik(2a_1-\mathcal{A})}\sum_{n=0}^{\infty}(-1)^nR_1^nR_2^{n+1}\nu^{2n+2},\\
\frac{1}{ik}\,\frac{P(z'=\mathcal{A},\omega)}{\partial z'}\bigg|_{z'=\mathcal{A}} &= e^{ik\mathcal{A}} - R_1e^{ik(2a_1-\mathcal{A})}\\
&\quad - \left(1-R_1^2\right)e^{ik(2a_1-\mathcal{A})}\sum_{n=0}^{\infty}(-1)^nR_1^nR_2^{n+1}\nu^{2n+2}.
\end{aligned} \tag{8.16}$$

After obtaining the values of the Green's function and wave field at the shallower boundary, we can use the Green's theorem of equation (2.5), with input from equations (8.15) and (8.16), to predict the wave field below the second reflector:

$$
\begin{aligned}
P(z,\omega) &= \frac{1}{\rho(z')}\left\{P(z',\omega)\frac{\partial G_0^{DN}(z,z',\omega)}{\partial z'} - G_0^{DN}(z,z',\omega)\frac{\partial P(z',\omega)}{\partial z'}\right\}\Bigg|_{z'=\mathcal{A}}^{z'=\mathcal{B}} \\
&= \frac{1}{\rho(z')}\left[G_0^{DN}(z,z',\omega)\frac{\partial P(z',\omega)}{\partial z'} - P(z',\omega)\frac{\partial G_0^{DN}(z,z',\omega)}{\partial z'}\right]_{z'=\mathcal{A}} \\
&= \frac{\rho_2 k}{\rho_0 k_2}e^{ika_1}\frac{R_1\nu^{-1}(R_2\lambda-\lambda^{-1})+\nu(\lambda-R_2\lambda^{-1})}{(1+R_1)(1+R_2)} \\
&- \frac{\rho_2 k}{\rho_0 k_2}e^{ika_1}R_1\frac{\nu^{-1}(R_2\lambda-\lambda^{-1})+R_1\nu(\lambda-R_2\lambda^{-1})}{(1+R_1)(1+R_2)} \\
&- \frac{\rho_2 k}{\rho_0 k_2}e^{ika_1}(1-R_1^2)\sum_{n=0}^{\infty}(-1)^n R_1^n R_2^{n+1}\nu^{2n+2}\frac{\nu^{-1}(R_2\lambda-\lambda^{-1})+R_1\nu(\lambda-R_2\lambda^{-1})}{(1+R_1)(1+R_2)}.
\end{aligned}
\tag{8.17}
$$

Since $\frac{\rho_2 k}{\rho_0 k_2} = \frac{\rho_2 c_2}{\rho_0 c_0} = \frac{\rho_1 c_1}{\rho_0 c_0}\frac{\rho_2 c_2}{\rho_1 c_1} = \frac{1+R_1}{1-R_1}\frac{1+R_2}{1-R_2}$, the equation above can be simplified as:

$$
P(z,\omega) = \frac{e^{ika_1}}{(1-R_1)(1-R_2)}\begin{pmatrix}
\left[R_1R_2\nu^{-1}+\nu\right]\lambda & - & \left[R_1\nu^{-1}+R_2\nu\right]\lambda^{-1} \\
-\left[R_1R_2\nu^{-1}+R_1^2\nu\right]\lambda & + & \left[R_1\nu^{-1}+R_1^2R_2\nu\right]\lambda^{-1} \\
-(1-R_1^2)\lambda\displaystyle\sum_{n=0}^{\infty}(-1)^n\left[R_1^nR_2^{n+2}\nu^{2n+1}+R_1^{n+1}R_2^{n+1}\nu^{2n+3}\right] & & \\
+(1-R_1^2)\lambda^{-1}\displaystyle\sum_{n=0}^{\infty}(-1)^n\left[R_1^nR_2^{n+1}\nu^{2n+1}+R_1^{n+1}R_2^{n+2}\nu^{2n+3}\right]. & &
\end{pmatrix}
\tag{8.18}
$$

Since

$$
\sum_{n=0}^{\infty}(-1)^n\left[R_1^nR_2^{n+2}\nu^{2n+1}+R_1^{n+1}R_2^{n+1}\nu^{2n+3}\right] = R_2^2\nu+(1-R_2^2)\sum_{n=0}^{\infty}(-1)^nR_1^{n+1}R_2^{n+1}\nu^{2n+3}, \tag{8.19}
$$

and

$$
\sum_{n=0}^{\infty}(-1)^n\left[R_1^nR_2^{n+1}\nu^{2n+1}+R_1^{n+1}R_2^{n+2}\nu^{2n+3}\right] = R_2\nu, \tag{8.20}
$$

equation (9.31) can be simplified as follows:

$$
\begin{aligned}
P(z,\omega) &= \frac{e^{ika_1}(1-R_1^2)\nu}{(1-R_1)(1-R_2)}\left(\lambda - R_2\lambda^{-1} - R_2^2\lambda + R_2\lambda^{-1} - (1-R_2^2)\lambda\sum_{n=0}^{\infty}(-1)^n R_1^{n+1}R_2^{n+1}\nu^{2n+2}\right) \\
&= \frac{e^{ika_1}(1-R_1^2)(1-R_2^2)}{(1-R_1)(1-R_2)}\lambda\sum_{n=0}^{\infty}(-1)^n R_1^n R_2^n \nu^{2n+1} \\
&= (1+R_1)(1+R_2)e^{ika_1}e^{ik_2(z-a_2)}\sum_{n=0}^{\infty}(-1)^n R_1^n R_2^n e^{ik_1(2n+1)(a_2-a_1)}.
\end{aligned}
$$

In the derivation above, we rewrite the trivial quantity 1 as the special case of $(-1)^n R_1^n R_2^n \nu^{2n}$ with $n = 0$. The expression above is exactly the wave field in the deepest layer: only the down-going wave is present with correct amplitude; the up-going waves cancel each other, as actually happened in the subsurface.

9 Downward continuation of both source and receiver

The original Green's theorem in this report is derived to downward continue the wave field (i.e., receivers) to the subsurface over a source-free region. It can also be used to downward continue the sources down to the subsurface by taking advantage of reciprocity: the recording is the same after the source and receiver locations are exchanged.

Assuming we have data on the measurement surface: $D(z_g, z_s)$ (its ω dependency is ignored), we can use $G_0^{DN}(z, z_g)$ to downward continue it from z_g to the target depth z:

$$
D(z, z_s) = \frac{1}{\rho(z_g)}\left\{\frac{\partial D(z_g, z_s)}{\partial z_g}G_0^{DN}(z, z_g) - D(z_g, z_s)\frac{\partial G_0^{DN}(z, z_g)}{\partial z_g}\right\}. \tag{9.1}
$$

Taking the $\frac{\partial}{\partial z_s}$ operation on equation (9.1), we have a similar procedure to downward continue $\frac{D(z_g,z_s)}{\partial z_s}$ to the subsurface:

$$
\frac{\partial D(z, z_s)}{\partial z_s} = \frac{1}{\rho(z_g)}\left\{\frac{\partial^2 D(z_g, z_s)}{\partial z_g \partial z_s}G_0^{DN}(z, z_g) - \frac{\partial D(z_g, z_s)}{\partial z_s}\frac{\partial G_0^{DN}(z, z_g)}{\partial z_g}\right\}. \tag{9.2}
$$

With equations (9.1) and (9.2), we downward continue the data D and its partial derivative over z_s to the subsurface location z. According to reciprocity, $D(z, z_s) = E(z_s, z)$, where $E(z_s, z)$ is resulted from exchanging the source and receiver locations in the experiment to generate D at the subsurface. The imaginary data $E(z_s, z)$ can be considered as the recording of receiver at z_s for a source located at z.

For this imaginary experiment, the source is located at depth z, according to the Green's theorem which is derived for a source-free region, we can downward continue the recording at z_s to any depth $Z \leq z$.

In seismic migration, we downward continue $E(z_s, z)$ to the same subsurface depth z with $G_0^{DN}(z, z_s)$ to have an experiment with coincident source and receiver:

$$\begin{aligned} E(z,z) &= \frac{1}{\rho(z_s)} \left\{ \frac{\partial E(z_s,z)}{\partial z_s} G_0^{DN}(z,z_s) - E(z_s,z) \frac{\partial G_0^{DN}(z,z_s)}{\partial z_s} \right\}, \\ &= \frac{1}{\rho(z_s)} \left\{ \frac{\partial D(z,z_s)}{\partial z_s} G_0^{DN}(z,z_s) - D(z,z_s) \frac{\partial G_0^{DN}(z,z_s)}{\partial z_s} \right\}. \end{aligned} \tag{9.3}$$

With the value of $D(z, z_s)$ and $\frac{\partial D(z,z_s)}{\partial z_s}$ in equations (9.2) and (9.1), we can simplify equation (9.3) as follows:

$$\begin{aligned} \rho(z_g)\rho(z_s)E(z,z) = {} & D(z_g,z_s) \frac{\partial G_0^{DN}(z,z_g)}{\partial z_g} \frac{\partial G_0^{DN}(z,z_s)}{\partial z_s} - \frac{\partial D(z_g,z_s)}{\partial z_s} \frac{\partial G_0^{DN}(z,z_g)}{\partial z_g} G_0^{DN}(z,z_s) \\ & + \frac{\partial^2 D(z_g,z_s)}{\partial z_g \partial z_s} G_0^{DN}(z,z_g) G_0^{DN}(z,z_s) - \frac{\partial D(z_g,z_s)}{\partial z_g} \frac{\partial G_0^{DN}(z,z_s)}{\partial z_s} G_0^{DN}(z,z_g). \end{aligned} \tag{9.4}$$

If the $z_s < z_g$ and there is no heterogeneity above z_s, the $\frac{\partial}{\partial z_s}$ operation on $D(z_g, z_s)$ is equivalent to multiplying $-ik$, in this case, equation (9.5) can be simplified further:

$$E(z,z) = -\frac{\frac{\partial G_0^{DN}(z,z_s)}{\partial z_s} + ikG_0^{DN}(z,z_s)}{\rho(z_s)} D(z,z_s).$$

As an example, the data in a 2-reflector model (with an ideal impulsive source located at z_s, the depth of receiver is $z_g > z_s$, the depth of reflector are a_1 and a_2, respectively) can be expressed as:

$$\begin{aligned} D(z_g,z_s) = {} & \frac{\rho_0}{2ik} \left\{ e^{ik(z_g - z_s)} + R_1 e^{ik(2a_1 - z_g - z_s)} \right\} \\ & + \frac{\rho_0}{2ik} \left\{ \left(1 - R_1^2\right) e^{ik(2a_1 - z_g - z_s)} \sum_{n=0}^{\infty} (-1)^n R_1^n R_2^{n+1} e^{ik_1(2n+2)[a_2 - a_1]} \right\}. \end{aligned} \tag{9.5}$$

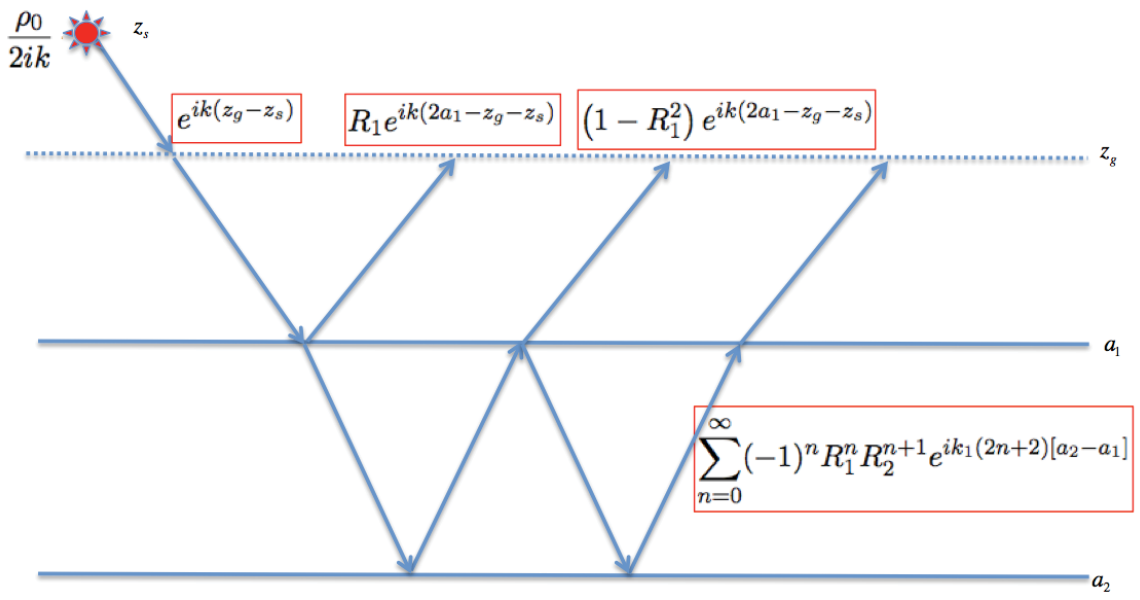

Figure 11: The history of various events in equation (9.5).

If we define $x = e^{ikz_s}$, $y = e^{ikz_g}$, $\sigma = e^{ikz}$, $\beta = \sum_{n=0}^{\infty}(-1)^n R_1^n R_2^{n+1} e^{ik_1(2n+2)[a_2-a_1]}$, and $\alpha = e^{ik(2a_1)}\left(R_1 + (1-R_1^2)\beta\right)$, the data can be expressed as:

$$\begin{aligned} D(z_g, z_s) &= \frac{\rho_0 x^{-1}}{2ik}\left\{y + \alpha y^{-1}\right\}, \\ \frac{\partial D(z_g, z_s)}{\partial z_g} &= \frac{\rho_0}{2} x^{-1}\left\{y - \alpha y^{-1}\right\}, \\ \frac{\partial D(z_g, z_s)}{\partial z_s} &= -\frac{\rho_0}{2} x^{-1}\left\{y + \alpha y^{-1}\right\}, \\ \frac{\partial^2 D(z_g, z_s)}{\partial z_g \partial z_s} &= \frac{\rho_0 k}{2i} x^{-1}\left\{y - \alpha y^{-1}\right\}. \end{aligned} \tag{9.6}$$

9.1 Above the first reflector

For $z < a_1$, the boundary values of the Green's function are:

$$\begin{array}{lll} G_0^{DN}(z,z_g) & = \rho_0 \frac{e^{ik(z-z_g)}-e^{ik(z_g-z)}}{2ik} & = \rho_0 \frac{\sigma y^{-1}-\sigma^{-1}y}{2ik}, \\ G_0^{DN}(z,z_s) & & = \rho_0 \frac{\sigma x^{-1}-\sigma^{-1}x}{2ik}, \\ \frac{\partial G_0^{DN}(z,z_s)}{\partial z_g} & & = \rho_0 \frac{\sigma y^{-1}+\sigma^{-1}y}{-2}, \\ \frac{\partial G_0^{DN}(z,z_s)}{\partial z_s} & & = \rho_0 \frac{\sigma x^{-1}+\sigma^{-1}x}{-2}. \end{array} \tag{9.7}$$

We have:

$$\begin{aligned} D(z,z_s) &= \frac{G_0^{DN}(z,z_g)\frac{\partial D(z_g,z_s)}{\partial z_g} - \frac{\partial G_0^{DN}(z,z_g)}{\partial z_g} D(z_g,z_s)}{\rho(z_g)} \\ &= \frac{\rho_0 x^{-1}}{4ik}\left(\sigma + \alpha\sigma^{-1} - \sigma^{-1}y^2 - \alpha\sigma y^{-2}\right) + \frac{\rho_0 x^{-1}}{4ik}\left(\sigma + \alpha\sigma^{-1} + \sigma^{-1}y^2 + \alpha\sigma y^{-2}\right) \\ &= \frac{\rho_0 x^{-1}}{2ik}\left(\sigma + \alpha\sigma^{-1}\right), \end{aligned} \tag{9.8}$$

and,

$$\frac{-1}{\rho(z_s)}\left(\frac{\partial G_0^{DN}(z,z_s)}{\partial z_s} + ikG_0^{DN}(z,z_s)\right) = \frac{\sigma x^{-1}+\sigma^{-1}x}{2} - \frac{\sigma x^{-1}+\sigma^{-1}x}{2} = \sigma^{-1}x. \tag{9.9}$$

And consequently, we have:

$$\begin{aligned} E(z,z) &= -\frac{1}{\rho(s)}\left(\frac{\partial G_0^{DN}(z,z_s)}{\partial z_s} + ikG_0^{DN}(z,z_s)\right) D(z,z_s) = \frac{1+\alpha\sigma^{-2}}{2ik/\rho_0} \\ &= \frac{\rho_0}{2ik}\left\{1 + e^{ik(2a_1-2z)}\left(R_1 + (1-R_1^2)\sum_{n=0}^{\infty}(-1)^n R_1^n R_2^{n+1} e^{ik_1(2n+2)[a_2-a_1]}\right)\right\}. \end{aligned} \tag{9.10}$$

The result above can be Fourier transformed into the time domain to have:

$$E(z,z,t) = -\frac{\rho_0 c_0}{2}\left\{\begin{array}{l} H(t) + R_1 H\left(t - \frac{2a_1-2z}{c_0}\right) \\ +(1-R_1^2)\sum\limits_{n=0}^{\infty}(-1)^n R_1^n R_2^{n+1} H\left(t - \frac{2a_1-2z}{c_0} - \frac{(2n+2)(a_2-a_1)}{c_1}\right) \end{array}\right\}. \tag{9.11}$$

The terms in the expression above can be interpreted as follows:

- The overall factor $-\frac{\rho_0 c_0}{2}$ is the amplitude of G_0^+ in the first medium.

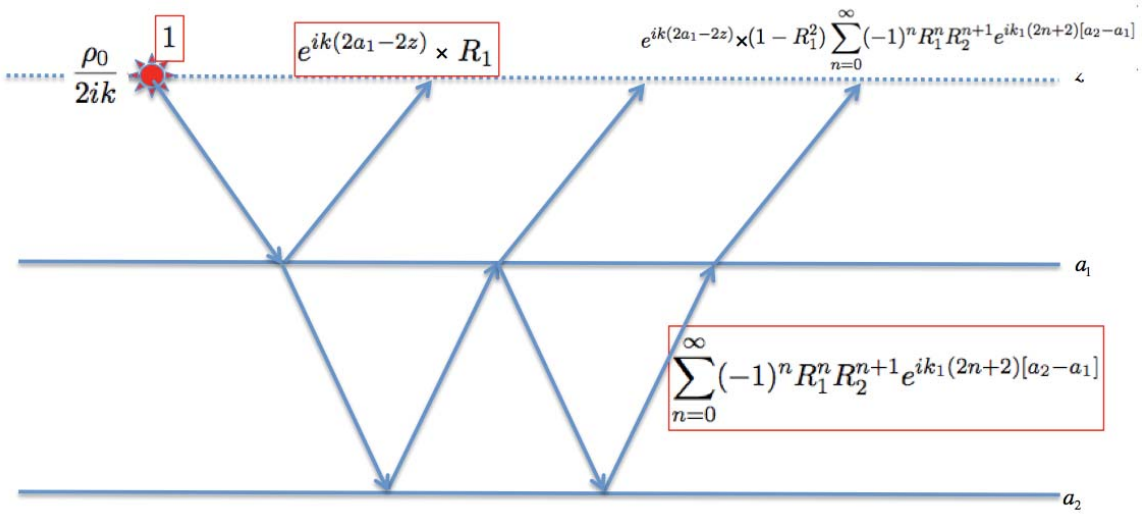

Figure 12: The history of various events in equation (9.10).

- The first term $H(t) = H\left(t - \frac{z-z}{c_0}\right)$ is propagation phase for the direct wave traveling from the source at z to a receiver coincide with the source at z. This term should be removed before applying the imaging condition.
- The second term $R_1 H\left(t - \frac{2a_1-2z}{c_0}\right)$ is the first primary.
- The third term $(1-R_1^2) \sum_{n=0}^{\infty} (-1)^n R_1^n R_2^{n+1} H\left(t - \frac{2a_1-2z}{c_0} - \frac{(2n+2)[a_2-a_1]}{c_1}\right)$ incorporate the second primary and all the internal multiples.

Balancing out the $-\frac{\rho_0 c_0}{2}$ factor, the data after removing the direct wave is denoted as $\mathcal{D}(z,t) \triangleq \frac{-2}{\rho_0 c_0} E(z,z,t) - H(t)$:

$$\mathcal{D}(z,t) = R_1 H\left(t - \frac{2a_1 - 2z}{c_0}\right) + (1-R_1^2) \sum_{n=0}^{\infty} (-1)^n R_1^n R_2^{n+1} H\left(t - \frac{2a_1 - 2z}{c_0} - \frac{(2n+2)(a_2-a_1)}{c_1}\right). \tag{9.12}$$

If we use the $t = 0$ imaging condition, we have:

$$\mathcal{D}(z,t) = \begin{cases} 0 & \texttt{if } (z < a_1) \\ R_1 & \texttt{if } (z = a_1) \end{cases} \tag{9.13}$$

In other words, we obtained the image of the first reflector at its actual depth a_1 with its correct reflection coefficient as amplitude.

9.2 Between the first and second reflectors

For $a_1 < z < a_2$, we have:

$$\begin{aligned} G_0^{DN}(z, z_g) &= \frac{\rho_1}{2ik_1}\frac{1}{1+R_1}\left((R_1\lambda - \lambda^{-1})\mu + (\lambda - R_1\lambda^{-1})\mu^{-1}\right), \\ \frac{\partial G_0^{DN}(z, z_g)}{\partial z_g} &= \frac{\rho_1 k}{2k_1}\frac{1}{1+R_1}\left((R_1\lambda - \lambda^{-1})\mu - (\lambda - R_1\lambda^{-1})\mu^{-1}\right), \end{aligned} \tag{9.14}$$

where $\lambda = e^{ik_1(z-a_1)}$, $\mu = e^{ik(z_g-a_1)}$. Using equations (9.14) and (9.6), we have:

$$\begin{aligned} D(z, z_s) &= \frac{1}{\rho(z_g)}\left(G_0^{DN}(z, z_g)\frac{\partial D(z_g, z_s)}{\partial z_g} - \frac{\partial G_0^{DN}(z, z_g)}{\partial z_g} D(z_g, z_s)\right) \\ &= \frac{\rho_0}{2ik}\frac{\rho_1 k x^{-1}}{\rho_0 k_1(1+R_1)}\left\{(\lambda - R_1\lambda^{-1})\mu^{-1}y - (R_1\lambda - \lambda^{-1})\mu\alpha y^{-1}\right\} \\ &= \frac{\rho_1 x^{-1}}{2ik_1(1+R_1)}\left\{(\lambda - R_1\lambda^{-1})e^{ika_1} - (R_1\lambda - \lambda^{-1})\alpha e^{-ika_1}\right\} \end{aligned} \tag{9.15}$$

If we define: $\beta = \sum_{n=0}^{\infty}(-1)^n R_1^n R_2^{n+1} e^{i(2n+2)[a_2-a_1]}$, we have: $\alpha = e^{2ika_1}\left(R_1 + (1-R_1^2)\beta\right)$, and the equation above can be simplified as:

$$\begin{aligned} D(z, z_s) &= \frac{\rho_1 x^{-1} e^{ika_1}}{2ik_1(1+R_1)}\left\{(\lambda - R_1\lambda^{-1}) - (R_1\lambda - \lambda^{-1})\left(R_1 + (1-R_1^2)\beta\right)\right\} \\ &= \frac{\rho_1 x^{-1} e^{ika_1}}{2ik_1}\frac{1-R_1^2}{1+R_1}\left\{\lambda - (R_1\lambda - \lambda^{-1})\beta\right\} \\ &= \frac{\rho_1 x^{-1} e^{ika_1}}{2ik_1}(1-R_1)\left\{\lambda + (\lambda^{-1} - R_1\lambda)\beta\right\} \\ &= \frac{\rho_0}{2ik}x^{-1}e^{ika_1}(1+R_1)\left\{\lambda + (\lambda^{-1} - R_1\lambda)\beta\right\} \end{aligned} \tag{9.16}$$

If we define: $\gamma = 1 - R_1\beta = \sum_{n=0}^{\infty}(-1)^n R_1^n R_2^n e^{ik_1(2n)(a_2-a_1)}$, the expression above can be rewritten as:

$$D(z, z_s) = \frac{\rho_0}{2ik}(1+R_1)e^{ik(a_1-z)}\left\{\lambda^{-1}\beta + \lambda\gamma\right\}. \tag{9.17}$$

The expression above can be verified as the following. The overall factor $\frac{\rho_0}{2ik}$ is the amplitude of the G_0^+ at the source. $e^{ik(a_1-z)}$ is the propagation from the source to the first reflector. $1+R_1$ is the transmission coefficient through the first reflector. The first term $\lambda^{-1}\beta$ can be expanded as:

$$\begin{aligned}\lambda^{-1}\beta &= e^{ik_1(a_1-z)}\sum_{n=0}^{\infty}(-1)^n R_1^n R_2^{n+1} e^{ik_1(2n+2)(a_2-a_1)} \\ &= R_2 e^{ik_1(2a_2-a_1-z)} - R_1 R_2^2 e^{ik_1(4a_2-3a_1-z)} + \cdots ,\end{aligned} \tag{9.18}$$

and incorporate all the up-going events. The second term $\lambda\gamma$ can be expanded as:

$$\begin{aligned}\lambda\gamma &= e^{ik_1(z-a_1)}\sum_{n=0}^{\infty}(-1)^n R_1^n R_2^n e^{ik_1(2n)(a_2-a_1)} \\ &= e^{ik_1(z-a_1)} - R_1 R_2 e^{ik_1(z+2a_2-3a_1)} + R_1^2 R_2^2 e^{ik_1(z+4a_2-5a_1)} + \cdots ,\end{aligned} \tag{9.19}$$

and incorporate all the down-going events. And,

$$\begin{aligned}G_0^{DN}(z,z_s) &= \frac{\rho_1}{2ik_1}\frac{1}{1+R_1}\left((R_1\lambda-\lambda^{-1})\xi + (\lambda - R_1\lambda^{-1})\xi^{-1}\right), \\ \frac{\partial G_0^{DN}(z,z_s)}{\partial z_s} &= \frac{\rho_1 k}{2k_1}\frac{1}{1+R_1}\left((R_1\lambda-\lambda^{-1})\xi - (\lambda - R_1\lambda^{-1})\xi^{-1}\right),\end{aligned} \tag{9.20}$$

where $\lambda = e^{ik_1(z-a_1)}$, $\xi = e^{ik(z_s-a_1)}$.

$$\begin{aligned}-\frac{1}{\rho(z_s)}\left(\frac{\partial G_0^{DN}(z,z_s)}{\partial z_s} + ikG_0^{DN}(z,z_s)\right) &= \frac{k\rho_1}{2k_1\rho_0}\frac{(\lambda^{-1}-R_1\lambda)\xi + (R_1\lambda^{-1}-\lambda)\xi^{-1}}{1+R_1} \\ &+ \frac{k\rho_1}{2k_1\rho_0}\frac{(\lambda^{-1}-R_1\lambda)\xi - (R_1\lambda^{-1}-\lambda)\xi^{-1}}{1+R_1} \\ &= \frac{k\rho_1}{k_1\rho_0}\frac{(\lambda^{-1}-R_1\lambda)\xi}{1+R_1}\end{aligned} \tag{9.21}$$

We have:

$$\begin{aligned}-\frac{1}{\rho(z_s)}\left(\frac{\partial G_0^{DN}(z,z_s)}{\partial z_s} + ikG_0^{DN}(z,z_s)\right)D(z,z_s) &= \frac{\rho_1}{2ik_1}\left\{\lambda^{-1}\beta+\lambda\gamma\right\}\left\{\lambda^{-1}-R_1\lambda\right\} \\ = \frac{\rho_1}{2ik_1}\left\{\beta\lambda^{-2} - R_1\gamma\lambda^2 + \gamma - \beta R_1\right\}&\end{aligned} \tag{9.22}$$

Let's check the physical meaning of the terms above. The first term:

$$\begin{aligned}\beta\lambda^{-2} &= \left[\sum_{n=0}^{\infty}(-1)^n R_1^n R_2^{n+1} e^{ik_1(2n+2)(a_2-a1)}\right] e^{ik_1(2a_1-2z)} \\ &= R_2 e^{ik_1(2a_2-2z)} - R_1 R_2^2 e^{ik_1(4a_2-2a_1-2z)} + R_1^2 R_2^3 e^{ik_1(6a_2-4a_1-2z)} + \cdots\end{aligned} \tag{9.23}$$

incorporates the upward reflections (from the second reflector) towards depth z from below (labeled as event 2, 6, 10, $\cdots$ in Figure 13). And the second term :

$$\begin{aligned}-R_1\gamma\lambda^2 &= -R_1\left[\sum_{n=0}^{\infty}(-1)^n R_1^n R_2^n e^{ik_1(2n)(a_2-a_1)}\right] e^{ik_1(2z-2a_1)} \\ &= -R_1 e^{ik_1(2z-2a_1)} + R_1^2 R_2 e^{ik_1(2z+2a_2-4a_1)} - R_1^3 R_2^2 e^{ik_1(2z+4a_2-6z_1)} + \cdots\end{aligned} \tag{9.24}$$

incorporate the downward reflections (from the first reflector) towards depth z from above (labeled as event 1, 5, 9, $\cdots$ in Figure 13). The rest of events can be interpreted as follows:

$$\begin{aligned}\gamma - \beta R_1 = 1 - 2\beta R1 &= 1 - 2R_1\sum_{n=0}^{\infty}(-1)^n R_1^n R_2^{n+1} e^{ik(2n+2)(a_2-a_1)} \\ &= 1 + 2\left[-R_1 R_2 e^{ik_1(2a_2-2a_1)}\right]^1 + 2\left[-R_1 R_2 e^{ik_1(2a_2-2a_1)}\right]^2 + 2\left[-R_1 R_2 e^{ik_1(2a_2-2a_1)}\right]^3 + \cdots\end{aligned} \tag{9.25}$$

where in the final expression above, the first term 1 is the propagation phase for the direct arrival from the source (this term is a unit since the source and receiver coincide). The second term $2\left[-R_1 R_2 e^{ik(2a_2-2a_1)}\right]^1$ represents two separate propagations labeled as event 3 and 4 in Figure 13, both events with distinct propagation history share the same propagation time. The third term $2\left[-R_1 R_2 e^{ik(2a_2-2a_1)}\right]^2$ represents two separate propagations labeled as event 7 and 8 in Figure 13, and again both events with distinct propagation history share the same propagation time.

The final result can be Fourier transformed into the time domain as:

$$E(z,z,t) = -\frac{\rho_1 c_1}{2}\left\{\begin{array}{l} H(t) + 2\sum\limits_{n=1}^{\infty}(-1)^n R_1^n R_2^n H\left(t - \frac{2n(a_2-a_1)}{c_1}\right) \\ + \sum\limits_{n=0}^{\infty}(-1)^{n+1} R_1^{n+1} R_2^n H\left(t - \frac{2z+2na_2-2(n+1)a_1}{c_1}\right) \\ + \sum\limits_{n=0}^{\infty}(-1)^n R_1^n R_2^{n+1} H\left(t - \frac{2(n+1)a_2-2na_1-2z}{c_1}\right) \end{array}\right\} \tag{9.26}$$

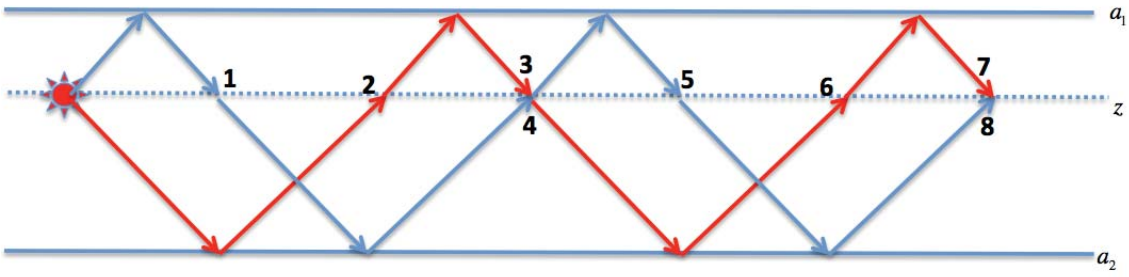

Figure 13: The diagram of events for an experiment with both source and receiver coincide at depth z which located between the first reflector at depth a_1 and the second reflector at depth a_2.

Balancing out the $-\frac{\rho_1 c_1}{2}$ factor, the data after removing the direct wave is denoted as $\mathcal{D}(z,t)\stackrel{\Delta}{=}\frac{-2}{\rho_1 c_1}E(z,z,t)-H(t)$:

$$\mathcal{D}(z,t)=\left\{\begin{array}{l} 2\sum\limits_{n=1}^{\infty}(-1)^n R_1^n R_2^n H\left(t-\frac{2n(a_2-a_1)}{c_1}\right) \\ +\sum\limits_{n=0}^{\infty}(-1)^{n+1} R_1^{n+1} R_2^n H\left(t-\frac{2z+2na_2-2(n+1)a_1}{c_1}\right) \\ +\sum\limits_{n=0}^{\infty}(-1)^{n} R_1^{n} R_2^{n+1} H\left(t-\frac{2(n+1)a_2-2na_1-2z}{c_1}\right) \end{array}\right\} \tag{9.27}$$

and after taking the $t=0$ imaging condition, we have:

$$\mathcal{D}(z,t)=\left\{\begin{array}{ll} -R_1 & \texttt{if } (z=a_1) \\ 0 & \texttt{if } (a_1<z<a_2) \\ R_2 & \texttt{if } (z=a_2) \end{array}\right. \tag{9.28}$$

Note that in the previous section, i.e., to image above the first reflector at a_1, we obtain the amplitude R_1 when z approach a_1 from above. In this section we image below the first reflector at a_1, the amplitude of the image is $-R_1$ when z approaches a_1 from below, as it should.

9.3 Below the second reflector

$$\begin{aligned} G_0^{DN}(z,z')\big|_{z'=z_g} &= \frac{\left[\nu^{-1}(R_2\lambda-\lambda^{-1})+R_1\nu(\lambda-R_2\lambda^{-1})\right]\mu+\left[R_1\nu^{-1}(R_2\lambda-\lambda^{-1})+\nu(\lambda-R_2\lambda^{-1})\right]\mu^{-1}}{2ik_2(1+R_1)(1+R_2)/\rho_2}, \\ \frac{\partial}{\partial z'}G_0^{DN}(z,z')\Big|_{z'=z_g} &= \frac{\left[\nu^{-1}(R_2\lambda-\lambda^{-1})+R_1\nu(\lambda-R_2\lambda^{-1})\right]\mu-\left[R_1\nu^{-1}(R_2\lambda-\lambda^{-1})+\nu(\lambda-R_2\lambda^{-1})\right]\mu^{-1}}{2k_2(1+R_1)(1+R_2)/(k\rho_2)}, \end{aligned} \tag{9.29}$$

where $\lambda \equiv e^{ik_2(z-a_2)}$, $\mu \equiv e^{ik(z_g-a_1)}$, and $\nu \equiv e^{ik_1(a_2-a_1)}$.

$$\begin{aligned} D(z,z_s) &= \frac{1}{\rho(z')}\left\{P(z',\omega)\frac{\partial G_0^{DN}(z,z',\omega)}{\partial z'} - G_0^{DN}(z,z',\omega)\frac{\partial P(z',\omega)}{\partial z'}\right\}\Bigg|_{z'=z_g}^{z'=\mathcal{B}} \\ &= \frac{1}{\rho(z')}\left[G_0^{DN}(z,z',\omega)\frac{\partial P(z',\omega)}{\partial z'} - P(z',\omega)\frac{\partial G_0^{DN}(z,z',\omega)}{\partial z'}\right]_{z'=z_g} \\ &= \frac{\rho_2}{2ik_2}e^{ik(a_1-z_s)}\frac{R_1\nu^{-1}(R_2\lambda-\lambda^{-1})+\nu(\lambda-R_2\lambda^{-1})}{(1+R_1)(1+R_2)} \\ &- \frac{\rho_2}{2ik_2}e^{ik(a_1-z_s)}\frac{\nu^{-1}(R_2\lambda-\lambda^{-1})+R_1\nu(\lambda-R_2\lambda^{-1})}{(1+R_1)(1+R_2)}\left\{R_1+(1-R_1^2)\beta\right\} \end{aligned} \tag{9.30}$$

Since $\frac{\rho_2 k}{\rho_0 k_2} = \frac{\rho_2 c_2}{\rho_0 c_0} = \frac{\rho_1 c_1}{\rho_0 c_0}\frac{\rho_2 c_2}{\rho_1 c_1} = \frac{1+R_1}{1-R_1}\frac{1+R_2}{1-R_2}$, the equation above can be simplified as:

$$D(z,z_s) = \frac{\rho_0 e^{ik(a_1-z_s)}/(2ik)}{(1-R_1)(1-R_2)}\left(\begin{array}{l} \left[R_1R_2\nu^{-1}+\nu\right]\lambda \;-\; \left[R_1\nu^{-1}+R_2\nu\right]\lambda^{-1} \\ -\left[R_1R_2\nu^{-1}+R_1^2\nu\right]\lambda \;+\; \left[R_1\nu^{-1}+R_1^2R_2\nu\right]\lambda^{-1} \\ -(1-R_1^2)\lambda\sum_{n=0}^{\infty}(-1)^n\left[R_1^nR_2^{n+2}\nu^{2n+1}+R_1^{n+1}R_2^{n+1}\nu^{2n+3}\right] \\ +(1-R_1^2)\lambda^{-1}\sum_{n=0}^{\infty}(-1)^n\left[R_1^nR_2^{n+1}\nu^{2n+1}+R_1^{n+1}R_2^{n+2}\nu^{2n+3}\right]. \end{array}\right) \tag{9.31}$$

Since

$$\sum_{n=0}^{\infty}(-1)^n\left[R_1^nR_2^{n+2}\nu^{2n+1}+R_1^{n+1}R_2^{n+1}\nu^{2n+3}\right] = R_2^2\nu+(1-R_2^2)\sum_{n=0}^{\infty}(-1)^nR_1^{n+1}R_2^{n+1}\nu^{2n+3}, \tag{9.32}$$

and

$$\sum_{n=0}^{\infty}(-1)^n\left[R_1^nR_2^{n+1}\nu^{2n+1}+R_1^{n+1}R_2^{n+2}\nu^{2n+3}\right] = R_2\nu, \tag{9.33}$$

equation (9.31) can be simplified as follows:

$$
\begin{aligned}
D(z,z_s) &= \frac{\rho_0 e^{ik(a_1-z_s)}(1-R_1^2)\nu}{2ik(1-R_1)(1-R_2)}\left(\lambda - R_2\lambda^{-1} - R_2^2\lambda + R_2\lambda^{-1} - (1-R_2^2)\lambda\sum_{n=0}^{\infty}(-1)^n R_1^{n+1}R_2^{n+1}\nu^{2n+2}\right)\\
&= \frac{\rho_0 e^{ik(a_1-z_s)}(1-R_1^2)(1-R_2^2)}{2ik(1-R_1)(1-R_2)}\lambda\sum_{n=0}^{\infty}(-1)^n R_1^n R_2^n \nu^{2n+1}\\
&= \frac{\rho_0(1+R_1)(1+R_2)}{2ik}e^{ik(a_1-z_s)}e^{ik_2(z-a_2)}\sum_{n=0}^{\infty}(-1)^n R_1^n R_2^n e^{ik_1(2n+1)(a_2-a_1)}.
\end{aligned}
$$

In the derivation above, we rewrite the trivial quantity 1 as the special case of $(-1)^n R_1^n R_2^n \nu^{2n}$ with $n=0$. The expression above is exactly the wave field in the deepest layer: only the down-going wave is present with correct amplitude; the up-going waves cancel with each other as actually happened in the subsurface. And the expression above can be simplified as:

$$
D(z,z_s) = \frac{\rho_0(1+R_1)(1+R_2)}{2ik}e^{ik(a_1-z_s)}e^{ik_1(a_2-a_1)}e^{ik_2(z-a_2)}\gamma
$$

After the downward continuation of the receiver, we can use the Green's theorem to downward continue the source:

$$
\begin{aligned}
G_0^{DN}(z,z')\big|_{z'=z_s} &= \frac{\left[\nu^{-1}(R_2\lambda-\lambda^{-1}) + R_1\nu(\lambda - R_2\lambda^{-1})\right]\xi + \left[R_1\nu^{-1}(R_2\lambda-\lambda^{-1}) + \nu(\lambda-R_2\lambda^{-1})\right]\xi^{-1}}{2ik_2(1+R_1)(1+R_2)/\rho_2},\\
\frac{\partial}{\partial z'}G_0^{DN}(z,z')\Big|_{z'=z_s} &= \frac{\left[\nu^{-1}(R_2\lambda-\lambda^{-1}) + R_1\nu(\lambda - R_2\lambda^{-1})\right]\xi - \left[R_1\nu^{-1}(R_2\lambda-\lambda^{-1}) + \nu(\lambda-R_2\lambda^{-1})\right]\xi^{-1}}{2k_2(1+R_1)(1+R_2)/(k\rho_2)},
\end{aligned}
\tag{9.34}
$$

where $\lambda \equiv e^{ik_2(z-a_2)}$, $\xi \equiv e^{ik(z_s-a_1)}$, and $\nu \equiv e^{ik_1(a_2-a_1)}$.

$$
-\frac{1}{\rho(z_s)}\left(\frac{\partial G_0^{DN}(z,z_s)}{\partial z_s} + ikG_0^{DN}(z,z_s)\right) = \frac{k\rho_2}{k_2\rho_0}\frac{\nu^{-1}(\lambda^{-1}-R_2\lambda) + R_1\nu(R_2\lambda^{-1}-\lambda)}{(1+R_1)(1+R_2)}\xi,
$$

and

$$
\begin{aligned}
-\frac{1}{\rho(z_s)}\left(\frac{\partial G_0^{DN}(z,z_s)}{\partial z_s} + ikG_0^{DN}(z,z_s)\right)D(z,z_s) = \frac{k\rho_2}{k_2\rho_0}&\frac{\nu^{-1}(\lambda^{-1}-R_2\lambda) + R_1\nu(R_2\lambda^{-1}-\lambda)}{(1+R_1)(1+R_2)}e^{ik(z_s-a_1)}\\
&\cdot\frac{\rho_0(1+R_1)(1+R_2)}{2ik}e^{ik(a_1-z_s)}e^{ik_1(a_2-a_1)}e^{ik_2(z-a_2)}\gamma
\end{aligned}
$$

The expression above can be simplified as:

$$\begin{aligned}
E(z,z) &= \frac{\rho_2}{2ik_2} e^{ik_1(a_2-a_1)} e^{ik_2(z-a_2)} \gamma \left\{ \nu^{-1}(\lambda^{-1} - R_2\lambda) + R_1\nu(R_2\lambda^{-1} - \lambda) \right\} \\
&= \frac{\rho_2}{2ik_2} \nu\lambda\gamma \left\{ \nu^{-1}(\lambda^{-1} - R_2\lambda) + R_1\nu(R_2\lambda^{-1} - \lambda) \right\} \\
&= \frac{\rho_2}{2ik_2} \left\{ 1 - R_2\lambda^2 + R_1R_2\nu^2 - R_1\lambda^2\nu^2 \right\} \gamma \\
&= \frac{\rho_2}{2ik_2} \left\{ 1 + R_1R_2\nu^2 - R_2\lambda^2 - R_1\lambda^2\nu^2 \right\} \gamma
\end{aligned}$$

Since: $\left(1 + R_1R_2\nu^2\right)\gamma = \left(1 - R_1R_2\nu^2\right) \sum_{n=0}^{\infty} \left[-R_1R_2\nu^2\right]^n = 1$, and:

$$\begin{aligned}
R_2\lambda^2\gamma = R_2\lambda^2 \sum_{n=0}^{\infty} (-1)^n R_1^n R_2^n \nu^{2n} &= R_2\lambda^2 + R_2\lambda^2 \sum_{n=1}^{\infty} (-1)^n R_1^n R_2^n \nu^{2n} \\
&= R_2\lambda^2 - R_2^2\lambda^2 \sum_{n=1}^{\infty} (-1)^n R_1^n R_2^{n-1} \nu^{2n+2}, \\
R_1\lambda^2\nu^2\gamma = R_1\lambda^2\nu^2 \sum_{n=0}^{\infty} (-1)^n R_1^n R_2^n \nu^{2n} &= \lambda^2 \sum_{n=0}^{\infty} (-1)^n R_1^{n+1} R_2^n \nu^{2n+2}, \\
\left\{ -R_2\lambda^2 - R_1\lambda^2\nu^2 \right\} \gamma = -R_2\lambda^2 - (1 - R_2^2)\lambda^2 \sum_{n=0}^{\infty} (-1)^n R_1^{n+1} R_2^n \nu^{2n+2}&.
\end{aligned}$$

The final downward continuation result can be expressed as:

$$\begin{aligned}
E(z,z) &= \frac{\rho_2}{2ik_2} \left\{ 1 - R_2\lambda^2 - (1 - R_2^2)\lambda^2 \sum_{n=0}^{\infty} (-1)^n R_1^{n+1} R_2^n \nu^{2n+2} \right\} \\
&= \frac{\rho_2}{2ik_2} \left\{ 1 - R_2\lambda^2 + (1 - R_2^2)\lambda^2 \sum_{n=0}^{\infty} (-1)^{n+1} R_1^{n+1} R_2^n \nu^{2n+2} \right\} \\
&= \frac{\rho_2}{2ik_2} \left\{ 1 - R_2 e^{ik_2(2z-2a_2)} + (1 - R_2^2) e^{ik_2(2z-2a_2)} \sum_{n=0}^{\infty} (-1)^{n+1} R_1^{n+1} R_2^n e^{ik_1(2n+2)(a_2-a_1)} \right\}.
\end{aligned}$$

In the results above, $\frac{\rho_2}{2ik_2}$ is the overall amplitude of G_0^+ in the third layer. The first term 1 is the propagation phase of the wave traveling from the source and receiver coincide at depth z. The second term $-R_2 e^{ik_1(2a_2-2a_1)}$ is the reflection from the second reflector at depth a_2 (here it has $-R_2$ as its reflection coefficient since both the source and receiver are located below the reflector).

The third term $(1-R_2^2)e^{ik_1(2a_2-2a_1)}\sum_{n=0}^{\infty}(-1)^{n+1}R_1^{n+1}R_2^n e^{ik_1(2n+2)(a_2-a_1)}$ contains infinite number of internal multiples generated between the first and second reflector.

$$E(z,z,t)=-\frac{\rho_2 c_2}{2}\left\{\begin{array}{l} H(t)-R_2H\left(t-\frac{2z-2a_2}{c_2}\right) \\ +(1-R_2^2)H\left(t-\frac{2z-2a_2}{c_2}-\frac{(2n+2)(a_2-a_1)}{c_1}\right)\end{array}\right\} \tag{9.35}$$

Balancing out the $-\frac{\rho_2 c_2}{2}$ factor, the data after removing the direct wave is denoted as $\mathcal{D}(z,t)\triangleq\frac{-2}{\rho_2 c_2}E(z,z,t)-H(t)$:

$$\mathcal{D}(z,t)=\left\{\begin{array}{l} -R_2H\left(t-\frac{2z-2a_2}{c_2}\right) \\ +(1-R_2^2)H\left(t-\frac{2z-2a_2}{c_2}-\frac{(2n+2)(a_2-a_1)}{c_1}\right)\end{array}\right\} \tag{9.36}$$

and after taking the $t=0$ imaging condition, we have:

$$\mathcal{D}(z,t)=\left\{\begin{array}{ll} -R_2 & \texttt{if } (z=a_2) \\ 0 & \texttt{if } (a_2<z)\end{array}\right. \tag{9.37}$$

Note that in the previous section, i.e., to image between the first and second reflectors, we obtain the amplitude R_2 when z approach a_2 from above. In this section we image below the second reflector at a_2, the amplitude of the image is $-R_2$ when z approaches a_2 from below, as it should.

10 Conclusions

A general and efficient procedure to compute the Green's function with vanishing Dirichlet and Neumann boundary conditions has been derived for a 1D medium of arbitrary complexity, and its effectiveness has been demonstrated with numerical examples that accurately predict the up-going and down-going wave field at depth using only the data on the shallower measurement surface. The density contribution to the Green's theorem and Green's function is accurately studied to better understand its role in imaging. In order to generalize the idea in this paper to a multidimensional earth, a finite-difference scheme is derived and validated by comparison with an analytic benchmark.

Several remarkable properties of the Green's function with double vanishing boundary conditions have been identified:

- The vanishing property of G_0^{DN} for $z>a$ unequivocally states that it is not necessary to know the medium's properties below a target to achieve the target's depth image. This conclusion is also stated in the paper "Finite volume model for migration" by Weglein et al. (2011a).

- G_0^{DN} contains no internal multiple and no source-generated reflections; this property agrees perfectly with not only the reflectionless approximation of WKBJ Green's function, but also with the idea of avoiding reflections and multiples in many current seismic imaging procedures.

We also have reported some very early and very positive news on the first wave theory RTM imaging tests, with a discontinuous reference medium and images that have the correct depth and amplitude (that is, producing the reflection coefficient at the correctly located target) with primaries and multiples in the data. That is an implementation of Weglein et al. (2011a;b) with creative implementation and testing and analysis.

11 Acknowledgments

Jim Mayhan and Jinlong Yang provided the proofreading of the manuscript. The authors would like to thank all M-OSRP members and sponsors. This work has been partially funded by NSFCMG award DMS-0327778 and DOE Basic Energy Sciences Award DE-FG02-05ER15697.

12 Appendix A: Classical Reflection Problem

In this appendix we derive and list the solution of the classical acoustic reflection problem. The medium properties are listed in Table 1. We denote $k = \omega/c_0$, $k_1 = \omega/c_1$, and the incident wave is $e^{ikz'}$. We assume the reflection and transmission waves are $Ae^{-ikz'}$ and $Be^{ik_1z'}$, respectively. In order to have a minimal framework for derivation, the philosophy here is to use the simplest possible form for the incident, reflection, and transmission waves. The complexities caused by flexible reflector depth are transferred to the parameters: A and B.

The boundary condition at the boundary $z' = a$ requires that:

$$\begin{aligned} e^{ika} + Ae^{-ika} &= Be^{ik_1a}, \\ (ik/\rho_0)e^{ika} + (-ik/\rho_0)Ae^{-ika} &= (ik_1/\rho_1)Be^{ik_1a}. \end{aligned} \tag{12.1}$$

The equations above can be simplified as:

$$\begin{aligned} e^{ika} + Ae^{-ika} &= Be^{ik_1a}, \\ e^{ika} - Ae^{-ika} &= \frac{\rho_0 k_1}{\rho_1 k} Be^{ik_1a}. \end{aligned} \tag{12.2}$$

Since $\frac{\rho_0 k_1}{\rho_1 k} = \frac{c_0\rho_0}{c_1\rho_1}$, we have:

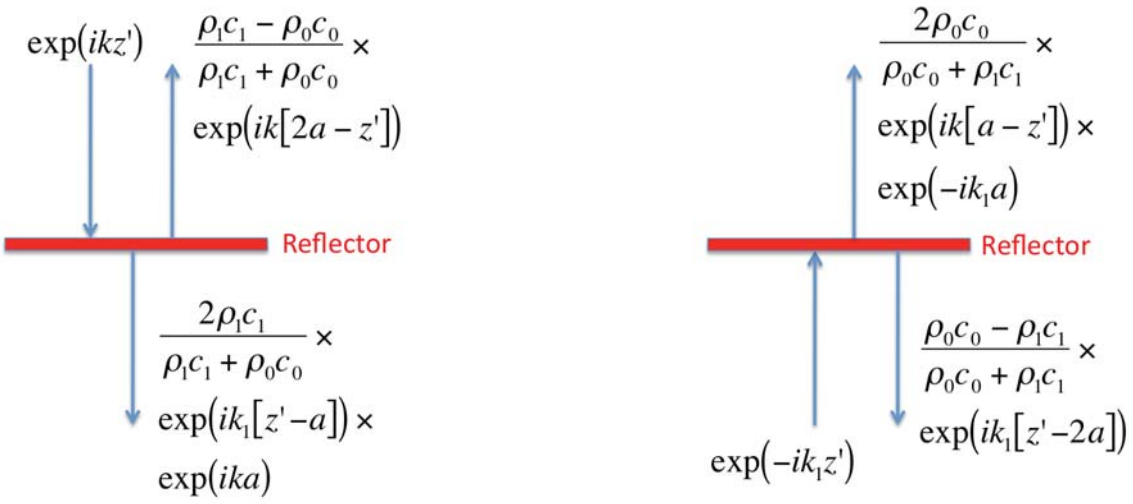

Figure 14: The solution of the two acoustic reflection problems in this appendix. Left: The down-going incident wave from the medium above; right: the up-going incident wave from the medium below.

$$\begin{aligned} e^{ika} + Ae^{-ika} &= Be^{ik_1 a}, \\ e^{ika} - Ae^{-ika} &= \frac{\rho_0 c_0}{\rho_1 c_1} Be^{ik_1 a}. \end{aligned} \tag{12.3}$$

Solving the above equations, we have:

$$\begin{aligned} A &= \frac{c_1\rho_1 - c_0\rho_0}{c_1\rho_1 + c_0\rho_0} e^{ik(2a)} = Re^{ik(2a)}, \\ B &= \frac{2c_1\rho_1}{c_1\rho_1 + c_0\rho_0} e^{i(k-k_1)a} = Te^{i(k-k_1)a}. \end{aligned} \tag{12.4}$$

If the incident wave comes from the second medium: $e^{-ik_1 z'}$, similarly we can assume the reflection wave being of the form $Ae^{ik_1 z'}$ and the transmission wave of the form $Be^{-ikz'}$.

$$\begin{aligned} e^{-ik_1 a} + Ae^{ik_1 a} &= Be^{-ika}, \\ (-ik_1/\rho_1)e^{-ik_1 a} + (ik_1/\rho_1)Ae^{ik_1 a} &= (-ik/\rho_0)Be^{-ika}. \end{aligned} \tag{12.5}$$

After a straightforward simplification we have:

$$\begin{aligned} e^{-ik_1 a} + Ae^{ik_1 a} &= Be^{-ika}, \\ e^{-ik_1 a} - Ae^{ik_1 a} &= \frac{k\rho_1}{k_1\rho_0} Be^{-ika}. \end{aligned} \tag{12.6}$$

Remove the ω dependency in $\frac{k\rho_1}{k_1\rho_0}$, to have:

$$\begin{aligned} e^{-ik_1 a} + Ae^{ik_1 a} &= Be^{-ika}, \\ e^{-ik_1 a} - Ae^{ik_1 a} &= \frac{\rho_1 c_1}{\rho_0 c_0} Be^{-ika}. \end{aligned} \tag{12.7}$$

The solution of the above equations is:

$$\begin{aligned} A &= \frac{c_0\rho_0 - c_1\rho_1}{c_0\rho_0 + c_1\rho_1} e^{-ik_1(2a)} = Re^{-ik_1(2a)}, \\ B &= \frac{2c_0\rho_0}{c_1\rho_1 + c_0\rho_0} e^{i(k-k_1)a} = Te^{i(k-k_1)a}. \end{aligned} \tag{12.8}$$

13 Appendix B: Confirmation that the Green's function (4.10) is the solution of the wave equation with vanishing Dirichlet and Neumann boundary conditions at the deeper boundary

In this case we have: $\mathcal{A} < a < \mathcal{B}$, and the acoustic wave equation is:

$$\left\{ \rho(z') \frac{\partial}{\partial z'} \left(\frac{\partial}{\rho(z')\partial z'} \right) - \frac{\omega^2}{c^2(z')} \right\} G_0(z, z', \omega) = \delta(z - z'). \tag{13.1}$$

Here we prove that the boundary conditions at the reflector are satisfied. First is the continuity of pressure. According to equation (4.10), the pressure immediately below the reflector can be obtained by setting z' in the expression for $z' > a$ (i.e., the second case) to a:

$$G_0(z, a+, \omega) = \rho_1 \frac{e^{ik_1(z-a)} - e^{ik_1(a-z)}}{2ik_1}. \tag{13.2}$$

while the pressure immediately above the reflector can be obtained by setting z' in the expression for $z' < a$ (i.e., the first case) to a:

$$G_0(z, a-, \omega) = \frac{\rho_1}{2ik_1} \left\{ \frac{Re^{ik_1(z-a)} - e^{ik_1(a-z)}}{1+R} + \frac{e^{ik_1(z-a)} - Re^{ik_1(a-z)}}{1+R} \right\}. \tag{13.3}$$

We can simplify the expression above as follows:

$$\begin{aligned} G_0(z,a-,\omega) &= \frac{\rho_1}{2ik_1}\left\{(1-R)e^{ik_1(z-a)} + \frac{-1-R}{1+R}e^{ik_1(a-z)} + \frac{R+R^2}{1+R}e^{ik_1(z-a)}\right\} \\ &= \frac{\rho_1}{2ik_1}\left\{(1-R+R)e^{ik_1(z-a)} - e^{ik_1(a-z)}\right\} \\ &= \frac{\rho_1}{2ik_1}\left\{e^{ik_1(z-a)} - e^{ik_1(a-z)}\right\} \\ &= G_0(z,a+,\omega). \end{aligned} \tag{13.4}$$

On the other hand, the continuity of $\frac{1}{\rho}\frac{\partial G_0^{DN}}{\partial z'}$ across the boundary can be verified in a similar fashion. The value of $\frac{1}{\rho}\frac{\partial G_0^{DN}}{\partial z'}$ immediately below the reflector is:

$$\frac{1}{\rho_1}\left.\frac{\partial G_0(z,z',\omega)}{\partial z'}\right|_{z'=a+} = \frac{-1}{\rho_1}\left\{e^{ik_1(z-a)} + e^{ik_1(a-z)}\right\}. \tag{13.5}$$

while the value of $\frac{1}{\rho}\frac{\partial G_0^{DN}}{\partial z'}$ immediately above the reflector can be obtained by setting z' in the expression for $z' < a$ (i.e., the first case) to a:

$$\frac{1}{\rho_0}\left.\frac{\partial G_0(z,z',\omega)}{\partial z'}\right|_{z'=a-} = \frac{c_1}{\rho_0 c_0}\left\{\frac{Re^{ik_1(z-a)} - e^{ik_1(a-z)}}{1+R} + \frac{Re^{ik_1(a-z)-e^{ik_1(z-a)}}}{1+R}\right\}. \tag{13.6}$$

We can simplify the expression above as follows:

$$\begin{aligned} \frac{1}{\rho_0}\left.\frac{\partial G_0(z,z',\omega)}{\partial z'}\right|_{z'=a-} &= \frac{c_1}{\rho_0 c_0}\left\{(R-1)e^{ik_1(z-a)} + \frac{R-R^2}{1+R}e^{ik_1(z-a)} + \frac{R-1}{1+R}e^{ik_1(a-z)}\right\} \\ &= \frac{c_1}{\rho_0 c_0}\left\{\frac{R-1}{R+1}e^{ik_1(z-a)} + \frac{R-1}{R+1}e^{ik_1(a-z)}\right\} \\ &= \frac{c_1}{\rho_0 c_0}\frac{R-1}{R+1}\left\{e^{ik_1(z-a)} + e^{ik_1(a-z)}\right\} \\ &= \frac{-1}{\rho_1}\left\{e^{ik_1(z-a)} + e^{ik_1(a-z)}\right\} \\ &= \frac{1}{\rho_1}\left.\frac{\partial G_0(z,z',\omega)}{\partial z'}\right|_{z'=a+}. \end{aligned} \tag{13.7}$$

The derivation above takes advantage of the following relations: since $R = \frac{\rho_1 c_1 - \rho_0 c_0}{\rho_1 c_1 + \rho_0 c_0}$, we have:

$$\frac{c_1}{\rho_0 c_0}\frac{R-1}{R+1} = \frac{c_1}{\rho_0 c_0}\frac{\frac{\rho_1 c_1 - \rho_0 c_0}{\rho_1 c_1 + \rho_0 c_0} - 1}{\frac{\rho_1 c_1 - \rho_0 c_0}{\rho_1 c_1 + \rho_0 c_0} + 1} = \frac{c_1}{\rho_0 c_0}\frac{-2\rho_0 c_0}{2\rho_1 c_1} = \frac{-1}{\rho_1}.$$

14 Appendix C: The causal acoustic Green's function used in this report

The analytic solution of the Green's function in equation (2.2) is available if both the velocity $c(z')$ and density $\rho(z')$ fields are constant: i.e., if $c(z') = c_0$ and $\rho(z') = \rho_0$. In this case the term $1/\rho(z') = 1/\rho_0$ becomes a constant and can be moved to the front of the $\partial/\partial z'$ operator, to have:

$$\frac{1}{\rho_0}\left\{\frac{\partial}{\partial z'}\frac{\partial}{\partial z'} + \frac{\omega^2}{c_0^2}\right\} G_0(z, z', \omega) = \delta(z - z').$$

Both terms on the left-hand side of the equation above contain the $\frac{1}{\rho_0}$ factor and the equation can be more succinctly written as:

$$\left\{\frac{\partial}{\partial z'}\frac{\partial}{\partial z'} + \frac{\omega^2}{c_0^2}\right\} G_0(z, z', \omega) = \rho_0\delta(z - z'). \tag{14.1}$$

Note that the equation above is identical to equation (27) of Weglein et al. (2011a), except for the extra density factor ρ_0 on the right-hand side, and the solution for equation (27) of Weglein et al. (2011a) is $\frac{e^{ik(z-z')}}{2ik}$ where $k = \omega/c_0$; our Green's function in equation (14.1) is:

$$G_0(z, z', \omega) = \frac{\rho_0}{2ik}e^{ik|z-z'|}, \tag{14.2}$$

where again, $k = \omega/c_0$.

References

Alford, R. M., K. R. Kelly, and D. M. Boore. "Accuracy of finite-difference modeling of the acoustic wave equation." Geophysics 39 (1974): 834–842.

Baysal, Edip, Dan D. Kosloff, and John W. C. Sherwood. "Reverse time migration." Geophysics 48 (1983): 1514–1524.

Clayton, R. W. and R. H. Stolt. "A Born-WKBJ inversion method for acoustic reflection data." Geophysics 46 (1981): 1559–1567.

Fletcher, R., P. Fowler, P. Kitchenside, and U. Albertin. "Suppressing unwanted internal reflections in prestack reverse-time migration." Geophysics 71 (2006): E79–E82.

Liu, F., G. Zhang, S. A. Morton, and J. P. Leveille. "An optimized wave equation for seismic modeling and reverse time migration." Geophysics 74 (2009): WCA153–WCA158.

Luo, Yi and Gerard T. Schuster. "Bottom-up target-oriented reverse-time datuming." CPS/SEG Geophysics Conference and Exhibition (2004): F55.

Vigh, Denes, E. William Starr, and Jerry Kapoor. "The role of reverse time migration in complex imaging." CSEG RECORDER (June 2009): 20–24.

Weglein, A. B., R. H. Stolt, and J. D. Mayhan. "Reverse-time migration and Green's theorem: Part I — The evolution of concepts, and setting the stage for the new RTM method." Journal of Seismic Exploration 20 (February 2011): 73–90.

Weglein, A. B., R. H. Stolt, and J. D. Mayhan. "Reverse time migration and Green's theorem: Part II — A new and consistent theory that progresses and corrects current RTM concepts and methods." Journal of Seismic Exploration 20 (May 2011): 135–159.

Whitmore, D. N. "Iterative depth imaging by back time propagation." 53^{rd} Annual International Meeting, SEG, Expanded Abstracts. . Society of Exploration Geophysicists, 1983. 382–385.

Multiples: signal or noise?

Arthur B. Weglein, M-OSRP, Physics Department, University of Houston

Summary

"The exclusive view" of seismic reflection data considers primaries as signal and multiples as noise. At the 2013 SEG "Recent Advances and the Road Ahead", a presentation entitled "Multiple Attenuation: Recent Advances and the Road Ahead (2013)" (also see Weglein, 2014) described the state of seismic multiple removal in terms of: (1) current industry capability, and (2) what are the significant and substantive open issues and challenges today. We described a three-pronged strategy that has the potential to close the current gap, for complex and complicated offshore and conventional and unconventional onshore plays. That entire activity and viewpoint is "the exclusive view" of seismic reflection data, where primaries are signal and multiples are a form of coherent noise that needs to be removed.

There is an alternative view, "the inclusive view" of processing seismic reflection data, where primaries and multiples are treated as signal. In that view both are considered useful, taken separately and/or taken together. "The inclusive view" is thought by some to provide advantage and added-value, over and beyond just using primaries as signal for seismic imaging. The inclusive view of utilizing both primaries and multiples, separately, or together, to enhance imaging has recently become a topic of increased discussion and activity. One purpose of this article is to examine this inclusive view and activity.

Seismic imaging

Since those pursuing the inclusive view are seeking added value in seismic imaging, we begin our discussion with a brief history of seismic imaging. That will allow us to define terms and place these recent "inclusive" efforts in perspective, and to assist in their examination and evaluation.

Let's begin by discussing the various concepts, objectives, and levels of ambition for seismic imaging. Migration has two ingredients: (1) a wave propagation component and (2) an imaging principle or concept. Jon Claerbout (Claerbout, 1971; Riley and Claerbout, 1976) was the initial and key wave-equation-migration imaging-concept pioneer and algorithm developer, and together with Stolt (1978) and Lowenthal et al. (1985), they introduced imaging conditions for locating reflectors at depth from surface-recorded data.

Imaging conditions

The three key imaging conditions that were introduced are:
(1) time and space coincidence of up and downgoing waves,
(2) the exploding-reflector model, and
(3) predicting a source and receiver experiment at a coincident-source-and-receiver subsurface point, and asking for time equals zero (the definition of Wave-Equation Migration (WEM)).
For a normal-incident spike plane wave on a horizontal reflector, these three imaging concepts are totally equivalent. However, a key point to make clear for this paper, is that for a non-zero-offset surface seismic-data experiment they are no longer equivalent, for either a one-dimensional or a multi-dimensional subsurface. For the purposes of determining quantitative information on the physical meaning of the image, the clear choice is predicting a source and receiver experiment at depth. Wave-equation migration (WEM) is defined as using the third imaging condition, (3), the predicted source and receiver experiment at depth at time equals zero. In anything beyond 1D normal-incidence or zero-offset data, the other two imaging concepts (for example, time coincidence of up and down waves) turn out to be asymptotic ray travel-time-curve "Kirchhoff" algorithms with a trajectory of image candidates, that are summed, looking for constructive addition for structural determination. Lost is the definitive "yes" or "no" to a point being an image provided by a source and receiver experiment at a coincident subsurface point. Stolt and his colleagues (Clayton and Stolt, 1981; Stolt and Weglein, 1985; Stolt and Benson, 1986) extended the experiment-at-depth concept to allow a separated source and receiver at time equals zero, to not only provide a definitive "yes" or "no" to any given subsurface point being a reflector, but, in addition, provide the angle-dependent reflection coefficient. The other imaging concepts cannot provide that imaging definitiveness nor the quantitative angle-dependent reflection-coefficient information at the image point. In addition, and in general all pre-stack versions, variants, and extensions of the first two imaging conditions listed above, whether for one-way waves or two-way waves, or for data consisting of primaries, or primaries and multiples, are always asymptotic or ray approximates of the third imaging condition. Asymptotic migration, resulting from adopting imaging conditions (1) or (2), will impose asymptotic forms of wave propagation that relate to ray theory and do not satisfy the ubiquitous space-filling propagation and illumination of wave theory and wave-theory migration.

The properties and benefits of Wave-Equation Migration (WEM) in comparison to asymptotic "Kirchhoff-like" migration are:
(1) Definitiveness of a subsurface point corresponding

to (or not corresponding to) structure from a predicted source and receiver experiment at that point;
(2) Quantitative angle-dependent reflection coefficient information at the imaged point; and
(3) Ubiquitous volume-filling wave propagation, coverage and illumination, compared to the limited propagation and illumination of ray theory.

RTM

When two-way migration was introduced by Whitmore, McMechan and their colleagues (Whitmore, 1983; McMechan, 1983), it was formulated and carried out first in post-stack and then in the pre-stack domain by running the data back in time (hence reversed time migration, or RTM) and the source field forward in time and then cross-correlating the two fields at zero lag. The post-stack and pre-stack versions were basically the earlier exploding-reflector model and the time coincidence of up and down-going wave-imaging concepts, respectively. That formulation of asymptotic RTM has become so widespread and ubiquitous that it has infected even one-way migration, with an unquestioned and unfortunately lock-step repeat, where the very meaning of migration has come to be defined as:

$$\mathbf{I}(\mathbf{x}) = \sum_{\mathbf{x_s}} \sum_{\omega} \frac{\mathbf{S}'(\mathbf{x},\mathbf{x_s};\omega)\mathbf{R}(\mathbf{x},\mathbf{x_s};\omega)}{\mathbf{S}'(\mathbf{x},\mathbf{x_s};\omega)\mathbf{S}(\mathbf{x},\mathbf{x_s};\omega)+\varepsilon^2}, \qquad (1)$$

where R is the back-propagated reflection data, S is the forward-propagated source wavefield, the zero-lag cross-correlation is indicated by the sum over angular frequency, ω, and the sum over sources adds candidate-image traveltime trajectories. S' is the complex conjugate of S, and ε is a stabilization parameter.

All current RTM methods correspond to asymptotic ray based migration, by adopting a version of imaging condition (1).

The conventional RTM method represented by equation (1), consists of back propagating the receiver field and forward propagating the source field, where each is carried out using the wave equation. However, the cross-correlation at zero lag is the grown-up version of imaging condition (1) and the imaging condition (1) is the place that the method entered the land of asymptotics and "Kirchhoff" ray theory.

All current RTM methods (for primaries and multiples) use variants and extensions or higher-order terms based on equation (1), and hence do not correspond to wave-equation migration.

That might come as a surprise to the very large number of researchers and those who apply equation (1) in oil and service companies that with all the wave-equation computer effort and expense to implement and utilize equation (1) that it doesn't correspond to wave-equation migration. The use of equation (1) is ubiquitous, but the imaging method it employs and represents and the RTM migration itself is ray-theoretic and is therefore not ubiquitous in its subsurface coverage and illumination.

Wave-equation migration (WEM) for two-way waves, for diving waves, or for migrating primaries and multiples

Neither the post- nor pre-stack current versions of RTM (captured in equation (1)) corresponded to predicting a source and receiver experiment at depth and hence neither is WEM RTM. We have a strong sense that many researchers that begin with migration forms such as equation (1) today, have no idea that they are starting with and remain in asymptotic rather than wave-equation migration concepts and algorithms. Weglein and his colleagues (Weglein et al., 2011a,b; Liu and Weglein, 2013) provided for two-way wave propagation the first source and receiver experiment at depth and wave-equation migration, *i.e.*, WEM RTM. Green's theorem provides a solid basis and firm foundation for predicting a source and receiver experiment at depth from the wavefield on an upper surface of a volume. That's how wave-equation migration RTM is formulated when required for either: (1) turning-wave primaries, and (2) for reflection data consisting of both primaries and multiples. The benefits and added value of WEM RTM compared to all current and conventional RTM methods (equation (1)) are the same benefits as between wave-equation migration and asymptotic or Kirchhoff forms for one-way waves for one-way-wave migration: (1) definitiveness on whether a point in the subsurface corresponds to structure, (2) the angle-dependent reflection coefficient at the image point, and (3) the subsurface coverage, and illumination of waves versus rays. Equation (2) describes WEM migration for one-way waves, where D is the surface data, and G_0^{-D} is the anti-causal Green's function that vanishes on the measurement surface. Equation (3) is WEM RTM where D in the integral is the surface data, and G_0^{DN} is the Green's function that along with its normal derivative vanishes on the lower surface and the walls of the volume.

$$D = \int_{S_s} \frac{\partial G_0^{-D}}{\partial z_s} \int_{S_g} \frac{\partial G_0^{-D}}{\partial z_g} D \, dS_g \, dS_s$$

(Green, 1-way waves) (2)

$$D = \int_{S_s} \left[\frac{\partial G_0^{DN}}{\partial z_s} \int_{S_g} \left\{ \frac{\partial G_0^{DN}}{\partial z_g} D + \frac{\partial D}{\partial z_g} G_0^{DN} \right\} dS_g + G_0^{DN} \frac{\partial}{\partial z_s} \int_{S_g} \left\{ \frac{\partial G_0^{DN}}{\partial z_g} D + \frac{\partial D}{\partial z_g} G_0^{DN} \right\} dS_g \right] dS_s$$

(Green, 2-way waves) (3)

Equation 2 is Stolt prestack one-way wave-equation migration, and equation 3 is wave-equation-migration RTM.

These new wave-equation-migration RTM methods (equation 3) provide for two-way wave propagation what earlier wave-equation migration methods (*e.g.*, Stolt, 1978) provided for one-way propagation (Weglein et al., 2011a; Stolt and Weglein, 2012).

Wave-Equation Migration Imaging for data consisting of primaries and multiples

In Figure 1, we illustrate (from Liu and Weglein, 2013) the result from applying equation (3) for WEM RTM to data that consists of all primaries and internal multiples, from a one-dimensional layered medium. The coincident source and receiver experiment at time equals zero is shown at different locations in the subsurface, predicting the correct location of structure. In addition, the correct reflection coefficient is provided on each side of each reflector, by the experiment being predicted for a source and a receiver slightly above or slightly below each reflector, respectively. Hence, to migrate with primaries and multiples, you are required to simply follow what George Green prescribed in 1828 (Green, 1828) for a closed surface adjusted by Weglein et al. (2011b) for surface reflection data with an accurately known discontinuous subsurface in the volume, and a Green's function that corresponds to properties in that volume and vanishes along with its normal derivative on all surfaces except the upper surface. There is no "crosstalk", no need for "secondary distributed sources" caused by data, no higher-order scattering theory allusions and incantations, or other *ad hoc* or unclear and/or unnecessary constructs, including unnecessarily separating primaries and multiples. It's all in equation (3). Equation (3) is the wave-equation migration formula that predicts a source and receiver in a volume with two-way wave propagation, and combined with an imaging condition predicts both structure and the angle-dependent reflection amplitude. That's the wave-equation migration method for any two-way wave propagation in the volume.

Hence, "the inclusive view" is not in any way new, or requiring new theory, in fact it was historically the first, the original, and classic focus and objective (*e.g.*, Green's theorem (1828)) of predicting a total wavefield inside a volume (*e.g.*, inside the earth) from total-wavefield surface measurements on the closed surface surrounding the volume.

Inclusive use of primaries and multiples to improve image illumination

Recent efforts at inclusive use of primaries and multiples were aimed at improved image illumination. Illumination seeks to improve the clarity and resolution of the located image at depth.

The first step would seem to require a firm theory for correct depth imaging with primaries and multiples. Only after the reflector location is in place are we reasonably concerned with issues of perhaps making the image clearer.

Having a better resolved and clearer but mislocated image is of dubious or no value.

Unfortunately, the methods currently put forth and pursued to realize "the inclusive view" for illumination do not hark back and begin their thinking and development with the solid foundation for wavefield prediction provided by Green (1828). Furthermore, the recent and current "inclusive view" activity very often has had shaky underpinnings, at best, and a lack of any clear and firm foundation and framework, with *ad hoc* constructs offered with confidence and conviction.

Those proposing to use primaries and multiples to enhance imaging have mainly confined their interest to improving the "illumination" for a structure map. Jon Claerbout famously and accurately observed, many years ago, that illumination is not an issue, in principle, for wave theory and wave-theory migration (WEM). Illumination is a fundamental and intrinsic issue for rays and all asymptotic (*e.g.*, Kirchhoff) migration methods and asymptotic RTM (equation (1)). Waves go everywhere and are space-filling. Rays don't. Where rays don't go, we have an intrinsic asymptotic-method-produced illumination issue. The conventional and ubiquitous industry-applied RTM methods, represented by equation (1), are all asymptotic migration methods. Current industry RTM methods certainly use the wave equation in running the data backwards and the source forward and cross correlating at zero lag. However, using the wave equation is not the same as being a wave-equation migration. Wave-equation migration predicts a source and receiver experiment at depth, and all current RTM methods do not meet that requirement and are not wave-equation migration. Hence, all the currently employed RTM methods (equation (1)) are, in principle, and on their own, contributing to an intrinsic illumination issue and challenge. Hence, at the outset, even with 100% perfect "illumination", asymptotic imaging provides a challenged image in terms of its ability to provide a reflection amplitude as a function of angle at the image point.

However, for those committed to asymptotic RTM and seeking to achieve improved "illumination" in order to better delineate structure by utilizing/including free-surface multiples using variants of equation (1), we recognize a certain added value, in particular, for relatively shallow targets (Berkhout and Verschuur, 1994, 1997; Whitmore et al., 2010, 2011b,a; Lu et al., 2011, 2013a,b; Lu and Whitmore, 2013; Ong et al., 2013). However, the latter methods also produce false events in the data (due to crosstalk) at deeper locations, and that issue can represent a serious downside. For example, imagine if such a generated false event interferes with a target primary. There doesn't seem to be a way, at the moment, to address that downside and to remove these false events. The basic reason those cross-talk-generated false images cannot be removed is there is no clear and firm wave-theory-based derivation of the method to begin with. Hence, we cannot go back and fix or avoid assumptions being made, that lead to injurious artifacts, since we don't have a starting point with a theory without those assumptions. Those crosstalk problems and artifacts occur whether the primaries and multiples are separated and utilized separately and then combined, or they are taken together at once (Wang et al., 2013).

Why did we want to remove multiples to begin with? Are those reasons any less valid today?

In general, it is important to remember why, in exploration seismology, we haven't used primaries and multiples for depth imaging and inversion. Have we overcome the fundamental reason for separating them and processing primaries? The simple and direct answer is "no". Primaries are much more accepting of an approximate, smooth velocity for imaging. We very often cannot provide an adequate smooth velocity for imaging primaries, even when multiples have been effectively removed. Providing an adequate smooth velocity for imaging diving waves (with state-of-the-art RTM) going down and under salt remains a tough and daunting problem. For primaries and multiples in your data, as in Figure 1, will require an accurate, discontinuous migration velocity with reflectors in the overburden for predicting a source and receiver experiment at depth, for wave-equation migration. Determining an accurate discontinuous velocity model is not a realistic assumption, not now, and not for anytime in the foreseeable future.

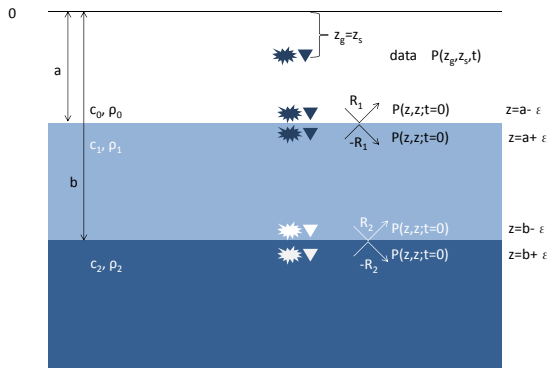

Fig. 1: *Imaging with primaries and internal multiples. A double Green's theorem is utilized with the data, and a Green's function that along with its normal derivative vanishes on the lower surface (and on the walls, in multi-D). That is what wave-equation migration means for waves that are two-way propagating in the medium.*

Wave-equation migration imaging with primaries and internal multiples requires an accurate, discontinuous velocity model (to achieve any imaging benefit and objective). Among those considering internal multiples to enhance illumination are: Berkhout and Verschuur (1994, 1997, 2012), Soni et al. (2012), Davydenko and Verschuur (2013a,b), Fleury and Snieder (2011, 2012), and Wang et al. (2013, 2014).

Conclusion: Multiples contain information. Does containing information qualify multiples as signal?

Yes, multiples contain information, but that's not the point. The point/problem is they contain too much information—containing information doesn't classify an event as signal; being able to reliably extract information from an event defines an event as signal. Multiples were and remain noise. Interest in illumination needs to start by selecting wave-equation migration and avoiding asymptotic migration; that selection of migration algorithms needs to come before considering placing different and additional events (*e.g.*, multiples), repeatedly and iteratively, into various forms of illumination-challenged migration (equation (1)).

The reason we separate primaries from multiples in exploration seismology is not due to lack of theory. The basic theory is almost 200 years old. It is due to the inability, in practice, to provide an adequate discontinuous velocity model necessary for the inclusive holistic and "all hold hands" whole-earth view. We need to be cognizant of that reality and to stay focused on delivering the next level of multiple-removal capability without requiring subsurface information. In general, we advocate a path that could require more data collected rather than detailed and accurate discontinuous subsurface information. The former is realizable and in general the latter is not. There are those who would respond "but the method being proposed will cost more for acquisition and for processing." The response: the cost of 3D acquisition and processing is considerably higher than their earlier 2D counterparts. However, 3D exploration makes good sense from the savings derived from a more successful drilling program, with fewer dry holes and more effective placement of development wells.

In our view, it is important: (1) to recognize and celebrate the progress in the field of removing multiples that has taken place over the past 20 years; and (2) to have a frank and forthright understanding of the serious and daunting challenges that remain and are beyond our collective current capability. The recent interest in using multiples to enhance illumination has shown some promise for shallow reflectors, and needs to be encouraged and pursued, but cannot be used as a distraction from the main, central and overriding high priority objective to fill the gap between the current challenges in removing multiples and our current ability. We have every confidence that (as with previous daunting challenges) the current challenge will be addressed, providing a new level of processing capability.

Below please find links for the SEG abstracts/posters/presentations and slides that relate to this communication.
http://mosrp.uh.edu/events/event-news/seg-annual-meeting-2013-2014
http://mosrp.uh.edu/news/seg-annual-meeting-2013-2014

Acknowledgments

The author would like to thank Lin Tang, Jinlong Yang and Jim Mayhan for assistance in preparing this article and M-OSRP sponsors for their support.

References

Berkhout, A. J., and D. J. Verschuur, 1994, Multiple technology: Part 2, migration of multiple reflections: 64th Annual International Meeting, SEG, Expanded Abstracts, 1497–1500.

———, 1997, Estimation of multiple scattering by iterative inversion, Part I: Theoretical considerations: Geophysics, **62**, 1586–1595.

———, 2012, Full wavefield migration - utilization of multiples in seismic migration: Presented at the 74th EAGE Conference & Exhibition, Expanded Abstracts.

Claerbout, J. F., 1971, Toward a unified theory of reflector mapping: Geophysics, **36**, 467–481.

Clayton, R. W., and R. H. Stolt, 1981, A Born-WKBJ inversion method for acoustic reflection data: Geophysics, **46**, 1559–1567.

Davydenko, M., and D. J. Verschuur, 2013a, Full wavefield migration, using internal multiples for undershooting: 73rd Annual International Meeting, SEG, Expanded Abstracts, 3741–3745.

———, 2013b, Full wavefield migration without dip limitation - using duplex waves in the imaging with multiples: Presented at the 75th EAGE Conference & Exhibition, Expanded Abstracts.

Fleury, C., and R. Snieder, 2011, Reverse-time-migration of multiply scattered seismic waves: 81st Annual International Meeting, SEG, Expanded Abstracts, 3382–3387.

———, 2012, Increasing illumination and sensitivity of reverse-time migration with internal multiples: Presented at the 74th EAGE Conference & Exhibition, Expanded Abstracts.

Green, G., 1828, An essay on the application of mathematical analysis to the theories of electricity and magnetism: Privately published. (Available online at `http://babel.hathitrust.org/cgi/pt?id=hvd.yl131n;view=1up;seq=9`).

Liu, F., and A. B. Weglein, 2013, The first *wave theory* RTM, examples with a layered medium, predicting the source and receiver at depth and then imaging, providing the correct location and reflection amplitude at every depth location, and where the data includes primaries and all internal multiples.: M-OSRP 2012-2013 Annual Report, 284–335.

Lowenthal, D., L. Lu, R. Roberson, and J. W. C. Sherwood, 1985, The wave equation applied to migration: Geophysical Prospecting, **24**, 380–399.

Lu, S., and N. D. Whitmore, 2013, Effects of acquisition geometry to 3d separated wavefield imaging: Presented at the 75th EAGE Conference & Exhibition, Expanded Abstracts.

Lu, S., N. D. Whitmore, H. LeGleut, and A. Long, 2013a, 3d high-resolution imaging using separated wavefields: Presented at the 75th EAGE Conference & Exhibition, Expanded Abstracts.

Lu, S., N. D. Whitmore, and A. A. Valenciano, 2013b, Challenges and opportunities in 3D imaging of sea surface related multiples: 83rd Annual International Meeting, SEG, Expanded Abstracts, 4111–4115.

Lu, S., N. D. Whitmore, A. A. Valenciano, and N. Chemingui, 2011, Imaging of primaries and multiples with 3d seam synthetic: 81st Annual International Meeting, SEG, Expanded Abstracts, 3217–3221.

McMechan, G. A., 1983, Migration by extrapolation of time dependent boundary values: Geophysical Prospecting, **31**, 413–420.

Ong, C., C. Lapilli, J. Perdomo, and R. Coates, 2013, Extended imaging and illumination in wave migrations: 83rd Annual International Meeting, SEG, Expanded Abstracts, 4116–4120.

Riley, D. C., and J. F. Claerbout, 1976, 2d multiple reflections: Geophysics, **41**, 592–620.

Soni, A. K., X. Staal, and E. Verschuur, 2012, VSP imaging using all multiples: Full wavefield migration approach: 72nd Annual International Meeting, SEG, Expanded Abstracts, 1–6.

Stolt, R. H., 1978, Migration by Fourier transform: Geophysics, **43**, 23–48.

Stolt, R. H., and A. K. Benson, 1986, Seismic migration: theory and practice: Geophysical Press.

Stolt, R. H., and A. B. Weglein, 1985, Migration and inversion of seismic data: Geophysics, **50**, 2458–2472.

———, 2012, Seismic imaging and inversion: Application of linear inverse theory: Cambridge University Press.

Wang, Y., X. Chang, and H. Hu, 2013, Simultaneous reverse time migration of primaries and multiples without multiples prediction: Presented at the 75th EAGE Conference & Exhibition, Expanded Abstracts.

———, 2014, Simultaneous reverse time migration of primaries and free-surface related multiples without multiple prediction: Geophysics, **79**, S1–S9.

Weglein, A. B., 2014, Multiple attenuation: strategy that addresses current challenges: E&P Magazine.

Weglein, A. B., R. H. Stolt, and J. D. Mayhan, 2011a, Reverse-time migration and Green's theorem: Part I — The evolution of concepts, and setting the stage for the new RTM method: Journal of Seismic Exploration, **20**, 73–90.

———, 2011b, Reverse time migration and Green's theorem: Part II — A new and consistent theory that progresses and corrects current RTM concepts and methods: Journal of Seismic Exploration, **20**, 135–159.

Whitmore, D. N., 1983, Iterative depth imaging by back time propagation: 53rd Annual International Meeting, SEG, Expanded Abstracts, 382–385.

Whitmore, N. D., A. Valenciano, S. Lu, and N. Chemingui, 2011a, Imaging of primaries and multiples with image space surface related multiple elimination: Presented at the 73rd EAGE Conference & Exhibition, Expanded Abstracts.

Whitmore, N. D., A. A. Valenciano, S. Lu, and N. Chemingui, 2011b, Deep water prestack imaging with primaries and multiples: Presented at the Twelfth International Congress of the Brazilian Geophysical Society, Sociedade Brasileira de Geofísica.

Whitmore, N. D., A. A. Valenciano, W. Sollner, and S.

Lu, 2010, Imaging of primaries and multiples using a dual-sensor towed streamer: 80th Annual International Meeting, SEG, Expanded Abstracts, 3187–3192.

Multiple attenuation: recent progress and a plan to address open, prioritized and pressing issues and challenges

Arthur B. Weglein, M-OSRP, Physics Department, University of Houston

Summary

This paper provides: (1) a brief overview of the current status of multiple attenuation in the petroleum industry; (2) recent progress for marine and on-shore plays; (3) open issues and pressing challenges and (4) a plan, and a schedule of delivery, of fundamental new capability to address these open issues and challenges.

Introduction

The demand for new and improved capability in removing multiples is driven by the portfolio of the petroleum industry and by current and anticipated future exploration trends. For example, the industry moved to deep water roughly 30 years ago. With that move, highly effective multiple-removal methods that were being applied industry-wide suddenly bumped up against their assumptions, when applied to deep water plays, and failed. (As an example, deconvolution is based on 1D and on statistical assumptions, the latter not satisfied in deep water.)

Since then, the overall industry trend to explore in progressively more complex and remote areas, with ill-defined and difficult-to-estimate subsurface properties and increasingly complex plays, is a constant that motivates the search for capabilities that will not require subsurface information. Methods that require various forms of subsurface information include, *e.g.*, F-K, Radon, and Feedback demultiple methods.

The inverse scattering series provides the opportunity to achieve all processing objectives directly and without subsurface information. The current inverse-scattering-series (ISS) internal-multiple-attenuation algorithm has a unique capability to predict the exact phase (time) and approximate amplitude of all internal multiples, at once, automatically, and without subsurface information. These properties separate the ISS internal-multiple-attenuation algorithm from all other methods, and make it the high-water mark of current internal-multiple effectiveness. That is, those ISS properties and strengths are what all other current demultiple methods (*e.g.*, Feedback loop methods, modeling and subtracting multiples, and filter methods) do not possess and cannot deliver (Weglein and Dragoset, 2005).

Carvalho (1992), Carvalho and Weglein (1994), Araújo (1994), Araújo et al. (1994), Weglein et al. (1997), and Weglein et al. (2003) developed ISS free-surface-multiple elimination algorithms and internal-multiple attenuation algorithms. Field-data applications demonstrated their effectiveness. Several marine and onshore data examples are noted below.

However, at every period in the history of E&P, the arrival of new capability to address the latest set of challenges has encouraged industry to explore in more difficult circumstances — situations never previously imagined, let alone considered, and beyond current capability to accommodate. That will once again demand a new and fundamentally higher level of capability and effectiveness. In this article, we describe how that's the state of affairs for multiple attenuation today.

The petroleum industry's current worldwide portfolio of both conventional and unconventional onshore plays, and of increasingly complex offshore plays — with new and unforeseen challenges — has returned and rejuvenated an interest in multiple removal (and a demand for substantially increased effectiveness). Multiple removal has come back to center stage, both for our petroleum-industry sponsors and concomitantly as a key and fundamental research project for the Mission-Oriented Seismic Research Program (M-OSRP).

Marine

Early marine field-data examples of the promise and delivery of ISS free-surface-multiple and internal-multiple algorithms can be found in the above-cited papers, SEG Abstracts, theses, and, *e.g.*, in Matson et al. (1999) and the Mississippi Canyon data tests in Weglein et al. (2003) pages R69 and R70.

Those algorithms were recently employed on data from offshore Brazil, and the results were reported in Ferreira (2011) (see Figure 1). One of the conclusions in those field-data tests at Petrobras was that "no other method was able to show similar effectiveness in attenuating the internal multiples generated by the salt layers."

Onshore

Fu et al. (2010a), Terenghi et al. (2011), and Luo et al. (2011) describe the motivation, evaluation, and comparison of different approaches to the removal of internal multiples on complex synthetic and onshore data. Fu et al. (2010a) concluded that "Their (ISS internal multiple algorithm) performance was demonstrated with complex synthetic and challenging land field data sets with encouraging results, where other internal multiple suppression methods were unable to demonstrate similar effectiveness."

Goodway (2013), Mackidd (2013), and Griffiths et al.

(2013) were among those that came to the same conclusion. A recent paper by Kelamis et al. (2013) presented at the International Petroleum Technology Conference in Beijing, China was entitled "Strategies of Land Internal Multiple Elimination based on Inverse Scattering Series."

Good news

At the 2013 post-convention SEG Internal Multiple Workshop (Thursday, September 26, 2013) it was positive and encouraging to see nine of the eleven presentations describe and exemplify the industry-wide impact and standalone capability (for complex offshore and onshore plays) of the inverse-scattering-series (ISS) internal-multiple-attenuator. ISS internal-multiple attenuation has become fully mainstream within the petroleum industry.

Challenge we face

With all this "good news", what could be the problem? Industry's portfolio/trend and focus today (and for the foreseeable future) makes it clear that a large and significant gap exists between the current challenge for the removal of free-surface multiples and internal multiples and the collective capabilities of the world-wide seismic exploration community (including, of course, M-OSRP). The specific issues are that: (1) the multiple generators and the subsurface properties are ill-defined and increasingly complex and (2) too often the multiple is proximal to or interfering with the primaries. The latter serious and significant issue can occur in many marine circumstances (*e.g.*, in the North Sea) and frequently occurs with onshore plays. That type of challenge of removing multiples proximal to, and/or overlapping with, primaries (without damaging primaries) is well beyond the collective capability of the petroleum industry, service companies and academic research groups and consortia to effectively address. It is not an issue that new and more complete data collection and acquisition will by itself address. We simply don't have the theory and fundamental concepts in place today that are needed for algorithm development, implementation and application. That's the basic reason we are unable to address the level of challenge we currently face worldwide in the petroleum industry. That's the bottom line. To adequately address the current industry challenge, we will need to be able to predict exactly the phase and amplitude of all internal multiples and surgically remove (eliminate) the multiples at all offsets, directly, and without subsurface information, and without damaging primaries. No one today is able to provide that for marine applications, let alone for the frequently more challenging onshore plays.

There is a need for new basic concepts and fundamental theory development that must begin with a frank and forthright recognition of the problem, its economic moment and significance, and the current technical gap. New concepts and algorithms will need to be produced, and then will be followed by addressing the practical application, implementation and compute issues.

The plan

At the 2013 SEG International Conference (Recent Advances and the Road Ahead Session), we proposed and described a three-pronged strategy (please see the links below) that M-OSRP will pursue as a direct response to that challenge. It will have the potential to provide the necessary step-change increase in capability, and thereby to respond effectively to this current and pressing problem. The level and scale of the challenge and the dividend that will derive from addressing it, motivates and galvanizes our efforts. Multiple removal has returned from being viewed as a relatively mature subject and project that helped M-OSRP "pay the rent" and is back to occupying center stage as a major research project and focus within M-OSRP.

The three-pronged strategy to respond to the current open issues and pressing challenges in removing multiples is as follows:
(1) Develop the ISS prerequisites for predicting the reference wave field (wavelet and radiation pattern) and producing de-ghosted data (in particular, for on-shore and ocean bottom acquisition) that are direct and do not require subsurface information;
(2) Develop internal-multiple-elimination algorithms from the inverse scattering series;
(3) Develop a replacement for the energy-minimization criteria for adaptive subtraction, that derives from, and always aligns with and serves, the inverse-scattering-series free-surface and internal-multiple algorithms.
This three-pronged strategy represents a consistent and aligned processing chain, with one single objective: providing a direct and practical solution to the removal of all multiples, without requiring any subsurface information, and without damaging primaries.

The plan is first to progress and deliver items (2) and (3) for marine applications (since item (1) is in relatively good shape for marine application), and simultaneously to progress item (1) for onshore plays. Then, we will return to onshore exploration with the full suite of (1), (2) and (3) ingredients in place. Our plan is to deliver in stages, with offshore delivery coming before onshore delivery.

Recent progress on the three-pronged plan to address current open issues and challenges

In discussing the second of the three prongs, that is, the upgrade of the ISS internal multiple attenuator, we need to begin with a review of its strengths and limitations. The first order ISS internal multiple attenuator always attenuates all internal multiples of first order from all reflectors at once, directly and without subsurface information, automatically and without interpretive intervention. That's a tremendous strength, and is a constant and holds independent of the circumstances and

complexity of the geology and the play. The primaries in the reflection data that enters the algorithm provides that delivery, without our requiring the primaries to be identified or in any way separated. The other events in the reflection data, that is, the internal multiples, when they enter the first order ISS internal multiple algorithm will alter and prep the higher order internal multiples and thereby assist and cooperate with higher order ISS internal multiple attenuation terms, to attenuate higher order internal multiples. That's a benefit and definite asset, and it's always in action and completely automatic. However, there is a downside, a limitation. There are cases when internal multiples that enter the first order attenuator can predict spurious or false events. That is a well-understood shortcoming of the leading order term, when taken in isolation, but is not an issue for the entire ISS internal multiple capability. It is anticipated by the ISS and higher order ISS internal multiple terms exist to precisely remove that issue of spurious event prediction, and taken together with the first order term, no longer experiences spurious event prediction. Chao Ma and Hong Liang provided those higher order terms and tests with complex multiple generators show the effectiveness of their spurious removal higher order ISS internal multiple attenuation algorithms (Liang et al., 2013; Ma and Weglein, 2013, 2014a,b). In a similar way, there are higher order ISS internal multiple terms that provide the elimination of internal multiples when taken together with the leading order attenuator term. Yanglei Zou has produced a general elimination algorithm for first order internal multiples in a 1D acoustic or elastic earth. Please see Zou and Weglein (2013), Zou and Weglein (2014a), Zou and Weglein (2014b), and Zou and Weglein (2014c).

The first tests that evaluated the ability of the ISS attenuator to perform in inelastic media showed it maintained its effectiveness in a medium where waves are attenuated and experiencing Q absorption, without any need or interest in knowing the absorptive mechanism (Wu and Weglein, 2014a). An outlined initial strategy for eliminating internal multiples in an inelastic medium is also described.

There are times, for example, in pre-salt plays in the North Sea, the deep water Gulf of Mexico, offshore Brazil and the Red Sea where the strategy and algorithms to eliminate internal multiples in an absorptive inelastic medium will be called for and necessary. There are other circumstances, for example, in certain on-shore and off-shore plays where elastic internal multiple elimination will be sufficient.

Jing Wu et al. (Wu and Weglein, 2014b) has contributed to extending off-shore Green's theorem preprocessing for wavelet estimation and deghosting to the on-shore elastic wave-field separation, in preparation for on-shore ISS internal multiple attenuation/elimination. Mayhan et al. (Mayhan et al., 2012; Mayhan and Weglein, 2013) has demonstrated the ability of Green's theorem marine preprocessing to be effective with SEAM data and marine field data. He reviewed and summarized the impact of that preprocessing on subsequent multiple removal (Zhang, 2007; Wang et al., 2012; Yang et al., 2013; Tang et al., 2013) that motives the on-shore extension. Jinlong Yang extended the ISS free surface and internal multiple algorithms to accommodate a source signature and radiation pattern (Yang et al., 2013; Yang and Weglein, 2014). Shih-Ying Hsu (Hsu et al., 2011) described the relative insensitivity of the ISS internal multiple attenuator to the near surface reference velocity. Lin Tang (Tang and Weglein, 2014) presented a method to use an invariance of Green's theorem preprocessing to back out the reference medium properties. Qiang Fu has contributed the first published results on applying the ISS internal multiple attenuator to field data from Saudi Aramco and Encana (Fu et al., 2010b; Fu and Weglein, 2014). Fang Liu (Liu and Weglein, 2013; Liu et al., 2011) has pioneered: (1) new wave equation migration methods for RTM and (2) ISS direct depth imaging without a velocity model, with viability demonstrated on the Kristin North Sea field data.

Below please find links for the SEG abstracts/posters/presentations and slides that relate to this communication.
http://mosrp.uh.edu/events/event-news/seg-annual-meeting-2013
http://mosrp.uh.edu/news/seg-annual-meeting-2013
http://mosrp.uh.edu/
http://arthurweglein.com

Summary

Today, the ISS internal-multiple attenuator combined with an energy-minimization adaptive subtraction is the most capable method for removing internal multiples. However, the current ISS attenuator-plus-adaptive-subtraction method will fail under the pressing and prioritized challenge of removing internal multiples that are proximal to and/or interfering with primaries. In this note, we describe a three-pronged strategy for providing an effective response to this pressing and prioritized challenge while retaining and adding to the strengths of the current ISS internal-multiple attenuator.

Acknowledgments

We thank the M-OSRP sponsors for their constant encouragement and strong support. We thank Dr. Jim D. Mayhan for his assistance in preparing this Abstract.

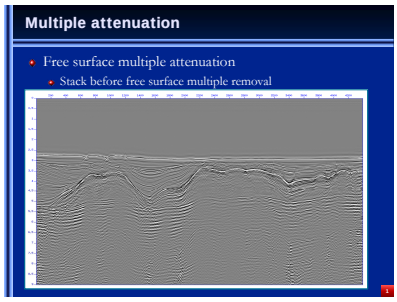

(a)

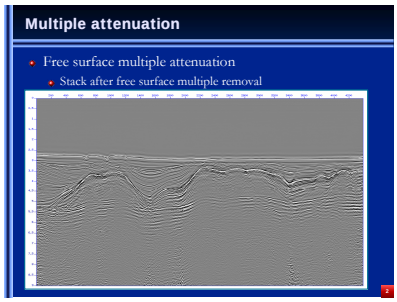

(b)

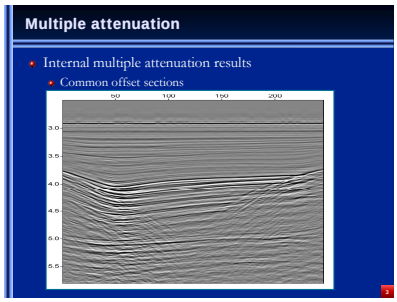

(c)

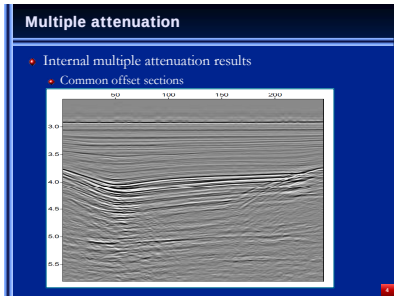

(d)

Fig. 1: *Stack before (a) and after (b) free-surface-multiple removal; common offset sections before (c) and after (d) internal-multiple attenuation (Ferreira, 2011).*

References

Araújo, F. V., 1994, Linear and non-linear methods derived from scattering theory: backscattering tomography and internal-multiple attenuation.: PhD thesis, Universidade Federal da Bahía, Brazil. (In Portuguese).

Araújo, F. V., A. B. Weglein, P. M. Carvalho, and R. H. Stolt, 1994, Inverse scattering series for multiple attenuation: An example with surface and internal multiples: 64th Annual International Meeting, SEG, Expanded Abstracts, Society of Exploration Geophysicists, 1039–1041.

Carvalho, P., and A. Weglein, 1994, Wavelet estimation for surface multiple attenuation using a simulated annealing algorithm: 64th Annual International Meeting, SEG, Expanded Abstracts, Society of Exploration Geophysicists, 1481–1484.

Carvalho, P. M., 1992, Free-surface multiple reflection elimination method based on nonlinear inversion of seismic data: PhD thesis, Universidade Federal da Bahia. (In Portuguese).

Ferreira, A., 2011, Internal multiple removal in offshore Brazil seismic data using the inverse scattering series: Master's thesis, University of Houston.

Fu, Q., Y. Luo, P. G. Kelamis, S. Huo, G. Sindi, S.-Y. Hsu, and A. B. Weglein, 2010a, The inverse scattering series approach towards the elimination of land internal multiples: 80th Annual International Meeting, SEG, Expanded Abstracts, Society of Exploration Geophysicists, 3456–3461.

———, 2010b, The inverse scattering series approach towards the elimination of land internal multiples: 80th Annual International Meeting, SEG, Expanded Abstracts.

Fu, Q., and A. B. Weglein, 2014, Inverse scattering series internal multiple attenuation on encana data: 84th Annual International Meeting, SEG, Expanded Abstracts. (Submitted).

Goodway, W., 2013, Preliminary results of synthetic and land internal multiple removal by inverse scattering. Presentation at the Post SEG Convention Workshop on Internal Multiples.

Griffiths, M., A. Pica, and B. Hung, 2013, Internal multiple removal solutions for multiple environments. Presentation at the Post SEG Convention Workshop on Internal Multiples.

Hsu, S.-Y., P. Terenghi, and A. B. Weglein, 2011, The properties of the inverse scattering series internal multiple attenuation algorithm: Analysis and evaluation on synthetic data with lateral variations, choosing reference velocity and examining its sensitivity to near surface properties: M-OSRP 2010-2011 Annual Report, 16–28.

Kelamis, P. G., Y. Luo, and A. B. Weglein, 2013, Strategies of land internal multiple elimination based on inverse scattering series: Technical Session 21: Recent Development in Seismic Imaging/Processing, International Petroleum Technology Conference, Beijing, China, 26-28 March 2013, Society of Exploration Geophysicists, 1–4.

Liang, H., C. Ma, and A. B. Weglein, 2013, General theory for accommodating primaries and multiples in internal multiple algorithm: Analysis and numerical tests: 83rd Annual International Meeting, SEG, Expanded Abstracts, Society of Exploration Geophysicists, 4178–4183.

Liu, F., X. Li, and A. B. Weglein, 2011, Addressing innate data limitations in ISS imaging algorithms: distinct data regularization methods to address different types of data limitations, to facilitate and allow specific ISS imaging steps and goals: 2010 M-OSRP Annual Report, 50–81.

Liu, F., and A. B. Weglein, 2013, The first *wave theory* RTM, examples with a layered medium, predicting the source and receiver at depth and then imaging, providing the correct location and reflection amplitude at every depth location, and where the data includes primaries and all internal multiples: 2012 M-OSRP Annual Report, 284–335.

Luo, Y., P. G. Kelamis, Q. Fu, S. Huo, G. Sindi, S.-Y. Hsu, and A. B. Weglein, 2011, Elimination of land internal multiples based on the inverse scattering series: The Leading Edge, **30**, 884–889.

Ma, C., and A. B. Weglein, 2013, One-dimensional analytic analysis of the effects of including internal multiples as part of input into the leading-order inverse scattering series (ISS) internal-multiple attenuation algorithm: comparison between free-surface and internal-multiple cases: M-OSRP 2012-2013 Annual Report, 123–145.

———, 2014a, Including higher-order inverse scattering series (ISS) terms to address a serious shortcoming/problem of the ISS internal-multiple attenuator: exemplifying the problem and its resolution: Presented at the 84th Annual International Meeting, SEG, Expanded Abstracts, Society of Exploration Geophysicists. (Submitted).

———, 2014b, Inverse scattering series (ISS) leading-order internal-multiple-attenuation algorithm and higher-order modification to accommodate primaries and internal multiples as input: 1-D normal incident test on interfering events, and extension to multi-D: Presented at the M-OSRP 2013-2014 Annual Report.

Mackidd, D., 2013, Multiples. . . the elephant in the room. Presentation at the Post SEG Convention Workshop on Internal Multiples.

Matson, K., D. Corrigan, A. Weglein, C.-Y. Young, and P. Carvalho, 1999, Inverse scattering internal multiple attenuation: Results from complex synthetic and field data examples: 69th Annual International Meeting, SEG, Expanded Abstracts, Society of Exploration Geophysicists, 1060–1063.

Mayhan, J. D., and A. B. Weglein, 2013, First application of Green's theorem-derived source and receiver deghosting on deep-water Gulf of Mexico synthetic (SEAM) and field data: Geophysics, **78**, WA77–WA89.

Mayhan, J. D., A. B. Weglein, and P. Terenghi, 2012, First application of Green's theorem derived source and receiver deghosting on deep water Gulf of Mexico synthetic (SEAM) and field data: 82nd Annual International Meeting, SEG, Expanded Abstracts, Society of Exploration Geophysicists, 1–5.

Tang, L., J. D. Mayhan, J. Yang, and A. B. Weglein, 2013, Using Green's theorem to satisfy data requirements of multiple removal methods: The impact of acquisition design: 83rd Annual International Meeting, SEG, Expanded Abstracts, Society of Exploration Geophysicists, 4392–4396.

Tang, L., and A. B. Weglein, 2014, Predicting reference medium properties from invariances in Green's theorem reference wave prediction: towards an on-shore near surface medium and reference wave prediction: Presented at the 84th Annual International Meeting, SEG, Expanded Abstracts, Society of Exploration Geophysicists. (Submitted).

Terenghi, P., S.-Y. Hsu, A. B. Weglein, and X. Li, 2011, Exemplifying the specific properties of the inverse scattering series internal-multiple attenuation method that reside behind its capability for complex onshore and marine multiples: The Leading Edge, **30**, 876–882.

Wang, Z., A. B. Weglein, J. D. Mayhan, P. Terenghi, and C. Rivera, 2012, Green's theorem derived deghosting: fundamental analysis, numerical test results, and impact on ISS free-surface multiple elimination: 82nd Annual International Meeting, SEG, Expanded Abstracts, Society of Exploration Geophysicists, 1–5.

Weglein, A. B., F. V. Araújo, P. M. Carvalho, R. H. Stolt, K. H. Matson, R. T. Coates, D. Corrigan, D. J. Foster, S. A. Shaw, and H. Zhang, 2003, Inverse scattering series and seismic exploration: Inverse Problems, **19**, R27–R83.

Weglein, A. B., and W. Dragoset, eds., 2005, Multiple attenuation: SEG. SEG Geophysics Reprint Series, No. 23.

Weglein, A. B., F. A. Gasparotto, P. M. Carvalho, and R. H. Stolt, 1997, An inverse-scattering series method for attenuating multiples in seismic reflection data: Geophysics, **62**, 1975–1989.

Wu, J., and A. B. Weglein, 2014a, The first test and evaluation of the ISS internal multiple attenuation algorithm for the attenuating medium: Presented at the 84th Annual International Meeting, SEG, Expanded Abstracts, Society of Exploration Geophysicists. (Submitted).

———, 2014b, Green's theorem based wavefield separation application on elastic/land: Presented at the 84th Annual International Meeting, SEG, Expanded Abstracts, Society of Exploration Geophysicists. (Submitted).

Yang, J., J. D. Mayhan, L. Tang, and A. B. Weglein, 2013, Accommodating the source (and receiver) array in free-surface multiple elimination algorithm: Impact on interfering or proximal primaries and multiples: 83rd Annual International Meeting, SEG, Expanded Abstracts, Society of Exploration Geophysicists, 4184–4189.

Yang, J., and A. B. Weglein, 2014, Incorporating source wavelet and radiation pattern into the ISS internal multiple attenuation algorithm: Presented at the 84th Annual International Meeting, SEG, Expanded Abstracts, Society of Exploration Geophysicists. (Submitted).

Zhang, J., 2007, Wave theory based data preparation for inverse scattering multiple removal, depth imaging and parameter estimation: analysis and numerical tests of Green's theorem deghosting theory: PhD thesis, University of Houston.

Zou, Y., and A. B. Weglein, 2013, A new method to eliminate first order internal multiples for a normal incidence plane wave on a 1d earth: SEG Technical Program Expanded Abstracts, 4136–4140.

———, 2014a, An algorithm for the elimination of all first-order internal multiples from all reflectors: 1D normal incidence and 1D pre-stack algorithm, discussion and numerical tests: Presented at the M-OSRP 2013-2014 Annual Report.

———, 2014b, The pre-stack 1D ISS internal multiple elimination algorithm for all reflectors Part I: strengths and limitations: Presented at the 84th Annual International Meeting, SEG, Expanded Abstracts, Society of Exploration Geophysicists. (Submitted).

———, 2014c, The pre-stack 1D ISS internal multiple elimination algorithm for all reflectors Part II: addressing the limitations: Presented at the 84th Annual International Meeting, SEG, Expanded Abstracts, Society of Exploration Geophysicists. (Submitted).

Internal multiple attenuation on Encana data

Qiang Fu and Arthur B. Weglein, M-OSRP, University of Houston

SUMMARY

The attenuation of internal multiple energy on land data is still one of the most challenging tasks in seismic data preprocessing. Low data quality and lack of velocity information of complicated structure (especially in near surface) on land data often result in poor predictions in many cases. Inverse Scattering Series (ISS) internal multiple attenuation is a very promising algorithm to attenuate internal multiple energy on land seismic exploration data. The key characteristic of this ISS-based methods is that they do not require any information about the subsurface, i.e., they are fully data driven. Internal multiples from all possible generators are predicted simultaneously from the input data. In this paper we apply Inverse Scattering Series (ISS) internal multiple attenuation algorithms on a land seismic data from Canada.

INTRODUCTION

Inverse Scattering Series (ISS) internal multiple attenuation is a data-driven internal multiple attenuation algorithm (Araújo et al., 1994; Weglein et al., 1997). The lack of any need for information about the medium through which the seismic wave propagates or the reflectors from which the internal multiples generate makes the algorithm feasible in areas with complicated geological structure. The algorithm predicts internal multiples for all horizons at once with no manual intervention required in the whole procedure. Weglein et al. (2003) provided a very comprehensive and detailed review on inverse scattering series applied on seismic exploration.

This ISS internal multiple-attenuation scheme is basically the first term in a subseries of the ISS that predicts the exact time and amplitude of all internal multiples without subsurface information. The ISS attenuation algorithm predicts the correct traveltimes and approximate amplitudes of all the internal multiples in the data, including converted-wave internal multiples (Coates and Weglein, 1996). Carvalho (1992) pioneered the free-surface ISS method and applied it to field data. Matson et al. (1999) were the first to apply the ISS internal multiple algorithm to marine towed-streamer field data. Matson (1997) and Weglein et al. (1997) extended the ISS methods for removing free-surface and internal multiples from ocean-bottom and land data. Fu et al. (2010) presented the first land field data example of ISS internal multiple algorithm. Terenghi (2011) showed a result of pre-stack field data internal multiple attenuation on Encana on-shore data.

THEORY

The ISS internal multiple attenuation algorithm in 2D starts with the input data, $D(k_g,k_s,\omega)$, that is deghosted and has all free-surface multiples eliminated. The parameters, k_g, k_s, and ω represent the Fourier conjugates to receiver, source and time, respectively. The ISS internal multiple attenuation algorithm for first order internal multiple prediction in a 2D earth is given by Araújo et al. (1994); Weglein et al. (1997):

$$\begin{aligned} b_3^{2D}(k_g,k_s,q_g+q_s) = \frac{1}{(2\pi)^2}\int_{-\infty}^{+\infty}\int_{-\infty}^{+\infty} dk_1 e^{-iq_1(z_g-z_s)} \\ dk_2 e^{-iq_2(z_g-z_s)} \\ \times \int_{-\infty}^{+\infty} dz_1 e^{i(q_g+q_1)z_1} b_1(k_g,k_1,z_1) \\ \times \int_{-\infty}^{z_1-\varepsilon} dz_2 e^{i(-q_1-q_2)z_2} b_1(k_1,k_2,z_2) \\ \times \int_{z_2+\varepsilon}^{+\infty} dz_3 e^{i(q_2+q_s)z_3} b_1(k_2,k_s,z_3). \end{aligned} \quad (1)$$

The quantity $b_1(k_g,k_s,z)$ corresponds to an un-collapsed migration (Weglein et al., 1997) of an effective incident plane-wave data which is given by $-2iq_sD(k_g,k_s,\omega)$ The vertical wavenumbers for receiver, q_g, and source q_s, are given by $q_i = sqn(\omega)\sqrt{\frac{\omega^2}{c_0^2}-k_i^2}$ for $i=(q,s)$; c_0 is the constant reference velocity; z_s and z_g are source and receiver depths; and z_i $(i=1,2,3)$ represents pseudodepth.

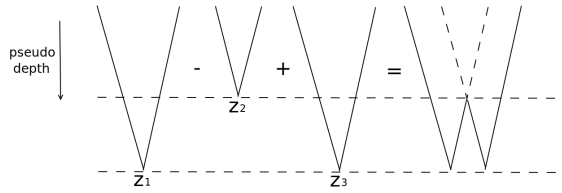

Figure 1: The sub-events of an internal multiple event. The internal multiple events(rightmost one) is constructed by three sub-events (left three) that satisfy the lower-higher-lower relationship in pseudodepth z_i $(i=1,2,3)$.

The construction of a first order internal multiple is illustrated in Figure 1. The first order internal multiple is composed of three sub-events that satisfy $z_1 > z_2$ and $z_3 > z_2$. The traveltime of the internal multiple is the sum of the traveltimes of the two deeper sub-events minus the traveltime of the shallower one. The parameter ε introduced in equation 1 to preclude $z_1 = z_2$ and $z_2 = z_3$ in the integrals. For band limited data, ε is related to the width of the wavelet. The output of equation 1, b_3, is divided by the obliquity factor and transformed back to the space-time domain. When we subtract the predicted internal multiples from the original input data (by adaptive subtraction), all first order internal multiples are attenuated and higher order internal multiples are altered.

DATA AND METHOD CHOSEN TO ACCOMMODATE THE DATA

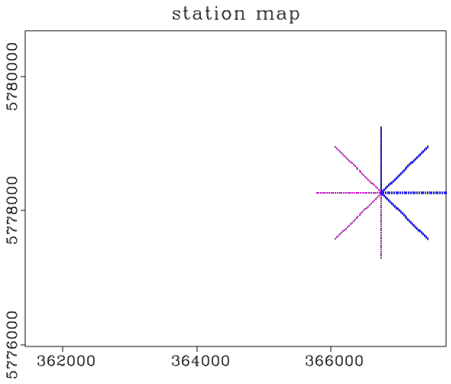

(a)

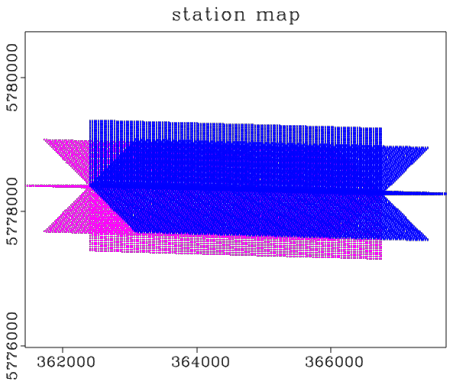

(b)

Figure 2: (a) Acquisition geometry map of the the first CMP gather of the data. (b) Acquisition geometry map of the whole Encana data. Red dots represent the source locations and the blue dots represent the receiver locations.

The Encana data is from the Western Canadian Sedimentary Basin, and it is situated over a restricted Devonian shelf basin. This shallow basin was initially connected to open marine waters. Pinnacle reefs grew in this marine environment and later filled with oil, making them a prime exploration target. The connection to the open marine later became restricted, causing the basin to fill with evaporates, which consist primarily of anhydrite today. The anhydrite acts as a lateral seal and cap rock for the porous reef reservoirs.

These reefs should be very easy to find in the seismic data. The basinal anhydrite produces a very strong peak reflection, but the response is almost reversed when there is a reef present, as the reef porosity has much lower acoustic impedance than the anhydrite. This is the case with the western part of this basin, where the reefs have all been found. On the East side of the basin, the situation is quite different. There, a Lower Cretaceous coal, which reaches 15 meters in thickness, produces severe multiple interference that obscures the entire Paleozoic section. Many reefs have been found there, but there have been many more dry holes drilled than successes, due to this interference. Most commercial multiple attenuation algorithms fail to remove this interference. Our goal here is to make the reefs clearly visible in seismic data in the East side of the basin as it does in the West side.

As mentioned in the previous section, Fu et al. (2010) tested the ISS internal multiple attenuation algorithm on the Arabian Peninsula land field data. Although Arabian Peninsula land field data in Fu et al. (2010) has better data quality, it also has much more complicated geological features. So it is hard to pick a single clear target to judge the internal multiple attenuation result. This Encana data is inferior in data quality (lower S/N ratio) and acquisition geometry (limited fold and offset range) comparing with the Arabian Peninsula data, but there is a very simple target or criterion - the disappeared target layer (the reef). The Encana data has four different azimuths, but this does not provide much help for the internal multiple attenuation task. Terenghi (2011) tested the same method on another Canadian field data, however, that data has large offset coverage.

The Encana data we use here is a multi-azimuth 2D survey line. Figure 2(b) shows the acquisition geometry of the data. And the geometry of the first CMP gather of this data is shown in Figure 2(a). All CMP stations of the data compose a straight line on the map, so this is a 2D survey line even though there are multiple azimuths in the data. The data is a relative old data (from mid 1990s), so it has a very low fold for each CMP gather (32 traces). The 2D ISS internal multiple predication algorithm requires a full coverage input (each shot gather has all receivers on the exact same stations, and we have a shot gather for each station. e.g. there is a trace between every stations pair.). If we want to perform the 2D ISS internal multiple predication, we would need to carry out a large amount of extrapolation to make a full 2D coverage data from the low fold data we have. That would not only be expensive for computation cost but also not reliable to "make" so much data by extrapolation. Given the structures of the whole survey line is fairly flat, the 1.5D pre-stack method would be a suitable choice for the internal multiple attenuation task on this data. In equation 1 we have shown 2D ISS internal multiple attenuation algorithm. The 1.5D ISS internal multiple attenuation algorithm is a straight forward extension of 2D algorithm, which can be described as below

$$
\begin{aligned}
b_3^{1.5D}(k_x;\omega) = \frac{1}{(2\pi)^4} e^{-iq(z_g-z_s)} e^{iq(z_g-z_s)} \\
\times \int_{-\infty}^{+\infty} dz_1 b_1(k_x,z_1) e^{2iqz_1} \\
\times \int_{-\infty}^{z_1-\varepsilon} dz_2 b_1(k_x,z_2) e^{-2iqz_2} \\
\times \int_{z_2+\varepsilon}^{+\infty} dz_3 b_1(k_x,z_3) e^{2iqz_3}. \qquad (2)
\end{aligned}
$$

The notation in equation 2 are the same as the one in equation 1. If we compare it with the 2D version, the only difference is that in 1.5D formula the output has only one horizontal spatial wavenumber index k_x rather than two (k_g and k_s). This is obvious since under the 1.5D assumption (flat-layer medium), all horizontal incident wavenumber should be equal to the re-

flected wavenumber ($k_g = k_1 = k_2 = k_s = k_x$). Hence there is only one horizontal spatial wavenumber k_x in equation 2.

RESULTS

Figure 3 and 4 show the input data in pre-stack and post-stack domains, respectively. As required by the ISS internal multiple attenuation algorithm, the data is first deghosted and has all free-surface multiples eliminated. In this case, the major multiple generator is the coal layer. We can see the reflector clearly in Figure 4 (in the vicinity of 1s) and the target layer (the reef) should be around 1.15s can not be seen in Figure 4.

Figure 5 and 6 show the internal multiple attenuation result in pre-stack and post-stack domains, respectively. The reference velocity c_0 used is the shallowest layer NMO velocity (averaged horizontally). After internal multiple attenuation, we can see that a significant amount of internal multiple energy is removed in the vicinity of 1.15s. However, we can still barely find the reef clearly. The result shows that there is marginal improvement of the target event after ISS internal multiple attenuation with this limited offset data.

Figure 7 and 8 are the predicted internal multiples in pre-stack and post-stack domains, respectively. Although the method knows nothing about the generator, the predicted internal multiples only appear below the main generator. Figure 7 shows the predicted internal multiples has primarily far offset component (with some near offset still visible). The near offset component is critical to obtain an effective internal multiple attenuation result. Therefore, the lack of near offset internal multiple prediction is an important reason we do not obtain very satisfactory result in this case. That is due to the fact that there is very limited offset coverage of the input data.

The data acquisition geometry consists of 4 different azimuths. We also tried to use the data of each azimuth separately and the results are not significantly different comparing the result by using data of all azimuths together. To use all azimuth data results a little better quality in the post-stack section and has 4 times higher fold comparing single azimuth data, which is increasing the S/N ratio.

CONCLUSIONS

We applied 1.5D pre-stack ISS internal multiple attenuation on Encana land seismic data and got marginal improvement of the target event. The result is not as satisfactory as the same ISS internal attenuation algorithm on the Arabian Peninsula data (Fu et al., 2010). This is due to the ISS internal multiple attenuation algorithm requiring a Fourier transform to be performed along the offset axis. That requires a reasonable offset range in the input data to avoid truncated effects. Considering the data acquisition geometry (32 traces per CMP gather and maximum offset 2000m), this is a positive and encouraging result. The ISS algorithm for the surface and internal multiple attenuation require reasonable data collection in terms of sampling and offset to be effective and to deliver its promise.

ACKNOWLEDGMENT

We thank David Mackidd and David Bonar of Encana for providing the data used in this paper and encouraging (1) the ISS internal multiple attenuation tests and (2) communicating these results to the geophysical community. We thank Dr. P. Terenghi for his useful and worthful comments and suggestions in reviewing this paper. We thank M-OSRP sponsors for their encouragement and support for our research. M-OSRP would like to thank Bill Goodway of Apache Corp, for his constant, strong and much appreciated encouragement and support for all the projects in our program.

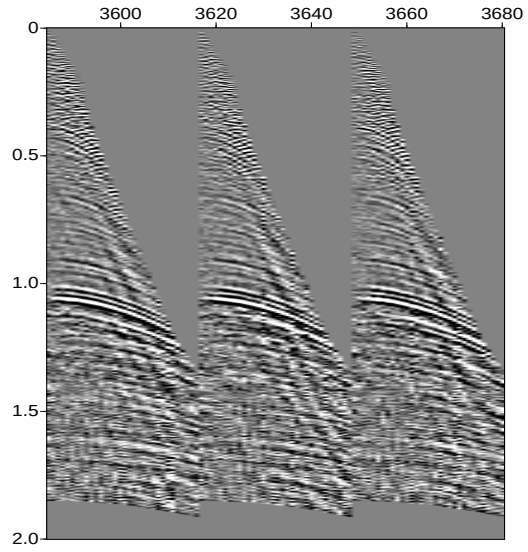

Figure 3: Three pre-stack gathers of of input data.

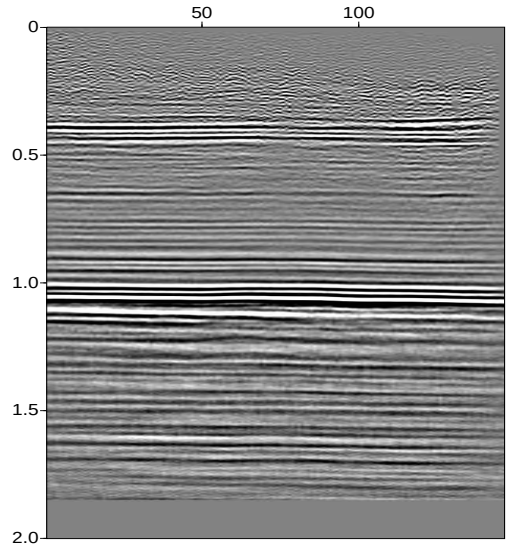

Figure 4: Stack section of input data.

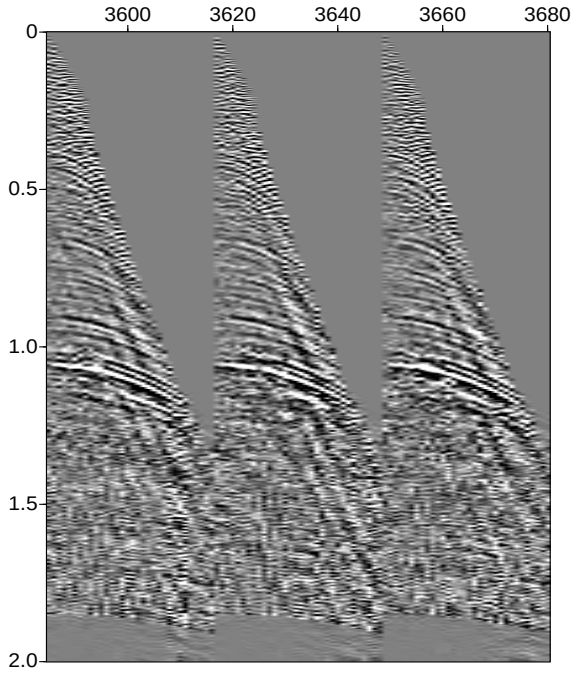

Figure 5: Three pre-stack gathers of internal multiple attenuation result.

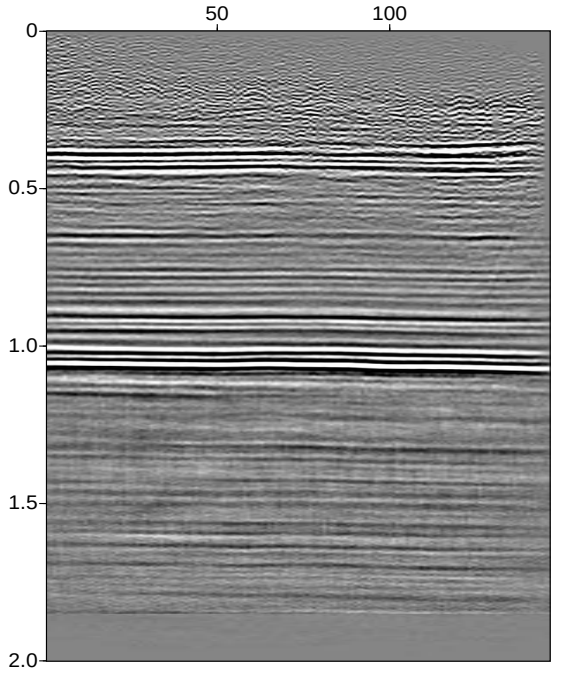

Figure 6: Stack section of internal multiple attenuation result.

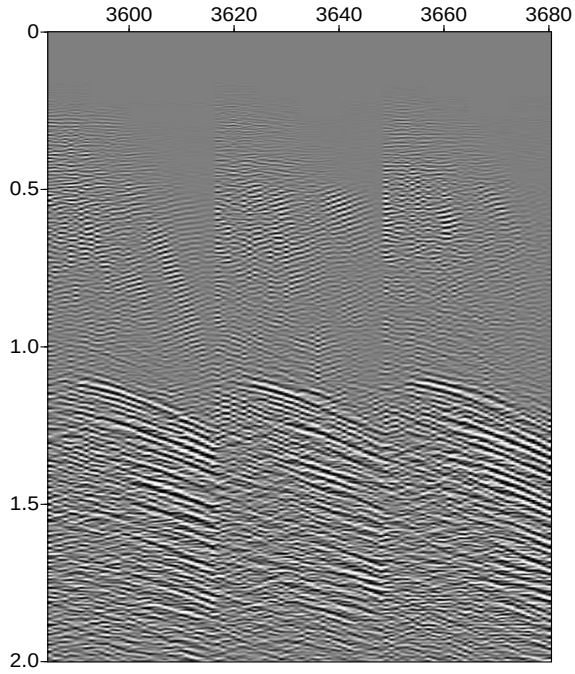

Figure 7: Three pre-stack gathers of internal multiple prediction.

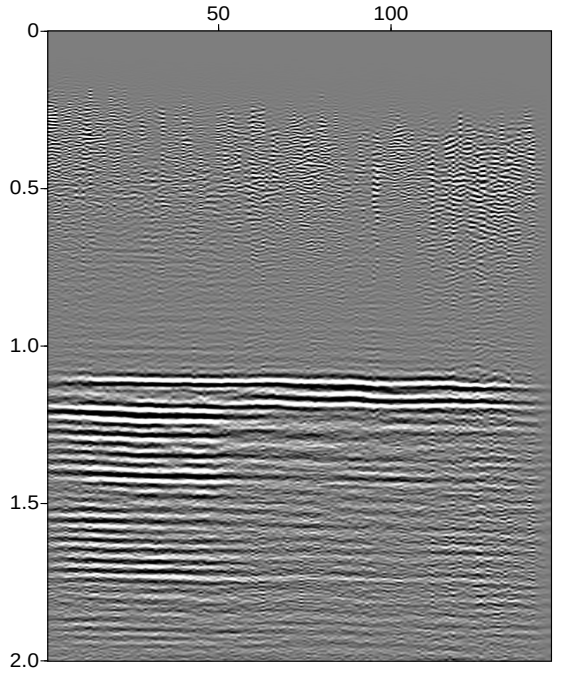

Figure 8: Stack section of internal multiple prediction.

REFERENCES

Araújo, F. V., A. B. Weglein, P. M. Carvalho, and R. H. Stolt, 1994, Inverse scattering series for multiple attenuation: An example with surface and internal multiples: 64th Annual International Meeting, SEG, Expanded Abstracts, 1039–1042.

Carvalho, P. M., 1992, Free-surface multiple reflection elimination method based on nonlinear inversion of seismic data: PhD thesis, Universidade Federal da Bahia.

Coates, R. T., and A. B. Weglein, 1996, Internal multiple attenuation using inverse scattering: Results from prestack 1 and 2d acoustic and elastic synthetics: 66th Annual International Meeting, SEG, Expanded Abstracts, 1522–1525.

Fu, Q., Y. Luo, P. G. Kelamis, S. Huo, G. Sindi, S.-Y. Hsu, and A. B. Weglein, 2010, The inverse scattering series approach towards the elimination of land internal multiples: 80th Annual International Meeting, SEG, Expanded Abstracts.

Matson, K., D. Corrigan, A. B. Weglein, C. Y. Young, and P. Carvalho, 1999, Inverse scattering internal multiple attenuation: Results from complex synthetic and field data examples: 69th Annual International Meeting, SEG, Expanded Abstracts, 1060–1063.

Matson, K. H., 1997, An inverse-scattering series method for attenuating elastic multiples from multicomponent land and ocean bottom seismic data: PhD thesis, University of British Columbia.

Terenghi, P., 2011, Informal m-osrp memo on "initial encana post-stack data iss attenuation tests".

Weglein, A. B., F. V. Araújo, P. M. Carvalho, R. H. Stolt, K. H. Matson, R. T. Coates, D. Corrigan, D. J. Foster, S. A. Shaw, and H. Zhang, 2003, Inverse scattering series and seismic exploration: Inverse Problems, R27–R83.

Weglein, A. B., F. A. Gasparotto, P. M. Carvalho, and R. H. Stolt, 1997, An inverse-scattering series method for attenuating multiples in seismic reflection data: Geophysics, **62**, 1975–1989.

Multiple removal and prerequisite satisfaction: current status and future plans

James D. Mayhan and Arthur B. Weglein, M-OSRP/Physics Department/University of Houston

Summary

In exploration seismology, as the geology probed by seismic waves becomes more complex, untangling multiples and primaries becomes more challenging. The inverse scattering series (ISS) has provided distinct algorithms for eliminating free-surface multiples and attenuating internal multiples without needing any subsurface information. To deliver their promise it is important to satisfy the prerequisites of these two algorithms. The free-surface-multiple-elimination algorithm assumes that its input has had the source wavelet deconvolved and ghosts removed. The internal-multiple algorithm requires deghosting and source-wavelet deconvolved and further assumes that its input data has had free-surface multiples removed. Fortunately, Green's theorem provides algorithms for estimating the source wavelet and removing ghosts that are consistent with the ISS algorithms, *i.e.*, they need no subsurface information and are multidimensional. The effects of meeting and not meeting the prerequisites of the demultiple algorithms are exemplified, and the current and future status of demultiple algorithms are discussed.

Introduction

The two purposes of this paper are (1) to review and exemplify the influence of prerequisite satisfaction for free-surface-multiple and internal-multiple algorithms with synthetic data corresponding to offshore plays, and (2) to motivate onshore methods for prerequisite satisfaction and describe early efforts to reach that goal.

As exploration for hydrocarbons has moved into areas with more complex geology, there are more instances in which multiples are proximal to or even overlapping primaries. Hence, demultiple algorithms are challenged to remove multiples without damaging proximal primaries. The inverse scattering series (ISS) can achieve all processing objectives directly and without subsurface information. In particular, the ISS free-surface-multiple-elimination method has the ability to accurately predict the phase and amplitude of free-surface multiples, if its prerequisites (source signature and deghosted data) are satisfied (Carvalho et al., 1992; Weglein et al., 1997, 2003). The current ISS internal-multiple-attenuation algorithm can predict the exact phase (time) and approximate amplitude of all internal multiples, at once, automatically, and without subsurface information (Araújo et al., 1994; Weglein et al., 2003), as has been demonstrated on marine field data (Carvalho and Weglein, 1994; Matson et al., 1999; Terenghi et al., 2011; Ferreira, 2011). Those ISS properties are what all other current demultiple methods (*e.g.*, Feedback loop methods, modeling and subtracting multiples, and filter methods) do not possess and cannot deliver (Weglein and Dragoset, 2005).

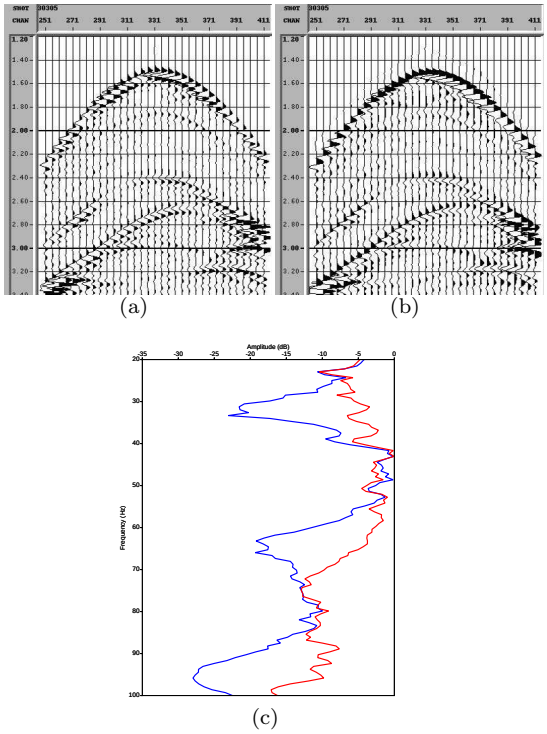

Fig. 1: *SEAM Phase I data, shot 130305: (a) recorded pressure wavefield at 17 m, (b) receiver-deghosted pressure wavefield at the air-water boundary using Green's theorem. The horizontal axis is trace number, and the vertical axis is time (s). Note the collapsed wavelet in the right panel. (c) Frequency spectra of 2D field data, shot 841: input hydrophones at 25 m (blue), receiver-deghosted pressure wavefield at the air-water boundary using Green's theorem (red). The receiver notches around 30 Hz, 60 Hz, and 90 Hz have been filled in. Input data courtesy of PGS. (Mayhan et al., 2011)*

The prerequisites for ISS demultiple algorithms can be met by Green's-theorem-based algorithms (Weglein and Secrest, 1990; Weglein et al., 2002; Zhang and Weglein, 2005, 2006; Zhang, 2007). The ability of Green's theorem to meet prerequisites has been tested on SEAM and field data (Mayhan and Weglein, 2013; Mayhan, 2013); we show examples in Figure 1. When prerequisites are satisfied, the prediction improves, as shown in Figures 2 and 4.

Free-surface-multiple removal with and without first removing ghosts is shown in Figure 2. Using the model shown in Figure 2(a), Figures 2(b) and 2(c) are the in-

put data with and without ghosts, respectively. Inputting them into the ISS free-surface-multiple-elimination algorithm, Figures 2(d) and 2(e) are their corresponding free-surface-multiple predictions. After subtracting from the input data, Figures 2(f) and 2(g) show the corresponding results after free-surface-multiple removal. If the input data are not deghosted, the ISS free-surface-multiple-removal method can predict the exact phase but only an approximate amplitude of free-surface multiples. After deghosting the data, we can see that all free-surface multiples are predicted exactly, and, through a simple subtraction, all are well eliminated, and, most importantly, primaries are not touched, as shown in Figure 2(g). Other examples of removing free-surface multiples with and without deghosting for simple synthetic data are given in Zhang (2007) and Wang et al. (2012) (Figure 3).

Free-surface-multiple elimination and internal-multiple attenuation with and without first removing the source wavelet are shown in Figure 4. Each column is plotted to the same scale. The left column uses the model in Figure 2(a), and the right column uses a model with no free surface and two reflectors. Figures 4(a), 4(c), and 4(e) show the input data and the predicted free-surface multiples using the free-surface-multiple-elimination algorithm with and without source wavelet deconvolution, and Figures 4(b), 4(d), and 4(f) show the input data and the predicted internal multiples using the internal-multiple-attenuation algorithm with and without source wavelet deconvolution. Figures 4(d) and 4(f) show that the internal-multiple-attenuation algorithm predicts the correct travel times but different amplitudes and shapes for the internal multiples. In Figure 4(d), the amplitude of the predicted internal multiple is comparable with the internal multiple in the input data, while the amplitude is totally different from that of the internal multiple in the input data in Figure 4(f). Deconvolving the source wavelet, as required by the internal-multiple-attenuation algorithm, significantly improves the amplitude and shape of the predicted internal multiple.

Current status

The current status of multiple removal for marine seismic data is summarized in Table 1. Row (1): Satisfying the prerequisites of the ISS (using Green's theorem) is relatively mature. Estimating the source wavelet and removing ghosts have been tested on simple synthetic data, SEAM data, and field data (Zhang, 2007; Mayhan, 2013). Row (2): Free-surface-multiple elimination is also mature. In principle, the ISS free-surface-multiple prediction algorithm gives the exact amplitude and phase of the free-surface multiples. Row (3): Internal-multiple attenuation is also mature; it was tested on field data by Matson et al. (1999), Terenghi et al. (2011), and Ferreira (2011). Work is underway to eliminate spurious events (Ma and Weglein, 2014) and move attenuation to elimination (Zou and Weglein, 2014a,b). Row (4): Adaptive subtraction using energy minimization is inconsistent; if multiples and primaries are separated, it works, but not if multiples are

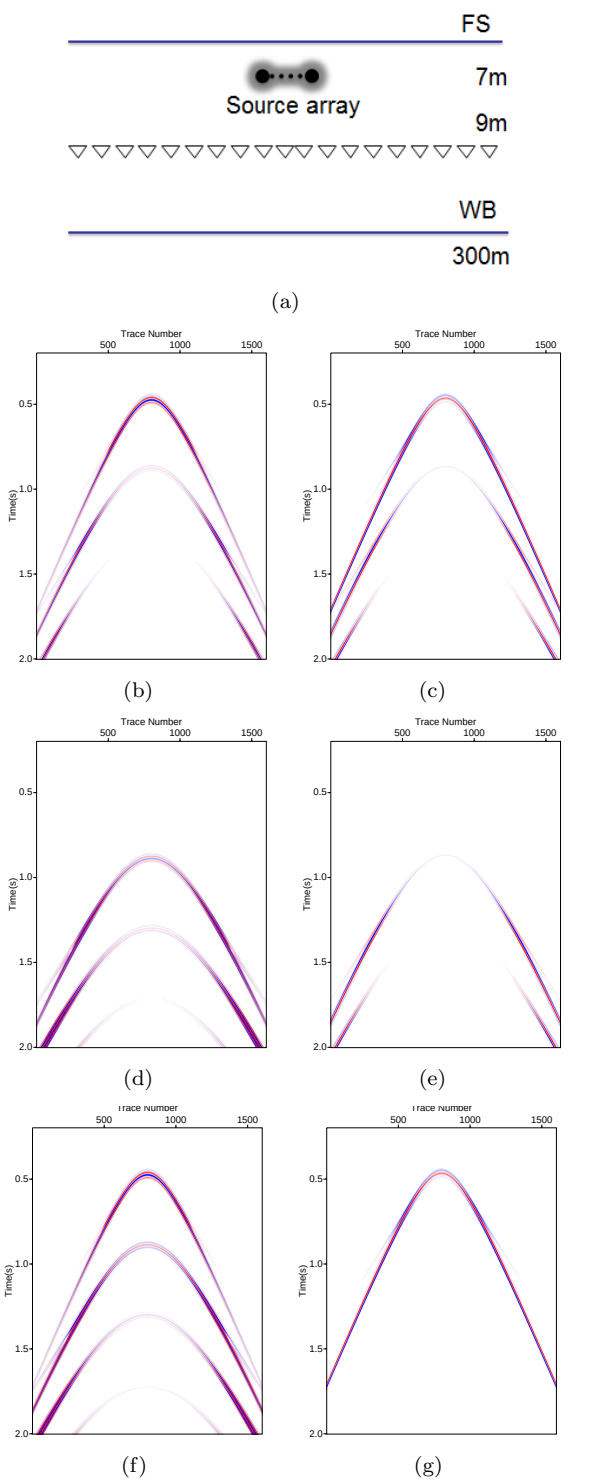

Fig. 2: *Free-surface-multiple removal with and without first removing ghosts: (a) model used to create input data; (b) & (c) input data with and without ghosts; (d) & (e) corresponding ISS free-surface-multiple prediction; (f) & (g) after free-surface-multiple removal through a simple subtraction. (Tang et al., 2013)*

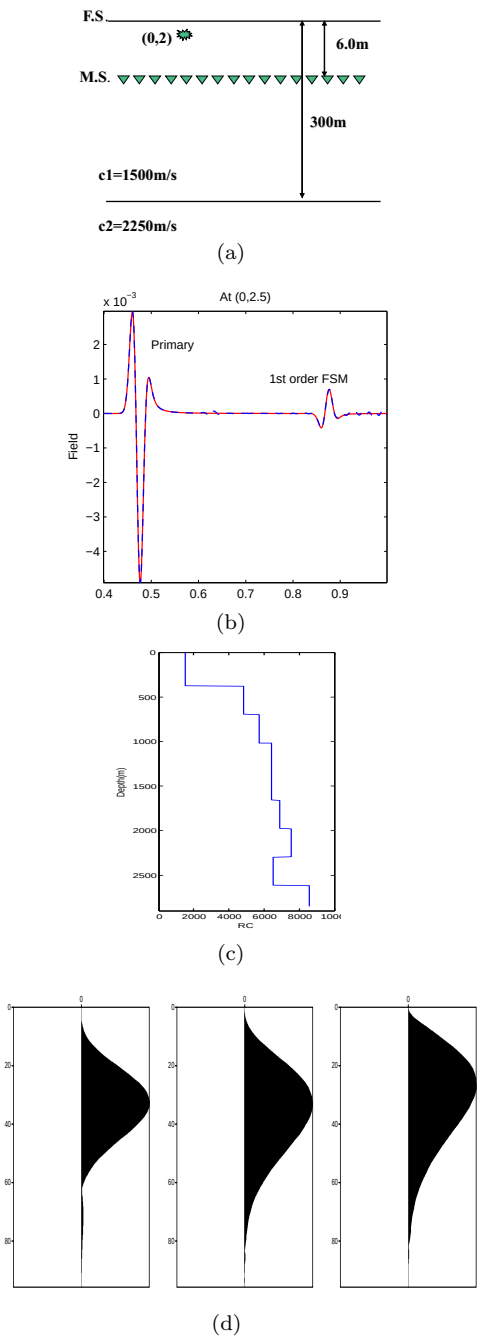

Fig. 3: *(a) The constant-density acoustic model used for panel (b). (b) Using receiver-array data, the calculated deghosting results (blue dash) are compared to the exact deghosting results (red solid). The direct wave has been removed before deghosting. Notice the small errors in amplitude. (Zhang, 2007) (c) The velocity model (provided by Total) used for panel (d). (d) Spectrum plots of their wavelets: The left panel is before deghosting, the middle panel is receiver deghosted, and the right panel is source and receiver deghosted. Both receiver deghosting and source deghosting recover more low-frequency information. (Wang et al., 2012)*

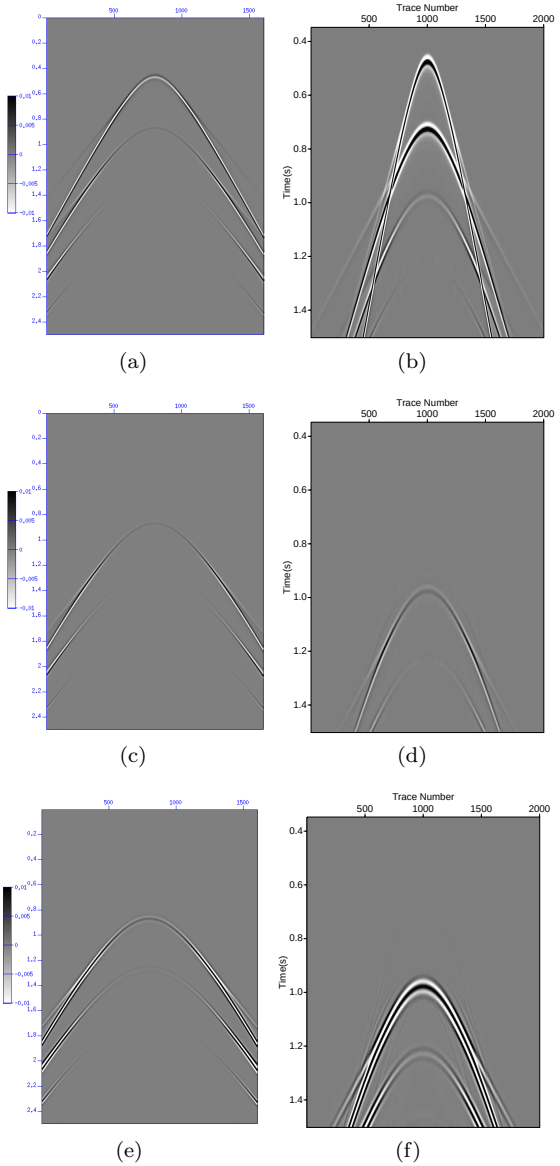

Fig. 4: *Impact of source wavelet on ISS free-surface-multiple removal: (a) input data, (c) and (e) predicted free-surface multiples with and without source wavelet deconvolution, respectively (Yang and Weglein, 2012). Impact of source wavelet on ISS internal-multiple attenuation: (b) input data, (d) and (f) predicted internal multiples with and without source wavelet deconvolution, respectively (Yang and Weglein, 2014).*

proximal to or overlapping primaries. A possible replacement for energy-minimization adaptive subtraction has been proposed for free-surface-multiples (Weglein, 2012).

The current capability of multiple removal for onshore seismic data is summarized in Table 2. Row (1): Using Green's theorem to satisfy ISS prerequisites, as is cur-

	Method	Comment/status
1	Prerequisites (estimate wavelet, deghost)	Relatively mature
2	Free-surface multiples	Eliminate
3	Internal multiples	Attenuate
4	Adaptive	Energy minimization

Table 1: *The current status of multiple removal (marine seismic data).*

rently performed for marine seismic data, is discussed in Wu and Weglein (2014b), and a method for finding the reference velocity in the near surface is discussed in Tang and Weglein (2014). Row (3): The results of testing ISS internal-multiple attenuation on land are encouraging; its "performance was demonstrated with complex synthetic and challenging land field data sets with encouraging results, where other internal multiple suppression methods were unable to demonstrate similar effectiveness" (Fu et al., 2010). Row (4): "The examples of this paper point to the pressing need to improve the prediction and reduce the reliance on adaptive steps, since the latter can fail precisely when you have interfering events." (Fu et al., 2010)

	Method	Comment/status
1	Prerequisites (estimate wavelet, deghost)	Find reference velocity iteratively
2	Free-surface multiples	Eliminate
3	Internal multiples	Attenuate
4	Adaptive	Energy minimization

Table 2: *The current capability of multiple removal (onshore seismic data).*

Future plans

There is a three-pronged strategy to address the current outstanding issues listed in Tables 1 and 2 (Weglein, 2014a,b). (1) Develop the ISS prerequisites for predicting the reference wavefield (wavelet and radiation pattern) and producing deghosted data (in particular, for onshore and ocean-bottom acquisition) that are direct and do not require subsurface information; (2) Develop ISS algorithms to reduce/eliminate so-called spurious events and to eliminate (vs. attenuate) internal multiples; and (3) Develop a replacement for the energy-minimization criteria for adaptive subtraction, that derives from, and always aligns with and serves, the inverse-scattering-series free-surface and internal-multiple algorithms. This three-pronged strategy represents a consistent and aligned processing chain, with one single objective: providing a direct and practical solution to the removal of all multiples, without requiring any subsurface information, and without damaging primaries. All three prongs are being progressed: (1) in Wu and Weglein (2014a,b), (2) in Zou and Weglein (2014a,b) and Ma and Weglein (2014), and (3) in Weglein (2012). This ideal status of multiple removal (marine seismic data) is summarized in Table 3.

	Method	Comment/status
1	Prerequisites (estimate wavelet, deghost)	Mature
2	Free-surface multiples	Eliminate
3	Internal multiples	Eliminate
4	Adaptive	Consistent with 1-3

Table 3: *The ideal status of multiple removal (marine seismic data).*

The energy-minimization adaptive-subtraction criteria, while not derived as a property of the free-surface-multiple-elimination or internal-multiple-attenuation criteria, is useful for completing the matching between multiple prediction and multiple, when events are separated and there are no higher-order multiples in the vicinity, and only a first-order algorithm is being used. Part of the three-pronged strategy is to use the terms in the respective ISS subseries that can accommodate the order of multiple anticipated in the target region. Given deghosted and wavelet-deconvolved data, there is a stable closed form that eliminates all orders of free-surface multiples at once (Weglein and Dragoset, 2005). With proximal and/or interfering events the energy-minimization criteria fails, independently of how it's implemented (because of interfering proximal events), and a new set of criteria is sought for the adaptive step that derives from and aligns with and always supports the multiple subseries. (A candidate for a replacement for energy-minimization adaptive for free-surface multiples is given in Weglein (2012).)

Conclusions

This paper gives (1) an overview of removing multiples from marine data and (2) motivation and preview for removing multiples from onshore data. In principle, the ISS free-surface-multiple prediction algorithm gives the exact amplitude and phase of the free-surface multiples, and the ISS internal-multiple-attenuation algorithm is the high-water mark of current internal-multiple-attenuation capability. The quality of their output assumes their requirements are met, *i.e.*, source wavelet deconvolved and ghosts removed.

Acknowledgements

We are grateful to M-OSRP's sponsors for their encouragement and support of this research.

References

Araújo, F. V., A. B. Weglein, P. M. Carvalho, and R. H. Stolt, 1994, Inverse scattering series for multiple attenuation: An example with surface and internal multiples: 64th Annual International Meeting, SEG, Expanded Abstracts, Society of Exploration Geophysicists, 1039–1041.

Carvalho, P., and A. Weglein, 1994, Wavelet estimation for surface multiple attenuation using a simulated annealing algorithm: 64th Annual International Meeting, SEG, Expanded Abstracts, Society of Exploration Geophysicists, 1481–1484.

Carvalho, P. M., A. B. Weglein, and R. H. Stolt, 1992, Nonlinear inverse scattering for multiple suppression: Application to real data. Part I: 62nd Annual International Meeting, SEG, Expanded Abstracts, Society of Exploration Geophysicists, 1093–1095.

Ferreira, A., 2011, Internal multiple removal in offshore Brazil seismic data using the inverse scattering series: Master's thesis, University of Houston.

Fu, Q., Y. Luo, P. G. Kelamis, S. Huo, G. Sindi, S.-Y. Hsu, and A. B. Weglein, 2010, The inverse scattering series approach towards the elimination of land internal multiples: 80th Annual International Meeting, SEG, Expanded Abstracts, Society of Exploration Geophysicists, 3456–3461.

Ma, C., and A. B. Weglein, 2014, Including higher-order inverse scattering series (ISS) terms to address a serious shortcoming/problem of the ISS internal-multiple attenuator: exemplifying the problem and its resolution: Presented at the 84th Annual International Meeting, SEG, Expanded Abstracts, Society of Exploration Geophysicists. (Submitted).

Matson, K., D. Corrigan, A. Weglein, C.-Y. Young, and P. Carvalho, 1999, Inverse scattering internal multiple attenuation: Results from complex synthetic and field data examples: 69th Annual International Meeting, SEG, Expanded Abstracts, Society of Exploration Geophysicists, 1060–1063.

Mayhan, J. D., 2013, Wave theoretic preprocessing to allow the Inverse Scattering Series methods for multiple removal and depth imaging to realize their potential and impact: methods, examples, and added value: PhD thesis, University of Houston.

Mayhan, J. D., P. Terenghi, A. B. Weglein, and N. Chemingui, 2011, Green's theorem derived methods for preprocessing seismic data when the pressure P and its normal derivative are measured: 81st Annual International Meeting, SEG, Expanded Abstracts, Society of Exploration Geophysicists, 2722–2726.

Mayhan, J. D., and A. B. Weglein, 2013, First application of Green's theorem-derived source and receiver deghosting on deep-water Gulf of Mexico synthetic (SEAM) and field data: Geophysics, **78**, WA77–WA89.

Tang, L., J. D. Mayhan, J. Yang, and A. B. Weglein, 2013, Using Green's theorem to satisfy data requirements of multiple removal methods: The impact of acquisition design: 83rd Annual International Meeting, SEG, Expanded Abstracts, Society of Exploration Geophysicists, 4392–4396.

Tang, L., and A. B. Weglein, 2014, Predicting reference medium properties from invariances in Green's theorem reference wave prediction: towards an on-shore near surface medium and reference wave prediction: Presented at the 84th Annual International Meeting, SEG, Expanded Abstracts, Society of Exploration Geophysicists. (Submitted).

Terenghi, P., X. Li, S.-Y. Hsu, and A. B. Weglein, 2011, 1D preprocessing of Kristin data: M-OSRP 2010-2011 Annual Report, 35–49.

Wang, Z., A. B. Weglein, J. D. Mayhan, P. Terenghi, and C. Rivera, 2012, Green's theorem derived deghosting: fundamental analysis, numerical test results, and impact on ISS free-surface multiple elimination: 82nd Annual International Meeting, SEG, Expanded Abstracts, Society of Exploration Geophysicists, 1–5.

Weglein, A. B., 2012, Short note: An alternative adaptive subtraction criteria (to energy minimization) for free surface multiple removal: M-OSRP 2011-2012 Annual Report, 375.

———, 2014a, Multiple attenuation: The status and a strategy that identifies and addresses current challenges: E&P Magazine.

———, 2014b, Multiples: Signal or noise?: E&P Magazine. (In preparation).

Weglein, A. B., F. V. Araújo, P. M. Carvalho, R. H. Stolt, K. H. Matson, R. T. Coates, D. Corrigan, D. J. Foster, S. A. Shaw, and H. Zhang, 2003, Inverse scattering series and seismic exploration: Inverse Problems, **19**, R27–R83.

Weglein, A. B., and W. Dragoset, eds., 2005, Multiple attenuation: SEG. SEG Geophysics Reprint Series, No. 23.

Weglein, A. B., F. A. Gasparotto, P. M. Carvalho, and R. H. Stolt, 1997, An inverse-scattering series method for attenuating multiples in seismic reflection data: Geophysics, **62**, 1975–1989.

Weglein, A. B., and B. G. Secrest, 1990, Wavelet estimation for a multidimensional acoustic or elastic earth: Geophysics, **55**, 902–913.

Weglein, A. B., S. A. Shaw, K. H. Matson, J. L. Sheiman, R. H. Stolt, T. H. Tan, A. Osen, G. P. Correa, K. A. Innanen, Z. Guo, and J. Zhang, 2002, New approaches to deghosting towed-streamer and ocean-bottom pressure measurements: 72nd Annual International Meeting, SEG, Expanded Abstracts, Society of Exploration Geophysicists, 2114–2117.

Wu, J., and A. B. Weglein, 2014a, The first test and evaluation of the ISS internal multiple attenuation algorithm for the attenuating medium: Presented at the 84th Annual International Meeting, SEG, Expanded Abstracts, Society of Exploration Geophysicists. (Submitted).

———, 2014b, Green's theorem based wavefield separation application on elastic/land: Presented at the 84th Annual International Meeting, SEG, Expanded Abstracts, Society of Exploration Geophysicists. (Submitted).

Yang, J., and A. B. Weglein, 2012, Incorporating source and receiver arrays in the inverse scattering series free-

surface multiple elimination algorithm: theory and examples that demonstrate impact: M-OSRP 2011-2012 Annual Report, 114–132.

———, 2014, Incorporating source wavelet and radiation pattern into the ISS internal multiple attenuation algorithm: Presented at the 84th Annual International Meeting, SEG, Expanded Abstracts, Society of Exploration Geophysicists. (Submitted).

Zhang, J., 2007, Wave theory based data preparation for inverse scattering multiple removal, depth imaging and parameter estimation: analysis and numerical tests of Green's theorem deghosting theory: PhD thesis, University of Houston.

Zhang, J., and A. B. Weglein, 2005, Extinction theorem deghosting method using towed streamer pressure data: analysis of the receiver array effect on deghosting and subsequent free surface multiple removal: 75th Annual International Meeting, SEG, Expanded Abstracts, Society of Exploration Geophysicists, 2095–2098.

———, 2006, Application of extinction theorem deghosting method on ocean bottom data: 76th Annual International Meeting, SEG, Expanded Abstracts, Society of Exploration Geophysicists, 2674–2678.

Zou, Y., and A. B. Weglein, 2014a, The pre-stack 1D ISS internal multiple elimination algorithm for all reflectors Part I: strengths and limitations: Presented at the 84th Annual International Meeting, SEG, Expanded Abstracts, Society of Exploration Geophysicists. (Submitted).

———, 2014b, The pre-stack 1D ISS internal multiple elimination algorithm for all reflectors Part II: addressing the limitations: Presented at the 84th Annual International Meeting, SEG, Expanded Abstracts, Society of Exploration Geophysicists. (Submitted).

Predicting reference medium properties from invariances in Green's theorem reference wave prediction: towards an on-shore near surface medium and reference wave prediction

Lin Tang and Arthur B. Weglein, University of Houston*

SUMMARY

The Inverse Scattering Series (ISS) methods require prerequisites to reach their potential. Seismic data preprocessing for ISS methods includes identifying and removing the reference wave, estimating the source wavelet and radiation pattern, and source and receiver deghosting. For on-shore seismic exploration, these preprocessing steps still have many serious challenges. To study how to determine the reference velocity for land application, this paper uses the marine environment and a point source as a starting point, and shows that the invariance of the estimated source signature for different output points below the cable could be a criterion to find the correct reference velocity. In addition, for the case of a source signature and radiation pattern, the invariance of the source wavelet in one radiation angle could be the criterion for having the right reference velocity.

INTRODUCTION

The current petroleum industry trend to deep water and complex geology, where primary and multiple events may often experience interfering or proximal with each other. In this case, removal of the multiple events becomes a big challenge. Inverse Scattering Series (ISS) methods offer a direct way of removing free-surface multiples and attenuating internal multiples without requiring any subsurface information. However, these methods have prerequisites that need to be satisfied. The prerequisites include identifying and removing the reference wave, estimating the source wavelet and radiation pattern, and source and receiver deghosting. In order to deliver the high fidelity of ISS multiple predictions, effective preprocessing methods need to be developed and improved (Zhang (2007), Mayhan et al. (2011), Mayhan and Weglein (2013), Tang et al. (2013), Yang et al. (2013)).

As seismic exploration goes to more complex and difficult onshore and offshore plays, there are more fundamental issues and challenges need to be resolved. Among these issues and challenges, removal of the reference wave on land is one pressing and important topic. Why do we need to remove the reference wave first? Scattering theory separates the real world into two parts: the reference medium, whose property is known, plus a perturbation. The wave that travels in the reference medium is called the reference wave, which does not experience the earth that we are interested in. So it is important to identify the reference wave and remove it before the following data processing steps, such as multiple removal and depth imaging. We need to identify it because it also contains the information of the source signature, which is essential information in the subsequent processing steps. ISS methods require that the reference medium agrees with the actual medium on and above the measurement surface (Weglein et al. (2003)). Green's theorem provides a good mathematical tool to achieve these prerequisites that are consistent with the ISS methods they are meant to serve.

For on-shore seismic application, the property of the medium near surface is often complicated and not easy to determine, e.g., because the conditions of rocks, soil or minerals in the near surface are not easy to define due to weathering. Strong ground roll could be generated that can obscure reflected seismic data. To remove the ground roll/reference wave, the physical properties of the near surface is needed. Our purpose in looking for a way to determine the velocity of near surface medium on land, is to provide a foundation for the study of on-shore seismic data preprocessing methods. It is part of the comprehensive Inverse Scattering Series multiple removal strategy.

In order to study the complex on-shore or ocean bottom near surface property, we propose to start from seeking criteria which can determine whether we have the correct reference medium information or not. The criteria could be the presence of some invariance that only the correct reference velocity would satisfy. We use a marine seismic application as a starting point to pursue this idea. First, consider an isotropic point source, which has an isotropic source wavelet in every radiation direction. Using Green's theorem, we can estimate the wavelet signature everywhere below the measurement surface. When using the correct reference velocity, the results for the wavelet should be invariant for all output points below the measurement surface. Thus, the value of reference velocity we use in the wavelet calculation that leads to an invariance of the estimated source wavelet is the correct reference velocity. Furthermore, instead of a single point source, in practice, source arrays which have angle radiation pattern are widely used in industry (Loveridge et al. (1984)). Then the invariance of the estimated wavelet will happen when estimating the wavelet at different points along one radiation angle. Similarly, only the correct reference velocity can lead to the invariance. Thus, the invariances of the source wavelet indicate that we have found the correct reference velocity.

This paper will discuss the criteria of predicting the reference medium properties from invariances in Green's theorem-based wavelet estimation, for both a point source and for source array cases. For a point source, the source wavelet estimated at any points beneath the measurement surface should stay the same, while for source array, estimated source wavelet results in one radiation angle should be invariant. These invariances could be criteria of having the correct reference velocity. Future study will extend this research from marine example to complex on shore elastic model.

THEORY

Green's theorem for wavelet estimation

The theory of wavelet estimation using Green's theorem was first described in Weglein and Secrest (1990). Assume that source $A(\omega)$ is placed at $\vec{r}_s$ and the receiver is at $\vec{r}$. The pressure wavefield P satisfies constant density acoustic wave equation in the frequency domain,

$$\left(\nabla^2+\frac{\omega^2}{c^2(\vec{r})}\right)P(\vec{r},\vec{r}_s,\omega)=A(\omega)\delta(\vec{r}-\vec{r}_s) \tag{1}$$

In scattering theory, we treat the actual medium as a combination of an unperturbed medium, called the reference medium, plus a perturbation. Introduce perturbation α defined by

$$\frac{1}{c^2(\vec{r})}=\frac{1}{c_0^2}[1-\alpha(\vec{r})],$$

where c_0 is the velocity in a homogeneous reference medium. Then Equation 1 becomes

$$\left(\nabla^2+\frac{\omega^2}{c_0^2}\right)P(\vec{r},\vec{r}_s,\omega)=\underbrace{\frac{\omega^2}{c_0^2}\alpha(\vec{r})P(\vec{r},\vec{r}_s,\omega)+A(\omega)\delta(\vec{r}-\vec{r}_s)}_{\rho}. \tag{2}$$

The right hand side of the equation can be viewed as the source of the wavefield P, which consists of two terms: the perturbation α, which generates scattered wave P_s, and the active source $A(\omega)$, the energy source that generates the wave, P. The corresponding Green's function satisfies,

$$\left(\nabla^2+\frac{\omega^2}{c_0^2}\right)G_0(\vec{r},\vec{r'},\omega)=\delta(\vec{r}-\vec{r'}). \tag{3}$$

Having a causal Green's function G_0^+, we can have wavefield P,

$$\begin{aligned}P(\vec{r},\omega) &= \int_\infty G_0^+(\vec{r},\vec{r'},\omega)\rho(\vec{r'},\omega)d\vec{r'}\\ &= \int_\infty G_0^+(\vec{r},\vec{r'},\omega)\frac{\omega^2}{c_0^2}\alpha(\vec{r'})P(\vec{r'},\omega)d\vec{r'}\\ &\quad +A(\omega)G_0^+(\vec{r},\vec{r}_s,\omega).\end{aligned} \tag{4}$$

The first term on the right hand side of Equation 4 is the source that generates the difference between the total wavefield P and the reference wavefield P_0, where $P_0=A(\omega)G_0$.

On the other hand, from Green's second identity, plugging P and G_0 in Equation 2 and Equation 3 in, we have,

$$\begin{aligned}&\int_V(P\nabla'^2G_0-G_0\nabla'^2P)d\vec{r'}\\ =&\int_V\left(P(\vec{r'},\vec{r}_s,\omega)\left[-\frac{\omega^2}{c_0^2}G_0(\vec{r'},\vec{r},\omega)+\delta(\vec{r}-\vec{r'})\right]\right.\\ &\left.-G_0(\vec{r'},\vec{r},\omega)\left[-\frac{\omega^2}{c_0^2}P(\vec{r'},\vec{r}_s,\omega)+\rho(\vec{r'})\right]\right)d\vec{r'}\\ =&\int_V P(\vec{r'},\vec{r}_s,\omega)\delta(\vec{r}-\vec{r'})d\vec{r'}\\ -&\int_V G_0(\vec{r'},\vec{r},\omega)\left[\frac{\omega^2}{c_0^2}\alpha(\vec{r'})P(\vec{r'},\vec{r}_s,\omega)+\delta(\vec{r'}-\vec{r}_s)A(\omega)\right]d\vec{r'}\\ =&\oint_S d\vec{S}\hat{n}\cdot\\ &\left[P(\vec{r'},\vec{r}_s,\omega)\nabla'G_0(\vec{r'},\vec{r},\omega)-G_0(\vec{r'},\vec{r},\omega)\nabla'P(\vec{r'},\vec{r}_s,\omega)\right]\end{aligned} \tag{5}$$

When choosing the volume as the infinite space below the measurement surface, and $\vec{r}$ is chosen to be below the measurement surface (inside the volume V), as shown in Figure 1. Equation 5 becomes

$$\begin{aligned}P(\vec{r},\vec{r}_s,\omega) &= \int_V G_0(\vec{r},\vec{r'},\omega)\frac{\omega^2}{c_0^2}\alpha(\vec{r'})P(\vec{r'},\vec{r}_s,\omega)d\vec{r'}\\ &\quad +\oint_S\left[P\nabla'G_0-G_0\nabla'P\right]\cdot\hat{n}dS.\end{aligned} \tag{6}$$

Choosing G_0^+ in Equation 6, let's compare Equation 6 and Equation 4. When the support of perturbation $\alpha(\vec{r})$ is within the volume V, the integral of α over infinity equals integral over volume V. Thus, with $\vec{r}$ inside the volume, the support of α within the volume, both Equations 6 and 4 should give the same wavefield. Therefore,

$$\begin{aligned}&A(\omega)G_0^+(\vec{r},\vec{r}_s,\omega)\\ =&\oint_S d\vec{S}\hat{n}\cdot\\ &\left[P(\vec{r'},\vec{r}_s,\omega)\nabla'G_0^+(\vec{r'},\vec{r},\omega)-G_0^+(\vec{r'},\vec{r},\omega)\nabla'P(\vec{r'},\vec{r}_s,\omega)\right].\end{aligned} \tag{7}$$

So source signature $A(\omega)$ can be estimated by a surface integral and then divided by the Green's function. Using Sommerfeld's radiation condition for G_0^+, the wavefield contribution at $\vec{r}$ in V from the infinite far away boundary vanishes. Then,

$$\begin{aligned}A(\omega) &= \frac{1}{G_0^+(\vec{r},\vec{r}_s,\omega)}\cdot\int_{m.s.}d\vec{S}\hat{n}\cdot\\ &\left[P(\vec{r'},\vec{r}_s,\omega)\nabla'G_0^+(\vec{r'},\vec{r},\omega)-G_0^+(\vec{r'},\vec{r},\omega)\nabla'P(\vec{r'},\vec{r}_s,\omega)\right].\end{aligned} \tag{8}$$

From Equation 8, we can see that the wavelet $A(\omega)$ is independent of the observation point $\vec{r}$. The estimation result of source wavelet should stay the same at any observation point $\vec{r}$ below the measurement surface . This condition will only hold when using the correct reference velocity. Therefore, the invariance of the estimated wavelet can be a criterion of having the correct reference velocity. Later, we will present test result to support this conclusion.

Radiation pattern

In the previous section, we focused on solving the wavelet from a point source at $\delta(\vec{r}-\vec{r}_s)$. In a more general case, a extended source array that consists of several point source could be used in seismic exploration. In this case, the source displays a radiation pattern in different radiation angles. The radiation pattern from a single effective point source could be estimated by assuming that $A(\omega)$ is a function of the radiation angle θ (using far field approximation).

Assume that a general extended source $\rho(\vec{r})$ as Figure 2 shows. Wavefield at $\vec{r}$ generated from this source array can be calculated from the integral,

$$P_0(\vec{r},\omega)=\int G_0(\vec{r},\vec{r'},\omega)\rho(\vec{r'})d\vec{r'}. \tag{9}$$

In 3D propagation, Green's function in frequency domain can be written as

$$G_0(\vec{r},\vec{r'},\omega) = \frac{e^{ik|\vec{r}-\vec{r'}|}}{|\vec{r}-\vec{r'}|}. \quad (10)$$

In the far field, $|\vec{r}| >> |\vec{r'}|$, we have approximation,

$$\begin{aligned} |\vec{r}-\vec{r'}| &= \sqrt{(\vec{r}-\vec{r'})^2} \\ &= \sqrt{r^2 - 2\vec{r}\cdot\vec{r'} + r'^2} \\ &= r[1 - \frac{2\vec{r}\cdot\vec{r'}}{r^2} + \frac{r'^2}{r^2}]^{1/2} \\ &= r(1 - \frac{\vec{r}\cdot\vec{r'}}{r^2} + \frac{r'^2}{2r^2} + ...) \\ &= r - \hat{n}\cdot\vec{r'} + O(\frac{1}{r}). \end{aligned} \quad (11)$$

The above equation uses Taylor series $(1+x)^{1/2} = 1 + \frac{1}{2}x + O(x^2)$, and $\hat{n}$ is the unit vector in the direction of $\vec{r}$. And similarly,

$$\frac{1}{|\vec{r}-\vec{r'}|} = \frac{1}{r} + \frac{\hat{n}\cdot\vec{r'}}{r^2} + ... = \frac{1}{r} + O(\frac{1}{r^2}). \quad (12)$$

Then in the far field, Equation 9 becomes

$$\begin{aligned} P_0(\vec{r},\omega) &= \int \frac{e^{ik(r-\hat{n}\cdot\vec{r'})}}{r}\rho(\vec{r'})d\vec{r'} \\ &= \frac{e^{ikr}}{r}\int e^{-ik\hat{n}\cdot\vec{r'}}\rho(\vec{r'})d\vec{r'} \\ &= \frac{e^{ikr}}{r}\tilde{\rho}(k\hat{n}). \end{aligned} \quad (13)$$

Therefore, in the far field if we process seismic data generated from the source array as if a point source, we can get the source wavelet

$$A(\omega,\theta) = \frac{P_0}{G_0} = \tilde{\rho}(k\hat{n}).$$

Since $\hat{n}$ is the direction from the source to the observation point, the estimated wavelet result will display variances in different radiation angle. While in one radiation angle, wavelet $A(\omega,\theta)$ will be the same. This could be a criterion of determining the correct reference velocity. If using a wrong reference velocity, this invariance at one radiation angle will not be satisfied.

POINT SOURCE

In this test, we use Cagnidard-de Hoop method to model over-under cable data. Then using Green's theorem of Equation 8, we estimate the wavelet, $A(\omega)$, at different points at a fixed depth below the cable. We predict the estimated wavelet results using different reference velocities:

(1) correct reference velocity $c_0 = 1500m/s$;
(2) wrong reference velocity $c_0 = 1490m/s$;
(3) further wrong reference velocity $c_0 = 1450m/s$.

The estimated reference wavefields P_0 are shown in Figure 3, and corresponding wavelet results in Figure 4. Figure 3 indicates that the wrong reference velocities also lead to errors in the prediction of P_0. The estimated source wavelet results show that when using the correct reference velocity, the wavelet displays invariance at different offset, while wrong velocities give different wavelet prediction at different output points.

Therefore, only the correct reference velocity can result in the invariance of estimated wavelet. When the velocities are further from the reference velocity, the errors of wavelet invariance also becomes larger. This conclusion will also help us in finding the correct reference velocity.

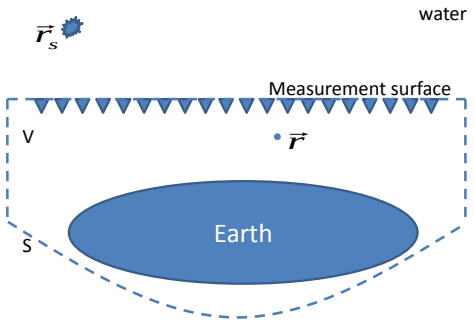

Figure 1: Volume chosen as half infinite space below the measurement surface.

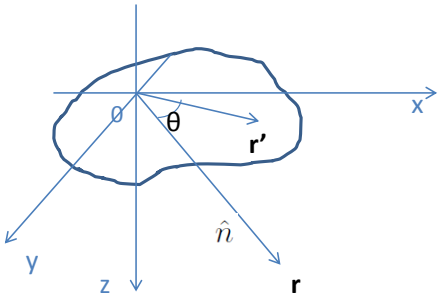

Figure 2: A general extended source.

SOURCE ARRAY

In this section, instead of a point source, data generated by a source array will be tested. The source array consists of 7 point sources separated at 3 m, as shown in Figure 5. First, we will estimate source wavelet along a horizontal cable, whose radiation angles are different. We predict source wavelet at depth 56 m, from offset 0 m to 606 m, whose radiation angles are from 0° to 85°. The results in Figure 5 show the radiation pattern in different offset (radiation angle). Next, we estimate the wavelet $A(\omega,\theta)$ in one radiation angle. The estimated wavelet in angle 5.8° using different velocities is shown in Figure 7.

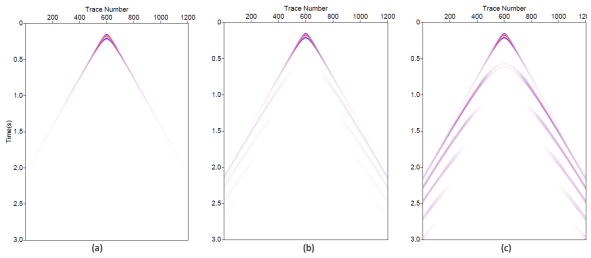

Figure 3: P_0 estimated using (a) correct $c_0 = 1500m/s$, (b) wrong $c_0 = 1490m/s$, (c) wrong $c_0 = 1450m/s$.

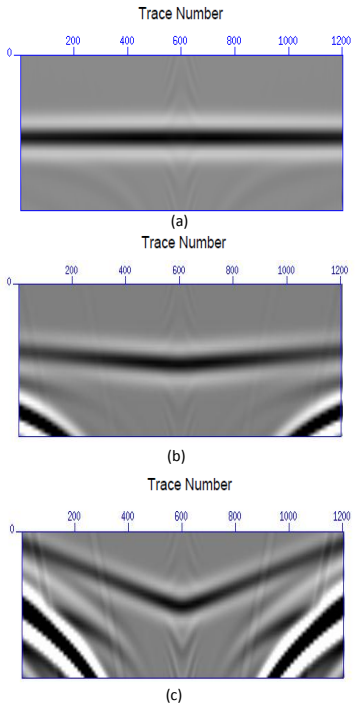

Figure 4: $A(t)$ estimated using (a) correct $c_0 = 1500m/s$, (b) wrong $c_0 = 1490m/s$, (c) wrong $c_0 = 1450m/s$

Similar to the conclusion above, we can see that only the correct velocity gives us the invariance of the source array wavelet in one angle, while the wrong reference velocity will lead to differences of the wavelet in one radiation angle.

CONCLUSIONS

We have shown that an output point invariance of the estimated wavelet using Green's theorem could be a criterion for determining the correct reference velocity. For a point source, the invariance occurs for the output point anywhere below the measurement surface, while for a source array, the invariance

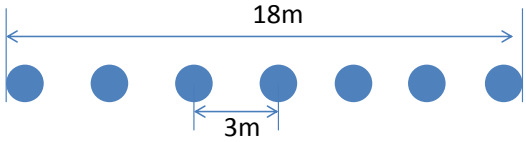

Figure 5: Source array

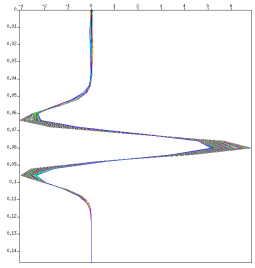

Figure 6: Radiation pattern of source array in Figure 5, estimated from offset 0m to 606m.

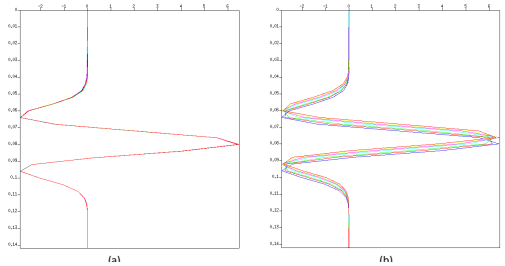

Figure 7: Wavelet estimated at depth 36m, 56m, 76m, 96m, 116m, 136m, 156m in the same radiation angle using (a) correct reference wave $c_0 = 1500m/s$ and (b) wrong reference velocity $c_0 = 1450m/s$.

is for output points along one radiation angle. Using marine seismic application as a starting point, this paper shows that invariances of Green's theorem-based wavelet estimation could be a criterion of determining the reference velocity. Using similar thinking, in the future study we will focus on solving the complex on-shore or ocean bottom near surface medium problems. For on-shore or ocean bottom problems, understanding of the near surface property could enable us to predict and remove the ground roll/reference wave on land, and thereby enhance the capability of subsequent multiple removal processing steps for the challenge of on-shore multiple attenuation.

ACKNOWLEDGEMENTS

We are grateful to all M-OSRP sponsors for encouragement and support in this research. We would like to thank Jinlong Yang and Chao Ma for reviewing this paper.

REFERENCES

Loveridge, M., G. Parks, L. Hatton, and M. Worthington, 1984, Effects of marine source array directivity on seismic data and source signature deconvlution: First Break, **2**, 16–22.

Mayhan, J., P. Terenghi, A. Weglein, and N. Chemingui, 2011, Green's theorem derived methods for preprocessing seismic data when the pressure p and its normal derivative are measured.: SEG Expanded Abstracts., 2722–2726.

Mayhan, J., and A. Weglein, 2013, First application of green's theorem-derived source and receiver deghosting on deep-water gulf of mexico synthetic (seam) and field data.: Geophysics, **78**, WA77–WA89.

Tang, L., J. Mayhan, J. Yang, and A. Weglein, 2013, Using green's theorem to satisfy data requirements of multiple removal methods: The impact of acquisition design.: SEG Expanded Abstracts., 4392–4396.

Weglein, A. B., F. V. Araújo, P. M. Carvalho, R. H. Stolt, K. H. Matson, R. T. Coates, D. Corrigan, D. J. Foster, S. A. Shaw, and H. Zhang, 2003, Inverse scattering series and seismic exploration: Inverse Problems, R27–R83.

Weglein, A. B., and B. G. Secrest, 1990, Wavelet estimation for a multidimensional acoustic earth model: Geophysics, **55**, 902–913.

Yang, J., J. Mayhan, L. Tang, and A. Weglein, 2013, Accommodating the source (and receiver) array in free-surface multiple elimination algorithm: Impact on interfering or proximal primaries and multiples.: SEG Expanded Abstracts., 4184–4189.

Zhang, J., 2007, Wave theory based data preparation for inverse scattering multiple removal, depth imaging and parameter estimation: analysis and numerical tests of green's theorem deghosting theory: PhD thesis, University of Houston.

Elastic Green's theorem preprocessing for on-shore internal multiple attenuation: theory and initial synthetic data tests

Jing Wu and Arthur B. Weglein, M-OSRP, University of Houston

SUMMARY

Prerequisites are important for the Inverse Scattering Series (ISS) multiple removal method, that assumes reference wave field has been removed and the source wavelet has been deconvolved. This paper derives the elastic Green's theorem reference wave prediction algorithm, which extends the off-shore acoustic to the on-shore elastic wave field separation, in preparation for on-shore ISS internal multiple attenuation.

INTRODUCTION

Weglein (2013) proposes a three-pronged strategy to respond to the current pressing challenges in removing multiples: (1) develop the ISS prerequisites for predicting the reference wave field and producing deghosted data that are direct and do not require subsurface information; (2) develop internal multiple elimination algorithms from the ISS; (3) develop a replacement for the energy-minimization criteria for adaptive subtraction. For part (1), Green's theorem preprocessing has documented effectiveness for off-shore plays (e.g., Weglein et al., 2002; Zhang, 2007; Mayhan et al., 2012; Mayhan and Weglein, 2013; Tang et al., 2013; Yang et al., 2013).

For on-shore plays, because of their complex structures with lateral variation, as well as significant ground roll, there are more fundamental issues and challenges for resolving the near surface problem. Among these issues and challenges, identification and removal of the reference wave is one pressing and essential topic. Scattering theory separates the real world into two parts: the reference medium, whose property is known, plus a perturbation. The wave that travels in the reference medium is called the reference wave, which does not experience the earth that we are interested in (Weglein et al., 2003; Tang and Weglein, 2014). Especially for on-shore, the ground roll as the main energy of the reference wave can obscure the reflections. In addition, the reference wave contains the source signature information, which is important and will be used for deconvolution before the subsequent ISS multiple removal. Therefore, it's an important step to identify and remove the reference wave field on land.

Matson (1997) provides the ISS free surface multiple elimination and internal multiple attenuation algorithms in PS space, i.e., by using potentials, rather than displacements. He assumes the reference wave has been removed by using linear mute; however, the linear mute may harm/destroy useful information, especially when the reference wave and the scattering wave are seriously interfering with each other. Weglein and Secrest (1990) propose the reference wave prediction method for the elastic media based on Green's theorem, and derive the wavelet estimation algorithm in displacement space. When the medium is assumed to consist of a homogeneous elastic whole space, Jiang et al. (2013) test the algorithm.

In order to simulate the land acquisition situation, we choose two homogeneous half spaces as the reference medium, an acoustic half-space over an elastic half-space. We locate the source in the acoustic medium and receivers in the elastic medium. The perturbation will be in the lower elastic half-space. By using Green's second identity, we derive the algorithm to separate the reference wave and scattering wave in PS space. In this paper, the algorithms are derived in both the space-frequency domain and the wavenumber-frequency domain. The wavelet can be estimated from the predicted reference wave. Numerical tests are shown to evaluate the accuracy of the algorithm for predicting the source wavelet for this acoustic over elastic half-space problem, that models the on-shore play acquisition. The results are positive and encouraging.

BACKGROUND FOR 2D ELASTIC MEDIUM

We are deriving the wave field separation method for on-shore application and we start with the elastic formulation. For convenience, the basis is changed from $\mathbf{u}=\begin{pmatrix} u_x \\ u_z \end{pmatrix}$ to $\Phi=\begin{pmatrix} \phi^P \\ \phi^S \end{pmatrix}$. $\mathbf{u}$ has x and z components; whereas Φ has potential components for P wave and S wave.

In PS space, the basic wave equations (Weglein and Stolt, 1995; Zhang, 2006) are

$$\hat{L}\Phi=\mathbf{F}, \tag{1}$$

$$\hat{L}\hat{G}=\delta, \tag{2}$$

$$\hat{L}_0\Phi_0=\mathbf{F}, \tag{3}$$

$$\hat{L}_0\hat{G}_0=\delta, \tag{4}$$

where $\hat{L}$ and $\hat{L}_0$ are the differential operators that describe the wave propagation in the actual and the reference media, respectively. $\mathbf{F}$ is the source term. $\hat{G}$ and $\hat{G}_0$ are the corresponding Green's function operators for the actual and reference media.

For a homogeneous medium,

$$\hat{L}_0=\begin{pmatrix} \bigtriangledown^2+\frac{\omega^2}{\alpha_0^2} & \\ & \bigtriangledown^2+\frac{\omega^2}{\beta_0^2} \end{pmatrix}=\begin{pmatrix} \hat{L}_0^P & \\ & \hat{L}_0^S \end{pmatrix}, \tag{5}$$

and

$$\hat{G}_0=\begin{pmatrix} \hat{G}_0^P & \\ & \hat{G}_0^S \end{pmatrix}. \tag{6}$$

Equations 5 and 6 are diagonal. However, in an actual inhomogeneous medium, $\hat{G}$ is no longer a diagonal matrix, but has a form

$$\hat{G}=\begin{pmatrix} \hat{G}^{PP} & \hat{G}^{PS} \\ \hat{G}^{SP} & \hat{G}^{SS} \end{pmatrix}. \tag{7}$$

For the superscripts, the right one represents the wave type of source side, whereas the left one represents the wave type of receiver side.

GREEN'S THEOREM WAVE FIELD SEPARATION ALGORITHM IN PS SPACE

Problem Description

Transforming the elastic wave equations from the displacement space to the PS space, we have

$$\hat{L}\Phi = \mathbf{F},$$
$$\hat{L}_0\hat{G}_0 = \delta,$$
$$\hat{L} = \hat{L}_0 - \hat{V}. \tag{8}$$

The basic form of these equations is the same as in the acoustic case. Based on the successful applications of Green's theorem wave field separation in the acoustic case (e.g., Zhang, 2007; Mayhan et al., 2012), it's feasible to apply Green's theorem wave field separation algorithm to the elastic medium in a similar way. The reference medium ($\hat{L}_0$) can be chosen for different objectives. To separate the reference and the scattering wave, the reference medium should be chosen equal to the actual medium above the measurement surface.

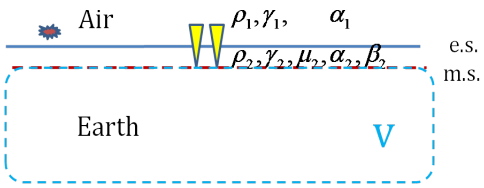

Figure 1: On-shore acquisition

For land acquisition, we assume that the source is located slightly above the earth's surface (e.s.), and the geophone is in the earth but close to the earth's surface shown as Fig.1. Actually, because of weathered layer and tundra, the property of near surface can be complicated, with lateral varying densities and velocities. For this initial study, we assume that the medium, which is below the earth's surface and above measurement surface (m.s.), is homogeneous. The reference wave can be predicted in any point inside the volume in Fig.1 by using Green's theorem.

Reference Wave Field Prediction in PS Space

In Fig.2, source ($\mathbf{r}_s$) is above the earth's surface, i.e., the boundary, receiver ($\mathbf{r}'$) is on the measurement surface, and the prediction location is represented by $\mathbf{r}$. The reference medium is chosen as a discontinuous two-half-space medium, above the boundary is homogeneous air, below is homogeneous elastic. A hemispherical surface integral upper bounded by the measurement surface will separate the total wave Φ into the reference wave Φ_0 and the scattering wave Φ_S. The prediction in the volume is the reference wave Φ_0 as shown in Fig.2.

The elastic Green's theorem algorithm in the space-frequency domain for the reference wave prediction in the volume is

$$\Phi_0(\mathbf{r},\mathbf{r}_s) = \oint \left(\Phi(\mathbf{r}',\mathbf{r}_s)\cdot\nabla'\hat{G}_0(\mathbf{r}',\mathbf{r}) - \nabla'\Phi(\mathbf{r}',\mathbf{r}_s)\cdot\hat{G}_0(\mathbf{r}',\mathbf{r})\right)\cdot\hat{n}dS', \tag{9}$$

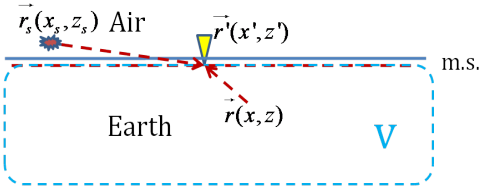

Figure 2: Volume enclosed (blue dashed line) for reference wave field prediction at $\mathbf{r}$ in the volume and $\mathbf{r}$ is under the measurement surface that is represented by $\mathbf{r}'$.

where $\Phi_0(\mathbf{r},\mathbf{r}_s) = \begin{pmatrix} \Phi_0^P(\mathbf{r},\mathbf{r}_s) \\ \Phi_0^S(\mathbf{r},\mathbf{r}_s) \end{pmatrix}$, $\Phi(\mathbf{r},\mathbf{r}_s) = \begin{pmatrix} \Phi^P(\mathbf{r},\mathbf{r}_s) \\ \Phi^S(\mathbf{r},\mathbf{r}_s) \end{pmatrix}$, and Green's function for the reference medium in the $(\mathbf{r},\omega)$ domain is

$$\begin{aligned}
&\hat{G}_0(\mathbf{r}',\mathbf{r}) \\
&= \begin{pmatrix} \hat{G}_0^P(\mathbf{r}',\mathbf{r}) + \hat{G}_0^{PP}(\mathbf{r}',\mathbf{r}) & \hat{G}_0^{PS}(\mathbf{r}',\mathbf{r}) \\ \hat{G}_0^{SP}(\mathbf{r}',\mathbf{r}) & \hat{G}_0^{S}(\mathbf{r}',\mathbf{r}) + \hat{G}_0^{SS}(\mathbf{r}',\mathbf{r}) \end{pmatrix} \\
&= \frac{1}{2\pi}\int e^{ik_x(x'-x)}dk_x \\
&\left(\begin{pmatrix} \frac{e^{iv_2|z'-z|}}{2iv_2} & 0 \\ 0 & \frac{e^{i\eta_2|z'-z|}}{2i\eta_2} \end{pmatrix} + \begin{pmatrix} \acute{P}\grave{P}\frac{e^{iv_2z}e^{iv_2z'}}{2iv_2} & \acute{S}\grave{P}\frac{e^{i\eta_2z}e^{iv_2z'}}{2i\eta_2} \\ \acute{P}\grave{S}\frac{e^{iv_2z}e^{i\eta_2z'}}{2iv_2} & \acute{S}\grave{S}\frac{e^{i\eta_2z}e^{i\eta_2z'}}{2i\eta_2} \end{pmatrix}\right)
\end{aligned}, \tag{10}$$

where $\acute{P}\grave{P}$, $\acute{P}\grave{S}$, $\acute{S}\grave{P}$, $\acute{S}\grave{S}$ represent the reflection coefficients along the boundary, respectively, and

$$v_2 = \begin{cases} \sqrt{k_{\alpha_2}^2 - k_x^2} & if \quad k_x < k_{\alpha_2} \\ i\sqrt{k_x^2 - k_{\alpha_2}^2} & if \quad k_x > k_{\alpha_2} \end{cases} \qquad k_{\alpha_2} = \frac{\omega}{\alpha_2} \quad ,$$

$$\eta_2 = \begin{cases} \sqrt{k_{\beta_2}^2 - k_x^2} & if \quad k_x < k_{\beta_2} \\ i\sqrt{k_x^2 - k_{\beta_2}^2} & if \quad k_x > k_{\beta_2} \end{cases} \qquad k_{\beta_2} = \frac{\omega}{\beta_2} \quad .$$

Since both Φ and $\hat{G}_0$ in the integral are tensors, the symbol $'\cdot'$ represents a tensor product.

If the measurement surface is horizontal, $\hat{n} = (0,-1)$, and it represents the outward normal vector directs upward. The algorithm can be simplified as:

$$\Phi_0(\mathbf{r},\mathbf{r}_s) = -\int \left(\Phi(\mathbf{r}',\mathbf{r}_s)\cdot\partial z'\hat{G}_0(\mathbf{r}',\mathbf{r}) - \partial z'\Phi(\mathbf{r}',\mathbf{r}_s)\cdot\hat{G}_0(\mathbf{r}',\mathbf{r})\right)dx'. \tag{11}$$

Using the reciprocity of Green's function and Fourier transforming over x, the algorithm in the wavenumber-frequency domain for the reference wave prediction in the volume can be obtained:

$$\tilde{\Phi}_0(k_x,z,\mathbf{r}_s) = -\tilde{\Phi}(k_x,z,\mathbf{r}_s)\cdot\partial z'\tilde{\hat{G}}_0^T(k_x,z,\mathbf{r}') + \partial z'\tilde{\Phi}(k_x,z,\mathbf{r}_s)\cdot\tilde{\hat{G}}_0^T(k_x,z,\mathbf{r}'), \tag{12}$$

where $\tilde{\hat{G}}_0^T$ is the transverse of $\tilde{\hat{G}}_0$.

With the separated reference wave from the total wave, the wavelet $A(\omega)$ can be estimated. Since

$$\begin{pmatrix} \Phi_0^P(\mathbf{r},\mathbf{r}_s,\omega) \\ \Phi_0^S(\mathbf{r},\mathbf{r}_s,\omega) \end{pmatrix} = \begin{pmatrix} A(\omega)\hat{G}_0^{PP}(\mathbf{r},\mathbf{r}_s,\omega) \\ A(\omega)\hat{G}_0^{SP}(\mathbf{r},\mathbf{r}_s,\omega) \end{pmatrix}, \tag{13}$$

$A(\omega)$ can be obtained by either

$$A(\omega) = \frac{\Phi_0^P(\mathbf{r},\mathbf{r}_s,\omega)}{\hat{G}_0^{PP}(\mathbf{r},\mathbf{r}_s,\omega)} \quad \text{or} \quad A(\omega) = \frac{\Phi_0^S(\mathbf{r},\mathbf{r}_s,\omega)}{\hat{G}_0^{SP}(\mathbf{r},\mathbf{r}_s,\omega)}, \tag{14}$$

where

$$\begin{aligned} \hat{G}_0^{PP}(\mathbf{r},\mathbf{r}_s,\omega) &= \frac{1}{2\pi}\int \grave{P}\grave{P}\frac{e^{-iv_1 z_s}e^{iv_2 z}}{2iv_1}e^{ik_x(x-x_s)}dk_x, \\ \hat{G}_0^{SP}(\mathbf{r},\mathbf{r}_s,\omega) &= \frac{1}{2\pi}\int \grave{P}\grave{S}\frac{e^{-iv_1 z_s}e^{i\eta_2 z}}{2iv_1}e^{ik_x(x-x_s)}dk_x, \end{aligned} \tag{15}$$

and $v_1 = \begin{cases} \sqrt{k_{\alpha_1}^2 - k_x^2} & if \quad k_x < k_{\alpha_1} \\ i\sqrt{k_x^2 - k_{\alpha_1}^2} & if \quad k_x > k_{\alpha_1} \end{cases} \qquad k_{\alpha_1} = \frac{\omega}{\alpha_1}$,

and $\grave{P}\grave{P}$, $\grave{P}\grave{S}$ represent the transmission coefficients along the boundary, respectively.

NUMERICAL EVALUATION

Since the methodology in this paper chooses the reference medium above the earth's surface to be acoustic, either fluid (water) or air can be chosen as the medium above the earth's surface. Those two cases would correspond to ocean bottom and on-shore applications, respectively. In this section, two models are chosen to evaluate Green's theorem wave field separation algorithm, one is water/elastic, and the other is air/elastic.

Water/Elastic Model

A water/elastic model is first selected to examine the accuracy of the algorithm. The parameters are listed in Table 1. The water/elastic boundary is at depth 0m, the source's depth is -5m, and the measurement's depth is 0m (on the boundary) but coupled with the lower elastic. The trace interval is 2m.

Layer Number	P Velocity (m/s)	S Velocity (m/s)	Density (kg/m^3)
1	1500	0	1000
2	2250	1200	2000

Table 1: The water/elastic model parameters

Since there is no perturbation from earth in this model, the reference medium is the same as the actual one. Therefore, if the prediction point in the elastic medium is close to depth 0m, the predicted reference wave should be the same as the total wave. This will serve as a criteria later to test the algorithm.

P wave is produced by source in the water, and transmitted P and S waves will be collected by the receivers in the elastic medium. The synthetic data are generated by multiplying a wavelet with the analytical forms of Green's function in the frequency domain (equation 13), shown in Fig.3(a) for PP and Fig.4(a) for SP. The most significant energy of the total wave is surface waves since source and receivers are very close to the boundary. The direct waves have relatively weaker energy.

The predicted reference P waves (PP0) and S waves (SP0) are listed in Fig.3(b) and Fig.4(b), respectively, and as anticipated are similar to the input data. Traces with offset 400m are extracted for further comparison, as shown in Fig.3(c) and Fig.4(c). The prediction results match well with input data, which confirm the effectiveness of our wave field separation algorithm.

After obtaining the reference wave, the wavelet can be estimated by using equation 14. The results of comparison between the actual wavelet (red line in Fig.3(d)) and the wavelet estimated from PP0 at offset 400m (blue line in Fig.3(d)), and the actual wavelet (red line in Fig.4(d)) and the wavelet estimated from SP0 at offset 400m (blue line in Fig.4(d)) further confirm the accuracy of the wavelet estimation algorithm.

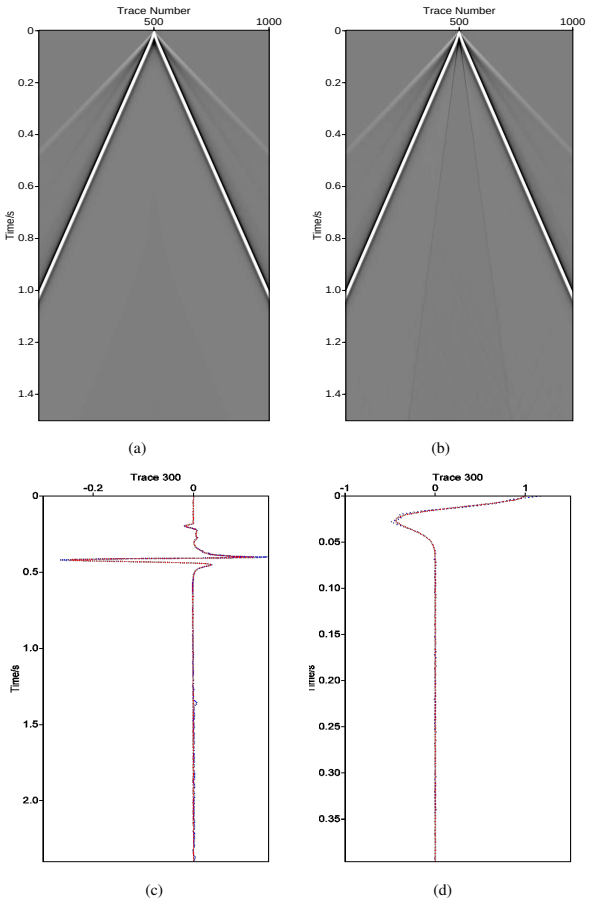

Figure 3: Numerical result for water/elastic model. (a): input data PP; (b): predicted reference wave PP0 at depth 0m; (c): traces with offset 400m, red line for PP, blue line for PP0; (d): actual wavelet (red line) and wavelet estimated from PP0 at offset 400m (blue line). Figures in (a) and (b) are in the same scale.

Air/Elastic Model

An air/elastic model is selected to examine the accuracy of the algorithm. The parameters are listed in Table 2. The depth of source is 0m, and we arrange the boundary as belonging to the upper half-space of air; whereas the depth of receiver is 5m and it is inside the elastic half-space. The prediction depth is chosen to be 25m. The result will confirm the theory that

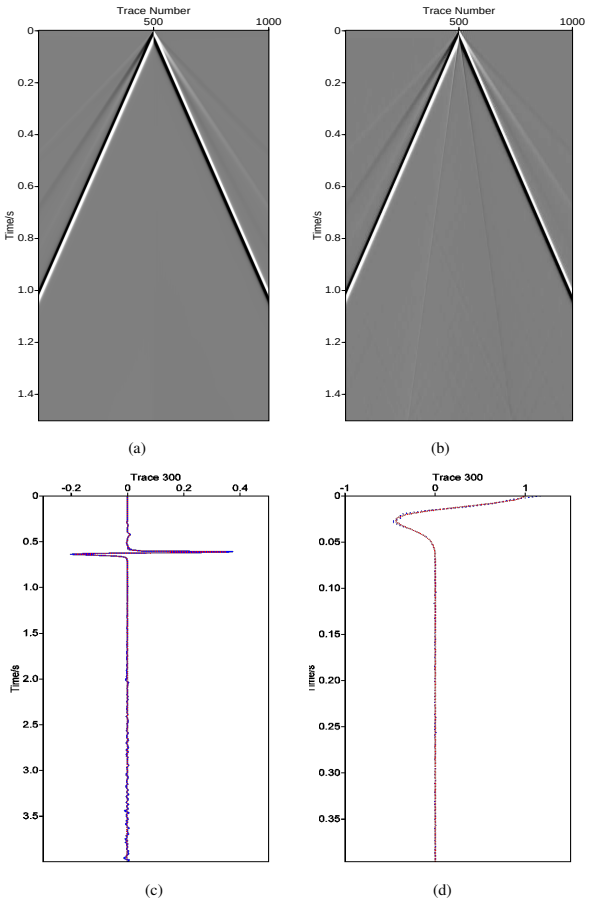

Figure 4: Numerical result for water/elastic model. (a): input data SP; (b): predicted reference wave SP0 at depth 0m; (c): traces with offset 400m, red line for SP, blue line for SP0; (d): actual wavelet (red line) and wavelet estimated from SP0 at offset 400m (blue line). Figures in (a) and (b) are in the same scale.

Green's theorem algorithm can predict the reference wave at any point in the volume, and the volume is upper bounded by the measurement surface. The trace interval is 2m.

Layer Number	P Velocity (m/s)	S Velocity (m/s)	Density (kg/m^3)
1	340	0	3
2	2250	1200	2000

Table 2: The air/elastic model parameters

The synthetic input data PP and SP are similarly generated as in the first case, as shown in Fig.5(a) and Fig.5(d). The predicted reference waves are shown in Fig.5(b) for PP0 and Fig.5(e) for SP0. In order to confirm the result, the analytical data (by multiplying the original wavelet with the analytical forms of Green's function in the frequency domain) for a receiver at depth 25m are also listed in Fig.5(c) and Fig.5(f).

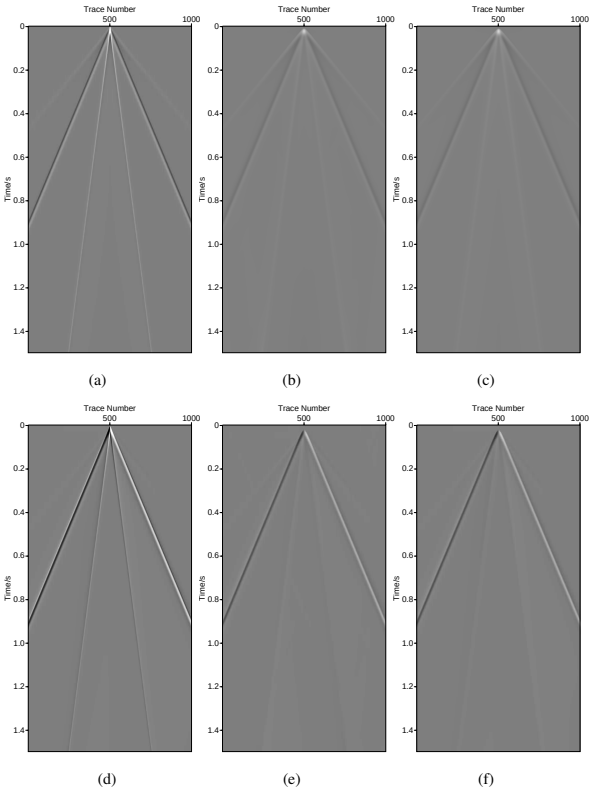

Figure 5: Numerical result for air/elastic model. (a): input data PP; (b): predicted reference wave PP0 at depth 25m; (c): analytical reference wave PP0 at depth 25m; (d): input data SP; (e): predicted reference wave SP0 at depth 25m; (f): analytical reference wave SP0 at depth 25m. All the figures are in the same scale.

CONCLUSION AND FUTURE PLAN

From the theoretical derivation and numerical tests in this paper, we understand that it's possible to apply the Green's theorem wave field separation algorithm on land. For on-shore application, the reference medium consists of two half spaces: one acoustic and the other elastic. This will provide a possible way to remove ground roll, which has the majority of the energy of the reference wave for on-shore acquisition. In order to apply Green's theorem to remove ground roll for practical complicated land acquisition data, a modified reference model and further research are required.

ACKNOWLEDGEMENTS

We are grateful to all M-OSRP sponsors for encouragement and support in this research.

REFERENCES

Jiang, T., P. Terenghi, and A. B. Weglein, 2013, Wavelet estimation and wavefield reconstruction in elastic media, without a subsurface model: Presented at the Mission-Oriented Seismic Research Program (M-OSRP) Annual Report.

Matson, K. H., 1997, An inverse-scattering series method for attenuating elastic multiples from multicomponent land and ocean bottom seismic data: PhD thesis, University of British Columbia.

Mayhan, J. D., P. Terenghi, A. B. Weglein, and C. Nizar, 2012, Green's theorem derived methods for preprocessing seismic data when the pressure P and its normal derivative are measured, *in* SEG Technical Program Expanded Abstracts: Soc. Expl. Geophys., 2722–2726.

Mayhan, J. D., and A. B. Weglein, 2013, First application of Greens theorem-derived source and receiver deghosting on deep-water Gulf of Mexico synthetic (SEAM) and field data, **78**, WA77WA89.

Tang, L., J. D. Mayhan, J. Yang, and A. B. Weglein, 2013, Using green's theorem to satisfy data requirements of multiple removal methods: The impact of acquisition design, *in* SEG Technical Program Expanded Abstracts: Soc. Expl. Geophys., 4392–4395.

Tang, L., and A. B. Weglein, 2014, Predicting reference medium properties from invariances in greens theorem reference wave prediction: towards an on-shore near surface medium and reference wave prediction, *in* SEG Technical Program Expanded Abstracts: Soc. Expl. Geophys., TBD.

Weglein, A. B., 2013, The multiple attenuation toolbox: Progress, challenges and open issues, *in* SEG Technical Program Expanded Abstracts: Soc. Expl. Geophys., 4493–4499.

Weglein, A. B., F. V. Araújo, P. M. Carvalho, R. H. Stolt, K. H. Matson, R. T. Coates, D. Corrigan, D. J. Foster, S. A. Shaw, and H. Zhang, 2003, Inverse scattering series and seismic exploration: Inverse Problems, R27–R83.

Weglein, A. B., and B. G. Secrest, 1990, Wavelet estimation for a multidimensional acoustic earth model: Geophysics, **55**, 902–913.

Weglein, A. B., S. A. Shaw, K. H. Matson, J. L. Sheiman, R. H. Solt, T. H. Tan, A. Osen, G. P. Correa, K. A. Innanen, Z. Guo, and J. Zhang, 2002, New approaches to deghosting towed-streamer and ocean-bottem pressure measurements: 72nd Annual International Meeting, SEG, Expanded Abstracts, 1016–1019.

Weglein, A. B., and R. H. Stolt, 1995, I. the wave physics of downward continuation, wavelet estimation and volume and surface scattering. ii. approaches to linear and nonlinear migration inversion: Mathematical Frontiers in Reflection Seismology: SEG/SIAM publication.

Yang, J., J. D. Mayhan, L. Tang, and A. B. Weglein, 2013, Accommodating the source (and receiver) array in free-surface multiple elimination algorithm: Impact on interfering or proximal primaries and multiples, *in* SEG Technical Program Expanded Abstracts: Soc. Expl. Geophys., 4184–4189.

Zhang, H., 2006, Direct non-linear acoustic and elastic inversion: Towards fundamentally new comprehensive and realistic target identification: PhD thesis, University of Houston.

Zhang, J., 2007, Wave theory based data preparation for inverse scattering multiple removal, depth imaging and parameter estimation: analysis and numerical tests of green's theorem deghosting theory: PhD thesis, University of Houston.

Incorporating the source wavelet and radiation pattern into the internal multiple attenuation algorithm

Jinlong Yang and Arthur B. Weglein, M-OSRP, University of Houston*

SUMMARY

The inverse scattering series internal multiple attenuation (ISS IMA) algorithm (Araújo et al., 1994; Weglein et al., 1997) is modified and extended by incorporating the source wavelet and radiation pattern in order to enhance the fidelity of the amplitude and phase predictions of the internal multiple. The modified ISS IMA algorithm is fully data-driven to predict all first-order internal multiples for all horizons at once, without requiring any subsurface information. In synthetic data tests, for data produced by a point source with a wavelet, the amplitude and shape of the predicted internal multiples are significantly improved by incorporating the source wavelet deconvolution. For data generated by a general source with a radiation pattern, the prediction is further improved by incorporating the source wavelet and radiation pattern into the algorithm. Therefore, the modified ISS IMA algorithm produces more accurate results when the data are generated by a frequency and angle dependent source.

INTRODUCTION

In seismic exploration, seismic reflection events are classified as primary or multiple, depending on whether the energy arriving at the receiver has experienced one or more upward reflections, respectively. Methods for seismic imaging and parameter estimation (inversion) assume that the data contain only primaries. Multiples are considered to be noise because they can interfere with primaries and/or be misinterpreted as primaries. Hence, multiple removal is a prerequisite to seismic imaging and inversion.

This abstract will focus on internal multiple attenuation and will analyze and test the impact of incorporating the source wavelet and radiation pattern on internal multiple prediction. The ISS IMA algorithm was first proposed by Araújo et al. (1994) and Weglein et al. (1997). It is a fully data-driven and model-type independent algorithm (Weglein et al., 2003), and it predicts the correct traveltimes and approximate amplitudes of all internal multiples at all depths at once. Matson et al. (1999) extended the theory for land and OBC applications. Ramírez and Weglein (2005) discussed how to extend the ISS IMA algorithm from attenuation toward elimination of multiples. Herrera and Weglein (2013) developed the 1-D ISS internal multiple elimination algorithm for internal multiple generated by a single shallowest reflector and Zou and Weglein (2013) further derived a general form of the ISS internal multiple elimination algorithm.

The ISS IMA algorithm has certain data requirements: (1) removal of the reference wavefield, (2) an estimation of the source wavelet and radiation pattern, (3) source and receiver deghosting, and (4) removal of the free-surface multiples. The first three requirements can be obtained by Green's theorem methods (Zhang and Weglein, 2005; Mayhan et al., 2012; Tang et al., 2013) and the free-surface multiples can be removed by the ISS free-surface multiple elimination algorithm (Carvalho, 1992; Weglein et al., 2003; Yang et al., 2013). Green's theorem methods and the ISS free-surface multiple elimination algorithm are consistent with the ISS IMA algorithm, since all are multidimensional wave-theoretic preprocessing methods and do not require subsurface information.

The ISS IMA algorithm assumes that the input data are spike wave. In other words, the input data have been deconvolved. If the input data are generated by a source wavelet instead of by a spike wave, the predicted internal multiple has convolved at least three source wavelets. Hence, the source wavelet has a significant effect on the amplitude and shape of the predicted internal multiple. In this paper, to improve the amplitude and the shape of a predicted internal multiple, the ISS IMA algorithm is extended to accommodate a source wavelet.

In addition, the ISS IMA algorithm assumes an isotropic point source, i.e., it assumes that the source has no variation of amplitude or phase with take-off angle. A large marine air-gun array will exhibit directivity and produce variations of the source signature (Loveridge et al., 1984). In on-shore exploration, even if there is no source array, the source can have radiation pattern or directivity. That directivity has significant effects on multiple removal or attenuation and AVO analysis. In seismic data processing, it is important that we characterize the source array's effect on any seismic processing methods. Therefore, to further improve the effectiveness of the ISS IMA algorithm, it is extended to accommodate a source wavelet and radiation pattern. The synthetic data tests show that accommodating the source wavelet and radiation pattern can enhance the fidelity of the amplitude and phase predictions of internal multiples.

THEORY

The ISS IMA algorithm (Araújo, 1994; Weglein et al., 1997, 2003) for first-order internal multiple prediction in a 2D earth is given by

$$\begin{aligned} b_3(k_g,k_s,\omega) &= \frac{1}{(2\pi)^2}\int_{-\infty}^{\infty}\int_{-\infty}^{\infty} dk_1 e^{-iq_1(z_g-z_s)} dk_2 e^{iq_2(z_g-z_s)} \\ &\times \int_{-\infty}^{\infty} dz_1 b_1(k_g,k_1,z_1) e^{i(q_g+q_1)z_1} \\ &\times \int_{-\infty}^{z_1-\varepsilon} dz_2 b_1(k_1,k_2,z_2) e^{-i(q_1+q_2)z_2} \\ &\times \int_{z_2+\varepsilon}^{\infty} dz_3 b_1(k_2,k_s,z_3) e^{i(q_2+q_s)z_3}, \end{aligned} \tag{1}$$

where ω, k_s and k_g are temporal frequency and the horizontal wavenumbers for source and receiver coordinates, respectively. q_s and q_g are the corresponding vertical source and re-

ceiver wavenumbers, respectively. $q_i = sgn(\omega)\sqrt{\omega^2/c_0^2 - k_i^2}$ for $i = (g,s)$; c_0 is the reference velocity. z_s and z_g are the source and receiver depths; and z_i ($i = 1,2,3$) represents pseudodepth (vertical depth of the water speed migration). The parameter ε is introduced to insure that the relations $z_1 > z_2$ and $z_3 > z_2$ are satisfied.

From the first-order equation of the inverse scattering series $D = G_0^d V_1 P_0^d$ (Weglein et al., 2003), which can be represented explicitly in 2-D case as

$$D(x_g,\varepsilon_g,x_s,\varepsilon_s,\omega) = \int dx_1 \int dz_1 \int dx_2 \int dz_2 \; G_0^d(x_g,\varepsilon_g,x_1,z_1,\omega) V_1(x_1,z_1,x_2,z_2,\omega) P_0^d(x_2,z_2,x_s,\varepsilon_s,\omega), \quad (2)$$

where the data D have been deghosted and the reference wavefield and free-surface multiples have been removed. G_0^d and P_0^d are the direct reference Green's function and the direct reference wavefield, respectively.

For a unit source, $P_0^d = G_0^d$. We take a Fourier transform over x_s and x_g on both sides of equation 2 and define b_1 as

$$b_1(k_g,k_s,q_g+q_s) \equiv \frac{V_1(k_g,q_g,k_s,q_s,\omega)}{-2iq_g} = -2iq_s D(k_g,k_s,\omega), \quad (3)$$

where b_1 represents effective plane-wave incident data and $D(k_g,k_s,\omega)$ is the Fourier-transformed prestack data. The input b_1 are introduced into equation 1 after an uncollapsed Stolt migration (Weglein et al., 1997) that takes $b_1(k_g,k_s,q_g+q_s)$ into the pseudodepth domain, $b_1(k_g,k_s,z_i)$, by using the reference velocity, c_0. Then, the first-order internal multiples $D_3(k_g,k_s,\omega)$, which are predicted by the ISS IMA algorithm (equation 1), are obtained by

$$D_3(k_g,k_s,\omega) = (-2iq_s)^{-1} b_3(k_g,k_s,q_g+q_s). \quad (4)$$

For an isotropic point source, $P_0^d = A(\omega)G_0^d$. Fourier transforming over x_s and x_g on both sides of equation 2 gives

$$b_1(k_g,k_s,q_g+q_s) = -2iq_s D(k_g,k_s,\omega)/A(\omega), \quad (5)$$

where $A(\omega)$ is the source signature. After b_3 has been predicted by equation 1, the first-order internal multiple is achieved by convolving the source wavelet $A(\omega)$ back

$$D_3(k_g,k_s,\omega) = (-2iq_s)^{-1} A(\omega) b_3(k_g,k_s,q_g+q_s). \quad (6)$$

For a general source with a radiation pattern (e.g., a source array), the direct reference wavefield P_0^d for a 2D case can be expressed as an integral of the direct reference Green's function G_0^d over all air-guns in an array,

$$P_0^d(x,z,x_s,z_s,\omega) = \int dx' dz' \rho(x',z',\omega) G_0^d(x,z,x'+x_s,z'+z_s,\omega), \quad (7)$$

where (x,z) and (x_s,z_s) are the prediction point and source point, respectively. (x',z') is the distribution of the source with respect to the source locator (x_s,z_s). Using the bilinear form of Green's function and Fourier transforming over x, we obtain the relationship between ρ and P_0^d as

$$P_0^d(k,z,x_s,z_s,\omega) = \rho(k,q,\omega)\frac{e^{iq|z-z_s|}}{2iq} e^{ikx}. \quad (8)$$

On the other hand, the reference wavefield P_0^d can be solved from the measured data by using Green's theorem method (Weglein and Secrest, 1990).

Since $k^2 + q^2 = \omega^2/c_0^2$, q is not a free variable, hence, we can not obtain $\rho(x,z,\omega)$ in space-frequency domain by taking an inverse Fourier transform on $\rho(k,q,\omega)$. However, the projection of the source signature $\rho(k,q,\omega)$ can be achieved directly from the direct reference wavefield P_0^d in the f-k domain, where the variable k or q represent the amplitude variations of the source signature with angles.

Substituting the projection of the source signature ρ into equation 2 and Fourier transforming over x_s and x_g gives

$$b_1(k_g,k_s,q_g+q_s) = -2iq_s D(k_g,k_s,\omega)/\rho(k_g,q_g,\omega). \quad (9)$$

Further details of obtaining ρ can be found in Yang et al. (2013) and Yang and Weglein (2013). The first-order internal multiple is calculated from b_3,

$$D_3(k_g,k_s,\omega) = (-2iq_s)^{-1}\rho(k_g,q_g,\omega) b_3(k_g,k_s,q_g+q_s). \quad (10)$$

All above derivations are 2D cases, and they can be directly extended to 3D. From the derivations, we can see that the kernel of the ISS IMA algorithm (equation 1) is not change and the source wavelet and radiation pattern are imported by equations 5 and 9. The predicted internal multiples D_3 are also affected by the source wavelet and radiation pattern in equations 6 and 10. If the source wavelet is not incorporated into the ISS IMA algorithm, the amplitudes and shapes of the predicted internal multiples are not comparable with those of the internal multiples in the input data. To improve the effectiveness of the internal multiple prediction, the ISS IMA algorithm should be modified for its input and output by accommodating the source wavelet and radiation pattern. This accommodation can enhance the fidelity of the amplitude and shape of the predictions of internal multiples.

NUMERICAL TESTS

In this section, we will present the numerical tests of the internal multiple prediction for the data generated by a point source and a general source with a radiation pattern. The numerical tests are based on a $1D$ acoustic model with varying velocity and constant density, as shown in Figure 1. The synthetic data that are generated by the finite-difference method. The data have one shot gather with 2001 traces, and each trace has 301 time samples, with $dt = 5ms$. The trace interval is $5m$.

The source wavelet effect on internal multiple prediction

For the data generated by a point source, the internal multiple will be predicted by using the ISS IMA algorithm with and without source wavelet deconvolution. Figure 2 shows the input data and their corresponding predicted internal multiples. They are plotted using the same scale. In the input data, the first two strongest events are the primaries, and the other events are internal multiples. Figures 2(b) and 2(c) show the predicted internal multiples using the ISS IMA algorithm with and without source wavelet deconvolution. From Figures 2(b) and 2(c),

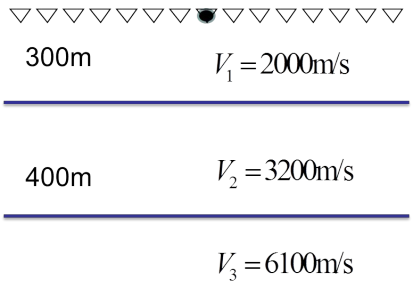

Figure 1: One-dimensional acoustic constant-density medium.

we can see that both algorithms predict the correct traveltimes, but they predict different amplitudes and shapes for the internal multiples. In Figure 2(b), the amplitude of the predicted internal multiple is comparable with the internal multiple in the input data, while the amplitude is totally different from that of the internal multiple in the input data in Figure 2(c).

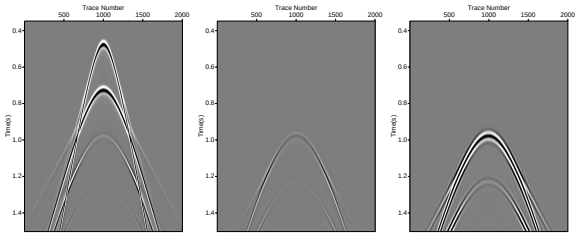

Figure 2: (a) The input data; (b) and (c) The internal multiples predicted by the ISS IMA algorithm with and without source wavelet deconvolution, respectively.

To see the details, we pick the middle trace (offset $= 0$) and the far trace (offset $= 1700m$) from each image in Figure 2. The time windows are chosen at $0.85s \sim 1.10s$ for the middle trace and at $1.05s \sim 1.25s$ for the far trace, as shown in Figure 3. For the middle trace, it can be seen that the shape of the internal multiple predicted by the ISS IMA algorithm without source wavelet deconvolution (Figure 3(c)) is totally different from that of the true internal multiple (Figure 3(a)). The predicted and true amplitudes are not comparable, either. This is because the predicted internal multiples convolve three wavelets. However, comparing Figure 3(b) with Figure 3(a), we can see that the amplitude and shape of the internal multiple predicted by the ISS IMA algorithm with source wavelet deconvolution are similar to those of the true internal multiple, as shown in Figure 4(a). It demonstrates that by accommodating the source wavelet deconvolution, the amplitude and shape of the predicted internal multiple are significantly improved for the internal multiple prediction. For the far-offset traces, we obtain the similar results, as shown in Figures 3(e) and 4(b).

From the numerical test, we conclude that by incorporating the source wavelet deconvolution, the ISS IMA algorithm produces more accurate and encouraging results for both zero offset and far offset. The predicted internal multiple has the correct traveltime, and the amplitude and shape are significantly improved. In addition, Liang et al. (2013) also discussed the source wavelet effect on the internal multiple prediction for the 1D normal incident model.

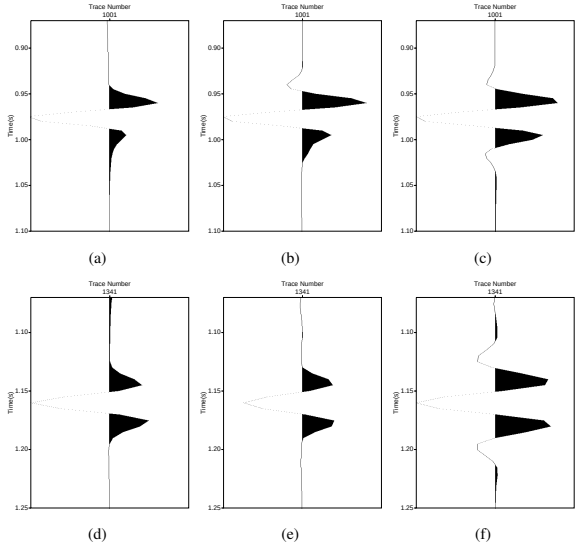

Figure 3: (a), (b), (c) The middle traces, and (d), (e), (f) the far traces, picked from the input data and the internal multiples predicted by the ISS IMA algorithm with and without source wavelet deconvolution.

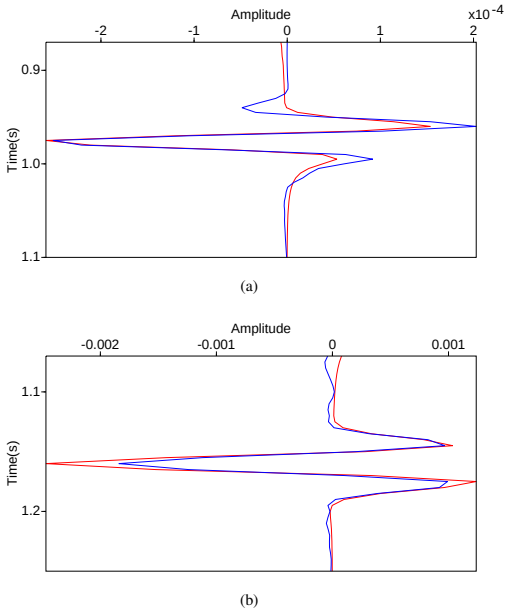

Figure 4: The comparison between the internal multiple (red) in the input data and the internal multiple (blue) predicted by the ISS IMA algorithm with source wavelet deconvolution at (a) zero offset and at (b) far offset ($1700m$).

The radiation pattern effect on internal multiple prediction

For the data generated by a general source with a radiation pattern (e.g., source array), we will predict the internal multiple using the ISS IMA algorithm with and without incorporating the source wavelet and radiation pattern. Here, the synthetic data are generated by a source array using the same model as Figure 1. The source array contains five point sources in one line with $20m$ range. Here, we assume that the source array only varies laterally with identical source signatures, but the assumption is not necessary in the ISS IMA algorithm.

Figure 5(a) shows the input data generated by the source array. Similar with the data generated by the point source, the first two strongest events are the primaries, and the other events are internal multiples. Figures 5(b) and 5(c) present the internal multiples predicted by using the ISS IMA algorithm with and without incorporating the source wavelet and radiation pattern. From Figures 5(b) and 5(c), we can see that both algorithms can predict the correct traveltime and an acceptable amplitude of the internal multiple.

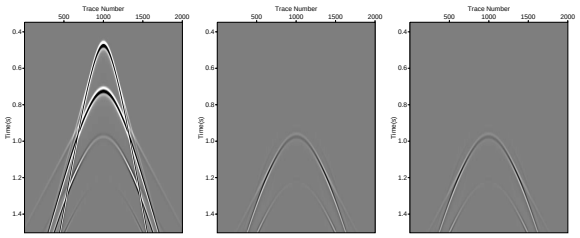

(a) (b) (c)

Figure 5: (a) The input data; (b) and (c) the internal multiples predicted by the ISS IMA algorithm with and without incorporating the source wavelet and radiation pattern.

To compare the internal multiple predictions in detail, the middle trace (offset $= 0$) and the far trace (offset $= 1700m$) are picked from each image in Figure 5. We choose the time windows at $0.85s \sim 1.10s$ for the middle trace and at $1.05s \sim 1.25s$ for the far trace, as shown in Figure 6. Comparing the middle and far traces, we can see that the amplitude and shape of the internal multiple predicted by the ISS IMA algorithm with and without incorporating the radiation pattern are very similar to those for the true internal multiple in the input data. Their comparisons are plotted in Figure 7. At zero offset, there are no visible differences, as shown in Figure 7(a), while at far offset, Figure 7(b) demonstrates that the amplitude of the internal multiple prediction is further improved by accommodating the radiation pattern. Therefore, for the general source data, the modified ISS IMA algorithm that incorporates the source wavelet and radiation pattern can enhance the accuracy and effectiveness of the amplitude prediction of the internal multiple.

CONCLUSIONS

The ISS IMA algorithm is modified and extended by accommodating the source wavelet and radiation pattern, which can be provided by the prerequisite. The ISS IMA modified algorithm enhances the fidelity of amplitude and phase predictions of the internal multiple. It retains all the merits of the original algorithm that is fully data-driven and does not require any subsurface information. In synthetic data tests, for data generated by a point source with a wavelet, the predictions of the amplitudes and shapes of internal multiples are significantly improved by incorporating the source wavelet deconvolution. For data generated by a general source with a radiation pattern, the prediction is further improved by incorporating the source wavelet and radiation pattern into the ISS IMA algorithm. We expect this extended ISS IMA algorithm to be relevant and useful for on-shore application, as well.

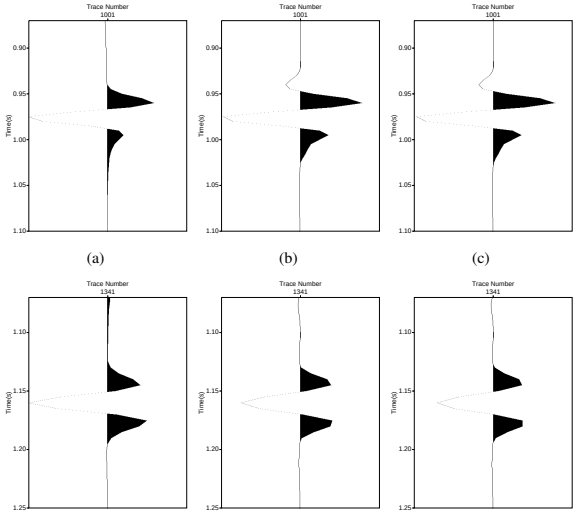

(a) (b) (c)

(d) (e) (f)

Figure 6: (a), (b), (c) The middle traces, and (d), (e), (f) the far traces, picked from the input data and the internal multiples predicted by the ISS IMA algorithm with and without incorporating the source wavelet and radiation pattern.

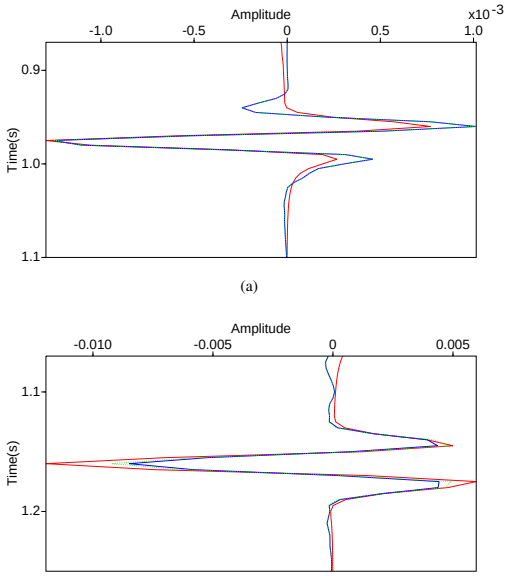

(a)

(b)

Figure 7: The comparison between the true internal multiple (red) in the input data and the internal multiple predicted by the ISS IMA algorithm with (green dash) and without (blue) incorporating the source wavelet and radiation pattern at (a) zero offset and at (b) far offset ($1700m$).

ACKNOWLEDGMENTS

We are grateful to all M-OSRP sponsors for their encouragement and support of this research.

REFERENCES

Araújo, F. V., 1994, Linear and non-linear methods derived from scattering theory: backscattered tomography and internal multiple attenuation: PhD thesis, Universidade Federal da Bahia.

Araújo, F. V., A. B. Weglein, P. M. Carvalho, and R. H. Stolt, 1994, Inverse scattering series for multiple attenuation: An example with surface and internal multiples: 64th Annual International Meeting, SEG, Expanded Abstracts, 1039–1042.

Carvalho, P. M., 1992, Free-surface multiple reflection elimination method based on nonlinear inversion of seismic data: PhD thesis, Universidade Federal da Bahia.

Herrera, W., and A. B. Weglein, 2013, Eliminating first-order internal multiples with downward reflection at the shallowest interface: Theory and initial examples: 83rd International Annual Meeting, SEG, Expanded Abstracts, 4131–4135.

Liang, H., C. Ma, and A. B. Weglein, 2013, General theory for accommodating primaries and multiples in internal multiple algorithm: Analysis and numerical tests: 83rd International Annual Meeting, SEG, Expanded Abstracts, 4178–4183.

Loveridge, M. M., G. E. Parkes, L. Hatton, and M. H. Worthington, 1984, Effects of marine source array directivity on seismic data and source signature deconvolution: First Break, **2**, 16–22.

Matson, K. H., D. C. Corrigan, A. B. Weglein, C. Y. Young, and P. M. Carvalho, 1999, Inverse scattering internal multiple attenuation: results from complex synthetic and field data examples: 69th Annual International Meeting, SEG, Expanded Abstracts, 1060–1063.

Mayhan, J. D., A. B. Weglein, and P. Terenghi, 2012, First application of Green's theorem derived source and receiver deghosting on deep water Gulf of Mexico synthetic (SEAM) and field data: 82nd Annual International Meeting, SEG, Expanded Abstracts, 1–5.

Ramírez, A. C., and A. Weglein, 2005, An inverse scattering internal multiple elimination method: Beyond attenuation, a new algorithm and initial tests: 75th International Annual Meeting, SEG, Expanded Abstracts, 2115–2118.

Tang, L., J. D. Mayhan, J. Yang, and A. B. Weglein, 2013, Using green's theorem to satisfy data requirements of inverse scattering series multiple removal methods: 83rd International Annual Meeting, SEG, Expanded Abstracts, 4392–4396.

Weglein, A. B., F. V. Araújo, P. M. Carvalho, R. H. Stolt, K. H. Matson, R. T. Coates, D. Corrigan, D. J. Foster, S. A. Shaw, and H. Zhang, 2003, Inverse scattering series and seismic exploration: Inverse Problems, R27–R83.

Weglein, A. B., F. A. Gasparotto, P. M. Carvalho, and R. H. Stolt, 1997, An inverse-scattering series method for attenuating multiples in seismic reflection data: Geophysics, **62**, 1975–1989.

Weglein, A. B., and B. G. Secrest, 1990, Wavelet estimation for a multidimensional acoustic earth model: Geophysics, **55**, 902–913.

Yang, J., J. D. Mayhan, L. Tang, and A. B. Weglein, 2013, Accommodating the source (and receiver) array in free-surface multiple elimination algorithm: impact on interfering or proximal primaries and multiples: 83rd International Annual Meeting, SEG, Expanded Abstracts, 4184–4189.

Yang, J., and A. B. Weglein, 2013, Incorporating the source array in the free-surface multiple elimination algorithm: impact on removing a multiple that interferes with a primary and first test of the source deconvolution on the internal multiple attenuation algorithm: M-OSRP Annual Report.

Zhang, J., and A. B. Weglein, 2005, Extinction theorem deghosting method using towed streamer pressure data: Analysis of the receiver array effect on deghosting and subsequent free surface multiple removal: 2095–2100.

Zou, Y., and A. B. Weglein, 2013, A new method to eliminate first order internal multiples for a normal incidence plane wave on a 1d earth: 83rd International Annual Meeting, SEG, Expanded Abstracts, 4136–4140.

Including higher-order Inverse Scattering Series terms to address a serious shortcoming/problem of the internal-multiple attenuator: exemplifying the problem and its resolution

*Chao Ma * and Arthur B. Weglein, M-OSRP/Physics Dept./University of Houston*

SUMMARY

The Inverse Scattering Series (ISS) internal-multiple-attenuation algorithm is often called upon due to its unique and unmatched ability to attenuate internal multiples. It can predict internal multiples (accurately in time and approximately in amplitude) that are generated by any reflectors below the free surface without needing sub-surface information. While this algorithm is the most capable algorithm currently available for attenuating internal multiples, there are an increasing number of offshore and onshore circumstances where the problem of removing internal multiples is beyond the current ISS internal-multiples-attenuation algorithm's ability to address. For example, an open issue and specific problem is removing internal multiples which are proximal to or interfering with the primaries (Weglein et al., 2011). This invites us to pursue solutions that can address this type of challenge. Recent work by Herrera and Weglein (2013) and Zou and Weglein (2013) extend the current ISS internal-multiple-attenuation algorithm to the ISS first-order internal-multiple-elimination algorithm. Ma et al. (2011) and Liang et al. (2013) show the spurious predictions (events that do not exist in the data) that the current ISS internal-multiple-attenuation algorithm can produce when the input data are generated by three or more reflectors, and internal multiples in the input data are treated as subevents. That spurious event issue is only a problem for the ISS leading-order term (the term used to derive the current ISS internal-multiple-attenuation algorithm), specific higher-order terms from ISS will remove those spurious events. We develop the new higher-order ISS internal-multiple-attenuation algorithm and show examples of how it can effectively address that limitation (spurious predictions) of the current ISS internal-multiple-attenuation algorithm while at the same time retaining the current algorithm's recognized strengths.

INTRODUCTION

The Inverse Scattering Series is a comprehensive seismic data-processing tool from which distinct task-specific subseries can be isolated to perform specific tasks (Weglein et al., 2003). For example, the current ISS leading-order internal-multiple-attenuation algorithm was first developed by Araujo et al. (1994) and Weglein et al. (1997) from the ISS internal-multiple-attenuation subseries. The strengths (always present independent of the circumstances and complexity of the geology and the play) of the ISS internal-multiple-attenuation algorithm are: (1) this algorithm does not need any sub-surface information for predicting the internal multiples, and (2) all first-order internal multiples generated by any reflectors below the free surface are predicted at once with accurate time and approximate amplitude. The tests on ISS internal-multiple-attenuation algorithm have shown promising results and unique value compared with other multiple-suppression methods (Fu et al., 2010; Hsu et al., 2010; Andre, 2011; Terenghi et al., 2011; Luo et al., 2011; Weglein et al., 2011; Kelamis et al., 2013). However, Weglein et al. (2011) point out limitations of the current ISS internal-multiple-attenuation algorithm: (1) this algorithm is always an attenuation algorithm, and (2) spurious predictions can occur only if there are three or more reflectors, and internal multiples in the input data are treated as subevents.

It should be mentioned that those two limitations will not always matter. For example, in the cases in which there are several strong internal-multiple generators, and primaries, internal multiples and spurious events are isolated from each other, the current ISS internal-multiple-attenuation algorithm, combined with the energy-minimization adaptive subtraction methods, will remove internal multiples and spurious events completely.

However, there are times when those two limitations do matter. For example, in some offshore (e.g., North Sea) and most on-shore (e.g., Middle East) plays with many internal multiple generators, internal multiples will be proximal to or interfere with primaries, the current ISS internal-multiple-attenuation algorithm plus energy-minimization adaptive subtraction methods will not remove internal multiples and spurious predictions. In these circumstances, a complete internal-multiple-elimination algorithm without spurious predictions is called upon.

In this paper, we will focus on addressing the second limitation (i.e., spurious predictions) and exemplifying that including the higher-order terms for addressing the spurious prediction will provide added values and better prediction results.

AN OVERVIEW OF THE ISS LEADING-ORDER INTERNAL MULTIPLE ATTENUATION ALGORITHM

We refer the current ISS internal-multiple-attenuation algorithm as ISS leading-order internal-multiple-attenuation algorithm (leading-order means this algorithm predicts internal multiples with the exact time but approximate amplitude). This algorithm starts with the input data, $D(k_g, k_s, \omega)$, in 2D, which are the Fourier transform of the deghosted prestack data, and with the wavelet deconvolved and direct wave and free-surface multiples removed. The second term is the prediction of the first-order internal multiples. In a 2D earth, this prediction is (Weglein et al.,

2003)

$$b_3(k_g,k_s,q_s+q_s) = \frac{1}{(2\pi)^2}\int_{-\infty}^{\infty}dk_1\int_{-\infty}^{\infty}dk_2 e^{-iq_1(z_g-z_s)}e^{iq_2(z_g-z_s)} \times \int_{-\infty}^{\infty}dz_1 b_1(k_g,k_1,z_1)e^{i(q_g+q_1)z_1} \times \int_{-\infty}^{z_1-\varepsilon}dz_2 b_1(k_1,k_2,z_2)e^{-i(q_1+q_2)z_2} \times \int_{z_2+\varepsilon}^{\infty}dz_3 b_1(k_2,k_s,z_3)e^{i(q_2+q_s)z_3}, \quad (1)$$

where k_s and k_g are the horizontal wavenumbers for the source and receiver coordinates, respectively; q_g and q_s are the vertical source and receiver wavenumbers defined by $q_i = sgn(\omega)\sqrt{\frac{\omega^2}{c_0^2}-k_i^2}$ for $i \in \{g,s\}$ (ω is the temporal freqency); z_s and z_g are source and receiver depths; and z_j ($i \in \{1,2,3\}$) represents pseudo-depth by using a reference velocity migration. The quantity $b_1(k_g,k_s,z)$ corresponds to an uncollapsed migration (Weglein et al., 1997) of effective plane-wave incident data.

The data with their first-order internal multiple attenuated are

$$D(k_g,k_s,\omega)+D_3(k_g,k_s,\omega), \quad (2)$$

where $b_3(k_g,k_s,\omega) = -2iq_sD_3(k_g,k_s,\omega)$.

For a 1-D earth and a normal incident plane wave, equation 1 reduces to

$$b_3(k) = \int_{-\infty}^{\infty}dz_1 e^{ikz_1}b_1(z_1)\int_{-\infty}^{z_1-\varepsilon}dz_2 e^{-ikz_2}b_1(z_2) \times \int_{z_2+\varepsilon}^{\infty}dz_3 e^{ikz_3}b_1(z_3). \quad (3)$$

The deghosted data, $D(t)$, for an incident plane wave, satisfy $D(\omega) = b_1(\frac{2\omega}{c_0})$, $D(\omega)$ is the temporal Fourier transform of $D(t)$, $b_1(z) = \int_{-\infty}^{\infty}e^{ikz}b_1(k)dk$, and $k = \frac{2\omega}{c_0}$ is the vertical wavenumber.

Equation 2 then reduces to

$$D(t)+D_3(t), \quad (4)$$

where $D_3(t)$ is Inverse Fourier transform of $D_3(\omega)$, and $D_3(\omega) = b_3(\frac{2\omega}{c_0})$, where $k = \frac{2\omega}{c_0}$.

The idea behind using equation 1 or equation 3 to predict the first-order internal multiple is to treat primaries (events that experience only one upward reflection) in the data as subevents, and to combine different subevents that satisfying the "lower(A)-higher(B)-lower(C)" requirement in the pseudo-depth domain (see Figure 1).

We denote the three primary-subevents combination as "*PPP*", where *P* stands for primary. Equation 1 or equation 3 can predict all first-order internal multiples without needing any subsurface information, and those predicted internal multiples will have an accurate time and an approximate amplitude. Its limitations (e.g., spurious predictions) and resolutions are pointed out in in Weglein et al. (2011). In the next section, we will briefly review the generation of those spurious predictions and the proposed algorithms to reduce them (Ma et al., 2011; Liang et al., 2013).

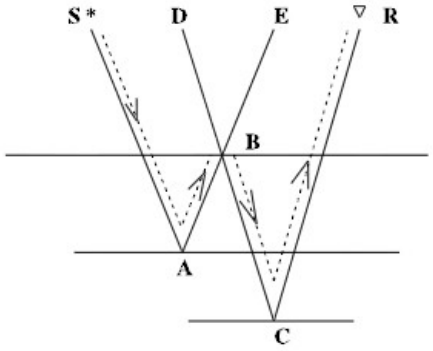

Figure 1: Combination of subevents for the first-order internal multiple (dashed line), $(SABE)_{time} + (DBCR)_{time} - (DBE)_{time} = (SABCR)_{time}$, figure adapted from Weglein et al. (2003)

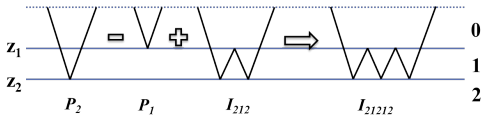

Figure 2a: In a two-reflector example, a "Primary – Primary – Internal multiple (*PPI*)" combination predicts a second-order internal multiple.

THE HIGHER-ORDER MODIFICATION OF THE ISS INTERNAL-MULTIPLE LEADING-ORDER ALGORITHM

The work of Araujo et al. (1994) and Weglein et al. (1997) focuses on the analysis of the leading-order prediction of first-order internal multiples (i.e., equation 1) by treating primaries in the data as subevents (see Figure 1). However, data consist of both primaries and internal multiples. Hence, when the data are input into equation 1, the internal multiples are inevitably also treated as subevents. When both primaries and internal multiples are treated as subevents,

$$\begin{aligned} b_3 &= b_1 * b_1 * b_1 \\ &= (P+I)(P+I)(P+I) \\ &= PPP+PPI+PIP+IPP+PII+IPI+IIP+III, \end{aligned} \quad (5)$$

where $*$ stands for the nonlinear interaction between the data (see equation 1), and *P* and *I* stand for primaries and internal multiples. Notice that we use the above expression to categorize different possible subevent combinations.

When internal multiples are treated as subevents, Zhang and Shaw (2010) use a two-reflector model to show that a second-order internal multiple can be predicted (see Figure 2a); Ma et al. (2011) and Liang et al. (2013) use three-reflector and four-reflector examples to show that spurious events are generated, respectively (see Figures 2b and 2c).

It is worth noting that because of the "lower-higher-lower" requirement of the algorithm (see Figure 1), the spurious event

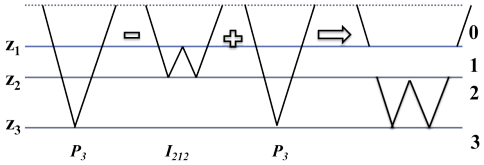

Figure 2b: In a three-reflector example, a "Primary – Internal multiple – Primary (*PIP*)" combination predicts a spurious event.

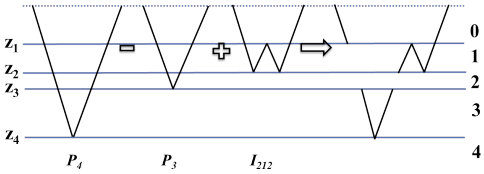

Figure 2c: In a four- reflector example, a "Primary – Primary – Internal multiple (*PPI*)" combination predicts another type of spurious event.

in Figure 2b (i.e., P_3–I_{212}–P_3), can be generated only when the arrival time of the third primary (P_3) is greater than that of the internal multiple (I_{212}). Otherwise, this spurious event would not be produced.

In Figure 2c, the condition for the prediction of spurious event (i.e., P_4–P_3–I_{212}) is that the arrival time of the third primary (P_3) is smaller than that of the internal multiple (I_{212}).

In order to eliminate the prediction of spurious events, we must remove the effects of internal multiples acting as subevents. The higher-order terms from ISS are isolated to address the two types of spurious events shown in 2b and 2c:

$$b_5^{PIP}(k) = \int_{-\infty}^{\infty} dz_1 e^{ikz_1} b_1(z_1) \int_{-\infty}^{z_1-\varepsilon} dz_2 e^{-ikz_2} b_3(z_2) \int_{z_2+\varepsilon}^{\infty} dz_3 e^{ikz_3} b_1(z_3), \quad (6)$$

and

$$b_5^{PPI}(k) = 2\int_{-\infty}^{\infty} dz_1 e^{ikz_1} b_3(z_1) \int_{-\infty}^{z_1-\varepsilon} dz_2 e^{-ikz_2} b_1(z_2) \int_{z_2+\varepsilon}^{\infty} dz_3 e^{ikz_3} b_1(z_3), \quad (7)$$

where $b_1(z)$ is the same as in equation 3, and $b_3(z) = \int_{-\infty}^{\infty} e^{ikz} b_3(k) dk$. The superscripts *PIP* and *PPI* in equations 6 and 7 indicate that higher-order terms, b_5^{PIP} and b_5^{PPI}, are included to address the spurious prediction generated by Primary–Internal multiple–Primary and Primary–Primary-Internal multiple, respectively. The factor of 2 is used in equation 7 because an internal multiple can act as a subevent in either the innermost integral or the outermost integral.

By including the higher-order terms in equations 6 and 7, the proposed new algorithm in 1-D is

$$D(t) + D_3(t) + D_5^{PIP}(t) + D_5^{PPI}(t), \quad (8)$$

where $D(t)$ and $D_3(t)$ are the same as in equation 4, and $D_5^{PIP}(t)$ and $D_5^{PPI}(t)$ are Inverse Fourier transforms of $D_3(\omega), D_5^{PIP}(\omega)$ and $D_5^{PPI}(\omega)$, respectively, and $D_5^{PIP}(\omega) = b_5^{PIP}(k)$ and $D_5^{PPI}(\omega) = b_5^{PPI}(k)$ with $k = \frac{2\omega}{c_0}$.

It should be mentioned that, in the cases where there are only three reflectors, only D_5^{PIP} is needed to address *PIP*-type spurious events because *PPI*-type spurious events arise only when there are four or more reflectors.

1-D NORMAL INCIDENT EXAMPLES WITH INTERFERING PRIMARIES AND INTERNAL MULTIPLES

In this section, we test both the D_5^{PIP} and D_5^{PPI} terms by using more realistic and practical synthetic data (generated by many reflectors with interfering primaries and internal multiples), compare the reference internal multiples to the prediction results with/without the inclusion of higher-order terms.

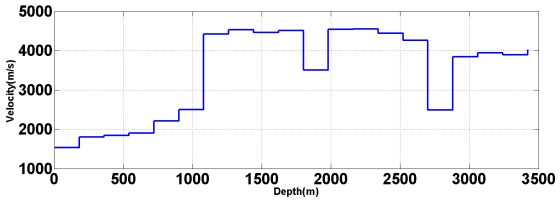

Figure 3: Velocity model used to generate synthetic data (courtesy of Saudi Arabian Oil Co.).

The first synthetic data are generated based on velocity model in Figure 3 by using reflectivity method with a ricker wavelet of peak frequency at 25 Hz .

The comparison is shown in Figure 4. When input contains only primaries, the leading-order algorithm predicts the first-order internal multiples very well (see Figure 4a). The prediction result shows degradation (because of the higher-order internal multiples and spurious events in the prediction) when the input contains both primaries and internal multiples (see Figure 4b). With the inclusion of higher-order terms, the prediction result improves (see Figure 4c).

In the second test, instead of comparing the prediction results with the reference internal multiples of **first-order**, we will

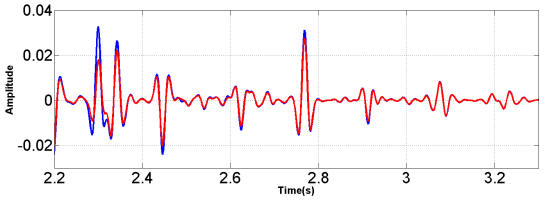

Figure 4a: Comparison between the reference first-order internal multiples (in blue) and leading-order prediction (in red) with primaries as input.

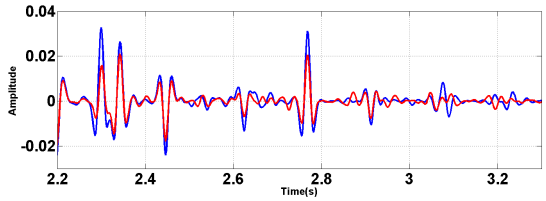

Figure 4b: Comparison between the reference first-order internal multiples (in blue) and leading-order prediction (in red) with primaries and internal multiples as input.

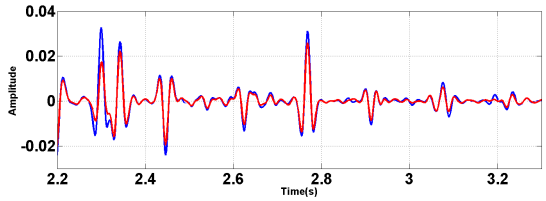

Figure 4c: Comparison between the reference first-order internal multiples (in blue) and leading-order plus higher-order prediction (in red) with primaries and internal multiples as input.

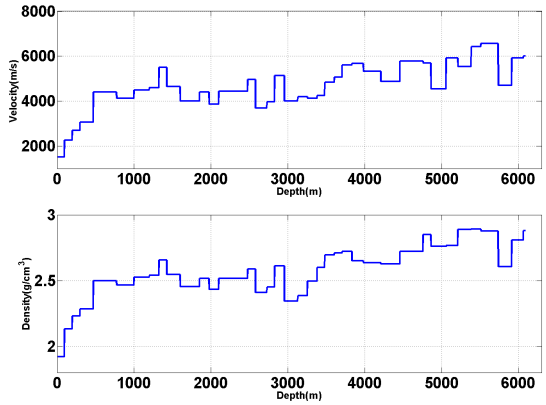

Figure 5: Velocity and density blocking from well-log data (courtesy of Kuwait Oil Company).

compare the prediction results with the reference internal multiples of **all orders**. The model (data courtesy of Kuwait Oil Company) is shown in Figure 5 with both velocity and density varying. We use reflectivity methods with a ricker wavelet of peak freqency at 25 Hz to generate the test data corresponding the model in Figure 5.

The comparison among the reference internal multiples (blue in Figure 6), leading-order prediction (red in Figure 6a), and leading-order plus higher-order prediction (red in Figure 6b) are shown in Figure 6 where arrows point to the significant improvements. Notice that the inputs for both predictions contain primaries and internal multiples. The results show that inclusion of higher-order terms improves the prediction results in the cases in which events are interfering with each other.

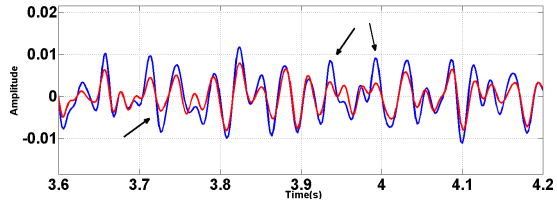

Figure 6a: Comparison between the reference internal multiples (in blue) and leading-order prediction (in red).

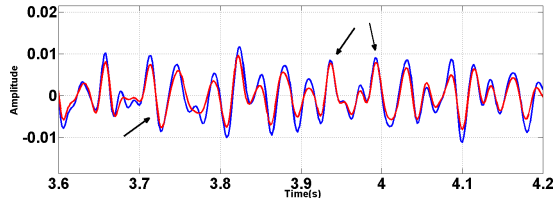

Figure 6b: Comparison between the reference internal multiples (in blue) and leading-order plus higher-order prediction (in red).

CONCLUSIONS

In this paper, we exemplified a serious shortcoming (i.e., spurious predictions) of the current ISS leading-order internal-multiple-attenuation algorithm. We develop, test and analyze the resolution with a new higher-order ISS algorithm that anticipates and removes the spurious events. This higher-order ISS internal-multiple-attenuation algorithm retains the strengths of the current leading-order ISS internal-multiple-attenuation algorithm and addresses one of its limitations.

The synthetic tests on the realistic well-log based data sets in this paper show the significance and value of including the higher-order ISS terms to address the spurious predictions.

ACKNOWLEDGMENTS

We are grateful to all M-OSRP sponsors for their encouragement and support of this research. We thank: (1) the Kuwait Oil Company (KOC) Exploration/Geosolution for permission to use their well log data in studies on the ISS method (in Figure 5); (2) KOC and WesternGeco/Schlumberger management for permission to cite the results of the study; (3) Clement Kostov and WG/SLB for a very valuable internship opportunity and experience during which Chao Ma carried out the study on the KOC data. Yi Luo and Saudi Arabian Oil Co. management are thanked for the velocity model in Figure 3. M-OSRP appreciates the close cooperation and collaboration with Panos Kelamis and his EXPEC ARC Geophysical Team, Saudi Arabian Oil Co..

REFERENCES

Andre, F., 2011, Internal multiple removal in offshore brrazil seismic data using the inverse scattering series: PhD thesis, University of Houston.

Araujo, F. V., A. B. Weglein, P. M. Carvalho, and R. H. Stolt, 1994, Inverse scattering series for multiple attenuation: An example with surface and internal multiples: SEG Technical Program Expanded Abstracts, 1039–1041.

Fu, Q., Y. Luo, P. G. Kelamis, S. Huo, G. Sindi, S.-Y. Hsu, and A. Weglein, 2010, The inverse scattering series approach towards the elimination of land internal multiples: SEG Technical Program Expanded Abstracts, **29**, 3456–3461.

Herrera, W., and A. Weglein, 2013, Eliminating first-order internal multiples with downward reflection at the shallowest interface: Theory and initial examples: SEG Technical Program Expanded Abstracts, 4131–4135.

Hsu, S., P. Terenghi, and A. B. Weglein, 2010, The properties of the inverse scattering series internal multiple attenuation algorithm: Analysis and evaluation on synthetic data with lateral variations, choosing reference velocity and examining its sensitivity to near surface properties: Mission-Oriented Seismic Research Program (M-OSRP) Annual Report, 1628.

Kelamis, P. G., Y. Luo, and A. Weglein, 2013, Strategies of land internal multiple elimination based on inverse scattering series: Presented at the 6th International Petroleum Technology Conference.

Liang, H., C. Ma, and A. Weglein, 2013, General theory for accommodating primaries and multiples in internal multiple algorithm: Analysis and numerical tests: SEG Technical Program Expanded Abstracts, 4178–4183.

Luo, Y., P. G.Kelamis, Q. Fu, S. Huo, G. Sindi, S.-Y. Hsu, and A. Weglein, 2011, Elimination of land internal multiples based on the inverse scattering series: The Leading Edge, **30**, 884–889.

Ma, C., H. Liang, and A. Weglein, 2011, Modifying the leading order iss attenuator of first-order internal multiples to accommodate primaries and internal multiples: fundamental concept and theory, development, and examples exemplified when three reflectors generate the data: Mission-Oriented Seismic Research Program (M-OSRP) 2011 Annual Report, 133–147.

Terenghi, P., S.-Y. Hsu, A. B.Weglein, and X. Li, 2011, Exemplifying the specific properties of the inverse scattering series internal-multiple attenuation method that reside behind its capability for complex onshore and marine multiples: The Leading Edge.

Weglein, A., S.-Y. Hsu, P. Terenghi, X. Li, and R. H. Stolt, 2011, Multiple attenuation: Recent advances and the road ahead (2011): The Leading Edge, 864–875.

Weglein, A. B., F. V. Araújo, P. M. Carvalho, R. H. Stolt, K. H. Matson, R. T. Coates, D. Corrigan, D. J. Foster, S. A. Shaw, and H. Zhang, 2003, Inverse scattering series and seismic exploration: Inverse Problems, R27–R83.

Weglein, A. B., F. A. Gasparotto, P. M. Carvalho, and R. H. Stolt, 1997, An inverse-scattering series method for attenuating multiples in seismic reflection data: Geophysics, **62**, 1975–1989.

Zhang, H., and S. Shaw, 2010, 1-d analytical analysis of higher order internal multiples predicted via the inverse scattering series based algorithm: SEG Expanded Abstracts, **29**, 3493–3498.

Zou, Y., and A. Weglein, 2013, A new method to eliminate first order internal multiples for a normal incidence plane wave on a 1d earth: SEG Technical Program Expanded Abstracts, 4136–4140.

The internal-multiple elimination algorithm for all reflectors for 1D earth Part I: strengths and limitations

Yanglei Zou, Arthur B. Weglein, M-OSRP/Physics Dept./University of Houston

SUMMARY

The ISS(Inverse-Scattering-Series) internal-multiple attenuation algorithm(Araújo et al. (1994) and Weglein et al. (1997)) can predict the correct time and approximate amplitude for all first-order internal multiples without any information of the earth. This algorithm is effective and can attenuate internal multiples in many cases. However, in certain places, both offshore and onshore, the multiple is often proximal to or interfering with the primaries. Therefore, the task of removing internal multiples without damaging primaries becomes more challenging and subtle and currently beyond the collective capability of the petroleum industry. Weglein et al. (2003) proposed a three-pronged strategy for providing an effective response to this pressing and prioritized challenge. One part of the strategy is to develop an internal-multiple elimination algorithm that can predict both the correct amplitude and correct time for all internal multiples. The ISS internal-multiple elimination algorithm for all first-order internal multiples generated from all reflectors in a 1D earth is proposed in part I of this paper. The primaries in the reflection data that enters the algorithm provides that elimination capability, automatically without our requiring the primaries to be identified or in any way separated. The other events in the reflection data, that is, the internal multiples, will not be helpful in this elimination scheme. That is a limitation of this new algorithm. In part II of this two part paper, we show how the ISS anticipates that shortcoming. Higher order ISS terms when combined with this new algorithm will provide elimination ability without the current shortcoming. The basic algorithm is developed,evaluated and tested in part I. The next version with higher order ISS terms that rewrites the elimination algorithm without a downside is presented and tested in part II. Moreover, this elimination algorithm based on the ISS internal-multiple attenuation algorithm is derived by using reverse engineering to provide the difference between eliminate and attenuate for a 1D earth. This particular elimination algorithm is model type dependent since the reverse engineering method is model type dependent. The ISS internal-multiple attenuation algorithm is model type independent and in future work we will pursue the development of an eliminator for a multi-dimensional earth by identifying terms in the inverse scattering series that have that purpose.

INTRODUCTION

The inverse-scattering-series allows all seismic processing objectives, such as free-surface-multiple removal and internal-multiple removal to be achieved directly in terms of data, without any estimation of the earth's properties. For internal-multiple removal, the ISS internal-multiple attenuation algorithm can predict the correct time and approximate and well-understood amplitude for all first-order internal multiples generated from all reflectors without any subsurface information. If the events in data are isolated, the energy minimization adaptive subtraction can fix the gap between attenuation algorithm and elimination algorithm plus all factors that are outside the assumed physics of the subsurface and acquisition, et al. However, in certain places, events often interfere with each other in both on-shore and off-shore seismic data. In these cases, the criteria of energy minimization adaptive subtraction may fail and completely removing internal multiples becomes more challenging and beyond the current capability of the petroleum industry.

For dealing with this challenging problem, Weglein et al. (2003) proposed a three-pronged strategy including (1)Develop the ISS prerequisites for predicting the reference wave field and to produce de-ghosted data Mayhan and Weglein (2014). (2)Develop internal-multiple elimination algorithms from ISS. (3)Develop a replacement for the energy-minimization criteria for adaptive subtraction. For the second part of the strategy, that is, to upgrade the ISS internal-multiple attenuator to eliminator, the strengths and limitations of the ISS internal-multiple attenuator are noted and reviewed. The ISS internal-multiple attenuator always attenuates all first-order internal multiples from all reflectors at once, automatically and without subsurface information. That is a tremendous strength, and is a constant and holds independent of the circumstances and complexity of the geology and the play. The primaries in the reflection data that enters the algorithm provides that delivery, automatically without our requiring the primaries to be identified or in any way separated. The other events in the reflection data, that is, the internal multiples, when they enter the ISS internal-multiple algorithm will alter the higher order internal multiples and thereby assist and cooperate with higher order ISS internal-multiple attenuation terms, to attenuate higher order internal multiples. However, there is a downside, a limitation. There are cases when internal multiples that enter the attenuator can predict spurious events. That is a well-understood shortcoming of the leading order term, when taken in isolation, but is not an issue for the entire ISS internal-multiple capability. It is anticipated by the ISS and higher order ISS internal multiple terms exist to precisely remove that issue of spurious event prediction, and taken together with the first order term, no longer experiences spurious event prediction. Ma et al. (2012) and Ma and Weglein (2014) provided those higher order terms and for spurious events removal. In a similar way, there are higher order ISS internal multiple terms that provide the elimination of internal multiples when taken together with the leading order attenuator term. There are early discussions in Ramírez (2007). And Wilberth Herrera and Weglein (2012) has derived an algorithm that can eliminate all first-order internal multiples generated at the shallowest reflector for 1D normal incidence. Part I of this paper proposes a general elimination algorithm for all first-order internal-multiples generated from all reflectors in a 1D earth. Similarly as the attenuator, The primaries in the reflection data that enters the algorithm

provides that elimination capability, automatically without our requiring the primaries to be identified or in any way separated. The other events in the reflection data, that is, the internal multiples, will not be helpful in this elimination scheme. That is a limitation of current algorithm. In part II of this two part paper, we show how the ISS anticipate that shortcoming. Higher order ISS terms when combined with the current algorithm will provide elimination ability without the current shortcoming. The basic algorithm is developed and explained in part I. The newer version with higher order ISS terms that rewrites elimination algorithm without a downside is presented and tested in part II. Moreover, this elimination algorithm based on the ISS internal-multiple attenuation algorithm is derived by using reverse engineering method. It is model type dependent since the reverse engineering method is model type dependent. The ISS internal-multiple attenuation algorithm is model type independent.

ISS INTERNAL-MULTIPLE ATTENUATION ALGORITHM AND ATTENUATION FACTOR FOR 1D NORMAL INCIDENCE

First, we can have a review of the ISS internal-multiple attenuation algorithm before we introduce the internal-multiple elimination algorithm. The ISS internal-multiple attenuation algorithm is first given by Araújo et al. (1994) Weglein et al. (1997). The 1D normal incidence version of the algorithm is presented as follows:

$$b_3^{IM}(k)=\int_{-\infty}^{\infty}dz e^{ikz}b_1(z)\int_{-\infty}^{z-\varepsilon_2}dz' e^{-ikz'}b_1(z')\int_{z'+\varepsilon_1}^{\infty}dz'' e^{ikz''}b_1(z''). \tag{1}$$

Where $b_1(z)$ which is closely related to the data is the water speed migration of the data due to a 1D normal incidence spike plane wave. ε_1 and ε_2 are two small positive number introduced to avoid self interaction. $b_3^{IM}(k)$ is the predicted internal multiples in the vertical wavenumber domain. This equation can predict the correct time and approximate amplitude of all first-order internal multiples.

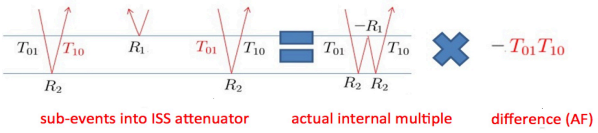

Figure 1: an example of the Attenuation Factor of a first-order internal multiple generated at the shallowest reflector, notice that all red terms are extra transmission coefficients

The procedure of predicting a first-order internal multiple generated at the shallowest reflector is shown in figure 1. The ISS internal-multiple attenuation algorithm uses three primaries in the data to predict a first-order internal multiple(Note that this algorithm is model type independent and it takes account all possible combinations of primaries that can predict internal multiples. These figures are just to show intuitively how it works). From the figure we can see, every sub event on the left hand side experiences several phenomena making its way

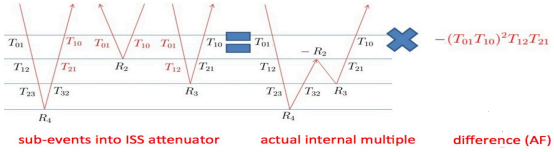

Figure 2: an example of the Attenuation Factor of a first-order internal multiple generated at the next shallowest reflector, notice that all red terms are extra transmission coefficients

down to the earth then back to the receiver. When compared with the internal multiple on the right hand side, the events on the left hand side have extra transmission coefficients as shown in red. Multiplying all those extra transmission coefficients, we get the attenuation factor $T_{01}T_{10}$ for this first-order internal multiple generated at the shallowest reflector. And all first-order internal multiples generated at the shallowest reflector have the same attenuation factor.

Figure 2 shows the procedure of predicting a first-order internal multiple generated at the next shallowest reflector. In this example, the attenuation factor is $(T_{01}T_{10})^2(T_{12}T_{21})$.

The attenuation factor, AF_j, in the prediction of internal multiples is given by the following:

$$AF_j=\begin{cases}T_{0,1}T_{1,0} & (for\ j=1)\\ \prod_{i=1}^{j-1}(T_{i-1,i}^2T_{i,i-1}^2)T_{j,j-1}T_{j-1,j} & (for\ 1<j<J)\end{cases} \tag{2}$$

The attenuation factor AF_j can also be performed by using reflection coefficients:

$$AF_j=\begin{cases}1-R_1^2 & (for\ j=1)\\ (1-R_1^2)^2(1-R_2^2)^2\cdots(1-R_{j-1}^2)^2(1-R_j^2) & (for\ 1<j<J)\end{cases} \tag{3}$$

The subscript j represents the generating reflector, and J is the total number of interfaces in the model. The interfaces are numbered starting with the shallowest location. The attenuation factor is directly related to the trajectory of the events, which forms the prediction of the internal multiple.

ISS INTERNAL-MULTIPLE ELIMINATION ALGORITHM FOR 1D NORMAL INCIDENCE

The discussion above demonstrates that all first-order internal multiples generated at the same reflector have the same attenuation factor. We can see the attenuation factor contains all transmission coefficients from the shallowest reflector down to the reflector generating the multiple. And from the examples(shown in figure 1 and 2) we can see the middle event contains all the information about those transmission coefficients .Therefore, our idea is to modify the middle term in the attenuation algorithm to remove the attenuation factor and make the attenuation algorithm an eliminator. That is from

$$b_3^{IM}(k) = \int_{-\infty}^{\infty} dz e^{ikz} b_1(z) \int_{-\infty}^{z-\varepsilon_2} dz' e^{-ikz'} b_1(z') \int_{z'+\varepsilon_1}^{\infty} dz'' e^{ikz''} b_1(z'') \quad (4)$$

to

$$b_E^{IM}(k) = \int_{-\infty}^{\infty} dz e^{ikz} b_1(z) \int_{-\infty}^{z-\varepsilon_2} dz' e^{-ikz'} F[b_1(z')] \int_{z'+\varepsilon_1}^{\infty} dz'' e^{ikz''} b_1(z'') \quad (5)$$

By introducing a new function called g(z) in which the amplitude of each event corresponds to a reflection coefficient, we find a way to construct $F[b_1(z)]$ by using $b_1(z)$ and g(z). After that, we find an integral equation about $b_1(z)$ and g(z). The $F[b_1(z)]$ is discovered Zou and Weglein (2013):

$$F[b_1(z)] = \frac{b_1(z)}{[1-(\int_{z-\varepsilon}^{z+\varepsilon} dz' g(z'))^2][1-\int_{-\infty}^{z-\varepsilon} dz' b_1(z') \int_{z'-\varepsilon}^{z'+\varepsilon} dz'' g(z'')]^2} \quad (6)$$

$$g(z) = \frac{b_1(z)}{1-\int_{-\infty}^{z-\varepsilon} dz' b_1(z') \int_{z'-\varepsilon}^{z'+\varepsilon} dz'' g(z'')} \quad (7)$$

To derive the $F[b_1(z)]$ from $b_1(z)$, g(z) must first be solved in equation (7). Thereafter, g(z) is integrated into equation (6). Now we will show one way to solve these equations. By iterating $g(z)$ in (7), we can get more accurate approximation. Substitute more accurate approximations of $g(z)$ into $F[b_1(z)]$, we will achieve or obtain higher orders of approximation of the elimination algorithm which can predict correct amplitude of first-order internal multiples generated at deeper reflectors.

ISS INTERNAL-MULTIPLE ELIMINATION ALGORITHM FOR 1D PRESTACK

Now we get the algorithm in 1D normal incidence and it lights the way to find an algorithm in 1D pre-stack. Let us discussed an example in a 2D world with 1D earth. In this example, the reflection coefficients and transmission coefficients are both angle dependent. With discussions about this example Zou and Weglein (2014), we find that the attenuation factors consist of angle dependent transmission coefficients. Following early discussions and work in Ramírez (2007) and Wilberth Herrera and Weglein (2012), we discovered the elimination algorithm in 1D pre-stack.

Below shows the 1D pre-stack internal-multiple elimination algorithm for acoustic medium (Note that the ISS internal-multiple attenuation algorithm is model type independent). Due to the angle dependent reflection coefficients, we can no longer just integrate the data in k-z domain to get the reflection coefficients as we did in 1D normal incidence, we need to go to k-q domain where each (k, q) corresponds to one reflection coefficient. The differences between the 1D pre-stack and 1D normal incidence algorithms are (1) the 1D pre-stack algorithm has one more variable k, and (2) use the reflection coefficients in the k-q domain instead of direct integral in k-z domain.

$$b_E^{IM}(k,2q) = \int_{-\infty}^{\infty} dz e^{2iqz} b_1(k,z) \int_{-\infty}^{z-\varepsilon_1} dz' e^{-2iqz'} F[b_1(k,z')] \times \int_{z'+\varepsilon_2}^{\infty} dz'' e^{2iqz''} b_1(k,z'')$$

$$F[b_1(k,z)] = \frac{1}{2\pi} \int_{-\infty}^{\infty} \int_{-\infty}^{\infty} dz' dq' \times \frac{e^{-iq'z} e^{iq'z'} b_1(k,z')}{[1-\int_{-\infty}^{z'-\varepsilon} dz'' b_1(k,z'') e^{iq'z''} \int_{z''-\varepsilon}^{z''+\varepsilon} dz''' g^*(k,z''') e^{-iq'z'''}]^2} \times \frac{1}{1-|\int_{z'-\varepsilon}^{z'+\varepsilon} dz'' g(k,z'') e^{iq'z''}|^2}$$

$$g(k,z) = \frac{1}{2\pi} \int_{-\infty}^{\infty} \int_{-\infty}^{\infty} dz' dq' \times \frac{e^{-iq'z} e^{iq'z'} b_1(k,z')}{1-\int_{-\infty}^{z'-\varepsilon} dz'' b_1(k,z'') e^{iq'z''} \int_{z''-\varepsilon}^{z''+\varepsilon} dz''' g^*(k,z''') e^{-iq'z'''}}$$

NUMERICAL TESTS FOR 1D PRESTACK ISS INTERNAL-MULTIPLE ELIMINATION ALGORITHM

We test the 1D pre-stack acoustic internal multiple elimination algorithm for a two-reflector model. Each layer has density $1.0g/cm^3$, $1.2g/cm^3$, $2.0g/cm^3$ and velocity 1500m/s 3000m/s and 4500m/s respectively. Figure 3 shows the data and figure 4 and 5 show the attenuation and elimination algorithm predictions respectively. Figure 6 to Figure 13 show different traces in different offsets (the elimination algorithm prediction (red) and attenuation algorithm prediction (green) compared to data (blue)). We can see the elimination algorithm keeps the correct time and can predict better amplitude.

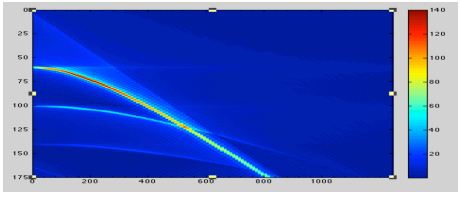

Figure 3: data

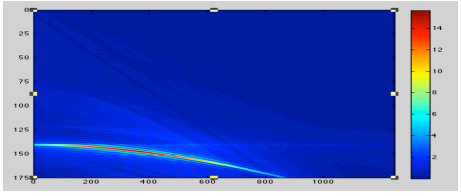

Figure 4: internal multiple attenuation prediction

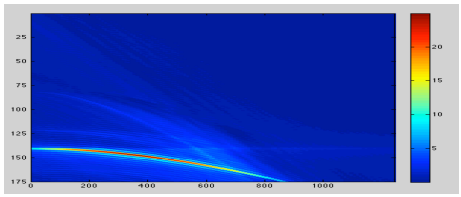

Figure 5: internal multiple elimination prediction

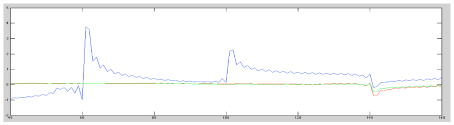

Figure 6: the elimination algorithm prediction (red) and attenuation algorithm prediction (green) compared to data (blue) at offset = 0m

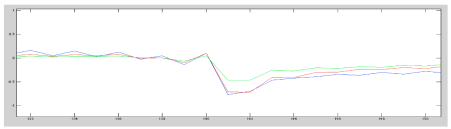

Figure 7: the elimination algorithm prediction (red) and attenuation algorithm prediction (green) compared to data (blue) at offset = 0m. After removing the tails of primaries.

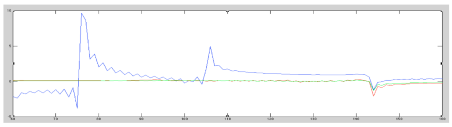

Figure 8: the elimination algorithm prediction (red) and attenuation algorithm prediction (green) compared to data (blue) at offset = 200m

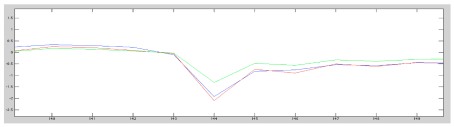

Figure 9: the elimination algorithm prediction (red) and attenuation algorithm prediction (green) compared to data (blue) at offset = 200m. After removing the tails of primaries.

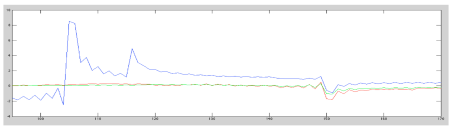

Figure 10: the elimination algorithm prediction (red) and attenuation algorithm prediction (green) compared to data (blue) at offset = 400m

CONCLUSION

The pre-stack 1D ISS internal multiple elimination algorithm for all first-order internal multiples from all reflectors is proposed in part I of this paper. Numerical tests are carried out to evaluate this new algorithm and to determine the strengths and limitations. The results shows the elimination algorithm can predict better amplitude of the internal multiples. In discussing the elimination algorithm, the primaries in the reflection data that enters the algorithm provides that elimination capability, automatically without our requiring the primaries to be identified or in any way separated. The other events in the reflection data, that is, the internal multiples, will not be helpful in this elimination scheme. That is a limitation of this new algorithm. In part II of this two part paper, we show how the ISS anticipates that shortcoming. Higher order ISS terms when combined with the current algorithm will provide elimination ability without the current shortcoming. The basic algorithm is developed and explained in part I. The newer version with higher order ISS terms that rewrites the elimination algorithm without a downside is presented and tested in part II.This algorithm is a part of the three-pronged strategy which is especially relevant and provide value when primaries and internal multiples are proximal to and/or interfere with each other in both on-shore and off-shore data.

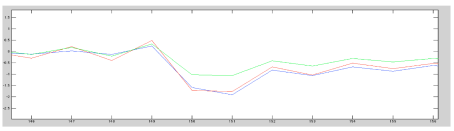

Figure 11: the elimination algorithm prediction (red) and attenuation algorithm prediction (green) compared to data (blue) at offset = 400m. After removing the tails of primaries.

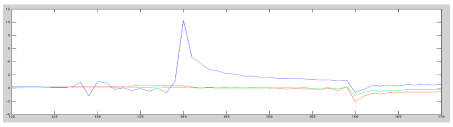

Figure 12: the elimination algorithm prediction (red) and attenuation algorithm prediction (green) compared to data (blue) at offset = 600m

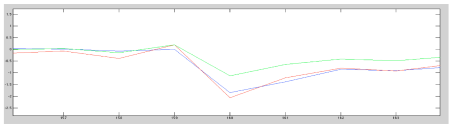

Figure 13: the elimination algorithm prediction (red) and attenuation algorithm prediction (green) compared to data (blue) at offset = 600m. After removing the tails of primaries.

ACKNOWLEDGMENTS

We are grateful to all M-OSRP sponsors for encouragement and support in this research. We would like to thank all our coworkers for their help in reviewing this paper and valuable discussions in this research program.

REFERENCES

Araújo, F. V., A. B. Weglein, P. M. Carvalho, and R. H. Stolt, 1994, Inverse scattering series for multiple attenuation: An example with surface and internal multiples: SEG Technical Program Expanded Abstracts, 1039–1041.

Ma, C., H. Liang, and A. B. Weglein, 2012, Modifying the leading order iss attenuator of first-order internal multiples to accommodate primaries and internal multiples: fundamental concept andtheory, development, and examples exemplified when three reflectors generatethe data: Mission Oriented Seismic Research Program Annual Report, 133–147.

Ma, C., and A. B. Weglein, 2014, Including higher-order inverse scattering series (iss) terms to address a serious shortcoming/problem of the iss internal-multiple attenuator: exemplifying the problem and its resolution: SEG Technical Program Expanded Abstracts.

Mayhan, J., and A. B. Weglein, 2014, Multiple removal and prerequisite satisfaction: current status and future plans: SEG Technical Program Expanded Abstracts.

Ramírez, A. C., 2007, 1.-inverse scattering subseries for removal of internal multiples and depth imaging primaries; 2.-green's theorem as the foundation of interferometry and guiding new practical methods and applications: PhD thesis, University of Houston.

Weglein, A. B., F. V. Araújo, P. M. Carvalho, R. H. Stolt, K. H. Matson, R. T. Coates, D. Corrigan, D. J. Foster, S. A. Shaw, and H. Zhang, 2003, Inverse scattering series and seismic exploration: Inverse Problems, R27–R83.

Weglein, A. B., F. A. Gasparotto, P. M. Carvalho, and R. H. Stolt, 1997, An inverse-scattering series method for attenuating multiples in seismic reflection data: Geophysics, **62**, 1975–1989.

Wilberth Herrera, Chao Ma, H. L. P. T., and A. B. Weglein, 2012, Progressing amplitude issues for testing 1d analytic data in leading order internal multiple algorithms: Mission Oriented Seismic Research Program Annual Report, 167–188.

Zou, Y., and A. B. Weglein, 2013, Internal multiple removal: an amplitude correction equation for internal-multiple attenuator(1d normal incidence): Mission Oriented Seismic Research Program Annual Report, 167–188.

———, 2014, An algorithm for the elimination of all first-order internal multiples from all reflectors: 1d noraml incidence and 1d pre-stack algorithm, discussion and numerical tests: Mission Oriented Seismic Research Program Annual Report.

The internal-multiple elimination algorithm for all reflectors for 1D earth Part II: addressing the limitations

Yanglei Zou, Arthur B. Weglein, M-OSRP/Physics Dept./University of Houston

SUMMARY

Driven by the demand for more capabilities in removing the internal multiples, the strengths and limitations of the ISS(Inverse-Scattering-Series) internal-multiple attenuation algorithm(Araújo et al. (1994) and Weglein et al. (1997)) are noted and reviewed. The ISS internal multiple attenuation algorithm has tremendous strength that it can predict the correct time and approximate amplitude for all first-order internal multiples without any information of the earth. As the first term in the internal-multiple elimination sub-series, the ISS internal-multiple attenuation algorithm has its own limitations, as noted in Weglein et al. (2003): in certain circumstances, it may generate spurious events Ma et al. (2012) and can not predict exact correct amplitude.That is a well-understood shortcoming of the leading order term, when taken in isolation, but is not an issue for the entire ISS internal multiple capability. In part I of this paper, a new elimination algorithm for all first-order internal multiples for one dimensional earth has been derived based on the ISS internal-multiple attenuation algorithm. This elimination algorithm based on the ISS internal-multiple attenuation algorithm is derived by using reverse engineering method. This elimination algorithm is model type dependent since the reverse engineering method is model type dependent while the ISS internal-multiple attenuation algorithm is model type independent. The primaries in the reflection data that enters this elimination algorithm provides that elimination capability, without requiring the primaries to be identified or in any way separated. The other events in the reflection data may alter the amplitude and need assist and cooperate with other ISS terms to completely eliminate the internal multiples. In part II of this paper, a modified strategy is proposed to address this limitation of the new elimination algorithm.

INTRODUCTION

The ISS internal-multiple attenuation algorithm(Araújo et al. (1994) and Weglein et al. (1997)) can predict the correct time and approximate amplitude for all first-order internal multiples without any information of the earth. This algorithm is effective and can attenuate internal multiples in many cases. However, in certain places, both offshore and onshore, the multiple is often proximal to or interfering with the primaries. Therefore, the task of removing internal multiples without damaging primaries becomes more challenging and subtle and currently beyond the collective capability of the petroleum industry. Weglein et al. (2003) proposed a three-pronged strategy for providing an effective response to this pressing and prioritized challenge. One part of the strategy is to develop an internal-multiple elimination algorithm that can predict both the correct amplitude and correct time for all internal multiples. Part I of this paper proposes a general elimination algorithm for all first-order internal-multiples generated from all reflectors in a 1D earth. The primaries in the reflection data that enters the algorithm provides that elimination capability, automatically without our requiring the primaries to be identified or in any way separated. The other events in the reflection data, that is, the internal multiples, will not be helpful in this elimination scheme. That is a limitation of current algorithm. In part II of this two part paper, we show how the ISS anticipate that shortcoming. Higher order ISS terms when combined with the current algorithm will provide elimination ability without the current shortcoming. The basic algorithm is developed and explained in part I. The newer version with higher order ISS terms that rewrites elimination algorithm without a downside is presented and tested in part II. In this part II, we will first give a review of both the internal multiple attenuator and eliminator, then we will propose a modified strategy with higher order terms from the inverse scattering series for addressing the limitations of the eliminator and test the strategy in a layered medium.

ISS INTERNAL-MULTIPLE ATTENUATION ALGORITHM AND ATTENUATION FACTOR FOR 1D NORMAL INCIDENCE

The ISS internal-multiple attenuation algorithm is first given by Araújo et al. (1994) and Weglein et al. (1997). The 1D normal incidence version of the algorithm is presented as follows:

$$b_3^{IM}(k)=\int_{-\infty}^{\infty}dz e^{ikz}b_1(z)\int_{-\infty}^{z-\varepsilon_2}dz' e^{-ikz'}b_1(z')\int_{z'+\varepsilon_1}^{\infty}dz'' e^{ikz''}b_1(z''). \tag{1}$$

Where $b_1(z)$ which is closely related to the data is the water speed migration of the data due to a 1D normal incidence spike plane wave. ε_1 and ε_2 are two small positive number introduced to avoid self interaction. $b_3^{IM}(k)$ is the predicted internal multiples in vertical wavenumber domain. This equation can predict the correct time and approximate amplitude of all first-order internal multiples.

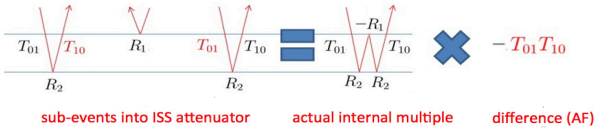

Figure 1: an example of the Attenuation Factor of a first-order internal multiple generated at the shallowest reflector, notice that all red terms are extra transmission coefficients

The procedure of predicting a first-order internal multiple generated at the shallowest reflector is shown in figure 1. The ISS internal-multiple attenuation algorithm uses three primaries in data to predict a first-order internal multiple. Multiplying all

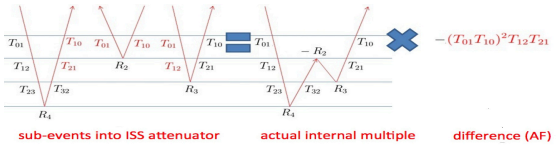

Figure 2: an example of the Attenuation Factor of a first-order internal multiple generated at the next shallowest reflector, notice that all red terms are extra transmission coefficients

those extra transmission coefficients, we get the attenuation factor $T_{01}T_{10}$ for this first-order internal multiple generated at the shallowest reflector. Figure 2 shows the procedure of predicting a first-order internal multiple generated at the next shallowest reflector. In this example, the attenuation factor is $(T_{01}T_{10})^2(T_{12}T_{21})$. The attenuation factor, AF_j, in the prediction of internal multiples is given by the following:

$$AF_j = \begin{cases} T_{0,1}T_{1,0} \quad (for\ j=1) \\ \prod_{i=1}^{j-1}(T^2_{i-1,i}T^2_{i,i-1})T_{j,j-1}T_{j-1,j} \quad (for\ 1<j<J) \end{cases} \tag{2}$$

The attenuation factor AF_j can also be performed by using reflection coefficients:

$$AF_j = \begin{cases} 1-R_1^2 \quad (for\ j=1) \\ (1-R_1^2)^2(1-R_2^2)^2\cdots(1-R_j^2) \quad (for\ 1<j<J) \end{cases} \tag{3}$$

The subscript j represents the generating reflector, and J is the total number of interfaces in the model.

ISS INTERNAL-MULTIPLE ELIMINATION ALGORITHM FOR 1D NORMAL INCIDENCE

The discussion above demonstrates that all first-order internal multiples generated at the same reflector have the same attenuation factor. We can see the attenuation factor contains all transmission coefficients from the shallowest reflector down to the reflector generating the multiple. Zou and Weglein (2013) proposed an elimination algorithm that can remove all the attenuation factors for all first-order internal multiples from all reflectors. The algorithm is shown as following:

$$F[b_1(z)] = \frac{b_1(z)}{[1-(\int_{z-\varepsilon}^{z+\varepsilon} dz' g(z'))^2][1-\int_{-\infty}^{z-\varepsilon} dz' b_1(z')\int_{z'-\varepsilon}^{z'+\varepsilon} dz'' g(z'')]^2} \tag{4}$$

$$g(z) = \frac{b_1(z)}{1-\int_{-\infty}^{z-\varepsilon} dz' b_1(z')\int_{z'-\varepsilon}^{z'+\varepsilon} dz'' g(z'')} \tag{5}$$

g(z) is a intermediate function to help construct the above close formula. To derive the $F[b_1(z)]$ from $b_1(z)$, g(z) must first be solved in equation (5). Thereafter, g(z) is integrated into equation (4). By iterating $g(z)$ in (5), we can get more accurate approximation. Substitute more accurate approximations of $g(z)$ into $F[b_1(z)]$, we will get higher orders of approximation of the elimination algorithm which can predict correct amplitude of first-order internal multiples generated at deeper reflectors.

First Type of Equation Approximation for g(z)

The simplest approximation for g(z) is presented as follows:

$$\begin{aligned} g(z) =& \frac{b_1(z)}{1-\int_{-\infty}^{z-\varepsilon} dz' b_1(z')\int_{z'-\varepsilon}^{z'+\varepsilon} dz'' g(z'')} \\ \approx& \frac{b_1(z)}{1-0} \\ \approx& b_1(z) \end{aligned} \tag{6}$$

Second Type of Equation Approximation for g(z)

A more accurate approximation for g(z) is presented as follows::

$$\begin{aligned} g(z) =& \frac{b_1(z)}{1-\int_{-\infty}^{z-\varepsilon} dz' b_1(z')\int_{z'-\varepsilon}^{z'+\varepsilon} dz'' g(z'')} \\ \approx& \frac{b_1(z)}{1-\int_{-\infty}^{z-\varepsilon} dz' b_1(z')\int_{z'-\varepsilon}^{z'+\varepsilon} dz'' b_1(z'')} \end{aligned} \tag{7}$$

Higher order approximations

By iterating $g(z)$ in (5), we can get more accurate approximation, as shown in figure 3. Substitute more accurate approximations of $g(z)$ into $F[b_1(z)]$, we will get better approximation of the elimination algorithm which can predict correct amplitude of first-order internal multiples generated at deeper reflectors.

First type approximation for $g(z)$	$g(z) = \frac{b_1(z)}{1-\int_{-\infty}^{z-\varepsilon} dz' b_1(z')\int_{z'-\varepsilon}^{z'+\varepsilon} dz'' g(z'')} \approx \frac{b_1(z)}{1-0} \approx b_1(z)$
Second type approximation for $g(z)$	$g(z) = \frac{b_1(z)}{1-\int_{-\infty}^{z-\varepsilon} dz' b_1(z')\int_{z'-\varepsilon}^{z'+\varepsilon} dz'' g(z'')} \approx \frac{b_1(z)}{1-\int_{-\infty}^{z-\varepsilon} dz' b_1(z')\int_{z'-\varepsilon}^{z'+\varepsilon} dz'' b_1(z'')}$
Third type approximation for $g(z)$	$g(z) = \frac{b_1(z)}{1-\int_{-\infty}^{z-\varepsilon} dz' b_1(z')\int_{z'-\varepsilon}^{z'+\varepsilon} dz'' g(z'')} \approx \frac{b_1(z)}{1-\int_{-\infty}^{z-\varepsilon} dz' b_1(z')\int_{z'-\varepsilon}^{z'+\varepsilon} dz'' \frac{b_1(z'')}{1-\int_{-\infty}^{z''-\varepsilon} dz''' b_1(z''')\int_{z'''-\varepsilon}^{z'''+\varepsilon} dz^{(4)} b_1(z^{(4)})}}$
...	...

Figure 3: different approximations for g(z)

ISS INTERNAL-MULTIPLE ELIMINATION ALGORITHM FOR 1D PRESTACK

In part I of this paper, a new algorithm dealing with the amplitude issue for all first-order internal multiples for one dimensional earth has been derived based on the ISS internal-multiple attenuation algorithm. The algorithm is shown as follows:

$$b_E^{IM}(k,2q) = \int_{-\infty}^{\infty} dz e^{2iqz} b_1(k,z) \int_{-\infty}^{z-\varepsilon_1} dz' e^{-2iqz'} F[b_1(k,z')] \times \int_{z'+\varepsilon_2}^{\infty} dz'' e^{2iqz''} b_1(k,z'')$$

$$F[b_1(k,z)] = \frac{1}{2\pi}\int_{-\infty}^{\infty}\int_{-\infty}^{\infty} dz'dq'$$
$$\times \frac{e^{-iq'z}e^{iq'z'}b_1(k,z')}{[1-\int_{-\infty}^{z'-\varepsilon} dz'' b_1(k,z'')e^{iq'z''}\int_{z''-\varepsilon}^{z''+\varepsilon} dz''' g^*(k,z''')e^{-iq'z'''}]^2}$$
$$\times \frac{1}{1-|\int_{z'-\varepsilon}^{z'+\varepsilon} dz'' g(k,z'')e^{iq'z''}|^2}$$

$$g(k,z) = \frac{1}{2\pi}\int_{-\infty}^{\infty}\int_{-\infty}^{\infty} dz'dq'$$
$$\times \frac{e^{-iq'z}e^{iq'z'}b_1(k,z')}{1-\int_{-\infty}^{z'-\varepsilon} dz'' b_1(k,z'')e^{iq'z''}\int_{z''-\varepsilon}^{z''+\varepsilon} dz''' g^*(k,z''')e^{-iq'z'''}}$$

A MODIFIED STRATEGY OF USING B_1+B_3 INSTEAD OF B_1 AS THE INPUT DATA FOR THE ELIMINATION ALGORITHM

The primaries in the reflection data that enters the elimination algorithm (both 1D normal incidence and 1D pre-stack) provides that elimination capability, automatically without our requiring the primaries to be identified or in any way separated. The other events in the reflection data, that is, the internal multiples, will not be helpful in this elimination scheme. That is a limitation of current algorithm. Now, we show the modified strategy and newer version of internal-multiple elimination algorithm. The limitation is due to internal multiples in the input data. Fortunately, we have a good approximations of the internal multiples (b_3) and if we use b_1+b_3 instead of b_1 as the input data for the elimination algorithm, we will be able to significantly reduce the errors due to the multiples in the data. In figure 4, b_1, which is very close to data, contains primaries, first-order internal multiples and higher-order internal multiples. We use the attenuation algorithm to predict first-order internal multiples(b_3) with correct time and approximate amplitude. Due to the multiples in the data, the attenuation algorithm also generates spurious events Ma et al. (2012) and makes prediction for higher-order multiples at the same time. However, the elimination algorithm assumes the data contains only primaries. Here is the strategy, since in b_1+b_3 the first-order internal multiples are attenuated and it is a good approximation for data with only primaries. If we use b_1+b_3 instead of b_1 for the elimination algorithm, the predicted spurious events and higher-order multiples due to first-order internal multiples in the data are also attenuated. All events in the red circle including other events are small compared with the first-order internal multiples and can be ignored.

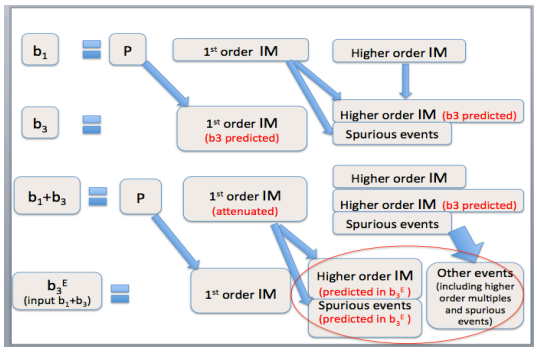

Figure 4: using b_1+b_3 instead of b_1 as the input data for the elimination algorithm

NUMERICAL TESTS ON A 34-REFLECTOR MODEL

In this section, we will test the modified strategy for a 34-reflector model under 1D normal incidence. And the modified strategy we proposed in this paper can be easily extended to the 1D pre-stack version. In figure 5, is a 34-reflector model. The input data is shown in figure 6. In this test we used a 40th approximation of the algorithm as shown in figure 7. We test the

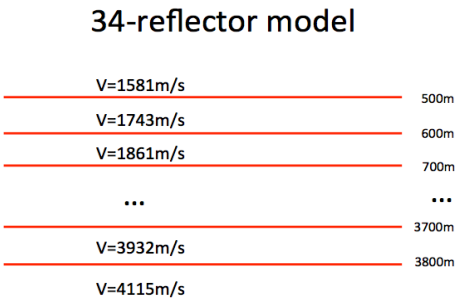

Figure 5: model

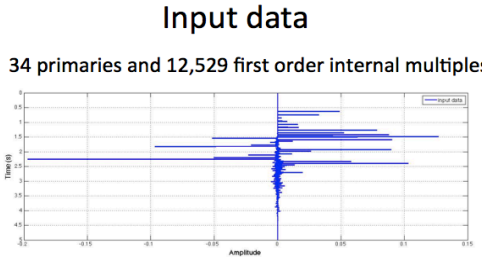

Figure 6: input data

ISS internal-multiple attenuation algorithm, the elimination algorithm with input b_1 and input b_1+b_3 respectively. From the result we conclude that using b_1+b_3 as the input significantly reduced errors and makes better prediction for all first-order internal multiples generated from all reflectors.

Figure 8,9,10 show the prediction of different algorithms/strategies compared with the input data. Figure 11,12,13 shows a small time interval of figure 8,9,10 respectively.

$$b_E^M(k) = \int_{-\infty}^{\infty} dz e^{ikz} b_1(z) \int_{-\infty}^{z-\varepsilon_2} dz' e^{-ikz'} F[b_1(z')] \int_{z'+\varepsilon_1}^{\infty} dz'' e^{ikz''} b_1(z'')$$

$$F[b_1(z)] = \frac{b_1(z)}{[1 - (\int_{z-\varepsilon}^{z+\varepsilon} dz' g(z'))^2][1 - \int_{-\infty}^{z-\varepsilon} dz' b_1(z') \int_{z'-\varepsilon}^{z'+\varepsilon} dz'' g(z'')]^2}$$

$$g(z) = \frac{b_1(z)}{1 - \int_{-\infty}^{z-\varepsilon} dz' b_1(z') \int_{z'-\varepsilon}^{z'+\varepsilon} dz'' g(z'')}$$

get g(z) by iteration

$$g_1(z) = b_1(z)$$

$$g_{n+1}(z) = \frac{b_1(z)}{1 - \int_{-\infty}^{z-\varepsilon} dz' b_1(z') \int_{z'-\varepsilon}^{z'+\varepsilon} dz'' g_n(z'')}$$

I used $g_{40}(z)$ in this test.

Figure 7: iteration to get $g_{40}(z)$

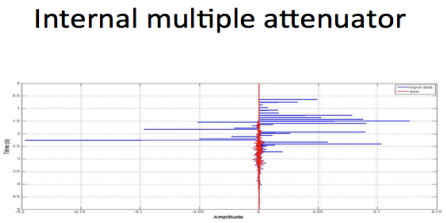

Figure 8: Internal multiple attenuator prediction(red) compared with the input data(blue)

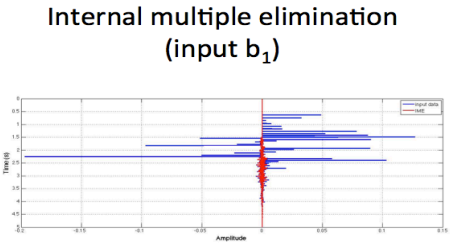

Figure 9: internal multiple elimination algorithm (with b_1 as the input data) prediction(red) compared with the input data(blue)

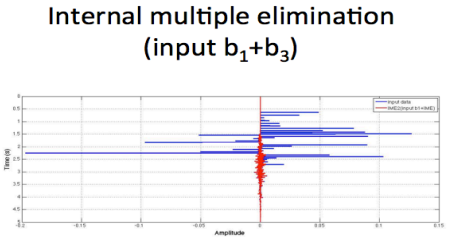

Figure 10: Internal multiple elimination algorithm (with $b_1 + b_3$ as the input data) prediction(red) compared with the input data(blue)

CONCLUSION

In part I of this paper, a new elimination algorithm for all first-order internal multiples for one dimensional earth has been derived based on the ISS internal-multiple attenuation algorithm. The primaries in the reflection data that enters this elimination algorithm provides that elimination capability, without requiring the primaries to be identified or in any way separated. The other events in the reflection data may alter the amplitude and need assist and cooperate with higher order ISS terms to completely eliminate the internal multiples. In this part II of this two part set of paper, a modified strategy is proposed to address this limitation of the current elimination algorithm. In the end we tested the strategy in a layered medium and the results are very encouraging.

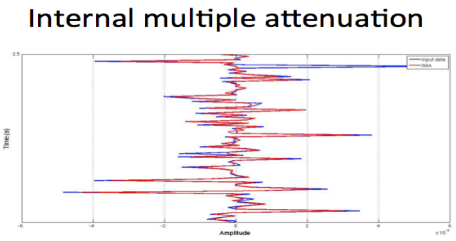

Figure 11: A small time interval of figure 8

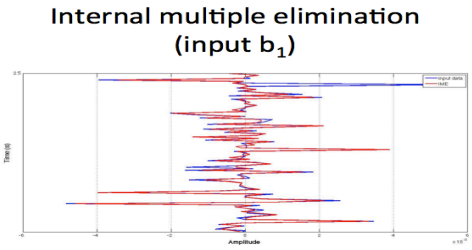

Figure 12: A small time interval of figure 9

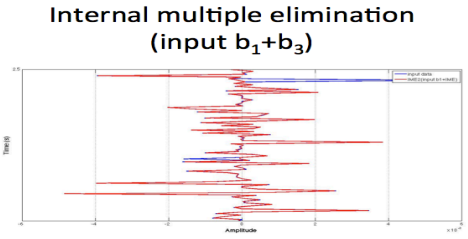

Figure 13: A small time interval of figure 10

ACKNOWLEDGMENTS

We are grateful to M-OSRP sponsors for encouragement and support in this research. And special thanks to Yi Luo and the Saudi Arabian Oil Co. for offering the velocity model used to generate the synthetic data in this paper.

REFERENCES

Araújo, F. V., A. B. Weglein, P. M. Carvalho, and R. H. Stolt, 1994, Inverse scattering series for multiple attenuation: An example with surface and internal multiples: SEG Technical Program Expanded Abstracts, 1039–1041.

Ma, C., H. Liang, and A. B. Weglein, 2012, Modifying the leading order iss attenuator of first-order internal multiples to accommodate primaries and internal multiples: fundamental concept andtheory, development, and examples exemplified when three reflectors generatethe data: Mission Oriented Seismic Research Program Annual Report, 133–147.

Weglein, A. B., F. V. Araújo, P. M. Carvalho, R. H. Stolt, K. H. Matson, R. T. Coates, D. Corrigan, D. J. Foster, S. A. Shaw, and H. Zhang, 2003, Inverse scattering series and seismic exploration: Inverse Problems, R27–R83.

Weglein, A. B., F. A. Gasparotto, P. M. Carvalho, and R. H. Stolt, 1997, An inverse-scattering series method for attenuating multiples in seismic reflection data: Geophysics, **62**, 1975–1989.

Zou, Y., and A. B. Weglein, 2013, Internal multiple removal: an amplitude correction equation for internal-multiple attenuator(1d normal incidence): Mission Oriented Seismic Research Program Annual Report, 167–188.

The first test and evaluation of the inverse scattering series internal multiple attenuation algorithm for an attenuating medium

Jing Wu and Arthur B. Weglein, M-OSRP, University of Houston

SUMMARY

In this paper, the Inverse Scattering Series (ISS) internal multiple attenuation algorithm is analytically and numerically evaluated on reflection data from an attenuating medium. All previous synthetic data tests on this algorithm have involved multidimensional acoustic and elastic media. The results for an attenuating medium show that the method retains its value to directly predict internal multiples (IM) with the exact phase and an approximate amplitude, without knowing the medium, and its anelastic properties.

INTRODUCTION

The inverse scattering series can achieve all processing objectives directly by using distinct isolated task-specific subseries and without subsurface information (Weglein et al. (2003)). ISS internal multiple attenuator has shown stand-alone capabilities on both marine and on-shore plays (e.g., Ferreira, 2011; Fu et al., 2010). To extend attenuation method to elimination, Zou and Weglein (2013) proposes a new algorithm to compensate for transmission loss in the attenuator. This new elimination method requires the input data to be wavelet deconvolved and assumes an elastic subsurface. Obviously, if the data are attenuated and broadened because of their propagation in the anelastic medium, Q compensation is the conventional step to recover the amplitudes before substituting the data into ISS internal multiple elimination algorithm. That can be a difficult step to effectively achieve in practice.

Q compensation based on ISS without Q information of the subsurface has demonstrated an early but encouraging effectiveness (e.g., Innanen and Weglein, 2003, 2005; Innanen and Lira, 2008). ISS Q compensation without Q method supposes that the input data contain primaries only, i.e., the internal multiple has been attenuated or eliminated for best before stepping into Q compensation algorithm.

This paper demonstrates that applying the industry standard ISS internal multiple attenuator to data from an anelastic earth will attenuate the multiples. The data with primary and relatively weak residual internal multiple can be substituted into the ISS Q compensation algorithm to obtain effective elastic data and then insert that data into the new elastic internal multiple elimination algorithm.

In this paper, for the first time the ISS internal multiple attenuator is tested on data from an attenuating medium. A two-reflector model with constant Q in each layer is used for analytical and numerical testing and evaluation. The result indicates that the prediction has the correct phase and an approximate amplitude. That is positive news for the ISS internal multiple attenuator and encourages developing an elimination method for the exploration plays where absorption is significant, e.g., pre-salt plays in the deep water Gulf of Mexico, off-shore Brazil, the Red Sea and the North Sea.

ANALYTICAL TEST OF ISS INTERNAL MULTIPLE ATTENUATION ALGORITHM ON DATA WITH Q

Q Definition

Based on Aki and Richards (2002), Q is used to represent the energy lost for a wave-field propagating, in one wave length, and is defined as

$$Q = \frac{2\pi E}{\Delta E}, \tag{1}$$

where E is the energy of the wave-field, and ΔE is the energy lost in a wavelength of propagation. With the definition of Q, the amplitude of wave-field A along propagation direction x can be represented as

$$A(x) = A_0 e^{-\frac{\omega}{2cQ}x}, \tag{2}$$

where A_0 is the amplitude without an absorption influence, ω is the angular frequency, and c is the velocity of the wave-field. The exponentially decaying term causes the attenuation and results in a wavelet broadening with a finite length, rather than the original spike. It is not difficult to understand that when Q decreases, the amplitude will decrease; on the other hand, when Q increases to infinity, there is no absorption.

Here, we assume that Q is frequency independent. In order to guarantee that the amplitude attenuates for negative frequency, it is convenient to replace ω with $|\omega|$, and then we have

$$A(x) = A_0 e^{-\frac{|\omega|}{2cQ}x}. \tag{3}$$

The dispersion is ignored here. That is convenient for later analytical calculations.

Analytical Test Under 1D Normal Incidence

Following the Q definition, we can express the wave-field in an anelastic medium analytically. In this section, the anelastic data will be used as input to test the ISS internal multiple attenuation algorithm analytically.

For 1D normal incidence, the ISS internal multiple attenuation algorithm (e.g., Araújo, 1994; Weglein et al., 1997, 2003) can be expressed as:

$$b_3(k_z) = \int_{-\infty}^{\infty} b_1(z) e^{ik_z z} dz \int_{-\infty}^{z-\varepsilon} b_1(z_1) e^{-ik_z z_1} dz_1 \int_{z_1+\varepsilon}^{\infty} b_1(z_2) e^{ik_z z_2} dz_2, \tag{4}$$

where the deghosted data, $D(t)$, for an incident spike wave, satisfies $D(\omega) = b_1(2\omega/c_0)$, and $b_1(z) = \int_{-\infty}^{\infty} b_1(k_z)e^{-ik_z z}dk_z$, $k_z = 2\omega/c_0$ is the vertical wavenumber, and $b_1(z)$ corresponds to an uncollapsed FK migration of the normal-incident spike plane-wave data. ε in the formula is used to make sure the events satisfy the lower-higher-lower relationship, and its value is chosen on the basis of the length of the wavelet.

A two-reflector model is provided below as an example, with the parameters listed in Fig.1, and with the depths of source and receiver both assumed to be zero.

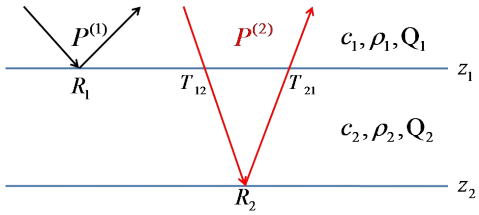

Figure 1: A two-reflector 1D model. $P^{(1)}$ and $P^{(2)}$ are primaries from the first and the second interface, respectively; R_1 and R_2 are reflection coefficients; T_{12} and T_{21} are transmission coefficients; c_1 and c_2 are the velocities; ρ_1 and ρ_2 are densities; and Q_1 and Q_2 are quality factors.

For a 1D model and a 1D normal-incident plane wave, two primaries in the data $D(\omega)$ can be represented as:

$$P^{(1)}(\omega) = R_1 e^{i\omega\frac{2z_1}{c_1}} e^{-|\omega|\frac{z_1}{c_1 Q_1}}, \quad (5)$$

$$P^{(2)}(\omega) = T_{12}R_2T_{21} e^{i\omega(\frac{2z_1}{c_1}+\frac{2(z_2-z_1)}{c_2})} e^{-|\omega|(\frac{z_1}{c_1 Q_1}+\frac{z_2-z_1}{c_2 Q_2})}. \quad (6)$$

The dispersion effect is not considered here in order to simplify the analytical calculation, i.e., the velocity does not change with frequency.

After migrating the data into the pseudo depth domain to get $b_1(z)$, we can substitute it into eqn.4. We further assume that the two primaries are isolated and ε is chosen reasonably to make sure there is no overlap between the two events among the integrals. The predicted internal multiple $b_3(k_z)$ can be obtained:

$$b_3(k_z) = (T_{12}R_2T_{21})^2 R_1 e^{ik_z(z_1+\frac{2c_1}{c_2}(z_2-z_1))} e^{-|k_z|(\frac{z_1}{2Q_1}+\frac{c_1}{c_2}\frac{z_2-z_1}{Q_2})} e^{-|k_z|\frac{z_1}{Q_1}}. \quad (7)$$

The actual first-order internal multiple in the k_z domain is

$$IM(k_z) = -T_{12}T_{21}R_2{}^2R_1 e^{ik_z(z_1+\frac{2c_1}{c_2}(z_2-z_1))} e^{-|k_z|(\frac{z_1}{2Q_1}+\frac{c_1}{c_2}\frac{z_2-z_1}{Q_2})}. \quad (8)$$

The relation between the predicted internal multiple and the actual internal multiple is

$$b_3(k_z) = -T_{12}T_{21} e^{-|k_z|\frac{z_1}{Q_1}} IM(k_z). \quad (9)$$

By using the ISS internal multiple attenuation algorithm, the multiple can be predicted with the correct phase and an approximate amplitude.

If the data are without the influence of Q absorption, then from Weglein et al. (2003), we can obtain the relation between predicted and actual internal multiple as

$$b_3(k_z) = -T_{12}T_{21}IM(k_z). \quad (10)$$

Comparing eqn.9 and eqn.10, it can be seen that the predicted amplitude is less accurate for input data with Q absorption than it is for data without Q; however, the phases are correct under both conditions.

NUMERICAL TEST OF ISS INTERNAL MULTIPLE ATTENUATION ALGORITHM ON DATA WITH Q

A two-reflector 1D model (Fig.1) will be used as an example to numerically test the effectiveness of ISS internal multiple attenuator on anelastic data. The parameters are listed in Table1.

Layer Number	Velocity (m/s)	Density (kg/m^3)	Travel Times (s)	Q Value
1	1500	1000	0.5	200
2	4000	1000	1.1	100
3	2000	1000		

Table 1: The parameters of a two-reflector 1D model

By using the parameters of Table 1, the synthetic data involving the Q value of each layer are generalized analytically without considering dispersion. The data include all the primaries and all the first-order internal multiples.

Substituting the input data b_1, shown as the blue line in Fig.2(a), into ISS internal multiple attenuation algorithm, we can predict internal multiple b_3, shown as the red line in Fig.2(a). Actually, the red line in Fig.2(a) is -b_3. It can be seen from eqn.9 that the polarity of b_3 is opposite to that of the actual internal multiple. In order to show the result more clearly, the predicted internal multiple and the actual internal multiple are compared in Fig.2(b). From the result, we can further establish that the prediction result matches well in phase and approximately in amplitude even with data from an attenuating medium, without knowing Q absorption properties.

DISCUSSION

In this paper, the ISS internal multiple attenuation algorithm is tested analytically and numerically using Q-influenced data, with the conclusion that the prediction will have the correct phase and an approximate amplitude.

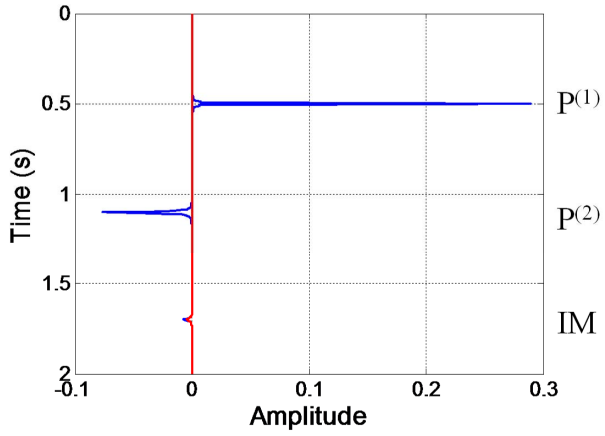

(a)

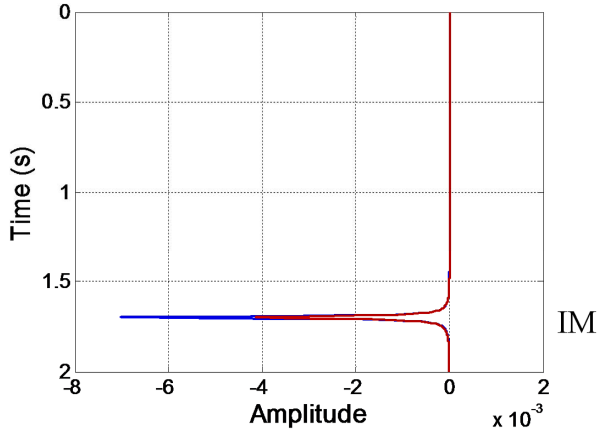

(b)

Figure 2: The numerical result of ISS internal multiple attenuation algorithm with anelastic data. (a): the input data b_1 (blue line) and the predicted multiple -b_3 (red line); (b): the actual internal multiple (blue line) and the predicted internal multiple -b_3 (red line).

The discussion in this paper gives us confidence that even for an attenuating medium, the ISS internal multiple attenuator can provide a result that retains the primary and partially removes the internal multiple. This is an important step in a strategy to eliminate internal multiples for both elastic and anelastic media. That will allow application for exploration plays where the geology exhibits significant absorption, e.g., pre-salt plays in the deep water Gulf of Mexico, off-shore Brazil, the Red Sea and the North Sea.

ACKNOWLEDGEMENTS

We are grateful to all M-OSRP sponsors for encouragement and support in this research.

APPENDIX A

B3 CALCULATION

The primaries in frequency domain can be expressed from eqn.5 and eqn.6. Since the migrated data in pseudo depth domain are required to substitute into the internal multiple attenuation algorithm, the variable should be changed from ω to $k_z = \frac{2\omega}{c_1}$:

$$P^{(1)}(k_z) = R_1 e^{ik_z z_1} e^{-|k_z|\frac{z_1}{2Q_1}}, \quad \text{(A-1)}$$

$$P^{(2)}(k_z) = T_{12}R_2T_{21} e^{ik_z(z_1+\frac{c_1}{c_2}(z_2-z_1))} e^{-|k_z|(\frac{z_1}{2Q_1}+\frac{c_1}{c_2}\frac{z_2-z_1}{2Q_2})}. \quad \text{(A-2)}$$

Then, Fourier transform is applied over k_z to pseudo depth domain to obtain

$$P^{(1)}(z) = \frac{R_1}{\pi}\frac{\frac{z_1}{2Q_1}}{(\frac{z_1}{2Q_1})^2+(z-z_1)^2}, \quad \text{(A-3)}$$

$$P^{(2)}(z) = \frac{T_{12}R_2T_{21}}{\pi}\frac{\frac{z_1}{2Q_1}+\frac{c_1}{c_2}\frac{z_2-z_1}{2Q_2}}{(\frac{z_1}{2Q_1}+\frac{c_1}{c_2}\frac{z_2-z_1}{2Q_2})^2+(z-(z_1+\frac{c_1}{c_2}(z_2-z_1))^2}. \quad \text{(A-4)}$$

$b_1(z) = P^{(1)}(z) + P^{(2)}(z)$, which will be substituted into ISS internal multiple attenuation algorithm to predict the internal multiple b_3.

Based on Weglein et al. (2003), the 1D ISS internal multiple attenuation algorithm is

$$b_3(k_z) = \int_{-\infty}^{\infty} b_1(z)e^{ik_z z}dz \int_{-\infty}^{z-\varepsilon} b_1(z_1)e^{-ik_z z_1}dz_1 \int_{z_1+\varepsilon}^{\infty} b_1(z_2)e^{ik_z z_2}dz_2, \quad \text{(A-5)}$$

where ε is used to make sure the events satisfy the lower-higher-lower relationship, and its value is chosen on the basis of the length of the wavelet.

For this model, there are two primaries in the data. Now I suppose these two events are isolated (Fig.A-1). The pseudo depth of the first event is z_1 with a length of 2a, whereas the pseudo depth of the second event is z_2' with a length of 2b. For ε in eqn.A-5 , it is chosen to satisfy $\varepsilon \geq max(2a, 2b)$ and $\varepsilon \leq (z_2' - b - (z_1 + a))$.

Kaplan et al. (2004) change the integral order of eqn.A-5 and rewrite the formula as:

$$b_3(k_z) = \int_{-\infty}^{\infty} b_1(z)e^{-ik_z z}[\int_{z+\varepsilon}^{\infty} b_1(z')e^{ik_z z'}dz']^2 dz. \quad \text{(A-6)}$$

Since $b_1(z) = P^{(1)}(z) + P^{(2)}(z)$, eqn.A-6 can be divided into two parts:

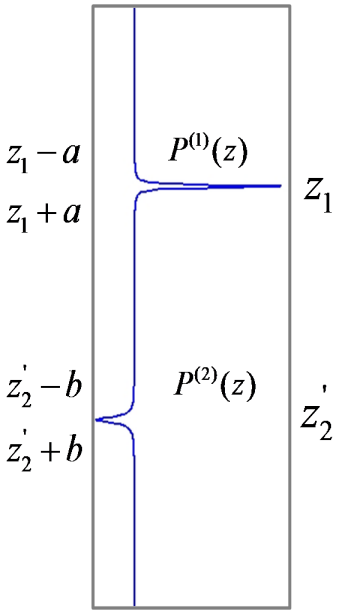

Figure A-1: A two-reflector model reflection record. $P^{(1)}$ and $P^{(2)}$ are primaries from the first and the second interface, respectively.

$$
\begin{aligned}
& b_3(k_z) \\
&= \int_{-\infty}^{\infty} P^{(1)}(z) e^{-ik_z z} [\int_{z+\varepsilon}^{\infty} b_1(z') e^{ik_z z'} dz']^2 dz \\
&+ \int_{-\infty}^{\infty} P^{(2)}(z) e^{-ik_z z} [\int_{z+\varepsilon}^{\infty} b_1(z') e^{ik_z z'} dz']^2 dz \\
&= \int_{z_1-a}^{z_1+a} P^{(1)}(z) e^{-ik_z z} [\int_{z+\varepsilon}^{\infty} b_1(z') e^{ik_z z'} dz']^2 dz \qquad (A-7-1) \\
&+ \int_{z_2'-b}^{z_2'+b} P^{(2)}(z) e^{-ik_z z} [\int_{z+\varepsilon}^{\infty} b_1(z') e^{ik_z z'} dz']^2 dz. \qquad (A-7-2)
\end{aligned}
\tag{A-7}
$$

For (A-7-1), the integral limitation of z is $[z_1 - a, z_1 + a]$. Consider the lower limit of the integral of z' and the constraint of ε,

$$z + \varepsilon \geq z_1 - a + \varepsilon \geq z_1 + a + 2a = z_1 + a,$$

and

$$z + \varepsilon \leq z_1 + a + \varepsilon \leq z_1 + a + z_2' - b - (z_1 + a) = z_2' - b.$$

We can see that the lower limit of the second integral should be after the end of the first event and before the beginning of the second event, i.e., in $[z + \varepsilon, \infty)$, the kernel of the second integral is $b_1(z') = P^{(2)}(z')$.

So

$$
\begin{aligned}
& (A-7-1) \\
&= \int_{z_1-a}^{z_1+a} P^{(1)}(z) e^{-ik_z z} [\int_{z+\varepsilon}^{\infty} b_1(z') e^{ik_z z'} dz']^2 dz \\
&= \int_{z_1-a}^{z_1+a} P^{(1)}(z) e^{-ik_z z} [\int_{z+\varepsilon}^{\infty} P^{(2)}(z') e^{ik_z z'} dz']^2 dz \\
&= \int_{-\infty}^{\infty} P^{(1)}(z) e^{-ik_z z} [\int_{-\infty}^{\infty} P^{(2)}(z') e^{ik_z z'} dz']^2 dz \\
&= (T_{12} R_2 T_{21})^2 R_1 e^{ik_z (z_1 + \frac{2c_1}{c_2}(z_2 - z_1))} e^{-|k_z|(\frac{z_1}{2Q_1} + \frac{c_1}{c_2}\frac{z_2 - z_1}{Q_2})} e^{-|k_z|\frac{z_1}{Q_1}}.
\end{aligned}
\tag{A-8}
$$

Similarly, for (A-7-2), the integral limitation of z is $[z_2' - b, z_2' + b]$. Consider the lower limit of the integral of z' and the constraint of ε,

$$z + \varepsilon \geq z_2' - b + \varepsilon \geq z_2' + b + 2b = z_2' + b.$$

The lower limit of the second integral should be after the end of the second event, i.e., in $[z + \varepsilon, \infty)$, the kernel the of second integral is $b_1(z') = 0$.

So

$$
\begin{aligned}
& (A-7-2) \\
&= \int_{z_2'-b}^{z_2'+b} P^{(2)}(z) e^{-ik_z z} [\int_{z+\varepsilon}^{\infty} b_1(z') e^{ik_z z'} dz']^2 dz \qquad (A-9) \\
&= 0.
\end{aligned}
$$

Now

$$
\begin{aligned}
& b_3(k_z) \\
&= (A-7-1) \\
&= (T_{12} R_2 T_{21})^2 R_1 e^{ik_z (z_1 + \frac{2c_1}{c_2}(z_2 - z_1))} e^{-|k_z|(\frac{z_1}{2Q_1} + \frac{c_1}{c_2}\frac{z_2 - z_1}{Q_2})} e^{-|k_z|\frac{z_1}{Q_1}}.
\end{aligned}
\tag{A-10}
$$

REFERENCES

Aki, K., and P. G. Richards, 2002, Quantitative seismology, second ed.: University Science Books.

Araújo, F. V., 1994, Linear and non-linear methods derived from scattering theory: backscattered tomography and internal multiple attenuation: PhD thesis, Universidade Federal da Bahia.

Ferreira, A., 2011, Internal multiple removal in offshore Brazil seismic data using the inverse scattering series: Master's thesis, University of Houston.

Fu, Q., Y. Luo, P. G. Kelamis, S. Huo, G. Sindi, S.-Y. Hsu, and A. B.Weglein, 2010, The inverse scattering series approach towards the elimination of land internal multiples: SEG Technical Program Expanded Abstracts, SEG, 3456–3461.

Innanen, K. A., and J. Lira, 2008, Direct non-linear q compensation of primaries in layered media: Theory and synthetic examples, *in* SEG Technical Program Expanded Abstracts: Soc. Expl. Geophys., 2957–2962.

Innanen, K. A., and A. B. Weglein, 2003, Construction of absorptive/dispersive wave fields with the forward scattering series: Journal of Seismic Exploration, **12**, 259–282.

———, 2005, Towards non-linear construction of a q-compensation operator directly from reflection seismic data, *in* SEG Technical Program Expanded Abstracts: Soc. Expl. Geophys., 1693–1696.

Kaplan, S. T., K. A. Innanen, E. Otnes, and A. Weglein, 2004, Internal multiple attenuation code-development and implementation: Mission-Oriented Seismic Research Program (M-OSRP) Annual Report, 83–102.

Weglein, A. B., F. V. Araújo, P. M. Carvalho, R. H. Stolt, K. H. Matson, R. T. Coates, D. Corrigan, D. J. Foster, S. A. Shaw, and H. Zhang, 2003, Inverse scattering series and seismic exploration: Inverse Problems, R27–R83.

Weglein, A. B., F. A. Gasparotto, P. M. Carvalho, and R. H. Stolt, 1997, An inverse-scattering series method for attenuating multiples in seismic reflection data: Geophysics, **62**, 1975–1989.

Zou, Y., and A. Weglein, 2013, A new method to eliminate first order internal multiples for a normal incidence plane wave on a 1D earth: SEG Technical Program Expanded Abstracts, SEG, 4136–4140.

The first *wave equation migration* RTM with data consisting of primaries and internal multiples: theory and 1D examples

Fang Liu and Arthur B. Weglein, Mission-Oriented Seismic Research Program, University of Houston

SUMMARY

Reverse time migration (RTM) is the cutting-edge imaging method used in seismic exploration. In earlier RTM publications, density was often chosen and used to balance a medium with velocity variation, such that the acoustic impedance − the product of velocity and density − stays constant. Thus, normal incidence reflections from sharp boundaries are avoided. In order to be more complete, consistent, realistic, and predictive, general velocity and density variations (not constrained by impedance matching) are intentionally included in our study so that we can test the impact of reflections on the Green's theorem-based wave-theory RTM algorithms.

The major objectives of this article are to advance our understanding and to provide concepts, added imaging capabilities, and new algorithms for RTM. Although our objective of extracting useful subsurface information from recorded data is not different from that of well-known previous RTM publications, our method is different.

Although all current methods utilize the wave equation, the imaging condition they call upon, the time and space coincidence of up- and down-going waves, ultimately results in an asymptotic or ray based algorithm. Current RTM application doesn't correspond to predicting a source and receiver experiment at depth at $t = 0$. That imaging principle is the defining property of wave equation migration (WEM). The method of this paper represents WEM for RTM.

In this paper, we also have some very early and very positive news on the first wave equation migration RTM imaging tests, with a discontinuous reference medium and images that have the correct depth and amplitude (that is, producing the reflection coefficient at the correctly located target) with primaries and multiples in the data. There is "no cross talk" or any other artifacts as reported by other methods that seek to migrate data with primaries and multiples. That is an implementation and analysis of Weglein et al. (2011a,b) with primaries and internal multiples in the data.

INTRODUCTION

One of the major early objectives of Reverse Time Migration (RTM) is to obtain a better image of salt flanks through diving waves than is obtained by one way migration imaging through the complex overburden. The key new capability of the RTM method compared with one-way migration algorithms is to allow two-way wave propagation in the imaging procedure. This article follows closely the idea established in Weglein et al. (2011a,b): achieving a Green's function with vanishing Dirichlet and Neumann boundary conditions at the deeper boundary, to eliminate the need for measurements at depth.

As stated in Whitmore (1983); Baysal et al. (1983); Luo and Schuster (2004); Fletcher et al. (2006); Liu et al. (2009) and Vigh et al. (2009), accurate medium properties above the target are required for the RTM procedure discussed in this article. The major difference is that in most RTM algorithms in the industry, a smoothed version of the velocity is used in the imaging procedure to avoid reflections from the velocity model itself, while the exact velocity models (often discontinuous) are used in all three examples in this article. We adopt the notations of the aforementioned articles as much as possible while introducing some minor modifications to allow smooth expansion/extension into new territory.

The major contributions of this article are:

- It provides two methods to calculate the Green's function with vanishing Dirichlet and Neumann boundary conditions for an arbitrary 1D medium.
- It incorporates the density variation for Green's theorem RTM.
- It provides the finite-difference scheme for calculating the Green's function that vanishes at the deeper boundary.
- It provides a two-way propagation and downward continuation of wave fields, by using Green's function with double vanishing boundary conditions.

The following notations are worth mentioning at the beginning: G_0^+ and G_0^- are used to denote causal and anti-causal Green's functions, respectively. G_0^{DN} is used to denote the Green's function with vanishing Dirichlet and Neumann boundary conditions at the deeper boundary. $k = \omega/c_0$ where c_0 is the constant velocity of the reference medium, and ω is the angular frequency.

THEORY

Green's theorem wave-field prediction with density variation

First, let us assume the wave propagation problem in a volume V bounded by a shallower depth A and deeper depth B:

$$\left\{ \frac{\partial}{\partial z'} \frac{1}{\rho(z')} \frac{\partial}{\partial z'} + \frac{\omega^2}{\rho(z')c^2(z')} \right\} D(z', \omega) = 0, \qquad (1)$$

where $A \le z' \le B$ is the depth, and $\rho(z')$ and $c(z')$ are the density and velocity fields, respectively. In exploration seismology, we let the shallower depth A be the measurement surface where the seismic acquisition takes place. The volume V is the finite volume defined in the "finite volume model" for migration, the details of which can be found in Weglein et al. (2011a). We measure D at the measurement surface $z' = A$, and the objective is to predict D anywhere between the shallower surface and another surface with greater depth, $z' = B$.

This can be achieved via the solution of the wave-propagation equation in the same medium by an idealized impulsive source or Green's function:

$$\left\{\frac{\partial}{\partial z'}\frac{1}{\rho(z')}\frac{\partial}{\partial z'}+\frac{\omega^2}{\rho(z')c^2(z')}\right\}G_0(z,z',\omega)=\delta(z-z'), \quad (2)$$

where z is the location of the source, and $A<z'<B$ and z increase in a downward direction. Abbreviating $G_0(z,z',\omega)$ as G_0, the solution for D in the interval $A<z'<B$ is given by Green's theorem:

$$D(z,\omega)=\frac{1}{\rho(z')}\left\{D(z',\omega)\frac{\partial G_0}{\partial z'}-G_0\frac{\partial D(z',\omega)}{\partial z'}\right\}\Bigg|_{z'=A}^{z'=B}, \quad (3)$$

where A and B are the shallower and deeper boundaries, respectively, of the volume to which the Green's theorem is applied. It is identical to equation (43) of Weglein et al. (2011a), except for the additional density contribution to the Green's theorem.

Note that in equation (3), the field values on the closed surface of the volume V are necessary for predicting the field value inside V. The surface of V contains two parts: the shallower portion $z'=A$ and the deeper portion $z'=B$. In seismic exploration, the need for data at $z'=B$ is not available. For example, one of the significant artifacts of the current RTM procedures is caused by this phenomenon: there are events necessary for accurate wave-field prediction that reach $z'=B$ but never return to $z'=A$. The solution, based on Green's theorem without any approximation, was first published in Weglein et al. (2011a) and Weglein et al. (2011b), the basic idea can be summarized as the following.

Since the wave equation is a second-order differential equation, its general solution has a great deal of freedom/flexibility. In other words, for a wave equation with a specific medium property, there are an infinite number of solutions. This freedom in choosing the Green's function has been taken advantage of in many seismic-imaging procedures. For example, the most popular choice in wave-field prediction is the physical solution G_0^+. In downward continuing an up-going wave field to a subsurface, the anti-causal solution G_0^- is often used.

If both G_0 and $\partial G_0/\partial z'$ vanish at the deeper boundary $z'=B$, where measurement is not available, then only the data at the shallower surface (i.e., the actual measurement surface) is needed in the calculation. We use G_0^{DN} to denote the Green's function with vanishing Dirichlet and Neumann boundary conditions at the deeper boundary.

Downward continuation of both source and receiver

The original Green's theorem in equation (3) is derived to downward continue the wave field (i.e., receivers) to the subsurface over a source-free region. It can also be used to downward continue the sources down to the subsurface by taking advantage of reciprocity: the recording is the same after the source and receiver locations are exchanged.

Assuming we have data on the measurement surface: $D(z_g,z_s)$ (its ω dependency is ignored), we can use $G_0^{DN}(z,z_g)$ to downward continue it from the receiver depth z_g to the target depth z:

$$D(z,z_s)=\frac{\frac{\partial D(z_g,z_s)}{\partial z_g}G_0^{DN}(z,z_g)-D(z_g,z_s)\frac{\partial G_0^{DN}(z,z_g)}{\partial z_g}}{\rho(z_g)}. \quad (4)$$

Taking the $\frac{\partial}{\partial z_s}$ operation on equation (4), we have a similar procedure to downward continue $\frac{D(z_g,z_s)}{\partial z_s}$ to the subsurface:

$$\frac{\partial D(z,z_s)}{\partial z_s}=\frac{\frac{\partial^2 D(z_g,z_s)}{\partial z_g\partial z_s}G_0^{DN}(z,z_g)-\frac{\partial D(z_g,z_s)}{\partial z_s}\frac{\partial G_0^{DN}(z,z_g)}{\partial z_g}}{\rho(z_g)}. \quad (5)$$

With equations (4) and (5), we downward continue the data D and its partial derivative over z_s to the subsurface location z. According to reciprocity, $D(z,z_s)=E(z_s,z)$, where $E(z_s,z)$ is resulted from exchanging the source and receiver locations in the experiment to generate D at the subsurface. The predicted data $E(z_s,z)$ can be considered as the recording of receiver at z_s for a source located at z.

For this predicted experiment, the source is located at depth z, according to the Green's theorem which is derived for a source-free region, we can downward continue the recording at z_s to any depth $Z\le z$.

In seismic migration, we downward continue $E(z_s,z)$ to the same subsurface depth z with $G_0^{DN}(z,z_s)$ to have an experiment with coincident source and receiver:

$$\begin{aligned}E(z,z)&=\frac{\frac{\partial E(z_s,z)}{\partial z_s}G_0^{DN}(z,z_s)-E(z_s,z)\frac{\partial G_0^{DN}(z,z_s)}{\partial z_s}}{\rho(z_s)},\\&=\frac{\frac{\partial D(z,z_s)}{\partial z_s}G_0^{DN}(z,z_s)-D(z,z_s)\frac{\partial G_0^{DN}(z,z_s)}{\partial z_s}}{\rho(z_s)}.\end{aligned} \quad (6)$$

If the $z_s<z_g$ and there is no heterogeneity above z_s, the $\frac{\partial}{\partial z_s}$ operation on $D(z_g,z_s)$ is equivalent to multiplying $-ik$, in this case, equation (6) can be further simplified:

$$E(z,z)=-\frac{\frac{\partial G_0^{DN}(z,z_s)}{\partial z_s}+ikG_0^{DN}(z,z_s)}{\rho(z_s)}D(z,z_s). \quad (7)$$

NUMERICAL EXAMPLES

As an example, for a 2-reflector model (with an ideal impulsive source located at z_s, the depth of receiver is $z_g>z_s$, the

Depth Range	Velocity	Density
$(-\infty, a_1)$	c_0	ρ_0
(a_1, a_2)	c_1	ρ_1
(a_2, ∞)	c_2	ρ_2

Table 1: The properties of an acoustic medium with two reflectors, at depth a_1 and a_2.

geological model is listed in Table 1), the data and its various derivatives can be expressed as:

$$\begin{aligned} D(z_g,z_s) &= \frac{\rho_0 x^{-1}}{2ik}\left\{y+\alpha y^{-1}\right\},\\ \frac{\partial D(z_g,z_s)}{\partial z_g} &= \frac{\rho_0}{2}x^{-1}\left\{y-\alpha y^{-1}\right\}\\ \frac{\partial D(z_g,z_s)}{\partial z_s} &= -\frac{\rho_0}{2}x^{-1}\left\{y+\alpha y^{-1}\right\},\\ \frac{\partial^2 D(z_g,z_s)}{\partial z_g \partial z_s} &= \frac{\rho_0 k}{2i}x^{-1}\left\{y-\alpha y^{-1}\right\}. \end{aligned} \tag{8}$$

where $x = e^{ikz_s}$, $y = e^{ikz_g}$, $\sigma = e^{ikz}$, $\alpha = e^{ik(2a_1)}\left(R_1 + (1-R_1^2)\beta\right)$, and $\beta = \sum_{n=0}^{\infty}(-1)^n R_1^n R_2^{n+1} e^{ik_1(2n+2)[a_2-a_1]}$. And $R_1 = \frac{c_1\rho_1 - c_0\rho_0}{c_1\rho_1 + c_0\rho_0}$, and $R_2 = \frac{c_2\rho_2 - c_1\rho_1}{c_2\rho_2 + c_1\rho_1}$ are the reflection coefficients from geological boundaries.

Above the first reflector

For $z < a_1$, the boundary values of the Green's function are:

$$\begin{array}{lll} G_0^{\boldsymbol{DN}}(z,z_g) & = \rho_0 \frac{e^{ik(z-z_g)} - e^{ik(z_g-z)}}{2ik} & = \rho_0 \frac{\sigma y^{-1} - \sigma^{-1} y}{2ik},\\ G_0^{\boldsymbol{DN}}(z,z_s) & & = \rho_0 \frac{\sigma x^{-1} - \sigma^{-1} x}{2ik},\\ \frac{\partial G_0^{\boldsymbol{DN}}(z,z_s)}{\partial z_g} & & = \rho_0 \frac{\sigma y^{-1} + \sigma^{-1} y}{-2},\\ \frac{\partial G_0^{\boldsymbol{DN}}(z,z_s)}{\partial z_s} & & = \rho_0 \frac{\sigma x^{-1} + \sigma^{-1} x}{-2}. \end{array} \tag{9}$$

After applying equation (8) into equation (7), we have:

$$E(z,z) = \frac{1 + e^{ik(2a_1-2z)}\left(R_1 + (1-R_1^2)\beta\right)}{2ik/\rho_0}. \tag{10}$$

The result above can be Fourier transformed into the time domain to have:

$$\begin{aligned} \frac{E(z,z,t)}{-\rho_0 c_0/2} = {} & H(t) + R_1 H(t-t_1) + (1-R_1^2)\times\\ & \sum_{n=0}^{\infty}(-1)^n R_1^n R_2^{n+1} H(t - t_1 - (2n+2)t_2) \end{aligned} \tag{11}$$

where, $t_1 = \frac{2a_1 - 2z}{c_0}$ and $t_2 = \frac{(a_2-a_1)}{c_1}$. Balancing out the $-\frac{\rho_0 c_0}{2}$ factor, the data after removing the direct wave is denoted as $\hat{D}(z,t) \triangleq \frac{-2}{\rho_0 c_0} E(z,z,t) - H(t)$:

$$\begin{aligned} \hat{D}(z,t) &= R_1 H(t-t_1)\\ &+ (1-R_1^2)\sum_{n=0}^{\infty}(-1)^n R_1^n R_2^{n+1} H(t - t_1 - (2n+2)t_2). \end{aligned} \tag{12}$$

If we use the $t = 0$ imaging condition, we have:

$$\hat{D}(z,t) = \begin{cases} 0 & \texttt{if } (z < a_1)\\ R_1 & \texttt{if } (z = a_1) \end{cases} \tag{13}$$

In other words, we obtained the image of the first reflector at its actual depth a_1 with its correct reflection coefficient as amplitude.

Between the first and second reflectors

For $a_1 < z < a_2$, we have:

$$\begin{aligned} G_0^{\boldsymbol{DN}}(z,z_g) &= \frac{(R_1\lambda - \lambda^{-1})\mu + (\lambda - R_1\lambda^{-1})\mu^{-1}}{2ik_1(1+R_1)/\rho_1},\\ \frac{\partial G_0^{\boldsymbol{DN}}(z,z_g)}{\partial z_g} &= \frac{(R_1\lambda - \lambda^{-1})\mu - (\lambda - R_1\lambda^{-1})\mu^{-1}}{2ik_1(1+R_1)/\rho_1}, \end{aligned} \tag{14}$$

where $\lambda = e^{ik_1(z-a_1)}$, $\mu = e^{ik(z_g-a_1)}$. Using equations (14) and (8), we have:The final result can be Fourier transformed into the time domain as:

$$\begin{aligned} \frac{E(z,z,t)}{-\rho_1 c_1/2} = {} & H(t) + 2\sum_{n=1}^{\infty}(-1)^n R_1^n R_2^n H\left(t - \tfrac{2n(a_2-a_1)}{c_1}\right)\\ & + \sum_{n=0}^{\infty}(-1)^{n+1} R_1^{n+1} R_2^n H\left(t - \tfrac{2z+2na_2-2(n+1)a_1}{c_1}\right)\\ & + \sum_{n=0}^{\infty}(-1)^n R_1^n R_2^{n+1} H\left(t - \tfrac{2(n+1)a_2-2na_1-2z}{c_1}\right) \end{aligned}$$

Balancing out the $-\frac{\rho_1 c_1}{2}$ factor, the data after removing the direct wave is denoted as $\hat{D}(z,t) \triangleq \frac{-2}{\rho_1 c_1} E(z,z,t) - H(t)$:

$$\hat{D}(z,t) = \begin{cases} 2\sum_{n=1}^{\infty}(-1)^n R_1^n R_2^n H\left(t - \frac{2n(a_2-a_1)}{c_1}\right)\\ + \sum_{n=0}^{\infty}(-1)^{n+1} R_1^{n+1} R_2^n H\left(t - \frac{2z+2na_2-2(n+1)a_1}{c_1}\right)\\ + \sum_{n=0}^{\infty}(-1)^n R_1^n R_2^{n+1} H\left(t - \frac{2(n+1)a_2-2na_1-2z}{c_1}\right) \end{cases}$$

and after taking the $t = 0$ imaging condition, we have:

$$\hat{D}(z,t) = \begin{cases} -R_1 & \texttt{if } (z = a_1)\\ 0 & \texttt{if } (a_1 < z < a_2)\\ R_2 & \texttt{if } (z = a_2) \end{cases} \tag{15}$$

Note that in the previous section, i.e., to image above the first reflector at a_1, we obtain the amplitude R_1 when z approach a_1 from above. In this section we image below the first reflector

at a_1, the amplitude of the image is $-R_1$ when z approaches a_1 from below, as it should.

Below the second reflector

For $z > a_1$, the boundary value of the Green's function is:

$$G_0^{DN}(z,z_g) = \frac{\left[\nu^{-1}(R_2\lambda - \lambda^{-1}) + R_1\nu(\lambda - R_2\lambda^{-1})\right]\mu + \left[R_1\nu^{-1}(R_2\lambda - \lambda^{-1}) + \nu(\lambda - R_2\lambda^{-1})\right]\mu^{-1}}{2ik_2(1+R_1)(1+R_2)/\rho_2},$$

where $\lambda \equiv e^{ik_2(z-a_2)}$, $\mu \equiv e^{ik(z_g-a_1)}$, and $\nu \equiv e^{ik_1(a_2-a_1)}$, $k_1 = \omega/c_1$.

The final downward continuation result can be expressed as:

$$E(z,z) = \frac{\rho_2}{2ik_2}\left\{ \begin{array}{l} 1 - R_2 e^{ik_2(2z-2a_2)} + (1-R_2^2)e^{ik_2(2z-2a_2)} \times \\ \sum_{n=0}^{\infty}(-1)^{n+1}R_1^{n+1}R_2^n e^{ik_1(2n+2)(a_2-a_1)} \end{array} \right. .$$

The time domain counterpart of the equation above is:

$$E(z,z,t) = -\frac{\rho_2 c_2}{2}\left\{ \begin{array}{l} H(t) - R_2 H\left(t - \frac{2z-2a_2}{c_2}\right) \\ +(1-R_2^2)H\left(t - \frac{2z-2a_2}{c_2} - \frac{(2n+2)(a_2-a_1)}{c_1}\right) \end{array} \right.$$

Balancing out the $-\frac{\rho_2 c_2}{2}$ factor, the data after removing the direct wave is denoted as $\hat{D}(z,t) \stackrel{\Delta}{=} \frac{-2}{\rho_2 c_2}E(z,z,t) - H(t)$:

$$\hat{D}(z,t) = \left\{ \begin{array}{l} -R_2 H\left(t - \frac{2z-2a_2}{c_2}\right) \\ +(1-R_2^2)H\left(t - \frac{2z-2a_2}{c_2} - \frac{(2n+2)(a_2-a_1)}{c_1}\right) \end{array} \right.$$

and after taking the $t = 0$ imaging condition, we have:

$$\hat{D}(z,t) = \left\{ \begin{array}{ll} -R_2 & \texttt{if } (z = a_2) \\ 0 & \texttt{if } (a_2 < z) \end{array} \right. \qquad (16)$$

Note that in the previous section, i.e., to image between the first and second reflectors, we obtain the amplitude R_2 when z approach a_2 from above. In this section we image below the second reflector at a_2, the amplitude of the image is $-R_2$ when z approaches a_2 from below, as it should.

CONCLUSIONS

A general and efficient procedure to compute the Green's function with vanishing Dirichlet and Neumann boundary conditions has been derived for a 1D medium of arbitrary complexity, and its effectiveness has been demonstrated with numerical examples that accurately predict the up-going and down-going wave field at depth using only the data on the shallower measurement surface. The density contribution to the Green's theorem and Green's function is accurately studied to better understand its role in imaging. In order to generalize the idea in this paper to a multidimensional earth, a finite-difference scheme is derived and validated by comparison with an analytic benchmark.

We also have reported some very early and very positive news on the first wave equation migration RTM imaging tests, with a discontinuous reference medium and images that have the correct depth and amplitude (that is, producing the reflection coefficient at the correctly located target) with primaries and multiples in the data. That is an implementation and analysis of Weglein et al. (2011a,b) with primaries and multiples in the data. There are no artifacts, "cross-talk" or other problems reported in the literature with other methods for migrating primaries and multiples for imaging and/or illumination (Weglein, 2014).

ACKNOWLEDGMENTS

Jim Mayhan and Jinlong Yang provided the proofreading of the manuscript. The authors would like to thank all M-OSRP members and sponsors. This work has been partially funded by NSFCMG award DMS-0327778 and DOE Basic Energy Sciences Award DE-FG02-05ER15697.

REFERENCES

Baysal, E., D. D. Kosloff, and J. W. C. Sherwood, 1983, Reverse time migration: Geophysics, **48**, 1514–1524.

Fletcher, R., P. Fowler, P. Kitchenside, and U. Albertin, 2006, Suppressing unwanted internal reflections in prestack reverse-time migration: Geophysics, **71**, E79–E82.

Liu, F., G. Zhang, S. A. Morton, and J. P. Leveille, 2009, An optimized wave equation for seismic modeling and reverse time migration: Geophysics, **74**, WCA153–WCA158.

Luo, Y., and G. T. Schuster, 2004, Bottom-up target-oriented reverse-time datuming: CPS/SEG Geophysics Conference and Exhibition, F55.

Vigh, D., E. W. Starr, and J. Kapoor, 2009, The role of reverse time migration in complex imaging: CSEG RECORDER, 20–24.

Weglein, A. B., 2014, Multiples: signal or noise?: Presented at the 84th Annual International Meeting, SEG, Expanded Abstracts, Society of Exploration Geophysicists. (Submitted).

Weglein, A. B., R. H. Stolt, and J. D. Mayhan, 2011a, Reverse-time migration and Green's theorem: Part I — the evolution of concepts, and setting the stage for the new RTM method: Journal of Seismic Exploration, **20**, 73–90.

———, 2011b, Reverse time migration and Green's theorem: Part II — a new and consistent theory that progresses and corrects current RTM concepts and methods: Journal of Seismic Exploration, **20**, 135–159.

Whitmore, D. N., 1983, Iterative depth imaging by back time propagation, *in* 53^{rd} Annual International Meeting, SEG, Expanded Abstracts: Society of Exploration Geophysicists, 382–385.

Multiple attenuation: The status and a strategy that identifies and addresses current challenges

Arthur B. Weglein

M-OSRP, Physics Department, University of Houston

5/20/2014

The demand for new and improved capability in removing multiples is driven by the portfolio of the petroleum industry and by current and anticipated future exploration trends. For example, the industry moved to deep water roughly 30 years ago. With that move, highly effective multiple-removal methods that were being applied industry-wide suddenly bumped up against their assumptions, when applied to deep water plays, and failed. (As an example, deconvolution is based on 1D and on statistical assumptions, the latter not satisfied in deep water.)

Since then, the overall industry trend to explore in progressively more complex and remote areas, with ill-defined and difficult-to-estimate subsurface properties and increasingly complex plays, is a constant that motivates the search for capabilities that will not require subsurface information. Methods that require various forms of subsurface information include, *e.g.*, F-K, Radon, and Feedback demultiple methods.

The inverse scattering series provides the opportunity to achieve all processing objectives directly and without subsurface information. The current inverse-scattering-series (ISS) internal-multiple-attenuation algorithm has a unique capability to predict the exact phase (time) and approximate amplitude of all internal multiples, at once, automatically, and without subsurface information. These properties separate the ISS internal-multiple-attenuation algorithm from all other methods, and make it the high-water mark of current internal-multiple effectiveness and explains its stand-alone capability. That is, those ISS properties and strengths are what all other current demultiple methods (*e.g.*, Feedback loop methods, modeling and subtracting multiples, and filter methods) do not possess and cannot deliver (Weglein and Dragoset, 2005).

Carvalho (1992), Carvalho and Weglein (1994), Araújo (1994), Araújo et al. (1994), Weglein et al. (1997), and Weglein et al. (2003) developed ISS free-surface-multiple elimination algorithms and internal-multiple attenuation algorithms. Field-data applications demonstrated their effectiveness. Several marine and onshore data examples are noted below.

However, at every period in the history of E&P, the arrival of new capability to address the latest set of challenges has encouraged industry to explore in yet more daunting circumstances — situations never previously imagined, let alone considered, and beyond current capability to accommodate. That will once again demand a new and fundamentally higher level of capability and effectiveness. In this article, we describe how that's the state of affairs for multiple attenuation today.

The petroleum industry's current worldwide portfolio of both conventional and unconventional onshore plays, and of increasingly complex offshore plays — with new and unforeseen daunting challenges — has returned and rejuvenated an interest in multiple removal (and a demand for substantially increased effectiveness). Multiple removal has come back to center stage, both for our petroleum-industry sponsors and concomitantly as a key and fundamental research project for the Mission-Oriented Seismic Research Program (M-OSRP) at the University of Houston.

1 Marine

Early marine field-data examples of the promise and delivery of ISS free-surface-multiple and internal-multiple algorithms can be found in the above-cited papers, SEG Abstracts, theses, and, *e.g.*, in the Mississippi Canyon data tests in Weglein et al. (2003) pages R69 and R70.

Those algorithms were recently employed on data from offshore Brazil, and the results were reported in Ferreira (2011) (see Figure 1). One of the conclusions in those field-data tests at Petrobras was that "no other method was able to show similar effectiveness in attenuating the internal multiples generated by the salt layers."

2 Onshore

Fu et al. (2010), Terenghi et al. (2011), and Luo et al. (2011) describe the motivation, evaluation, and comparison of different approaches to the removal of internal multiples on complex synthetic and onshore data. Fu et al. (2010) concluded that "Their (ISS internal multiple algorithm) performance was demonstrated with complex synthetic and challenging land field data sets with encouraging results, where other internal multiple suppression methods were unable to demonstrate similar effectiveness."

Goodway (2013), Mackidd (2013) and Griffiths et al. (2013) were among those that came to the same conclusion. A recent paper by Kelamis et al. (2013) presented at the International Petroleum Technology Conference in Beijing, China was entitled "Strategies of Land Internal Multiple Elimination based on Inverse Scattering Series."

3 Good news

At the 2013 post-convention SEG Internal Multiple Workshop (Thursday, September 26, 2013) it was positive and encouraging to see nine of the eleven presentations describe and exemplify the industry-wide impact and stand-alone capability (for complex offshore and onshore plays) of the inverse-scattering-series (ISS) internal-multiple-attenuator. ISS internal-multiple attenuation has become fully mainstream within the petroleum industry.

4 Challenge we face

With all this "good news", what could be the problem? Industry's portfolio/trend and focus today (and for the foreseeable future) makes it clear that a large and significant gap exists between the current challenge for the removal of free-surface multiples and internal multiples and the collective capabilities of the world-wide seismic exploration community (including, of course, M-OSRP). The specific issues are that: (1) the multiple generators and the subsurface properties are ill-defined and increasingly complex and (2) too often the multiple is proximal to or interfering with the primaries. The latter serious and significant issue can occur in many marine circumstances (*e.g.*, in the North Sea) and frequently occurs with onshore plays. **That type of challenge of removing multiples proximal to, and/or overlapping with, primaries (without damaging primaries) is well beyond the collective capability of the petroleum industry,**

service companies and academic research groups and consortia to effectively address. It is not an issue that new and more complete data collection and acquisition will by itself address. We simply don't have the theory and fundamental concepts in place today that are needed for algorithm development, implementation and application. That's the basic reason we are unable to address the level of challenge we currently face worldwide in the petroleum industry. That's the bottom line. To adequately address the current industry challenge, we will need to be able to predict exactly the phase and amplitude of all internal multiples and thereby surgically remove (eliminate) the multiples at all offsets, directly, and without subsurface information, and without damaging primaries. No one today is able to provide that for marine applications, let alone for the even more challenging onshore plays.

There is a need for new basic concepts and fundamental theory development that must begin with a frank and forthright recognition of the problem, its economic moment and significance, and the current technical gap. We must recognize the problem we face today and our collective inability to address it. New concepts and algorithms will need to be produced, and then will be followed by addressing the practical application and implementation issues.

5 The plan

At the 2013 SEG International Conference (Recent Advances and the Road Ahead Session), we proposed and described a three-pronged strategy (please see the link and slides below) that M-OSRP will pursue as a direct response to that challenge. It will have the potential to provide the necessary step-change increase in capability, and thereby to respond effectively to this current and pressing problem. The level and magnitude of the challenge, and the potential for opening and delineating new petroleum reserves and achieving improved drilling success rates all underlie our commitment to developing and delivering fundamental new concepts and algorithms that offer a step-change increase in capability. Multiple removal has returned from being viewed as a relatively mature subject and project that helped M-OSRP "pay the rent" and is back to occupying center stage as a major research project and focus within M-OSRP. We feel that our background and experience gives us a good chance to develop, and to deliver, the next level of required capability.

The three-pronged strategy to respond to the current open issues and pressing challenges in removing multiples is as follows:

(1) Develop the ISS prerequisites for predicting the reference wave field (wavelet and radiation pattern) and producing de-ghosted data (in particular, for on-shore and ocean bottom acquisition) that are direct and do not require subsurface information;

(2) Develop internal-multiple-elimination algorithms from the inverse scattering series;

(3) Develop a replacement for the energy-minimization criteria for adaptive subtraction, that derives from, and always aligns with and serves, the inverse-scattering-series free-surface and internal-multiple algorithms.

This three-pronged strategy represents a consistent and aligned processing chain, with one single objective: providing a direct and practical solution to the removal of all multiples, without requiring any subsurface information, and without damaging primaries.

The plan is first to progress and deliver items (2) and (3) for marine applications (since item (1) is in relatively good shape for marine application), and simultaneously to progress item (1) for onshore plays. Then, we will return to onshore exploration with the full suite of (1), (2) and (3) ingredients in place. Our plan is to deliver in stages, with offshore delivery coming before onshore delivery.

Below please find links for the SEG abstracts/posters/presentations and slides that relate to this communication.

http://mosrp.uh.edu/events/event-news/seg-annual-meeting-2013

http://mosrp.uh.edu/news/seg-annual-meeting-2013

http://mosrp.uh.edu/

http://arthurweglein.com

6 Summary

Today, the ISS internal-multiple attenuator combined with an energy-minimization adaptive subtraction is the most capable method for removing internal multiples. However, the current ISS attenuator-plus-adaptive-subtraction method will fail under the pressing and prioritized challenge of removing internal multiples that are proximal to and/or interfering with primaries. In this note, we describe a three-pronged strategy for providing an effective response to this pressing and prioritized challenge while retaining and adding to the strengths of the current ISS attenuator.

7 Acknowledgments

The author would like to thank Dr. Jim D. Mayhan for his assistance in preparing this article.

8 References

References cited in this article can be found in: http://mosrp.uh.edu/research/publications/ep-magazine-2014

9 Figure captions

Figure 1: Stack before (a) and after (b) free-surface-multiple removal; common offset sections before (c) and after (d) internal-multiple attenuation (Ferreira, 2011).

Multiple attenuation

- Free surface multiple attenuation
  - Stack before free surface multiple removal

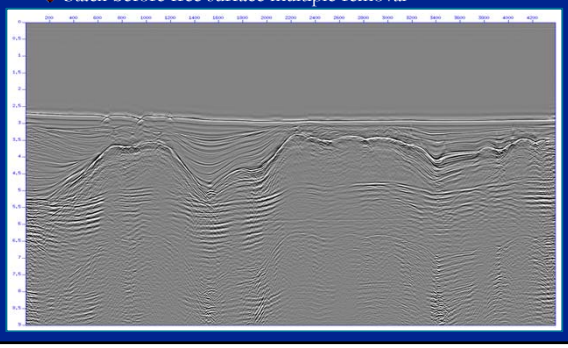

1

Multiple attenuation

- Free surface multiple attenuation
  - Stack after free surface multiple removal

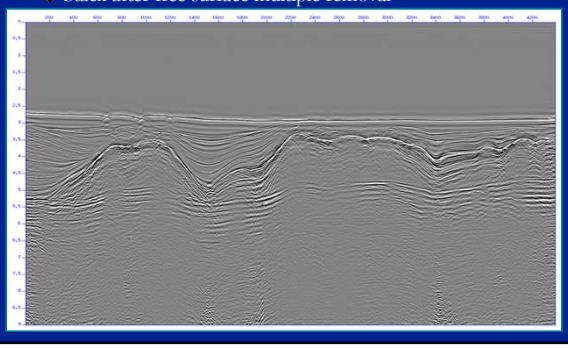

2

Multiple attenuation

- Internal multiple attenuation results
  - Common offset sections

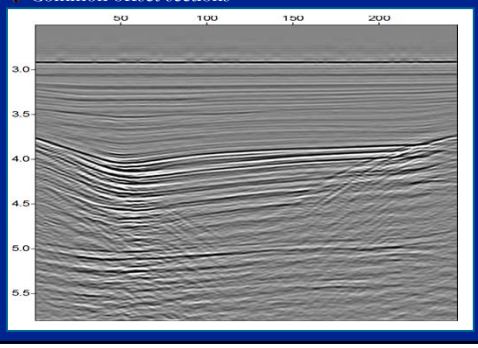

3

Multiple attenuation

- Internal multiple attenuation results
  - Common offset sections

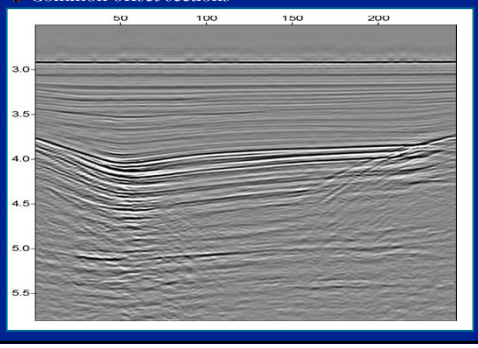

4

Are we seriously considering treating multiples as signal?

Arthur B. Weglein

M-OSRP, Physics Department, University of Houston

5/20/2014

This article is an Executive Summary of an invited presentation, "Multiples: signal or noise?", at the upcoming 2014 SEG Conference and Convention, "Recent Advances and the Road Ahead: Special Session".

This is the second of a two-article set. In the first of these two articles, that appeared in the April, 2014 *E&P Magazine*, we described the state of seismic multiple removal: (1) the current capability; (2) the challenges and (3) a strategy to directly respond to the current challenges. That article relates to "the exclusive view" of seismic reflection data, where primaries are signal and multiples are noise to be removed.

There is an alternative view, "the inclusive view" of processing seismic reflection data, where primaries and multiples are treated as signal and used for seismic imaging. This article examines the recent activity within the inclusive view.

Migration has two ingredients: (1) a wave-propagation component and (2) an imaging principle or concept. Jon Claerbout (Claerbout, 1971; Riley and Claerbout, 1976) was the initial and key wave-equation-migration imaging-concept pioneer, and together with Stolt (1978) and Lowenthal et al. (1985), were among those who introduced imaging conditions for locating reflectors at depth from surface-recorded data.

The three key imaging conditions that were introduced are:
(1) time and space coincidence of up and downgoing waves,
(2) the exploding-reflector model, and
(3) predicting a source and receiver experiment at a coincident-source-and-receiver subsurface point, and asking for time equals zero (the definition of Wave-Equation Migration (WEM)).

For a normal-incident spike plane wave incident on a horizontal reflector, these three imaging concepts are totally equivalent. For a non-zero-offset surface-seismic-data experiment they are no longer equivalent. Wave-equation migration (WEM) is defined as using the third imaging condition, (3), predicting a source and receiver experiment at depth at time equals zero. Imaging conditions (1) and (2) are the basis of asymptotic approximate, ray travel-time-curve "Kirchhoff-like" algorithms.

The properties and benefits of Wave-Equation Migration (WEM) (condition (3)) in comparison to asymptotic "Kirchhoff-like" migration (from imaging conditions (1) and (2)) are:

(1) Definitiveness as to whether or not to a subsurface point corresponds to structure;

(2) Angle-dependent reflection coefficient at the imaged point; and

(3) Ubiquitous wave propagation and wave illumination, compared to limited propagation and illumination of asymptotic ray-theory migration.

All current RTM methods correspond to asymptotic ray-based migration, derived from imaging condition (1).

The currently applied RTM methods consist of back propagating the receiver field and forward propagating the source field, where each is carried out using the wave equation. However, the cross-correlation at zero lag is imaging condition (1) and that step is when the RTM method entered asymptotics and "Kirchhoff" ray theory.

That might come as a surprise to RTM researchers and users, given the immense wave-equation computation and expense to implement, to hear that current RTM is not wave equation migration (WEM).

We provided (Weglein et al., 2011a, 2011b; Liu and Weglein, 2013) the first prediction of a source and receiver experiment at depth for two-way wave propagation, that is, the first WEM RTM. WEM RTM is designed for: (1) turning-wave primaries, and (2) for reflection data consisting of primaries and multiples. The added value of WEM RTM compared to all current RTM methods are the same three benefits as between wave-equation migration and asymptotic ray Kirchhoff migration, for one-way waves, listed above.

In Figure 1, we illustrate (from Liu and Weglein, 2013) the result from applying the first WEM RTM algorithm to data that consists of primaries and all internal multiples, from a one-dimensional layered medium. The output of the WEM RTM (coincident source and receiver experiment at time equals zero) is shown at different locations in the subsurface, with the correct location of structure. In addition, the correct reflection coefficient is provided on each side of each reflector, by the experiment being predicted

for a coincident source and a receiver slightly above or slightly below each reflector, respectively. Hence, to migrate with primaries and multiples, you simply follow what George Green prescribed in 1828, extended by Weglein et al. (2011b) for exploration seismology where the measured wavefield data is only available on the upper surface of the volume. There is no need for "secondary distributed sources" caused by data, higher-order "scattering theory" allusions and incantations, or other *ad hoc* or unclear ill-defined constructs, including unnecessarily separating primaries and multiples. And no "crosstalk" artifacts or other imponderable and irreconcilable problems arise.

Hence, the theory for WEM imaging with data from "the inclusive view" is not really very new in concept. We simply arranged for Green's theorem to require data only on the upper surface, leading to the first WEM RTM.

Recent efforts in the use of primaries and multiples are aimed at improved image illumination.

A good place to start that discussion is with a method that inputs primaries and multiples and correctly locates reflectors in depth. Correct location comes before good illumination; a misplaced but well illuminated image is of little or no value.

Claerbout famously observed, many years ago, that illumination is not an issue, in principle, for wave theory and wave-theory migration (WEM). Illumination is a fundamental and intrinsic issue for rays and all asymptotic (*e.g.*, Kirchhoff) migration methods and asymptotic RTM. Waves go everywhere and are space-filling. Rays don't. Where rays don't go, we have an intrinsic asymptotic-method-produced illumination issue. All currently applied RTM methods are asymptotic migration. Current industry RTM methods certainly use the wave equation in running the data backwards and the source forward and cross correlating at zero lag. However, using the wave equation is not the same as being a wave-equation migration. Wave-equation migration predicts a source and receiver experiment at depth, and all current RTM methods do not meet that requirement and are not wave-equation migration. Hence, all the currently employed RTM methods are, on their own (for primaries, or primaries and multiples), contributing to an algorithmic-induced limited-illumination issue.

Unfortunately, the methods currently put forth and pursued to realize "the inclusive view" for illumination do not hark back and begin their development with the solid wavefield prediction provided by Green (1828). The recent and current "inclusive view" activity very often has shaky underpinnings, at best, and a lack of any clear and firm technical foundation and framework, with *ad hoc* constructs, offered with full confidence and conviction.

The current “inclusive” activity is, without exception, using variants of asymptotic RTM for primaries, multiples, or primaries and multiples for improved illumination. However, these methods produce false images at depth (due to crosstalk), a serious downside. There doesn’t seem to be a way to address that downside and to remove these false events. The reason those “illumination” enhanced imaging methods cannot be advanced and improved to remove the crosstalk-generated false images is there is no clear wave-theory-based starting point and derivation of the method, to begin with. If there was, we could then back up, avoid the unacceptable assumption, and fix it.

Looking for a theory? George Green in (1828) basically provided the theory for imaging data with primaries and multiples: that’s the place to start. That thinking led to WEM RTM and the results in Figure 1, correct migration-inversion images without cross-talk artifacts.

Why have we treated primaries as signal and multiples as a form of noise? Primaries are much more accepting of an approximate, smooth velocity for structural imaging. We very often cannot provide an adequate smooth velocity for imaging primaries. Providing an adequate smooth velocity for imaging diving waves going down and under salt remains a tough and daunting problem. For primaries and multiples in your data, as in Figure 1, will require an accurate, discontinuous migration velocity model for predicting a source and receiver experiment at depth, for wave-equation migration. Determining an accurate discontinuous velocity model is not a realistic assumption, not now, and not for anytime in the foreseeable future.

Wave-equation migration imaging with primaries and internal multiples requires an accurate, discontinuous velocity model.

When considering imaging primaries and multiples we recommend thinking “what would George Green do? ”

Multiples contain information. Are they signal? Of course multiples contain information, but that’s not the point. The point is they contain too much information. Containing information doesn’t classify an event as signal; being able to reliably extract information from an event defines an event as signal.

The reason we separate primaries from multiples in exploration seismology is not due to lack of theory. The basic theory is almost 200 years old. It is due to the inability, in practice, to provide an adequate discontinuous velocity model necessary for the inclusive holistic view.

While we recognize the value that current asymptotic RTM illumination efforts have demonstrated for shallow reflectors using free-surface multiples, we advocate: (1) starting with WEM RTM that best serve illumination objectives, (2) see what illumination with primaries will provide, and (3) then perhaps consider adding multiples to the mix, following a Green's theorem prescription. That approach will never produce "crosstalk" or other irreconcilable false images.

We need to maintain a balance and perspective and not to be distracted by the "inclusive view" vogue and fashion, to lose our way and start to seriously think of multiples as signal. They are not. And it's not personal. The point is that the accurate and discontinuous subsurface information they require to be considered signal is unattainable. Far beyond unobtainable. Multiples were and remain noise. In general, new proposed seismic methods and strategies that will require more detailed subsurface information are headed in exactly in the wrong direction: technically and historically.

We recommend maintaining our focus on the real, tough, adult and pressing challenges of finding significantly more effective methods to remove multiples, directly and without subsurface information. That brings us full circle, back to the first of these two *E&P Magazine* articles. That's where our primary focus and attention resides.

Below please find a link for the SEG abstracts/posters/presentations and slides that relate to this communication.
http://mosrp.uh.edu/events/event-news/seg-annual-meeting-2013-2014

The link below has relevant references for the April 2014 and May 2014 *E&P* articles:
http://mosrp.uh.edu/research/publications/ep-magazine-2014

Acknowledgments

We thank Lin Tang, Jinlong Yang and Jim Mayhan for assistance in preparing this article. M-OSRP sponsors are thanked for their encouragement and support.

Figure caption

Figure 1: WEM RTM imaging with primaries and internal multiples. Result is a correct migration-inversion above and below each reflector, with no "crosstalk" false images.

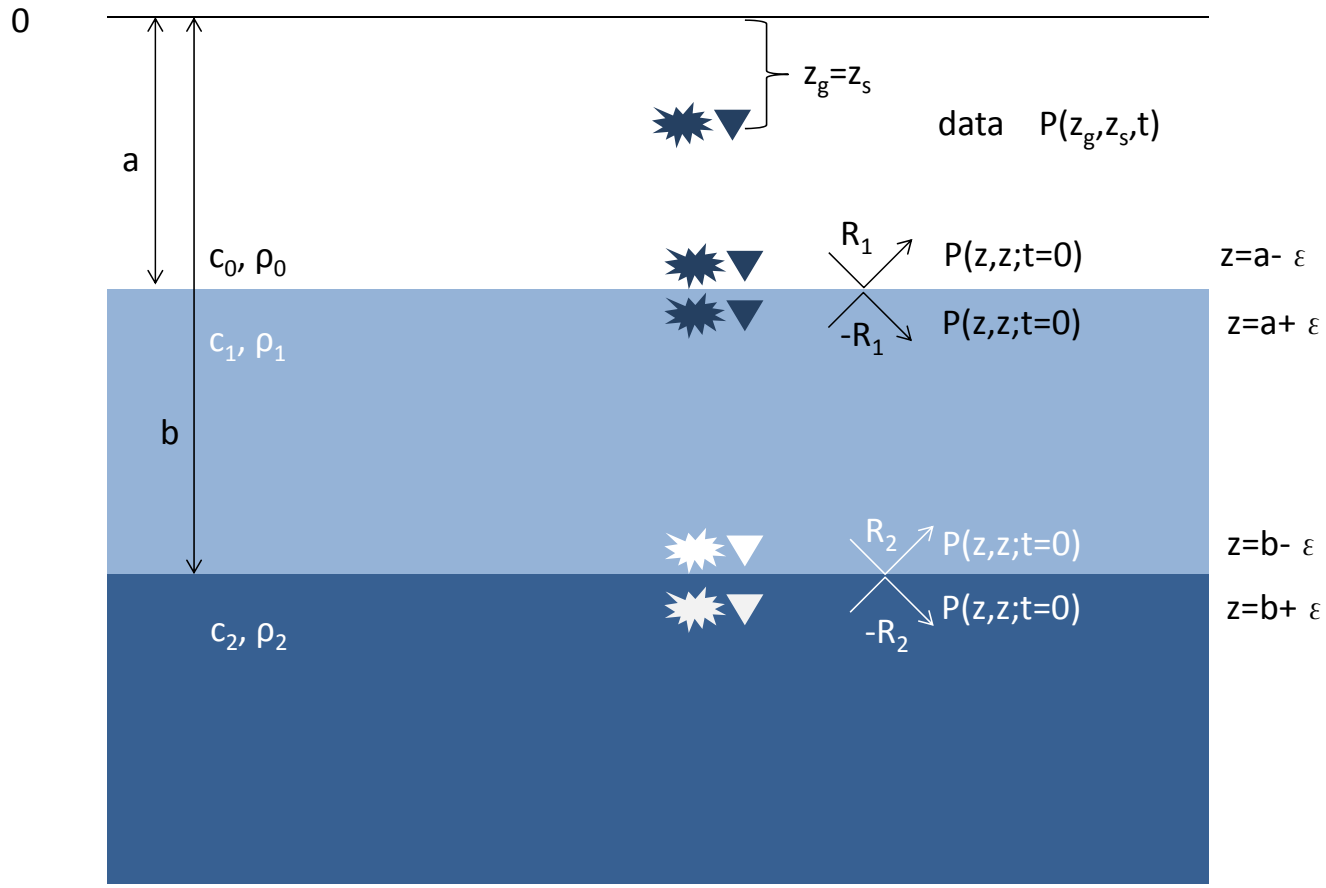
0
a
b
c_0, ρ_0
c_1, ρ_1
c_2, ρ_2
$z_g=z_s$
data $P(z_g,z_s,t)$
R_1
$-R_1$
$P(z,z;t=0)$
$P(z,z;t=0)$
z=a- ε
z=a+ ε
R_2
$-R_2$
$P(z,z;t=0)$
$P(z,z;t=0)$
z=b- ε
z=b+ ε

A timely and necessary antidote to indirect methods and so-called P-wave FWI

ARTHUR B. WEGLEIN, University of Houston

Editor's note: The following article brings to light a cautionary concern (and a set of fundamental and substantive issues, related to indirect methods, in general, that benefits from a broader and deeper understanding and perspective), regarding the validity of basic assumptions made in FWI. It was slated to appear in the special section on FWI in September. The article also describes and exemplifies a direct inverse method for the same FWI-type objectives. However as that issue was fully subscribed, given the popularity of FWI, it was decided, in conjunction with the section's guest editors (Antoine Guitton, Tariq Alkhalifah, and Chris Liner) that the article appear in the October TLE. *In the introduction to the FWI section, the guest editors pose some admonitory questions: "Are we heading in the right direction? Are we in the right valley? Or within a bigger context, is FWI the way to go?" In this context, Weglein's article is a timely and pertinent riposte that will be of significant interest and may elicit a degree of controversy to those working in the FWI field.*

A central purpose of this article is to bring an alternative voice, perspective, and understanding to the latest geophysical stampede, technical bubble, and self-proclaimed seismic cure-all, the so-called "full-waveform inversion" or FWI. If you think this is exaggerated, I refer to the advertisement/announcement of the 2013 SEG Workshop on FWI whose opening line is, "Full-waveform inversion has emerged as the final and ultimate solution to the Earth resolution and imaging objective."

Besides representing language, attitude, and a viewpoint that have no place anywhere in science, and, in particular, in exploration seismology, the fact is that the method, as put forth, is from a fundamental and basic-principle point of view (aside from, and well before, any practical considerations and track record of added-value are considered) hardly deserving of the label "inversion", let alone all the other extreme and unjustified claims and attributes, as being the "deliverance" and the last and final word on the subject.

From a direct-inversion point of view, and for the algorithms that are derived for solving the exact same problem of estimating, for example, the location of velocity anomalies and shallow hazards, and velocity changes at the top and base salt, all the current approaches to so-called full-waveform inversion are: (1) always using the wrong data, (2) always using the wrong algorithms, and (3) all too often, using the wrong Earth model, as well. Making this clear is one purpose of this article.

The issue being discussed in this article is not a matter of semantics and is not a labeling/mislabeling issue; it is the substantive issue of what data and what algorithms are called for by direct inversion to achieve certain seismic processing objectives. In particular, the focus here is on objectives that rely on the amplitude of reflection data as a function of incident angle to determine changes in, e.g., P-wave velocity, AVO parameters, or so-called FWI.

Another purpose of this article is to propose and exemplify an alternative and direct inverse solution that actually deserves the label "inversion" and could be useful for those goals and objectives, and perhaps can actually earn, deserve, and warrant a label of FWI, although never as the "ultimate and final solution." The direct-inversion approach provides not only a method but also a framework and platform for understanding when it will and will not work. All current so-called FWI methods are indirect model-matching methods, and indirect methods can never provide that capability and clarity. Model-matching run backward, or solving a forward problem in an inverse sense, resides behind all the current indirect P-wave-only so-called FWI and is never equivalent to a direct inverse solution for any nonlinear problem, nor does it even represent a fully and completely aligned goal and property of a direct inverse solution.

A third and perhaps the most important goal of this article is to provide a new, comprehensive overview and bridge for these two approaches for those who may be following, applying, and/or considering the current so-called indirect model-matching FWI approach and those proposing, interested in, or providing a road to a direct inverse methodology. It will be shown how these two approaches have the same starting point, and in fact, have the same exact generalized Taylor series expansion for modeling data and for expressing the actual data in terms of a reference model and reference data and the difference between actual and reference properties. The two approaches differ in how they view each of the same terms of that forward series. One view of those individual terms leads to a Taylor series form that does not allow a direct inverse series and that leaves as the only option the running of a forward (linear truncated) series in an inverse sense. That forward description viewed as only a generalized Taylor series results in, and provides no other choice other than, an indirect model-matching approach (e.g., as seen in AVO and the so-called FWI methods). This is the mainstream/conventional view of the forward description as a Taylor series, and, while easy to understand, that view precludes a direct inverse, and therefore explains the widespread use of indirect model-matching approaches. Another view of those individual terms in the forward Taylor series that derives from the fundamental equation of scattering theory (the Lippmann-Schwinger equation) recognizes that the forward Taylor series is a special class of generalized Taylor series—a generalized geometric series. Further, it is a geometric series for a forward problem, and it has a geometric series for a direct inverse solution. Without understanding and calling upon the scattering-theory equation, that recognition of the forward series as being geometric is not possible, and a direct inverse solution would not be achievable. All of the consequences and differences between the forward model-matching approach leading to methods such as so-called FWI and the direct inverse methods, derived from the inverse scattering series, have that simple, accessible, and understandable origin. The details, arguments, and examples behind these three objectives and goals are provided below.

Let's begin. Seismic processing is an inverse problem, in which measurements on or near the surface of the Earth are used to make inferences about the nature of the subsurface that are relevant to the exploration and production of hydrocarbons.

There was a time, not too long in the past, when a discussion of any method for solving inverse or data-processing problems always began with a definition of direct and indirect methods. The latter was deemed the less respectable and the lesser choice between the two, considered out of desperation and resignation and offered with hesitation and apology. It was associated among "inversionists" with searching and model matching rather than with seeking a direct, clear, and definitive solution through a math-physics analysis.

It appears that earlier, healthy understanding and respect for the framework and definitiveness of direct inverse methods have largely given way or have been pushed aside, with serious and substantive negative and injurious conceptual and practical consequences. Among the latter manifestations and consequences is the totally mislabeled and ubiquitous phenomenon of so-called "full-wave inversion" (FWI) methods. Among FWI references are Brossier et al. (2009), Crase et al. (1990), Gauthier et al. (1986), Nolan and Symes (1997), Pratt (1999), Pratt and Shipp (1999), Sirgue et al. (2010), Symes (2008), Tarantola (1984, 1986), Valenciano et al. (2006), Vigh and Starr (2008), and Zhou et al. (2012).

This note advocates (whenever possible) direct methods for solving processing problems and providing prerequisites. Direct methods offer many conceptual and practical benefits over indirect methods. Advantages of direct methods begin with actually knowing that you are solving the problem that you are interested in solving.

How can you recognize a direct versus an indirect method? Consider the quadratic equation

$$ax^2 + bx + c = 0, \tag{1}$$

and the solution

$$x = (-b \pm \sqrt{b^2 - 4ac}) / 2a. \tag{2}$$

Equation 2 is a direct solution for the roots of Equation 1. On the other hand, if you see a cost function involved in a solution, the solution is indirect. Also, if you see a modeling equation being solved in an inverse sense, or an iteratively linear updating, those are each direct indicators of an indirect solution and a model-matching approach, which too often can start with an incorrect or insufficient modeling equation and a matching of fundamentally inadequate data. The only time that a forward problem solved in an inverse sense can be equivalent to a direct inverse solution is when the direct inverse solution is linear. For example, locating reflectors at depth with a known velocity model is linear, and, hence, e.g., (asymptotic) RTM is a modeling run backward (i.e., in an inverse sense) to directly determine structure. Another transparent example is given by the forward geometric series

$$S = ar + ar^2 + ar^3 + \ldots = \frac{ar}{1-r} \qquad when\,|\,r\,|\!<1 \tag{3}$$

and the inverse

$$r = \frac{S/a}{1+S/a} = S/a - (S/a)^2 + (S/a)^3 \ldots \tag{4}$$
$$= r_1 + r_2 + r_3 + \cdots \text{ when } |S/a|. < 1$$

If, rather than these nonlinear relationships among S, a, and r, we instead imagine an exact linear relationship that S, a, and r might satisfy, e.g.,

$$S = ar, \tag{5}$$

then we have the forward problem of solving for S given a and r, and the inverse problem becomes solving for r in terms of S and a. The direct inverse solution $r = S/a$ is equivalent to the forward problem solved in an inverse sense, solving $S = ar$ for r in terms of S and a. However, if the forward relationship assumed among S, a, and r is a quadratic relationship (an approximate of the actual nonlinear forward problem given by Equation 3), we have

$$S = ar + ar^2. \tag{6}$$

Then, solving the forward problem, Equation 6, in an inverse sense is a quadratic solution with *two* roots that can be real or imaginary, whereas the solution to Equation 4 is a *single* real solution for r. In place of Equation 6, think of the linearized forward Zoeppritz equation for R_{PP} solved in an inverse sense, and the point is clear. This simple and transparent example demonstrates a pitfall of thinking that a direct inversion is equivalent to a forward problem solved in an inverse sense. Another example, pointed out in Weglein et al. (2009), is the direct inverse solution for predicting and removing free-surface and internal multiples, from the inverse-scattering series, where these two distinct algorithms are independent not only of subsurface information, they are also independent of whether we assume the Earth is acoustic, elastic, anelastic, heterogeneous, and anisotropic. The multiple-removal algorithms (which are direct and nonlinear) do not change one line of code when you change your mind about the Earth model type you want to consider. Can you imagine a model-matching and subtraction method or linear-updating method for predicting and removing multiples, with any cost function, L_1, L_2, L_P, that would be independent of subsurface properties and the type of Earth model you are using to generate the synthetic data? It is hard to overstate the significance of this point. The widely recognized benefit to industry from effectively removing free-surface and internal multiples using algorithms derived from the inverse scattering series, for offshore and onshore plays, never would have occurred if the indirect inversion, model-matching, and iterative updating, and FWI-like thinking, were the approaches pursued for removing multiples.

In general, we look at inversion as a set of tasks: free-surface and internal-multiple removal, depth imaging, and nonlinear AVO. For the purposes of this article and for discussing FWI, the focus is entirely on how the ISS addresses that parameter estimation task in isolation, and as if all other tasks (e.g., multiple removal) had been previously achieved.

Indirect methods such as flat common-image gathers (CIG) were developed as a response to the inability to directly solve for and adequately provide a velocity model for depth imaging, and those CIGs represent a necessary condition at the image that an accurate velocity would satisfy. References for CIGs are Anderson et al. (2012), Baumstein et al. (2009), Ben-Hadj-ali et al. (2008, 2009), Biondi and Sava (1999), Biondi and Symes (2004), Brandsberg-Dahl et al. (1999), Chavent and Jacewitz (1995), Fitchner (2011), Guasch et al. (2012), Kapoor et al. (2012), Rickett and Sava (2002), Sava et al. (2005), Sava and Fomel (2003), Sirgue et al. (2009, 2010, 2012), Symes and Carazzone (1991), Tarantola (1987), and Zhang and Biondi (2013). Many wrong velocity models can and will also satisfy a flat common-image-gather criterion, especially under complex imaging circumstances. Indeed, unquestioned faith in the power of satisfying the flat CIG criterion can and does contribute to dry-hole drilling. Mathematicians who work on the latter types of CIG problems would better spend their time describing the underlying lack of a necessary and sufficient condition, and the consequences, rather than dressing up and obfuscating the necessary but insufficient condition in fancy, rigorous, and abstract new clothes.

It seems that the recent surge of interest in estimating changes in velocity is fueled by: (1) the improved ability to produce low-frequency and low-vertical-wavenumber information from new acquisition and improved deghosting; (2) the implicit admission of serious problems with methods to estimate velocity models (e.g., with tomography, iterative flat CIG searching, and the like); and, of course, (3) the persistent and unacceptable dry-hole drilling rate. Today, for example, we basically remain fixed and without significant progress (at a one-in-ten success rate) in drilling successful exploration wells in the deep-water Gulf of Mexico (Hawthorn, 2009; Iledare and Kaiser, 2007).

Indirect methods should be considered only when direct methods are not available or are inadequate, or when you cannot figure out how to solve a problem directly. Indirect methods are often and reasonably employed to allow a channel or an adjustment (a dial) for phenomena and components of reality that are outside and external to the physics of the system you have chosen and defined. Of course, there always are, and always will be, phenomena outside your assumed and adopted physics and system that must be accommodated and that are ignored at your peril. That's the proper realm and role for indirect methods. Even then, however, they need to be applied judiciously and always with scrutiny of what resides behind cost-function-criteria assumptions. When a direct method to predict the amplitude and phase of free-surface multiples, such as inverse-scattering-series free-surface-multiple removal, includes the obliquity factor, and has the direct satisfaction of prerequisites such as source and receiver deghosting and wavelet estimation, then the better the direct method of providing the prerequisites performs, the better the free-surface demultiple provides the amplitude and phase of the free-surface multiples. If at any stage you decide you can "roll in" obliquity, source and receiver deghosting, and wavelet estimation into a catch-all energy-minimization adaptive subtraction, you run into the serious problem: No matter how much better you achieve a satisfaction of energy minimization, you still have no guarantee that that improved energy minimization aligns with and supports free-surface-multiple removal while preserving primaries. In fact, removal of multiples can increase "energy" (e.g., when you have destructive interference between a primary and a multiple), and it is widely understood that the energy-minimization criteria are among today's greatest impediments to effectively removing free-surface and internal multiples for complex onshore and marine plays. The criteria behind the indirect adaptive step matter. Within the area of free-surface and internal-multiple attenuation, the rush to and overreliance on energy-minimization adaptive subtraction contributes to the inability to effectively and surgically remove multiples at all offsets and without damaging primaries. That specific issue was discussed in a recent report to the M-OSRP consortium on seeking adaptive criteria (Weglein, 2012) that serve as an alternative and replacement for energy minimization for free-surface multiple removal. However, the trend of using indirect methods for phenomena and processing goals within the system, and for providing prerequisites within the system, is in general a conceptual and practical mistake. There has been a dangerous and growing tendency to solve everything inside and outside the system by using indirect methods and cost functions. Of course the need for ever-faster computers is universally recognized and supported. However, the growth in computational physics, often at the expense of mathematical physics, and the availability of ever-faster computers, encourages the rush to "cost functions" and to searching without thinking, and thus represents a ubiquitous, misguided, and unfortunate trend, with "solutions" that aren't. When we give up on physics and determinism, we look at statistics and searching, and indirect methods become a "natural" choice and are always readily available, along with their drawbacks and consequences.

A direct method provides a framework of precise data needs, and it delivers a straight-ahead formula that takes in your data and actually solves and explicitly and directly outputs the solution that you seek. Indirect methods can never provide that clarity or confidence. Model-matching and iterative updating by any fancy name, such as a new "Frechet derivative," and the so-called "full-wave inversion," are model-matching and are never, ever, equivalent to a direct inversion for the Earth's elastic mechanical property changes. The distinction is significant and has both conceptual and mercantile consequences.

Here is an example of the difference. Suppose someone said that you could take a single seismic trace that is a single function of time, and invert simultaneously for velocity and density, each as a function of depth in a 1D Earth.

Today, you might reasonably be cautious and concerned because the dimension of the data is less than the overall dimension of the quantities you seek to determine. We have learned as an industry to be dubious in the latter single-trace, solve-for-two-functions-of-depth case. We look skeptically at those who would model-match and pull all kinds of arcane cost functions and generalized inverses together, using different norms and constraints and full-wave predictions of that single trace that can be model-matched with amplitude and

phase so that we can call that model-matching scheme "full-waveform inversion." Why can't we solve for density and velocity uniquely from a single trace, because we can certainly model the single trace from knowing the velocity and density as a function of depth? That's a beginning and an example of thinking that solving a forward problem in an inverse sense is in some way actually solving the inverse problem. What came along in that earlier time, as a response to this question, were direct acoustic inversion methods that said that inverting for velocity and density as functions of depth from a single trace is impossible, or at least that it is impossible to provide the unique and actual velocity and density as a function of depth. That direct-inversion framework convinced many (hopefully most) people that the one-trace-in, two-functions-out approach is not a question or an issue of which indirect algorithm or L_p cost function you are using. It is more basic and stands above algorithm; it's an inadequate-data issue. No algorithm with that single-trace data input should call itself "inversion," even if that single trace was model-matched and iteratively updated and computed with amplitude and phase and, with too much self-regard, labels itself as "full-wave inversion." We learned to stop running that single trace through search algorithms for velocity and density—and that lesson was absorbed within our collective psyches in our industry—for whatever the cost function and local or global minimum you employed. Using the wrong and fundamentally inadequate data closes the book and constitutes the end of the story. Thus, we learned to look for and respect dimension between the data and the sought-after parameters we want to identify. That is a good thing, but it turns out that it's not a good-enough thing. In fact, direct acoustic wavefield inversion for a 1D Earth requires all the traces for a given shot record in order to determine one or more parameters (e.g., V_p and density) as a function of depth.

This article will show (in a similar way) that the fact that you can solve the forward Zoeppritz equations (or a linear approximate) for a PP reflection coefficient as a function of incident angle and the changes in λ, μ, and ρ across the reflector does not imply that you can solve for changes in λ, μ, and ρ in terms of the PP reflection coefficient as a function of angle. A direct inverse for the changes in λ, μ, and ρ demands all multicomponent sources and receivers, or, equivalently, PP, PS, SP, and SS data.

These conditions on data requirements hold for any processing/inverse problem in which the reference or background medium is elastic—e.g., for all amplitude analysis, including AVO and so-called FWI and all ISS multiple removal and imaging with ocean-bottom or onshore acquisition. See Li et al. (2011), Liang et al. (2010), Matson (1997), Matson and Weglein (1998), Weglein et al. (2003), and H. Zhang (2006).

"Inadequate data" means something much more basic and fundamental than limitations due to sampling, aperture, and bandwidth. That is, indirect solutions can (and often do) input data that are fundamentally inadequate from a basic and direct inverse perspective and understanding. The indirect

methods then search locally and globally around error surfaces with Frechet derivatives and conjugate gradients, and they keep hordes of math, physics, geophysics, and computer scientists busy using giant and super-fast computers looking at outputs and 3D color displays, and being convinced that with all the brainpower and resources that are invested, they are on track and are on their way to solving the problem. What's wrong with linear iterative updating? What's wrong begins with understanding the meaning of a linear inverse. Even in cases in which the data are adequate—e.g., cases with P-wave data and an acoustic inverse model—the algorithms that a direct inverse provides for explicit linear and each nonlinear estimate of changes in P-wave velocity and density, will differ at the first nonlinear step and at every subsequent step, with the nonlinear iterative linear estimate of these changes in physical properties. The linear, quadratic, cubic, … estimates of physical properties from a direct inverse method are explicit and unique (a generalized Taylor/geometric series) and order-by-order in the data and will not agree with an iterative linear update. Hence, although the iterative linear updating is nonlinear in the data, it does not represent a direct inverse solution. Further, the terms in the direct solution are analytically determined in terms of the first term, whereas iterative linear updating requires generalized inverses, SVD, cost functions, and numerical solutions. They could not be more different. If you had an alternative to the solution of the quadratic equation and it produced different roots from those produced by the direct quadratic formula, (Equation 2), would you call it "an inverse solution for the roots?" That's the issue, and it's that simple.

For the elastic inverse case, the difference is yet more serious. A direct inverse solution for the P-velocity, V_P, shear velocity, V_S, and density, ρ, and a linear iterative method, will already differ at the linear step, and that difference and resulting gap grow at each nonlinear step and estimate.

When it comes to directly inverting for changes in elastic properties and density, there are direct and explicit formulas for the linear and nonlinear estimates. The same single unchanged direct inverse ISS set of equations that derived the algorithms for free-surface and internal-multiple removal—and have demonstrated standalone capability (see, e.g., Ferreira, 2011; Luo et al., 2011; and Weglein et al., 2003, 2011)—have also provided the ISS depth imaging (Weglein et al. 2011, 2012) and direct inversion for Earth mechanical properties. In Zhang (2006), we find the first direct nonlinear equations for estimating the changes in elastic properties for a 1D Earth.

The mathematical origin of linear inverse theory (and linear iterative inversion) begins with a Taylor series of the recorded data, $D(m)$, from the actual Earth. Those data depend on the Earth properties characterized by the label m and the synthetic data $D(m_0)$ from an estimate or reference value of those properties that we label, m_0. To relate $D(m)$ and $D(m_0)$, we introduce a Taylor series

$$D(m) = D(m_0) + D'(m_0)\Delta m + \frac{D''(m_0)}{2}\Delta m^2 + \ldots, \quad (7)$$

in which the derivatives are Frechet derivatives. A linearized form of Equation 7 is considered

$$D(m) = D(m_0) + D'(m_0)\Delta m_1^1, \quad (8)$$

where the Frechet derivative,

$$D'(m_0) = \frac{D(m_0 + \varepsilon\Delta m) - D(m_0)}{\varepsilon\Delta m} \quad (9)$$

is approximated by a finite-difference approximation involving data at m_0 and data at a nearby model, $m_0+\varepsilon\Delta m$. Δm_1^1 means the first linear estimate of Δm, with the subscript standing for linear and the superscript for the first estimate. The matrix inversion of Equation 8 for Δm_1^1 leads to a new approximate $m_0+\Delta m_1^1$, and

$$D(m) - D(m_0 + \Delta m_1^1) = D'(m_0 + \Delta m_1^1)\Delta m_1^2. \quad (10)$$

The process is repeated and is the basis of iterative linear inversion. Properties of that process related to convergence to m are spelled out in Blum (1972), page 536, with issues where the constants such as M that appear in the convergence criteria are unknown.

Another starting point for this type of perturbative approach is from scattering theory, where $D(m)$ relates to the actual Green's function, G, and $D(m_0)$ relates to the reference Green's function, G_0, and $V = m–m_0$. The identity among G, G_0, and V is called the Lippmann-Schwinger or Scattering Equation (see, e.g., Taylor 1972)

$$G = G_0 + G_0VG \quad (11)$$

and an expansion of Equation 11 for G in terms of G_0 and V produces

$$G = G_0 + G_0VG_0 + G_0VG_0VG_0 + \ldots. \quad (12)$$

Keys and Weglein (1983) provide the formal association between $D'(m_0)\Delta m$ and G_0VG_0. Equation 7 is a Taylor series in Δm, and as such that series does not have an available inverse series. However, because Equation 12 (which follows from the scattering Equation 11) is a geometric series in $r = VG_0$ and $a = G_0$, then a geometric series for $S = G–G_0$ in terms of a and r—$S = ar/(1–r)$—has an inverse series $r = (S/a)/(1+S/a)$ with terms

$$r_1 = S/a$$

$$r_2 = -(S/a)^2$$

$$r_3 = (S/a)^3$$

$$r_4 = -(S/a)^4$$

$$\ldots .$$

A unique expansion of VG_0 in orders of measurement values of $(G-G_0)$ is

$$VG_0 = (VG_0)_1 + (VG_0)_2 + \ldots \quad (13)$$

The scattering-theory equation allows that forward series form the opportunity to find a direct inverse solution. Substituting Equation 13 into Equation 12 and setting the terms of equal order in the data to be equal, we have $D = G_0 V_1 G_0$, where the higher order terms are $V_2, V_3, \ldots$, as given in Weglein et al. (2003) page R33 Equations 7—14.

For the elastic equation, V is a matrix and the relationship between the data and V_1 is

$$\begin{pmatrix} D^{PP} & D^{PS} \\ D^{SP} & D^{SS} \end{pmatrix} = \begin{pmatrix} G_0^P & 0 \\ 0 & G_0^S \end{pmatrix} \begin{pmatrix} V_1^{PP} & V_1^{PS} \\ V_1^{SP} & V_1^{SS} \end{pmatrix} \begin{pmatrix} G_0^P & 0 \\ 0 & G_0^S \end{pmatrix}$$

$$V_1 = \begin{pmatrix} V_1^{PP} & V_1^{PS} \\ V_1^{SP} & V_1^{SS} \end{pmatrix}$$

$$V = \begin{pmatrix} V^{PP} & V^{PS} \\ V^{SP} & V^{SS} \end{pmatrix}$$

$$V = V_1 + V_2 + \ldots$$

where V_1, V_2 are linear, quadratic contributions to V in terms of the data,

$$D = \begin{pmatrix} D^{PP} & D^{PS} \\ D^{SP} & D^{SS} \end{pmatrix}.$$

The changes in elastic properties and density are contained in $V = \begin{pmatrix} V^{PP} & V^{PS} \\ V^{SP} & V^{SS} \end{pmatrix}$, and that leads to direct and explicit solutions for the changes in mechanical properties in orders of the data, $D = \begin{pmatrix} D^{PP} & D^{PS} \\ D^{SP} & D^{SS} \end{pmatrix}$,

$$\frac{\Delta\lambda}{\lambda} = \left(\frac{\Delta\lambda}{\lambda}\right)_1 + \left(\frac{\Delta\lambda}{\lambda}\right)_2 + \ldots$$

$$\frac{\Delta\mu}{\mu} = \left(\frac{\Delta\mu}{\mu}\right)_1 + \left(\frac{\Delta\mu}{\mu}\right)_2 + \ldots$$

$$\frac{\Delta\rho}{\rho} = \left(\frac{\Delta\rho}{\rho}\right)_1 + \left(\frac{\Delta\rho}{\rho}\right)_2 + \ldots$$

The ability of the forward series to have a direct inverse series derives from (1) the identity among G, G_0, V provided by the scattering equation and then (2) the recognition that the forward solution can be viewed as a geometric series for the data, D, in terms of VG_0. The latter derives the direct inverse series for VG_0 in terms of the data.

Viewing the forward problem and series as the Taylor series (Equation 7) in terms of Δm does not offer a direct inverse series, and hence there is no choice but to solve the forward series in an inverse sense. It is that fact that results in all current AVO and FWI methods being modeling methods that are solved in an inverse sense. Among references that solve a forward problem in an inverse sense in P-wave AVO are Beylkin and Burridge (1990), Boyse and Keller (1986),

Burridge et al. (1998), Castagna and Smith (1994), Clayton and Stolt (1981), Foster et al. (2010), Goodway (2010), Goodway et al. (1997), Shuey (1985), Smith and Gidlow (2000), Stolt (1992), and Stolt and Weglein (1985). The intervention of the explicit relationship among G, G_0, and V (the scattering equation) in a Taylor series-like form produces a geometric series and a direct inverse solution.

The linear equations are:

$$\begin{pmatrix} \hat{D}^{PP} & \hat{D}^{PS} \\ \hat{D}^{SP} & \hat{D}^{SS} \end{pmatrix} = \begin{pmatrix} \hat{G}_0^P & 0 \\ 0 & \hat{G}_0^S \end{pmatrix} \begin{pmatrix} \hat{V}_1^{PP} & \hat{V}_1^{PS} \\ \hat{V}_1^{SP} & \hat{V}_1^{SS} \end{pmatrix} \begin{pmatrix} \hat{G}_0^P & 0 \\ 0 & \hat{G}_0^S \end{pmatrix} \quad (14)$$

$$\hat{D}^{PP} = \hat{G}_0^P \hat{V}_1^{PP} \hat{G}_0^P \quad (15)$$

$$\hat{D}^{PS} = \hat{G}_0^P \hat{V}_1^{PS} \hat{G}_0^S \quad (16)$$

$$\hat{D}^{SP} = \hat{G}_0^S \hat{V}_1^{SP} \hat{G}_0^P \quad (17)$$

$$\hat{D}^{SS} = \hat{G}_0^S \hat{V}_1^{SS} \hat{G}_0^S \quad (18)$$

$$\tilde{D}^{PP}\left(k_g, 0; -k_g, 0; \omega\right) = -\frac{1}{4}\left(1 - \frac{k_g^2}{v_g^2}\right)\tilde{a}_\rho^{(1)}\left(-2v_g\right) - \frac{1}{4}\left(1 + \frac{k_g^2}{v_g^2}\right)\tilde{a}_\gamma^{(1)}\left(-2v_g\right) + \frac{2k_g^2\beta_0^2}{\left(v_g^2 + k_g^2\right)\alpha_0^2}\tilde{a}_\mu^{(1)}\left(-2v_g\right) \quad (19)$$

$$\tilde{D}^{PS}\left(v_g, \eta_g\right) = -\frac{1}{4}\left(\frac{k_g}{v_g} + \frac{k_g}{\eta_g}\right)\tilde{a}_\rho^{(1)}\left(-v_g - \eta_g\right) - \frac{\beta_0^2}{2\omega^2}k_g\left(v_g + \eta_g\right)\left(1 - \frac{k_g^2}{v_g\eta_g}\right)\tilde{a}_\mu^{(1)}\left(-v_g - \eta_g\right) \quad (20)$$

$$\tilde{D}^{PS}\left(v_g, \eta_g\right) = \frac{1}{4}\left(\frac{k_g}{v_g} + \frac{k_g}{\eta_g}\right)\tilde{a}_\rho^{(1)}\left(-v_g - \eta_g\right) + \frac{\beta_0^2}{2\omega^2}k_g\left(v_g + \eta_g\right)\left(1 - \frac{k_g^2}{v_g\eta_g}\right)\tilde{a}_\mu^{(1)}\left(-v_g - \eta_g\right) \quad (21)$$

and

$$\tilde{D}^{SS}\left(k_g, \eta_g\right) = \frac{1}{4}\left(1 - \frac{k_g^2}{\eta_g^2}\right)\tilde{a}_\rho^{(1)}\left(-2\eta_g\right) - \left[\frac{\eta_g^2 + k_g^2}{4\eta_g^2} - \frac{2k_g^2}{\eta_g^2 + k_g^2}\right]\tilde{a}_\mu^{(1)}\left(-2\eta_g\right), \quad (22)$$

where $a_\gamma^{(1)}$, $a_\mu^{(1)}$, and $a_\rho^{(1)}$ are the linear estimates of the changes in bulk modulus, shear modulus, and density, respectively. The direct quadratic nonlinear equations are

$$\begin{pmatrix} \hat{G}_0^P & 0 \\ 0 & \hat{G}_0^S \end{pmatrix} \begin{pmatrix} \hat{V}_2^{PP} & \hat{V}_2^{PS} \\ \hat{V}_2^{SP} & \hat{V}_2^{SS} \end{pmatrix} \begin{pmatrix} \hat{G}_0^P & 0 \\ 0 & \hat{G}_0^S \end{pmatrix} = -\begin{pmatrix} \hat{G}_0^P & 0 \\ 0 & \hat{G}_0^S \end{pmatrix} \begin{pmatrix} \hat{V}_1^{PP} & \hat{V}_1^{PS} \\ \hat{V}_1^{SP} & \hat{V}_1^{SS} \end{pmatrix} \begin{pmatrix} \hat{G}_0^P & 0 \\ 0 & \hat{G}_0^S \end{pmatrix} \begin{pmatrix} \hat{V}_1^{PP} & \hat{V}_1^{PS} \\ \hat{V}_1^{SP} & \hat{V}_1^{SS} \end{pmatrix} \begin{pmatrix} \hat{G}_0^P & 0 \\ 0 & \hat{G}_0^S \end{pmatrix}, \quad (23)$$

$$\hat{G}_0^P \hat{V}_2^{PP} \hat{G}_0^P = -\hat{G}_0^P \hat{V}_1^{PP} \hat{G}_0^P \hat{V}_1^{PP} \hat{G}_0^P - \hat{G}_0^P \hat{V}_1^{PS} \hat{G}_0^S \hat{V}_1^{SP} \hat{G}_0^P, \quad (24)$$

$$\hat{G}_0^P \hat{V}_2^{PS} \hat{G}_0^S = -\hat{G}_0^P \hat{V}_1^{PP} \hat{G}_0^P \hat{V}_1^{PS} \hat{G}_0^S - \hat{G}_0^P \hat{V}_1^{PS} \hat{G}_0^S \hat{V}_1^{SS} \hat{G}_0^S, \quad (25)$$

$$\hat{G}_0^S \hat{V}_2^{SP} \hat{G}_0^P = -\hat{G}_0^S \hat{V}_1^{SP} \hat{G}_0^P \hat{V}_1^{PP} \hat{G}_0^P - \hat{G}_0^S \hat{V}_1^{SS} \hat{G}_0^S \hat{V}_1^{SP} \hat{G}_0^P, \quad (26)$$

$$\hat{G}_0^S \hat{V}_2^{SS} \hat{G}_0^S = -\hat{G}_0^S \hat{V}_1^{SP} \hat{G}_0^P \hat{V}_1^{PS} \hat{G}_0^S - \hat{G}_0^S \hat{V}_1^{SS} \hat{G}_0^S \hat{V}_1^{SS} \hat{G}_0^S. \quad (27)$$

Because $\hat{V}_1^{PP}$ relates to $\hat{D}^{PP}$, $\hat{V}_1^{PS}$ relates to $\hat{D}^{PS}$, and so on, the four components of the data will be coupled in the nonlinear elastic inversion. We cannot perform the direct nonlinear inversion without knowing all components of the data. Thus, the direct nonlinear solution determines the data needed for a direct inverse. That, in turn, defines what a linear estimate means. That is, a linear estimate of a parameter is an estimate of a parameter that is linear in data that can directly invert for that parameter. Because D_{PP}, D_{PS}, D_{SP}, and D_{SS} are needed to determine a_γ, a_μ, and a_ρ directly, a linear estimate for any one of these quantities requires simultaneously solving Equations 19–22. See, e.g., Weglein et al. (2009) for further detail.

Those direct nonlinear formulas are like the direct solution for the quadratic equation mentioned above and solve directly and nonlinearly for changes in V_P, V_S, and density in a 1D elastic Earth. Stolt and Weglein (2012), present the linear equations for a 3D Earth that generalize Equations 19-22. Those formulas prescribe precisely what data you need as input, and they dictate how to compute those sought-after mechanical properties, given the necessary data. There is no search or cost function, and the unambiguous and unequivocal data needed are full multicomponent data—PP, PS, SP, and SS—for all traces in each of the P and S shot records. The direct algorithm determines first the data needed and then the appropriate algorithms for using those data to directly compute the sought-after changes in the Earth's mechanical properties. Hence, any method that calls itself inversion (let alone full-wave inversion) for determining changes in elastic properties, and in particular the P-wave velocity, V_P, and that inputs only P-data, is more off base, misguided, and lost than the methods that sought two or more functions of depth from a single trace. You can model-match P-data until the cows come home, and that takes a lot of computational effort and people with advanced degrees in math and physics computing Frechet derivatives, and requires sophisticated L_p norm cost functions and local or global search engines, so it must be reasonable, scientific, and worthwhile. Why can't we use just PP data to invert for changes in V_P, V_S, and density, because Zoeppritz says that we can model PP from those quantities, and because we have, using PP-data with angle variation, enough dimension? As stated above, data dimension is good, but not good enough for a direct inversion of those elastic properties.

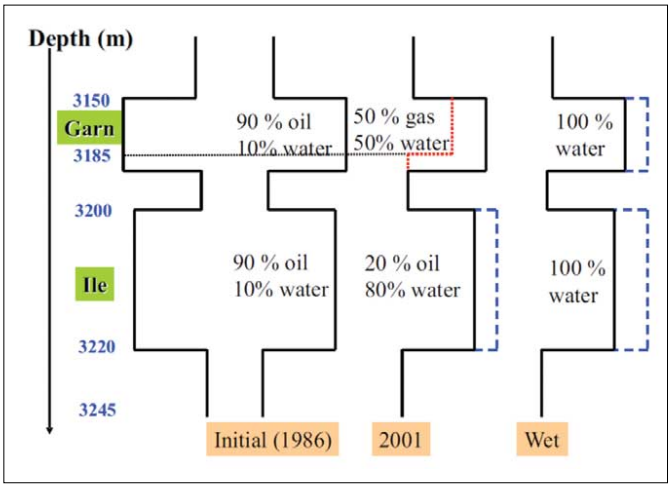

Figure 1. *Synthetic well log A-52.*

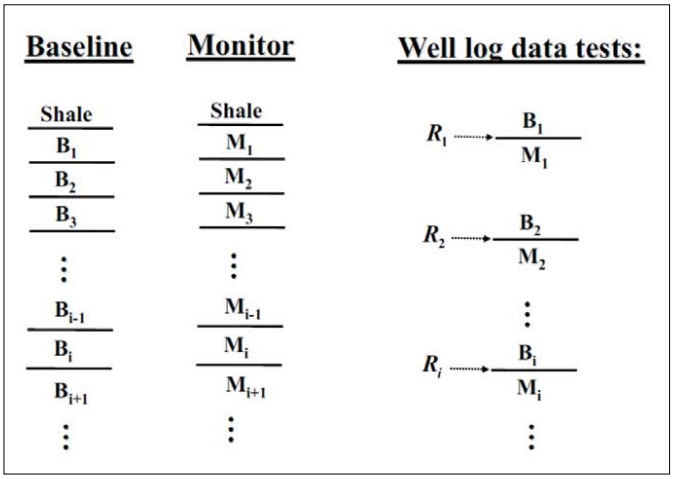

Figure 2. *The baseline, monitor, and input reflection coefficients.*

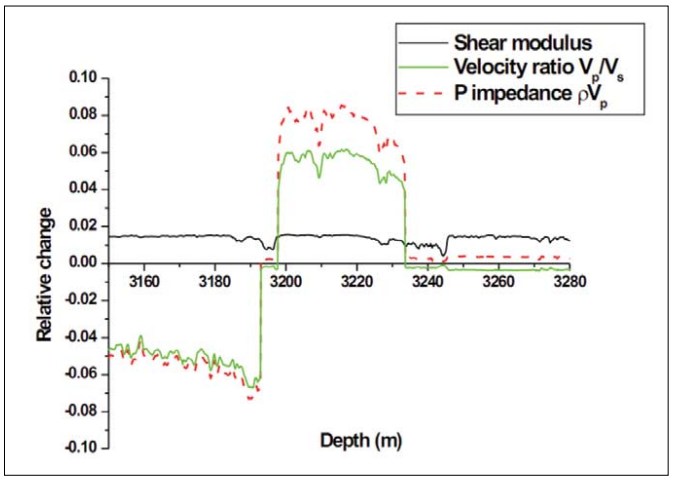

Figure 3. *Comparison of actual changes in shear modulus, P-impedance, and velocity ratio V_p/V_S. The baseline is the log data in 1986 and the monitor is the log data in 2001.*

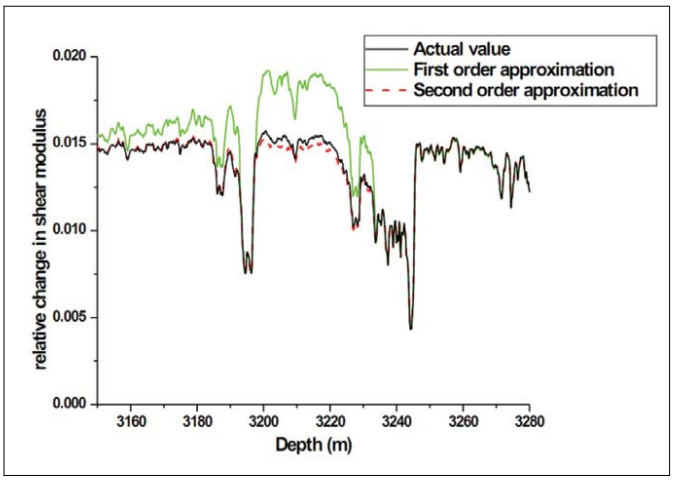

Figure 4. *Comparison of first- and second-order approximations of relative change in shear modulus. The baseline is the log data in 1986 and the monitor is the log data in 2001.*

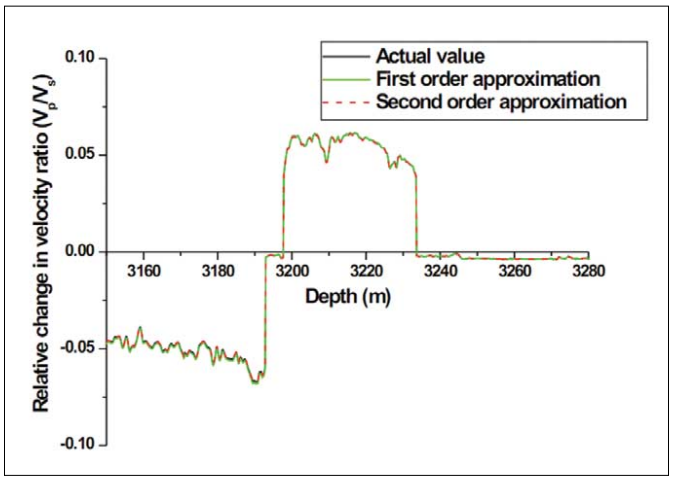

Figure 5. *Comparison of first- and second-order approximations of relative change in V_p/V_S. The baseline is the log data in 1986 and the monitor is the log data in 2001.*

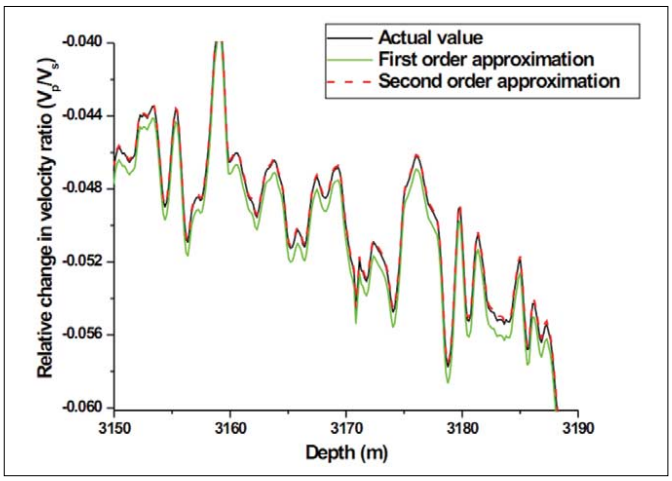

Figure 6. *Zoomed-in comparison of first- and second-order approximations of relative change in V_p/V_S. The baseline is the log data in 1986 and the monitor is the log data in 2001.*

The direct inverse is nonlinear. Iterative linear is nonlinear. But iterative linear inversion is not in any way equivalent to a direct nonlinear inversion. The further evidence that iterative linear inverse is not a direct elastic inverse solution, is that you can iteratively linear invert P-wave data. Hence, you can have the fundamentally inadequate data and perform iterative linear updating. That's not possible with a direct inverse method. The framework, data needs, and algorithms provided by direct inversion all matter. If you iteratively linear invert multicomponent data, you would not be performing a direct inversion, and your nonlinear estimates would not agree with the unique nonlinear terms provided by a direct solution. Multicomponent data are important, but the direct inverse algorithm of that data is essential. The framework of a direct method helps you understand what will allow things to work in principle, and, equally important, it helps you identify the issue or problem when things don't work. Indirect methods, on the other hand, can never match that definiteness, clarity, and value. When we use just P-wave data with an acoustic or elastic model-matching FWI for shallow-hazard detection or velocity estimation at top salt, and then issues arise, perhaps the framework and requirements described in this note might be among the issues behind a lack of predictive stability and usefulness.

In "Wave theory modeling of P-waves in a heterogeneous elastic medium" (Weglein 2012), a single-channel P-wave formalism is presented as a way to model P-waves in amplitude and phase without needing to model and predict shear waves. This P-only wave-modeling method is intractable as a parameter-estimation inverse procedure, blocked at the first and linear term. That supports the need for all multicomponent data in a direct inverse for estimating changes in the Earth's mechanical properties. If one somehow remained insistent that P-data were adequate for a direct elastic inverse, one would have to provide a response to that linear, intractable inverse step. Further, those direct and explicit nonlinear formulas are derivable only from the direct inverse machinery of the inverse scattering series (please see the References section).

Using P-wave data with amplitude and phase for an acoustic Earth model flies in the face of 40 years of AVO experience, which says that the elastic Earth is the minimum realistic Earth model for any amplitude-dependent algorithm or processing method. Using P-wave data for an elastic Earth model, with algorithms that utilize amplitude and phase, violates the necessary multicomponent data needs prescribed by direct inversion of V_P, V_S, and density. Having the adequate data (defined by a direct-inversion framework) is better than not having the necessary and sufficient data and is a good place to start. However, even when one is starting with the indicated multicomponent data, the train can still be taken off the track by indirect search and iterative linear-updating algorithms, when direct inverse algorithms are indicated and available. Iterative linear updating of multicomponent data is a model-matching indirect method and is never equivalent to a direct inversion of those data.

Some might say in response that P-wave FWI with either an acoustic or elastic medium, followed by use of some search algorithm, represents "an approximation," and what's wrong with approximations? The answer is precisely that "What IS wrong with the approximation?" If you purposefully or inadvertently ignore (or wish away) the framework and algorithms that a direct solution to the elastic parameter estimation provides, you will never know what you are ignoring and dropping and what your approximation is approximating, nor will you know what value your method actually represents and means, and how you could improve the reliability of your prediction.

In summary, so-called P-wave FWI is something less than advertised and is in general the wrong (acoustic) Earth model, the wrong data, and the wrong method—but besides that, it has a lot going for it.

In Zhang (2006), the direct elastic inverse was applied to a 4D application and the term beyond linear was able to help distinguish a pressure change from a fluid change. This line of research continued in Li (2011) and Liang (2010). This is comparatively illustrated with synthetic log data in Zhang's Figures 1 through 6 (which are included in this article).

Epilog

A direct method to find the route from where you are to where you want to go—e.g., for a scheduled meeting—would use MapQuest, while an indirect method would seek and search and stop at every possible location in the city until you arrive somewhere where someone seems to be happy to see you, and you have a toolbox of L_p cost functions to define "happy." A direct solution, in contrast to indirect methods, does not require or ever raise the issue of necessary but insufficient conditions or cost functions, and it's not a "condition" or property. It's a solution, a construction. Nothing beats that for clarity, efficiency, and effectiveness. The direct MapQuest inversion communication and message to the current indirect P-wave FWI methods is that the latter are searching for the meeting in the wrong city.

The message of this article is that direct inversion provides a framework, and a set of data requirements and algorithms, that not only have produced a standalone capability (with model-type independent algorithms) for removing free-surface and internal multiples, without subsurface information, but also for establishing the requirements for all seismic processing methods that depend on amplitude analysis, such as AVO and so-called FWI. Being frank, we wish these requirements were not the case, because it makes our lives more complicated and difficult—but the conclusions are inescapable. When the framework, data requirements, and direct methods are not satisfied, we have a clear and understandable reason for the resulting failure and for what we might do to provide more reliable and useful predictive capability. Direct and indirect methods both play an essential role in an effective seismic processing strategy: where the former accommodates the physics within the system, and the latter provides a channel for real-world phenomena beyond the assumed physics. TLE

References

Anderson, J. E., L. Tan, and D. Wang, 2012, Time-reversal checkpointing methods for RTM and FWI: Geophysics, **77**, no. 4, S93–S103, http://dx.doi.org/10.1190/geo2011-0114.1.

Baumstein, A., J. E. Anderson, D. L. Hinkley, and J. R. Krebs, 2009,

Scaling of the objective function gradient for full-wavefield inversion: 79th Annual International Meeting, SEG, Expanded Abstracts, 2243–2247, http://dx.doi.org/10.1190/1.3255307

Beylkin, G. and R. Burridge, 1990, Linearized inverse scattering problem of acoustics and elasticity: Wave Motion, **12**, no. 1, 15–22, http://dx.doi.org/10.1016/0165-2125(90)90017-X.

Ben-Hadj-ali, H., S. Operto, and J. Virieux, 2008, Velocity model building by 3D frequency-domain, full-waveform inversion of wide-aperture seismic data: Geophysics, **73**, no. 5, VE101–VE117, http://dx.doi.org/10.1190/1.2957948.

Ben-Hadj-ali, H., S. Operto, and J. Vireux, 2009, Efficient 3D frequency-domain full-waveform inversion (FWI) with phase encoding: 71st Conference and Exhibition, EAGE, Extended Abstracts, P004.

Biondi, B. and P. Sava, 1999, Wave-equation migration velocity analysis: 69th Annual International Meeting, SEG, Expanded Abstracts, 1723–1726, http://dx.doi.org/10.1190/1.1820867.

Biondi, B. and W. Symes, 2004, Angle-domain common-image gathers for migration velocity analysis by wavefield-continuation imaging: Geophysics, **69**, no. 5, 1283–1298, http://dx.doi.org/10.1190/1.1801945.

Blum, E. K., 1972, Numerical analysis and computation: Theory and practice: Addison-Wesley.

Boyse, W. E. and J. B. Keller, 1986, Inverse elastic scattering in three dimensions: The Journal of the Acoustical Society of America, **79**, no. 2, 215–218, http://dx.doi.org/10.1121/1.393561.

Brandsberg-Dahl, S., M. de Hoop, and B. Ursin, 1999, Velocity analysis in the common scattering-angle/azimuth domain: 69th Annual International Meeting, SEG, Expanded Abstracts, 1715–1718, http://dx.doi.org/10.1190/1.1820865.

Brossier, R., S. Operto, and J. Virieux, 2009, Robust elastic frequency-domain full-waveform inversion using the L1 norm: Geophysical Research Letters, **36**, no. 20, L20310, http://dx.doi.org/10.1029/2009GL039458.

Burridge, R., M. de Hoop, D. Miller, and C. Spencer, 1998, Multiparameter inversion in anisotropic elastic media: Geophysical Journal International, **134**, 757–777.

Castagna, J. and S. Smith, 1994, Comparison of AVO indicators: A modeling study: Geophysics, **59**, no. 12, 1849–1855, http://dx.doi.org/10.1190/1.1443572.

Chavent, G. and C. Jacewitz, 1995, Determination of background velocities by multiple migration fitting: Geophysics, **60**, no. 2, 476–490, http://dx.doi.org/10.1190/1.1443785.

Clayton, R. W. and R. H. Stolt, 1981, A Born-WKBJ inversion method for acoustic reflection data: Geophysics, **46**, no. 11, 1559–1567, http://dx.doi.org/10.1190/1.1441162.

Crase, E., A. Pica, M. Noble, J. McDonald, and A. Tarantola, 1990, Robust elastic nonlinear waveform inversion: Application to real data: Geophysics, **55**, no. 5, 527–538, http://dx.doi.org/10.1190/1.1442864.

Ferreira, A., 2011, Internal multiple removal in offshore Brazil seismic data using the inverse scattering series: Master's thesis, University of Houston.

Fitchner, A., 2011, Full seismic waveform modeling and inversion: Springer-Verlag.

Foster, D., R. Keys, and F. Lane, 2010, Interpretation of AVO anomalies: Geophysics, **75**, no. 5, 75A3–75A13, http://dx.doi.org/10.1190/1.3467825.

Gauthier, O., J. Virieux, and A. Tarantola, 1986, Two dimensional nonlinear inversion of seismic waveforms: Geophysics, **51**, no. 7, 1387–1403, http://dx.doi.org/10.1190/1.1442188.

Goodway, B., 2010, The magic of Lamé: The Leading Edge, **29**, no. 11, 1432, http://dx.doi.org/10.1190/tle29111432.1.

Goodway, B., T. Chen, and J. Downton, 1997, Improved AVO fluid detection and lithology discrimination using Lamé petrophysical parameters; "λρ", "μρ", and "λ/μ fluid stack", from P and S inversions: 67th Annual International Meeting, SEG, Expanded Abstracts, 183–186, http://dx.doi.org/10.1190/1.1885795.

Guasch, L., M. Warner, T. Nangoo, J. Morgan, A. Umpleby, I. Stekl, and N. Shah, 2012, Elastic 3D full-waveform inversion: 82nd Annual International Meeting, SEG, Expanded Abstracts, 1–5, http://dx.doi.org/10.1190/segam2012-1239.1.

Hawthorn, A., 2009, Real time seismic measurements whilst drilling-A drilling optimization measurement for subsalt wells: EAGE Subsalt Imaging Workshop.

Iledare, O. O. and M. J. Kaiser, 2007, Competition and performance in oil and gas lease sales and development in the U.S. Gulf of Mexico OCS Region, 1983–1999: OCS Study MMS 2007-034.

Kapoor, S., D. Vigh, H. Li, and D. Derharoutian, 2012, Full-waveform inversion for detailed velocity model building: 74th Annual Conference and Exhibition, EAGE, Extended Abstracts, W011.

Keys, R. G. and A. B. Weglein, 1983, Generalized linear inversion and the first Born theory for acoustic media: Journal of Mathematical Physics, **24**, no. 6, 1444–1449, http://dx.doi.org/10.1063/1.525879.

Li, X., F. Liu, and A. B. Weglein, 2011, Dealing with the wavelet aspect of the low frequency issue: A synthetic example: M-OSRP 2010 Annual Meeting, 82–89.

Li, X., 2011, I. Multiparameter depth imaging using the inverse scattering series; II. Multicomponent direct nonlinear inversion for elastic earth properties using the inverse scattering series: PhD thesis, University of Houston.

Liang, H., A. B. Weglein, and X. Li, 2010, Initial tests for the impact

of matching and mismatching between the Earth model and the processing model for the ISS imaging and parameter estimation: M-OSRP 2009 Annual Meeting, 165–180.

Luo, Y., P. Kelamis, Q. Fu, S. Huo, G. Sindi, S.-Y. Hsu, and A. Weglein, 2011, Elimination of land internal multiples based on the inverse scattering series: The Leading Edge, **30**, no. 8, 884–889, http://dx.doi.org/10.1190/1.3626496.

Matson, K. H., 1997, An inverse-scattering series method for attenuating elastic multiples from multicomponent land and ocean bottom seismic data: PhD thesis, University of British Columbia.

Nolan, C. and W. Symes, 1997, Global solution of a linearized inverse problem for the wave equation: Communications on Partial Differential Equations, **22**, no. 5–6, 919–952, http://dx.doi.org/10.1080/03605309708821289.

Pratt, R., 1999, Seismic waveform inversion in the frequency domain, Part I: Theory and verification in a physical scale model: Geophysics, **64**, no. 3, 888–901, http://dx.doi.org/10.1190/1.1444597.

Pratt, R. and R. Shipp, 1999, Seismic waveform inversion in the frequency domain, Part 2: Fault delineation in sediments using crosshole data: Geophysics, **64**, no. 3, 902–914, http://dx.doi.org/10.1190/1.1444598.

Rickett, J. and P. Sava, 2002, Offset and angle-domain common image-point gathers for shot-profile migration: Geophysics, **67**, no. 3, 883–889, http://dx.doi.org/10.1190/1.1484531.

Sava, P., B. Biondi, and J. Etgen, 2005, Wave-equation migration velocity analysis by focusing diffractions and reflections: Geophysics, **70**, no. 3, U19–U27, http://dx.doi.org/10.1190/1.1925749.

Sava, P. and S. Fomel, 2003, Angle-domain common-image gathers by wavefield continuation methods: Geophysics, **68**, no. 3, 1065–1074, http://dx.doi.org/10.1190/1.1581078.

Shuey, R. T., 1985, A simplification of the Zoeppritz equations: Geophysics, **50**, no. 4, 609–614, http://dx.doi.org/10.1190/1.1441936.

Sirgue, L., O. I. Barkved, J. P. Van Gestel, O. J. Askim, and J. H. Kommedal, 2009, 3D waveform inversion on Valhall wide-azimuth OBC: 71st Annual Conference and Exhibition, EAGE, Extended Abstracts, U038.

Sirgue, L., O. I. Barkved, J. Dellinger, J. Etgen, U. Albertin, and J. H. Kommedal, 2010, Full-waveform inversion: the next leap forward in imaging at Valhall: First Break, **28**, 65–70.

Sirgue, L., B. Denel, and F. Gao, 2012, Challenges and value of applying FWI to depth imaging projects: 74th Conference and Exhibition, EAGE, Extended Abstracts.

Smith, G. and M. Gidlow, 2000, A comparison of the fluid factor with λ and μ in AVO analysis: 70th Annual International Meeting, SEG, Expanded Abstracts, 122–125, http://dx.doi.org/10.1190/1.1815615.

Stolt, R. H., 1989, Seismic inversion revisited, in J. Bee Bednar, L. R. Lines, R. H. Stolt, and A. B. Weglein, eds, Proceedings of the geophysical inversion workshop: Society for Industrial and Applied Mathematics, 3–19.

Stolt, R. H. and A. B. Weglein, 1985, Migration and inversion of seismic data: Geophysics, **50**, no. 12, 2458–2472, http://dx.doi.org/10.1190/1.1441877.

Stolt, R. H. and A. B. Weglein, 2012, Seismic imaging and inversion, volume 1: Cambridge University Press.

Symes, W., 2008, Migration velocity analysis and waveform inversion: Geophysical Prospecting, **56**, no. 6, 765–790, http://dx.doi.org/10.1111/j.1365-2478.2008.00698.x.

Symes, W. W. and J. J. Carazzone, 1991, Velocity inversion by differential semblance optimization: Geophysics, **56**, no. 5, 654–663, http://dx.doi.org/10.1190/1.1443082.

Tarantola, A., 1986, A strategy for nonlinear elastic inversion of seismic reflection data: Geophysics, **51**, no. 10, 1893–1903, http://dx.doi.org/10.1190/1.1442046.

Tarantola, A., 1987, Inverse problem theory: Method for data fitting and model parameter estimation: Elsevier.

Taylor, J. R., 1972, Scattering theory: the quantum theory of nonrelativistic collisions: John Wiley and Sons.

Valenciano, A., B. Biondi, and A. Guitton, 2006, Target-oriented wave-equation inversion: Geophysics, **71**, no.4, A35–A38, http://dx.doi.org/10.1190/1.2213359.

Vigh, D. and E. W. Starr, 2008, 3D prestack plane-wave, full-waveform inversion: Geophysics, **73**, no. 5, VE135–VE144, http://dx.doi.org/10.1190/1.2952623.

Weglein, A.B., 2012, Short note: An alternative adaptive subtraction criteria (to energy minimization) for free surface multiple removal: M-OSRP 2011 Annual Report, 375.

Weglein, A. B., 2012, Short note: A formalism for (1) modeling the amplitude and phase of pressure waves from a heterogeneous elastic medium and (2) selecting and predicting P-wave events that have only experienced pressure-wave episodes in their history: M-OSRP 2011 Annual Report, 364–370.

Weglein, A. B., S.-Y. Hsu, P. Terenghi, X. Li, and R. H. Stolt, 2011, Multiple attenuation: Recent advances and the road ahead (2011): The Leading Edge, **30**, no. 8, 864–875, http://dx.doi.org/10.1190/1.3626494.

Weglein, A. B., F. Liu, X. Li, P. Terenghi, E. Kragh, J. Mayhan, Z. Wang, J. Mispel, L. Amundsen, H. Liang, L. Tang, and S.-Y. Hsu, 2012, Inverse scattering series direct depth imaging without the velocity model: first field data examples: Journal of Seismic Exploration, **21**, 1–28.

Weglein, A. B., H. Zhang, A. C. Ramirez, F. Liu, and J. Lira, 2009, Clarifying the underlying and fundamental meaning of the approximate linear inversion of seismic data: Geophysics, **74**, no. 6, WCD1–WCD13, http://dx.doi.org/10.1190/1.3256286.

Weglein, A. B. and K. Matson, 1998, Inverse-scattering interval multiple attenuation: an analytic example and subevent interpretation in S, Hassanzadeh, ed., Mathematical methods in geophysical imaging: SPIE, 1008–1017.

Weglein, A. B., F. V. Araújo, P. M. Carvalho, R. H. Stolt, K. H. Matson, R. T. Coates, D. Corrigan, D. J. Foster, S. A. Shaw, and H. Zhang, 2003, Inverse scattering series and seismic exploration: Inverse Problems, **19**, no. 6, R27–R83, http://dx.doi.org/10.1088/0266-5611/19/6/R01.

Weglein, A. B., D. J. Foster, K. H. Matson, S. A. Shaw, P. M. Carvalho, and D. Corrigan, 2002, Predicting the correct spatial location of reflectors without knowing or determining the precise medium and wave velocity: initial concept, algorithm and analytic and numerical example: Journal of Seismic Exploration, **10**, 367–382.

Zhang, H., 2006, Direct nonlinear acoustic and elastic inversion: towards fundamentally new comprehensive and realistic target identification: PhD thesis, University of Houston.

Zhang, Y. and B. Biondi, 2013, Moveout-based wave-equation migration velocity analysis: Geophysics, **78**, no. 2, U31–U39, http://dx.doi.org/10.1190/geo2012-0082.1.

Zhou, H., L. Amundsen, and G. Zhang, 2012, Fundamental issues in full-waveform inversion: 82nd Annual International Meeting, SEG, Expanded Abstracts, http://dx.doi.org/10.1190/segam2012-0878.1.

Acknowledgments: I thank the M-OSRP sponsors for their support, and Jim Mayhan, Hong Liang, Di Chang, and Lin Tang for their help in preparing this article.

Corresponding author: aweglein@Central.UH.EDU